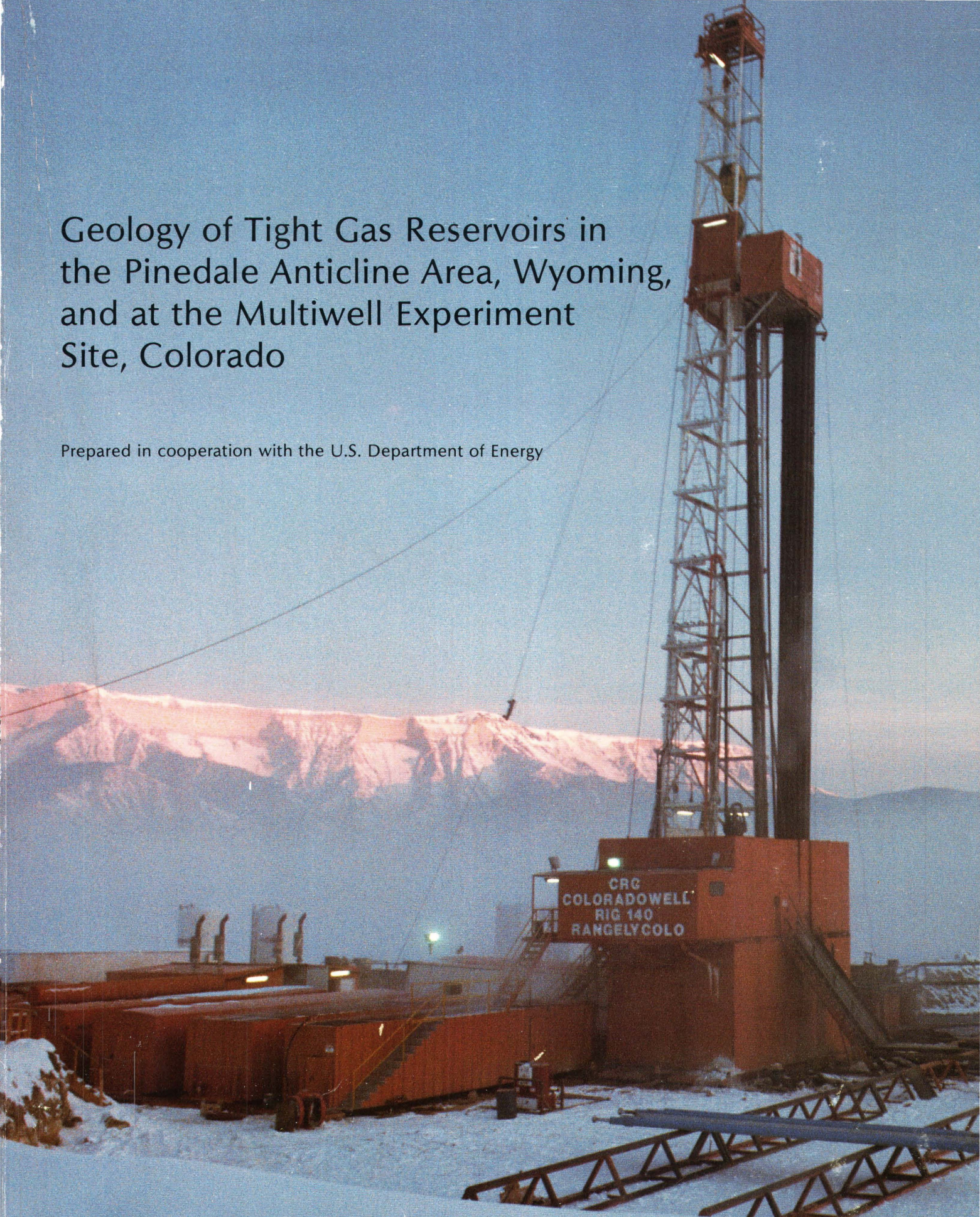


Geology of Tight Gas Reservoirs in the Pinedale Anticline Area, Wyoming, and at the Multiwell Experiment Site, Colorado

Prepared in cooperation with the U.S. Department of Energy



U.S. GEOLOGICAL SURVEY BULLETIN 1886

Front Cover: CER Corporation, MWX-2 well, Piceance basin, Colorado. The Eocene Wasatch and Green River Formations form the Roan Cliffs in the background. (Photograph by Allan R. Sattler, Sandia National Laboratories, Albuquerque, New Mexico.)

Back Cover: El Paso Natural Gas, Wagon Wheel no. 1 well, Green River basin, Wyoming. In the background are Precambrian rocks of the Wind River Mountains. (Photograph by Jack Shaughnessy, Consulting Geologist, Amarillo, Texas.)

Cover designed by Loretta J. Ulibarri

Geology of Tight Gas Reservoirs in the Pinedale Anticline Area, Wyoming, and at the Multiwell Experiment Site, Colorado

Edited by B.E. LAW and C.W. SPENCER

Prepared in cooperation with the U.S. Department of Energy

U.S. GEOLOGICAL SURVEY BULLETIN 1886

DEPARTMENT OF THE INTERIOR
MANUEL LUJAN, JR., Secretary



U.S. GEOLOGICAL SURVEY
Dallas L. Peck, Director

Any use of trade, product, or firm names in this publication is for descriptive purposes only and does not imply endorsement by the U.S. Government.

UNITED STATES GOVERNMENT PRINTING OFFICE: 1989

For sale by the
Books and Open-File Reports Section
U.S. Geological Survey
Federal Center
Box 25426
Denver, CO 80225

Library of Congress Cataloging-in-Publication Data

Geology of tight gas reservoirs in the Pinedale anticline area, Wyoming, and at the Multiwell Experiment site, Colorado / edited by B.E. Law and C.W. Spencer.

p. cm. — (U.S. Geological Survey bulletin ; 1886)

“Prepared in cooperation with the U.S. Department of Energy.”

Bibliography: p.

Supt. of Docs. no.: I 19.3: 1886

1. Gas reservoirs—Colorado—Piceance Creek Watershed. 2. Gas reservoirs—Green River Watershed (Wyo.—Utah) 3. Gas, Natural—Geology—Colorado—Piceance Creek Watershed. 4. Gas, Natural—Geology—Green River Watershed (Wyo.—Utah) I. Law, B. E. II. Spencer, Charles Winthrop, 1930– III. United States, Dept. of Energy. IV. Title: Pinedale anticline area, Wyoming. V. Title: Multiwell Experiment Site, Colorado. VI. Series.

QE75.B9no. 1886

[TN880]

557.3 s—dc20

[553.2'85'0978785]

89-600155
CIP

CONTENTS

[Letters designate chapters]

- (A) Introduction, by B.E. Law and C.W. Spencer.
- (B) Structural and stratigraphic framework of the Pinedale anticline, Wyoming, and the Multiwell Experiment site, Colorado, by B.E. Law and R.C. Johnson.
- (C) Comparison of overpressuring at the Pinedale anticline area, Wyoming, and the Multiwell Experiment site, Colorado, by Charles W. Spencer.
- (D) Mineral composition, petrography, and diagenetic modifications of lower Tertiary and Upper Cretaceous sandstones and shales, northern Green River basin, Wyoming, by Richard M. Pollastro.
- (E) Thermal history and provenance of rocks in the Wagon Wheel No. 1 well, Pinedale anticline, northern Green River basin—evidence from fission-track dating, by Nancy D. Naeser.
- (F) Analysis of vitrinite maturation and Tertiary burial history, northern Green River basin, Wyoming, by Warren W. Dickinson.
- (G) Thermal maturity patterns in the northern Green River basin, Wyoming, by M.R. Lickus, M.J. Pawlewicz, B.E. Law, and W.W. Dickinson.
- (H) Gamma-ray well-log anomaly in the northern Green River basin of Wyoming, by Stephen E. Prenskey.
- (I) Quantitative model for overpressured gas resources of the Pinedale anticline, Wyoming, by R.R. Charpentier, B.E. Law, and S.E. Prenskey.
- (J) Petrology and isotope geochemistry of mineralized fractures in Cretaceous rocks—evidence for cementation in a closed hydrologic system, by Janet K. Pitman and Warren W. Dickinson.
- (K) Reservoir sedimentology of rocks of the Mesaverde Group, Multiwell Experiment site and east-central Piceance basin, northwest Colorado, by John C. Lorenz.
- (L) Thermal history of selected coal beds in the Upper Cretaceous Mesaverde Group and Tertiary Wasatch Formation, Multiwell Experiment site, Colorado, in relation to hydrocarbon generation, by Vito F. Nuccio and Ronald C. Johnson.
- (M) Fluid inclusion evidence for paleotemperatures within the Mesaverde Group, Multiwell Experiment site, Piceance basin, Colorado, by Charles E. Barker.
- (N) Rock-Eval analysis of sediments and ultimate analysis of coal, Mesaverde Group, Multiwell Experiment site, Piceance basin, Colorado, by Charles E. Barker.
- (O) Azimuthal vertical seismic profiles at the Multiwell Experiment site, northwest Colorado, by Myung W. Lee.

CONVERSION FACTORS FOR SOME SI METRIC AND U.S. UNITS OF MEASURE

To convert from	To	Multiply by
Feet (ft)	Meters (m)	0.3048
Miles (mi)	Kilometers (km)	1.609
Pounds (lb)	Kilograms (kg)	0.4536
Degrees Fahrenheit (°F)	Degrees Celsius (°C)	Temp °C = (temp °F - 32) / 1.8

Chapter A

Introduction

By B.E. LAW and C.W. SPENCER

Prepared in cooperation with the U.S. Department of Energy

U.S. GEOLOGICAL SURVEY BULLETIN 1886

GEOLOGY OF TIGHT GAS RESERVOIRS IN THE PINEDALE ANTICLINE AREA, WYOMING,
AND AT THE MULTIWELL EXPERIMENT SITE, COLORADO

CONTENTS

Pinedale anticline **A1**
Multiwell Experiment **A3**
References cited **A6**

FIGURES

1. Map of central Rocky Mountain region of Utah, Wyoming, and Colorado showing location of Pinedale anticline and Multiwell Experiment site **A2**
2. Map showing wells drilled in the Pinedale anticline area, northern part of Green River basin, Wyoming **A3**
3. Diagram showing relative location of MWX wells in the Piceance basin of Colorado **A5**

TABLE

1. Wells drilled in Pinedale anticline area, Sublette County, Wyoming **A4**

Introduction

By B.E. Law and C.W. Spencer

Low-permeability (tight) gas reservoirs are rocks that have an estimated in situ permeability to gas of 0.1 millidarcy (mD) or less. Within the United States, these reservoirs contain major resources of gas. The National Petroleum Council (NPC) (1980) estimated the in-place gas resource for tight reservoirs in the United States at about 924.0 trillion cubic feet (TCF). More recent estimates of the gas resource in the Greater Green River basin of Wyoming, Colorado, and Utah, and in the Piceance basin of Colorado indicate that the NPC estimates for these basins are very conservative. In the Greater Green River basin, estimates of the in-place gas resource for tight reservoirs range from 3,600 to 6,800 TCF, and the mean estimate is 5,063 TCF (Law and others, 1989); in the Piceance basin, estimates of the in-place gas resource range from 274.5 to 605.0 TCF, and the mean estimate is 419.5 TCF (Johnson and others, 1987).

In 1977, the U.S. Geological Survey, in cooperation with the U.S. Department of Energy, initiated geologic investigations of low-permeability (tight) gas reservoirs in the Rocky Mountain region. The overall objectives of these efforts are to geologically characterize tight sandstone reservoirs and to estimate gas resources in selected basins. In order to accomplish these objectives, our efforts focused on small areas containing several wells or on individual wells containing large amounts of high-quality data. Two such areas that have been extensively studied are the Pinedale anticline in the northern part of the Green River basin of Wyoming and the Multiwell Experiment site in the Piceance basin of Colorado (fig. 1).

Results of the geologic investigations indicate that the tight gas-bearing reservoirs in these areas have experienced similar depositional, structural, burial, and thermal histories. Some of the relationships between the occurrences of gas and geologic characteristics are dissimilar, however, because of slight differences in the timing, intensity, and duration of geologic processes in each area. Thus, the purpose of this publication is to provide both geologic data and interpretations of tight gas reservoirs for two well-studied areas that will contribute to an improved understanding of unconventional reservoirs in other areas.

PINEDALE ANTICLINE

The Pinedale anticline is in the northern part of the Green River basin of Wyoming (figs. 1, 2). The first well drilled on the Pinedale anticline was completed in 1939 to a depth of 10,000 ft (3,048 m) by the California Company. Since that time, 19 additional wells have been drilled on the anticline (fig. 2). Specific locations and pertinent well data are shown in table 1. Most of the wells have been drilled to depths of 10,000–12,000 ft (3,058–3,658 m) in the Upper Cretaceous Lance Formation. The deepest well is the El Paso Natural Gas Company Wagon Wheel No. 1 well, which was drilled to 19,000 ft (5,791 m) into the Upper Cretaceous Baxter Shale. All the wells have encountered extensive thicknesses of gas-saturated rocks, and data obtained from the Wagon Wheel well conclusively demonstrate the occurrence of a thick gas-bearing interval below a depth of about 8,000 ft (2,438 m). The indicated in-place gas resource contained in low-permeability reservoirs in the Pinedale anticline area is about 159.0 TCF (Charpentier and others, 1987; this volume).

As a consequence of the extensive testing and coring conducted in the Wagon Wheel well, most of the geological interpretations in the Pinedale area are derived from data obtained from this well. Within the depth interval of 5,000 to 18,000 ft (1,524–5,486 m), approximately 900 ft (274 m) of rock was cored. The cored intervals are shown on figure 3 of Law and Johnson (this volume). Data derived from cores in the Wexpro and American Hunter wells (table 1) were also incorporated into these investigations.

The Wagon Wheel well, completed in 1970, was proposed as part of a nuclear stimulation project. It was intended to be the fourth nuclear experiment following the Gasbuggy, Rulison, and Rio Blanco detonations in the San Juan basin of New Mexico and the Piceance basin of Colorado. Plans for detonation of a nuclear device in the Wagon Wheel well were abandoned, however, due to environmental considerations and disappointing test results obtained from the previous three experiments. This project, including drilling and testing results, is discussed by Martin and Shaughnessy (1969) and Shaughnessy and Butcher (1973, 1974). Several other geologic studies conducted in the Wagon Wheel area are discussed in Law (1984).

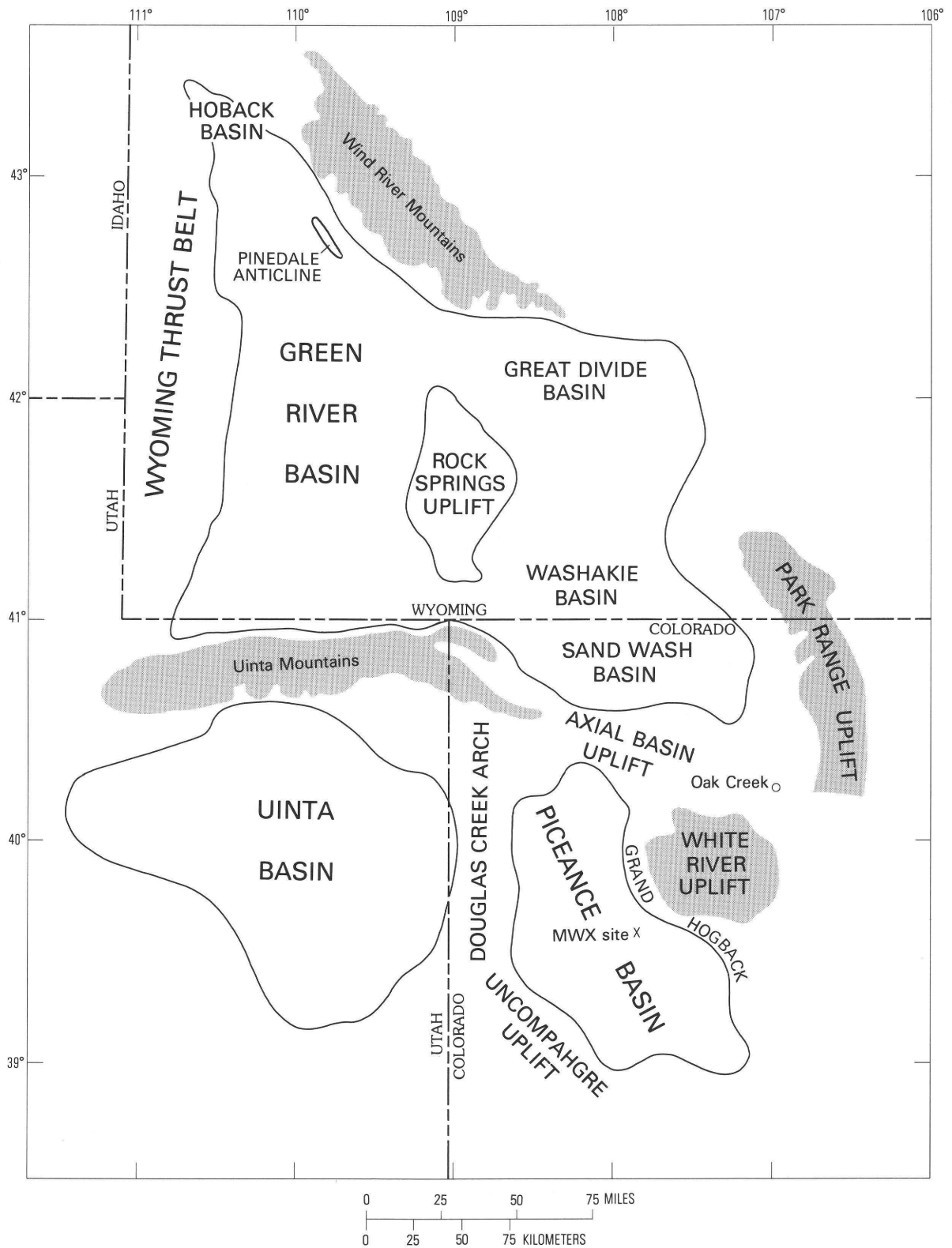


Figure 1. Central Rocky Mountain region of Utah, Wyoming, and Colorado showing location of Pinedale anticline and Multiwell Experiment (MWX) site.

Five wells currently are producing in the Pinedale anticline area and several other wells are shut-in (fig. 2, table 1). Gas production, with minor amounts of con-

densate, is from low-permeability lenticular sandstones in the Lance Formation below a depth of about 8,000 ft (2,438 m). The reservoirs require hydraulic-fracture

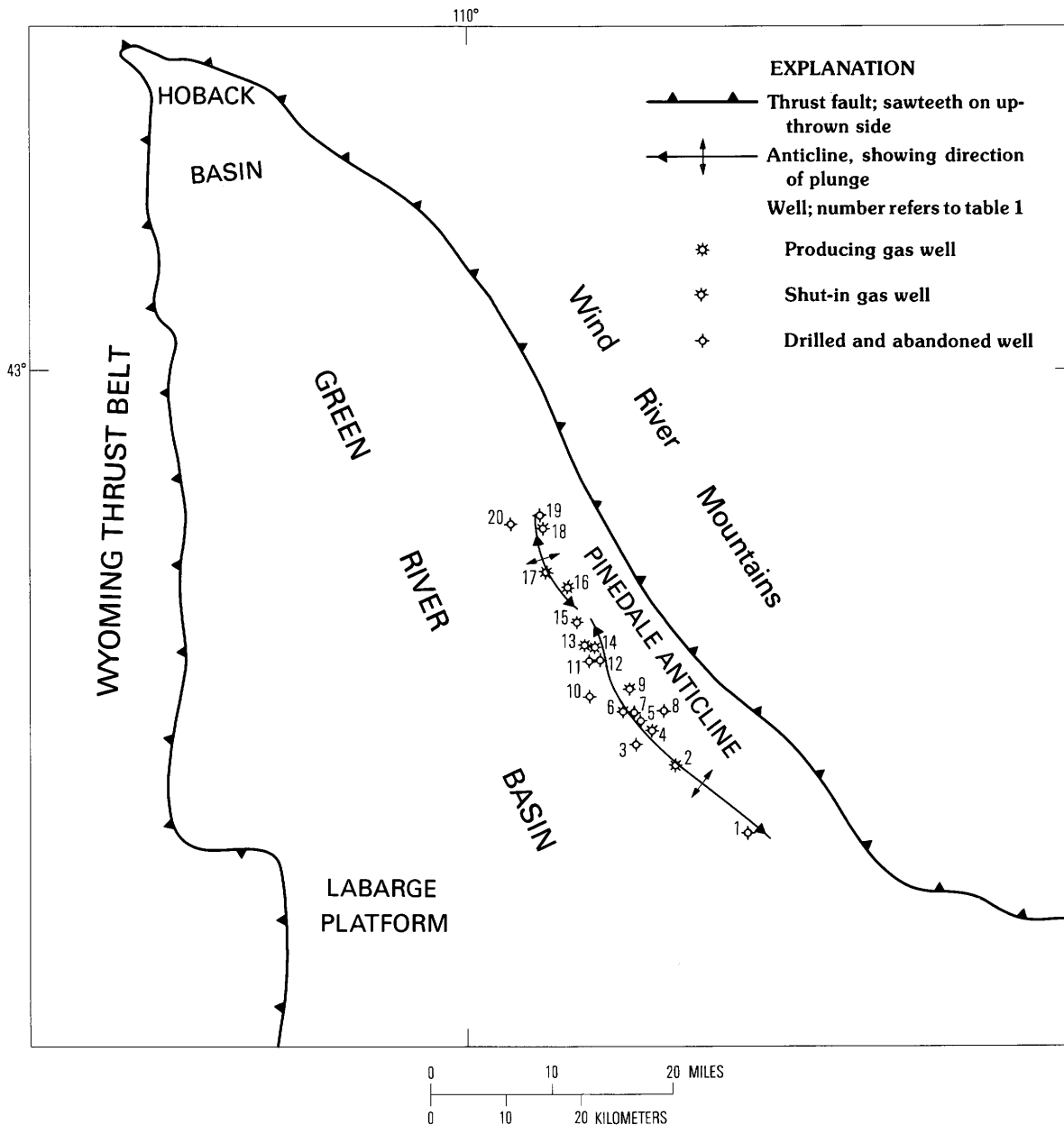


Figure 2. Wells drilled in the Pinedale anticline area of the northern part of the Green River basin, Wyoming. Detailed location information for wells shown in table 1.

stimulation for sustained economic production rates. Initial gas production rates are highly variable. Maximum rates of 1.5 million cubic feet per day (MMCFD) from single reservoirs and about 2.5 MMCFD from multiple reservoirs have been reported.

MULTIWELL EXPERIMENT

The U.S. Department of Energy (DOE) conducted a field-oriented, enhanced gas recovery research experiment in the southern part of the Piceance basin of

Colorado. This project is called the Multiwell Experiment (MWX) and was undertaken as a major part of the Department's Fossil Energy Western Gas Sands Subprogram. The main purpose of the research is to provide new and improved technology for the identification of natural gas in tight-gas reservoirs and to develop economically viable and reliable methods to recover the gas (Northrop and others, 1984; Spencer, 1984). The MWX site is on the south side of the valley of the Colorado River (fig. 1) at a surface kelly-bushing elevation of about 5,355 ft (1,630 m). Three closely spaced (115–215 ft, 35–66 m), extensively cored and logged wells

Table 1. Wells drilled in Pinedale anticline area, Sublette County, Wyoming

[Locations of wells shown on figure 2. Kelly bushing and total depth in feet. Status: D&A, drilled and abandoned; Prod., producing well; SI, shut-in well. Leaders (---) indicate no data]

Map no.	Well name	Operator	Location	Kelly bushing	Total depth	Formation at total depth	Status
1	Unit 1	Texaco	NE1/4SW1/4 sec. 25, T. 29 N., R. 107 W.	7,134	11,008	Lance	D&A
2	New Fork 1	American Hunter	SW1/4NE1/4 sec. 25, T. 30 N., R. 108 W.	7,338	10,989	Lance	Prod.
3	Pinedale 6	El Paso Natural Gas	SE1/4NW1/4 sec. 21, T. 30 N., R. 108 W.	7,294	11,057	Lance	D&A
4	Pinedale 7	El Paso Natural Gas	SE1/4NE1/4 sec. 15, T. 30 N., R. 108 W.	7,369	10,270	Lance	SI
5	Pinedale 1	El Paso Natural Gas	NE1/4SE1/4 sec. 6, T. 30 N., R. 108 W.	7,196	10,550	Lance	D&A
6	Wagon Wheel 1	El Paso Natural Gas	SE1/4NW1/4 sec. 5, T. 30 N., R. 108 W.	7,089	19,000	Baxter	SI
7	Pinedale 5	El Paso Natural Gas	C SE1/4 sec. 5, T. 30 N., R. 108 W.	7,056	15,018	Rock Springs	D&A
8	New Fork 2	American Hunter	SW1/4NE1/4 sec. 2, T. 30 N., R. 108 W.	7,282	11,986	Lance	D&A
9	Pinedale 2	El Paso Natural Gas	SE1/4 sec. 29, T. 31 N., R. 108 W.	7,034	10,694	Lance	SI
10	New Fork 4	American Hunter	NW1/4SE1/4 sec. 35, T. 31 N., R. 109 W.	6,957	11,550	Lance	D&A
11	Government 1	California Company	SW1/4NE1/4 sec. 14, T. 31 N., R. 109 W.	---	10,000	Lance	D&A
12	Pinedale 3	El Paso Natural Gas	C NW1/4 sec. 13, T. 31 N., R. 109 W.	6,982	11,009	Lance	D&A
13	Jensen 1	Leonard Hay	SW1/4NW1/4 sec. 11, T. 31 N., R. 109 W.	6,932	10,320	Lance	Prod.
14	Jensen 2	Leonard Hay	SE1/4SE1/4 sec. 11, T. 31 N., R. 109 W.	---	10,310	Lance	Prod.
15	Pinedale 4	El Paso Natural Gas	C NW1/4 sec. 34, T. 32 N., R. 109 W.	7,204	11,123	Lance	SI
16	Mesa 2	Wexpro	SE1/4NW1/4 sec. 16, T. 32 N., R. 109 W.	7,474	12,190	Lance	Prod.
17	Mesa 1	Wexpro	NE1/4NE1/4 sec. 7, T. 32 N., R. 109 W.	7,525	12,050	Lance	Prod.
18	Pinedale 8	Mountain Fuel	NE1/4SW1/4 sec. 20, T. 33 N., R. 109 W.	7,448	10,500	Lance	SI
19	Unit 1	Stanolind	NW1/4SE1/4 sec. 17, T. 33 N., R. 109 W.	---	7,797	Unnamed Tertiary	D&A
20	Baumgartner Fed. 21-24	Black Hawk Resources	NE1/4NW1/4 sec. 24, T. 33 N., R. 110 W.	7,344	11,238	Lance	D&A

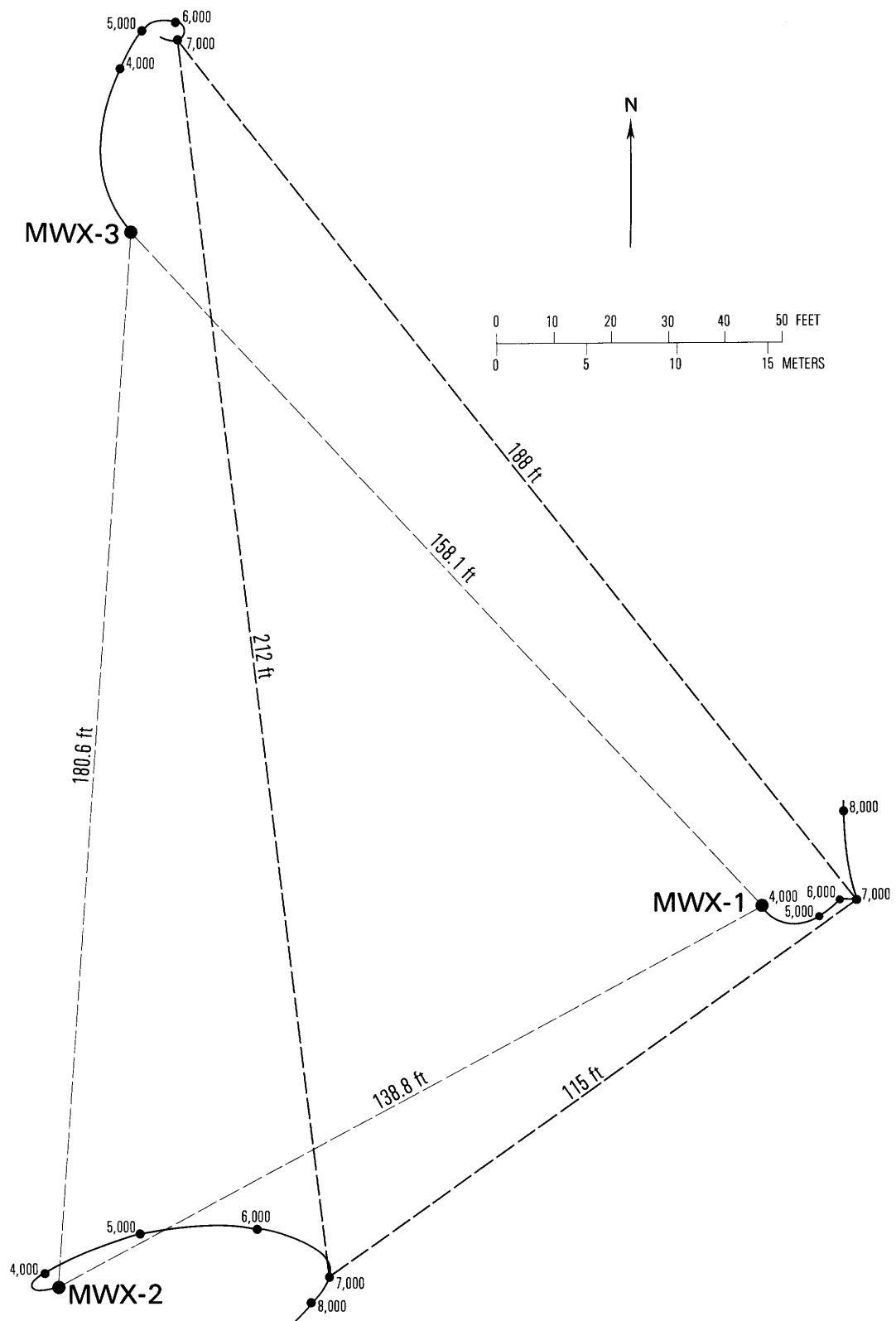


Figure 3. Relative location of MWX wells in the Piceance basin of Colorado. Large circles adjacent to well labels represent surface locations; small circles represent locations of well bore at depth (in feet) indicated. Modified from Mann (1984, fig. 7).

were drilled. They are designated CER Nos. 1, 2, and 3 MWX and are all located in the northwest quarter of sec. 34, T. 6 S., R. 94 W., Garfield County, Colorado. The wells were spudded in the upper part of the Tertiary Wasatch Formation and reached total depths of from 7,565 to 8,350 ft (2,306–2,545 m), at or near the base of the Upper Cretaceous Mesaverde Group. Figure 3 shows the location of the three wells relative to each other at the surface and at various depths. As can be seen in this figure, the well bores deviate only slightly from vertical and have only minor lateral drift with depth. In the discussions and chapters that follow, these wells will be referred to as MWX-1, MWX-2, and MWX-3. Many of the geologic studies conducted at the MWX site are discussed in Spencer and Keighin (1984).

One of the main reasons the MWX wells were drilled so close together was to facilitate well-interference production testing in tight sandstone reservoirs. The basic approach was to perforate and produce gas from one of the three wells and then observe the pressure response or pressure interference in the two adjacent (observation) wells. The close spacing and extensive well coring also provide data on the lateral and vertical variations of reservoir characteristics and on the distribution of natural fractures in "blanket" marine sandstone and lenticular fluvial reservoirs. The primary-objective reservoirs studied, however, are the lenticular sandstones in the fluvial part of the Mesaverde Group because:

1. Low-permeability, gas-bearing reservoirs in Upper Cretaceous fluvial sandstone occur in sequences, often thicker than 5,000 ft (1,524 m), in the Piceance basin and many other Tertiary basins in the Rocky Mountain region. Furthermore, some Rocky Mountain basins, such as the Greater Green River basin, have more than 14,000 ft (4,270 m) of strata containing mostly tight gas sandstones.

2. Artificial stimulation (hydraulic fracturing) has been relatively unsuccessful in lenticular rock sequences and somewhat more successful in the so-called "blanket" marine reservoirs of Cretaceous age in the Rockies.

Studies at MWX can be generally grouped into five disciplines: (1) geology, (2) geophysics, (3) rock mechanics, (4) borehole geophysical-log interpretation, and (5) well-testing and well-data diagnostics (Clark, 1983; Searls and others, 1983; Branagan and others, 1984; Northrup and others, 1984; Sattler, 1984; Spencer, 1984; Warpinski and others, 1984). There is considerable interrelationship and interaction among the various disciplines. The distribution of natural fractures vertically and areally, for example, is a very important aspect of the recovery of gas from tight reservoirs. Natural fracture analysis and the prediction of orientation of induced hydraulic fractures at the MWX site involves integration of regional tectonic information, surface fracture mapping, thermal and pressure history, rock mechanics, geophysics, core

study, borehole well-log analysis, well-testing, and fracture diagnostics. Interpretation of porosity and water saturation values from borehole geophysical logs requires integration of laboratory-measured core porosity, grain density, and water saturation data and petrographic, petrologic, and stratigraphic data.

REFERENCES CITED

- Branagan, P., Cotner, G., and Lee, S.J., 1984, Interference testing of naturally fractured Cozzette Sandstone; a case study at the DOE MWX site: Society of Petroleum Engineers/Gas Research Institute/Department of Energy Unconventional Gas Recovery Symposium, Dallas, Tex., Proceedings, p. 359–366.
- Charpentier, R.R., Law, B.E., and Prenskey, S.E., 1987, Quantitative model of overpressured gas resources of the Pinedale anticline, Wyoming: Society of Petroleum Engineers/Department of Energy Joint Symposium on Low-Permeability Reservoirs, Denver, Colo., 1987, Proceedings, p. 153–164.
- Clark, J.A., 1983, The prediction of hydraulic fracture azimuth through geological, core, and analytical studies: Society of Petroleum Engineers/Department of Energy Symposium on Low-Permeability Gas Reservoirs, Dallas, Tex., Proceedings, p. 107–114.
- Johnson, R.C., Crovelli, R.A., Spencer, C.W., and Mast, R.F., 1987, An assessment of gas resources in low-permeability sandstones of the Upper Cretaceous Mesaverde Group, Piceance basin, Colorado: U.S. Geological Survey Open-File Report 87–357, 26 p.
- Law, B.E., ed., 1984, Geological characteristics of low-permeability Upper Cretaceous and lower Tertiary rocks in the Pinedale anticline area, Sublette County, Wyoming: U.S. Geological Survey Open-File Report 84–753, 107 p.
- Law, B.E., Spencer, C.W., Crovelli, R.A., Mast, R.F., Dolton, G.L., Charpentier, R.R., and Wandrey, C.J., 1989, Gas resource estimates of overpressured low-permeability Cretaceous and Tertiary sandstone reservoirs in the Greater Green River basin, Wyoming, Colorado, and Utah: Wyoming Geological Association Field Conference Guidebook, p. 39–61.
- Mann, R.L., 1984, Multiwell Experiment Drilling Review, *in* Frohne, K-H., ed., Western Gas Sands Subprogram review: Morgantown, U.S. Department of Energy DOE/METC/84–3, p. 155–164.
- Martin, W.B., and Shaughnessy, J., 1969, Project Wagon Wheel, *in* Symposium on Tertiary rocks of Wyoming: Wyoming Geological Association Field Conference, 21st, Guidebook, p. 145–152.
- National Petroleum Council, 1980, Tight gas reservoirs, part I, *in* Unconventional gas resources: Washington, D.C., National Petroleum Council, 222 p., with appendices.
- Northrop, D.A., Sattler, A.R., Mann, R.L., and Frohne, K-H., 1984, Current status of the Multiwell Experiment: Society of Petroleum Engineers/Gas Research Institute/Department of Energy Unconventional Gas Recovery Symposium, Dallas, Tex., Proceedings, p. 351–358.

- Sattler, A.R., 1984, The Multiwell Experiment core program, II: Society of Petroleum Engineers/Gas Research Institute/Department of Energy Unconventional Gas Recovery Symposium, Dallas, Tex., Proceedings, p. 2235-2244.
- Searls, C.A., Lee, M.W., Miller, J.J., Albright, J.N., Fried, J., and Applegate, J.K., 1983, A coordinated seismic study of the Multiwell Experiment site: Society of Petroleum Engineers/Department of Energy Symposium on Low Permeability Gas Reservoirs, Dallas, Tex., Proceedings, p. 115-120.
- Shaughnessy, J., and Butcher, R.H., 1973, Geology of Project Wagon Wheel Nuclear Stimulation Project, *in* Fassett, J.E., ed., Cretaceous and Tertiary rocks of the southern Colorado Plateau: Four Corners Geological Society, p. 185-196.
- _____, 1974, Geology of Wagon Wheel Nuclear Stimulation Project, Pinedale field, Wyoming: American Association of Petroleum Geologists Bulletin, v. 58, no. 11, p. 2250-2259.
- Spencer, C.W., 1984, Overview of U.S. Department of Energy Multiwell Experiment, Piceance Creek basin, Colorado, *in* Spencer, C.W., and Keighin, C.W., eds., Geologic studies in support of the U.S. Department of Energy Multiwell Experiment, Garfield County, Colorado: U.S. Geological Survey Open-File Report 84-757, p. 1-13.
- Spencer, C.W., and Keighin, C.W., eds., 1984, Geologic studies in support of the U.S. Department of Energy Multiwell Experiment, Garfield County, Colorado: U.S. Geological Survey Open-File Report 84-757, 134 p.
- Warpinski, N.R., Branagan, P., and Wilmer, R., 1984, In situ stress measurements at DOE's Multiwell Experiment, *in* Frohne, K-H., ed., Western Gas Sands Subprogram review: Morgantown, U.S. Department of Energy, DOE/METC 84-3, p. 181-189.

Chapter B

Structural and Stratigraphic Framework of the Pinedale Anticline, Wyoming, and the Multiwell Experiment Site, Colorado

By B.E. LAW and R.C. JOHNSON

Prepared in cooperation with the U.S. Department of Energy

U.S. GEOLOGICAL SURVEY BULLETIN 1886

GEOLOGY OF TIGHT GAS RESERVOIRS IN THE PINEDALE ANTICLINE AREA, WYOMING,
AND AT THE MULTIWELL EXPERIMENT SITE, COLORADO

CONTENTS

Abstract	B1
Introduction	B1
Pinedale anticline	B1
Structure	B1
Stratigraphy	B3
Cretaceous rocks	B3
Tertiary rocks	B6
Multiwell Experiment site	B6
Structure	B6
Stratigraphy	B6
Cretaceous rocks	B6
Tertiary rocks	B8
References cited	B9

FIGURES

1. Map showing structure contours of top of Cretaceous rocks, northern Green River basin **B1**
2. Cross section through northern Green River basin, extending from Wyoming thrust belt northeast to Wind River Mountains **B2**
- 3-4. Charts showing:
 3. Stratigraphic sequence and cored intervals, El Paso Natural Gas Company Wagon Wheel No. 1 well, northern Green River basin **B3**
 4. Stratigraphic correlation for Pinedale anticline, MWX site, and intermediate areas **B4**
- 5-6. Maps showing:
 5. Location of Greater Green River basin and Piceance basin and Western Interior epeiric seaway during Late Cretaceous time **B5**
 6. Structure contours of top of the Rollins and Trout Creek Sandstone Members of the Iles Formation of the Mesaverde Group, Piceance basin **B7**
7. Cross section through Piceance basin including MWX site **B8**
8. Chart showing stratigraphic sequence and cored intervals, MWX-1 and MWX-2 wells, Piceance basin **B9**

Structural and Stratigraphic Framework of the Pinedale Anticline, Wyoming, and the Multiwell Experiment Site, Colorado

By B.E. Law and R.C. Johnson

Abstract

Both the Pinedale anticline and the U.S. Department of Energy Multiwell Experiment site are located in Rocky Mountain foreland basins that have experienced similar styles of deformation during the Laramide orogeny but have significantly different structural complexity. The Pinedale anticline is a large, thrust-rooted fold that formed in response to structural deformation associated with the evolution of the adjacent Wind River Mountains. The Multiwell site, by contrast, is in a structurally simple area near the synclinal axis of the Piceance basin.

Gas-bearing reservoirs occur in marine and nonmarine clastic sequences that are about 4,200 ft (1,280 m) thick at the Multiwell site and more than 10,000 ft (3,000 m) thick in the Pinedale anticline area. These rocks were deposited in and adjacent to the western margin of the Western Interior seaway during early Campanian to late Maestrichtian time.

INTRODUCTION

The structural and stratigraphic framework of the Pinedale anticline area and U.S. Department of Energy Multiwell Experiment (MWX) site is known with varying degrees of certainty. The structural and stratigraphic setting of the MWX area is fairly well known (Lorenz, 1983, 1984; Johnson and Nuccio, 1984, 1986; Johnson, 1987, 1989), but considerably less is known about the Pinedale area. The most significant previously published structural and stratigraphic studies relevant to the Pinedale area are by Martin and Shaughnessy (1969), Shaughnessy and Butcher (1973, 1974), Law and Nichols (1982), Shuster and Steidtmann (1983), Law (1984), and Hagen and others (1985).

During the course of recent investigations in the Pinedale and MWX areas, data were obtained from well logs and cores, particularly from the Pinedale area, that necessitate modification of the existing geologic framework. For this reason and in order to place the other reports in this volume in the proper geologic setting, we will describe the structural and stratigraphic framework of each area.

PINEDALE ANTICLINE

Structure

The Pinedale anticline is in the Rocky Mountain foreland in the northern part of the Green River basin, between the Idaho-Utah-Wyoming thrust belt to the west and the Wind River Mountains to the northeast (Law and Spencer, this volume, fig. 1). The northern part of the Green River basin formed during the Laramide orogeny in response to tectonic loading by thrusting events in the

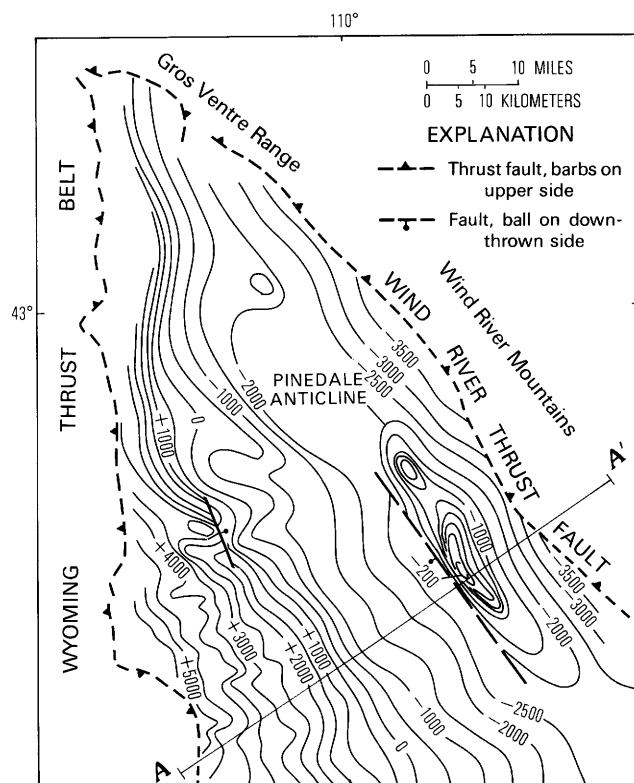


Figure 1. Structure contours of the top of Cretaceous rocks, northern Green River basin, Wyoming. Contour interval, 100 and 500 ft. Line of section A-A' (fig. 2) also shown.

Idaho-Utah-Wyoming thrust belt and by uplift of the Wind River Mountains (Jordan, 1981; Hagen and others, 1985).

The Pinedale anticline is the largest structural feature in the northern Green River basin. It is about 35 mi (56 km) long and 6 mi (10 km) wide. Its structural configuration is shown in the structure contour map of the northern Green River basin (fig. 1) and in cross section A-A' (fig. 2), which extends from the Wyoming thrust belt northeastward to the Wind River Mountains. The anticline is asymmetric in that its west flank is steeper than its east flank. Structural relief at the top of Cretaceous rocks is about 2,000 ft (610 m), with two areas of local closure. According to Shaughnessy and Butcher (1973, 1974), the west flank of the anticline is bounded by a buried, high-angle, east-dipping reverse or thrust fault (fig. 2) that flattens out at depth. Shaughnessy and Butcher indicated about 600 ft (182 m) of displacement across the fault and believe the fault intersects the El Paso Natural Gas Wagon Wheel No. 1 borehole at a depth of about 18,000 ft (5,486 m). Examination of the two deepest cores from the well (17,163-17,193, 17,959-17,996 ft) shows increasingly steeper dips and increasing fracture frequency, both of which indicate proximity to a fault. Surface expression of the anticline in the Eocene Wasatch Formation is subtle, and, dips of 1°-2° are locally present on the flanks of the structure.

The Pinedale anticline is a thrust-rooted detachment structure that probably formed in response to

southwest-directed compression associated with structural deformation of the Wind River Mountains. The parallel trend of the fold axis, the asymmetry of the anticline, and the geometric similarities between the west-bounding fault and the Wind River thrust are consistent with this interpretation. Based on this interpretation, the structural evolution of the Pinedale anticline is inferred from structural and stratigraphic data to be related to uplift and erosion of the Wind River Mountains.

Structural growth of the Wind River Mountains probably was episodic and may have begun as long ago as 90 Ma (Shuster, 1986; Shuster and Steidtmann, 1988), prior to the Laramide orogeny. Love (1960) and Berg (1961) both concluded that uplift of the Wind River Mountains began during Late Cretaceous time. Keefer (1965) observed that the Wind River Mountains probably began to rise at the beginning of Paleocene time and that, by middle to late Paleocene time, the Precambrian core of the range had been breached. These conclusions are supported by Shuster and Steidtmann (1988). Independent investigations by Prenskey (1984, this volume) of a unique, regionally occurring gamma-ray response in Paleocene rocks of the northern Green River basin indicate that, by early to middle Paleocene time, the Precambrian crystalline core of the Wind River Mountains was exposed and shedding arkosic debris into the adjacent basin.

Definitive evidence of the earliest syntectonic sedimentation related to uplift and erosion of the Wind

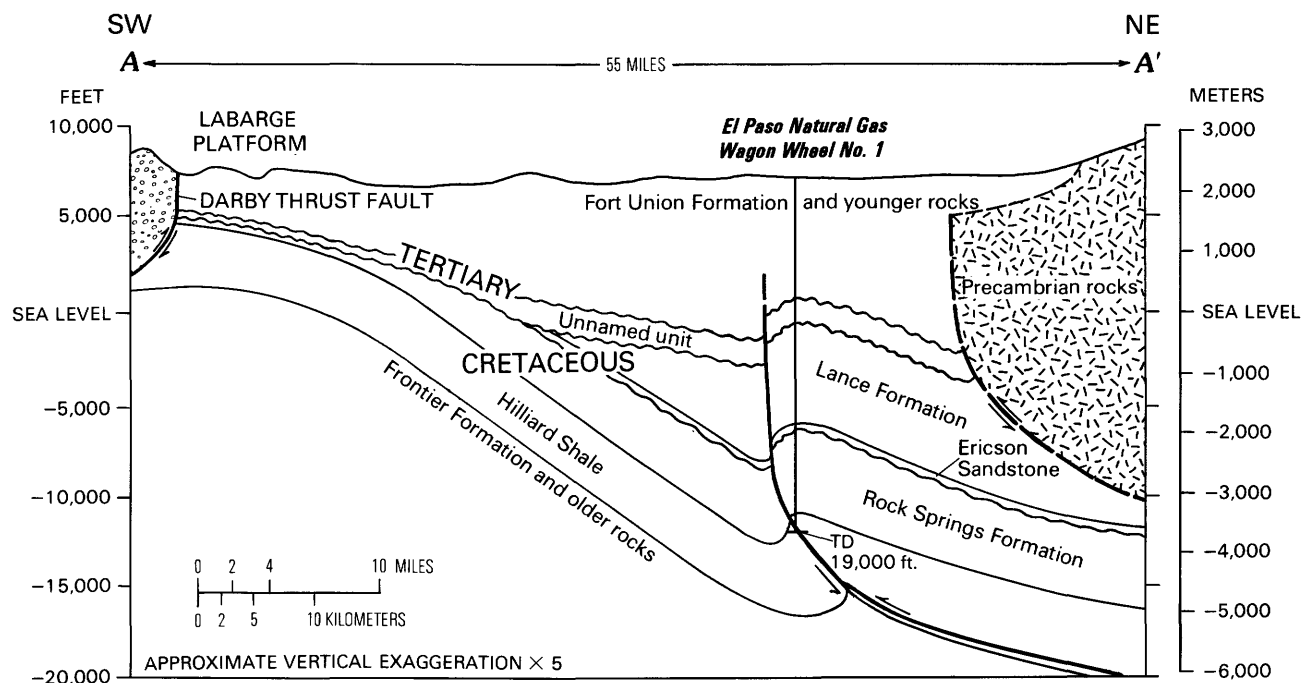


Figure 2. Cross section through the northern Green River basin, extending from the Wyoming thrust belt northeast to the Wind River Mountains. High-angle reverse fault on west side of Pinedale anticline from Martin and Shaughnessy (1969) and Shaughnessy and Butcher (1973, 1974). TD, total depth of well. Line of section shown in figure 1.

River Mountains is lacking in the Pinedale anticline area, but mineralogical compositions of the Upper Cretaceous Lance Formation as determined by Pollastro (this volume) indicate that the Wind River Mountains probably began to supply sediments to the adjacent basin during deposition of the Lance Formation. Core-derived mineralogical data from wells in the Pinedale anticline show that the Lance contains detrital limestone and dolomite grains (Law and others, 1986; Pollastro, this volume). Although the source of the Lance cannot conclusively be demonstrated, its composition is compatible with a Wind River Mountains source. Thus, structural growth of the Pinedale anticline, which is assumed to be genetically linked to deformation associated with the Wind River Mountains, probably began during Late Cretaceous and continued through Eocene time.

Stratigraphy

Most of the stratigraphic data for the Pinedale anticline area are from the El Paso Natural Gas Company Wagon Wheel No. 1 well. This well was drilled to a total depth of 19,000 ft (5,791 m) and was extensively cored and logged; it is presented in this report as the stratigraphic reference well for the Pinedale area (fig. 3). The stratigraphic nomenclature used in the Pinedale anticline area for Cretaceous rocks is mostly from the area of the Rock Springs uplift and is based on stratigraphic correlations shown in figure 4. Stratigraphic correlations of Upper Cretaceous rocks in the Pinedale area, at Oak Creek in the southeastern part of the Sand Wash basin of Colorado, and at the MWX site in the Piceance basin of Colorado are also shown.

Cretaceous Rocks

About 11,500 ft (3,505 m) of Upper Cretaceous rocks was penetrated in the Wagon Wheel well and includes, in ascending order, the Hilliard Shale, Rock Springs Formation, Ericson Sandstone, and Lance Formation. With the exception of the Hilliard Shale and the lower 800–1,000 ft (244–305 m) of the Rock Springs Formation, the entire sequence was deposited in nonmarine environments adjacent to the western margin of the Western Interior seaway (fig. 5) in response to thrusting events in the Wyoming thrust belt and uplift of the adjacent Wind River Mountains (fig. 1). East and southeast of the Pinedale anticline, these rocks grade into and intertongue with marine, marginal-marine, and nonmarine rocks.

Hilliard Shale.—The Hilliard Shale is composed mostly of gray shale that grades upward to silty and sandy shale. About 700 ft (213 m) of Hilliard Shale was

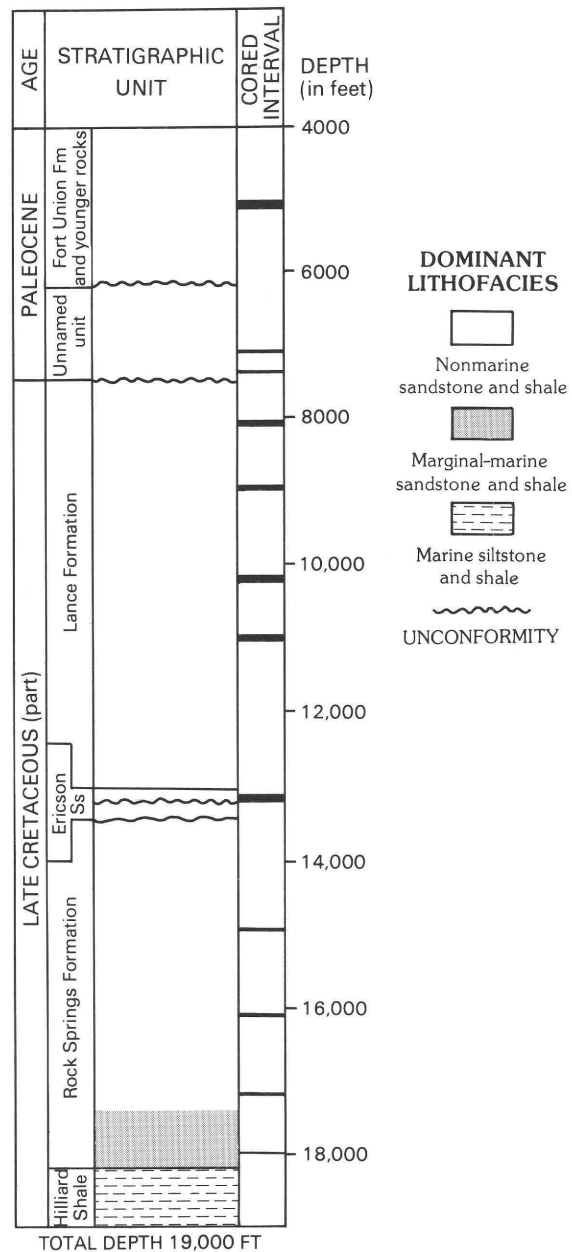
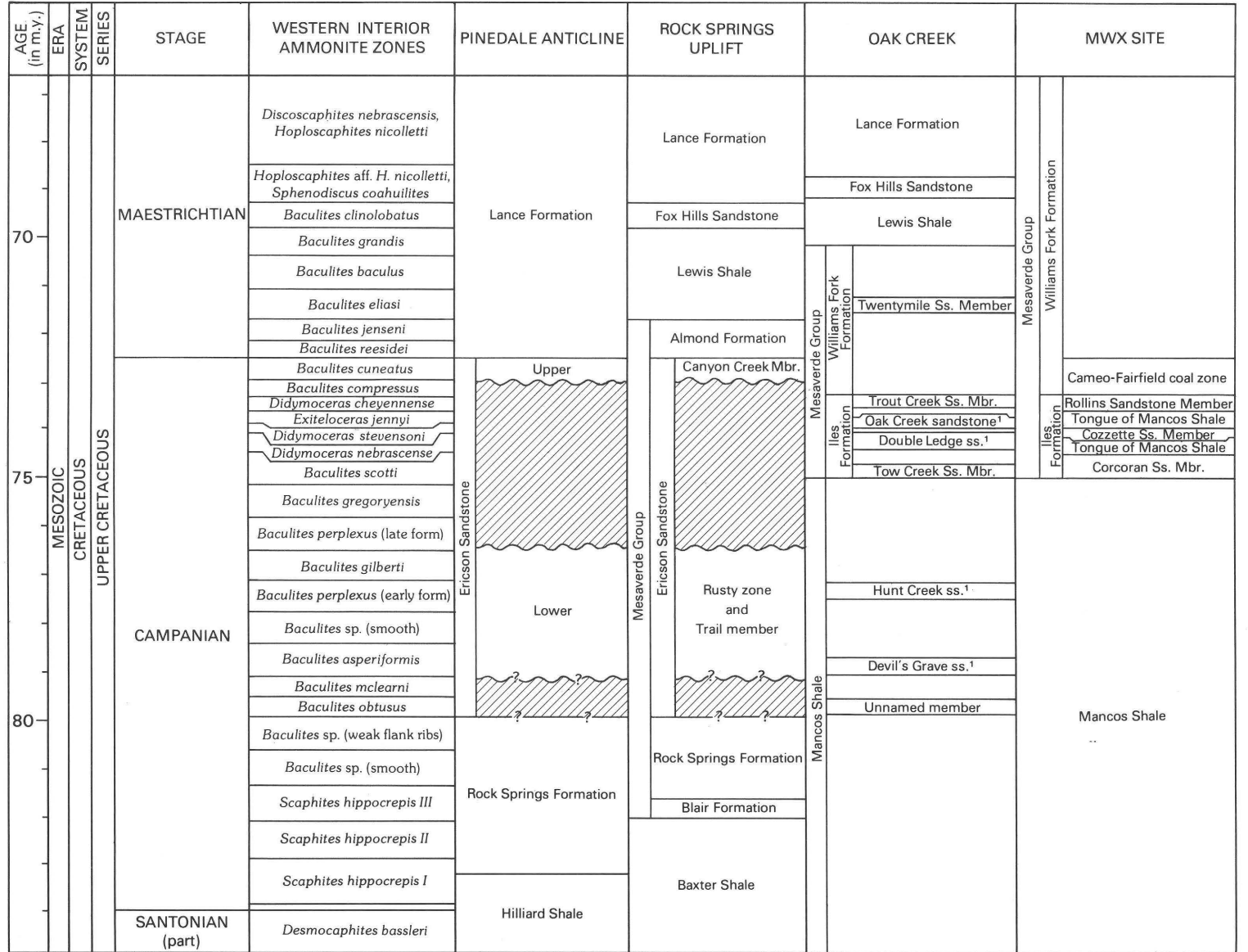


Figure 3. Stratigraphic sequence and cored intervals, El Paso Natural Gas Company Wagon Wheel No. 1 well, northern Green River basin, Wyoming. Location of well shown in figure 2.

penetrated in the Wagon Wheel well, but wells west of the Pinedale anticline indicate that the total thickness of the Hilliard Shale is about 3,500 ft (1,067 m). The upper part of the Hilliard Shale was deposited in a shallow-water marine environment. The Hilliard Shale is, in part, equivalent to the Baxter Shale in the Rock Springs uplift and to the Mancos Shale in the Oak Creek and MWX areas (fig. 4). In the Wagon Wheel well, the top of the Hilliard is at a depth of about 18,270 ft (5,569) (fig. 3).



¹Unranked unit

Figure 4. Stratigraphic correlation chart for Pinedale anticline, Green River basin, and MWX site, Piceance basin. Stratigraphy of intermediate areas also shown. Location of areas shown in Law and Spencer (this volume, fig. 1).

Rock Springs Formation.—In surface exposures in the Rock Springs uplift and in core from the Wagon Wheel well, the Rock Springs Formation is composed of tan to light-gray, fine- to medium-grained sandstone, siltstone, shale, carbonaceous mudstone, and coal. Its lower contact intertongues with the underlying Hilliard Shale, and in well logs this contact is placed at the base of predominantly sandstone bearing rocks. The Rock Springs Formation is about 4,800 ft (1,463 m) thick and can be subdivided into three parts. The lower part is 800–1,000 ft (244–305 m) thick and consists of intertonguing sandstone and shale deposited in shallow-water marine and marginal-marine environments. The middle part is about 2,450 ft (747 m) thick and consists of sandstone, siltstone, shale, and coal deposited in middle- to lower-delta-plain environments. The upper part is about 1,550 ft (472 m) thick and consists of interbedded sandstone, siltstone, and mudstone deposited in alluvial-plain environments. The Rock Springs Formation in the Pinedale anticline area is equivalent to the upper part of the Baxter Shale, Blair Formation and Rock Springs Formation in the Rock Springs uplift area and to the middle part of the Mancos Shale in the Oak Creek and MWX areas (fig. 4). In the Wagon Wheel well, the depth to the top of the Rock Springs is about 13,465 ft (4,104 m) (fig. 3).

Ericson Sandstone.—The Ericson Sandstone is composed mostly of sandstone and lesser amounts of siltstone and mudstone. In the Pinedale area, the Ericson is divided into two parts. The lower part is 290 ft (88 m) thick and is a sandstone that has interbeds of siltstone and shale deposited in meandering- and braided-stream systems. The nature of the contact with the underlying Rock Springs Formation is uncertain; in the western part of the Green River basin, the contact probably is unconformable; farther to the east, it probably is conformable. The lower part of the Ericson is equivalent to the Rusty zone and Trail Member of the Ericson Sandstone in the Rock Springs uplift area, to the intertonguing sandstones and shales in the upper part of the Mancos Shale in the Oak Creek area, and to the upper part of the Mancos Shale in the MWX area. In the Wagon Wheel well, the depth to the top of the lower Ericson is about 13,165 ft (4,013 m) (fig. 3).

The upper part of the Ericson is about 100 ft (30 m) thick and is a conglomeratic sandstone. It is more quartz rich and contains less siltstone and shale than the lower part. The upper part is predominantly light to medium gray and consists of very fine to coarse grained quartzose sandstone that contains granules of chert, quartzite, and siltstone. Sedimentological characteristics of the upper part, as determined from both cores and outcrops, indicate deposition in a braided-stream system. Regional stratigraphic relationships (Law, 1979; Law and Nichols, 1982; Law and others, 1983; Bucurel-White, 1983)

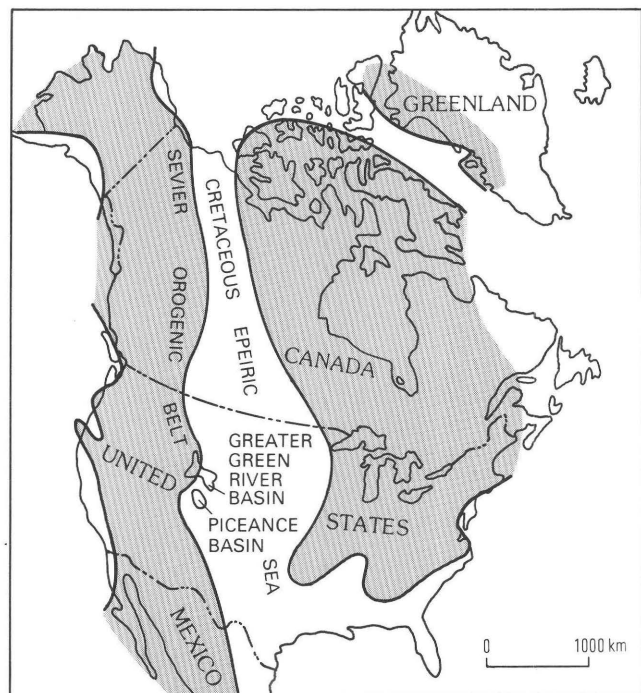


Figure 5. Location of Greater Green River basin and Piceance basin and Western Interior epeiric seaway during Late Cretaceous time. Modified from Gill and Cobban (1973).

suggest that the contact between the lower and upper parts is unconformable. The upper part of the Ericson is equivalent to the Canyon Creek zone of the Ericson Sandstone in the Rock Springs uplift area, to the lower part of the Williams Fork Formation in the Oak Creek area, and to part of the Cameo-Fairfield coal zone of the Williams Fork Formation in the MWX area (fig. 4). In the Wagon Wheel well, the depth to the top of the upper Ericson is about 13,065 ft (3,982 m) (fig. 3).

Lance Formation.—In the Wagon Wheel well, the Lance Formation is about 5,500 ft (1,692 m) thick and is composed of tan to brown, fine- to medium-grained sandstone, siltstone, shale, and carbonaceous mudstone. The Lance is interpreted to have been deposited in an alluvial-plain environment. Its lower contact is conformable with the underlying Ericson Sandstone, and its upper contact is unconformable with overlying Tertiary rocks. The lower part of the Lance in the Pinedale area is temporally equivalent to the Almond Formation, Lewis Shale and Fox Hills Sandstone in the Rock Springs uplift area, to the upper part of the Williams Fork Formation, Lewis Shale, Fox Hills Sandstone and Lance Formation in the Oak Creek area, and to the Williams Fork Formation above the Cameo-Fairfield coal zone at the MWX site (fig. 4). In the Wagon Wheel well, the depth to the top of the Lance is about 7,520 ft (2,292 m) (fig. 3).

Lower Tertiary rocks in the Pinedale anticline area were deposited in dominantly fluvial environments. Depositional patterns in these rocks are more complex than those in Cretaceous rocks because of multiple source terranes, the emergence of adjacent highlands, and the development of internal basin drainage during the Tertiary. Our discussion of Tertiary rocks is restricted to the lower Tertiary inasmuch as younger Tertiary rocks are not gas bearing.

Probably the most significant departure from previous stratigraphic studies in the Pinedale area is the identification of the Cretaceous-Tertiary boundary. In southwestern Wyoming, the base of the Tertiary is marked by a regional unconformity (Roehler, 1961; Ritzma, 1965; Dorr and others, 1977; Beaumont, 1979), and throughout most of the region the oldest Tertiary unit is the Paleocene Fort Union Formation or its equivalent. In the subsurface of the northern Green River and Great Divide basins, however, an older unnamed Tertiary interval has been identified on the basis of well-log correlations and palynology (Law, 1979; Law and Nichols, 1982; Bucurel-White, 1983). In the Pinedale area, studies by Martin and Shaughnessy (1969) and Shaughnessy and Butcher (1973, 1974) indicate that the Cretaceous-Tertiary boundary is at a depth of about 10,000 ft (3,048 m) in the Wagon Wheel well; however, more recent stratigraphic and palynological studies by Law (1979) and Law and Nichols (1982) indicate that the boundary is at a depth of 7,520 ft (2,302 m).

Unnamed unit.—The unnamed unit consists of interbedded conglomerate, sandstone, siltstone, and mudstone. In the Pinedale area, it unconformably overlies the Lance Formation and is 1,285–1,510 ft (391–460 m) thick. The siliciclastic sediments of this unit were derived from the Wind River Mountains and deposited in alluvial-plain and fluvial-deltaic environments. The age of the unit is uncertain but probably is early to middle Paleocene. In the Wagon Wheel well, the depth to the top of the unnamed unit is about 6,215 ft (1,894 m) (fig. 3).

Fort Union Formation and younger rocks.—The Fort Union Formation and younger rocks consist of interbedded conglomerate, sandstone, siltstone, mudstone, and carbonaceous mudstone. Coal beds, commonly associated with the lower part of the Fort Union Formation in the Rock Springs uplift area and elsewhere, are not present in the Pinedale area, presumably because of facies changes related to the proximity of source terranes in the nearby Wind River Mountains. Regionally, the base of the Fort Union is unconformable, but in the vicinity of the Pinedale anticline the nature of the contact with the underlying unnamed unit is uncertain. The Fort Union Formation and younger rocks were deposited in dominantly fluvial environments, and the age of these rocks is middle Paleocene to Eocene.

Structure

The Multiwell Experiment (MWX) site is in the Rulison gas field on the gently dipping southwest flank of the Piceance basin near its structural axis (Law and Spencer, this volume, fig. 1) (fig 6). The Piceance basin is a Laramide structural and sedimentary basin that was subsiding from the latest Cretaceous through about the end of the Eocene. It is bounded on the northwest by the Uinta uplift, on the east by the White River uplift, on the southeast by the Sawatch Mountains uplift, on the south by the San Juan volcanic field, and on the southwest by the Uncompahgre uplift.

The Piceance basin is highly asymmetric; it has gently dipping west and southwest flanks and a sharply upturned east flank. The structural axis of the basin is just west of the steeply dipping east flank. The east flank, called the Grand Hogback, is believed to be underlain by a deep-seated west-thrusting reverse or normal thrust fault (Gries, 1983).

Stratigraphy

Cretaceous Rocks

The principal low-permeability gas-bearing interval at the MWX site is the Upper Cretaceous Mesaverde Group. At the MWX site, the Mesaverde is about 4,200 ft (1,280 m) thick and is approximately equivalent to the upper half of Upper Cretaceous low-permeability reservoirs in the Pinedale anticline area (fig. 4). The stratigraphic sequence penetrated at the MWX site is shown in figures 7 and 8 and includes, in ascending order, the Corcoran, Cozzette and Rollins Sandstone Members of the Iles Formation and the Williams Fork Formation. These Upper Cretaceous rocks were deposited in and adjacent to the Western Interior seaway during the Late Cretaceous (fig. 5). Rapid subsidence during the Late Cretaceous caused a major marine incursion, and an epeiric seaway covered much of the foreland basin, including the area of the Piceance and Green River basins. During this marine incursion, about 5,500 ft (1,680 m) of marine Mancos Shale was deposited in the MWX area. The Mancos Shale conformably underlies the Mesaverde throughout the Piceance basin.

Iles Formation of the Mesaverde Group.—At the MWX site, the Iles Formation of the Mesaverde Group extends upward from the underlying Mancos Shale through the marginal-marine Rollins Sandstone Member (equivalent to the Trout Creek Member at Oak Creek) and consists of a series of transgressive and regressive marine cycles. The Iles Formation was deposited during

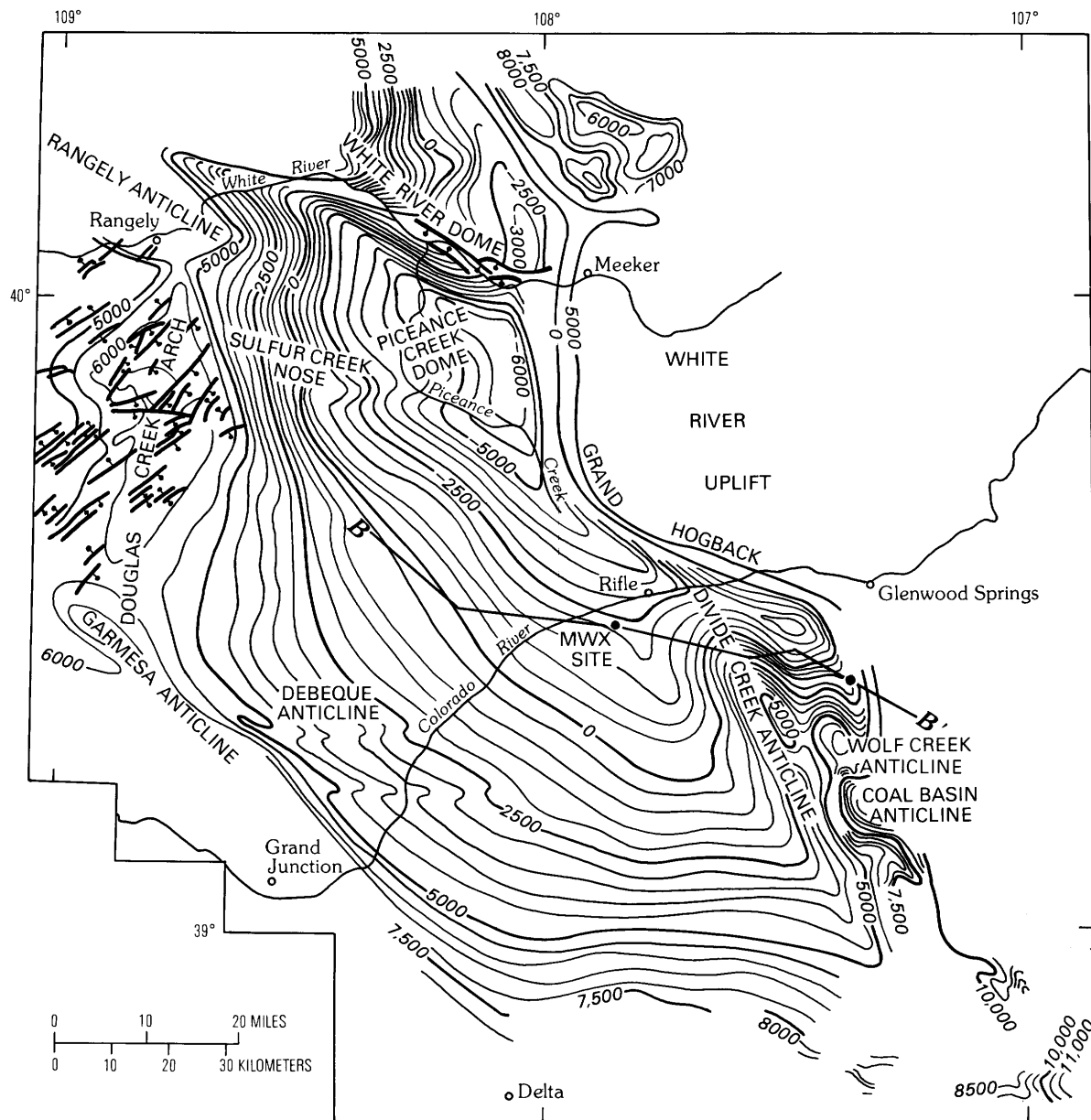


Figure 6. Structure contours of the top of the Rollins and Trout Creek Sandstone Members of the Iles Formation of the Mesaverde Group, Piceance basin. Contours in feet. Line of section B-B' (fig. 7) also shown.

late Campanian time, during which a series of clastic sediment wedges were deposited in response to orogenic activity in the Sevier orogenic belt farther to the west (Fouch and others, 1983). During deposition of the Iles Formation, there were several marine transgressions and regressions.

The three major regressive cycles recognized at the MWX site are, in ascending order, the Corcoran, Cozzette, and Rollins Sandstone Members of the Iles Formation. Tongues of transgressive marine shale separate each of the three cycles. The Corcoran and Cozzette cycles prograded from northwest to southeast across the MWX area and undergo a facies change into Mancos

Shale about 25–30 mi (40–48 km) southeast of the MWX site. The position of maximum regression of the Rollins or Trout Creek cycle is east of the Grand Hogback, and, although the orientation of the strandline is difficult to determine, it appears that the Rollins cycle prograded from west to east across the MWX area.

At the MWX site, the Corcoran is about 135 ft (41 m) thick, the Cozzette about 165 ft (50 m) thick, and the Rollins about 135 ft (41 m) thick. Throughout most of the southern part of the Piceance basin, the Corcoran and Cozzette regressive cycles are very complex, and commonly each cycle contains more than one shoreface sandstone sequence, as well as lenticular channel sandstones

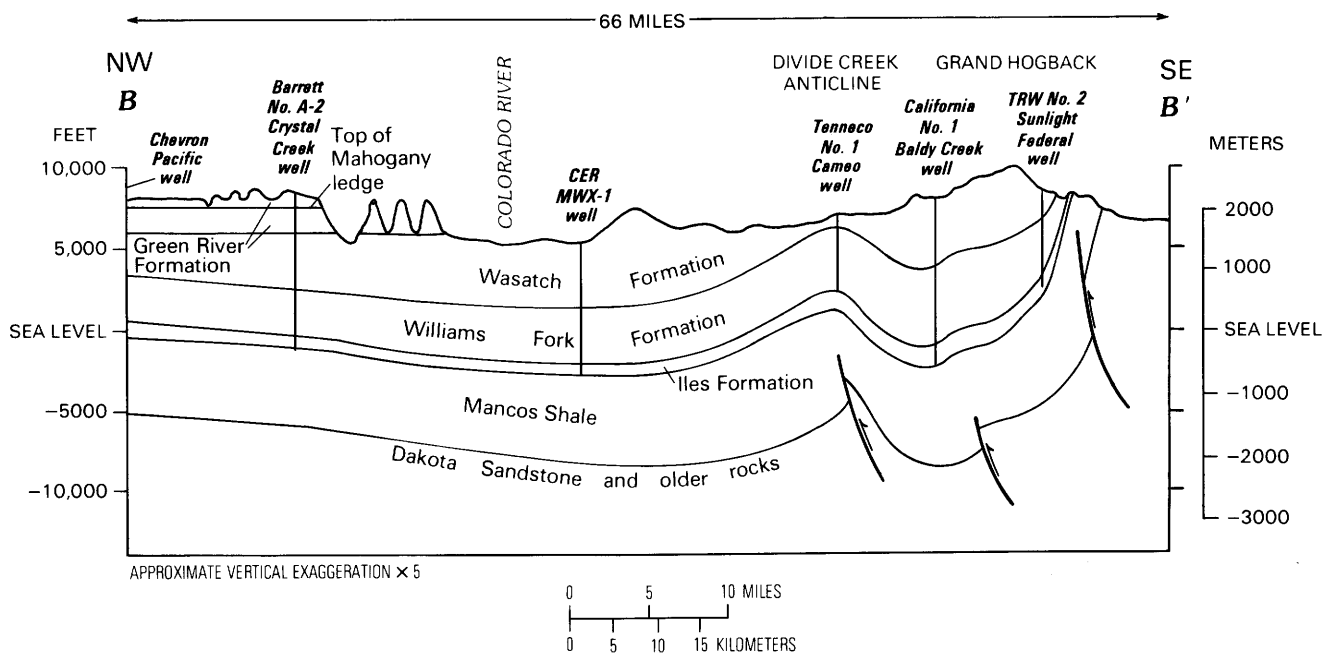


Figure 7. Cross section through Piceance basin including MWX site. Line of section shown in figure 5.

and some coal. At the MWX site, both the Corcoran and Cozzette contain two shoreface sequences (Lorenz, this volume). In contrast, the Rollins consists of a single coarsening-upward shoreface sandstone. The individual shoreface sandstones in the Corcoran and the Cozzette are probably blanket sandstones from a reservoir point of view but are regionally less persistent than the Rollins shoreface sandstone and can seldom be traced over large areas.

Williams Fork Formation of the Mesaverde Group.—About 3,500 ft (1,066 m) of Upper Cretaceous Campanian and Maestrichtian nonmarine rocks of the Williams Fork Formation overlies the Iles Formation in the MWX area. The lower 800 ft (244 m) of the Williams Fork consists mostly of carbonaceous shale and coal deposited in a coastal-plain or delta-plain (paludal) environment. Most of the thick coal beds are in the Cameo-Fairfield coal zone, which makes up about the lower 450 ft (137 m) of this sequence. The Cameo-Fairfield is present in all but the northwesternmost part of the Piceance basin and is by far the most significant coal zone in the basin. At the MWX site, about 80 ft (24 m) of coal occurs in the Cameo-Fairfield coal zone. About 2,700 ft (823 m) of mostly fluvial point-bar and overbank deposits overlies the paludal sequence. Lorenz (1983, this volume) recognized a 550-ft-thick (168 m) transition zone between the underlying paludal and overlying fluvial rocks that he referred to as the coastal zone, and he suggested that there is some marine influence in the uppermost 350 ft (107 m) of the Williams Fork.

Tertiary Rocks

A major regional unconformity is present at the base of Tertiary rocks throughout most, if not all, of the Piceance basin (Johnson and May, 1978, 1980). A considerable thickness of Mesaverde rocks was probably eroded during this period of beveling in many parts of the basin (Johnson, 1989). The thickness of section eroded at MWX is not known, but, because the MWX site is near the trough of the basin, the amount of beveling at the site is probably much less than that on the flanks (Johnson, 1989).

The lithology of the lower Tertiary rocks overlying the unconformity at MWX has not been described in detail but is probably similar to that of lower Tertiary rocks in nearby wells (Johnson and others, 1979) and on outcrops at Rifle Gap (Donnell, 1969; Johnson, 1982).

Wasatch Formation.—About 2,400 ft (732 m) of Paleocene-age Atwell Gulch Member of the Wasatch Formation overlies the Cretaceous-Tertiary unconformity at MWX (Donnell, 1969). The lower 770 ft (235 m) of the Atwell Gulch consists of interbedded gray mudstone and conglomeratic sandstone. Pebbles and cobbles in the basal conglomerate at MWX are mostly varicolored chert, whereas andesite and dacite pebbles and cobbles predominate throughout the rest of the interval. The conglomeratic interval thickens toward the southeastern margin of the basin and was probably derived from the Sawatch uplift to the southeast. The remaining 1,730 ft (527 m) of Atwell Gulch consists of drab-colored mudstone and a few lenticular channel sandstones.

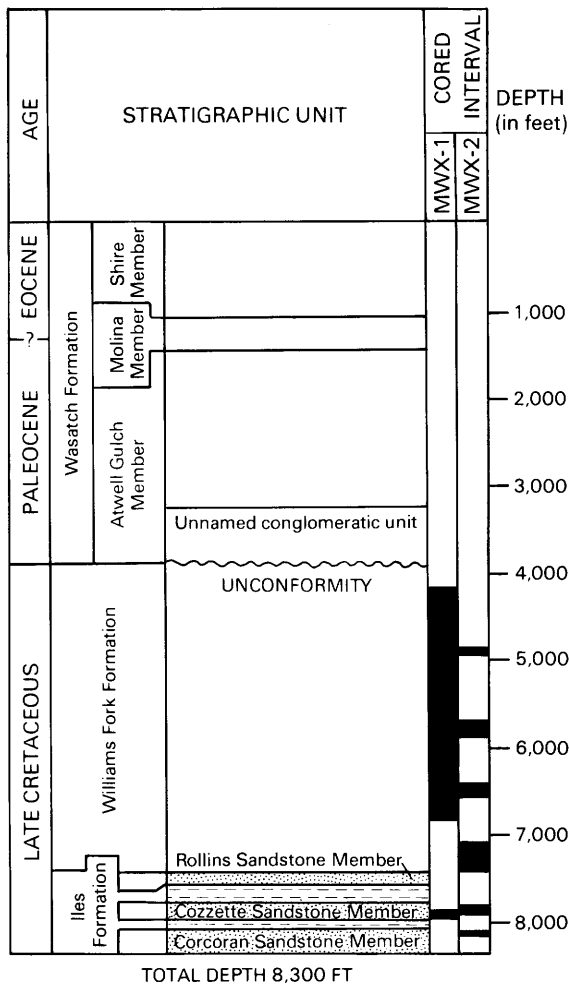


Figure 8. Stratigraphic sequence and cored intervals, MWX-1 and MWX-2 wells, Piceance basin, Colorado. Unlabeled units between Rollins and Cozette and Cozette and Corcoran are tongues of Mancos Shale.

A thin remnant of the Molina Member of the Wasatch Formation overlies the Atwell Gulch Member at MWX (Donnell, 1969; Johnson, 1979). The Molina Member is the sandiest interval in the Wasatch and has been identified along both the east and west flanks of the basin, where it consists of interbedded conglomeratic sandstone and gray mudstone. Pebbles consist mostly of varicolored chert and quartzite. At MWX, only the very persistent basal sandstone of the Molina Member (depth of 1,485–1,505 ft in MWX-1) can be identified with certainty. Two sandstones above the basal sandstone in the MWX-1 well may also be Molina sandstones. Thus far, attempts to date the Molina Member using palynomorphs have been unsuccessful (Johnson and May, 1978).

The remaining 1,100 ft (335 m) of lower Tertiary rocks at MWX is included in the Shire Member of the Wasatch Formation. The Shire Member consists of varicolored mudstone and sparse lenticular channel sandstones

and has been dated as early Eocene in age (Wood, 1962; Donnell, 1969; Newman, 1974; Johnson and May, 1978). It is exposed at the surface at MWX, extends about 1,200 ft (366 m) up the sides of nearby canyon walls, and is overlain by the Eocene Green River Formation.

REFERENCES CITED

- Beaumont, E.A., 1979, Depositional environments of Fort Union sediments (Tertiary, northwest Colorado) and their relation to coal: *American Association of Petroleum Geologists Bulletin*, v. 63, no. 2, p. 194–217.
- Berg, R.B., 1961, Laramide tectonics of the Wind River Mountains, in Wiloth, G.J., ed., *Symposium on Late Cretaceous rocks, Wyoming and adjacent areas: Wyoming Geological Association Field Conference, 16th, 1961, Guidebook*, p. 70–80.
- Bucurel-White, H., 1983, Section C-C', subsurface and surface correlations of some Upper Cretaceous and Tertiary rocks from the northwest flank of the Rock Springs uplift to the Rawlins uplift, Great Divide basin, Wyoming: U.S. Geological Survey Open-File Report 83-418, 2 sheets.
- Donnell, J.R., 1969, Paleocene and lower Eocene units in the southern part of the Piceance Creek basin, Colorado: U.S. Geological Survey Bulletin 1274-M, p. M1–M18.
- Dorr, J.A., Jr., Spearing, D.R., and Steidtmann, J.R., 1977, Deformation and deposition between a foreland uplift and an impinging thrust belt, Hoback basin, Wyoming: *Geological Society of American Special Paper 177*, 82 p.
- Fouch, T.D., Lawton, T.F., Nichols, D.J., Cashion, W.B., and Cobban, W.A., 1983, Patterns and timing of synorogenic sedimentation in Upper Cretaceous rocks of central and northeast Utah, in Reynolds, M.W., and Dolly, E.D., eds, *Mesozoic paleogeography of the West-Central United States: Society of Economic Paleontologists and Mineralogists Rocky Mountain Paleogeography Symposium, 2nd, Denver, Colo.*, 1983, p. 305–336.
- Gill, J.R., and Cobban, W.A., 1973, Stratigraphy and geologic history of the Montana Group and equivalent rocks, Montana, Wyoming, and North and South Dakota: U.S. Geological Survey Professional Paper 776, 37 p.
- Gries, Robbie, 1983, Oil and gas prospecting beneath Precambrian of foreland thrust plates in Rocky Mountains: *American Association of Petroleum Geologists Bulletin*, v. 67, no. 1, p. 1–28.
- Hagen, E.S., Shuster, M.W., and Furlong, K.P., 1985, Tectonic loading and subsidence of intermontane basins; Wyoming foreland province: *Geology*, v. 13, p. 585–588.
- Johnson, R.C., 1982, Measured section of Upper Cretaceous Mesaverde Formation and lower part of the lower Tertiary Wasatch Formation, Rifle Gap, Garfield County, Colorado: U.S. Geological Survey Open-File Report 85-590, 11 p.
- _____, 1987, Geologic history and hydrocarbon potential of Late Cretaceous-age low-permeability reservoirs, Piceance basin, western Colorado: U.S. Department of Energy, Fossil Energy, DOE/MC/20422–2337, 97 p.

- _____. 1989, Geologic history and hydrocarbon potential of Late Cretaceous-age, low-permeability reservoirs, Piceance basin, western Colorado: U.S. Geological Survey Bulletin 1787-E, 51 p.
- Johnson, R.C., Granica, M.P., and Dessenberger, N.C., 1979, Cross section B-B' of Upper Cretaceous and lower Tertiary rocks, southern Piceance Creek basin, Colorado: U.S. Geological Survey Miscellaneous Field Investigations Map MF-1130-B, 2 sheets.
- Johnson, R.C., and May, F., 1978, Preliminary stratigraphic studies of the upper part of the Mesaverde Group, the Wasatch Formation, and the lower part of the Green River Formation, Debeque area, Colorado, including environments of deposition and investigation of palynomorph assemblages: U.S. Geological Survey Miscellaneous Field Studies Map MF-1050, 2 sheets.
- _____. 1980, A study of the Cretaceous-Tertiary unconformity in the Piceance Creek basin, Colorado; the underlying Ohio Creek Formation (Upper Cretaceous defined as a member of the Hunter Canyon or Mesaverde Formation): U.S. Geological Survey Bulletin 1482-B, 27 p.
- Johnson, R.C., and Nuccio, V.F., 1984, Late Cretaceous through early Tertiary general stratigraphy and structural geology of the Piceance Creek basin, Colorado, *in* Spencer, C.W., and Keighin, C.W., eds., Geologic studies in support of the U.S. Department of Energy Multiwell Experiment, Garfield County, Colorado: U.S. Geological Survey Open-File Report 84-757, p. 14-20.
- _____. 1986, Structural and thermal history of the Piceance Creek basin, western Colorado, in relation to hydrocarbon occurrence in the Mesaverde Group, *in* Spencer, C.W., and Mast, R.F., eds., Geology of tight gas reservoirs: American Association of Petroleum Geologists Studies in Geology 24, p. 165-206.
- Jordan, T.E., 1981, Thrust loads and foreland basin evolution, Cretaceous, western United States: American Association of Petroleum Geologists Bulletin, v. 65, no. 12, p. 2506-2520.
- Keefer, W.R., 1965, Stratigraphy and geologic history of the uppermost Cretaceous, Paleocene, and lower Eocene rocks in the Wind River basin, Wyoming: U.S. Geological Survey Professional Paper 495-A, p. A1-A77.
- Law, B.E., 1979, Section B-B', subsurface and surface correlations of some Upper Cretaceous and Tertiary rocks, northern Green River basin, Wyoming: U.S. Geological Survey Open-File Report 79-1689, 2 sheets.
- _____. 1984, Structure and stratigraphy of the Pinedale anticline, Wyoming, *in* Law, B.E., ed., Geological characteristics of low-permeability Upper Cretaceous and lower Tertiary rocks in the Pinedale anticline area, Sublette County, Wyoming: U.S. Geological Survey Open-File Report 84-753, p. 6-15.
- Law, B.E., Bucurel-White, H., and Bader, J.W., 1983, Sedimentological aspects of stratigraphic correlations in the Upper Cretaceous Ericson Sandstone, Greater Green River basin, Wyoming, Colorado, and Utah: Geological Society of America Abstracts with Programs, v. 15, no. 5, p. 333.
- Law, B.E., and Nichols, D.J., 1982, Subsurface stratigraphic correlations of some Upper Cretaceous and lower Tertiary rocks, northern Green River basin, Wyoming [abs.], *in* Steidtmann, J.R., ed., Subsurface practices in geology and geophysics: Laramie, Wyo., University of Wyoming, Department of Geology and Geophysics, Earth Science Bulletin 15, p. 17.
- Law, B.E., Pollastro, R.M., and Keighin, C.W., 1986, Geologic characterization of low-permeability gas reservoirs in selected wells, Greater Green River basin, Wyoming, Colorado, and Utah, *in* Spencer, C.W., and Mast, R.F., eds., Geology of tight gas reservoirs: American Association of Petroleum Geologists Studies in Geology 24, p. 253-270.
- Lorenz, J.C., 1983, Reservoir sedimentology in Mesaverde rocks of the Multi-Well Experiment site: Sandia National Laboratories Report SAND83-1078, 36 p.
- _____. 1984, Reservoir sedimentology of Mesaverde rocks at the MWX site, *in* Spencer, C.W., and Keighin, C.W., eds., Geologic studies in support of the U.S. Department of Energy Multiwell Experiment, Garfield County, Colorado: U.S. Geological Survey Open-File Report 84-757, p. 21-32.
- Love, J.D., 1960, Cenozoic sedimentation and crustal movement in Wyoming: American Journal of Science, v. 258-A, p. 204-214.
- Martin, W.B., and Shaughnessy, J., 1969, Project Wagon Wheel, *in* Symposium on Tertiary rocks of Wyoming: Wyoming Geological Association Field Conference, 21st, Guidebook, p. 145-152.
- Newman, K.R., 1974, Palynomorph zones in early Tertiary formations of the Piceance Creek and Uinta basins, Colorado and Utah, *in* Murray, D.K., ed., Guidebook to the energy resources of the Piceance Creek basin, Colorado: Rocky Mountain Association of Geologists Field Conference Guidebook 25, p. 47-56.
- Premsky, S.E., 1984, A gamma-ray log anomaly associated with the Cretaceous-Tertiary boundary in the northern Green River basin, Wyoming, *in* Law, B.E., ed., Geological characteristics of low-permeability Upper Cretaceous and lower Tertiary rocks in the Pinedale anticline area, Sublette County, Wyoming: U.S. Geological Survey Open-File Report 84-753, p. 22-35.
- Ritzma, H.R., 1965, Fossil soil at base of Paleocene rocks, southern Rock Springs uplift, Wyoming, *in* Sedimentation of Late Cretaceous and Tertiary outcrops, Rock Springs uplift: Wyoming Geological Association Field Conference, 19th, 1965, Guidebook, p. 137-139.
- Roehler, H.W., 1961, The Late Cretaceous-Tertiary boundary in the Rock Springs uplift, Sweetwater County, Wyoming, *in* Symposium on Late Cretaceous rocks, Wyoming and adjacent areas: Wyoming Geological Association Field Conference, 16th, 1961, Guidebook, p. 96-100.
- Shaughnessy, J., and Butcher, R.H., 1973, Geology of Project Wagon Wheel nuclear stimulation project, *in* Fassett, J.E., ed., Cretaceous and Tertiary rocks of the southern Colorado Plateau: Four Corners Geological Society, p. 185-196.
- _____. 1974, Geology of Wagon Wheel nuclear stimulation project, Pinedale field, Wyoming: American Association of Petroleum Geologists Bulletin, v. 58, no. 11, p. 2250-2259.

- Shuster, M.W., 1986, The origin and sedimentary evolution of the northern Green River basin, western Wyoming: Laramie, University of Wyoming, Ph.D. thesis, 323 p.
- Shuster, M.W., and Steidtmann, J.R., 1983, Origin and development of northern Green River basin; a stratigraphic and flexural study [abs.]: American Association of Petroleum Geologists Bulletin, v. 67, no. 8, p. 1356.
- 1988, Tectonic and sedimentary evolution of the northern Green River basin, western Wyoming, *in* Schmidt, C.J., and Perry, W.J., Jr., eds., Interaction of the Rocky Mountain foreland and the Cordilleran thrust belt: Geological Society of America Memoir 171, p. 515-529.
- Wood, A.E., 1962, The early Tertiary rodents of the Family Paramyidae: American Philosophical Society Transactions, v. 52, p. 261.

Chapter C

Comparison of Overpressuring at the Pinedale Anticline Area, Wyoming, and the Multiwell Experiment Site, Colorado

By CHARLES W. SPENCER

Prepared in cooperation with the U.S. Department of Energy

U.S. GEOLOGICAL SURVEY BULLETIN 1886

GEOLOGY OF TIGHT GAS RESERVOIRS IN THE PINEDALE ANTICLINE AREA, WYOMING,
AND AT THE MULTIWELL EXPERIMENT SITE, COLORADO

CONTENTS

Abstract	C1
Introduction	C1
Methods of study	C2
Pinedale area	C3
Multiwell Experiment site	C4
Comparison of overpressuring in the Pinedale and MWX areas	C12
Summary and conclusions	C12
References cited	C14

FIGURES

1. Map showing distribution of overpressuring in Greater Green River basin, Wyoming, Utah, and Colorado C3
2. Graphs showing subsurface pressure, temperature, and vitrinite reflectance, El Paso Natural Gas No. 1 Wagon Wheel well, on the crest of the Pinedale anticline C4
3. Drill-stem test chart from test run in Upper Cretaceous Lance Formation, El Paso Natural Gas No. 1 Wagon Wheel, between depths of 10,978 and 11,070 ft C5
4. Cross plot of interpreted reservoir pressure and depth for six wells drilled on Pinedale anticline C6
5. Interpreted pressure profile for MWX wells C7
- 6-7. Temperature logs for MWX-1 well measured by Los Alamos National Laboratories:
 6. From high-resolution, and openhole geophysical logs and an openhole drill-stem test C8
 7. Six months after hole was cased C9
8. Differential temperature gradient log for MWX-1 well C10
9. Graph showing vitrinite reflectance of kerogen extracts obtained from MWX wells as a function of depth C11
10. Profile through MWX area showing topographic relief in Colorado River valley C12
11. Graph showing pressure gradients in Pinedale and MWX areas C13

Comparison of Overpressuring at the Pinedale Anticline Area, Wyoming, and the Multiwell Experiment Site, Colorado

By Charles W. Spencer

Abstract

Abnormally high reservoir pressures occur in many Rocky Mountain basins in deep, hot (>200 °F, 93 °C), low-permeability (tight) reservoir sequences. Although the pressuring fluid phase is usually natural gas, some overpressured oil and gas reservoirs are also present. The high pressure is interpreted to be caused by active or recently active generation of hydrocarbons at a rate that exceeds hydrocarbon loss.

Comparison of overpressuring in Upper Cretaceous tight gas sandstone reservoirs at the Pinedale area, Sublette County, Wyo., and at the U.S. Department of Energy Multiwell Experiment site, Garfield County, Colo., indicates that although these two areas have experienced different paleothermal histories, many similarities exist between the areas. Both have been cooled below their maximum levels of paleoheating, and this cooling has resulted in the interpreted development of shallow zones of inactive or residual overpressuring. These shallow zones are intervals where gas is no longer being generated and is being lost by diffusion and gas-phase migration. Below these inactive zones, pressure-causing gas generation is actively occurring at temperatures higher than about 200 °F (93 °C). In the active generation zones, pressures are variable but higher than those in the inactive zones. Pressure variations in the active zones are related to rock permeability and organic richness and to the ability of source rocks to generate gas at a rate that exceeds gas loss.

In both areas, maximum pressures are about equal to the fracture gradient of the sandstone reservoirs. High pore pressures may be a factor in the development of natural fractures. Limited studies of fracture-filling cements at the Multiwell site indicate that the fractures formed at elevated temperatures and at a time when reservoir waters were gas saturated.

Inconclusive data from the deep, highly overpressured parts of the Multiwell Experiment wells suggest that some retardation of thermal maturation (vitrinite reflectance) may have occurred. Data from the Pinedale wells, however, do not suggest suppression of vitrinite reflectance.

INTRODUCTION

Overpressured low-permeability (tight) gas reservoirs are common in the deeper parts of many Rocky Mountain basins (Spencer 1983, 1987). Pore pressure or

reservoir pressure, as it is more commonly described, is often expressed in terms of a pressure gradient in psi/ft (kPa/m). In freshwater reservoirs, normal pressure is about 0.43 psi/ft (9.73 kPa/m), and if reservoir pressures exceed 0.5 psi/ft (11.31 kPa/m), the reservoirs usually are considered to be overpressured (reservoirs containing highly saline water are exceptions to this generalization). Upper Cretaceous sandstone, shale, and coal strata are substantially overpressured at both the Pinedale anticline area in the Green River basin of southwestern Wyoming and the U.S. Department of Energy Multiwell Experiment (MWX) site in the Piceance basin of northwestern Colorado (Law and Spencer, this volume, fig. 1); maximum reservoir pressures in both areas are about 0.8 psi/ft (18.1 kPa/m). Both areas are in regionally overpressured basins that have been studied by the U.S. Geological Survey (USGS) in cooperation with the U.S. Department of Energy's Western Tight Gas Sands Subprogram.

Although a variety of factors can cause overpressuring (Fertl, 1976), the generally accepted causes of most overpressuring are dewatering (compaction) of shales (Harkins and Baugher, 1969) or alteration of "montmorillonite" (smectite) to a less hydrated mixed-layer illite-smectite mineralogy (Powers, 1967; Burst, 1969). Both concepts assume that water is the pressuring mechanism, but in most tight reservoirs oil or gas is the dominant pressuring fluid phase. In fact, overpressured water is rarely encountered in Rocky Mountain reservoirs, and the active or recently active generation of hydrocarbons at a rate that exceeds loss by migration is believed to be the most likely cause of overpressuring in rock sequences where overpressured water is generally not encountered (Meissner, 1976, 1978a, b; Law and others, 1980) and is the most likely cause of overpressuring in both the Pinedale (Law, 1984a; Spencer, 1984a) and MWX areas (Spencer, 1987).

Regionally overpressured tight gas-bearing rock sequences in the Rocky Mountain basins have the following characteristics in common.

1. Hydrocarbons are almost always the mobile reservoir-pressuring fluid.

2. Overpressuring mostly occurs in rock sequences having present-day temperatures of about 200 ± 10 °F (93 ± 6 °C) or higher. Some residual or "inactive" (Law, 1984a) overpressuring occurs at lower temperatures; this phenomenon will be discussed later in the report.

3. Overpressuring only occurs in tight rock sequences.

4. Organic-rich source beds are still capable of generating hydrocarbons at rates that exceed loss by migration.

5. Minimum vitrinite reflectance in oil (R_o) of the kerogen in these rock sequences is usually greater than 0.6 percent in very rich oil-prone source beds and greater than 0.7 percent in very rich gas-prone source beds. In relatively organically lean oil-prone source beds, the minimum R_o is usually greater than 0.7 percent and in lean gas-prone sedimentary rocks greater than 0.8 percent. A relationship may exist, however, between thermal maturation and permeability (B.E. Law, written commun., 1986), and as noted previously overpressuring only occurs in tight rocks. If the rock sequence is either very organically lean or nonorganic, regional overpressuring will not occur.

6. Local structure and stratigraphy are of secondary importance in the occurrence of overpressuring.

7. Reservoirs rarely have discrete gas-water or oil-water contacts and commonly produce no water.

8. Natural fracturing is necessary for high gas production rates.

9. *Maximum* pressure gradients in an area are about equal to the natural-fracture gradient of the rocks.

10. Most classical hydrodynamic concepts and models developed for conventional blanket reservoirs do not apply to overpressured sequences, except that oil and gas in high-pressure sequences tend to migrate from high pressure to lower pressure.

11. Overpressured strata are commonly in the center of the basin.

12. Water-bearing reservoirs having normal to sub-normal pressure are usually updip from overpressured, deep rocks.

Acknowledgments.—The support of the U.S. Department of Energy Morgantown Energy Technology Center is gratefully acknowledged. R.A. Ullrich, El Paso Natural Gas Company provided core samples and well data from the Wagon Wheel No. 1 well. Paul Branagan supplied MWX pressure and other data. B.E. Law and R.R. Charpentier reviewed this paper and provided constructive comments.

METHODS OF STUDY

Reservoir pressures in the Pinedale anticline and MWX areas do not represent isolated data points but are parts of a study of regionally overpressured tight-gas basins. In conventional rocks, reservoir pressure is generally easily estimated or calculated because the rocks have good permeability. Reservoir pressures are calculated by extrapolation of drill-stem test (DST) shut-in pressures to an undisturbed original pressure or by long-term measurement of cased-hole, shut-in pressures. In tight-gas reservoirs, in situ permeability to gas is very low ($0.1 < 0.0001$ mD) and the usual methods of measuring reservoir pressure may not be adequate. In the MWX wells, numerous cased-hole pressure measurements were obtained during rock-stress tests and other well tests, but in the Pinedale area only a few extrapolatable DSTs are available.

In gas reservoirs and especially in tight gas reservoirs, accurate static pressure calculations are impeded by the fact that gas is highly compressible. After a well is flowed (pressure drawdown), the well is shut in and gas recompression occurs in the hole (wellbore storage) and in the formation (afterflow). Shut-in times of many weeks or months may be required to estimate pressures in tight reservoirs because of the compressibility of gas and the low permeability. Drill-stem tests can indicate, therefore, *minimum* levels of high pressure but generally cannot be used to estimate true pressure.

Fracture permeability greatly enhances both rock-matrix permeability and the rock-surface area evaluated by a DST, but probably no more than 10 percent of the DSTs run in tight reservoir sequences in the Rocky Mountain region evaluate rock sequences that are highly fractured at the well bore. Some DSTs in fractured reservoirs can be used to estimate true reservoir pressure; however, other methods to detect overpressuring should also be used, including correlation of data from drilling-mud weights, drilling-time charts (d-exponent), and mud-log gas shows and kicks. Estimation of pore pressure by using borehole geophysical logs of Tertiary and Cretaceous rocks in the Rocky Mountain region is not yet reliable (S.E. Prenskey, oral commun., 1984).

Mud weights and gas shows are the two most widely available sources of data to indicate overpressuring. With experience, the *top* of overpressuring can be accurately identified by using these data, but caution must be used when attempting to estimate *maximum* reservoir pressures within the overpressured interval. Various operators have their own approaches to drilling high-pressured, tight rocks. Some operators drill "underbalanced"; that is, they drill using mud weights known to be less than true reservoir pressure. Drilling underbalanced greatly enhances drill-bit penetration rates. Some operators will unknowingly drill underbalanced, but most try to use

mud weights equivalent to the reservoir pressure of the section being penetrated. Balanced drilling permits good bit penetration rates, minimizes the potential for well blowouts, and reduces the chances of accidentally fracturing the open part of the hole by mud weights that exceed the formation fracture gradient.

PINEDALE AREA

The Pinedale area (fig. 1) includes wells on and adjacent to the northwest-trending Pinedale anticline. The area is in the northwest part of the greater Green River basin and has been studied in detail because of the availability of deep well and core information (Law, 1984b).

Abnormally high pressures in the northwest part of the Greater Green River basin were noted by Rathbun (1968) and Rathbun and Dickey (1969). The northern Green River basin is between the southwest-thrusted Wind River Mountains uplift and the east-thrusted Wyoming thrust belt, and Rathbun and Dickey believed that the overpressuring was caused by tectonic compression. They also believed that borehole-geophysical logs could be used to identify a conductivity anomaly associated with overpressuring in the northern Green River basin, but most of their interpretation of abnormal pressures was based on mud-weight data. Computer processing of well logs by Prenskey and Dickinson (1986) indicates that borehole-geophysical logs are not a reliable means to identify overpressuring in the well-consolidated rocks of the northern Green River basin. Overpressuring in the basin is regionally distributed and not confined to tectonically stressed localities (fig. 1). Limited data suggest that pressures are normal just in front of and beneath the thrust along most of the southwest side of the Wind River Mountains uplift. The occurrence of apparently normal pressures adjacent to the Wind River Mountains thrust is probably related to loss of gas caused by vertical fracturing in rocks adjacent to and under the thrust.

The El Paso Natural Gas No. 1 Wagon Wheel well was drilled in sec. 5, T. 30 N., R. 108 W., Sublette County, Wyo.. The well was drilled on the axis of the Pinedale anticline and was in the Upper Cretaceous Hilliard Shale at total depth of 19,000 ft (5,791 m). Figure 2A shows a plot of interpreted subsurface temperature and pressure gradients of the well, and figure 2B shows a plot of vitrinite reflectance data correlated with depth. The pressure interpretation is based mostly on mud weight and other data compiled from mud logs, well logs, and borehole mud weights determined from DST hydrostatic pressures. None of the DST shut-in pressure data was extrapolatable because of the low permeability of the reservoirs tested, but a few DST's had sufficient pressure buildup during initial shut-in times such that the

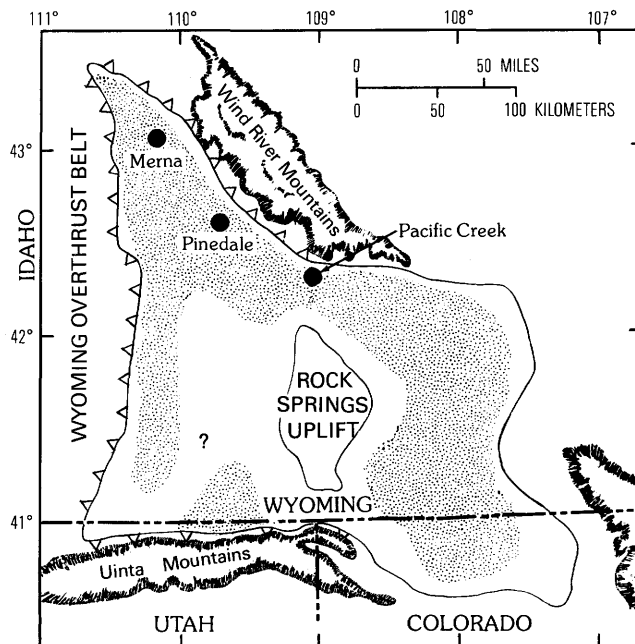


Figure 1. Generalized distribution of overpressuring (pattern) in the Greater Green River basin of Wyoming, Utah, and Colorado. Query (?) indicates overpressuring uncertain.

overpressuring could be clearly verified even though its *maximum* amount could not be determined. Figure 3 shows a DST chart from the well, run in the Upper Cretaceous Lance Formation between depths of 10,978 and 11,070 ft (3,346.1–3,374.1 m). A visual interpretation of the initial shut-in curve and pressure data confirms the presence of abnormally high reservoir pressure. The initial shut-in pressure was 6,805 psi (46.9 MPa) at a gauge depth of 11,066 ft (3,372.9 m), and the pressure was increasing at the time the shut-in period ended (point A). The true reservoir pressure is slightly higher than the maximum hydrostatic pressure (point B) of 7,600 psi (52.4 MPa). Although the DST pressure data are not extrapolatable, I believe that the well was being drilled slightly underbalanced at the time the test was run, and therefore the true reservoir pressure is greater than 7,600 psi (52.4 MPa). Consequently, the reservoir pressure gradient is greater than 0.69 psi/ft (15.61 kPa/m). This DST yielded gas to the surface in 55 minutes at a rate too low to gauge and recovered 2,800 ft (853.4 m) of water cushion and 90 ft (27.4 m) of slightly gas-cut mud.

The pressure-depth plot (fig. 2A) shows several inflections in the pressure gradient with depth. The first inflection is at about 8,000 ft (2,438 m) in the Lance Formation and marks the top of the abnormally high pressure interval. Another inflection is at about 10,400 ft (3,170 m), and a third is at about 15,000 ft (4,572 m), adjacent to a coal zone in the middle of the Rock Springs Formation (Law, 1984a). Law described the interval between 8,030 ft (2,447.5 m) and 10,400 ft (3,170 m) as a

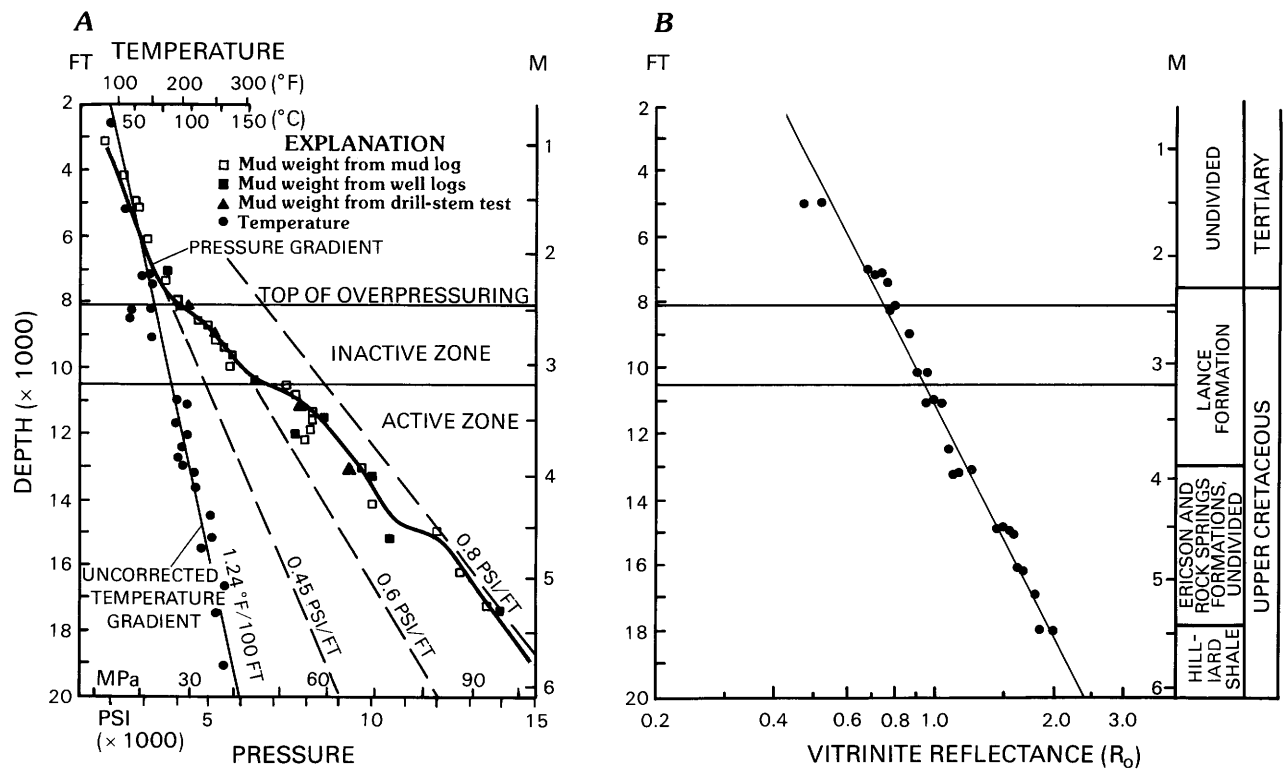


Figure 2. Subsurface pressure, temperature, and vitrinite reflectance, El Paso Natural Gas No. 1 Wagon Wheel well, on the crest of the Pinedale anticline, sec. 5, T. 30 N., R. 108 W., Sublette County, Wyo. A, Pressure and uncorrected temperature. Modified from Law (1984a, fig. 12). Location of well shown in Law and Spencer (this volume, fig. 1). Temperature data from Wagon Wheel and other nearby wells. B, Vitrinite reflectance (in percent) of kerogen extracts from core of Wagon Wheel well.

zone of inactive gas generation and interprets the source beds in this zone to have been formerly at sufficiently high temperature (>190 °F, >88 °C) to have generated gas. He believed the source beds were overpressured at the time of gas generation and gas generation ceased when a cooling event caused the source beds to cool below the 190–200 °F (88–93 °C) critical minimum temperature for gas generation. The uncorrected temperature at 8,000 ft (2,438 m) is now about 150 °F (66 °C) and the corrected temperature about 175 °F (79 °C). The inactive zone represents a residual overpressured interval, and a similar zone is interpreted to exist at the MWX site.

The pressure-gradient increase at about 10,400 ft (3,170 m) in the No. 1 Wagon Wheel is at a present-day corrected subsurface temperature of approximately 200 °F (93 °C), interpreted to be the estimated minimum temperature necessary for significant gas generation from humic-rich source beds still capable of gas generation at a rate that exceeds pressure loss. The vitrinite reflectance (R_0) at the top of the inactive zone is about 0.74 percent (fig. 2B), and the highest vitrinite reflectance value measured in the well is 2.0 percent at about 18,000 ft (5,486 m).

The No. 1 Wagon Wheel site was a proposed site for nuclear stimulation and, consequently, the well was drilled with considerable concern to keep reservoir pressures and mud weights as close to a balanced condition as

possible. For this reason, the general pressures for the Pinedale anticline are best shown by this profile (fig. 2A); other wells in the area may show some differences in reservoir pressure. Figure 4 shows mud-weight profiles for several other wells in the anticline area. This compilation shows that most of the mud weights were adjusted to the pressure variations in a similar manner. Somewhat lower mud weights were used to drill the El Paso Natural Gas No. 5 Pinedale Unit well in the interval from about 10,000 ft to 13,060 ft (3,050–3,980 m). This well is only about 0.5 mi (0.8 km) southeast of the No. 1 Wagon Wheel well. It is interpreted that the No. 5 Pinedale Unit well was drilled underbalanced to a depth of 13,060 ft (3,981 m) and the casing was set, at which point drilling was resumed in an apparently balanced condition to total depth.

It is not unusual to encounter an apparently normally pressured well in an area where most wells are overpressured. The normally pressured well may be the result of loss of pressure caused by extensive vertical fracturing.

MULTIWELL EXPERIMENT SITE

The deeper parts of the Piceance basin of northwestern Colorado, including the area of the Multiwell Experiment (MWX) site, are interpreted to be regionally

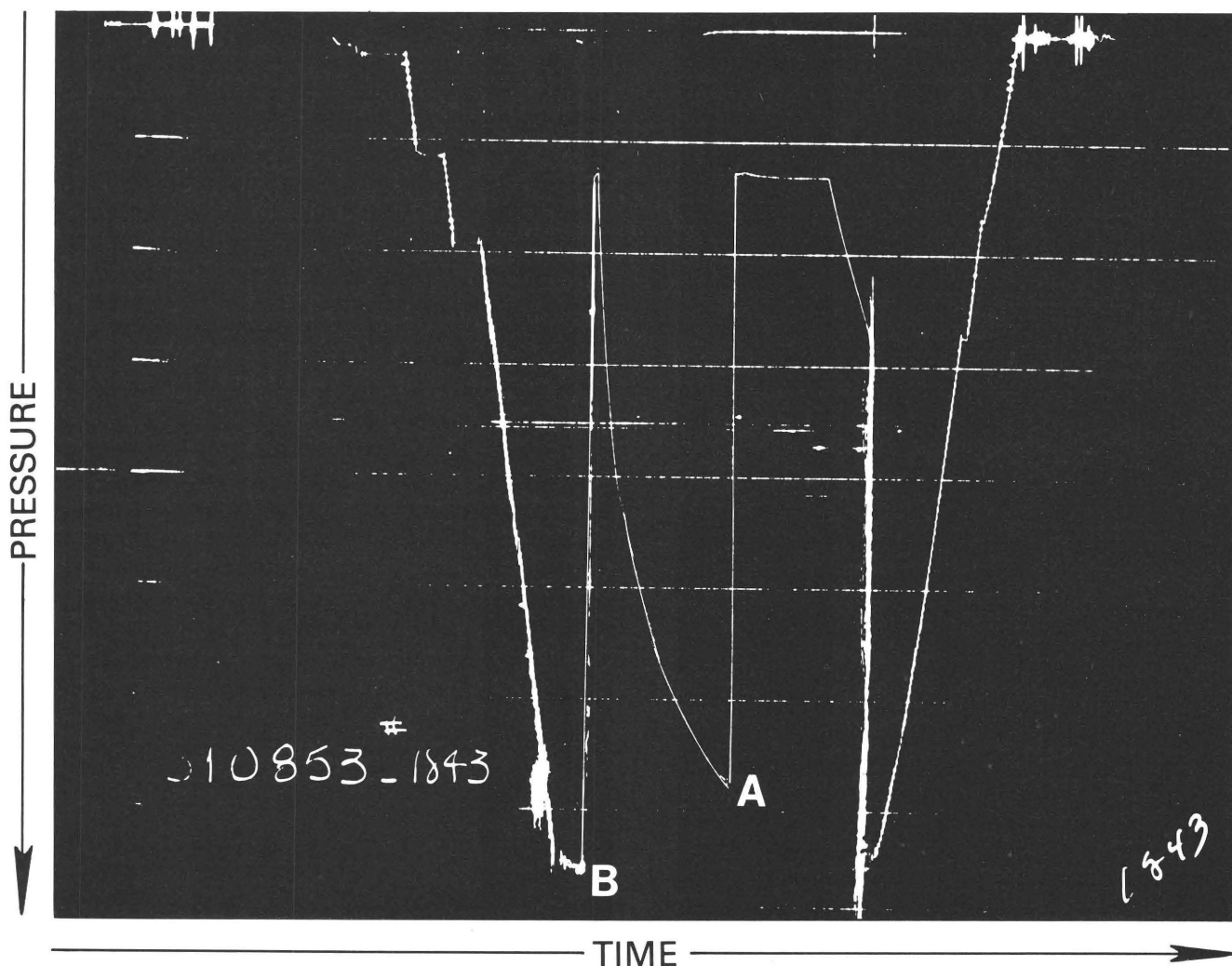


Figure 3. Drill-stem test chart from test run in Upper Cretaceous Lance Formation, El Paso Natural Gas No. 1 Wagon Wheel, between depths of 10,978 and 11,070 ft (3,346.1–3,374.1 m). Initial shut-in pressure (point A), 6,805 psi (46.9 MPa); maximum mud hydrostatic pressure (point B), 7,600 psi (52.4 MPa).

overpressured (Spencer, 1987). The MWX site is in the valley of the Colorado River, about 6.5 mi (10.5 km) southwest of Rifle, Colo. (Law and Spencer, this volume, fig. 1). The U.S. Department of Energy supported the drilling of three closely spaced wells at this site in order to advance knowledge of well-log interpretation, artificial stimulation (hydraulic fracturing), and recovery of natural gas from tight gas reservoirs (Northrop and others, 1984; Warpinski and others, 1985). The MWX wells are the *only* wells drilled in the basin for which the operator has attempted to obtain good pressure and temperature data throughout a thick sequence of tight rocks. The three wells are located in a triangle and are quite close (115–215 ft, 35–66 m) to each other (Spencer, 1984b). They are designated as the CER Nos. 1, 2, and 3 MWX and are in the NW1/4 sec. 34, T. 6 S., R. 94 W., Garfield County, Colo. In this volume, the wells are referred to as the MWX-1, -2, and -3. The wells were spudded in the upper part of the Tertiary

Wasatch Formation and reached total depths at or near the base of the Upper Cretaceous Mesaverde Group. Many geologic and engineering studies have been conducted at the MWX site (Spencer and Keighin, 1984).

A series of experiments involving in situ stress testing and hydraulic fracturing were conducted (Branagan and others, 1984; Warpinski and others, 1984; Branagan and others, 1985). As a result of this research and other unpublished studies (Paul Branagan, written commun., 1986), a considerable amount of reservoir-pressure and fracture-gradient data have been developed. Figure 5 shows the interpreted pressure profile for the MWX wells and the fracture gradients for various lithologies.

The top of the overpressured interval is in gas-bearing sandstones in the fluvial part of the Mesaverde Group at a depth of about 5,600 ft (1,707 m) and a present-day temperature of 165 °F (74 °C). It is interpreted that overpressuring from the 165 °F (74 °C) line to the 200 °F

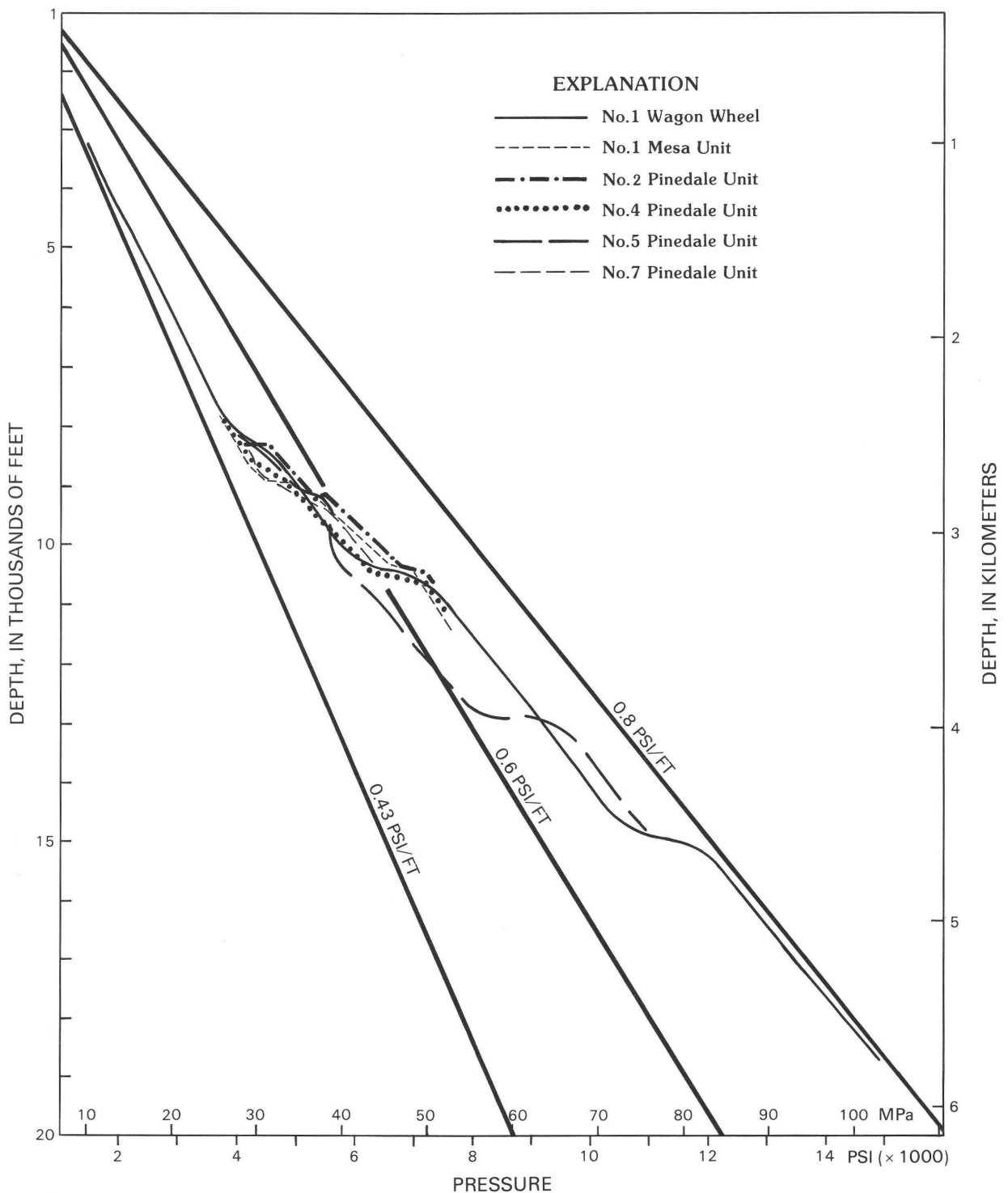


Figure 4. Cross plot of interpreted reservoir pressure and depth for six wells drilled on Pinedale anticline. Data mostly compiled from drilling-mud weights and gas shows from mud logs. Modified from Spencer (1984a). Locations of the wells shown in Law and Spencer (this volume, fig. 1).

(93 °C) line represents a zone of residual overpressuring and that little or no gas is being generated in this interval. The gas pressure in this interval probably is being depleted by migration along fractures and by diffusion. This low-temperature overpressuring in thermally mature rocks is

similar to the “inactive zone” of overpressuring described by Law (1984a) in the Pinedale area in the Green River basin. The interpreted top of “active” present-day overpressuring at MWX is at a depth of 7,024 ft (2,141 m) and a temperature of 200 °F (93 °C).

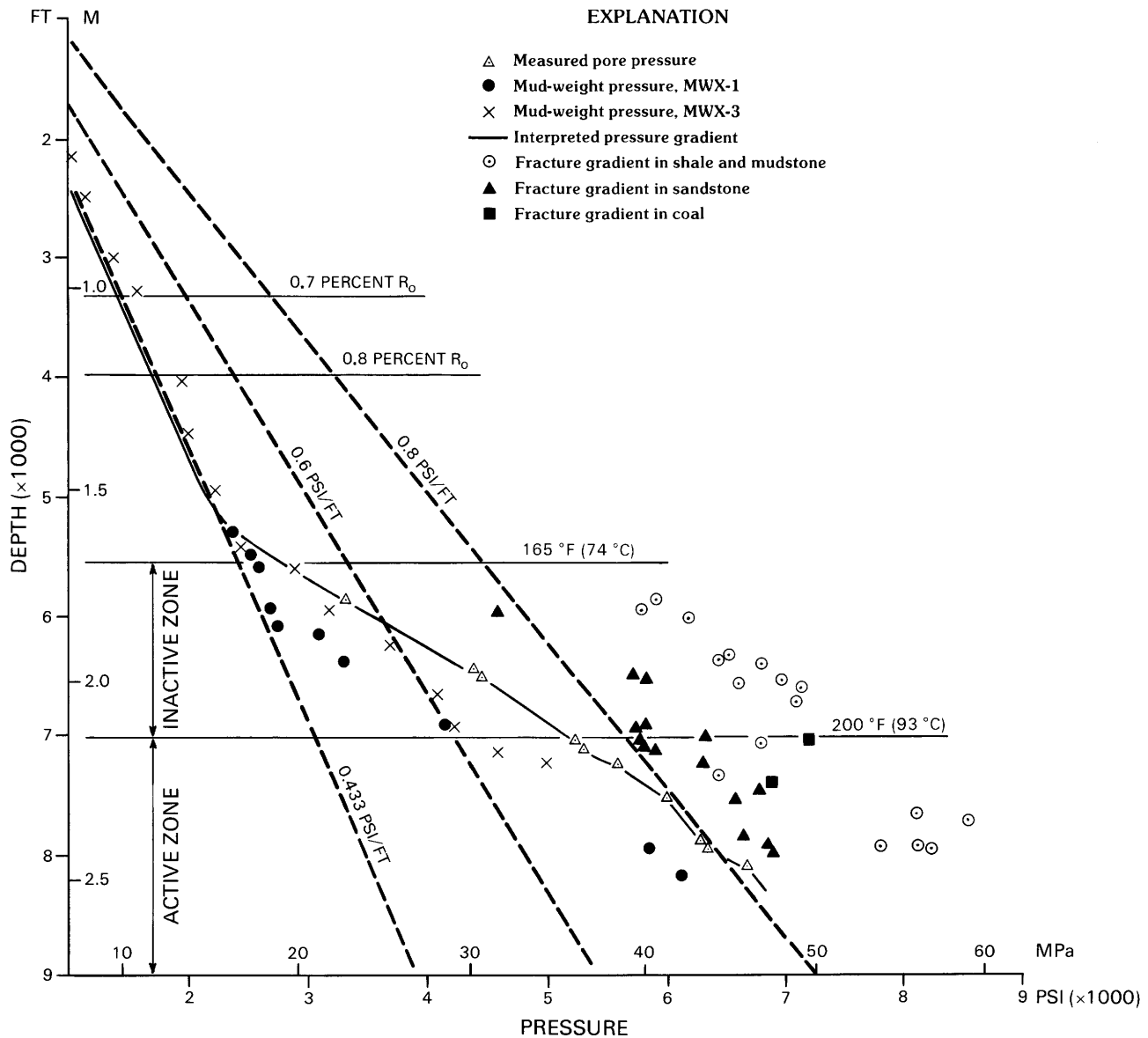


Figure 5. Interpreted pressure profile for MWX wells, Piceance basin, sec. 34, T. 6 S., R. 94 W., Garfield County, Colo. Measured pore pressure and fracture-gradient data from stress and other tests (Warpinski and others, 1984; Paul Branagan, written commun., 1986, 1987). Fracture gradients for mudstone and shale are higher than that for sandstone. Vitrinite reflectance values of 0.7 and 0.8 R_o from Bostick and Freeman (1984).

The temperature data were derived from high-resolution temperature logs run in the MWX-1 well by Los Alamos National Laboratory (LANL) six months after the hole was cased (Bostick and Freeman, 1984). Figure 6 shows a plot of the LANL data and borehole-geophysical log maximum bottom-hole temperatures from the MWX open-hole logs. The standard American Association of Petroleum Geologists (AAPG) bottom-hole temperature correction for these log depths is also shown (Meissner, 1978a). This correction is necessary because the circulation of drilling mud cools the borehole. At depths of less than 7,000 ft (2,134 m), the AAPG-corrected temperatures are within 10 °F (6 °C) of the

LANL temperatures and tend to be slightly higher than the LANL data. Below 7,000 ft (2,134 m), there are a few points that suggest a spread of corrected temperature data higher and lower than the LANL temperatures. Many factors can affect the maximum log temperatures and the amount of correction needed. Although this study cannot resolve these differences, these discrepancies are recognized as a source of error in interpreting the exact temperature of the top of overpressuring when only open-hole maximum log temperatures are available.

The increase in temperature gradient at a depth of about 7,000 ft (2,130 m) is probably caused by the low thermal conductivity of a sequence of Mesaverde coal

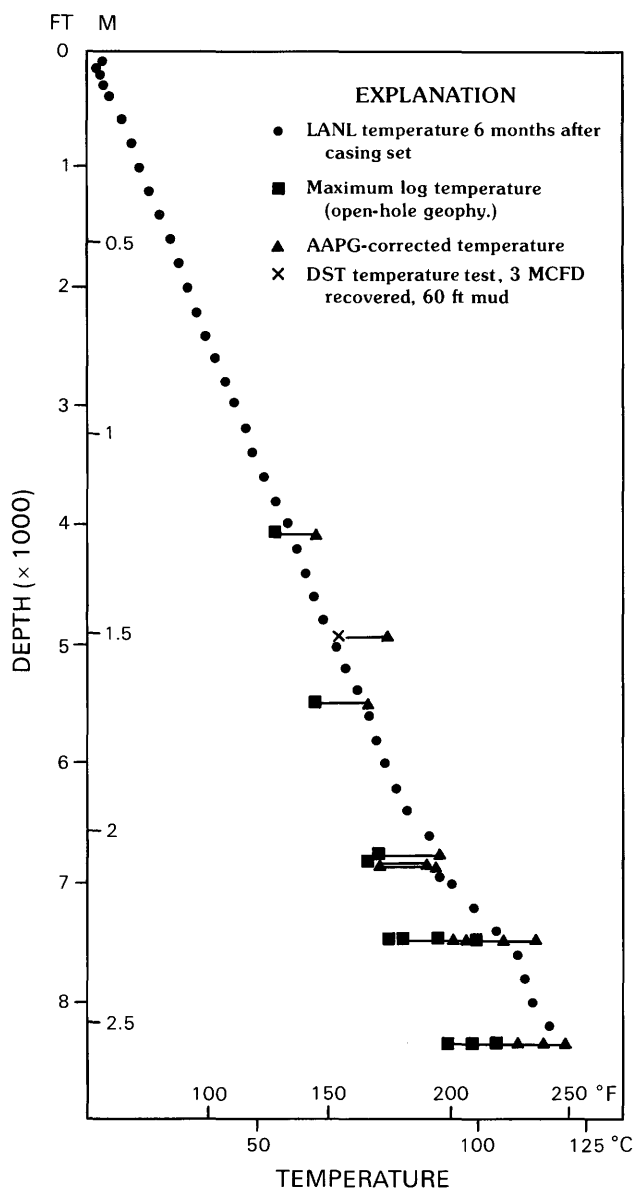


Figure 6. Temperature log for MWX-1 well. Temperatures from Los Alamos National Laboratories (LANL) high-resolution log, openhole geophysical logs, and an openhole drill-stem test (DST). Standard American Association of Petroleum Geologists (AAPG) (Meissner, 1979a) correction applied.

beds from about 6,900 ft (2,103 m) to 7,455 ft (2,272 m). This major coal zone is approximately correlative with the Cameo-Fairfield coal zone (Nuccio and Johnson, 1983, 1984a). Several thin coals are present above this main coal zone. Figure 7 shows the temperature profile for the MWX-1 well and the changes in temperature gradients associated with the coaly interval above the Rollins Sandstone Member of the Iles Formation. Figure 8 shows the actual variations in the differential temperature gradient caused by lithologic changes and, especially, the high gradients associated with the low thermal

conductivity of the coals. The increase in subsurface temperatures below the coal zone must have persisted through geologic time and should have caused a corresponding increase in the gradient of vitrinite reflectance levels in the underlying source beds.

Vitrinite reflectance values (fig. 9) (Bostick and Freeman, 1984) show that no such apparent increase in the trend of vitrinite reflectance values has occurred in the overpressured coal zone and underlying highly pressured rocks (fig. 5). (For an MWX vitrinite profile having more data points, see Nuccio and Johnson, this volume.) Vitrinite reflectance values below depths of about 7,000 ft (2,130 m) appear to be suppressed. This suppression may have significance in interpreting rates of thermal maturation in organic-rich rocks that have experienced long-term levels of hydrocarbon-caused, abnormally high pressure. Cecil and others (1977) conducted laboratory studies of coalification and proposed that thermal maturation can be retarded in closed thermodynamic (high-pressure) systems. Extrapolation of their laboratory tests to the MWX site suggests that pressure-caused vitrinite suppression may have occurred. Although the data are presently inconclusive, it is speculated that organic-rich source rocks (coals) are capable of generating hydrocarbons with consequent abnormally high pressures over a geologically long period of time, and that kerogen maturation of source rocks might be suppressed in a prolonged high-pressure environment in which the maturation products (gas and gas condensate) cannot easily leave the site of origin. This maturation suppression may be similar to other thermochemical reactions that can be intentionally suppressed by increasing the partial pressure of the evolved gas reaction products. For example, calcium carbonate calcinates at a higher temperature if the partial pressure of carbon dioxide is increased.

Anomalously low vitrinite reflectance values also have been noted in lipid-rich (oil-prone) source beds (Hutton and Cook, 1980; Walker and others, 1983; Nuccio and Johnson, 1984b). The conditions that produce these low values may or may not be related to abnormally high paleopressures because suppression has been noted in low-temperature, very low maturity lipid-rich oil shales (Nuccio and Johnson, 1984b) that probably have not been overpressured. At the MWX site, vitrinite from coaly matter in dominantly gas prone rocks was used. No obvious suppression of vitrinite reflectance values is seen in the Wagon Wheel No. 1 well in the Pinedale area (fig. 2B).

The reservoir-pressure profile (fig. 5) shows the approximate depth of the 0.7- and 0.8-percent vitrinite reflectance in oil (R_o) levels projected by Bostick and Freeman (1984) by using core data. Additional vitrinite values for MWX samples are shown in Nuccio and Johnson (this volume). Tertiary rocks in the MWX wells are organically very lean; consequently, overpressuring

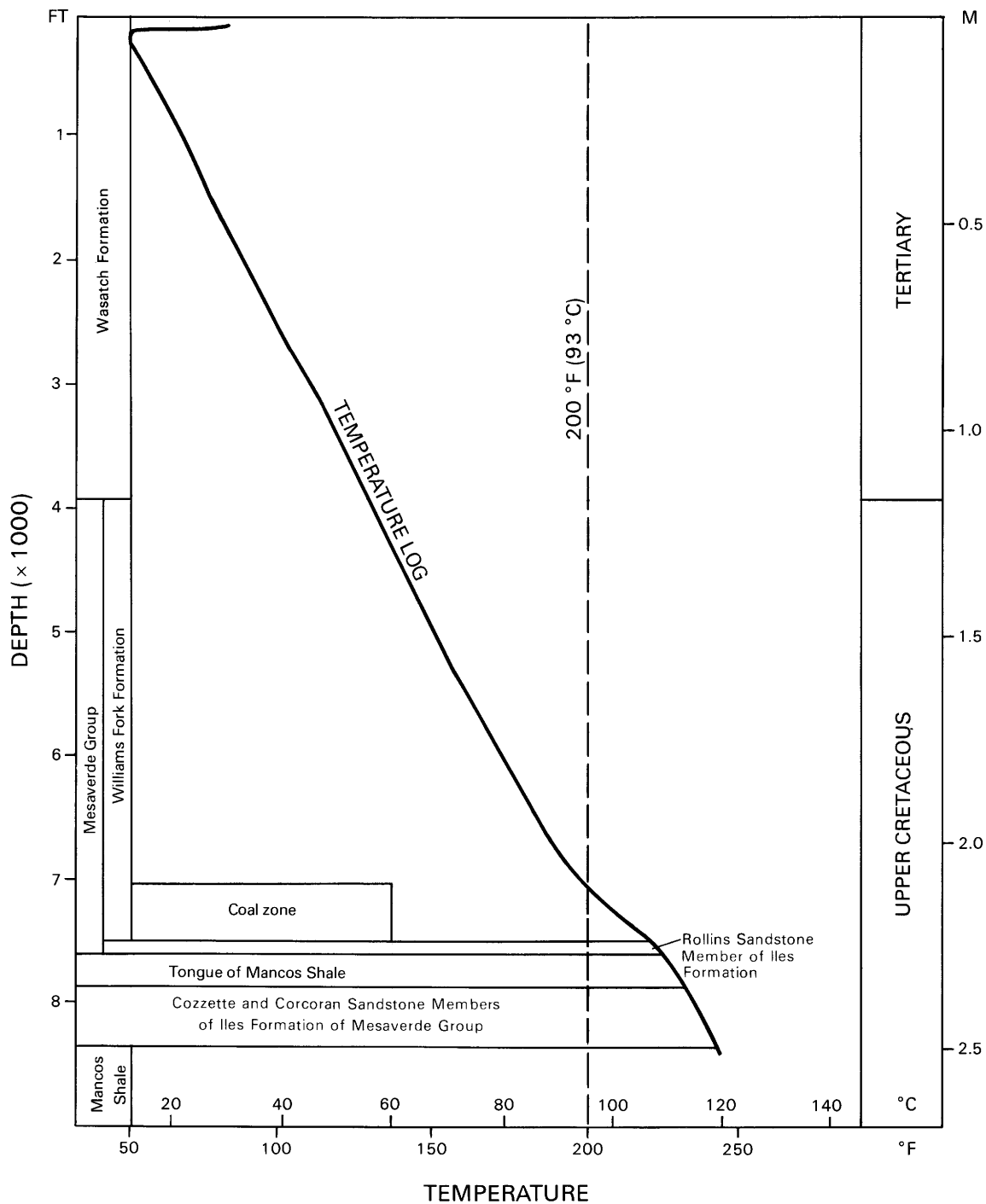


Figure 7. Temperature log for MWX-1 well. Measured by Los Alamos National Laboratory 6 months after hole was cased. Temperature gradient change in coal zone of Mesaverde Group shown.

as the result of active hydrocarbon generation probably never occurred in Tertiary rocks at MWX. The 0.8-percent level is, however, at a present-day well depth of about 4,000 ft (1,220 m) in Mesaverde rocks that include dark-gray to black organic shales and mudstones. The top of the Mesaverde and the base of the Tertiary is at a present-day depth of 3,900 ft (1,189 m) based on

correlations by R.C. Johnson (oral commun., 1982). Maximum burial probably occurred about 9-10 m.y. ago (Bostick and Freeman, 1984; Nuccio and Johnson, 1984a), and at that time the top of the overpressured zone probably was as shallow as the present 4,000-ft (1,220 m) depth in the MWX wells. After maximum burial, the Colorado River eroded 4,000-5,000 ft

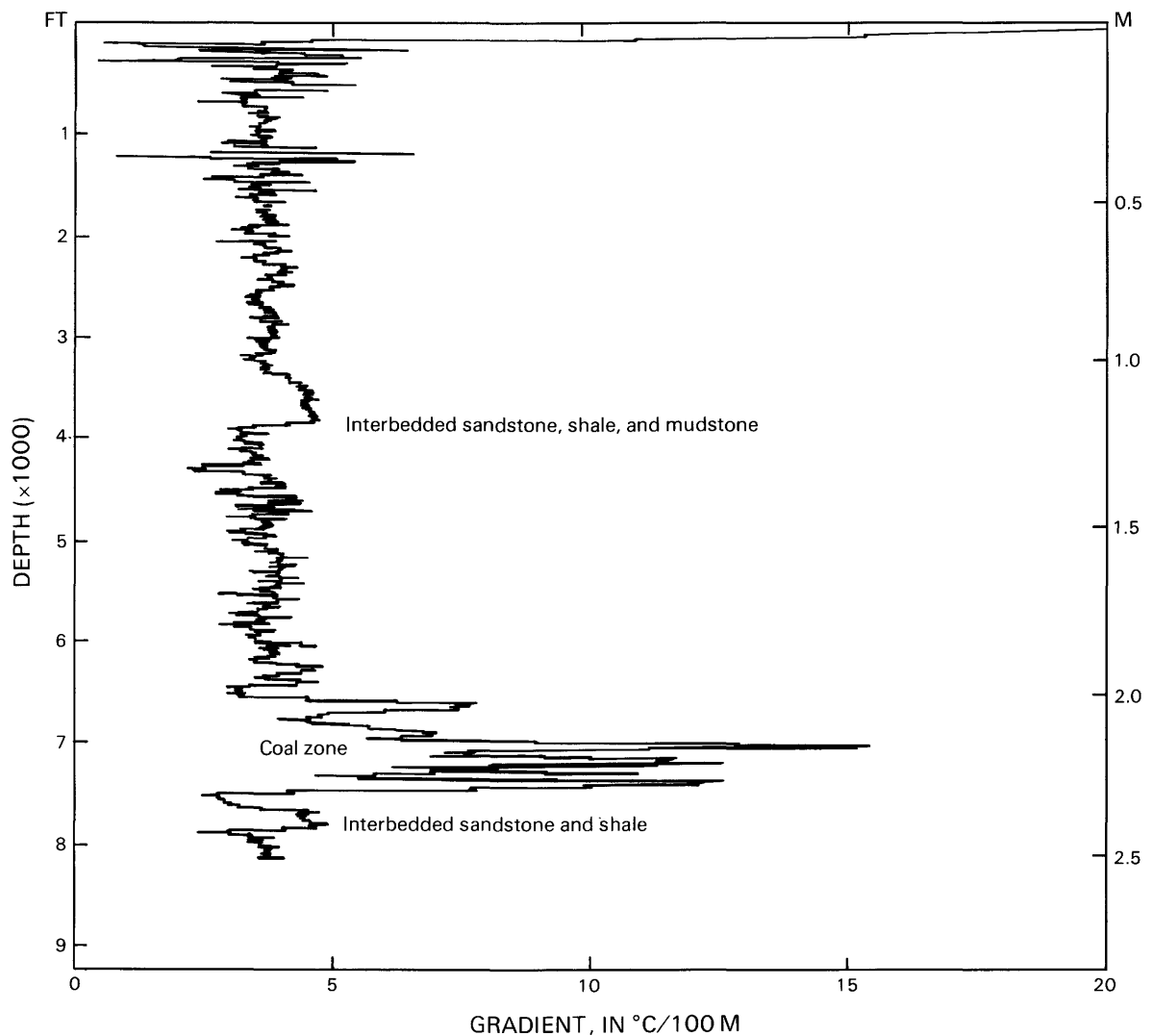


Figure 8. Differential temperature gradient log for MWX-1 well showing strong gradient increases across coal zone in Mesaverde Group. Temperature log measured by Los Alamos National Laboratories shown in figure 7.

(1,220–1,520 m) of rocks to the present elevation at the well site. This erosion caused considerable cooling of the rock sequence, and it is interpreted that as the rocks cooled gas generation ceased in the upper part of the Mesaverde Group. Reservoir pressure began to decrease in the MWX rocks because of gas diffusion and migration in the interval between the present 4,000-ft (1,220 m) depth to the top of active generation at about 7,000 ft (2,130 m). This pressure decay continued and the present-day top of interpreted inactive overpressure is at a depth of 5,600 ft (1,707 m). Pressures at depths less than 5,600 ft (1,707 m) are shown as normal in figure 5; however, pressures in gas reservoirs shallower than about 5,000 ft actually may be slightly subnormal on the basis of studies by Meissner (1978b) and Law and Dickinson (1985) in other basins.

The high topographic relief in the MWX area (fig. 10) complicates the use of pressure gradients as a means

to describe reservoir pressure. If a reservoir has the same pressure at two locations, one in a valley and the other on a mesa, then the pressure gradient of the well drilled in the valley will be higher than that in the well drilled on the mesa. In cases such as these, it is helpful to evaluate abnormal pressure in terms of a calculated potentiometric surface. For example, the calculated freshwater potentiometric surface of rocks at the base of the Mesaverde Group is 12,408 ft (3,782 m) above sea level. The nearest exposure of equivalent rocks is at an elevation of about 6,000 ft (1,830 m) at Rifle Gap, 12 mi (19 km) northeast of the MWX site. It is unlikely, therefore, that abnormal pressures at the MWX site are caused by recharge by meteoric water. In theory, any fluid movement should be toward the outcrops at Rifle Gap.

Overpressuring as a possible cause of natural fracturing has been proposed by Chaney (1949), Meissner (1978b), Hedberg (1980), and Law and others (1980).

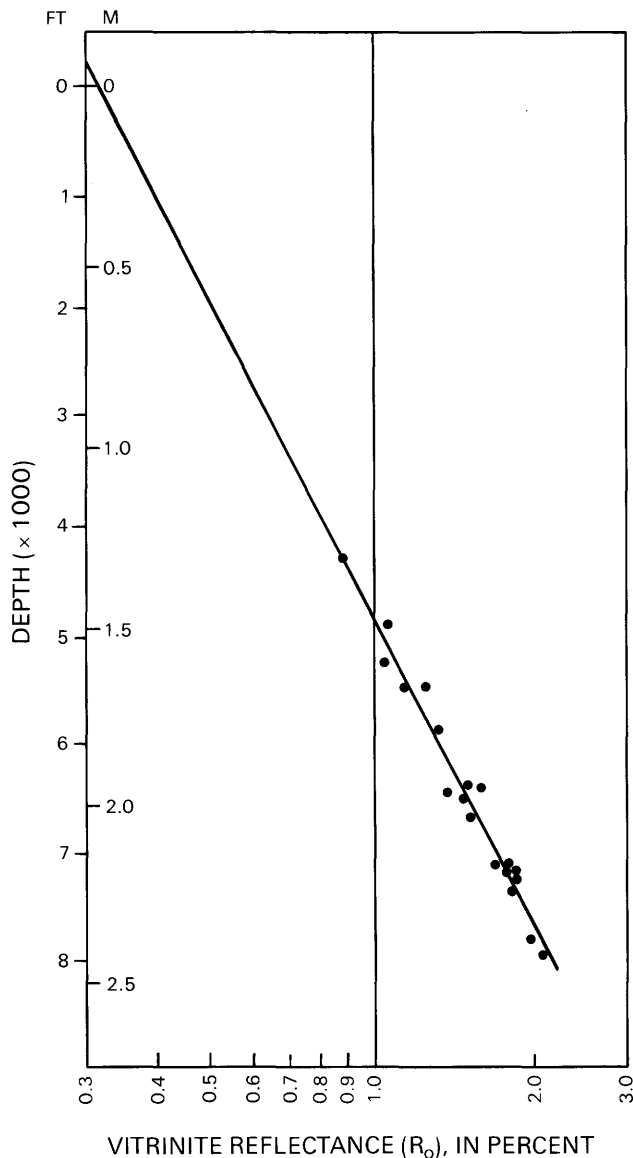


Figure 9. Vitrinite reflectance of kerogen extracts obtained from MWX wells. Modified from Bostick and Freeman (1984, fig. 3).

Based on maximum pressures at MWX and other sites, it would seem that gas (and oil) migration in many low-permeability reservoirs may be controlled by pressure-induced fractures in the sandstones and that the shales serve as confining seals and source beds. Fracture-gradient data obtained from measurement of instantaneous shut-in pressures in the MWX wells, compiled by Warpinski and others (1984) and Paul Branagan (written commun., 1985), are shown on the pore-pressure profile (fig. 5) and were used to measure minimum rock stress; that is, the approximate pressure at which a natural or artificial fluid-driven fracture will propagate. These data show that the fracture gradient is lowest in sandstone and high but variable in shale and mudstone.

The gradients were measured only in two coals, but both seem to be higher than most measured in sandstones. These data suggest that, if abnormal pressures can cause natural fractures, the limiting maximum pore pressure in a sandstone reservoir is controlled by the sandstone fracture gradient. It is also interpreted that pressure caused by hydrocarbon generation in coal, mudstone, and shale hydrocarbon-source beds is probably higher than that in adjacent sandstones. Therefore, source beds having a high fracture gradient can be pressurized by gas generation to a higher level than can adjacent sandstones. When the source bed-fracture gradient is exceeded, the pressure is probably rapidly released into the lower fracture gradient sandstone. This rapid release causes the sandstones to fracture and the gas and other fluids to migrate.

There are many calcite-cemented and open natural fractures in the MWX core. Pitman and Sprunt (1984) studied ¹³C and ¹⁸O stable isotopes of the cements and concluded that carbon becomes slightly heavier with depth but isotopically light oxygen remains relatively constant. According to them, the isotope trends may reflect fracture cementation at different times but under somewhat similar conditions of depth and temperature. This conclusion is consistent with the concept that some or many of the natural fractures were caused by overpressuring initiated by large volumes of gas (and some water) being generated in the source beds as the rocks were progressively heated (buried). Pitman and Dickinson (this volume) discuss isotopic compositions of calcite fracture-filling cements in closed hydrologic systems at Pinedale and MWX.

Fluid inclusions in the MWX calcite fracture-filling cements have been studied by C.E. Barker (oral commun., 1984). In this technique, rock thin sections are heated until the inclusion liquid expands and the associated gas bubble in the inclusion goes into solution. The temperature at which the gas completely dissolves is called the homogenization temperature and is inferred to be approximately the minimum temperature at which the cement, or mineral, was precipitated. All the inclusions in calcite-filled fractures from deep core samples from the MWX and Pinedale areas that Barker studied burst (decrepitated) or deformed prior to reaching the homogenization temperature. Barker concluded the gas had low solubility in the liquid and the internal pressure of the inclusion exceeded the strength of the crystal. He also concluded from crushing-stage studies that the inclusion gases are methane and that the calcite was precipitated from methane-saturated water under relatively high pressure and temperature. This last conclusion also somewhat supports the concept of fracture cementation from gas-saturated water at elevated temperature and pressure but does not necessarily prove the fractures were initiated by abnormal pressures.

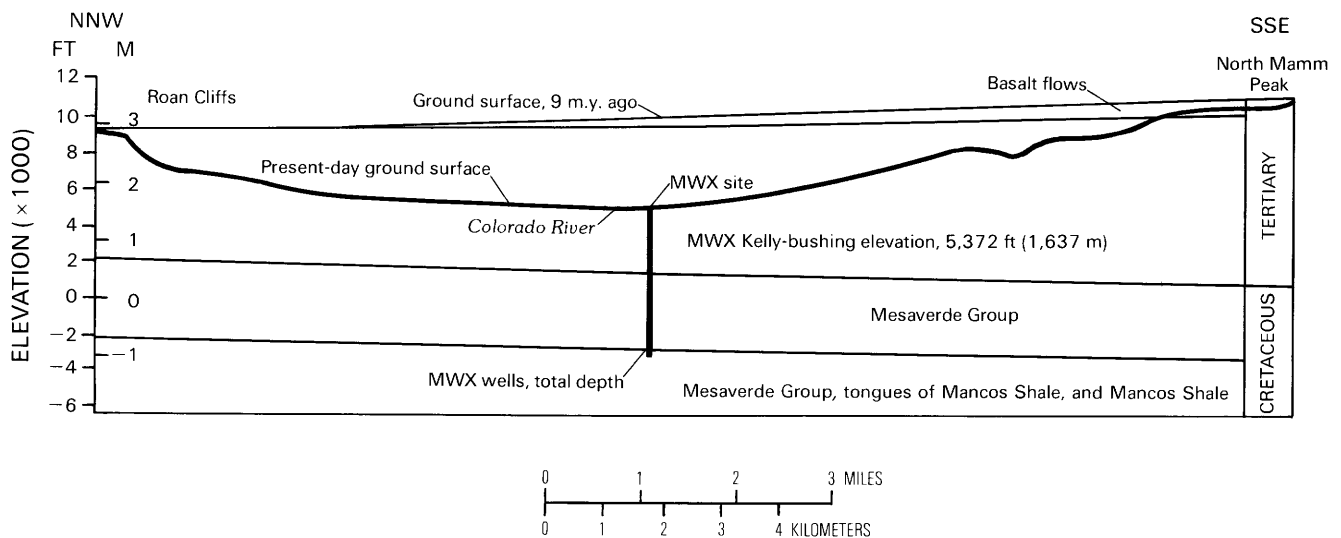


Figure 10. Profile through MWX area showing topographic relief in Colorado River valley. Modified from Bostick and Freeman (1984, fig. 4).

COMPARISON OF OVERPRESSURING IN THE PINEDALE AND MWX AREAS

As noted earlier, overpressuring in the Pinedale and MWX areas does not represent isolated occurrences but comprises better than normal data sites within regions of abnormally high pressure. Pressure gradients at the two locations can be compared by adjusting the gradients at both sites to the top of the 200 °F (93 °C) subsurface temperature points. In this manner, pressure gradient changes can be evaluated irrespective of *actual* reservoir pressure and differences in drill depths and temperature gradients (fig. 11). Both locations have an interpreted shallow zone of inactive or residual overpressure. This zone is about 2,400 ft (730 m) thick in the Wagon Wheel No. 1 well and about 1,400 ft (430 m) thick at the MWX site. Assuming the factors controlling overpressuring are correctly understood, then the relative thicknesses of the inactive zones are, in part, related to pressure loss owing to gas-phase migration and diffusion after gas generation ceased. Because the stratigraphy and reservoir character of both areas are similar, pressure loss should be greater at the site where the generation had ceased for the longest period of time, and indeed this seems to be the case. Rocks at the MWX site started cooling about 10 m.y. ago (Bostick and Freeman, 1984; Nuccio and Johnson 1984a), and the original top of high pressure is interpreted to have been as shallow as 4,000 ft (1,220 m) (Spencer, 1987). The pressure between 4,000 and 5,600 ft (1,220–1,707 m) in the MWX wells appears to have decayed to normal or subnormal pressures, and active pressure maintenance is interpreted to be occurring at and beneath the 200 °F (93 °C) present-day subsurface temperature level.

The extent to which the MWX inactive zone is being charged by vertical gas migration from the active zone is not known. It is not likely that this effect occurs for more than a few hundred feet above the active zone because of the extremely low permeability of the horizontally bedded sealing shales and mudstones. Most of the pressure probably is being lost by slow diffusion through shale beds and by lateral gas migration in the sandstone reservoirs, which, although very tight, have slightly better matrix and fracture permeability than the argillaceous seals.

The cooling event in the Pinedale area started more recently than that at the MWX site. On the basis of fission-track annealing studies, the rocks at the Wagon Wheel No. 1 started cooling only about 2–4 m.y. ago (Naeser, 1986), as compared with 10 m.y. ago for the MWX site. This more recent cooling seems to be a reasonable explanation for the somewhat thicker inactive zone in the Wagon Wheel No. 1 well, as compared with that in the MWX wells (fig. 11). The more recent cooling also helps explain why the maturation level (R_0 0.74 percent) equivalent to the onset of significant gas generation (Law, 1984a) is about at the top of the inactive zone in the Wagon Wheel well. Conversely, the 0.7- to 0.8-percent vitrinite reflectance levels in the MWX wells are well above the top of the inactive zone (fig. 11).

SUMMARY AND CONCLUSIONS

A comparison of overpressuring in the Pinedale and MWX areas shows many similarities in spite of some significant differences in depths to the top of the overpressuring zone, vitrinite reflectance levels, thermal and pressure gradients, thickness of the inactive zone, and

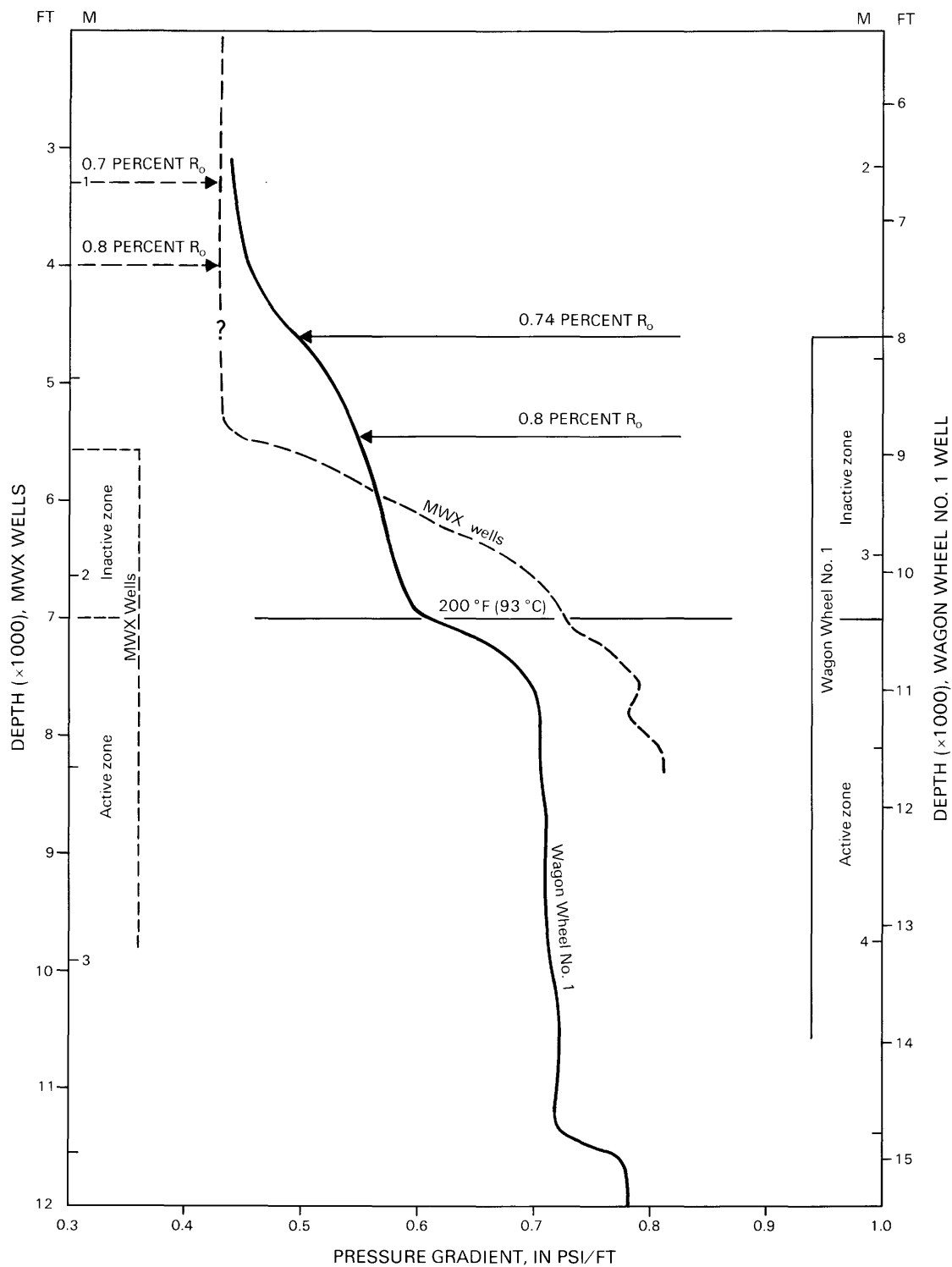


Figure 11. Pressure gradients in Pinedale and MWX areas. Gradients adjusted to common 200 °F (93 °C) subsurface temperature datum.

geologic time since the latest cooling of the rocks began. All these differences can be readily explained if the concepts of pressure-causing gas generation are recognized and accepted as a working model.

All the wells drilled on or near the Pinedale anticline encountered overpressured tight gas reservoirs to varying degrees. In the Wagon Wheel No. 1 well, the maximum reservoir pressure encountered (based on mud

weights) is about 14,800 psi (102 MPa) at 19,000 ft (5,791.2 m). This pressure is equal to a gradient of almost 0.8 psi/ft (18.1 kPa/m). Measured maximum gradients in the active gas generation zone at the MWX site are slightly higher than 0.8 psi/ft (18.1 kPa/m). These pressure gradients are about the same as those needed to artificially fracture tight sandstones in most Rocky Mountain Cretaceous-age rocks. No reliable fracture-gradient data exist for the Pinedale area, but much data exists for the MWX site (fig. 5). At MWX, fracture gradients in shale and mudstone are generally much higher than those in sandstone. Fracture-gradients in the sandstones most likely control the maximum amount of overpressuring and the high reservoir pressures probably cause some of the natural fractures.

Meissner (1978b) and Law and others (1980) proposed that hydrocarbons can be generated in low-permeability sequences at a rate more rapid than pressure loss until the fracture gradient of the rocks is exceeded, at which time the gas (or oil) migrates out of the reservoirs and thereby reduces the pressure. The pressure is reduced to the closure stress, the fractures close, and pressure build-up begins again.

Analyses of wells in the Pinedale area and the MWX site confirm the concepts of overpressuring caused by active gas generation developed by Law and others (1980) for similar tight gas reservoirs in the Pacific Creek area (fig. 1). Using these concepts, the depth to the top of the overpressured zone in tight gas reservoir sequences can be predicted, but the degree of overpressuring is less predictable. The information from these two areas also provides some measure of the rate of pressure decay (gas loss and gas shrinkage due to cooling) in tight rock sequences. In the Pinedale area, the originally, actively overpressured rocks have been cooling during the last 2 to 4 m.y. The rate of heat flow also may have decreased slightly because the top of the 200 °F (93 °C) active gas generation zone is now about 2,400 ft (730 m) below the 0.74-percent R_0 level at the top of the zone of inactive overpressuring. At the MWX site, erosion and cooling started about 9–10 m.y. ago, and the pressure has returned to normal or below normal through 1,600 ft (488 m) of strata interpreted to have been originally overpressured. The inactive zone at MWX is now about 1,400 ft (430 m) thick and the top of the zone or active gas generation is about 3,000 ft (915 m) below the interpreted top of the zone of active overpressuring at the time of maximum heating.

This research enables engineers and scientists to: (1) locate the main interval of gas saturation (almost all reservoirs in tight-gas overpressured sequences are gas saturated), (2) predict the approximate depth at which overpressuring will occur and thereby predict the depth at which intermediate casing should be set, (3) anticipate the maximum pressure that may be encountered during

drilling (maximum pressure is about equal to the fracture gradient of the sandstone reservoirs), and (4) provide a paleopressure model for paleohydrologic and other studies. Determination of high-pressure areas is important in petroleum exploration and resource assessment because the higher pressure provides more reservoir energy to produce hydrocarbons and because more gas can be stored in given gas-saturated pore volume at higher pressures.

At the MWX site, vitrinite reflectance levels of coaly organic matter appear to be slightly suppressed in the deep, highly overpressured parts of the wells. Although data are presently inconclusive, prolonged abnormally high gas pressure may have caused this apparent suppression of thermal maturation.

REFERENCES CITED

- Bostick, N.H., and Freeman, V.L., 1984, Tests of vitrinite reflectance and paleotemperature models at the Multiwell Experiment site, Piceance Creek basin, Colorado, *in* Spencer, C.W., and Keighin, C.W., eds., *Geologic studies in support of the U.S. Department of Energy Multiwell Experiment, Garfield County, Colorado*: U.S. Geological Survey Open-File Report 84-757, p. 110-120.
- Branagan, P., Cotner, G., and Lee, S.J., 1984, Interference testing of naturally fractured Cozzette Sandstone; a case study at the DOE MWX site: Society of Petroleum Engineers Unconventional Gas Recovery Symposium, Pittsburgh, Pa., 1984, Proceedings, p. 359-366.
- Branagan, P.T., Cipolla, C.L., Lee, S.J., and Wilmer, R.H., 1985, Comprehensive well testing and modeling of pre- and post-fracture well performance of the MWX lenticular tight gas sands: Society of Petroleum Engineers/U.S. Department of Energy Joint Symposium on Low Permeability Reservoirs, Denver, Colo., 1985, SPE/DOE Proceedings 13867, p. 191-202.
- Burst, J.F., 1969, Diagenesis of Gulf Coast clayey sediments and its possible relation to petroleum migration: *American Association of Petroleum Geologists Bulletin*, v. 53, no. 1, p. 73-93.
- Cecil, B.C., Stanton, R.W., and Robbins, E.I., 1977, Geologic factors controlling coalification and hydrocarbon maturation [abs.]: *American Association of Petroleum Geologists Bulletin*, v. 61, no. 5, p. 775.
- Chaney, P.E., 1949, Abnormal pressures, lost circulation; Gulf Coast's top drilling problem: *Oil and Gas Journal*, v. 47, no. 51, p. 210-215.
- Fertl, W.H., 1976, Abnormal formation pressure environments, *in* Fertl, F.H., ed., *Abnormal formation pressures; implications to exploration, drilling, and producing of oil and gas resources; Developments in petroleum science 2*: New York, Elsevier, p. 1-48.
- Harkins, K.L., and Baugher, J.W., 1969, Geological significance of abnormal formation pressures: *Journal of Petroleum Technology*, v. 21, p. 961-966.

- Hedberg, H.D., 1980, Methane generation and petroleum migration, *in* Roberts, W.H., III, and Cordell, R.J., eds., Problems of petroleum migration: American Association of Petroleum Geologists Studies in Geology 10, p. 179-206.
- Hutton, A.C., and Cook, A.C., 1980, Influence of alginite on the reflectance of vitrinite from Joadja, NSW, and some other coals and oil shales containing alginite: *Fuel*, v. 59, p. 711-714.
- Law, B.E., 1984a, Relationships of source-rock, thermal maturity, and overpressuring to gas generation and occurrence in low-permeability Upper Cretaceous and lower Tertiary rocks, Greater Green River basin, Wyoming, Colorado, and Utah, *in* Woodward, J., Meissner, F.F. and Clayton, J.L., eds., Hydrocarbon source rocks of the greater Rocky Mountain region: Rocky Mountain Association of Geologists Symposium, Denver, Colo., 1984, p. 469-490.
- _____.ed., 1984b, Geological characteristics of low-permeability Upper Cretaceous and Lower Tertiary rocks in the Pinedale anticline area, Sublette County, Wyoming: U.S. Geological Survey Open-File Report 84-753, 107 p.
- _____.1984c, Structure and stratigraphy of the Pinedale Anticline, Wyoming, *in* Law, B.E., ed., Geological characteristics of low-permeability Upper Cretaceous and lower Tertiary rocks in the Pinedale anticline area, Sublette County, Wyoming: U.S. Geological Survey Open-File Report 84-753, p. 6-15.
- Law, B.E., and Dickinson, W.W., 1985, Conceptual model for origin of abnormally pressured gas accumulations in low-permeability reservoirs: *American Association of Petroleum Geologists Bulletin*, v. 69, no. 8, p. 1295-1304.
- Law, B.E., Spencer, C.W., and Bostick, N.H., 1980, Evaluation of organic matter, subsurface temperature and pressure in low-permeability Upper Cretaceous and lower Tertiary sandstones in Pacific Creek area, Sublette and Sweetwater Counties, Wyoming: *The Mountain Geologist*, v. 17, no. 2, p. 23-35.
- Meissner, F.F., 1976, Abnormal electric resistivity and fluid pressure in Bakken Formation, Williston basin, and its relation to petroleum generation, migration and accumulation [abs.]: *American Association of Petroleum Geologists Bulletin*, v. 60, no. 8, p. 1403-1404.
- _____.1978a, Patterns of source-rock maturity in nonmarine source-rocks of some typical Western Interior basins: Rocky Mountain Association of Geologists Continuing Education Lecture Series, Chapter IX, p. 1-37.
- _____.1978b, Petroleum geology of the Bakken Formation, Williston basin, North Dakota and Montana: *Montana Geological Society Annual Conference*, 24th, 1978, p. 207-227.
- Naeser, N.D., 1986, Neogene thermal history of the northern Green River basin, Wyoming; evidence from fission-track dating, *in* Gautier, D.L., ed., Roles of organic matter in sediment diagenesis: *Society of Economic Paleontologists and Mineralogists Special Publication* 38, p. 65-72.
- Northrop, D.A., Sattler, A.R., Mann, R.L., and Frohne, K.H., 1984, Current status of the Multiwell Experiment: *Society of Petroleum Engineers Unconventional Gas Recovery Symposium*, Pittsburgh, Pa., 1984, SPE/DOE/GRI Proceedings 12868, p. 351-358.
- Nuccio, V.F., and Johnson, R.C., 1983, Preliminary thermal maturity map of the Cameo-Fairfield or equivalent coal zone through the Piceance Creek basin, Colorado: U.S. Geological Survey Miscellaneous Field Studies Map MF-1575, scale 1:253,440, 2 sheets.
- _____.1984a, Thermal maturation and burial history of the Upper Cretaceous Mesaverde Group, including the Multiwell Experiment (MWX), Piceance Creek basin, Colorado, *in* Spencer, C.W., and Keighin, C.W., eds., *Geologic studies in support of the U.S. Department of Energy Multiwell Experiment, Garfield County, Colorado*: U.S. Geological Survey Open-File Report 84-757, p. 102-109.
- _____.1984b, Retardation of vitrinite reflectance in Green River oil shales, Piceance Creek basin, northwestern Colorado [abs.]: *American Association of Petroleum Geologists Bulletin*, v. 68, no. 4, p. 513.
- Pitman, J.K., and Sprunt, E.S., 1984, Origin and occurrence of fracture-filling cements in the Upper Cretaceous Mesaverde Formation at MWX, Piceance Creek basin, Colorado, *in* Spencer, C.W. and Keighin, C.W., eds., *Geologic studies in support of the U.S. Department of Energy Multiwell Experiment, Garfield County, Colorado*: U.S. Geological Survey Open-File Report 84-757, p. 87-101.
- Powers, M.C., 1967, Fluid-release mechanisms in compacting marine mudrocks and their importance in oil exploration: *American Association of Petroleum Geologists Bulletin*, v. 51, no. 7, p. 1240-1254.
- Prensky, S.E., and Dickinson, W.W., 1986, Computer-generated well-log data plots assist in regional subsurface evaluation, northern Green River basin: *Geobyte*, v. 1, no. 2, p. 52-58.
- Rathbun, F.C., 1968, Abnormal pressures and conductivity anomaly northern Green River basin, Wyoming: *Society of Petroleum Engineers Annual Fall Meeting*, 43rd, Houston, Tex., 1968, SPE Paper 2205, p. 1-8.
- Rathbun, F.C., and Dickey, P., 1969, Abnormal pressures and conductivity anomaly, northern Green River basin, Wyoming: *The Log Analyst*, v. 10, no. 4, p. 3-8.
- Spencer, C.W., 1983, Overpressured reservoirs in Rocky Mountain region [abs.]: *American Association of Petroleum Geologists Bulletin*, v. 67, no. 8, p. 1356-1357.
- _____.1984a, Overpressured tight gas reservoirs in the Pinedale anticline area, Sublette, County, Wyoming, *in* Law, B.E., ed., Geological characteristics of low-permeability Upper Cretaceous and lower Tertiary rocks in the Pinedale anticline area, Sublette County, Wyoming: U.S. Geological Survey Open-File Report 84-753, p. 51-59.
- _____.1984b, Overview of U.S. Department of Energy Multiwell Experiment, Piceance Creek basin, Colorado, *in* Spencer, C.W. and Keighin, C.W., eds., *Geologic studies in support of the U.S. Department of Energy Multiwell Experiment, Garfield County, Colorado*: U.S. Geological Survey Open-File Report 84-757, p. 1-13.
- _____.1987, Hydrocarbon generation as a mechanism for overpressuring in the Rocky Mountain region: *American Association of Petroleum Geologists Bulletin*, v. 71, no. 4, p. 368-388.
- Spencer, C.W., and Keighin, C.W., eds., 1984, *Geologic studies in support of the U.S. Department of Energy Multiwell Experiment, Garfield County, Colorado*: U.S. Geological Survey Open-File Report 84-757, 134 p.

- Walker, A.L., McCulloch, T.H., Petersen, N.F., and Stewart, R.J., 1983, Discrepancies between anomalously low reflectance of vitrinite and other maturation indicators from an upper Miocene oil source rock, Los Angeles basin, California [abs.]: American Association of Petroleum Geologists Bulletin, v. 67, no. 3, p. 565.
- Warpinski, N.R., Branagan, P.T., Sattler, A.R., Lorenz, J.C., Northrop, D.A., Mann, R.L., and Frohne, K-H., 1985, Fracturing and testing case study of paludal, tight, lenticular gas sands: Society of Petroleum Engineers/ U.S. Department of Energy Symposium on Low Permeability Reservoirs, Denver, Colo., 1985, Proceedings, p. 267-278.
- Warpinski, N.R., Branagan, Paul, and Wilmer, R., 1984, In situ stress measurements at DOE's Multi-Well Experiment, *in* Frohne, K-H., ed., Western gas sands sub-program review, technical proceedings: U.S. Department of Energy, DOE/METC 84-3, p. 181-189.

Chapter D

Mineral Composition, Petrography, and Diagenetic Modifications of Lower Tertiary and Upper Cretaceous Sandstones and Shales, Northern Green River Basin, Wyoming

By RICHARD M. POLLASTRO

Prepared in cooperation with the U.S. Department of Energy

U.S. GEOLOGICAL SURVEY BULLETIN 1886

GEOLOGY OF TIGHT GAS RESERVOIRS IN THE PINEDALE ANTICLINE AREA, WYOMING,
AND AT THE MULTIWELL EXPERIMENT SITE, COLORADO

CONTENTS

Abstract	D1
Introduction	D1
Location and stratigraphy of wells	D2
Methodology	D3
Results	D4
Tertiary rocks	D6
Early Tertiary-Late Cretaceous interval	D7
Wagon Wheel No. 1 well	D7
New Fork wells	D22
Upper Cretaceous rocks	D22
General mineralogy and diagenetic overview	D22
Lance Formation	D24
Ericson Sandstone	D27
Rock Springs Formation	D28
Specific diagenetic phases and events	D32
Laumontite and associated framboidal pyrite and chlorite	D32
Interstratified chlorite/smectite (corrensite) in sandstone	D34
Alteration of feldspars to chert-chalcedony	D34
Summary	D35
References cited	D38

FIGURES

1. Map showing structural features of the northern Green River basin and location of wells used in study **D2**
- 2-6. Charts showing:
 2. Generalized stratigraphy in northern Green River basin **D3**
 3. General and unit- or depth-specific sequences of paragenesis for sandstones from El Paso Natural Gas Company Wagon Wheel No. 1 and American Hunter New Fork Nos. 1, 2, and 4 wells **D5**
 4. Paragenetic sequence for laumontite-bearing sandstones of Fort Union Formation in Wagon Wheel No. 1 well **D5**
 5. Paragenetic sequence for quartzarenites of Ericson Sandstone in Wagon Wheel No. 1 well **D6**
 6. General paragenetic sequence for Upper Cretaceous sandstones in WASP well **D6**
7. Thin section photomicrographs of sandstones of Fort Union Formation in Wagon Wheel No. 1 well **D16**
8. Scanning electron micrographs of clays in sandstones of Fort Union Formation from Wagon Wheel No. 1 well **D17**
- 9-11. Thin section photomicrographs of:
 9. Lower Tertiary sandstones from Wagon Wheel No. 1 well **D18**
 10. Lower Tertiary sandstones from Wagon Wheel No. 1 well **D19**
 11. Lower Tertiary sandstones, Wagon Wheel No. 1 and New Fork No. 1 wells **D20**

12. Scanning electron micrographs of authigenic clay minerals in sandstones **D21**
13. Thin section photomicrographs of sandstones **D23**
- 14-15. Thin section photomicrographs of sandstones:
 14. From the Rock Springs and Lance Formations, New Fork No. 2 and WASP wells **D25**
 15. Lance Formation and Ericson Sandstone, Wagon Wheel No. 1 and WASP wells **D26**
16. Graphs showing clay-mineral relationships between sandstones and shales from the Lance Formation, Wagon Wheel No. 1 well, as determined by X-ray powder diffraction **D27**
- 17-22. Thin section photomicrographs of:
 17. Quartzarenites from the Ericson Sandstone, Wagon Wheel No. 1 well **D29**
 18. Sandstones from the Ericson Sandstone and Rock Springs Formation, Wagon Wheel No. 1 and WASP wells **D30**
 19. Sandstones from the Rock Springs Formation, Wagon Wheel No. 1 well **D31**
 20. Sandstones from the Rock Springs Formation, WASP and Wagon Wheel No. 1 wells **D33**
 21. Relic feldspar grains in sandstones **D36**
 22. Feldspar grains being replaced by silica **D37**

TABLES

1. Location, and stratigraphic units cored from wells used in this study, northern Green River basin **D3**
- 2-4. Mineralogical data for samples from:
 2. El Paso Natural Gas Company Wagon Wheel No. 1 well **D8**
 3. Inexco A-1 WASP well **D12**
 4. American Hunter New Fork Nos. 1, 2, and 4 wells **D14**

Mineral Composition, Petrography, and Diagenetic Modifications of Lower Tertiary and Upper Cretaceous Sandstones and Shales, Northern Green River Basin, Wyoming

By Richard M. Pollastro

Abstract

Mineralogic and petrologic studies of lower Tertiary and Upper Cretaceous rocks of the northern Green River basin reveal several depositional and diagenetic relations. Although lower Tertiary sandstones are typically arkosic, average feldspar content decreases progressively with depth and most Upper Cretaceous sandstones contain little feldspar. Some original feldspar in both lower Tertiary and Upper Cretaceous sandstones has been dissolved or altered to calcite, silica, or kaolinite. Below depths of 16,000 ft (4,900 m), however, detrital feldspars are unaltered and feldspar content increases to as much as 15 weight percent of the rock.

Lower Tertiary and Upper Cretaceous shales from the study area typically are enriched in mixed-layer illite/smectite (I/S) and discrete illite; chlorite and kaolinite are much less abundant. Shales from the Ericson Sandstone, however, are enriched in kaolinite indicating a major change in detrital source material. Clay-mineral assemblages in sandstones above a depth of 16,000 ft (4,900 m) are typically kaolinite and chlorite rich. These clay minerals in sandstones are mostly coarser, authigenic, pore-lining or pore-filling cements. The absence of kaolinite below 16,000 ft suggests that the stability of kaolinite may be controlled by maximum burial conditions.

The conversion of smectite to illite is a major diagenetic reaction in both sandstones and shales. As precursor smectite-bearing clays (defined here as I/S) become more illitic with depth, illitic and sericitic overgrowths become more abundant on shale clasts, feldspar grains, and earlier I/S clay cements. Products of the smectite-to-illite reaction also contribute to the formation of other authigenic carbonate, clay-mineral, and silica phases.

Early stages of diagenesis in these sandstones commonly involve compaction and precipitation of pyrite and subsequent quartz overgrowths and (or) I/S cements. These earliest stages are commonly followed by cementation and replacement by iron-free and iron-bearing calcite cements; iron-bearing calcite commonly replaces iron-free calcite. Dolomite cements also increase in abundance in deeper samples. Dissolution of calcite cements produces much of the secondary intergranular porosity, and the dissolution of feldspars, chert, and shale clasts commonly produces significant intragranular porosity. In the case

of quartz-rich, quartz-cemented sandstones, relatively high intragranular (moldic) porosity is attained at depths greater than 13,000 ft (3,900 m), mostly from the dissolution of chert grains.

INTRODUCTION

The allogenic and authigenic mineral assemblages of sandstone and shale can help provide a physical, chemical, and petrologic history of both depositional and postdepositional (diagenetic) environments. Quantitative or semiquantitative analysis of these assemblages reveals important mineralogical differences, lithological relationships, and the intensity of a particular diagenetic stage. During the past two decades, the diagenesis of sandstone and shale has received considerable attention. Of particular interest are studies that relate the effects of diagenesis on both reservoir quality and the source-rock potential of organic-rich shale by evaluating organic-matter type, amount, and maturation (Scholle and Schluger, 1979; Longstaffe, 1981; McDonald and Surdam, 1984; Gautier, 1986). Combined studies of inorganic and organic diagenesis may also provide insight into the timing of generation and migration of hydrocarbons.

Studies of clay minerals are important to the understanding of inorganic diagenesis (Burst, 1969; Perry and Hower, 1970; Weaver and Beck, 1971; Hower and others, 1976; Weaver, 1979; Hower, 1981). For example, the conversion of smectite to illite (illitization of smectite) through a mixed-layer or interstratified illite/smectite (I/S) series (as defined by X-ray powder diffraction profiles) is considered the major clay-mineral reaction that occurs as sedimentary rocks are progressively buried. The maximum extent of this reaction can provide information on the chemical or thermal intensity of diagenesis, as well as on the chemical constituents that may be related to stages of dissolution and precipitation of various

minerals phases in sandstone, shale, and bentonite beds (Hower and others, 1976; Boles and Franks, 1979; Hoffman and Hower, 1979; Millikan and others, 1981; Altaner and others, 1984; Nadeau and others, 1984; Pollastro, 1985; Pollastro and Barker, 1986).

Recent stratigraphic, geochemical, mineralogic, and petrologic studies on the tight-gas sandstones, shales, and coals of the Green River basin of Wyoming (Law, 1979, 1984a, b; Dickinson, 1984, 1985, this volume; Keighin, 1984; Pollastro, 1985; Law and others, 1986; Naeser, 1986; Pollastro and Barker, 1986; Schuster, 1986; Law and Johnson, this volume), particularly in the area of the Pinedale anticline, provide much of the framework for large-scale basin analysis and petroleum geology. None of these studies, however, relate the clay mineralogy and bulk-rock mineralogy and petrology to regional diagenetic stages.

In this study, basic mineralogic relationships and spatial, textural, and morphologic observations are used to characterize the depositional and burial history of Upper Cretaceous and lower Tertiary sandstones and shales from the northern Green River basin. The interpretations of this study are limited to data obtained from five wells. Most of the data are from the El Paso Natural Gas

Company Wagon Wheel No. 1 well (Law, 1984a; Law and Johnson, this volume, fig. 1) and are used as a mineralogic and stratigraphic reference set. This report presents a comprehensive mineralogic analysis of both sandstones and shales and describes and interprets the stages of diagenesis in tight-gas sandstone reservoirs in the area. The distribution and processes that cause dissolution porosity in these rocks will be discussed in a later report.

Acknowledgments.—I thank Christopher J. Schenk and C. William Keighin for their critical reviews of the manuscript and helpful suggestions for improvement, the U.S. Department of Energy and B.E. Law for allowing the opportunity to work on the low-permeability sandstones of the Green River basin, and B.E. Law for his encouragement and support throughout the study.

LOCATION AND STRATIGRAPHY OF WELLS

Location information for the wells used in this study is shown in table 1, and well locations are shown in figure 1. As previously mentioned, most of the data in the study are from the El Paso Natural Gas Company Wagon Wheel

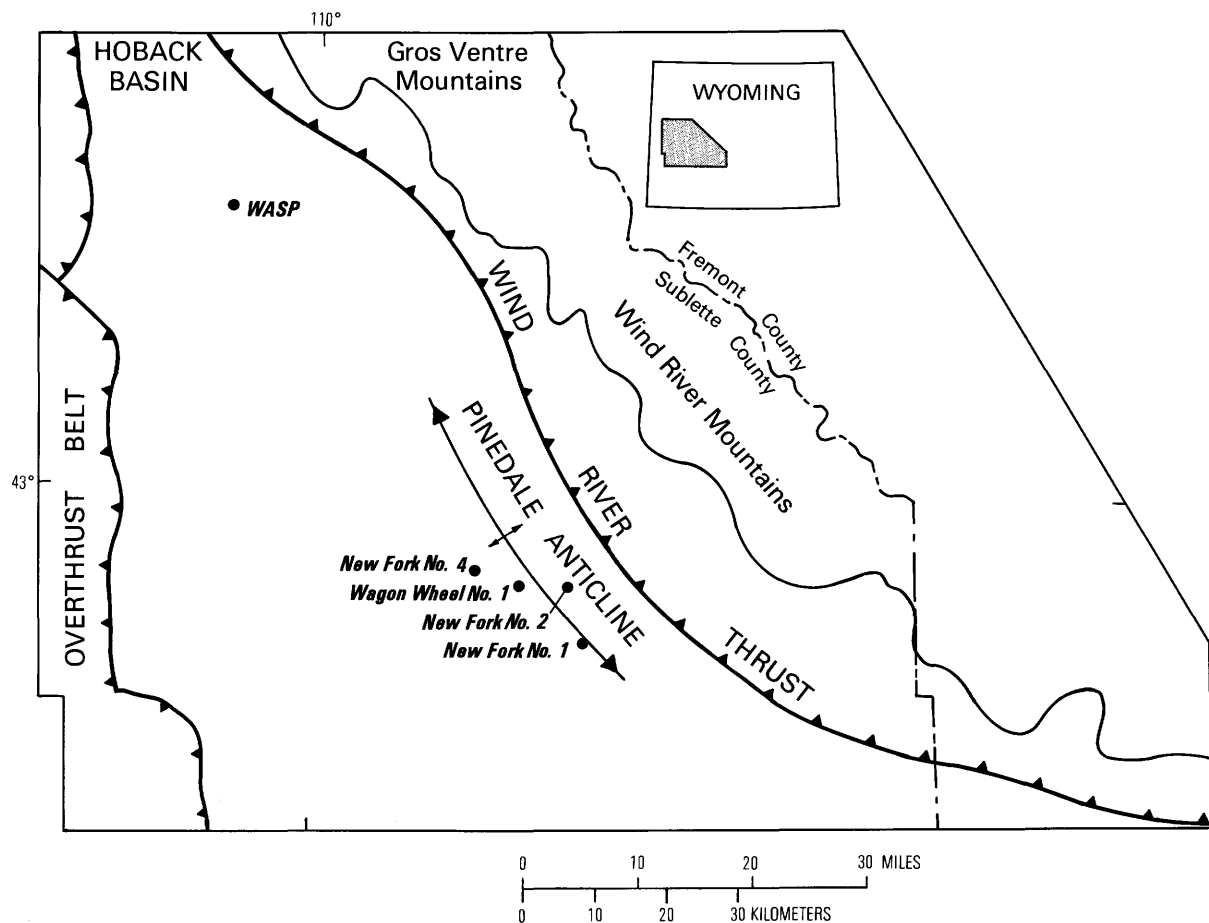


Figure 1. Structural features of the northern Green River basin and location of wells used in study. Location information for wells and stratigraphic units cored shown in table 1.

Table 1. Locations of wells and stratigraphic units cored from wells used in this study, northern Green River basin [Location of wells shown in figure 1]

Well	Location	Stratigraphic units cored
El Paso Natural Gas Wagon Wheel No. 1	Sec. 5, T. 30 N., R. 108 W.	Rock Springs, Ericson, Lance, unnamed Tertiary unit, Fort Union
Inexco A-1 WASP (Belco Petroleum 3-28 Merna)	Sec. 28, T. 36 N., R. 112 W.	Rock Springs, Ericson, Lance
American Hunter New Fork No. 1	Sec. 25, T. 30 N., R. 108 W.	Lance, unnamed Tertiary unit
American Hunter New Fork No. 2	Sec. 2, T. 30 N., R. 108 W.	Lance, unnamed Tertiary unit
American Hunter New Fork No. 4	Sec. 35, T. 31 N., R. 109 W.	Lance, unnamed Tertiary unit

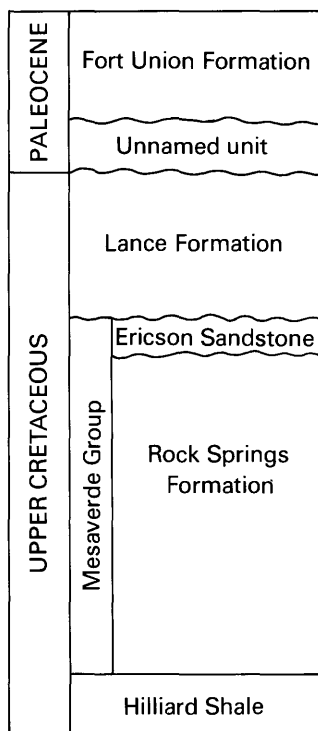


Figure 2. Generalized stratigraphy in the northern Green River basin. Modified from Law and others (1986).

No. 1 well. This well, on the crest of the Pinedale anticline, was originally planned for the nuclear stimulation of tight gas-bearing sandstones. Twelve sections of core, totaling about 900 ft (275 m), were taken at selected intervals at depths ranging from 5,000 to 18,000 ft (1,525–5,485 m) (Law and others, 1986), and for the present study approximately 180 sandstone and shale samples were analyzed. A total of 60 core samples from three American Hunter wells (designated New Fork Nos. 1, 2, and 4) drilled in the area of the Pinedale anticline were also studied. Approximately 90 sandstone and shale samples were analyzed from the Inexco A-1 WASP (Wyoming Atomic Stimulation Project) well. The WASP well, also planned for nuclear stimulation, is about 60 mi (97 km) northwest of the Wagon Wheel well. This well

was later drilled deeper and renamed the Belco Petroleum 3-28 Merna well.

The stratigraphy and structural evolution of the northern Green River basin has been described by Martin and Shaughnessy (1969), Shaughnessy and Butcher (1973, 1974), Law (1979, 1984a), Schuster and Steidtmann (1983), Schuster (1986), and Law and Johnson (this volume). A simplified stratigraphic section is shown in figure 2.

In the deepest part of the Greater Green River basin, sedimentary rocks ranging from Cambrian through Tertiary in age reach a maximum thickness of about 32,000 ft (9,750 m). In the wells studied, cores were taken from lower Tertiary and Upper Cretaceous, interbedded, discontinuous, low-permeability sandstone and shale between depths of 5,000 to 18,000 ft (1,500–5,500 m). Most of these rocks were deposited in nonmarine environments. The only exception is the lower 1,600 ft (490 m) of the Wagon Wheel well drilled in the marginal-marine lower part of the Rock Springs Formation. Upper Cretaceous rocks include the Rock Springs Formation, Ericson Sandstone, and Lance Formation. Tertiary rocks in ascending order include an unnamed unit and the Fort Union Formation. (See Law and Johnson, this volume, for stratigraphic nomenclature.) All of the above mentioned units were studied from the Wagon Wheel well; the WASP core was taken from the lowermost 1,200 ft (365 m) of the Lance Formation and from parts of the Ericson Sandstone and Rock Springs Formation. The three New Fork wells were cored from the lower Tertiary unnamed unit and from the upper part of the Lance Formation. Cores recovered from the New Fork Nos. 2 and 4 wells have been interpreted to contain the Cretaceous-Tertiary (K-T) unconformity (B.E. Law, oral communication, 1986).

METHODOLOGY

X-ray powder diffractometry (XRD) and acid-soluble carbonate analysis were performed on half of a 1-in.-diameter (2.5 cm) cored plug sampled from the original core of each well; the adjacent half of each plug was used for thin section preparation.

Samples were washed and scrubbed to remove surficial contaminants, dried, and then ground to <35 mesh. Each sample was split by using a Jones splitter into two portions, one for whole-rock XRD analysis and one for carbonate dissolution and clay-mineral analysis.

Carbonate was dissolved in 1N HCl and the residue filtered and washed with distilled water immediately after effervescence stopped in order to minimize solution of noncarbonate minerals (Pollastro, 1977). The insoluble residue was dried overnight at 65 °C. The weight percent of the residue was then determined. A small part of the residue was spot checked for undissolved carbonate with 6N HCl.

Qualitative and semiquantitative estimates of the minerals in whole rock were made through XRD analysis of randomly oriented powders that were ground to <44 μm (<325 mesh) and packed into the back of aluminum specimen holders. A fine texture was imparted onto the surface to be irradiated in an attempt to maximize random orientation of the grains (Schultz, 1978a). Semiquantitative estimates of the amount (in weight percent) of total phyllosilicates and individual minerals were calculated by comparison with several prepared mixtures of the same minerals having similar XRD characteristics and by the procedures outlined by Schultz (1964) and Hoffman (1976) with some modification. In order to check the carbonate results, the semiquantitative relative weight-percent values calculated for total carbonates by XRD were compared with those determined by chemical dissolution.

Oriented clay aggregates of the <2- and <0.25- μm (equivalent spherical diameter) fractions were prepared by using a modified filter-membrane-peel technique (Pollastro, 1982) similar to that described by Drever (1973). Semiquantitative XRD analysis of the clay-size fractions was made by using the method of Schultz (1964) with some modification (Pollastro, 1985).

Although I am aware that the interpretation of XRD patterns for I/S clay does not conform with the concept of interparticle diffraction (Nadeau and others, 1984), the currently accepted terminology for these interstratified clay minerals (as described by Reynolds, 1980) will be used for convenience. Composition and ordering of the I/S clay was determined on oriented, ethylene glycol-saturated specimens of both the <2- and <0.25- μm fractions by using the methods of Reynolds and Hower (1970) and Schultz (1978b). Ordering types were defined by using the "Reichweite" (R) notation (as described by Reynolds, 1980). Most diffractograms of naturally occurring I/S clay can be categorized into one of three ordering types (or any mixture of these types) of interstratification (Reynolds and Hower, 1970): (1) random I/S ($R=0$), (2) allevardite or short-range-ordered I/S ($R=1,2$), or (3) Kalkberg or long-range-ordered I/S ($R\geq 3$).

Thin section and scanning electron microscopy (SEM) analyses of sandstones were used as reconnaissance methods for qualitative and descriptive petrographic analysis and to identify general diagenetic and petrophysical relationships. Two matched thin sections were prepared from each sandstone plug. One was impregnated with blue epoxy to aid in recognizing porosity and stained with potassium ferrocyanide and alizarin red for the identification of carbonate phases following the procedure described by Dickson (1966). The other section was impregnated with clear epoxy and stained with potassium cobaltinitrite to distinguish between potassium and plagioclase feldspar. SEM samples of freshly fractured rock chips were air dusted, mounted on aluminum stubs, and sputter coated with $\approx 100 \text{ \AA}$ of gold/palladium.

RESULTS

Although the mineralogic composition of the sandstones and shales in this study is relatively simple, their diagenetic history is complex. Numerous diagenetic events have occurred since the deposition of many of these rocks, and their original compositions have been partly or extensively modified. Diagenetic events or stages identified in the sandstones of this study are not necessarily restricted to a particular lithologic unit. Original characteristics, such as feldspar content or the presence of ductile lithic grains and rock fragments, produce specific chemical or physical constraints that create an environment more or less susceptible to change during deep burial. Specific sedimentologic factors may also control or limit the degree and spatial extent of diagenesis. Moreover, it is important to note that the degree or extent of diagenesis may vary from one sandstone to another and over relatively short vertical distances.

Pollastro (1985) and Pollastro and Barker (1986) have outlined the diagenesis, nature, and significance of the smectite-to-illite reaction for both sandstone and shale in the Wagon Wheel well, and I will only discuss the smectite-to-illite reaction as it relates to petrographic textures or other diagenetic events. The diagenetic events and modifications identified in this study are summarized in figures 3–6. Similar diagenetic events have occurred in rocks from both the area of the Pinedale anticline and the WASP well. In general, however, equivalent rocks recovered from wells in the Pinedale area are at a more advanced stage of diagenesis—that is, thermally and compositionally more mature—than those from the area of the WASP well because those in the Pinedale section have been buried much deeper. These differences in thermal maturation and diagenetic extent are shown in mean random vitrinite reflectance values (Law, 1984), clay-mineral data, and interpretations of paragenesis from petrographic analysis.

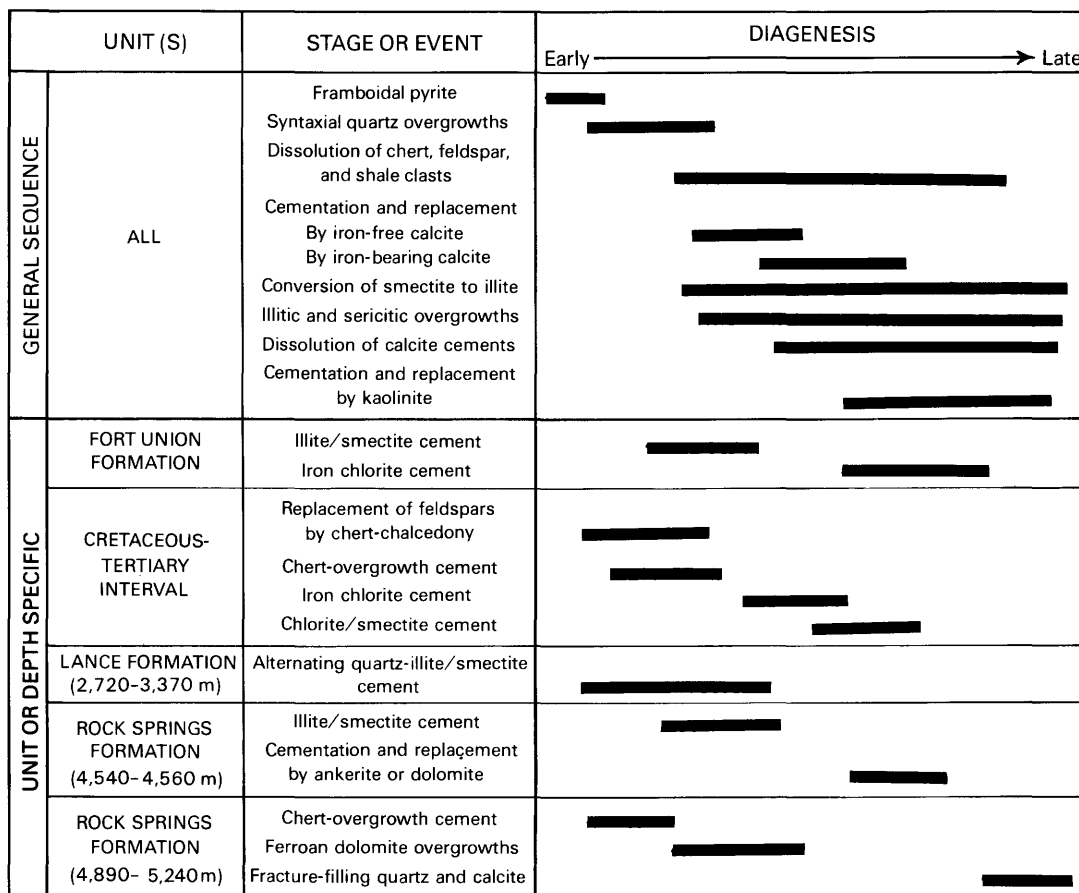


Figure 3. General and unit- or depth-specific sequences of paragenesis for sandstones from the El Paso Natural Gas Company Wagon Wheel No. 1 and American Hunter New Fork Nos. 1, 2, and 4 wells.

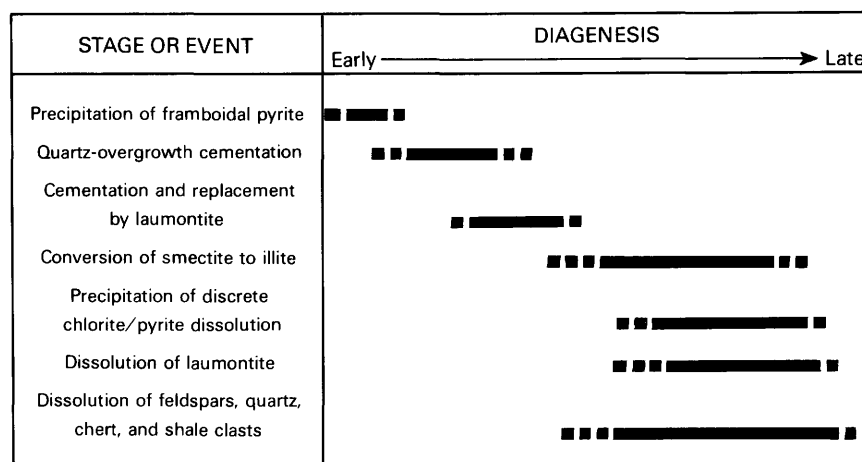


Figure 4. Paragenetic sequence for laumontite-bearing sandstones of the Fort Union Formation in the Wagon Wheel No. 1 well.

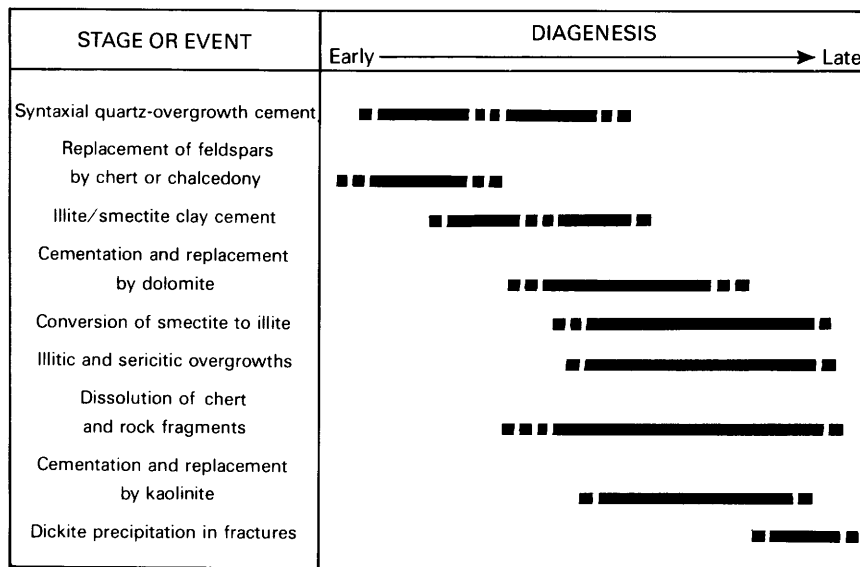


Figure 5. Paragenetic sequence for quartzarenites of the Ericson Sandstone in the Wagon Wheel No. 1 well.

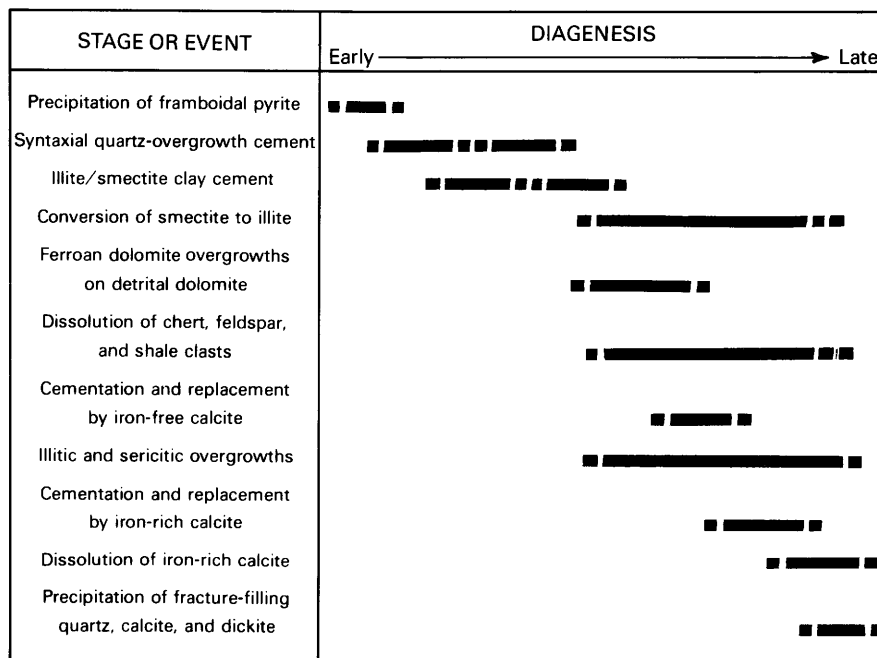


Figure 6. General paragenetic sequence for Upper Cretaceous sandstones in the WASP well.

Tertiary Rocks

Mineralogical data from XRD for each of the wells are shown in tables 2–4; paragenetic sequences for the Tertiary rocks are shown in figure 3. Tertiary rocks were cored from the Wagon Wheel and New Fork Nos. 1, 2, and 4 wells; however, only the lowermost Tertiary rocks are represented in the New Fork cores. In the Wagon

Wheel well, Tertiary sandstones are primarily feldspathic, many are conglomeratic, and most are classified as lithic arkoses. Sandstones of the Fort Union Formation (table 2) sampled from the Wagon Wheel well average about 50 weight percent feldspar and contain little or no carbonate; quartz content is about 25–30 weight percent. Biotite grains are abundant and glauconite is common. As a result of early compaction, poor sorting, and high

clay matrix content (fig. 7A), most of the sandstones from the Fort Union have little macroporosity.

The dominant clay minerals are randomly interstratified I/S ($R=0$) and discrete chlorite; little discrete illite or kaolinite was observed. Most of the discrete clay-size chlorite is iron rich, as interpreted by XRD characteristics (Pollastro, 1984). The chlorite has weak to absent odd-number basal reflections (001, 003, 005, and so forth) and very strong even-number basal reflections. The interbedded shales consist mostly of expandable I/S clay and contain less feldspar and clay-size chlorite than adjacent sandstones (table 2).

Diagenesis in sandstones of the Fort Union Formation involves early compaction of feldspathic sands having clay-rich matrices. Few remnants of calcite, either as cement or a replacement phase, were observed in thin section, and little or no calcite was detected by XRD (table 2). The little calcite that remains selectively and partially replaces feldspar or infills dissolution voids (fig. 7B). Dissolution of the clayey matrix produced intergranular porosity; some intragranular porosity was also created from the dissolution of shale clasts and framework feldspars (fig. 7B). Early cements also include smectite-rich I/S coatings on framework grains. I/S clay cement also drapes or bridges secondary pores (fig. 8A).

Feldspar grains commonly are altered and appear sericitized (fig. 7A). Closer examination of these feldspars using the SEM shows that they are being altered to a smectitic clay (figs. 8B, C). As discussed later, these clay-altered feldspar grains are more susceptible to dissolution and (or) sericitization (smectite to illite) with deeper burial because the early formed, smectitic clay crystals create nucleation sites for dissolution or illite growth.

About 10 ft (3 m) of the core from the Fort Union Formation in the Wagon Wheel well contains sandstones cemented by laumontite. The paragenetic sequence for these sandstones is summarized in figure 4. Although cementation by laumontite is interpreted to have occurred relatively early in the burial history of these sandstones, laumontite formation postdates compaction of ductile glauconite and brittle biotite grains and precipitation of syntaxial quartz overgrowth cement. Laumontite partly to almost completely replaces feldspars and etches, corrodes, and embays framework quartz grains, particularly in areas where cementation is extensive (fig. 7C). Later dissolution of laumontite cement creates extensive intergranular and intragranular secondary porosity (fig. 7D). Iron-rich chlorite replaces laumontite and lines secondary pores. The authigenic chlorite commonly coexists with framboidal pyrite (fig. 8D); however, chlorite probably formed much later.

Lower Tertiary unnamed sandstones from 7,040 to 7,140 ft (2,150–2,180 m) in the Wagon Wheel well contain shale clasts and grains of chert, biotite, and glauconite. Many of the sandstones from this interval are

cemented by calcite (fig. 9A). In contrast, sandstones containing little or no calcite have intergranular spaces filled with fine, clay-rich matrix (fig. 9B). Detrital carbonate grains are occasionally found in these sandstones; rarely, sandstones contain isolated rhombs of dolomite. Total feldspar content in this group of sandstones and shales is about 20–25 weight percent; potassium feldspar typically is more abundant than plagioclase, and quartz content is about 30–45 weight percent (table 2). Although the addition of carbonate to the bulk-rock analysis appears to dilute all other phases in these sandstones, there is a real decrease in the relative weight percent of feldspar and an increase in quartz content, as compared to sandstones above from the Fort Union Formation in the Wagon Wheel well. Dissolution and (or) replacement of feldspars by calcite, smectitic clay, or other phases account for some of the decrease in feldspar abundance (fig. 9B, C).

Early Tertiary–Late Cretaceous Interval

Law (1979) and Law and Nichols (1982) reported that the Cretaceous–Tertiary (K–T) unconformity is at a depth of about 7,520 ft (2,302 m) in the Wagon Wheel well. In the American Hunter New Fork wells, this unconformity is at depths of from 8,300 to 8,700 ft (2,530–2,650 m) (B.E. Law, oral communication, 1986). The bulk mineralogy of Tertiary sandstones from the New Fork wells is similar to that in the Wagon Wheel well. In general, the most significant difference in mineralogy from Tertiary rocks to Upper Cretaceous rocks is an increase in total feldspar content. This change in feldspar content occurs near, or coincident with, the K–T unconformity and can often be recognized on gamma-ray logs (Prensky, 1984; this volume); it is best shown in the XRD data from the Wagon Wheel well (table 2). The significance of this abrupt change in feldspar content is not well understood. The sudden increase in feldspar content may, however, reflect unroofing of Phanerozoic rocks of the Wind River Mountains and incipient deposition of arkosic debris from granitic crystalline Precambrian rocks in the core of the Wind River Mountains (Schuster and Steidtmann, 1983; Prensky, 1984, this volume; Schuster, 1986).

Wagon Wheel No. 1 Well

In the lowermost Tertiary sandstones in the Wagon wheel well, at depths from 7,340 to 7,400 ft (2,240–2,260 m), total feldspar content is less than 10 weight percent of the bulk rock, detrital dolomite is common, and kaolinite is abundant as an intergranular cement and replacement phase. The total quartz content of these sandstones, a significant portion of which is from chert

Table 2. Mineralogical data for samples from El Paso Natural Gas Company Wagon Wheel No. 1 well

[Analyzed using X-ray powder diffraction. Sample designation indicates depth from surface to sample; suffix refers to lithology: s, sandstone; shl, shale. All stratigraphic units are formations except Ericson Sandstone, and unnamed Tertiary unit. Data in relative weight percent. Sol Carb, soluble carbonate; Cal, calcite; Dol, dolomite; Carb, other carbonate minerals; Plag, plagioclase; K-spar, potassium feldspar, I/S, illite-smectite; Kaol, kaolinite; Chl, chlorite; C/S, chlorite-smectite; L, laumontite; A, ankerite; S, siderite; P, pyrite. tr, trace; leaders (--), none detected; nd, not determined]

Sample designation	Stratigraphic unit	Sol Carb	Whole rock							<2- μ m clay fraction					
			Clay	Quartz	Cal	Dol	Carb	Plag	K-spar	Other	Illite	I/S	Kaol	Chl	C/S
5001.0s	Fort Union	--	20	26	--	--	--	30	24	--	4	73	6	17	--
5020.5s	Fort Union	--	17	30	--	--	--	28	18	7-L	9	2	--	89	--
5028.2shl	Fort Union	--	55	20	--	--	--	13	12	--	11	74	--	15	--
5058.9s	Fort Union	--	18	31	--	--	--	31	20	--	3	58	--	39	--
5072.5shl	Fort Union	--	33	25	--	--	--	21	18	3-P	6	77	--	17	--
7046.3s	Tertiary	21	15	30	21	--	--	17	17	--	3	80	7	10	--
7048.5shl	Tertiary	--	55	25	--	--	--	7	13	3-P	9	54	--	37	--
7054.6s	Tertiary	--	35	31	--	--	--	13	21	--	12	61	--	27	--
7057.2s	Tertiary	tr	23	41	2	--	--	14	20	--	3	64	--	31	--
7061.4s	Tertiary	14	25	30	14	--	--	10	21	--					
7066.7s	Tertiary	4	25	35	4	--	--	19	17	--	3	25	11	14	47
7083.3shl	Tertiary	tr	43	33	2	--	--	7	15	--	18	46	13	23	--
7093.0s	Tertiary	18	21	36	18	--	--	10	15	--	8	28	14	21	29
7095.0shl	Tertiary	tr	50	25	2	--	--	9	14	--	33	34	--	--	33
7100.7s	Tertiary	--	33	40	--	--	--	8	19	--	5	23	--	--	72
7102.9s	Tertiary	12	34	30	9	3	--	9	15	--	5	18	5	18	27
7106.5s	Tertiary	43	19	19	43	--	--	6	13	--	18	50	19	13	--
7108.2s	Tertiary	--	38	40	--	--	--	3	19	--	8	34	34	24	--
7110.5s	Tertiary	--	35	38	--	--	--	7	20	--	2	20	11	30	37
7114.2s	Tertiary	10	18	37	10	--	--	16	19	--	2	20	11	30	37
7116.1shl	Tertiary	--	48	30	--	--	--	8	14	--	13	30	15	16	26
7120.4s	Tertiary	--	28	44	--	--	--	13	15	--	9	42	--	28	21
7125.0s	Tertiary	5	25	43	6	--	--	12	14	--	8	40	11	14	27
7129.6s	Tertiary	18	18	45	18	--	--	6	13	--	6	48	13	14	19
7130.2shl	Tertiary	8	54	24	8	--	--	5	11	--	27	53	4	9	7
7134.1shl	Tertiary	3	70	16	1	2	--	3	9	--	-15	56	13	16	--
7137.2shl	Tertiary	--	50	28	--	--	--	6	14	--	14	37	25	24	--
7340.6s	Tertiary	8	17	65	8	--	--	4	6	--	10	12	27	25	26
7343.6s	Tertiary	10	18	55	10	--	--	7	10	--	6	11	38	40	5
7350.0s	Tertiary	7	17	41	4	3	--	15	20	--	11	27	19	10	33
7355.0s	Tertiary	6	25	64	4	2	--	3	2	--	9	38	10	15	28
7358.8s	Tertiary	6	17	73	5	1	--	2	2	--	12	22	--	35	31
7366.3s	Tertiary	20	15	50	20	--	--	7	8	--	11	10	24	19	36
7375.8s	Tertiary	8	15	73	7	1	--	2	2	--	10	18	8	31	33
7378.5s	Tertiary	6	15	72	5	1	--	3	4	--	11	12	--	77	--
7382.8s	Tertiary	14	26	55	9	5	--	2	3	--	21	59	9	11	--
7384.0shl	Tertiary	12	58	28	7	5	--	--	2	--	33	51	9	7	--
7388.0shl	Tertiary	20	57	21	15	5	--	--	2	--	29	62	3	6	--
7392.2shl	Tertiary	15	44	39	11	4	--	--	2	--	22	64	6	8	--
7395.0shl	Tertiary	18	56	24	13	5	--	--	2	--	30	59	4	7	--
8030.1s	Lance	--	33	63	1	--	--	1	2	--	19	37	23	21	--
8037.0shl	Lance	16	52	31	10	6	--	--	1	--	23	61	9	7	--
8045.2s	Lance	--	30	68	1	--	--	1	--	--	19	22	20	40	--
8050.8s	Lance	--	24	72	1	--	--	3	--	--	23	41	23	13	--
8059.1s	Lance	2	27	70	3	--	--	--	--	--	19	29	26	26	--

Table 2. Continued

Sample designation	Stratigraphic unit	Sol Carb	Whole rock								<2- μ m clay fraction				
			Clay	Quartz	Cal	Dol	Carb	Plag	K-spar	Other	Illite	I/S	Kaol	Chl	C/S
8063.0s	Lance	--	31	67	--	--	--	2	--	--	43	30	14	13	--
8066.5s	Lance	14	36	47	9	5	--	2	1	--	23	56	11	10	--
8070.2s	Lance	10	40	47	6	4	--	1	2	--	28	54	8	8	--
8073.4shl	Lance	11	64	23	7	4	--	1	1	--	27	61	7	5	tr
8076.9s	Lance	19	18	62	17	2	--	1	--	--	13	51	24	12	tr
8084.6s	Lance	10	14	73	11	--	--	2	--	--	22	29	27	22	tr
8088.2s	Lance	9	15	74	9	--	--	1	1	--	22	34	29	15	--
8094.5s	Lance	9	20	69	9	--	--	2	--	--	33	24	22	21	tr
8100.1s	Lance	10	18	70	10	--	--	2	--	--	15	17	19	28	21
8107.3s	Lance	10	17	72	10	--	--	1	--	--	15	16	35	12	22
8113.2s	Lance	10	20	69	10	--	--	1	--	--	18	38	15	13	1
8117.0shl	Lance	3	56	38	3	--	--	2	--	--	28	50	16	6	--
8124.2s	Lance	20	15	63	19	1	--	1	1	--	15	21	32	16	16
8128.1s	Lance	19	14	65	19	--	--	2	--	--	19	21	48	18	tr
8131.6s	Lance	7	18	73	7	--	--	2	--	--	12	22	24	17	25
8134.3s	Lance	12	25	60	12	--	--	2	1	--	16	47	16	21	--
8135.8shl	Lance	12	44	42	10	2	--	1	1	--	17	64	13	6	--
8136.5shl	Lance	7	61	32	4	2	--	1	--	--	16	66	12	6	--
8920.5shl	Lance	6	49	38	3	3	--	5	2	--	46	47	--	7	--
8925.8s	Lance	4	25	66	3	1	--	4	1	--	25	23	--	52	--
8931.5s	Lance	10	30	56	6	4	--	4	--	--	28	56	4	12	--
8934.7s	Lance	22	16	59	21	2	--	2	--	--	23	45	25	7	--
8944.1s	Lance	12	12	73	10	2	--	2	1	--	25	42	19	14	--
8954.3s	Lance	9	15	75	7	2	--	1	--	--	26	46	14	14	--
8962.1s	Lance	12	14	71	9	3	--	3	--	--	22	40	16	22	--
8971.6s	Lance	8	25	65	6	2	--	2	--	--	12	61	12	12	--
8980.8s	Lance	8	16	74	3	5	--	2	--	--	29	56	8	11	--
8984.4shl	Lance	6	45	47	4	2	--	2	2	--	29	36	22	29	--
8988.8s	Lance	15	11	72	12	3	--	2	--	--	20	33	10	37	--
9001.3shl	Lance	5	68	26	2	2	--	1	1	--	41	52	3	4	--
10142.6s	Lance	7	27	60	6	4	--	3	--	--	33	28	14	25	--
10145.3shl	Lance	10	35	45	1	9	--	10	--	--	57	37	3	3	--
10153.4s	Lance	11	14	75	8	3	--	2	--	--	42	36	--	24	--
10163.8s	Lance	8	17	73	6	2	--	3	--	--	36	33	--	31	--
10171.2s	Lance	6	18	73	4	2	--	3	--	--	29	28	6	37	--
10173.5shl	Lance	6	52	38	2	4	--	3	--	--	52	34	6	8	--
10190.5s	Lance	6	14	78	3	3	--	2	--	--	26	24	--	50	--
10193.8s	Lance	--	70	28	--	--	--	2	--	--	60	35	--	5	--
10204.0shl	Lance	--	45	52	--	--	--	3	--	--	60	33	--	7	--
10212.2s	Lance	9	32	57	2	6	--	3	--	--	42	27	16	15	--
10217.6s	Lance	13	10	74	11	3	--	2	--	--	35	33	--	32	--
10235.0s	Lance	6	15	77	4	2	--	2	--	--	26	26	--	32	--
10245.0s	Lance	8	24	65	4	4	--	3	--	--	44	29	--	27	--
10252.3shl	Lance	9	50	38	2	7	--	3	--	--	63	30	1	6	--
10971.1s	Lance	16	25	57	10	6	--	2	--	--	35	35	15	15	--
10977.7s	Lance	17	13	65	15	2	--	2	3	--	36	35	7	22	--
10984.6s	Lance	6	18	74	4	2	--	2	--	--	32	31	--	37	--
10993.9s	Lance	2	10	85	2	1	--	2	--	--	23	21	8	48	--
10995.3shl	Lance	2	67	28	--	2	--	3	--	--	54	39	3	4	--
11003.8s	Lance	11	22	65	7	4	--	2	--	--	22	24	8	46	--

Table 2. Continued

Sample designation	Stratigraphic unit	Sol Carb	Whole rock								<2- μ m clay fraction				
			Clay	Quartz	Cal	Dol	Carb	Plag	K-spar	Other	Illite	I/S	Kaol	Chl	C/S
11007.8s	Lance	12	27	58	8	5	--	2	--	--	38	34	10	18	--
11017.3s	Lance	12	35	50	6	6	--	3	--	--	37	37	25	12	--
11018.2shl	Lance	8	53	40	1	3	--	3	--	--	55	33	2	10	--
11024.8shl	Lance	16	52	28	2	14	--	2	--	--	53	37	4	6	--
11027.8s	Lance	21	23	54	14	7	--	2	--	--	33	26	17	24	--
11032.6shl	Lance	--	58	40	--	--	--	2	--	--	50	41	2	7	--
11035.0s	Lance	10	24	60	4	6	--	4	--	--	27	23	19	31	--
11044.0s	Lance	9	15	75	3	5	--	2	--	--	27	14	13	46	--
11046.8shl	Lance	9	72	20	--	4	--	4	--	--	71	21	3	5	--
11051.3shl	Lance	7	65	25	--	7	--	3	--	--	57	33	5	5	--
11056.5s	Lance	9	10	79	6	3	--	2	--	--	45	23	12	20	--
11066.3shl	Lance	2	85	12	--	--	--	3	--	--	56	35	4	5	--
11068.1shl	Lance	18	46	35	10	8	--	1	--	--	50	31	5	14	--
13097.3shl	Ericson	--	66	34	--	--	--	--	--	--	19	32	35	14	--
13100.9s	Ericson	--	11	89	--	--	--	--	--	--	32	8	21	48	--
13104.1s	Ericson	--	7	93	--	--	--	--	--	--	56	6	15	23	--
13108.9s	Ericson	--	7	93	--	--	--	--	--	--	59	18	10	13	--
13114.5shl	Ericson	--	42	56	--	--	--	1	1	--	26	16	50	8	--
13119.0s	Ericson	--	10	90	--	--	--	--	--	--	22	21	30	27	--
13124.2s	Ericson	--	8	92	--	--	--	--	--	--	26	10	38	26	--
13129.0s	Ericson	--	11	89	--	--	--	--	--	--	30	10	30	30	--
13136.0s	Ericson	--	7	93	--	--	--	--	--	--	53	28	13	6	--
13141.4s	Ericson	--	10	90	--	--	--	--	--	--	29	33	14	14	--
13144.5s	Ericson	--	12	88	--	--	--	--	--	--	22	14	41	23	--
13150+-s	Ericson	--	8	92	--	--	--	--	--	--	66	11	11	12	--
13162.0s	Ericson	--	25	75	--	--	--	tr	--	--	61	10	11	18	--
13167.0s	Ericson	--	20	80	--	--	--	--	--	--	39	27	25	9	--
13170.0s	Ericson	--	30	70	--	--	--	tr	--	--	43	24	21	11	--
13176.0s	Ericson	--	25	73	--	--	--	2	--	--	30	21	32	17	--
13179.0s	Ericson	--	25	74	--	--	--	1	--	--	32	16	36	16	--
13184.0s	Ericson	--	25	75	tr	--	--	--	--	--	40	18	27	15	--
13190.0s	Ericson	nd	21	70	--	8	--	1	--	--	23	26	32	19	--
13197.0s	Ericson	nd	23	71	--	6	--	tr	--	--	30	26	28	16	--
13198.0shl	Ericson	--	53	47	--	--	--	--	--	--	42	33	20	5	--
14897.8shl	Rock Springs	28	46	24	11	17	--	2	--	--	64	29	4	3	--
14902.3shl	Rock Springs	nd	67	27	3	1	--	2	1	--	66	23	6	5	--
14906.2shl	Rock Springs	24	50	26	6	17	--	1	--	--	73	18	5	4	--
14914.1shl	Rock Springs	--	66	31	--	--	--	2	1	--	70	20	2	8	--
14918.4shl	Rock Springs	nd	54	27	2	20	--	2	--	--	54	33	4	9	--
14920.9s	Rock Springs	47	17	34	7	18	22-A	1	--	--	40	22	4	34	--
14923.8shl	Rock Springs	27	48	23	9	18	--	2	--	--	55	34	8	8	--
14927.0s	Rock Springs	28	25	46	9	19	--	1	--	--	40	25	32	3	--
14930.3shl	Rock Springs	--	66	32	--	--	--	2	--	--	51	32	10	7	--
14932.5shl	Rock Springs	nd	65	26	--	6	--	2	1	--	60	33	3	4	--
14939.5shl	Rock Springs	--	64	35	--	--	--	1	--	--	48	37	11	4	--
14942.5shl	Rock Springs	24	54	22	4	--	19-A	1	--	--	55	37	6	2	--
14946.1s	Rock Springs	24	34	41	4	20	--	1	--	--	55	39	14	2	--
14951.3s	Rock Springs	19	25	56	5	9	5-S	tr	--	--	79	17	2	2	--
16062.1shl	Rock Springs	25	25	45	8	17	--	4	1	--	47	31	--	22	--
16065.2s	Rock Springs	26	22	48	12	14	--	3	1	--	52	14	--	34	--

Table 2. Continued

Sample designation	Stratigraphic unit	Sol Carb	Whole rock								<2- μ m clay fraction				
			Clay	Quartz	Cal	Dol	Carb	Plag	K-spar	Other	Illite	I/S	Kaol	Chl	C/S
16068.5shl	Rock Springs	17	54	24	2	15	--	4	1	--	68	25	--	7	--
16072.5s	Rock Springs	17	23	51	7	10	--	7	2	--	56	16	--	29	--
16076.5s	Rock Springs	16	24	52	5	12	--	5	2	--	43	16	--	43	--
16078.8shl	Rock Springs	16	40	39	2	14	--	4	1	--	76	16	--	8	--
16083.6s	Rock Springs	13	21	61	2	11	--	4	1	--	45	14	--	41	--
16087.0s	Rock Springs	16	20	59	1	15	--	5	--	--	44	17	--	39	--
16094.8s	Rock Springs	15	27	50	5	10	--	4	4	--	52	21	--	27	--
16098.0s	Rock Springs	14	31	49	5	9	--	5	1	--	58	21	--	21	--
16101.9shl	Rock Springs	19	36	37	4	15	--	5	3	--	60	27	--	13	--
16104.5s	Rock Springs	26	26	40	10	16	--	4	4	--	56	15	--	29	--
16106.8s	Rock Springs	26	25	43	12	15	--	3	2	--	56	27	--	17	--
16110.0shl	Rock Springs	18	53	25	4	14	--	4	--	--	63	25	--	12	--
16112.1s	Rock Springs	23	20	51	10	13	--	4	2	--	48	17	--	35	--
16115.3shl	Rock Springs	nd	54	3	3	15	--	4	1	--	66	33	--	11	--
16116.6shl	Rock Springs	20	39	35	4	16	--	4	2	--	71	13	--	16	--
16117.8s	Rock Springs	23	25	46	3	20	--	4	2	--	70	10	--	20	--
16118.0s	Rock Springs	26	28	40	10	16	--	4	2	--	68	12	--	20	--
16168.8s	Rock Springs	27	15	48	13	15	--	8	1	--	74	15	--	11	--
17172.3shl	Rock Springs	21	44	27	5	17	--	6	1	--	76	16	--	8	--
17173.3s	Rock Springs	28	27	37	14	15	--	7	--	--	79	9	--	12	--
17176.1s	Rock Springs	21	20	47	8	14	--	8	3	--	70	24	--	6	--
17178.5s	Rock Springs	20	17	52	6	14	--	9	2	--	62	20	--	11	--
17183.2s	Rock Springs	15	21	53	2	14	--	8	2	--	64	16	--	20	--
17187.0shl	Rock Springs	18	60	22	--	14	--	4	--	--	74	17	--	9	--
17959.0s	Rock Springs	32	21	32	20	12	--	15	--	--	67	21	--	12	--
17960.0shl	Rock Springs	21	45	26	10	12	--	7	--	--	74	12	--	14	--
17965.0s	Rock Springs	28	29	34	12	16	--	6	3	--	72	17	--	11	11

Table 3. Mineralogical data for samples from Inexco A-1 WASP well

[Analyzed using X-ray powder diffraction. Sample designation indicates depth from surface to sample; suffix refers to lithology: s, sandstone; shl, shale. All stratigraphic units are formations except Hilliard Shale and unnamed Tertiary unit. Data in relative weight percent. Sol Carb, soluble carbonate; Cal, calcite; Dol, dolomite; Carb, other carbonate minerals; Plag, plagioclase; K-spar, potassium feldspar; I, illite; I/S, illite-smectite; Kaol, kaolinite; Chl, chlorite; A, ankerite. tr, trace; leaders (--), none detected; nd, not determined]

Sample designation	Stratigraphic unit	Sol		Whole rock						<2- μ m clay fraction				Percent illite in I/S
		Carb	Clay	Quartz	Cal	Dol	Carb	Plag	K-spar	Illite	I/S	Kaol	Chl	
10446.4shl	Lance	7	48	44	3	2	--	3	--	25	41	24	25	81
10462.5s	Lance	14	24	60	10	3	--	3	--	8	27	36	27	75
10509.2shl	Lance	14	53	31	6	6	--	4	--	33	55	7	5	80
10510.0s	Lance	23	27	52	12	5	--	4	--	12	49	25	12	75
10530.5s	Lance	tr	32	63	1	--	--	4	1	21	32	24	21	82
10541.3s	Lance	9	17	72	6	2	--	3	--	17	32	33	18	80
10576.5shl	Lance	19	60	23	10	6	--	1	--	nd	nd	nd	nd	nd
11339.6shl	Lance	--	72	25	--	1	--	2	--	31	60	5	4	80
11356.4s	Lance	1	34	61	1	--	--	3	1	20	49	20	11	79
11388.2s	Lance	--	41	57	tr	--	--	2	--	23	50	17	10	82
11445.4s	Lance	8	23	68	6	2	--	1	--	20	36	32	12	80
11488.1shl	Lance	12	55	30	6	4	2	2	1	31	55	7	7	80
11504.5s	Lance	--	21	72	5	1	--	1	--	31	37	5	27	75
11546.0s	Lance	32	18	52	23	6	--	1	tr	28	56	10	6	80
11629.0shl	Lance	--	74	25	--	--	--	1	--	46	47	3	4	80
11625.7s	Lance	10	33	55	6	3	--	3	--	15	39	30	18	80
11656.0shl	Lance	--	63	36	--	--	--	1	--	36	57	3	4	85
11678.0s	Ericson	10	70	20	7	1	--	1	--	14	43	29	14	80
11736.1s	Ericson	6	30	64	2	2	--	2	--	26	33	27	14	82
11759.0s	Ericson	14	16	70	11	2	--	1	--	22	31	29	18	80
11969.2s	Ericson	8	15	78	5	1	--	1	--	33	44	4	19	82
11989.4s	Ericson	6	24	70	4	2	--	tr	--	20	38	14	28	80
12042.0shl	Rock Springs	--	23	76	--	--	--	--	tr	38	51	6	5	80
12055.3s	Rock Springs	--	57	42	tr	tr	--	tr	--	32	40	16	12	80
12128.0s	Rock Springs	5	22	74	3	1	--	--	--	29	50	8	13	78
12147.1s	Rock Springs	5	35	60	3	2	--	--	--	27	45	16	12	78
12153.9s	Rock Springs	4	25	72	1	2	--	tr	tr	17	30	12	41	78
12220.0s	Rock Springs	8	20	73	7	tr	--	--	--	18	30	27	25	78
12274.8shl	Rock Springs	--	53	47	--	--	--	--	--	26	64	6	4	80
12296.2s	Rock Springs	6	18	76	3	2	1	--	--	19	18	52	18	78
12336.1s	Rock Springs	2	24	75	1	tr	--	--	--	21	23	16	40	78
12374.0shl	Rock Springs	--	68	30	--	--	--	1	1	28	56	9	7	80
12396.4s	Rock Springs	6	21	73	4	2	--	tr	--	16	22	21	41	82
12432.5shl	Rock Springs	10	64	28	2	3	3	tr	tr	31	46	13	10	80
12451.9s	Rock Springs	--	45	55	tr	--	--	tr	--	24	42	22	12	78
12494.9s	Rock Springs	--	17	82	tr	1	--	--	--	29	15	24	32	82
12531.2s	Rock Springs	--	29	69	tr	tr	--	tr	1	19	25	25	31	82
12542.0s	Rock Springs	1	28	71	1	--	--	tr	--	40	38	7	15	80
12552.0s	Rock Springs	--	34	66	--	--	--	tr	1	21	27	35	17	78
13002.3s	Rock Springs	3	43	54	--	2	1	tr	--	23	44	20	13	80
13003.4shl	Rock Springs	4	43	54	--	2	1	tr	--	25	51	14	10	82
13100.1s	Rock Springs	6	28	67	3	2	--	tr	--	26	42	18	14	80
13128.1shl	Rock Springs	--	55	43	--	--	--	1	1	40	30	22	8	82
13127.4s	Rock Springs	--	18	82	--	--	--	--	--	29	36	16	19	82
13181.2s	Rock Springs	--	14	86	--	--	--	--	--	nd	nd	nd	nd	nd

Table 3. Continued

Sample designation	Stratigraphic unit	Sol Carb	Whole rock							<2- μ m clay fraction				Percent illite in I/S
			Clay	Quartz	Cal	Dol	Carb	Plag	K-spar	Illite	I/S	Kaol	Chl	
13199.0shl	Rock Springs	5	63	32	--	2	1	1	1	41	47	4	8	82
13224.8s	Rock Springs	--	30	70	--	--	--	tr	--	43	47	20	10	85
13251.6shl	Rock Springs	--	32	66	1	--	--	1	--	35	22	34	9	82
13264.0s	Rock Springs	--	26	74	tr	tr	--	tr	tr	13	9	6	72	82
13306.5s	Rock Springs	--	26	74	--	--	--	tr	--	17	5	--	78	nd
13311.6shl	Rock Springs	--	45	54	tr	tr	--	1	tr	25	56	12	7	87
13364.6s	Rock Springs	3	34	64	2	--	--	--	tr	35	23	24	18	85
13366.1shl	Rock Springs	18	46	37	1	15	--	1	--	35	44	12	9	80
13391.9s	Rock Springs	22	25	55	6	12	2	tr	tr	36	14	37	13	87
13396.0s	Rock Springs	18	18	67	7	5	3	tr	tr	35	13	35	17	80
13415.8shl	Rock Springs	9	62	28	2	4	3	1	tr	47	41	5	7	80
13473.2s	Rock Springs	23	29	50	6	15	--	tr	tr	32	27	32	9	82
13475.5shl	Rock Springs	--	46	54	--	--	--	--	tr	27	47	15	11	nd
13506.2s	Rock Springs	--	31	68	--	--	--	tr	--	52	29	8	11	85
13533.4s	Rock Springs	11	24	65	8	3	--	tr	tr	51	27	--	22	85
13542.3shl	Rock Springs	23	49	34	6	10	--	1	tr	53	27	--	20	82
13579.5s	Rock Springs	7	25	68	2	5	--	tr	tr	29	44	3	24	85
13670.3shl	Rock Springs	21	60	26	3	7	4	tr	--	56	32	--	12	85
13684.3s	Rock Springs	10	22	68	6	4	--	tr	--	34	39	12	15	80
13731.5s	Rock Springs	10	26	64	4	5	--	tr	tr	37	30	--	33	78
13737.9shl	Rock Springs	7	33	61	2	3	--	tr	--	30	47	5	18	80
13811.1s	Rock Springs	1	43	57	tr	--	--	tr	tr	46	37	9	8	80
13866.0s	Rock Springs	23	27	53	9	8	3	tr	--	31	45	18	6	82
13881.6s	Rock Springs	15	18	70	8	6	--	tr	tr	29	43	12	16	80
13884.2shl	Rock Springs	16	60	24	4	11	1	--	--	46	42	4	8	82
13924.0shl	Rock Springs	--	61	37	tr	--	--	1	1	48	39	5	8	80
13941.8s	Rock Springs	--	67	33	--	--	--	tr	tr	20	51	22	7	82
13952.9shl	Rock Springs	19	61	21	5	7	6-A	tr	tr	46	42	4	8	85
13969.0s	Rock Springs	12	21	70	--	7	2	--	tr	40	37	5	18	78
13987.0s	Rock Springs	18	20	62	11	5	2	tr	--	30	39	6	25	80
14020.6shl	Rock Springs	9	61	29	--	9	--	1	--	46	44	4	6	78
14026.7s	Rock Springs	23	29	50	6	13	--	1	1	32	46	16	6	80
14043.2s	Rock Springs	21	25	53	15	5	5	tr	--	37	51	--	12	75
14091.5s	Rock Springs	18	20	62	7	9	2	--	--	31	30	6	33	78
14104.5shl	Rock Springs	7	53	40	--	6	--	tr	--	39	40	7	4	82
14110.4s	Rock Springs	2	33	65	1	--	--	1	--	33	32	--	35	82
14121.6s	Rock Springs	5	34	62	tr	3	1	tr	tr	35	40	11	14	82
14131.6s	Rock Springs	9	25	68	5	2	--	tr	--	26	56	--	18	80
14159.2s	Rock Springs	31	20	50	13	17	--	tr	tr	33	36	25	6	82
14198.0s	Rock Springs	13	21	68	6	5	tr	tr	tr	36	51	10	3	80
14241.9s	Rock Springs	20	29	53	7	9	2	--	--	39	44	14	3	75
14286.0shl	Rock Springs	22	48	32	4	15	--	1	--	47	40	6	7	80
14327.2s	Rock Springs	28	38	36	13	13	--	tr	tr	39	45	10	6	80
14341.6shl	Rock Springs	--	52	46	tr	tr	--	1	1	36	56	4	4	nd
14352.2s	Rock Springs	18	32	52	7	9	--	--	--	34	44	17	5	78
14358.7s	Rock Springs	25	35	42	8	15	1	--	--	40	32	22	6	80

Table 4. Mineralogical data for samples from American Hunter New Fork Nos. 1, 2, and 4 wells

[Analyzed using X-ray powder diffraction. Sample designation indicates well number and depth from surface to sample; suffix refers to lithology: s, sandstone; shl, shale. All stratigraphic units are formations except for unnamed Tertiary unit. Data in relative weight percent. Sol Carb, soluble carbonate; Cal, calcite; Dol, dolomite; Carb, other carbonate minerals; Plag, plagioclase; K-spar, potassium feldspar, I/S, illite-smectite; Kaol, kaolinite; Chl, chlorite; C/S, chlorite-smectite; P, pyrite. tr, trace; leaders (--), none detected]

Sample designation	Stratigraphic unit	Sol Carb	Whole rock								<2- μ m clay fraction				
			Clay	Quartz	Cal	Dol	Carb	Plag	K-spar	Other	Illite	I/S	Kaol	Chl	C/S
1-7951.4s	Tertiary	20	13	63	12	6	--	3	3	--	23	21	39	17	--
1-7953.2s	Tertiary	15	11	65	11	7	--	3	3	--	7	32	30	30	--
1-7961.2s	Tertiary	12	39	49	6	4	--	tr	2	--	26	60	9	5	--
1-7965.1s	Tertiary	18	19	61	16	2	--	1	1	--	12	45	29	14	--
1-7969.8s	Tertiary	15	18	47	8	6	--	11	18	--	10	28	45	17	--
1-7975.2s	Tertiary	8	13	67	6	5	--	3	6	--	20	30	28	22	--
1-8150.0s	Tertiary	12	21	60	7	5	--	2	5	--	8	32	48	12	--
1-8152.5s	Tertiary	14	18	41	9	8	--	8	16	--	13	11	65	12	--
1-8460.7s	Lance	8	16	74	8	2	--	tr	--	--	11	27	45	17	--
1-8486.6s	Lance	11	18	72	6	4	--	tr	--	--	17	29	38	16	--
2-8451.3s	Tertiary	13	18	30	20	5	--	11	16	--	12	38	43	7	--
2-8439.5s	Tertiary	7	14	40	8	1	--	22	15	--	14	32	32	22	--
2-8461.4s	Tertiary	2	16	47	3	1	--	18	15	--	13	39	19	29	--
2-8706.3s	Tertiary	14	17	65	3	11	--	1	3	--	35	36	17	12	--
2-8710.0s	Tertiary	32	10	45	22	10	--	7	6	--	15	9	--	75	--
2-8713.9s	Lance	11	19	68	8	2	--	3	--	--	14	41	27	19	--
2-8715.5s	Lance	13	24	60	8	5	--	2	1	--	16	31	20	32	--
2-8752.3s	Lance	26	31	38	7	17	--	1	6	--	35	42	11	12	--
2-9204.5s	Lance	20	12	67	18	2	--	1	--	--	12	27	44	17	--
2-9217.5s	Lance	16	25	59	9	6	--	1	--	--	13	53	20	14	--
2-9238.3s	Lance	20	12	67	19	2	--	tr	--	--	9	24	48	19	--
4-8260.0s	Tertiary	21	14	63	21	--	--	2	--	--	7	30	27	10	26
4-8263.8s	Tertiary	13	24	38	14	1	--	9	14	--	3	34	23	3	28
4-8269.0s	Tertiary	8	17	55	12	--	--	12	4	--	3	5	62	11	19
4-8271.0s	Lance	6	31	61	7	--	--	2	--	--	--	--	4	96	--
4-8271.1s	Lance	12	26	54	12	--	--	8	--	--	--	--	--	100	--
4-8274.0shl	Lance	8	53	36	7	3	--	--	1	--	24	65	7	4	--
4-8274.1shl	Lance	11	59	28	7	3	--	1	2	--	16	72	8	4	--
4-8280.0shl	Lance	10	65	25	7	2	--	tr	tr	--	25	63	7	5	--
4-8281.0shl	Lance	tr	67	31	1	--	--	tr	1	--	35	51	8	6	--
4-8287.0s	Lance	2	28	68	3	--	--	--	1	--	13	22	18	46	--
4-8288.3shl	Lance	--	49	47	--	--	--	2	2	--	26	42	21	10	--
4-8290.0shl	Lance	1	65	31	2	1	--	--	1	--	26	54	12	7	--
4-8292.0shl	Lance	--	65	35	--	--	--	--	--	--	44	43	10	4	--
4-8510.0s	Lance	10	16	73	11	--	--	tr	--	--	20	22	44	13	--
4-8516.0s	Lance	16	27	51	16	--	--	4	--	2	15	19	45	22	--
4-8517.0s	Lance	19	26	55	16	2	--	1	--	--	18	17	--	65	--
4-8520.0shl	Lance	12	57	35	4	3	--	--	1	--	35	48	11	6	--
4-8526.0shl	Lance	tr	79	20	--	tr	--	tr	1	--	35	45	11	9	--
4-8534.0shl	Lance	--	57	40	--	--	--	--	tr	--	31	42	17	10	--
4-8535.0shl	Lance	--	72	25	--	--	--	--	--	2-P	37	50	9	4	--
4-10272.2s	Lance	8	24	66	6	2	--	2	--	--	15	46	26	14	--
4-10280.0shl	Lance	6	58	35	1	3	--	2	1	tr-P	40	43	11	6	--
4-10282.2s	Lance	18	17	64	15	2	--	2	--	--	22	37	28	13	--
4-10287.5s	Lance	6	27	65	4	2	--	2	--	--	20	28	21	32	--

Table 4. Continued

Sample designation	Stratigraphic unit	Sol Carb	Whole rock								<2- μ m clay fraction				
			Clay	Quartz	Cal	Dol	Carb	Plag	K-spar	Other	Illite	I/S	Kaol	Chl	C/S
4-10291.0s	Lance	7	17	75	6	1	--	1	--	--	19	47	17	17	--
4-10302.0shl	Lance	13	72	20	6	2	--	tr	--	--	48	39	6	7	--
4-10310.3s	Lance	10	28	59	7	3	--	3	--	--	20	52	11	17	--
4-10315.8s	Lance	7	23	67	6	1	--	3	tr	--	15	55	10	20	--
4-10316.0shl	Lance	--	59	39	--	--	--	2	--	--	48	42	5	4	--
4-10329.0s	Lance	5	38	56	2	2	--	2	tr	--	38	40	13	8	--
4-10523.3s	Lance	7	26	64	7	2	--	1	tr	--	25	34	--	40	--
4-10524.3s	Lance	9	14	76	8	1	--	1	tr	--	22	35	13	30	--
4-10524.4s	Lance	8	25	70	6	1	--	1	--	--	24	34	--	42	--
4-10543.0s	Lance	11	28	59	9	2	--	2	--	--	22	61	9	7	--
4-10556.4s	Lance	6	17	74	6	1	--	2	--	--	32	37	16	15	--
4-10565.4s	Lance	9	23	67	4	2	--	2	--	--	19	53	5	23	--
4-10567.0s	Lance	3	29	67	3	tr	--	1	--	--	27	31	--	42	--

grains, is 55–75 weight percent. The shales from this interval in the Wagon Wheel well are more illitic than those higher in the section (table 2). I/S and discrete illite comprise about 80–90 relative weight percent of the clay minerals in the <2- μ m fraction.

Many of the samples from the unnamed Tertiary unit and the uppermost part of the Lance Formation exhibit extensive diagenetic modification. Similar types and degrees of diagenesis can be correlated with equivalent units and depths in the New Fork wells of the Pinedale area. The particular intensity of diagenesis in this interval is defined by extensive physical and chemical modifications in sandstone samples from core recovered at depths beginning about 7,340 ft (2,240 m) in the Wagon Wheel well. Lower Tertiary unnamed sandstones cored from the interval above, at 7,040–7,140 ft (2,150–2,180 m) exhibit much less diagenetic change than sandstones below 7,340 ft.

Thin section and SEM analysis of core samples 7,343.6 and 8,084.6 from the Wagon Wheel well core (table 2) illustrate the maximum extent of diagenesis across the K–T interval in the Pinedale area. These diagenetic events are diagrammed in figure 3. Early compaction produced deformation fabrics, including squashing of ductile pelitic grains and rock fragments and the fracturing, crushing, and interpenetration of brittle framework grains (fig. 9D). Well-developed syntaxial overgrowths on quartz framework grains formed prior to other diagenetic stages. Chert overgrowth cement was observed on a few grains (fig. 10A). Schuster (1986) reported that chert cement is ubiquitous in lower Tertiary sandstones of the Pinedale anticline, but in this study chert cement was rare and limited in extent when present. Kaolinite cement replacing calcite was found to be ubiquitous, however, and, because of its microcrystalline texture and low birefringence in thin section, it can easily

be mistaken for chert or other forms of microcrystalline quartz (figs. 10B, C), particularly if SEM analysis of the samples is not performed.

Chloritic clay cements commonly form rims around framework quartz and most syntaxial quartz overgrowths (fig. 10D). The precipitation of discrete chlorite cement is interpreted as the next stage in the paragenetic sequence. Although much of this discrete chlorite cement coexists with mixed-layer chlorite/smectite (C/S), the C/S is interpreted to have formed later, as discussed later.

Precipitation of discrete chlorite clay was followed by cementation of sandstone by iron-free calcite. Calcite also partly replaced feldspars, chert, and shale fragments (fig. 9D). Iron-free calcite was later dissolved and (or) replaced by iron-bearing calcite cement; the iron content of these cements, as revealed by staining, increases with depth into sandstones of the Lance Formation (fig. 11A).

The later dissolution of calcite created extensive intergranular and intragranular secondary porosity. Feldspars, chert, and shale and carbonate fragments were also extensively dissolved (fig. 11B). Replacement of much of the intergranular calcite cement by kaolinite resulted in a complex network of microporosity (fig. 11B). Precipitation of C/S (mainly corrensite) was contemporaneous with formation and dissolution of iron-bearing calcite. C/S is a cement in many of the sandstones in the interval between 7,060 and 8,130 ft (2,150–2,480 m) (Pollastro and Barker, 1986). Although the C/S coexists with late authigenic quartz overgrowths, it postdates most authigenic quartz because the clay commonly drapes quartz crystals or etches quartz overgrowths (fig. 12A). In some cases, however, quartz crystal growth probably was inhibited by the presence of C/S clay; therefore, multiple stages of quartz precipitation were also likely.

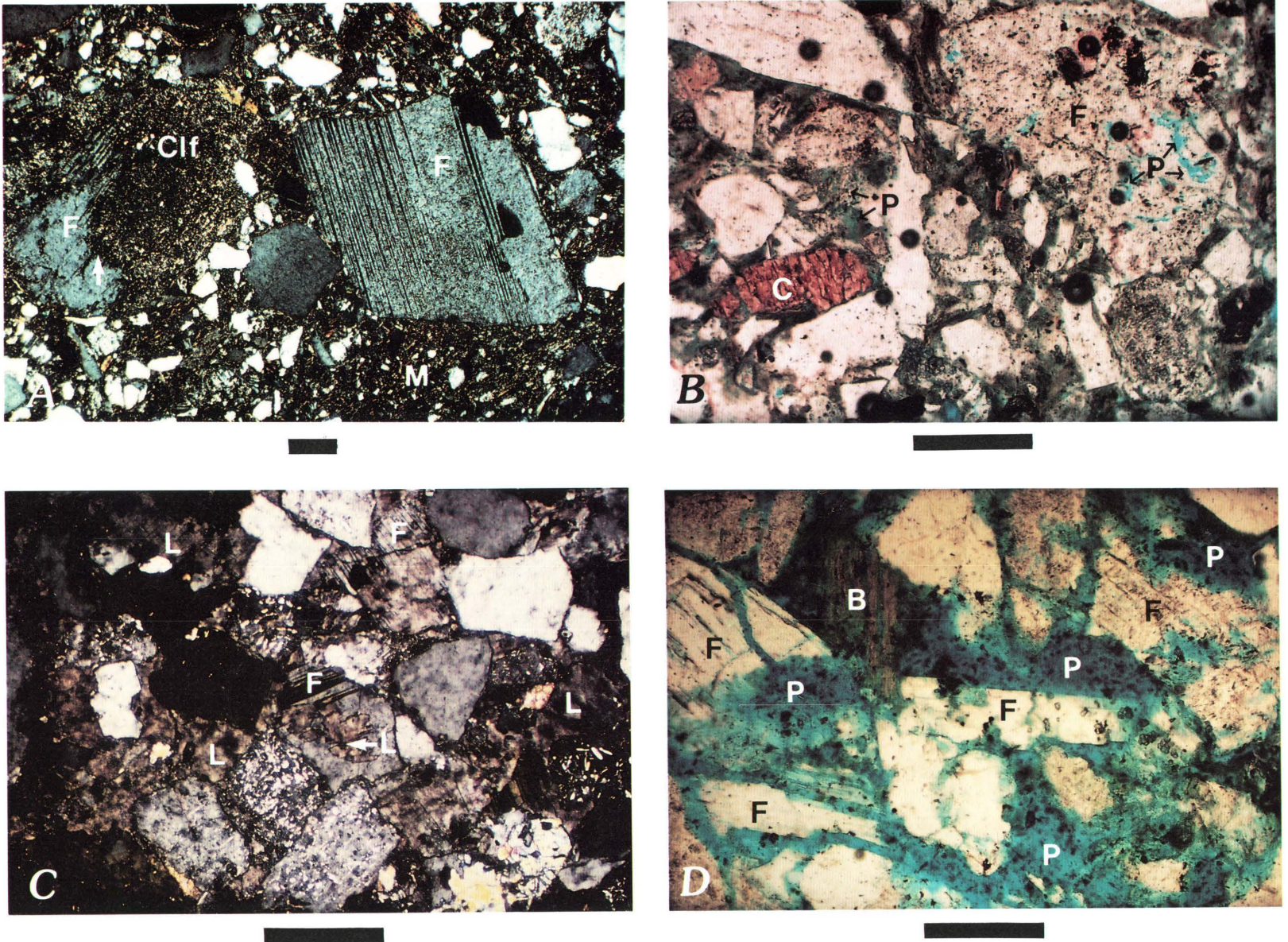


Figure 7. Thin section photomicrographs of sandstones of the Fort Union Formation in the Wagon Wheel No. 1 well. Scale bars 0.2 mm. *A*, Poorly sorted, lithic arkose having high clay matrix (M) and clay-altered feldspars (Clf) (crossed nicols). F, feldspar. *B*, Intergranular and intragranular dissolution porosity (P) in lithic arkose showing remnants of calcite (C). F, feldspar. *C*, Laumontite (L) cement replacing feldspars (F) in sandstone. *D*, Extensive dissolution porosity (P) after removal of laumontite. F, feldspar; B, biotite.

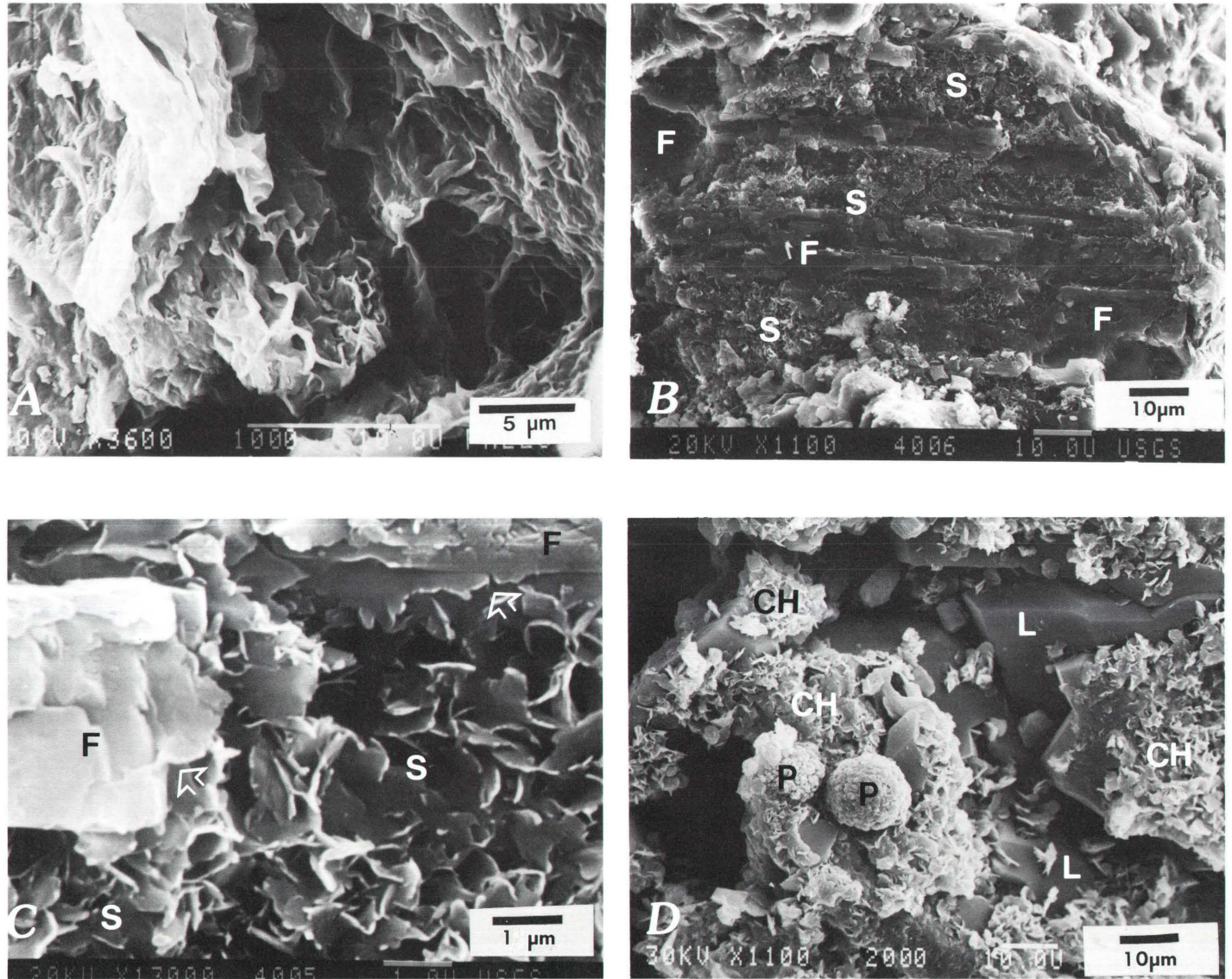


Figure 8. Scanning electron micrographs of clays in sandstones of the Fort Union Formation from the Wagon Wheel No. 1 well. A, Smectite grain-coating cement. B, Feldspar (F) grain altered by smectitic clay (S). Q, quartz. C, Higher magnification of B. D, Framboidal pyrite (P) in laumontite (L) cement showing chlorite (CH) replacing laumontite.

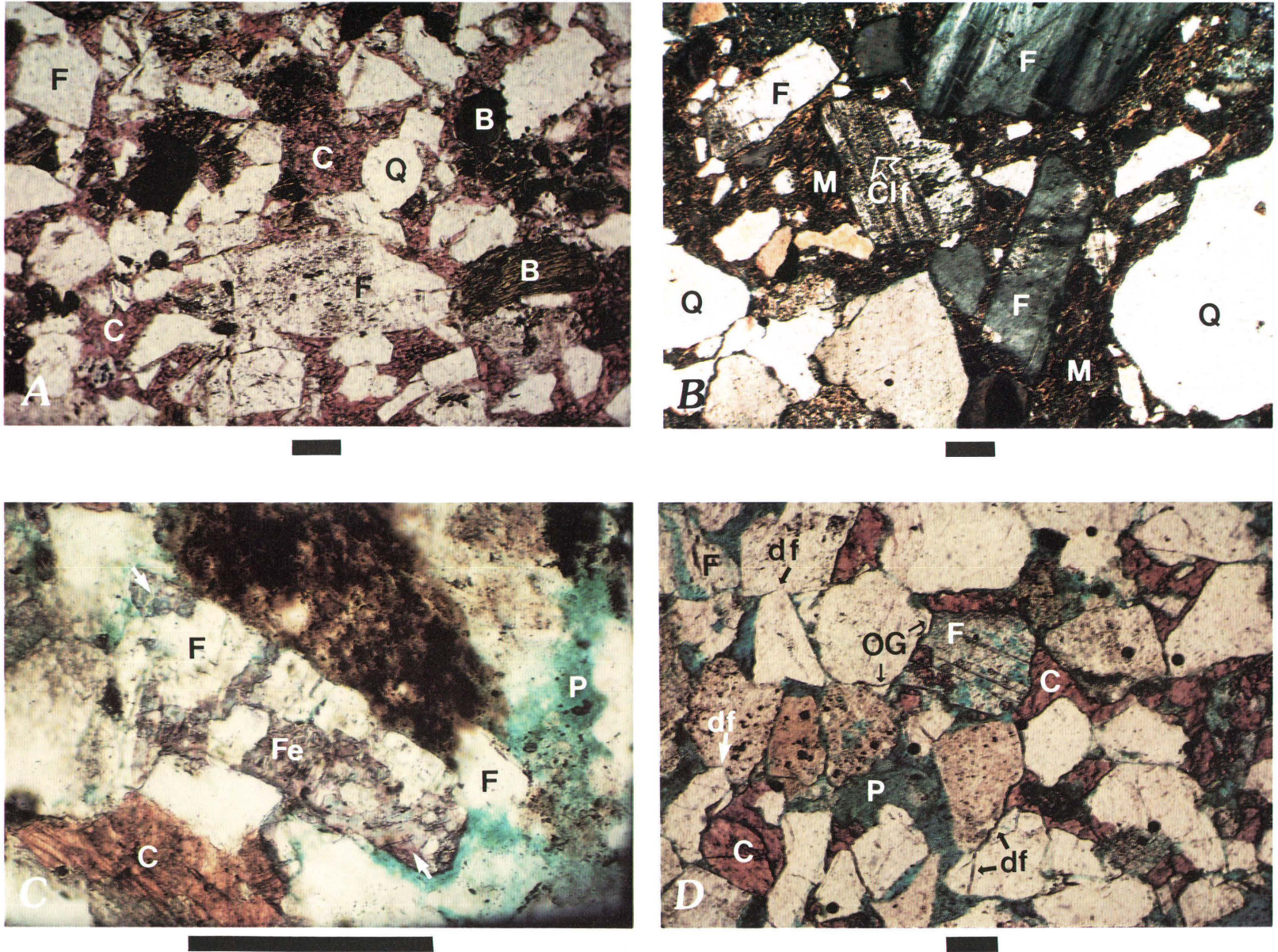


Figure 9. Thin section photomicrographs of lower Tertiary sandstones from the Wagon Wheel No. 1 well. Scale bars 0.2 mm. *A*, Calcite (C) extensively cemented sandstone having essentially little or no porosity. Q, quartz; B, biotite; F, feldspar. *B*, Poorly sorted sandstone having high clay matrix (M) and clay-altered feldspars (Clf) (crossed nicols). F, feldspar; Q, quartz. *C*, Replacement of feldspars (F) by iron-free calcite (C) and ferroan (Fe) calcite (arrows). Note intergranular dissolution porosity (P). *D*, Deformation fabrics (df) and dissolution porosity (P) in sandstone cemented by iron-free calcite (C). Note quartz overgrowth (OG) cement and dissolution and replacement of feldspars (F) by calcite.

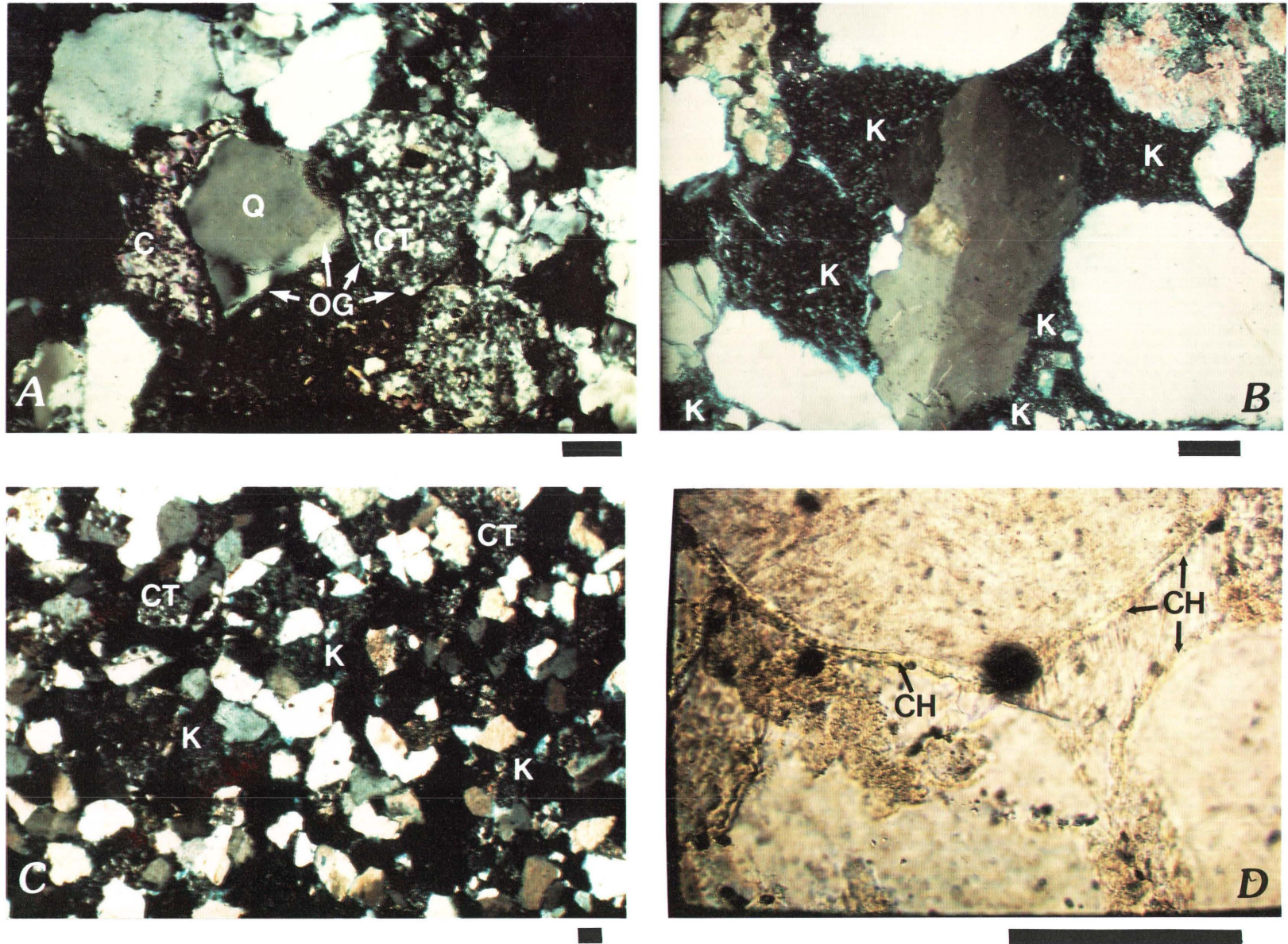


Figure 10. Thin section photomicrographs of lower Tertiary sandstones from the Wagon Wheel No. 1 well. Scale bars 0.1 mm. *A*, Calcite (C) cement after overgrowths (OG) on quartz (Q) and chert (CT) (crossed nicols). *B*, Extensive kaolinite (K) cement showing resemblance to chert (crossed nicols). *C*, Extent and similarity of microcrystalline chert (CT) and kaolinite (K) (crossed nicols). *D*, Grain-coating chlorite (CH) cement.

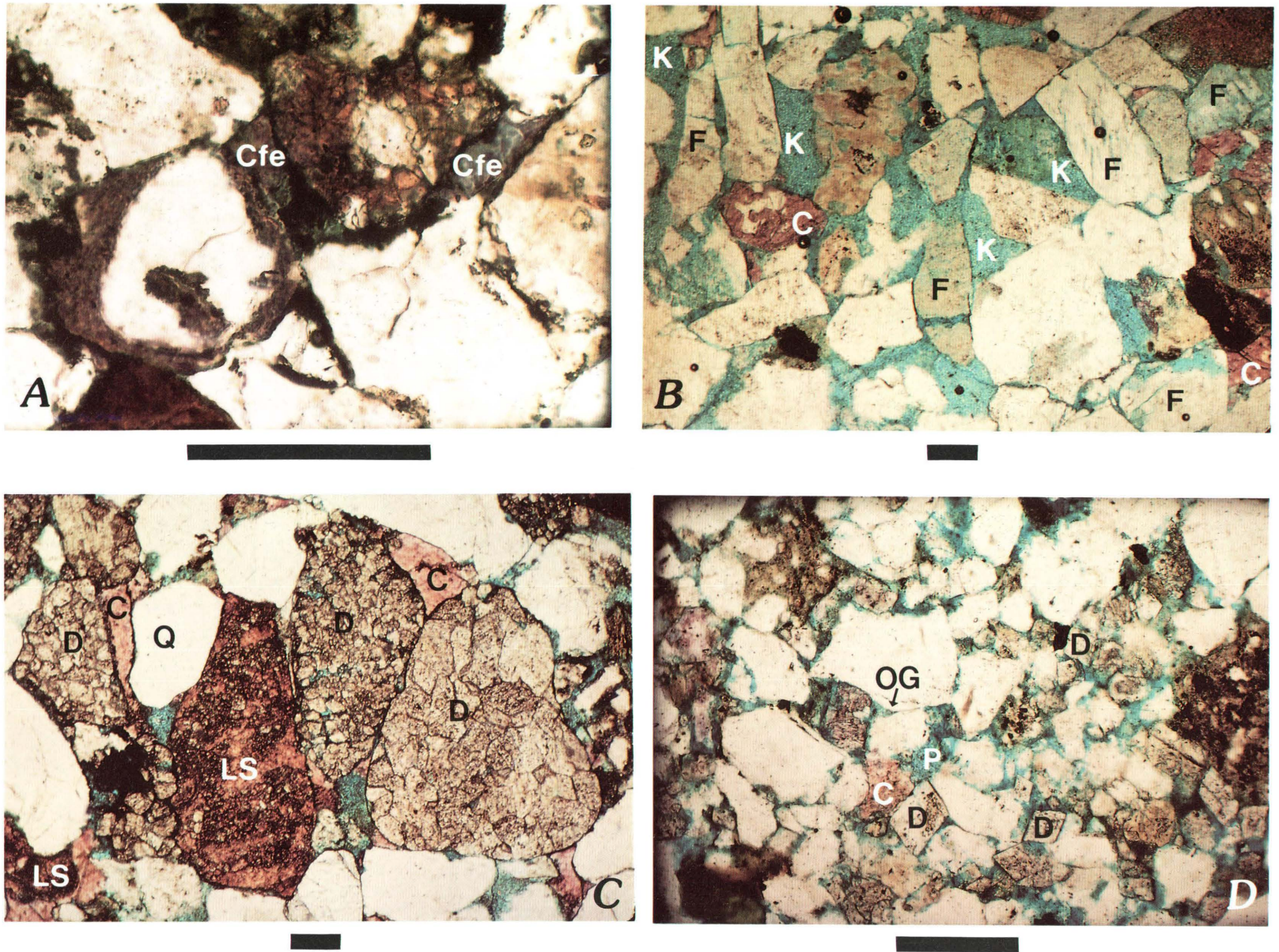


Figure 11. Thin section photomicrographs of lower Tertiary sandstones. Scale bars 0.2 mm. *A*, Ferroan calcite (Cfe) cement. Wagon Wheel No. 1 well. *B*, High secondary porosity (blue) resulting from dissolution of calcite (C) cement and dissolution of feldspars (F) and other grains mostly replaced or infilled by kaolinite (K). Wagon Wheel No. 1 well, 7,366 ft. *C*, Coarse-grained sandstone containing abundant detrital limestone (LS) and dolomite (D) grains partly cemented by calcite (C). Q, quartz. New Fork No. 1 well, 7,970 ft. *D*, Rhombic detrital dolomite (D) grains in sandstone exhibiting dissolution porosity (P) and remnants of calcite (C) cement. Note quartz overgrowths (OG).



Figure 12. Scanning electron micrographs of authigenic clay minerals in sandstones. *A*, Chlorite/smectite (CS) and terminated quartz (Q) crystals in close association with kaolinite (K). Wagon Wheel No. 1 well. *B*, Coarse, vermicular kaolinite as pore-filling cement. Wagon Wheel No. 1 well. *C*, kaolinite (K) replacing earlier-formed calcite (C) cement. Ericson Sandstone, WASP well, 11,760 ft. *D*, Chlorite/smectite (CS) honeycombs on earlier formed platelets of chlorite (CH). Wagon Wheel No. 1 well.

The extent of diagenesis in sandstones from the K-T interval is variable: the high intensity of diagenesis was certainly selective to particular sandstones. Many sandstones within the same interval show few diagenetic events and are still well cemented with iron-free or iron-bearing calcite. The minor secondary porosity that exists in sandstones well cemented by calcite is primarily intragranular and formed by the partial dissolution of feldspars, chert, and sedimentary rock fragments. These local variations in the intensity of diagenesis may be controlled by sedimentologic factors.

New Fork Wells

The feldspar content of Tertiary rocks in the New Fork wells varies from 2 to 40 weight percent and total clay content averages 15–20 weight percent. Carbonate minerals, mostly calcite, were observed in all Tertiary sandstone samples; XRD analysis indicates that dolomite contents are as high as 10 weight percent. Although no Tertiary shales were analyzed from the New Fork cores, shaley siltstones having clay contents of more than 30 weight percent (as calculated by XRD) (New Fork sample 1-7961.2, table 4) and clayey matrices observed in thin section show a marked increase in discrete illite and I/S. The direct relationship between increases in discrete illite and I/S and an increase in detrital clay in sandstone suggests that shales from this interval have a similar clay-mineral assemblage. This illite-I/S assemblage is similar to that for equivalent rocks from the Wagon Wheel well.

Detrital limestone and dolomite grains and other sedimentary rock fragments are abundant in Tertiary sandstones from the New Fork Nos. 1 and 2 wells, particularly in the coarser sandstones (fig. 11C). Although most of the detrital dolomite consists of well-rounded polycrystalline grains, individual rhombs of detrital dolomite commonly are dispersed throughout the finer grained sandstones (fig. 11D). Detrital carbonate grains were likely derived from Paleozoic carbonate rocks. Rhombs of authigenic dolomite also occur as overgrowths on detrital dolomite grains or as replacements in chert fragments (fig. 13A). Similar petrographic characteristics for dolomite from the Wagon Wheel well were reported by Dickinson (1984, 1985).

The style and intensity of diagenesis in the lower Tertiary sandstones and sandstones from the Lance Formation in the three New Fork wells, a depth range of 7,950 to 10,570 ft (2,420–3,220 m), are similar in many aspects to those for the K-T interval described in the Wagon Wheel well between depths of 7,240 and 11,070 ft (2,240–3,370 m) and are summarized in figure 3. Most sandstones of the New Fork cores from this interval contain significant secondary porosity. They are characterized by well-formed, early quartz (fig. 13B) and rare minor chert overgrowth cementation. Silica

cementation was usually followed by the precipitation of I/S clay around overgrowths and other framework grains. C/S also formed in some of the sandstones from this interval (table 4).

Calcite and kaolinite are major cements in Tertiary sandstones from the New Fork wells (fig. 13B). Framework feldspar grains have been extensively dissolved or replaced, and sometimes infilled by calcite and (or) altered to kaolinite (fig. 13C). The dissolution of calcite cement and silicate framework grains (primarily feldspars and chert) are the common causes of intergranular and intragranular secondary porosity, respectively. The extent of dissolution is variable, however, and thus the amount of intragranular secondary porosity is unpredictable among sandstones from any one interval.

Upper Cretaceous Rocks

General Mineralogy and Diagenetic Overview

In the Wagon Wheel well, total feldspar content generally decreases to less than 5 weight percent of the bulk rock in Upper Cretaceous sandstones and shales at depths less than 16,000 ft (4,900 m), as compared to the 20–25 weight percent in Tertiary rocks immediately above the Cretaceous-Tertiary unconformity (tables 2–4). Typically, 2–3 weight percent plagioclase is present, and potassium feldspar is absent or present only in trace amounts; however, rocks deeper than 16,000 ft (4,900 m) in the Wagon Wheel well contain as much as 15 weight percent total feldspar in some samples (table 2).

The diagenesis of Upper Cretaceous rocks from the Wagon Wheel well varies in some aspects from unit to unit, but many diagenetic events are common to most units; these are shown in the upper part of figure 3. Additional or unique diagenetic events are shown in the lower part of figure 3. Early diagenesis of Upper Cretaceous sandstones from the Wagon Wheel well typically involved compaction, framboidal pyrite formation, and the precipitation of quartz overgrowth and smectitic clay cements. These earliest stages were followed by partial dissolution of framework grains and cementation by calcite. Iron-bearing calcite commonly replaced earlier iron-free calcite, and dissolution of both calcite cements and feldspar, chert, and shale grains typically followed. The replacement of calcite cement and (or) feldspar, chert, and lithic grains (shale clasts) by kaolinite or the precipitation of kaolinite cement in secondary pores was almost ubiquitous during later stages of burial.

In the WASP well, the paragenetic sequence and extent of diagenesis in sandstones from the Lance Formation and Ericson Sandstone and most sandstones from the Rock Springs Formation are similar through the depth interval cored (10,450–14,360 ft; 3,180–4,380 m) and are

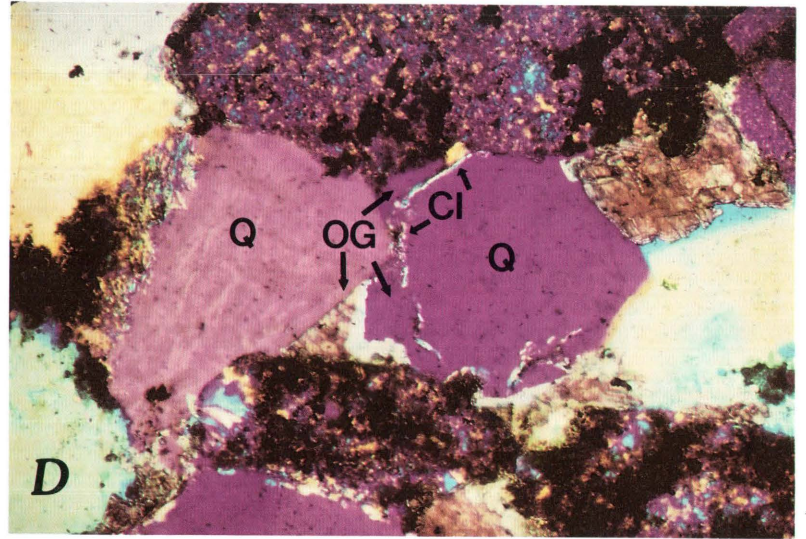
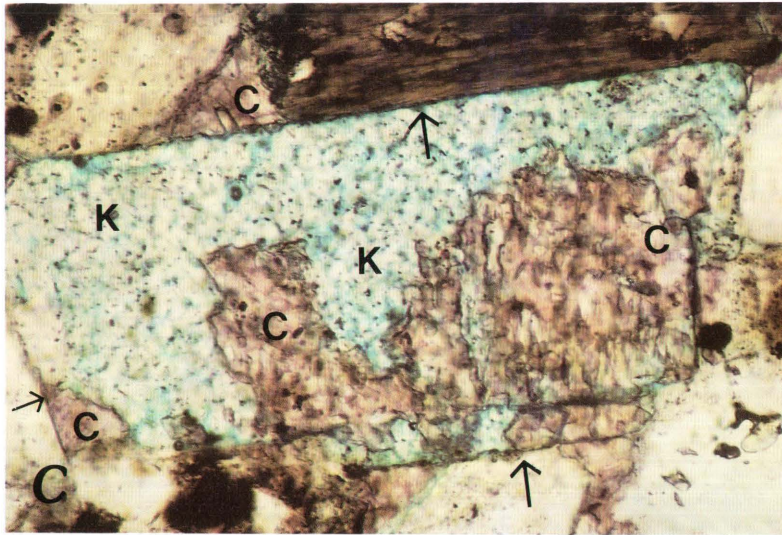
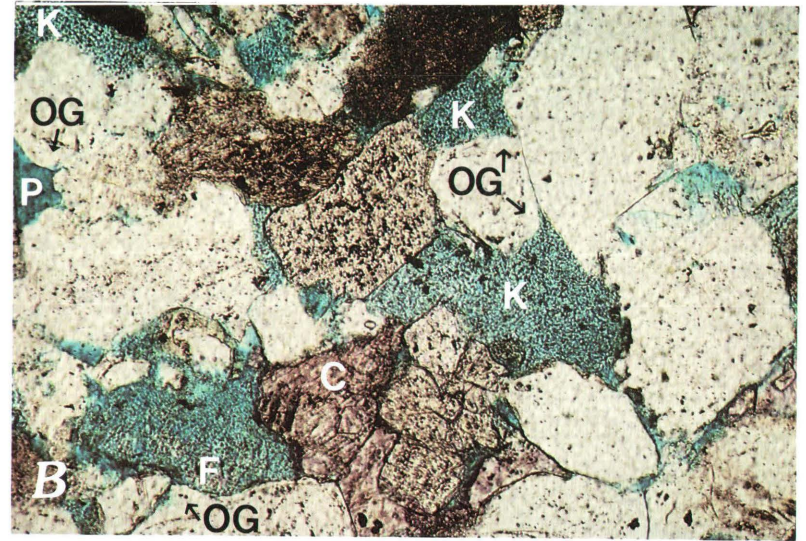
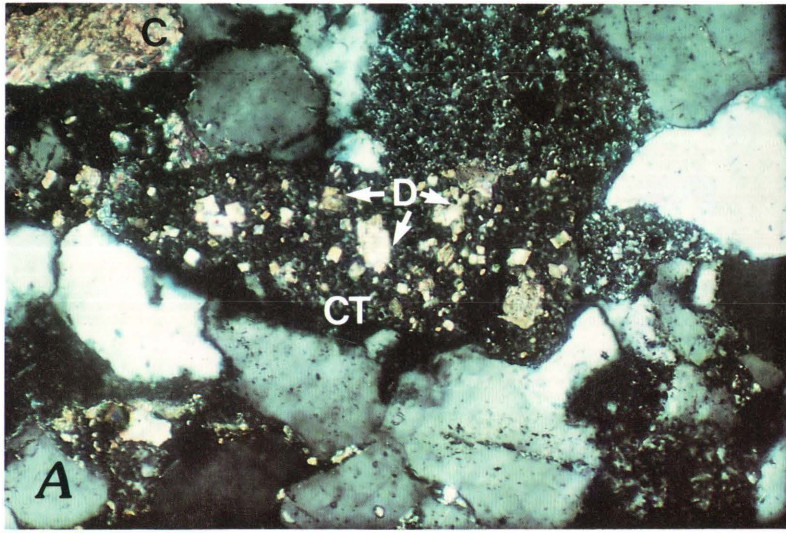


Figure 13. Thin section photomicrographs of sandstones. Scale bars 0.1 mm. *A*, dolomite (D) rhombs replacing chert (CT) in sandstone cemented by calcite (C) (crossed nicols). *B*, Quartz-overgrowth cement (OG) and porosity (P) from dissolution of feldspar (F) and later calcite (C) cement prior to replacement by kaolinite (K). *C*, Relic outline of rectangular feldspar (arrows) replaced by calcite (C) and kaolinite (K). Unnamed Tertiary unit, New Fork No. 4 well, 8,260 ft. *D*, Alternating quartz-overgrowth (OG) and clay (Cl) cements (crossed nicols, accessory plate). Q, quartz. Rock Springs Formation, WASP well, 12,514 ft.

summarized in figure 6. Most of the diagenetic stages are similar to those in the generic sequence described above for the Wagon Wheel well (fig. 3). Diagenesis of Upper Cretaceous sandstones of the WASP well generally began with the formation of quartz overgrowths; the development of these overgrowths was sometimes preceded or interrupted by the precipitation of smectitic grain-coating clay (fig. 13D). Many of the sandstones are characterized by ferroan dolomite overgrowths on detrital dolomite grains. The ferroan dolomite overgrowth cements are easily recognized after carbonate staining. These overgrowths commonly are extensive, and can fill a significant volume of primary pore space (fig. 14A). Formation of these overgrowths of ferroan dolomite postdated formation of quartz overgrowths but predated cementation by calcite (fig. 14B). These diagenetic events were almost always followed by calcite cementation. Wherever iron-free calcite cement formed, it commonly was replaced by iron-bearing calcite cement. Fractures formed late in the burial history, probably during uplift and erosion (Pollastro and Barker, 1986), and were filled by quartz, then dickite, and finally calcite (fig. 14C). Detailed descriptions for each of the Upper Cretaceous units from these wells follow.

Lance Formation

The Lance Formation is represented in core samples from all five wells. Sandstones typically consist of 60–70 weight percent quartz, as calculated by XRD. Chert and chalcedony are abundant and are framework grains or microcrystalline replacements of earlier phases. Volcanic quartz grains, including some having beta habit, were observed in some sandstones (fig. 14D). Clay content varies from about 10 to 35 weight percent of the bulk rock; however, the very clay-rich sandstones commonly contain shale clasts or laminae.

Diagenesis within the Lance Formation between the cored intervals from about 8,920 ft to 11,070 ft (2,720–3,370 m) in the Wagon Wheel well is summarized in figure 3. Sandstones from this interval contain at least two alternating generations of quartz and I/S clay cement. After formation of the second generations of quartz and I/S cement, calcite cement was precipitated and chert and shale clasts were replaced by calcite. The later dissolution of calcite cement, chert, and sedimentary rock fragments created some moderate secondary porosity. If feldspar was an original component of these rocks, most has been altered because little or no feldspar was detected in the analysis. Replacement of many partly to completely dissolved rock fragments by I/S and discrete illite suggests cannibalization (usually by solution) of earlier, more expandable clay and reprecipitation as a more illitic assemblage (Pollastro, 1985). Authigenic pore-lining and pore-filling chlorite was also

precipitated after calcite dissolution and is closely associated with the progressive growth of illitic cements.

Calcite and dolomite are common constituents to the sandstones of the Lance Formation in samples from all of the wells studied (tables 2–4). Much of the carbonate material is detrital limestone fragments and polycrystalline dolomite grains (fig. 15A); rhombic dolomite grains are also common, particularly in some of the finer, clay-rich siltstones. When observed in thin section, most sandstones and siltstones containing more abundant carbonate (>10 weight percent of bulk rock as calculated by XRD) are partly or extensively cemented by iron-free or iron-bearing calcite (fig. 15B). Iron-bearing calcite cements commonly replace earlier iron-free calcite cement. In contrast, however, iron-free calcite fills fractures that formed very late in the burial history (Dickinson, 1985; Pollastro and Barker, 1986).

Kaolinite is a common cement in many of the sandstones, and, as in the Tertiary rocks, it replaces feldspar, chert grains, rock fragments, and calcite cements. Kaolinite cement commonly is extensive (fig. 15C). It typically occurs as coarse crystals in books and vermicules or as individual pseudo-hexagonal plates (fig. 12B). Because of its coarse nature in many of the sandstones, the weight percent of kaolinite relative to other clay minerals in the rock may be grossly underestimated because the XRD data only calculates the amount of kaolinite in the <2- μ m fraction. Other authigenic clay mineral phases in sandstones of the Lance Formation are I/S, C/S, and discrete illite. In many cases, these clay phases are overgrowths on a precursor clay substrate (Pollastro, 1985).

Shale samples from the Lance Formation are dominated by I/S and discrete illite clay; little kaolinite and (or) discrete chlorite were observed in the shales. This relationship is shown in the XRD data for the Lance Formation in all wells (tables 2–4). Chlorite and kaolinite, however, are abundant in sandstones, particularly cleaner sandstones; that is, those containing less than 20 weight percent phyllosilicate minerals. This relationship is demonstrated by a crossplot of XRD data for an interval of the Lance Formation. The data show an almost inverse relationship between the amount of <2- μ m discrete chlorite and discrete illite (fig. 16A). A comparison of the lithology of these samples and the XRD data shows that the most chlorite rich sandstones are the cleanest and that those sandstones containing the most discrete illite are true shales. Intermediate compositions include shale-laminated sandstones and lithic sandstones containing an abundance of shale clasts.

Crossplots of total phyllosilicate content for the bulk rock versus relative weight percent discrete illite (fig. 16B) or discrete chlorite (fig. 16C) also demonstrate well-defined clay-mineral populations for both sandstone and shale. This relationship can be explained by considering

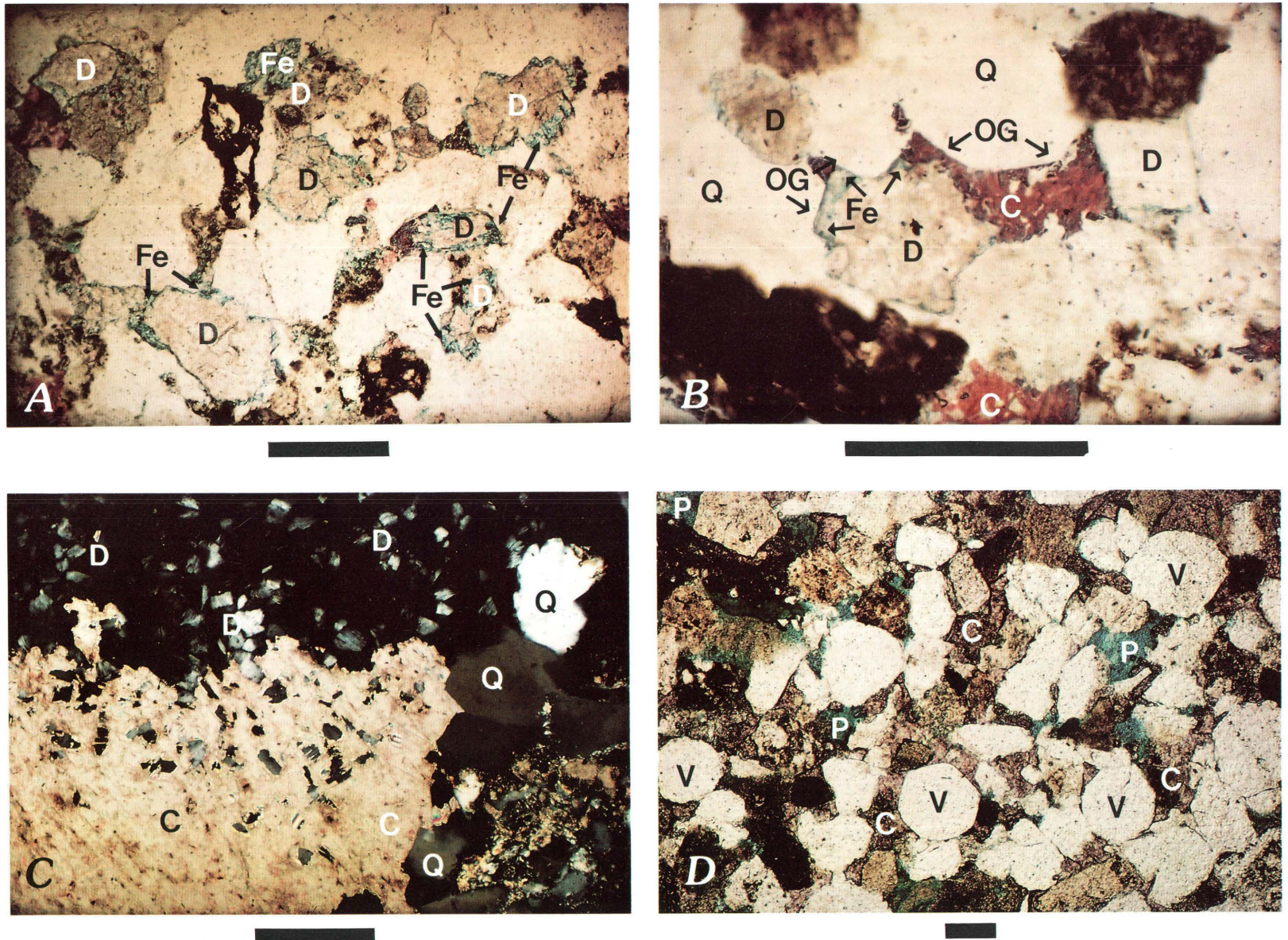


Figure 14. Thin section photomicrographs of sandstones. Scale bars 0.2 mm. *A*, Detrital dolomite (D) with ferroan (Fe) dolomite overgrowths (stained blue). Rock Springs Formation, WASP well, 13,553 ft. *B*, Genesis of cements. Earliest quartz overgrowth (OG) cement on quartz (Q) grains, followed by ferroan dolomite (Fe) overgrowths on detrital dolomite (D), then intergranular calcite (C) cement. Rock Springs Formation, WASP well. *C*, Cements filling fracture. Order of genesis: quartz (Q), dickite (D), and calcite (C) (crossed nicols). Rock Springs Formation, WASP well, 13,612 ft. *D*, Volcanic quartz (V) grains having beta habit, secondary porosity (P), and calcite (C) cement. Lance Formation, New Fork No. 2 well.

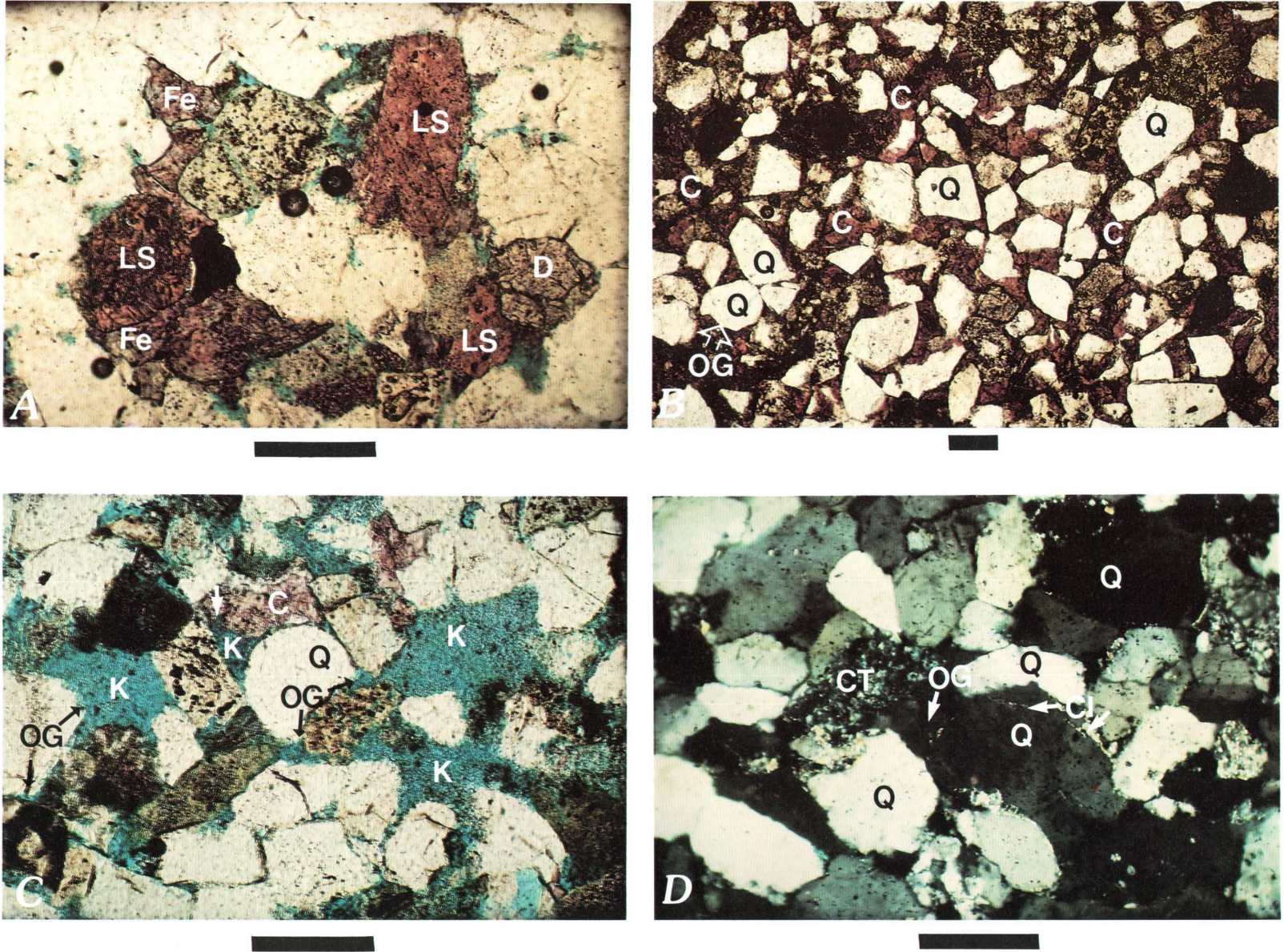


Figure 15. Thin section photomicrographs of sandstones. Scale bars 0.2 mm. *A*, Detrital limestone (LS) and dolomite (D) in ferroan (Fe) calcite-cemented sandstone of Lance Formation. Wagon Wheel No. 1 well, 10,153 ft. *B*, Low-porosity sandstone showing quartz overgrowths (OG) on quartz (Q) prior to calcite (C) cement. Lance Formation, WASP well, 11,546 ft. *C*, Quartz overgrowths (OG) and replacement of calcite (C) cement (arrows) and grains by kaolinite (K). Q, quartz. Lance Formation, Wagon Wheel No. 1 well, 8,124 ft. *D*, Quartzarenite comprised mainly of quartz (Q) and chert (CT) grains with clay (Cl) and quartz-overgrowth (OG) cements. Ericson Sandstone, Wagon Wheel No. 1 well, 13,124 ft.

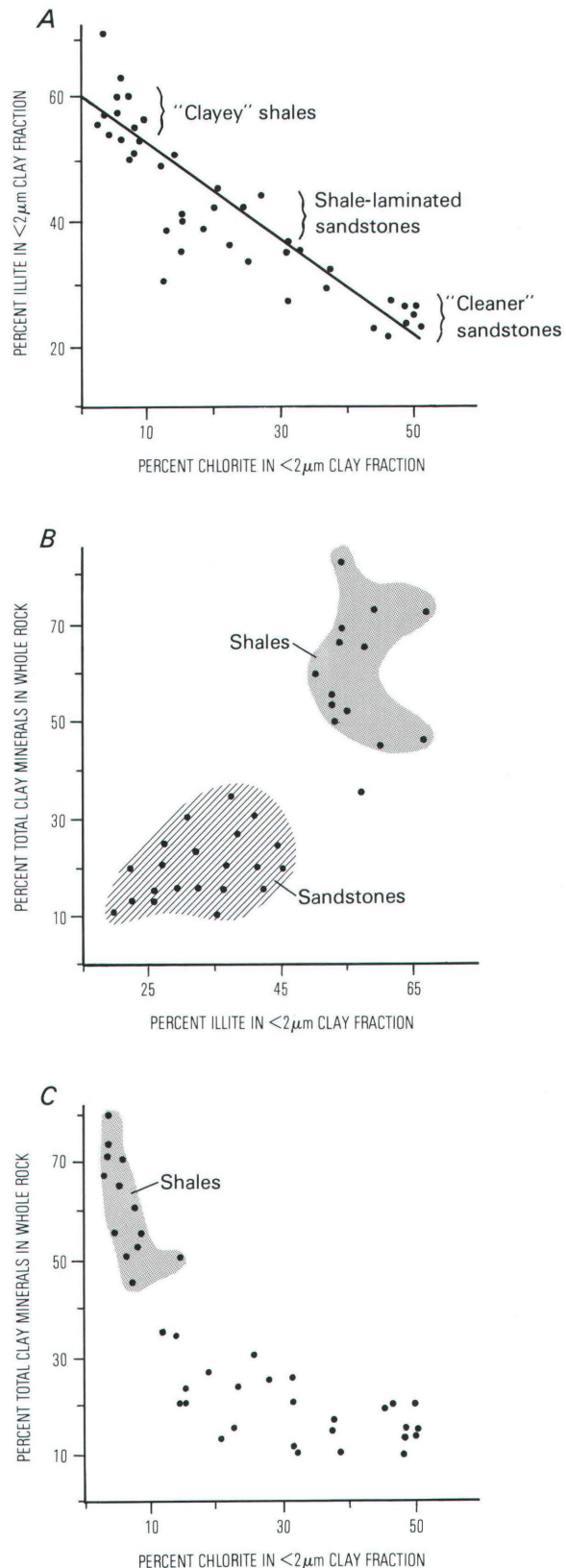
the origin for many of the clay minerals in sandstone versus those in shale. Detritus of the shales from the Lance Formation was derived from sources containing free silica (quartz, chert, and so forth), mica (mostly discrete illite), smectite, and (or) I/S; some detrital carbonate (typically 5–10 weight percent) is also common. Few chlorite or kaolinite clay minerals were common to the source area and, therefore, deposited in the shales. In sandstones, however, kaolinite is pervasive as an authigenic cement or replacement phase, as discussed earlier, and was observed throughout the entire Lance Formation at all localities in this study. Discrete iron-rich chlorite is also an authigenic clay common to these low-permeability sandstones. The weight ratio of chlorite and kaolinite to the total clay-mineral population in these sandstones is probably underestimated from the XRD data because many of the individual clay particles, as measured from thin section and SEM analysis, is greater than $2\ \mu\text{m}$ in diameter (fig. 12B). Therefore, these relationships between sandstone and shale clay mineralogy are probably more significant than the data plotted in figure 16 because the analysis only accounts for relative weight percent as determined from the $<2\text{-}\mu\text{m}$ clay mineralogy.

Ericson Sandstone

The Ericson Sandstone was sampled from core of the Wagon Wheel and WASP wells. In the northern Green River basin, the Ericson is subdivided into an upper unit, referred to as the Canyon Creek zone, and a lower unit, the Trail zone (Law, 1984b; Law and Johnson, this volume). The nonmarine sandstones of the Ericson are more continuous than the more common, lenticular Upper Cretaceous low-permeability sandstones in this area. Compositionally, the sandstones of the Ericson are more arenitic than the more lithic sandstones of the Lance Formation and other Mesaverde units in this part of the basin (Gautier and Pollastro, 1982; Edman and Surdam, 1985). There is some textural evidence suggesting that feldspars were present in many of the Upper Cretaceous sandstones sampled from the Wagon Wheel and WASP wells. This evidence will be discussed below.

In the Wagon Wheel well, the upper zone of the Ericson contains quartzarenites that average about 90 weight percent quartz, as determined by XRD (table 2). These sandstones are composed primarily of detrital quartz, chert fragments, and occasional shale clasts (fig. 15D). Parts of the lower zone in the Wagon Wheel well (sample 13132 and deeper, table 2), however, contain sandstones having 20–30 weight percent total clay, as calculated by XRD; this clay is predominantly mica and kaolinite minerals.

Figure 16. Clay-mineral relationships between sandstones and shales from the Lance Formation, Wagon Wheel No. 1 well, as determined by X-ray powder diffraction. A, Relative weight



percent illite versus chlorite. B, Total clay in whole rock versus relative weight percent illite in clay fraction. C, Total clay in whole rock versus relative weight percent chlorite in clay fraction.

The diagenetic stages interpreted for quartzarenites of the Ericson Sandstone are shown in figure 5 for the Pinedale area and figure 6 for the WASP samples. Multiple stages of syntaxial quartz overgrowths interrupted by stages of clay cement around framework quartz grains are typical of sandstones of the Ericson (fig. 15D). Quartz cementation filled most primary intergranular porosity in many sandstones of the Ericson, and subsequent dissolution of chert grains and shale clasts produced intragranular pores (fig. 17A). The only porosity in quartzarenite sandstones is intragranular secondary porosity that formed by dissolution of chert and rock fragments (figs. 17A, B). Because of the dissolution of less stable rock fragments and chert grains (both which are microcrystalline composites and therefore contain numerous reactive surfaces relative to framework quartz grains and quartz overgrowth cement), sandstones of the Ericson have higher porosity than sandstones in adjacent formations. Therefore, the quartz-rich sandstones of the Ericson have potential for better porosities than other reservoir rocks at depths greater than 10,000 ft (3,050 m).

Highly illitic clay coats many of the quartz grains. Grains having a sericitic appearance or coarse illitic overgrowths account for a major part of the micaceous material. Many of the sericitic grains are shale clasts that probably contained a precursor smectitic clay. During deep burial diagenesis, these grains were converted to a more illitic composition with lath-shaped overgrowths (Pollastro, 1985). Shale clasts also may have served as nuclei for further crystal growth of intergranular illitic or sericitic cements (fig. 17C).

Authigenic kaolinite is common in sandstones of the Ericson. Chert grains are commonly altered to booklets and vermicules of kaolinite (fig. 17D). Coarse-crystalline dickite, probably of hydrothermal origin, fills late-formed fractures in some sandstones of the Ericson at a depth of about 13,200 ft (4,020 m) in the Wagon Wheel well.

Sandstones of the Ericson in the WASP core are generally coarser and contain more lithic fragments than those from the Wagon Wheel well. These characteristics are consistent with a closer proximity to a source area to the northwest (B.E. Law, oral commun., 1987). Very quartz rich sandstones are distinctively absent in samples from the WASP core, as compared to samples from the Wagon Wheel core. Detrital dolomite occurs in sandstones of the Ericson from the WASP well; it is less common than in those from the Wagon Wheel well and occurs only in sandstones from the lower zone. Dolomite rhombs commonly replace chert or are overgrowths on polycrystalline detrital dolomite grains, and sparry or rhombic dolomite partly to completely replaces quartz and chert grains (fig. 18A). Calcite is rare or absent in Ericson samples from the Wagon Wheel well. In the WASP core, however, all sandstones of the Ericson contain calcite

cement; this calcite is commonly partly dissolved or sometimes replaced by kaolinite (figs. 12C, 18B).

Shales of the Ericson from the Wagon Wheel well are enriched in kaolinite relative to all other shales in this study (table 2). No shale samples from the Ericson were analyzed in the WASP core.

Rock Springs Formation

Mesaverde Group rocks referred to as "Undivided" by Law (1984b) are designated as the Rock Springs Formation in this report (Law and Johnson, this volume) and are represented in samples from the Wagon Wheel and WASP wells. Seventy-three samples of the Rock Springs Formation were analyzed from the WASP core from 12,050 to 14,350 ft (3,670–4,370 m), and thirty-seven samples were analyzed from the Wagon Wheel well from about 14,000 to 17,965 ft (4,270–5,470 m) (table 2).

Sandstones from the Rock Springs Formation in the Wagon Wheel well typically are finer grained than those from the WASP well and contain 45–50 weight percent quartz, 25 weight percent total clay, and 20–25 weight percent carbonate minerals. Sandstones of the Rock Springs Formation commonly are rich in sedimentary rock fragments, particularly carbonate grains and shale clasts; chert is also a major component. Early quartz overgrowth cementation is common to lithic sandstones of the Rock Springs Formation. A few quartzarenite sandstones, petrographically similar to the quartz-rich sandstones of the upper part of the Ericson from the Wagon Wheel well, are present in the WASP core. These sandstones are extensively cemented by silica and contain mostly secondary moldic porosity from the dissolution of chert and shale clasts (fig. 18C).

Rock Springs sandstones from the Wagon Wheel well are rich in detrital dolomite (fig. 18D); dolomite content averages about 15 weight percent, as determined by XRD. Limestone rock fragments are also common. Ankerite or siderite may also coexist with dolomite. In core samples from the WASP well, dolomite increases from about 2 to 15 weight percent downsection. Detrital dolomite is both rhombic and polycrystalline and commonly has micritic or sparry overgrowths of ferroan dolomite; micritic dolomite or ankerite cement sometimes replaces or encompasses framework grains (fig. 19A). Iron-free and iron-bearing calcite cements are usually present, and the more iron bearing varieties commonly replace iron-free calcite (fig. 19B).

Sandstones from the Rock Springs Formation in the Wagon Wheel well contain distinctly more feldspar than do other Upper Cretaceous sandstones higher in the section. Below a depth of about 16,000 ft (4,900 m), plagioclase and potassium feldspar, combined, may comprise as much as 10 weight percent of the rock (table 2).

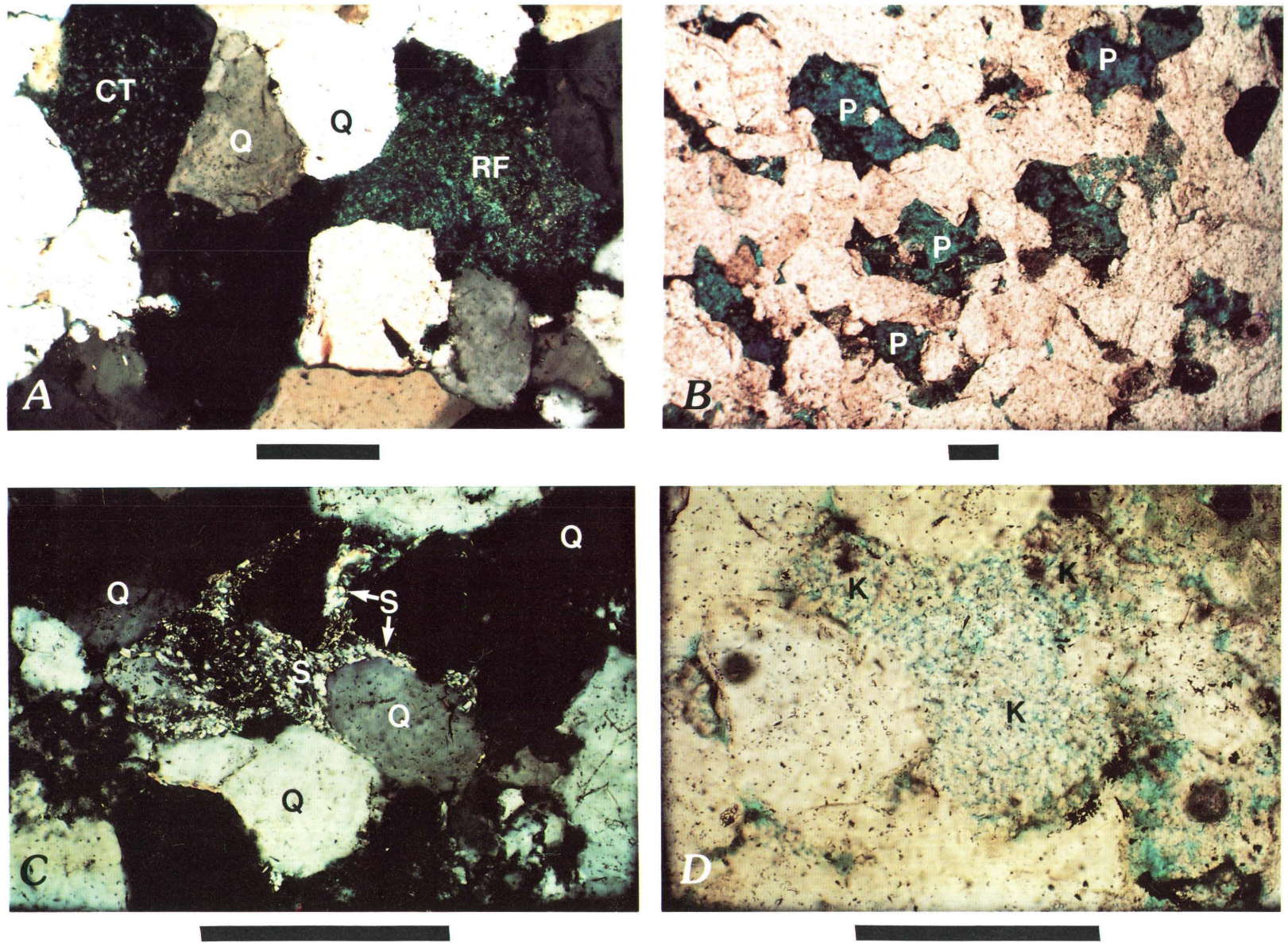


Figure 17. Thin section photomicrographs of quartzarenites from the Ericson Sandstone, Wagon Wheel No. 1 well. Scale bars 0.2 mm. *A, B*, Porosity (P) from dissolution of chert (CT) and shale fragments (RF) in quartz (Q) sandstone. 13,109 ft. *C*, Sericitic (S) overgrowths from sericitized grain in quartz (Q) sandstone. 13,124 ft. *D*, Chert grain or shale clast altered to kaolinite (K).

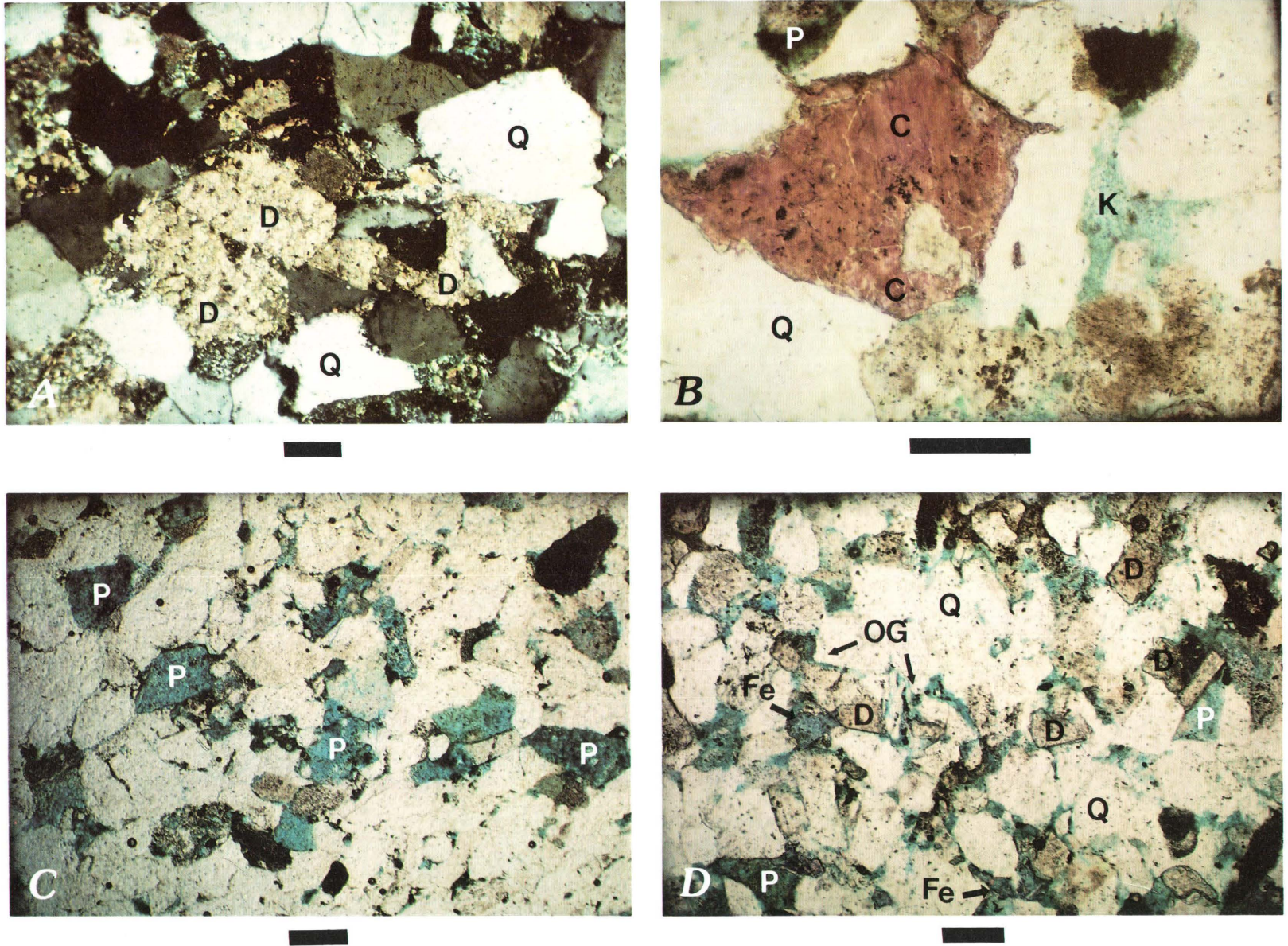


Figure 18. Thin section photomicrographs of sandstones. Scale bars 0.1 mm. *A*, Extensive replacement of chert and cementation by dolomite (D) (crossed nicols). Q, quartz. Lower part of Ericson Sandstone, Wagon Wheel No. 1 well, 13,197 ft. *B*, Dissolution porosity (P) and cementation by calcite (C) and kaolinite (K). Q, quartz. Ericson Sandstone, WASP well, 11,757 ft. *C*, Moldic porosity (P) in quartzarenite. Rock Springs Formation, WASP well, 13,181 ft. *D*, Quartz overgrowth (OG) and ferroan (Fe) calcite cements in sandstone containing abundant detrital rhombic dolomite (D) grains. Note extensive dissolution porosity (P). Q, quartz. Rock Springs Formation, Wagon Wheel No. 1 well, 16,084 ft.

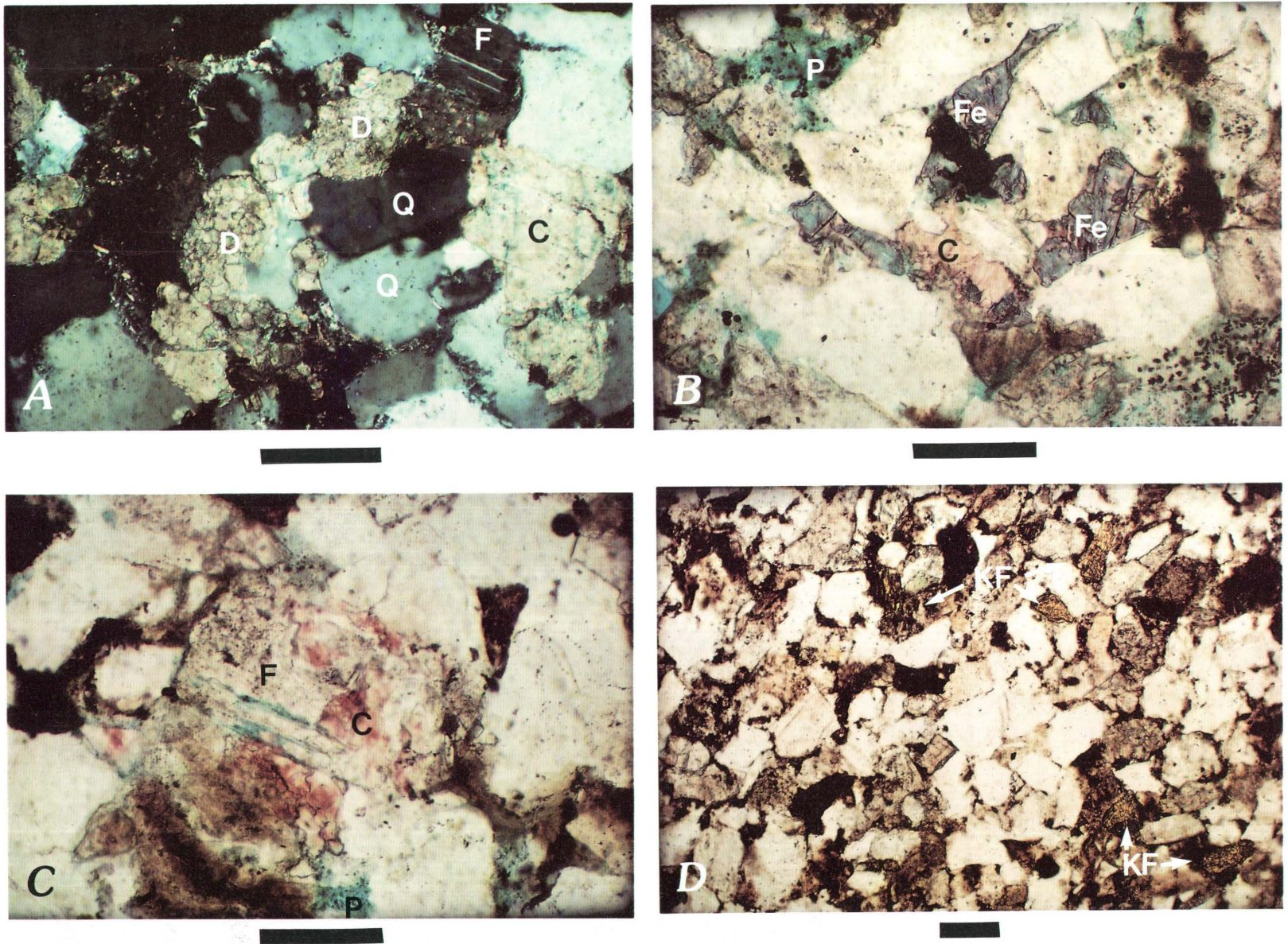


Figure 19. Thin section photomicrographs of sandstones, Rock Springs Formation, Wagon Wheel No. 1 well. Scale bars 0.1 mm. *A*, Dolomite (D) and calcite (C) cements replacing framework feldspar (F) and quartz (Q) (crossed nicols). 16,087 ft. *B*, Ferroan (Fe) calcite cement after iron-free calcite (C). Note porosity (P) infilled by blue epoxy. 16,087 ft. *C*, Dissolution of feldspar (F) and replacement or infilling by calcite (C). 16,095 ft. *D*, Abundance of potassium feldspar (KF) (stained yellow). 16,076 ft.

These feldspars may be partly or completely replaced by calcite; in some samples, calcite cement fills earlier dissolution pores in the grains (fig. 19C). Both potassium feldspar and plagioclase grains are commonly unaltered (fig. 19D). Other common mineral grains are biotite and glauconite.

The common clay minerals in sandstones of the Rock Springs Formation are illite, illitic I/S (table 3), and iron-rich chlorite. Kaolinite was found in almost all sandstones from the WASP core and to a depth of about 14,950 ft (4,560 m) in the Wagon Wheel well. Illitic clay cement was observed between stages of quartz overgrowth cementation in many of the sandstones. Clay cementation may have occurred relatively early in the burial history and, therefore, the original clay-mineral composition may have been modified during deep burial diagenesis (Pollastro, 1985). Illitic or sericitic clay overgrowths also occur as elongate or lathlike crystals on shale clasts and as coatings on framework grains. This micaceous clay sometimes grows outward crystallizing from the framework grain nucleus to form a late intergranular cement (fig. 20A).

Diagenesis of sandstones from the Rock Springs Formation in the Wagon Wheel well can be separated into two different sequences by depth and is shown in figure 3. Sandstones from the upper sequence, from 14,890 to 14,950 ft (4,340–4,560 m), exhibit less quartz overgrowth cementation than those from 16,060 to 17,970 ft (4,890–5,480 m). Authigenic kaolinite is common to sandstones in the upper cored interval and is absent in sandstones below 16,000 ft (4,900 m). Ankerite and siderite cements are common in the upper sequence; dolomite is more common in sandstones of the lower sequence (table 2). Sandstones below 16,000 ft (4,900 m) contain unusually well preserved feldspars, more extensively developed syntaxial quartz overgrowths, and rare occurrences of chert cement. Late diagenetic features in the lower sequence include precipitation of pore-filling chlorite and infilling of fractures by quartz and iron-free calcite.

Porosity in sandstones from the Rock Springs Formation is essentially secondary and produced through the dissolution of intergranular cements, framework chert, and shale clasts (fig. 20B). The dissolution of feldspars, where present, also contributes to the development of some moldic porosity.

Illite and I/S are the major clay minerals in shales of the Rock Springs Formation. Chlorite and kaolinite each comprise less than 10 relative weight percent of the <2- μ m clay minerals of the shales from the Wagon Wheel well. Kaolinite and chlorite are more abundant in shales from the WASP well, where they commonly exceed 20 relative weight percent of the <2- μ m clay minerals. The relative increase in abundance of kaolinite and chlorite in WASP shales is consistent with a closer proximity to provenance, assuming kaolinite and chlorite in these

shales are primarily detrital components. In the Wagon Wheel well, kaolinite is not present in either shale or sandstone samples below 16,060 ft (4,900 m), and the relative amount of clay-size chlorite markedly increases below that depth (table 2). This relationship may indicate that kaolinite is not stable at high temperatures produced by deep burial, as first suggested by Hower and others (1976).

Two sandstone and one shale sample of the Rock Springs Formation were analyzed from the Wagon Wheel well at depths from 17,960 to 17,970 ft (5,477–5,480 m). The sandstones are extensively cemented by carbonate minerals; total carbonate averages about 30 weight percent of the bulk rock, as calculated by XRD (table 2). Dolomite is commonly more abundant than calcite; rhombs of detrital dolomite are dispersed throughout the sections, and micritic to sparry dolomite overgrowths form intergranular cements or sometimes replace feldspars, quartz, chert, or shale fragments (fig. 20C). Intergranular iron-free and iron-bearing calcite cements are present; iron-bearing calcite cement always replaces iron-free calcite. It also replaces dolomite rhombs, chert, and other rock fragments.

Relative to most other Upper Cretaceous sandstones in the Wagon Wheel well, distinctly more feldspar is in the Rock Springs Formation. Many of the feldspars are well preserved. Plagioclase is in amounts as high as 15 weight percent of the bulk rock, as calculated by XRD (table 2). Stained thin sections reveal the presence of unaltered potassium feldspar in moderate quantities (fig. 20D). Because of the relative abundance of feldspars at this depth, the possibility of albitization or other authigenic feldspar formation was investigated for these sandstones. No evidence for this process was found and it is interpreted that the feldspars in the Rock Springs Formation are original detrital components that have been preserved throughout its burial history.

Specific Diagenetic Phases and Events

Laumontite and Associated Framboidal Pyrite and Chlorite

Laumontite-bearing sandstones are in the Fort Union Formation in the Wagon Wheel well, at a depth of about 5,000 ft (1,520 m). Burial reconstruction for the area of the well (Pollastro and Barker, 1986) suggests that approximately 5,600 ft (1,700 m) of section has been eroded. The total maximum burial estimated for laumontite-bearing sandstones of the Fort Union Formation in the Wagon Wheel well therefore is about 10,600 ft (3,230 m), a depth that corresponds to a calculated maximum burial temperature for these rocks of 90 °C (Pollastro and Barker, 1986, fig. 9). Many recent studies report the formation of laumontite very

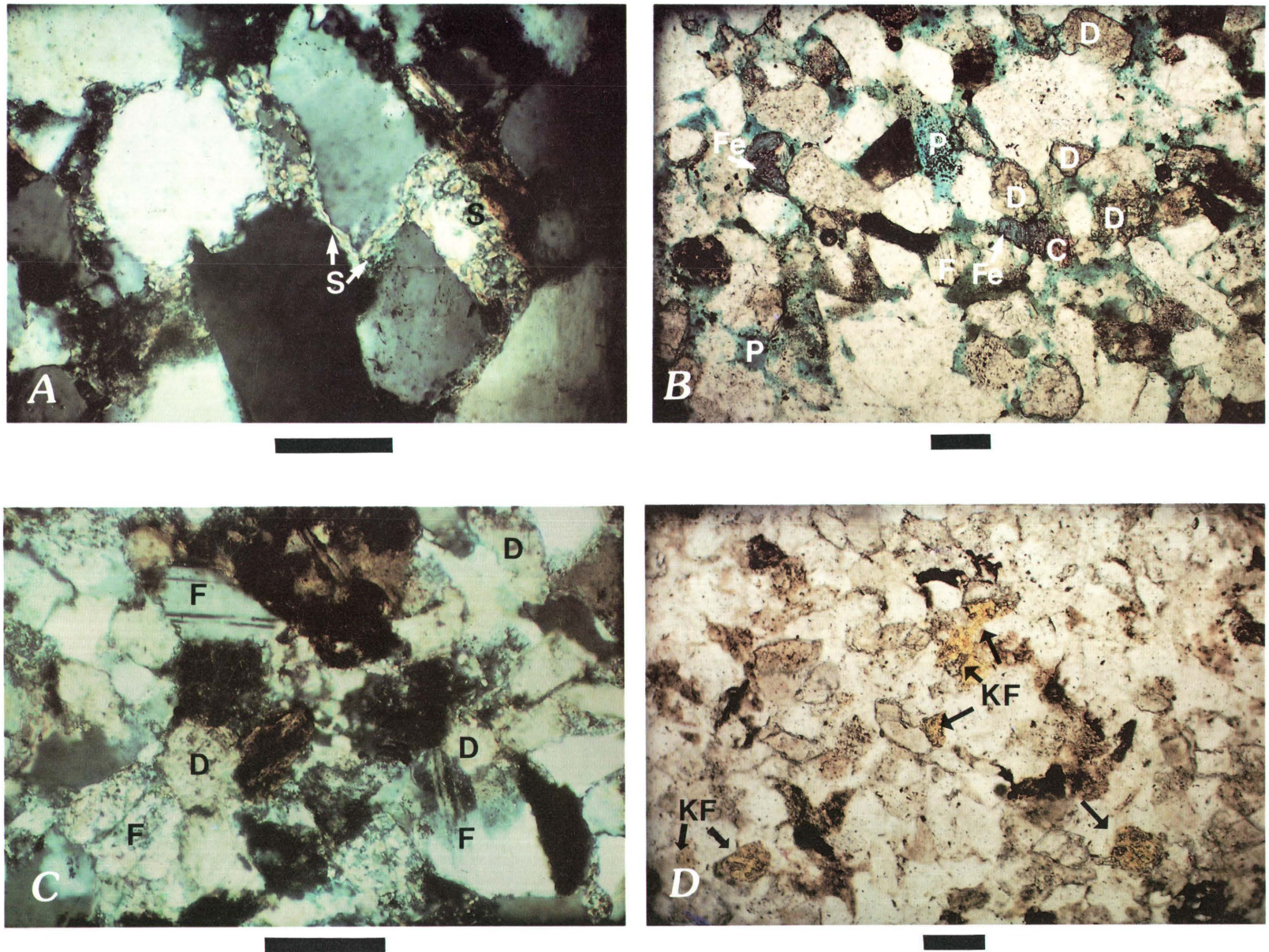


Figure 20. Thin section photomicrographs of sandstones. Scale bars 0.1 mm. *A*, Intergranular sericite (S) overgrowths nucleating from sericitized grains (crossed nicols). Rock Springs Formation, WASP well, 13,255 ft. *B*, Detrital dolomite (D) rhombs showing ferroan (Fe) calcite cement after iron-free calcite (C). Note dissolution porosity (P). F, feldspar. Rock Springs Formation, Wagon Wheel No. 1 well, 16,084 ft. *C*, Original feldspars (F) being replaced by dolomite (D) in sandstone (crossed nicols). Rock Springs Formation, Wagon Wheel No. 1 well, 17,959 ft. *D*, Yellow-stained potassium feldspars (KF) in deep sandstone. Rock Springs Formation, Wagon Wheel No. 1 well, 17,965 ft.

late in the burial history and in the deep subsurface (Crossy and others, 1984; Helmold and van de Kamp, 1984) or in environments having temperatures that approach or mark the onset of metamorphism (Ghent, 1979).

McCulloh and others (1981) studied the Sespe Hot Springs, Calif., and reported laumontite formation between temperatures of 43 and 89 °C. They concluded that laumontite can crystallize at any depth between the surface and 22,000 ft (6,700 m) and that its formation is dependent upon wherever the appropriate combination of temperature, fluid pressure, and fluid composition are met and mineralogically immature, permeable, and porous rocks have reacted sufficiently with interstitial water having exceptionally low $p\text{CO}_2$. They also stated that the derivation of laumontite from any precursor zeolite is not required and that the concept of depth zonation of zeolitic minerals in burial diagenesis, as suggested by Miyashiro and Shido (1970) and others, is not necessarily valid with respect to this mineral. It is interpreted here that laumontite in the sandstones of the Fort Union Formation from the Wagon Wheel well likely formed early in the burial history of the rocks, when primary intergranular porosity was high and temperatures were much less than 90 °C, probably by processes similar to those of the Sespe Hot Springs.

Framboidal pyrite and authigenic chlorite are also associated with laumontite cement (fig. 8D). The formation of framboidal pyrite in sedimentary rocks is reported to occur shortly after burial of the sediment by sulfate-reducing bacteria. (See review by Berner, 1984.) Dispersed, intergranular, framboidal pyrite associated with laumontite in the study area may have precipitated (1) in primary intergranular pores shortly after deposition of the sediment and then later was enclosed within the laumontite cement or (2) in close association with the laumontite from warm hydrothermal fluids. The former interpretation is more likely because in thin sections of several other sandstones, texturally similar framboidal pyrite was observed enclosed by early calcite cement. The pyrite probably acted as a source of iron for the later formation of chlorite clay; in thin section concentrations of chlorite are found within reddish-brown stained areas where pyrite framboids either are concentrated or have been partly or completely dissolved.

Interstratified Chlorite/Smectite (corrensite) in Sandstones

Interstratified chlorite/smectite (C/S), mainly corrensite, is in sandstones between a sampled depth interval from 7,080 to 8,130 ft (2,150–2,480 m) in the Wagon Wheel well. Corrensite in these rocks is thought to have formed, at least in part, by reacting from a precursor chlorite cement. This interpretation of a chlorite precursor is evidenced texturally by a honeycomb morphology,

characteristic of smectite, superimposed on or mixed with an earlier "house of cards" morphology that is characteristic of discrete chlorite (fig. 12D). This interpretation is also supported by the occurrence of early discrete chlorite cements in sandstones of the Fort Union Formation above this interval and the Lance Formation below this interval. Pollastro (1985) reported similar relationships for the evolution of I/S clay in the Wagon Wheel well. Iron for the formation of C/S may have been available during the precipitation and (or) dissolution of iron-bearing calcite; the dissolution of ferromagnesian minerals and pyrite are other possible sources of iron.

The smectite-to-illite reaction may have supplied iron, magnesium, and silica for the formation of discrete chlorite, C/S, and quartz because the conversion from random I/S to short-range-ordered I/S occurred, to a large extent, in this depth interval (Pollastro, 1985; Pollastro and Barker, 1986). Authigenic I/S is also found lining pores and coating grains, but I/S cement is not as pervasive as C/S. Aluminous-rich pore fluids certainly were present because the C/S is always in immediate proximity to, or coexists with, authigenic kaolinite (fig. 8A). Corrensite in the Wagon Wheel core probably formed at temperatures greater than 90 °C, coincident with the change from randomly interstratified I/S ($R=0$) to short-range-ordered I/S ($R=1$) (Pollastro and Barker, 1986). Temperatures of formation for both the formation of C/S and short-range-ordered I/S ($R=1$) are in good agreement with those documented from other studies (Velde, 1972; Hoffman and Hower, 1979; Weaver, 1979).

Alteration of Feldspars to Chert-Chalcedony

Some textural evidence suggests that feldspars were present in sandstones of the Ericson Sandstone and the Lance and Rock Springs Formations in the northern Green River basin. Feldspars probably were replaced by microcrystalline silica, as evidenced by rectangular grains of chert or chalcedony that resemble relic feldspars (figs. 21A, B). Feldspars may have altered directly to chert or chalcedony or, in part, through an intermediate stage after calcite. Recently, Morad and Aldahan (1987) described early diagenetic direct replacement of feldspars by fine-crystalline quartz in Proterozoic sandstones of the Visingso Group in Norway and Sweden. Earlier studies by Wallace (1976), Odom and others (1979), and Heald and Lares (1973) also report the diagenetic replacement of feldspar by quartz. Walker (1962) reported on the reversible nature of chert-calcite replacement in sedimentary rocks and suggested that feldspars may first be replaced by calcite and then the calcite replaced by chert.

Textural and petrographic evidence in this study that supports the interpretation of replacement of feldspars by quartz or at least suggests that feldspars were once present in any of these sandstones includes: (1) the

limited variety of framework grains (mainly quartz and chert) and the absence of feldspar in many Upper Cretaceous fluvial sandstones from these wells; (2) the rectangular outline of many chert grains (many have straight, parallel, opposing sides, a habit characteristic of feldspar) in Upper Cretaceous sandstones from the wells (figs. 21A, B); (3) the orientation of microcrystalline quartz in chert and chalcedony grains along what may be relic feldspar twin lamellae (fig. 21C, D); and (4) textural relationships that suggest direct replacement of feldspar by microcrystalline quartz or chalcedony (figs. 22A, B).

SUMMARY

Lower Tertiary sandstones of the northern Green River basin are rich in feldspars and sedimentary rock fragments and can be generally classified as lithic arkoses. The average feldspar content of these sandstones is about 50 weight percent (as calculated by XRD) in the Fort Union Formation and progressively decreases to less than 10 weight percent in lowermost Tertiary sandstones near the Cretaceous-Tertiary unconformity. Although this progressive reduction in feldspar content in the bulk rock is generally due to a relative decrease in detrital feldspar and increase in silica framework grains, present mineralogical compositions can be partly explained by diagenetic modifications. Feldspar dissolution and an increase in authigenic phases, mostly carbonate and clay-mineral cements and replacement phases, produces a relative decrease in total feldspar content.

Typical clay-mineral suites of lower Tertiary sandstones consist of expandable interstratified illite/smectite, kaolinite, and iron-rich chlorite; interbedded shales are dominated by expandable interstratified illite/smectite and discrete illite clay. The conversion of smectite to illite in interstratified illite/smectite plays a major role, however, in the progressive burial of these clay minerals.

The change from lower Tertiary to Upper Cretaceous rocks in this area is consistent with a decrease in feldspar content. In Tertiary sandstones, plagioclase and potassium feldspar grains, together with quartz, form the major framework. In Upper Cretaceous sandstones, quartz, chert, and detrital carbonate minerals are the major framework grains. Samples of sandstone and shale taken from core recovered above 15,000 ft (4,570 m) in the Wagon Wheel well contain less than 5 weight percent feldspar and typically average 2-3 weight percent. Although this reduction in feldspar content is again mostly due to a change in source material, dissolution and replacement of feldspars by carbonate minerals, silica, and kaolinite contribute to their near disappearance. In samples taken below present-day depths of 16,000 ft (4,900 m) and to about 18,000 ft (5,500 m) in the Wagon

Wheel well, detrital feldspar may comprise as much as 15 weight percent of the sandstone. The excellent preservation of feldspars at these depths is not well understood, but sedimentologic factors may control diagenetic extent.

Upper Cretaceous shales are dominated by interstratified illite/smectite and discrete illite clay. Shales from the Ericson Sandstone, however, are enriched in kaolinite and chlorite relative to most other Upper Cretaceous shales. Chlorite and kaolinite are typically authigenic and are most abundant in sandstones.

The typical early stages of diagenesis involve compaction, framboidal pyrite formation, and precipitation of smectitic clay and quartz overgrowth cements. These earliest stages are followed by partial dissolution of framework grains and cementation by calcite. Iron-bearing calcites replaced earlier iron-free calcites. Dissolution of calcite cements and feldspar, chert and shale grains, coupled with the replacement or precipitation of kaolinite, typically follow in the sequence. The illitization of smectite from earlier expandable-clay cements or in shale clasts is a dynamic diagenetic process with progressive burial. The development of illitic and sericitic overgrowths by precipitation or solution and recrystallization during deep burial is also a prevalent diagenetic process in most of these sandstones. Finally, quartz, dickite, and calcite fill fractures formed late in the burial history of these rocks.

Specific diagenetic events are limited to particular units or intervals. These include the precipitation of the zeolite laumontite and the clay mineral corrensite and the replacement of feldspars by chert or chalcedony. Laumontite in sandstones of the Fort Union Formation from the Wagon Wheel well is interpreted to have formed early at temperatures below 90 °C, whereas corrensite is interpreted to have formed much later in the burial history at temperatures in excess of 90 °C. Early replacement of feldspars by chert or chalcedony is suggested by textural evidence and in some cases may have resulted in changes in sandstone composition.

Ferroan calcite cements become progressively more abundant with increased burial depth in these rocks. The paragenetic relationship of iron-rich calcite cements evolving from iron-free calcite cement in burial sequences has been reported in sandstone cores from the Wagon Wheel well by Dickinson (1984; 1985) and in sandstones from other basins (Boles, 1978; Land and Dutton, 1978; Pitman and others, 1982; Burley and Kantorowicz, 1986). Remnants of iron-free calcites commonly are enclosed by iron-bearing cements. The dissolution and replacement of calcite is consistent in sandstones from all wells and intervals and is evidenced by remnants or relics of iron-free calcite and (or) iron-bearing calcite cements in sandstones containing secondary intergranular pores or replaced by kaolinite cement, by dissolution of detrital limestone grains, and by complete or partial dissolution of calcite

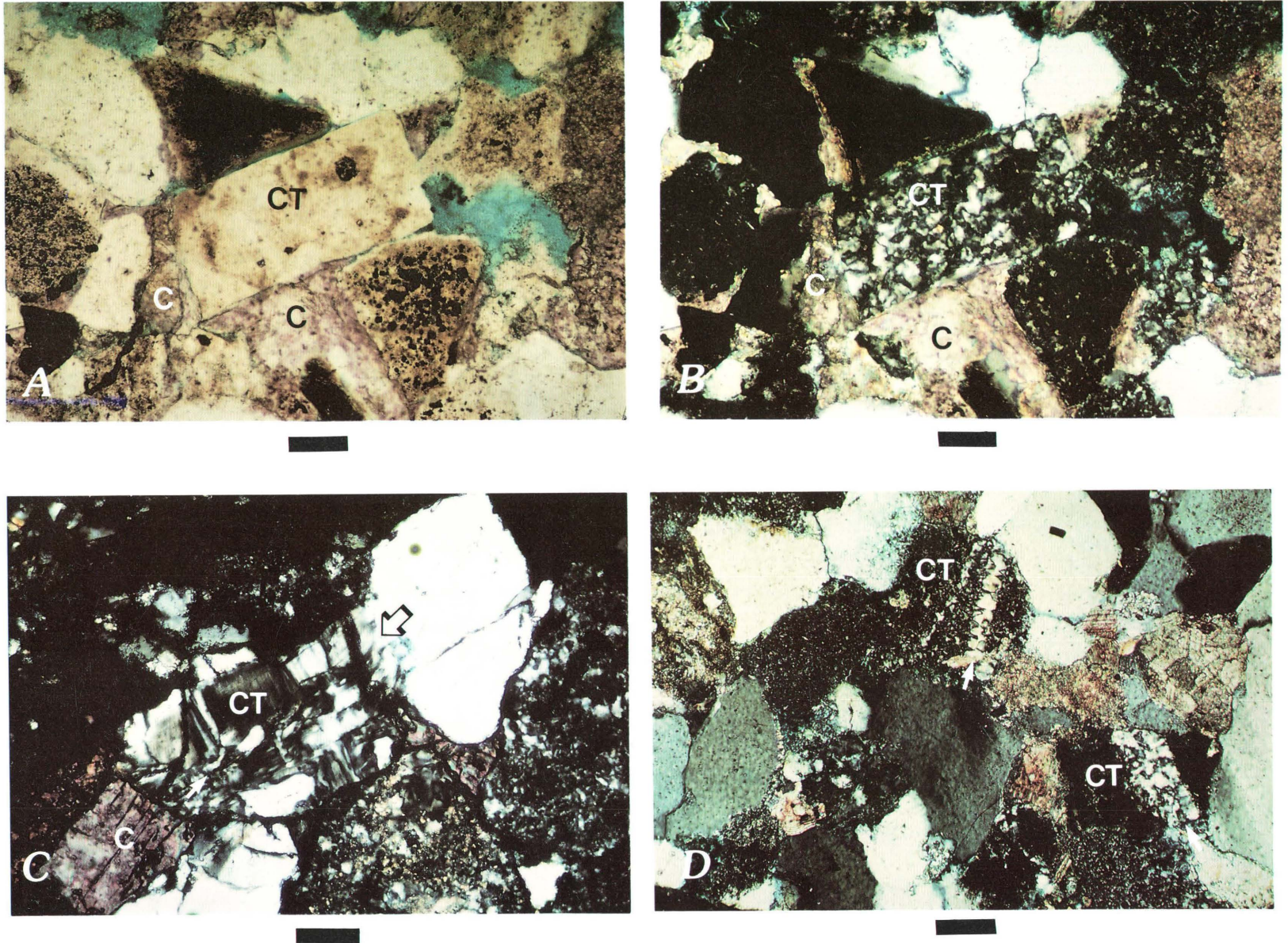


Figure 21. Thin section photomicrographs of relic feldspar grains in sandstones. Scale bars 0.1 mm. *A, B*, Rectangular chert-chalcedony (CT) grain resembling relic feldspar in sandstone partly cemented by calcite (C). *C, D*, Chert-chalcedony (CT) grains with appearance of replacement after feldspar along twin lamellae (small arrows) in sandstone cemented by calcite (C). Note alteration boundary (large arrow) in C (crossed nicols).

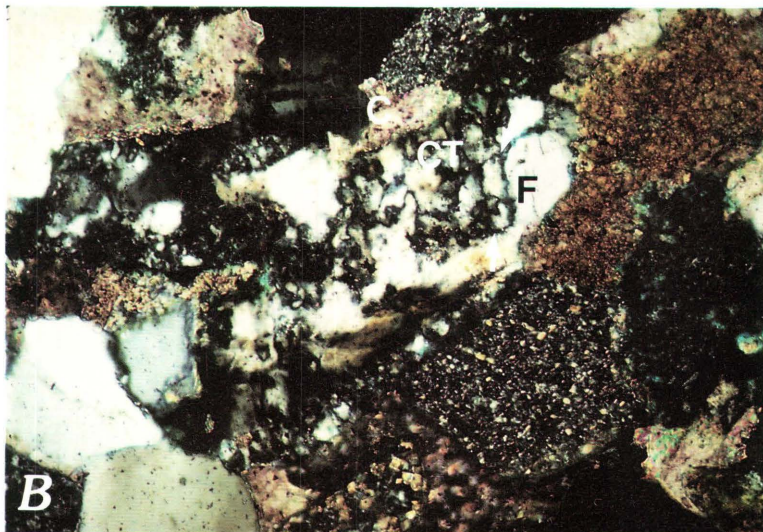


Figure 22. Thin section photomicrographs of feldspar grains being replaced by silica. Scale bars 0.1 mm (crossed nicols). Note alteration boundary (arrows) in both photos. *A*, Feldspar (F) replaced by chert-chalcedony (CT) and calcite (C). Lance Formation, New Fork No. 2 well, 9,238 ft. *B*, Partial replacement of feldspar (F) by chert-chalcedony (CT) and calcite (C). Ericson Sandstone, WASP well, 11,759 ft.

cement in polycrystalline detrital dolomite grains. Ferroan dolomite cements are also common and usually occur as overgrowths on grains of detrital dolomite.

Porosity in these sandstones is mainly secondary and produced by dissolution processes. The dissolution of intergranular calcite cement is probably the most important process in producing secondary porosity in most of these sandstones. Intragranular or moldic porosity may also be extensive but is usually of secondary importance in lithic sandstones. In quartzarenites or very quartz rich

(>80 weight percent quartz) sandstones, however, porosity is mainly moldic. The original intergranular porosity in these quartz-rich sandstones usually is completely destroyed by extensive early quartz cementation. At depth, any porosity in these sandstones is usually intragranular (moldic) and was created by the dissolution of mainly chert grains. For this reason, quartz-rich sandstones containing abundant chert have a high porosity potential; permeabilities in quartzarenites, however, may be much lower than those in lithic sandstones having

mainly intergranular secondary porosity and fewer permeability barriers.

REFERENCES CITED

- Altaner, S., Aronson, J.L., Whitney, C.G., and Hower, J., 1984, Model for K-bentonite formation: evidence from zoned K-bentonite in the Disturbed Belt, Montana: *Geology*, v. 12, p. 312-415.
- Berner, R.A., 1984, Sedimentary pyrite formation: *Geochimica et Cosmochimica Acta*, v. 48, p. 605-615.
- Boles, J.R., 1978, Active ankerite cementation in the subsurface Eocene of southwest Texas: *Contributions to Mineralogy and Petrology*, v. 68, p. 13-22.
- Boles, J.R., and Franks, S.G., 1979, Clay diagenesis in Wilcox sandstones of southwest Texas; implications of smectite diagenesis on sandstone cementation: *Journal of Sedimentary Petrology*, v. 49, p. 55-70.
- Burley, S.D., and Kantorowicz, J.D., 1986, Thin section and S.E.M. textural criteria for the recognition of cement-dissolution porosity in sandstones: *Sedimentology*, v. 33, p. 587-604.
- Burst, J.F., 1969, Diagenesis of Gulf Coast clayey sediments and its possible relation to petroleum migration: *American Association of Petroleum Geologists Bulletin*, v. 53, p. 73-93.
- Crossey, L.J., Frost, B.R., and Surdam, R.C., 1984, Secondary porosity in laumontite-bearing sandstones, *in* McDonald, D.A., and Surdam, R.C., eds., *Clastic diagenesis: American Association of Petroleum Geologists Memoir 37*, p. 225-236.
- Dickinson, W.D., 1984, Isotope geochemistry of carbonate minerals in Upper Cretaceous and Tertiary sandstones from the Pinedale anticline, Wyoming, *in* Law, B.E., ed., *Geological characteristics of low-permeability Upper Cretaceous and lower Tertiary rocks in the Pinedale anticline area, Sublette County, Wyoming: U.S. Geological Survey Open-File Report 84-753*, p. 95-107.
- , 1985, Isotope geochemistry of carbonate minerals in non-marine rocks, northern Green River basin, Wyoming: *U.S. Geological Survey Open-File Report 85-532*, 103 p.
- Dickson, J.A.D., 1966, Carbonate identification and genesis as revealed by staining: *Journal of Sedimentary Petrology*, v. 36, p. 491-505.
- Drever, J., 1973, The preparation of oriented clay mineral specimens for X-ray diffraction analysis by a filter membrane peel technique: *American Mineralogist*, v. 58, p. 395-406.
- Edman, J.D., and Surdam, R.C., 1986, Organic-inorganic interactions as a mechanism for porosity enhancement in the Upper Cretaceous Ericson Sandstone, Green River basin, Wyoming, *in* Gautier, D.L., *Roles of organic matter in sediment diagenesis: Society of Economic Paleontologists and Mineralogists Special Publication 38*, p. 85-109.
- Gautier, D.L., ed., 1986, *Roles of organic matter in sediment diagenesis: Society of Economic Paleontologists and Mineralogists Special Publication 38*, 203 p.
- Gautier, D.L., and Pollastro, R.M., 1982, Petrology and mineralogy in relation to reservoir properties in the EPNG No. 1 Wagon Wheel well, Green River basin, Wyoming [abs.], *in* Steidtmann, J.R., ed., *Subsurface practices in geology and geophysics: Laramie, University of Wyoming, Department of Geology and Geophysics, Earth Science Bulletin 15*, p. 8.
- Ghent, E.D., 1979, Problems in zeolite facies, geothermometry, geobarometry, and fluid compositions, *in* Scholle, P.A., and Schluger, P.R., eds., *Aspects of diagenesis: Society of Economic Paleontologists and Mineralogists Special Publication 26*, p. 81-87.
- Heald, M.T., and Larese, R.E., 1973, The significance of the solution of feldspar in porosity development: *Journal of Sedimentary Petrology*, v. 43, p. 458-460.
- Helmold, K.P., and van de Kamp, P.C., 1984, Diagenetic mineralogy and controls on albitization and laumontite formation in Paleogene arkoses, Santa Ynez Mountains, California, *in* McDonald, D.A., and Surdam, R.C., eds., *Clastic diagenesis: American Association of Petroleum Geologists Memoir 37*, p. 239-276.
- Hoffman, J., 1976, Regional metamorphism and K-Ar dating of clay minerals in Cretaceous sediments of the disturbed belt of Montana: Cleveland, Ohio, Case Western Reserve University, Ph.D. thesis, 266 p.
- Hoffman, J., and Hower, J., 1979, Clay mineral assemblages as low-grade metamorphic geothermometers; application to the thrust faulted disturbed belt of Montana, U.S.A., *in* Scholle, P.A., and Schluger, P.K. eds., *Aspects of diagenesis: Society of Economic Paleontologists and Mineralogists Special Publication 26*, p. 55-79.
- Hower, J., 1981, Shale diagenesis, *in* Longstaffe, F.J., ed., *Clays and the resource geologist: Mineralogical Association of Canada, Short Course Handbook*, v. 6, p. 60-80.
- Hower, J., Eslinger, E., Hower, M., and Perry, E., 1976, The mechanism of burial diagenetic reactions in argillaceous sediments; 1, mineralogical and chemical evidence: *Geological Society of America Bulletin*, v. 87, p. 725-737.
- Keighin, C.W., 1984, Petrographic and selected reservoir characteristics of some Tertiary and Cretaceous sandstones, Pinedale anticline, Sublette County, Wyoming, *in* Law, B.E., eds., *Geological characteristics of low-permeability Upper Cretaceous and lower Tertiary rocks in the Pinedale anticline area, Sublette County, Wyoming: U.S. Geological Survey Open-File Report 84-753*, p. 16-21.
- Land, L.S., and Dutton, S.P., 1978, Cementation of a Pennsylvanian deltaic sandstone, isotopic data: *Journal of Sedimentary Petrology*, v. 48, p. 1167-1176.
- Law, B.E., 1979, Section B-B'; subsurface and surface correlations of some Upper Cretaceous and Tertiary rocks, northern Green River basin, Wyoming: *U.S. Geological Survey Open-File Report 79-1689*, 2 sheets.
- , 1984a, Structure and stratigraphy of the Pinedale anticline, Wyoming, *in* Law, B.E., ed., *Geological characteristics of low-permeability Upper Cretaceous and lower Tertiary rocks in the Pinedale anticline area, Sublette County, Wyoming: U.S. Geological Survey Open-File Report 84-753*, p. 6-16.

- _____. 1984b, Relationships of source-rock, thermal maturity, and overpressuring to gas generation and occurrence in low-permeability Upper Cretaceous and lower Tertiary rocks, Greater Green River basin, Wyoming, Colorado, and Utah, *in* Woodward, Jane, Meissner, F., and Clayton, J., eds., Symposium on hydrocarbon source rocks of the greater Rocky Mountain region: Rocky Mountain Association of Geologists, p. 469-490.
- Law, B.E., and Nichols, D., 1982, Subsurface stratigraphic correlations of some Upper Cretaceous and lower Tertiary rocks, northern Green River basin, Wyoming [abs.], *in* Steidtmann, J.R., ed., Subsurface practices in geology and geophysics: Laramie, University of Wyoming, Department of Geology and Geophysics, Earth Science Bulletin 15, p. 17.
- Law, B.E., Pollastro, R.M., and Keighin, C.W., 1986, Geologic characteristics of low-permeability gas reservoirs in selected wells, greater Green River basin, Wyoming, Colorado, and Utah, *in* Spencer, C.W., and Mast, R.F., Geology of tight gas reservoirs: American Association of Petroleum Geologists Studies in Geology 24, p. 253-269.
- Longstaffe, F.J., ed., 1981, Clays and the resource geologist: Mineralogical Association of Canada, Short Course Handbook, v. 6, 199 p.
- Martin, W. B., and Shaughnessy, J., 1969, Project Wagon Wheel: Wyoming Geological Association Symposium on Tertiary Rocks of Wyoming, 21st Field Conference, Guidebook, p. 145-152.
- McCulloh, T.H., Frizzel, B.A., Jr., Stewart, R.J., and Barnes, I., 1981, Precipitation of laumontite with quartz, thenardite, and gypsum at Sespe Hot Springs, Western Transverse Ranges, California: Clays and Clay Minerals, v. 29, p. 353-364.
- McDonald, D.A., and Surdam, R.C., eds., 1984, Clastic diagenesis: American Association of Petroleum Geologists Memoir 37, 434 p.
- Millikan, K.L., Land, L.S., and Loucks, R.G., 1981, History of burial diagenesis determined from isotopic geochemistry, Frio Formation, Brazoria County, Texas: American Association of Petroleum Geologists Bulletin, v. 65, p. 1397-1413.
- Miyashiro, A., and Shido, F., 1970, Progressive metamorphism in zeolite assemblages: Lithos, v. 3, p. 251-260.
- Morad, S., and Aldahan, A.A., 1987, Diagenetic replacement of feldspars by quartz in sandstones: Journal of Sedimentary Petrology, v. 57, p. 488-493.
- Nadeau, P.H., Wilson, M.J., McHardy, W.J., and Tait, J.M., 1984, Interparticle diffraction; a new concept for interstratified clays: Clay Minerals, v. 19, 757-769.
- Naeser, N.D., 1986, Neogene thermal history of the northern Green River basin, Wyoming; evidence from fission-track dating, *in* Gautier, D.L., ed., Roles of organic matter in sediment diagenesis: Society of Economic Paleontologists and Mineralogists Special Publication 38, p. 65-72.
- Odom, I.E., Willand, T.N., and Lassin, R.J., 1979, Paragenesis of diagenetic minerals in the St. Peter sandstone (Ordovician), Wisconsin and Illinois, *in* Scholle, P.A., and Schluger, P.R., eds., Aspects of diagenesis: Society of Economic Paleontologists and Mineralogists Special Publication 26, p. 425-443.
- Perry, E.A., and Hower, J., 1970, Burial diagenesis of Gulf Coast pelitic sediments: Clays and Clay Minerals, v. 18, p. 165-177.
- Pitman, J.K., Fouch, T.D., and Goldhaber, M.B., 1982, Depositional setting and diagenetic evolution of Tertiary unconventional reservoir rocks, Uinta basin, Utah: American Association of Petroleum Geologists Bulletin, v. 66, p. 1581-1596.
- Pollastro, R.M., 1977, A reconnaissance analysis of the clay mineralogy and major element geochemistry in the Silurian and Devonian carbonates of western New York; a vertical profile: State University of New York at Buffalo, M.A. thesis, 120 p.
- _____. 1982, A recommended procedure for the preparation of oriented clay-mineral specimens for X-ray diffraction analysis; modifications to Drever's filter-membrane-peel technique: U.S. Geological Survey Open-File Report 82-71, 10 p.
- _____. 1984, Mineralogy of selected sandstone/shale pairs and sandstones from the Multiwell Experiment; interpretations from X-ray diffraction and scanning electron microscopy analyses, *in* Spencer, C.W., and Keighin, C.W., eds., Geologic studies in support of the U.S. Department of Energy Multiwell Experiment, Garfield County, Colorado: U.S. Geological Survey Open-File Report 84-757, p. 67-74.
- _____. 1985, Mineralogical and morphological evidence for the formation of illite at the expense of illite/smectite: Clays and Clay Minerals, v. 33, p. 265-274.
- Pollastro, R.M., and Barker, C.E., 1986, Application of clay-mineral, vitrinite reflectance, and fluid inclusion studies to the thermal and burial history of the Pinedale anticline, Green River basin, Wyoming, *in* Gautier, D.L., ed., Roles of organic matter in sediment diagenesis: Society of Economic Paleontologists and Mineralogists Special Publication 38, p. 73-83.
- Prensky, S.E., 1984, A gamma-ray log anomaly associated with the Cretaceous-Tertiary boundary in the northern Green River basin, Wyoming, *in* Law, B.E., ed., Geologic characteristics of low-permeability Upper Cretaceous and lower Tertiary rocks in the Pinedale anticline area, Sublette County, Wyoming: U.S. Geological Survey Open-File Report 84-753, p. 22-35.
- Reynolds, R.C., Jr., 1980, Interstratified clay minerals, *in* Brindley, G. W., and Brown, G., eds., Crystal structure of clay minerals and their X-ray identification: Mineralogical Society of London, p. 247-303.
- Reynolds, R.C., Jr., and J. Hower, 1970, The nature of interlayering in mixed-layer illite-montmorillonite: Clays and Clay Minerals, v. 18, p. 25-36.
- Ritzma, H.R., 1965, Fossil zone at base of Paleocene rocks, southern Rock Springs uplift, Wyoming: Wyoming Geological Survey Annual Field Conference, 19th, Guidebook, p. 137-139.
- Roehler, H.W., 1961, The late Cretaceous-Tertiary boundary in the Rock Springs uplift, Sweetwater County, Wyoming: Wyoming Geological Association Annual Field Conference, 16th, Guidebook, p. 96-100.
- Scholle, P.A., and Schluger, P.A., eds., 1979, Aspects of diagenesis: Society of Economic Paleontologists and Mineralogists Special Publication 26, 443 p.

- Schultz, L.G., 1964, Quantitative interpretation of mineralogical composition from X-ray and chemical data for the Pierre Shale: U.S. Geological Survey Professional Paper 391-C, 31 p.
- _____, 1978a, Sample packer for randomly oriented powders in X-ray diffraction analysis: *Journal of Sedimentary Petrology*, v. 48, p. 627-629.
- _____, 1978b, Mixed-layer clay in the Pierre Shale and equivalent rocks, northern Great Plains region: U.S. Geological Survey Professional Paper 1064-A, 28 p.
- Schuster, M.W., 1986, The origin and sedimentary evolution of the northern Green River basin, western Wyoming: Laramie, University of Wyoming, Ph.D. thesis, 323 p.
- Schuster, M.W., and Steidtmann, J.R., 1983, Origin and development of northern Green River basin; a stratigraphic and flexural study: *American Association of Petroleum Geologist Bulletin*, v. 67, p. 1356.
- Shaughnessy, J., and Butcher, R.H., 1973, Geology of Project Wagon Wheel Nuclear Stimulation Project, *in* Fassett, J.E., ed., *Cretaceous and Tertiary rocks of the southern Colorado Plateau: Durango, Colo.*, Four Corners Geological Society, p. 185-196.
- _____, 1974, Geology of Wagon Wheel Nuclear Stimulation Project, Pinedale field, Wyoming: *American Association of Petroleum Geologists Bulletin*, v. 58, p. 2250-2259.
- Velde, B., 1972, Phase equilibria for dioctahedral expandable phases in sediments and sedimentary rocks: *International Clay Conference, Madrid, Spain, 1972, Proceedings; National Research Council of Spain*, p. 235-248.
- Walker, T.R., 1962, Reversible nature of chert-carbonate replacement in sedimentary rocks: *Geological Society of America Bulletin*, v. 73, p. 237-242.
- Wallace, C.A., 1976, Diagenetic replacement of feldspar by quartz in the Uinta Mountain Group, Utah and its geochemical implications: *Journal of Sedimentary Petrology*, v. 46, p. 847-861.
- Weaver, C.E., 1979, Geothermal alteration of clay minerals and shales: Office of Nuclear Waste Isolation, Technical Report 21, 176 p.
- Weaver, C.E., and Beck, K.C., 1971, Clay water diagenesis during burial; how mud becomes gneiss: *Geological Society of America Special Paper* 134, 96 p.

Chapter E

Thermal History and Provenance of Rocks in the Wagon Wheel No. 1 Well, Pinedale Anticline, Northern Green River Basin—Evidence from Fission-Track Dating

By NANCY D. NAESER

Prepared in cooperation with the U.S. Department of Energy

U.S. GEOLOGICAL SURVEY BULLETIN 1886

GEOLOGY OF TIGHT GAS RESERVOIRS IN THE PINEDALE ANTICLINE AREA, WYOMING,
AND AT THE MULTIWELL EXPERIMENT SITE, COLORADO

CONTENTS

Abstract	E1
Introduction	E1
The fission-track method	E2
Annealing of fission tracks	E2
Application to sedimentary basins	E3
Thermal history	E3
Provenance studies	E5
Methods	E6
Laboratory procedures	E6
Present-day temperatures in the Wagon Wheel No. 1 well	E8
Fission-track data	E8
Apatite ages	E8
Zircon ages	E9
Thermal history	E9
Provenance of the sediments	E10
Conclusions	E11
References cited	E11

FIGURES

1. Map showing structural features of the Green River basin E2
- 2-6. Diagrams showing:
 2. Temperatures required to anneal fission tracks in apatite E4
 3. Expected decrease in apparent apatite age with increasing temperature and depth at time of maximum burial heating E5
 4. Expected distribution of apparent apatite ages in sedimentary rocks after uplift and (or) cooling E5
 5. Depth and present-day temperature of samples for fission-track studies from Wagon Wheel No. 1 well E6
 6. Fission-track ages and corrected present-day temperatures for detrital apatite and zircon from Wagon Wheel No. 1 well E7
7. Histograms of fission-track ages of zircon grains in six samples from the Wagon Wheel No. 1 well E9

TABLES

1. Depth, stratigraphic position, and present-day temperature of samples from Wagon Wheel No. 1 well, northern Green River basin, Wyoming E7
2. Apatite and zircon fission-track ages, Wagon Wheel No. 1 well, northern Green River basin, Wyoming E8

Thermal History and Provenance of Rocks in the Wagon Wheel No. 1 Well, Pinedale Anticline, Northern Green River Basin—Evidence From Fission-Track Dating

By Nancy D. Naeser

Abstract

Fission-track ages of detrital apatite from Upper Cretaceous and lower Tertiary sedimentary rocks in the El Paso Natural Gas Wagon Wheel No. 1 well in the northern Green River basin of Wyoming indicate that the rocks have undergone significant cooling. Apatite data suggest that the latest phase of cooling began about 4–2 Ma and involved a relatively rapid temperature decrease of at least 20 °C. The timing of this cooling is consistent with evidence for a period of widespread uplift and erosion in the Green River basin beginning in the Pliocene.

Zircon fission-track data suggest that most of the Upper Cretaceous and lowermost Paleocene rocks in the well had a similar provenance. A significant change in provenance occurs within Paleocene rocks and probably coincided with exposure and erosion of the crystalline core of the Wind River Mountains to the northeast.

INTRODUCTION

In the present study, the thermal history and provenance of rocks in the northern Green River basin of Wyoming are interpreted by using fission-track ages of detrital apatite and zircon separated from core from the El Paso Natural Gas Wagon Wheel No. 1 well (fig. 1). The well was drilled to a depth of 19,000 ft (5,791 m) into the Upper Cretaceous Hilliard Shale and is the deepest well on the Pinedale anticline. The well penetrated about 11,500 ft (3,505 m) of Upper Cretaceous rocks from the Lance Formation to the Hilliard Shale. All but the lowermost 1,600 ft (488 m), including all of the rocks sampled for this study, were deposited in nonmarine environments in an eastward-prograding wedge of siliciclastic rocks derived primarily from western source terranes. By latest Cretaceous-early Tertiary time, deposition in the Pinedale area was more complex in that structural uplift on the basin margins provided multiple

source terranes for the dominantly fluvial sediments. Since Eocene time, there has been no net deposition in the northern Green River basin (Rice and Gautier, 1983; Shuster and Steidtmann, 1983; Law, 1984a, b; Pollastro and Barker, 1984a, 1986; Dickinson and Law, 1985; Law and others, 1986; Dickinson, this volume; Law and Johnson, this volume; Pollastro, this volume).

The Pinedale anticline trends northwest; it is about 35 mi (56 km) long and 6 mi (10 km) wide and has structural relief of about 2,000 ft (610 m). Its structural evolution is most likely related to movement on the Wind River thrust fault, which is parallel with and to the northeast of the anticline (fig. 1). Growth of the anticline may have begun as early as 90 Ma (Shuster, 1986), but the main period of structural deformation probably occurred during Laramide deformation (Law and Johnson, this volume).

Several lines of evidence, which will be reviewed later, suggest that rocks in the Wagon Wheel well have cooled below their maximum paleotemperature. The fission-track study was undertaken to help clarify the cooling history, to provide input to paleopressure studies (Law, 1984c; Spencer, this volume), and to study the provenance of the rocks encountered in the well.

Acknowledgments.—This research was done in cooperation with the U.S. Department of Energy Morgantown Energy Technology Center and with B.E. Law, U.S. Geological Survey. It was supported in part by the U.S. Geological Survey Evolution of Sedimentary Basins Program.

I thank R.A. Ullrich of the El Paso Natural Gas Company and B.E. Law for providing samples from the Wagon Wheel well; L.R. Mahrt and J.R. Shannon, U.S. Geological Survey, for performing mineral separations; and T.H. McCulloh, Mobil Exploration and Producing Services, for providing corrected present-day temperatures of the samples.

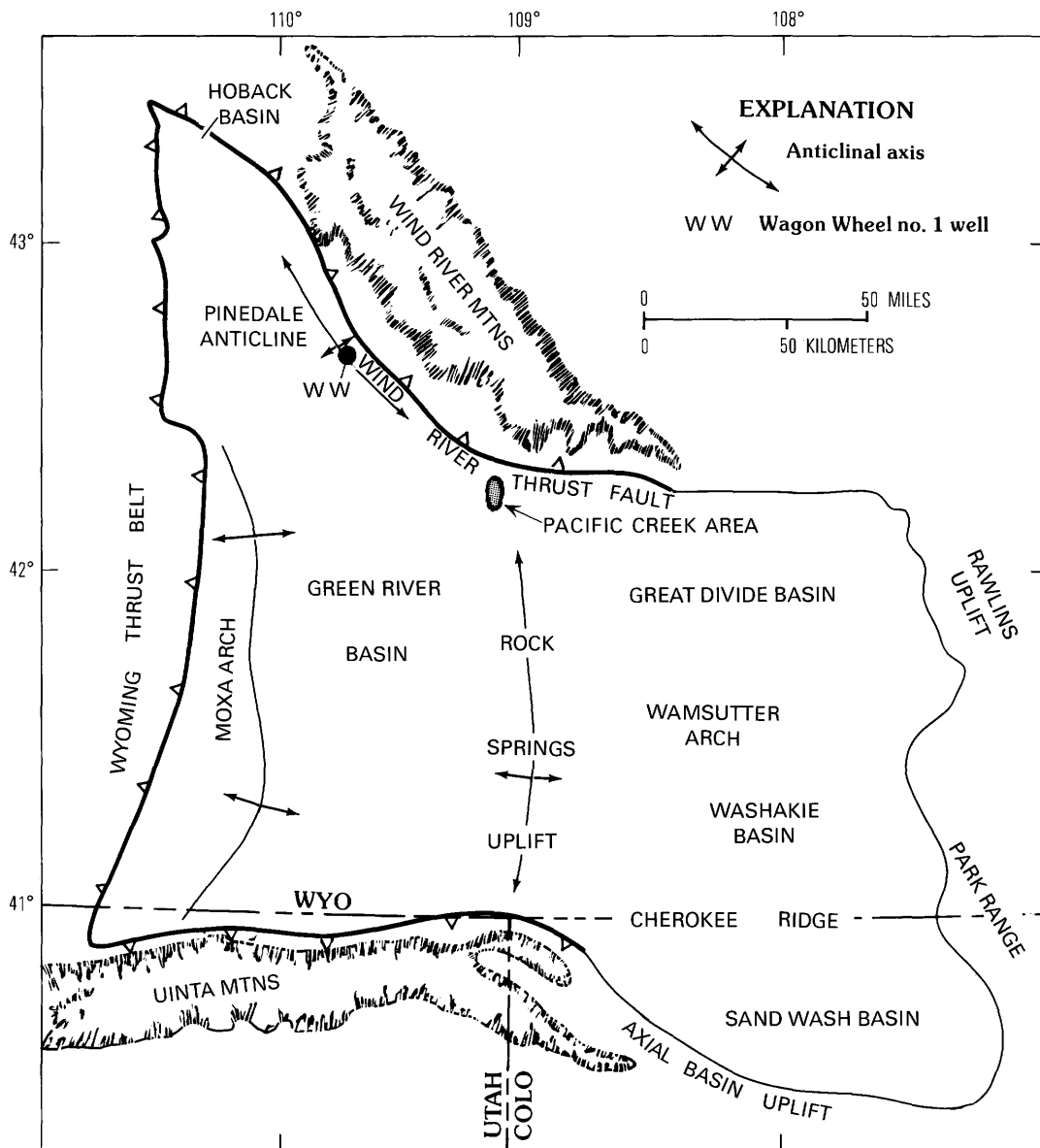


Figure 1. Structural features of the Green River basin, northern Wyoming. Location of El Paso Natural Gas Company Wagon Wheel No. 1 well (WW) also shown. Modified from Law (1984a).

THE FISSION-TRACK METHOD

A fission track is the zone of intense damage that forms when a fission fragment travels through a solid. Several naturally occurring isotopes fission spontaneously, but only ^{238}U has a fission half-life (9.9×10^{15} yr) sufficiently short to produce significant numbers of spontaneous tracks during a time period of geologic interest.

Trace amounts of uranium are in a number of common minerals, and, because ^{238}U fissions spontaneously at a constant rate, fission tracks can be used to date these minerals. The age of a mineral is calculated by determining the number of spontaneous tracks intersecting a polished surface of the mineral and the amount of

uranium that produced those tracks (Naeser, 1976, 1979a; Naeser and others, 1989). The two minerals most commonly dated by the fission-track method are apatite and zircon.

Annealing of Fission Tracks

If a mineral containing spontaneous fission tracks is heated to a sufficiently high temperature, the ions displaced along the damage zone of the track move back to normal crystallographic positions in the mineral and the zone is partly to totally repaired. The repair of the damage zone results in the progressive shortening and

ultimate disappearance of the fission track. The reduction in the number of spontaneous tracks produces an anomalously young fission-track age, as compared, for example, to fission-track ages determined for unannealed minerals or to biotite potassium-argon (K-Ar) ages for the same sample.

The two most important factors controlling the temperature at which annealing of fission tracks occurs are the mineral involved—different minerals anneal at different temperatures—and the duration of heating—the longer a mineral is heated, the lower the temperature required to totally anneal its tracks. Temperature-time relationships that are probably most applicable to geologic problems have been obtained by determining the temperatures at which minerals are totally annealed (that is, yield a zero age) in drill holes in areas where the approximate duration of heating of the rocks is known. The most complete drill-hole data available are for apatite, and studies by Naeser (1981) indicate that total annealing of fission tracks in apatite occurs at temperatures that range from about 105 °C for long-term heating over a period of about 10^8 years duration to 150 °C for heating over a period of 10^5 years (fig. 2).

Drill-hole data predict slightly longer heating times for any given temperature than do data extrapolated from laboratory annealing experiments (fig. 2). Laboratory data do not take into account the number of new tracks that form during long-term geologic annealing (Sanford, 1981). In addition, laboratory data are based on essentially square-pulse heating and thus may underestimate heating time for most geologic annealing. On the other hand, heating times are commonly difficult to estimate for drill-hole samples, and the times used in drill-hole calibrations may be too long (Harrison, 1985); if so, the actual “effective” heating times (Hood and others, 1975) applicable to most long-term geologic annealing probably are intermediate between the times indicated by the drill-hole data and those indicated by the extrapolated laboratory data (fig. 2).

The temperatures at which fission tracks in zircon are totally annealed are not as well known as those for apatite. Limited data show that temperatures are higher than for apatite and are probably in the range of 160–240 °C for heating over periods of geologic time (>1 million years) (Harrison and others, 1979; Hurford, 1985; cf. Zeitler, 1985).

APPLICATION TO SEDIMENTARY BASINS

Fission tracks in apatite and zircon have been used in a variety of studies in basin analysis (Naeser and others, 1989). The widespread occurrence of apatite and zircon in the detrital suites of sedimentary rocks and the close correspondence between apatite and zircon annealing

temperatures and the temperatures at which oil is generated (Hood and others, 1975; Waples, 1980; Naeser and others, 1989) make fission-track analysis an attractive method for studying the overall thermal history and more localized temperature anomalies in sedimentary basins. Thermal history information is most often provided by apatite because most of the rocks sampled in sedimentary basins have not been subjected to temperatures sufficient to anneal zircon. The presence of unannealed zircons sets some limits, however, on maximum paleotemperatures, and the ages of the individual unannealed zircon grains can be used to determine the provenance of sedimentary rocks and to date marker horizons such as volcanic ashes within sedimentary sequences.

Thermal History

Naeser (1979b) first suggested that fission-track annealing could be used to study the thermal history of a sedimentary basin and described the expected trend of fission-track ages with depth in sedimentary rocks. This trend typically is somewhat more complicated than that for basement rocks because the grains that comprise sedimentary rocks can be of widely differing ages. The grains may be equal in age to the stratigraphic age of the rock, as in the case of grains derived from contemporaneous volcanism, but much more commonly the grains will be older.

Figures 3 and 4 illustrate relationships between depth and age for sedimentary sequences that are at their maximum burial temperature or have cooled below maximum paleotemperature. In a sedimentary sequence at maximum temperature (fig. 3), fission-track ages for apatites from shallow rocks at relatively low temperatures will not have been affected by annealing during burial of the sediments (zone of no annealing), and the ages of individual apatite grains in these rocks will reflect the age(s) of the source rocks for the detrital grains. The composite apatite age (see later discussion) calculated for each individual sample in this zone may remain relatively constant with depth (as depicted in fig. 3) but more commonly will vary somewhat depending on the age(s) of the detrital grains counted in a given sample. In rock subjected to progressively higher temperatures as a result of deeper burial, apatite will undergo partial annealing and yield progressively younger ages (zone of partial annealing). Within this zone, the apparent apatite ages will become younger than the stratigraphic age of the rock and will finally decrease to zero at the depth where the temperature for total annealing is attained for a sufficient time (zone of total annealing).

Drill-hole annealing data and extrapolated laboratory data (fig. 2) suggest that, for heating durations on the order of 10^5 to 10^8 years, the zone of

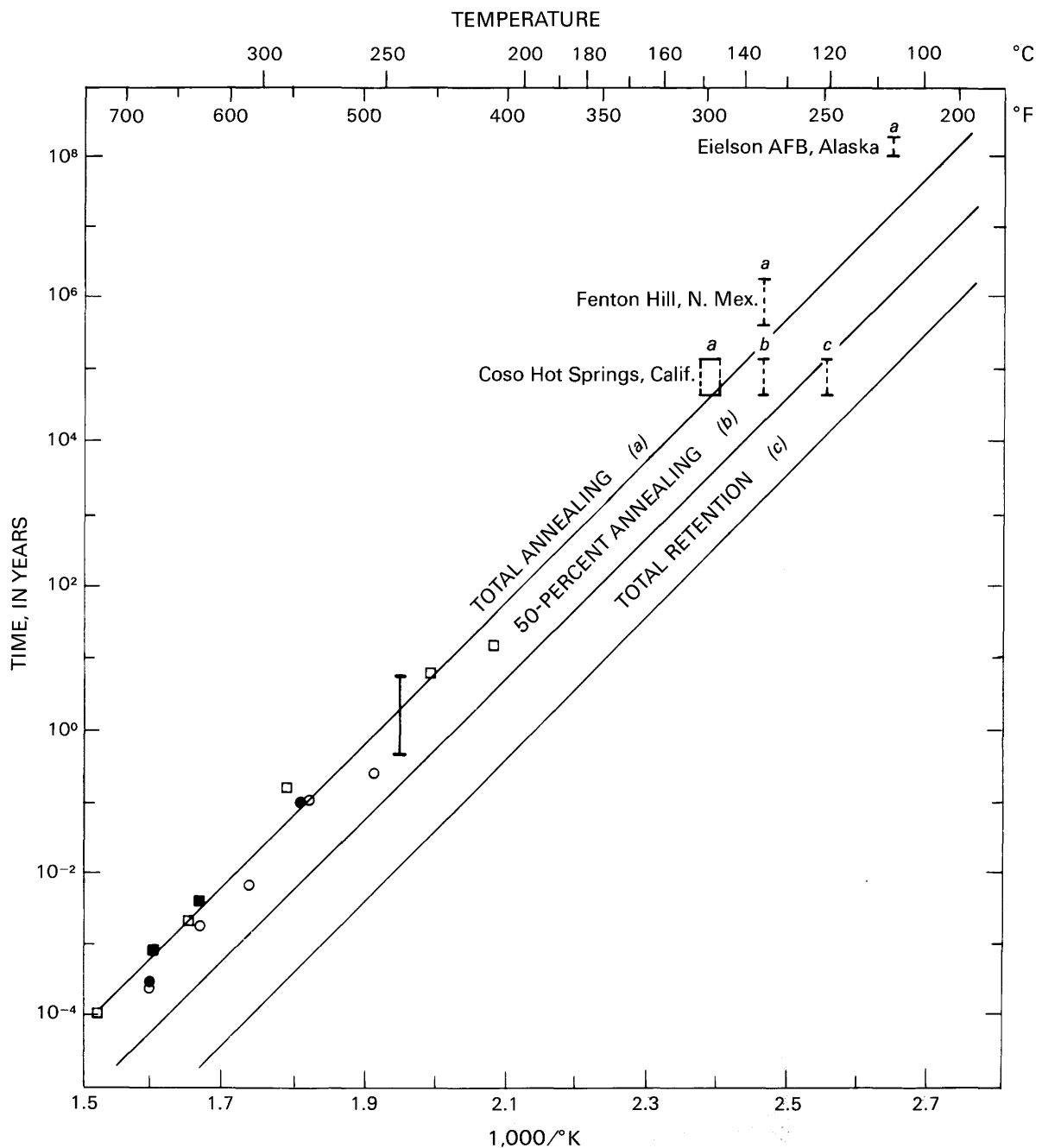


Figure 2. Temperatures required to anneal fission tracks in apatite for short (laboratory experiments) to very long (geologic) heating periods. Temperatures for geologic annealing (dashed vertical bars) (Naeser, 1981) were determined by dating apatite from drill holes in three areas where approximate duration of heating is known. Total annealing temperatures predicted by laboratory experiments were determined by using fading rates established by Naeser and Faul (1969) (open circles), Reimer (1972) (solid circles), Märk and others (1973)

(open squares), and Zimmermann and Gaines (1978) (solid squares). Extrapolation of laboratory data (solid lines) based on rate constant for fission-track annealing determined from least-squares fit of laboratory data by Zimmermann and Gaines (1978). Solid vertical bar represents 95-percent confidence interval for least-squares fit. *a*, *b*, and *c* on solid lines and dashed vertical bars identify data for total annealing (*a*), 50 percent annealing (*b*), and total retention (*c*) of fission tracks. Modified from Sanford (1981, fig. 2).

partial annealing for apatite spans a temperature interval of only 30–35 °C. It must be emphasized that the actual temperatures covered by this zone depend, as does

the temperature for total annealing, on the duration of heating. At a temperature of 105 °C, for example, apatite heated for 10⁸ years will be totally annealed, but apatite

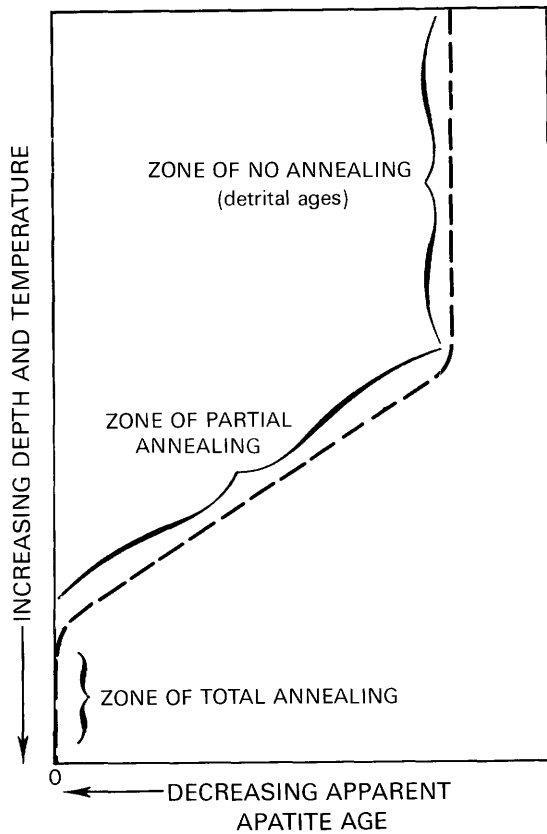


Figure 3. Expected decrease in apparent apatite age with increasing temperature and depth in sedimentary sequence at time of maximum burial heating. Temperature at which apatite age decreases to zero depends on length of time rock has been heated near its present-day temperature (see fig. 2). Drill-hole and extrapolated laboratory data (fig. 2) indicate annealing occurs over 30–35 °C temperature interval. Modified from Naeser (1979b).

heated for only 10^5 years will show little or no age reduction as a result of annealing.

When a sedimentary sequence cools below the maximum paleotemperature, in response to either uplift and erosion or a decrease in the geothermal gradient, apatite from the zone of total annealing will once again begin to accumulate tracks and to record a fission-track age (fig. 4). The recorded apatite age, the slope of the temperature-age plot, and the thickness of the zone of cooling ages give information on the time, rate, and amount of cooling, respectively.

Zircon fission-track ages should generate curves similar to those shown in figures 3 and 4, but annealing will occur at higher temperatures than in apatite.

Research on apatites from the Otway Basin, Australia, and other areas shows that the reduction in mean track length and change in track length distribution that produce the observed age decrease with progressive annealing can in themselves provide important

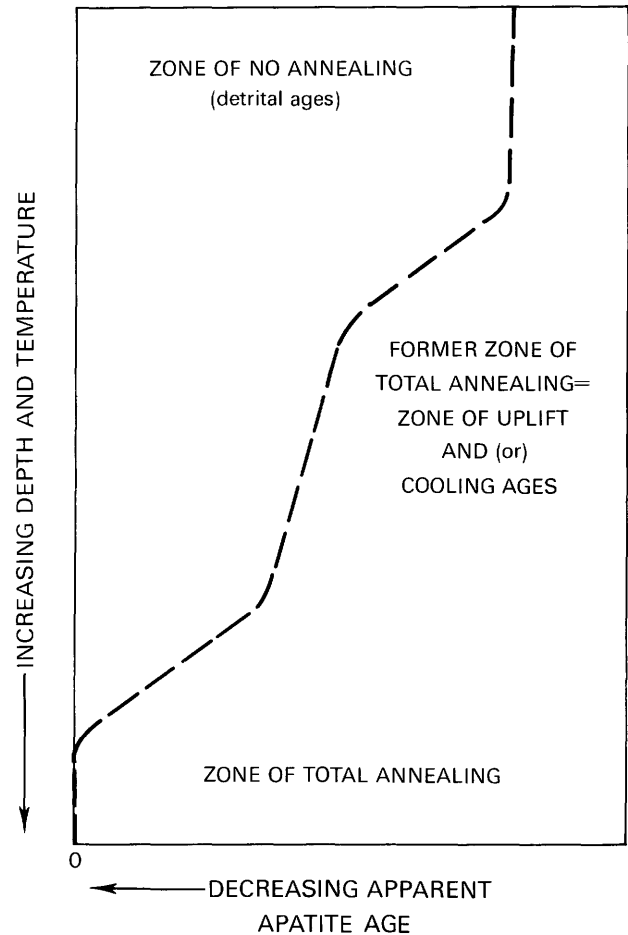


Figure 4. Expected distribution of apparent apatite ages in sedimentary rocks after uplift and (or) cooling. Modified from Naeser (1979b).

information about thermal history (Duddy and Gleadow, 1982; Gleadow and others, 1983; Gleadow, Duddy, Green, and Hegarty, 1986; Gleadow, Duddy, Green, and Lovering, 1986; Green and others, 1989). If a reasonably complete age profile cannot be obtained through a sedimentary sequence or if the ages alone are ambiguous, length measurements can often provide valuable insight into the thermal history. Track-length measurements may not be possible or practical in young or low-uranium apatite having low spontaneous track density, and this problem is compounded in rocks having a low yield of apatite. Samples from the Wagon Wheel well exemplify rocks in which apatite track-length measurements are not possible or practical.

Provenance Studies

In sedimentary rocks in which zircon has been unaffected by postdepositional annealing of fission tracks, the ages of the individual zircon grains provide much

information about the parent rocks of the sediments. Within a detrital grain suite, for example, it may be possible to correlate individual age populations to probable parent rocks in order to delineate sediment transport patterns in a basin (Zeitler and others, 1982, 1986; Hurford and others, 1984; Johnson, 1984; Baldwin and Harrison, 1985; Yim and others, 1985; Baldwin and others, 1986). Changes in the zircon suite through time can be used to reconstruct changes in the sedimentation pattern, to define different source areas, and to reconstruct the uplift and erosion history of the parent rocks (Zeitler and others, 1982, 1986; Cervený, 1986; Cervený and others, 1988).

METHODS

Laboratory Procedures

Samples for fission-track analysis were taken from 12 sandstone core samples recovered from the Wagon Wheel No. 1 well between depths of about 5,038 and 16,090 ft (1,536–4,904 m), from rocks of the lower Tertiary Fort Union Formation to the Upper Cretaceous Rock Springs Formation (figs. 5, 6, table 1).

The amount of core available for processing varied from 64 to 195 g. Apatite and (or) zircon were separated from the samples by using heavy liquid and magnetic separation techniques (Naeser, 1986, fig. 5). Grains coarser than about 74 μm (200 mesh; very fine sand size) can be dated by using the fission-track method. Samples from the Wagon Wheel well were sieved to 74 to 180 μm or 74 to 850 μm (+200 to -80, or +200 to -20 mesh) size fractions before they were treated with heavy liquids. This entire fraction was used when possible, but in several samples only the 74 to 125 μm (+200 to -115 mesh) size fraction yielded a sufficiently pure separation (greater than 80 percent apatite or zircon) for dating. In most samples, the fraction lighter than methylene iodide required further treatment with a bromoform-methylene iodide mix (sp gr = 3.037) and with handpicking in order to improve the segregation of apatite from contaminating grains. In most samples from the Wagon Wheel well, zircon is more abundant than apatite. The apatite yield varied from less than 50 to about 200 grains, many of which were not suitable for fission-track analysis.

Both apatite and zircon were dated by using the external detector method; a low-uranium-content muscovite was used as the detector, and samples were counted at $\times 1500$ magnification using a $\times 100$ oil immersion lens (Naeser, 1976, 1979a; Naeser and others, 1989). Thermal neutron fluence was determined from a calibrated muscovite detector covering a glass dosimeter¹ placed at the top and bottom of each irradiation tube. The fluences were calibrated against the copper value determined by

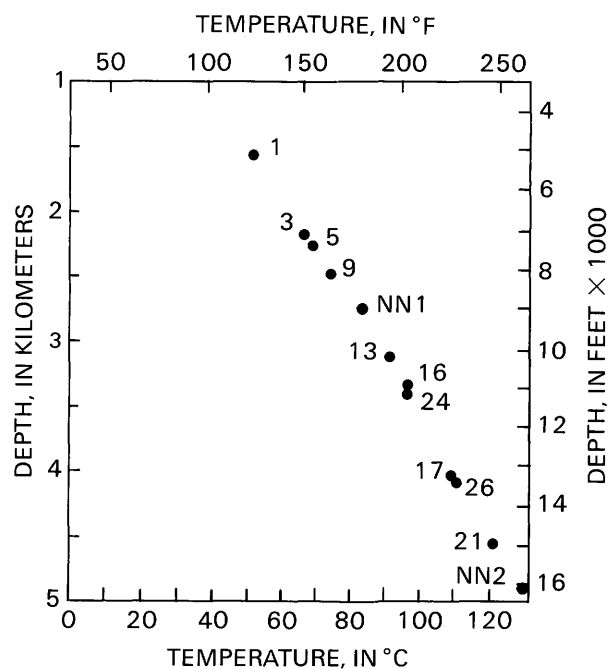


Figure 5. Depth and present-day temperature (corrected) of samples for fission-track studies from Wagon Wheel No. 1 well. Sample information in table 1; sample numbers without alphabetic prefix, WWH.

the National Bureau of Standards (Carpenter and Reimer, 1974), and the fluence for each sample was calculated by interpolation between the values determined for the standards. This method of fluence determination, if used in conjunction with a fission-decay constant of $7.03 \times 10^{-17} \text{ yr}^{-1}$ (Roberts and others, 1968) and with laboratory procedures followed in the U.S. Geological Survey fission-track laboratory, consistently yields fission-track ages that are concordant with K-Ar ages of coexisting phases in rapidly cooled (volcanic and hypabyssal) rocks (Naeser and others, 1977).

The apatite and zircon fission-track ages for each of the Wagon Wheel samples (table 2, fig. 6) were calculated by using the sums of the spontaneous and induced tracks counted in the individual grains in the sample to calculate the values for spontaneous track density (ρ_s) and induced track density (ρ_i), respectively, in the fission-track age equation (Price and Walker, 1963; Naeser, 1967). The uncertainty in the age was calculated by combining the Poisson errors on the spontaneous and induced track counts and on the track counts in the detector covering the dosimeter (Lindsey and others, 1975; McGee and others, 1985). These methods are commonly

¹Zircon, National Bureau of Standards (NBS) glass standard SRM 962, 37.38 ± 0.08 ppm uranium; apatite, NBS glass standard SRM 963, 0.823 ± 0.002 ppm uranium, or USGS glass standard calibrated against SRM 963.

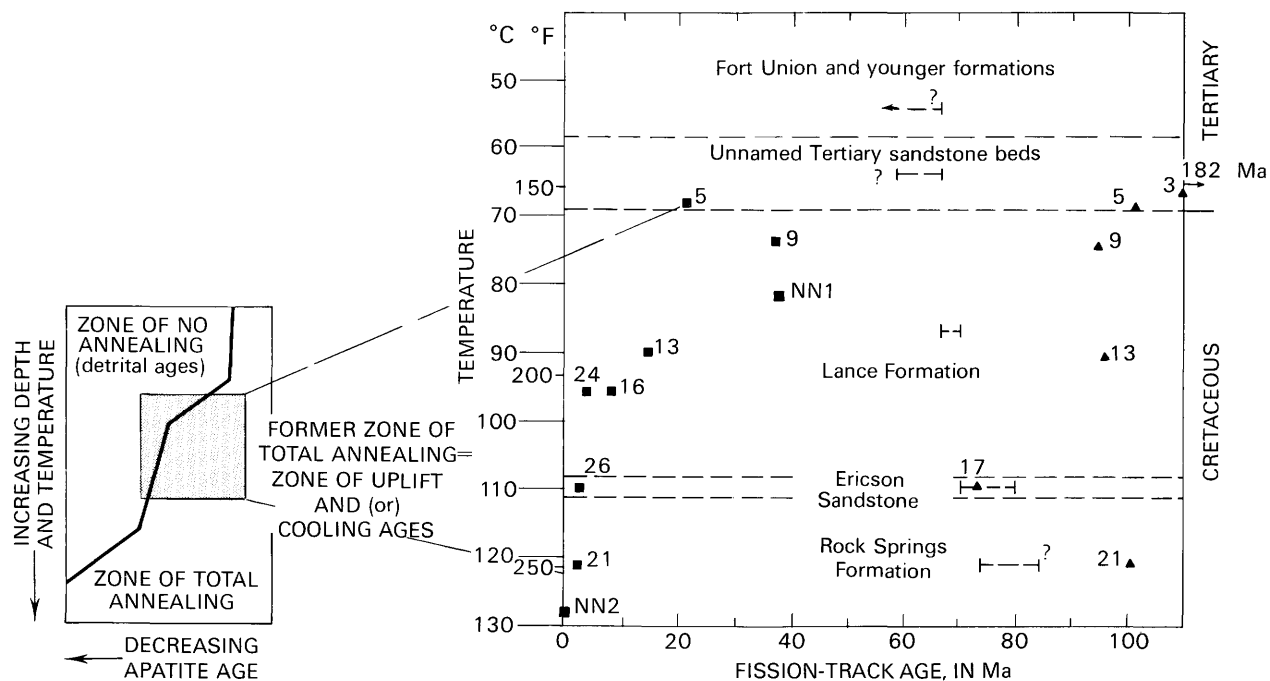


Figure 6. Fission-track ages and corrected present-day temperatures for detrital apatite (squares) and zircon (triangles) from sandstones from Wagon Wheel No. 1 well, as compared to theoretical pattern of ages expected in rocks that have undergone cooling (fig. 4). Sample WWH-17 is from upper part of Ericson Sandstone, sample WWH-26 from lower part. Dashed horizontal bar in each stratigraphic

unit indicates approximate time of deposition of unit as determined from K-Ar ages of Cretaceous ammonite zones (Obradovich and Cobban, 1975; recalculated for new K-Ar constants); correlations shown in Weimer (1961), Law (1984b), and Law and Johnson (this volume); time scale of Palmer (1983). Sample information in table 1; sample numbers without alphabetic prefix, WWH.

Table 1. Depth, stratigraphic position, and present-day temperature of samples from Wagon Wheel No. 1 well, northern Green River basin, Wyoming [Location of well shown in fig.1]

Sample	Depth (feet)	Depth (meters)	Stratigraphic unit ¹	Present-day temperature (°C)	
				Log	Corrected ²
WWH-1	5,038	1,536	Fort Union Formation	44	50
WWH-3	7,061	2,152	Unnamed Tertiary sandstone beds	59	66
WWH-5	7,340	2,237	Unnamed Tertiary sandstone beds	61	68
WWH-9	8,087	2,465	Lance Formation	67	74
NN1	8,960	2,731	Lance Formation	73	81
WWH-13	10,165	3,098	Lance Formation	81	90
WWH-16	11,027	3,361	Lance Formation	84	96
WWH-24	11,057	3,370	Lance Formation	84	96
WWH-17	13,100	3,993	Ericson Sandstone (upper part)	101	109
WWH-26	13,197	4,022	Ericson Sandstone (lower part)	102	110
WWH-21	14,950	4,557	Rock Springs Formation	114	121
NN2	16,090	4,904	Rock Springs Formation	122	128

¹From Law (1984b) and B.E. Law (oral commun., 1984, 1987). Fort Union Formation indicates interval described as "Fort Union and younger formations" in Law (1984b).

²See text for description of correction technique.

used to calculate age and uncertainty in fission-track dating, but they may not be strictly applicable to sedimentary rock samples in which the detrital grains were most likely derived from more than one age population. The "age" calculated from the ages of

individual detrital grains in a sedimentary rock is in fact a composite age and has no real meaning in a stratigraphic sense.

Despite the wide range in individual grain ages in most of the samples (Naeser, 1986, table 2), the

Table 2. Apatite and zircon fission-track ages, Wagon Wheel No. 1 well, northern Green River basin, Wyoming [Location of well shown in figure 1; sample locality data shown in table 1. ρ_s , spontaneous track density; ρ_i , induced track density (two times measured density); t , tracks; n , neutrons; ϕ , neutron fluence (see text for method of determination); number in parentheses is number of tracks counted]

Sample	Number of grains counted	ρ_s ($\times 10^6 t/cm^2$)	ρ_i ($\times 10^6 t/cm^2$)	ϕ ($\times 10^{15} n/cm^2$)	Age ¹ ($\times 10^6$ years)
Apatite					
WWH-5	8	0.299 (94)	5.73 (902)	6.72 (2,354)	20.9±4.6
WWH-9	10	0.213 (91)	2.31 (494)	6.61 (2,354)	36.3±8.4
NN1	8	0.321 (77)	5.45 (654)	10.4 (3,723)	36.5±8.9
WWH-13	9	0.093 (28)	2.53 (380)	6.51 (2,354)	14.3±5.6
WWH-16	6	0.047 (5)	2.23 (119)	6.40 (2,354)	8.0±7.3
WWH-24	6	0.036 (8)	2.05 (230)	3.67 (2,726)	3.8±2.7
WWH-26	11	0.023 (8)	2.03 (354)	3.61 (2,726)	2.4±1.7
WWH-21	9	0.025 (5)	3.50 (357)	6.30 (2,354)	2.6±2.3
NN2	6	0 (0)	4.25 (251)	10.3 (3,723)	0
Zircon					
WWH-3	5	22.33 (394)	7.43 (65)	1.03 (4,424)	181.9±49.0
WWH-5	9	12.48 (1,578)	6.53 (413)	0.889 (6,340)	100.9±11.4
WWH-9	9	10.28 (1,078)	6.60 (346)	1.01 (4,424)	94.4±12.0
WWH-13	9	11.04 (1,472)	6.92 (461)	1.01 (4,424)	95.8±10.6
WWH-17	9	9.69 (931)	7.91 (380)	1.01 (4,424)	73.6±9.2
WWH-21	4	13.55 (477)	10.12 (142)	1.01 (4,424)	100.7±19.5

¹Age is ± 2 standard deviations. Age is calculated from fission-track age equation (Price and Walker, 1963; Naeser, 1967) using sums of the spontaneous and the induced track counts obtained for all grains counted in sample and the following values: $\lambda_D = 1.55 \times 10^{-10} \text{ yr}^{-1}$; $\lambda_F = 7.03 \times 10^{-17} \text{ yr}^{-1}$ (Roberts and others, 1968); $\sigma = 580 \times 10^{-24} \text{ cm}^2$; $I = 7.252 \times 10^{-3}$. Standard deviation is calculated by combining Poisson errors on spontaneous and induced counts and counts in detector covering dosimeter (Lindsey and others, 1975; McGee and others, 1985).

composite age calculated for the first six grains counted in any given sample gives a reasonable estimate of the composite "age" for that sample and does not change significantly with the inclusion of additional individual grain ages.

Present-Day Temperatures in the Wagon Wheel No. 1 Well

Two sets of temperatures are given in table 1: (1) temperatures interpolated from log data and (2) corrected temperatures that have been adjusted from the log data by T.H. McCulloh (written commun., 1982) using the procedures outlined in Bostick and others (1978, p. 74–75) and McCulloh and Beyer (1979).

The uncertainty associated with individual corrected temperatures is about ± 3 °C from the surface to depths of 10,000 ft (3,048 m) and about ± 5 °C from depths of 10,000 to 19,000 ft (3,048–5,791 m) (T.H. McCulloh, oral commun., 1982). Corrected temperatures are 6–12 °C higher than temperatures interpolated from the drill-hole logs and closely match temperatures that would be obtained if correction procedures of the American Association of Petroleum Geologists Geothermal Survey of North America were used (Kehle and others, 1970; Kehle, 1972).

FISSION-TRACK DATA

Apatite Ages

Apatite ages were determined for nine samples from the Wagon Wheel well (fig. 6, table 2). Sample WWH-17, from the upper part of the Upper Cretaceous Ericson Sandstone, yielded insufficient apatite for an age determination.

The time of deposition of Cretaceous sedimentary units sampled in the Wagon Wheel well is known with some confidence because the units can be correlated to ammonite zones, the ages of which have been determined by K-Ar dating of associated bentonite layers (Weimer, 1961; Obradovich and Cobban, 1975; Law, 1984b; Law and Johnson, this volume). The unnamed Tertiary rocks (table 1) underlie the Paleocene Fort Union Formation and thus are older than the Eocene-Paleocene boundary (57.8 Ma) and younger than the Tertiary-Cretaceous boundary (66.4 Ma) (Palmer, 1983).

Comparison of stratigraphic and fission-track ages in the Wagon Wheel well indicates that all of the composite apatite ages calculated for the samples (fig. 6) and almost all of the individual apatite grain ages are younger than the stratigraphic age of the sedimentary unit from which they were collected. This relationship indicates that significant annealing of the apatite has occurred during

burial of the sediments. If the zone of no annealing shown in figures 3 and 4 is preserved in the Wagon Wheel well, it must be above the shallowest sample analyzed (WWH-5; 7,340 ft, 2,237 m) because even that sample contains partially annealed apatite.

Apatite fission-track ages calculated for samples from the Wagon Wheel well show two distinct trends (fig. 6). In the upper part of the sampled interval, the apatite ages generally decrease with increasing temperature and approach zero at a temperature of slightly more than 96 °C. At this point, the trend in ages changes abruptly and the ages remain almost constant or decrease slightly, from about 4 to 2 Ma, over a temperature interval of at least 20 °C, down through sample WWH-21. Apatite from the deepest sample in the drill hole (NN2) is totally annealed; that is, it contained no spontaneous fission tracks and yielded a zero age.

Zircon Ages

Zircon ages were determined for six samples from the Wagon Wheel well (figs. 6, 7, table 2). Sample WWH-16 yielded insufficient zircon for an age determination, and sample WWH-1 could not be dated because the zircon is metamict.

The composite zircon fission-track age calculated for each of the Wagon Wheel samples and all but a few of the individual zircon grain ages are equal to or older than the depositional age of the unit from which they were sampled (figs. 6, 7). This relationship suggests that no significant annealing of the zircon has occurred in any of the samples since deposition.

Lack of significant zircon annealing is also suggested by the fact that the composite zircon ages calculated for most of the samples are indistinguishable from one another (table 2, fig. 7). Some variation exists in the range of the individual zircon grain ages in the samples (fig. 7), but, for most samples, no obvious correlation can be made between the calculated sample age or the range in individual grain ages and the present-day temperature (or depth) of the sample. Samples WWH-17, -3, and -1 appear to be exceptions. Sample WWH-17, from the upper part of the Ericson Sandstone, yielded a significantly younger composite zircon age than did many of the samples, and it apparently contains a lower percentage of old (older than about 110 Ma) zircons (fig. 7). As noted below, this may result, at least in part, from the provenance of this sandstone. Samples WWH-1 and WWH-3, from the upper part of the Tertiary section sampled in the Wagon Wheel well, contain detrital zircon suites that appear to be older than those in the underlying rocks. All of the zircons in WWH-1 are metamict and are probably of considerable age. In sample WWH-3, no zircon grains younger than 100 Ma were

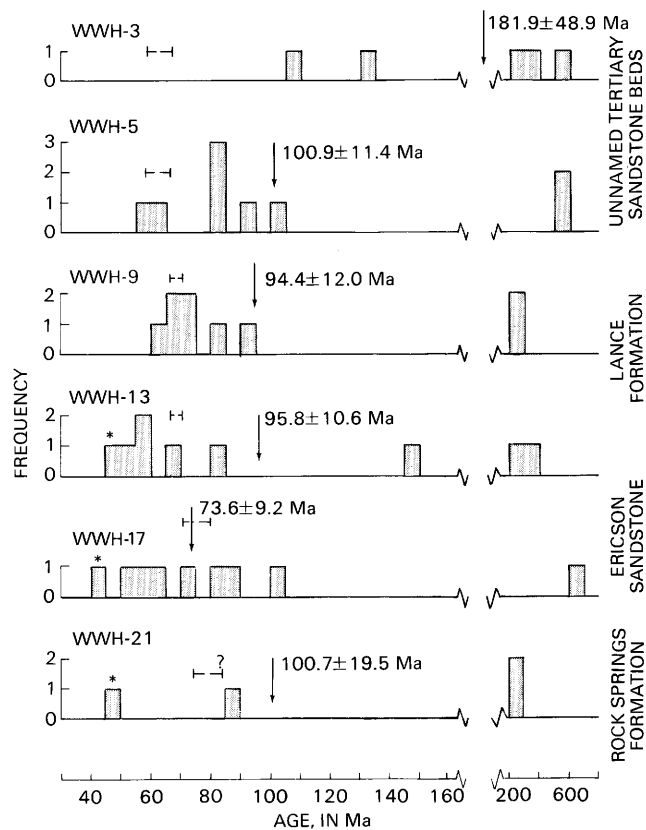


Figure 7. Histograms of fission-track ages of individual zircon grains in six samples from the Wagon Wheel No. 1 well (Naeser, 1986). Composite age (± 2 standard deviations) calculated for each sample (fig. 6, table 2) indicated by arrow. Bar indicates approximate time of deposition of unit from which sample was collected (see text and fig. 6). Asterisk (*) indicates age is younger than stratigraphic age and does not overlap stratigraphic age at two standard deviations; all other ages are equal to or older than stratigraphic age.

observed and the percentage of metamict grains is significantly higher than in the underlying samples. Again, the provenance of these units is probably different.

THERMAL HISTORY

Because of the temperature-time dependency in annealing (fig. 2), the degree of annealing observed in the apatite from the upper part of the Wagon Wheel well (as deep as the almost totally annealed apatite at about 96 °C) may have been produced by the rocks either being near their present-day (or a lower) temperature for a long period of time (at least 10^8 yr) (see fig. 2), or being at a higher temperature for a shorter time before they cooled to their present-day temperature.

The rocks in the upper part of the drill hole are latest Cretaceous (Lance Formation) and younger in age (less than about 70 Ma) (Weimer, 1961; Obradovich and

Cobban, 1975; Law, 1984b; Law and Johnson, this volume) (fig. 6). According to the burial reconstruction of Pollastro and Barker (1986, fig. 10) for the Pinedale anticline, the rocks were buried rapidly to maximum depth at about 37 Ma, and since that time no net sediment deposition has occurred. Even if the rocks had remained at maximum depth until the present time, such that present-day temperature equaled maximum temperature, they would have been near that temperature for considerably less than 10^8 years (see also Dickinson, this volume). We therefore are left with the second explanation; that is, cooling has occurred in the rocks.

The trend of the apatite ages at temperatures greater than about 96 °C provides evidence for the nature of this cooling. These ages vary little with depth down through sample WWH-21 and are believed to record the timing of an episode of relatively rapid cooling (the zone of uplift and (or) cooling shown in figures 4 and 6). The apatite ages suggest that at least the latest phase of cooling in the rocks began about 4–2 Ma and involved a relatively rapid decrease in temperature of at least 20 °C.

The total amount of cooling since 4–2 Ma cannot be interpreted with certainty because the temperature of the deepest sample in the drill hole (NN2) is presently sufficiently high (128 °C) that, even if the apatite had initially retained tracks following cooling, these tracks would probably have been subsequently totally annealed. However, fission-track data from shallower samples in the Wagon Wheel well, above the zone of cooling ages, help place some constraints on the amount of cooling since 4–2 Ma. For example, apatite in sample WWH-13, which is presently at a (corrected) temperature of 90 °C, yields a composite age of 14.3 ± 5.6 m.y., indicating that it was not totally annealed prior to the Pliocene cooling. Pollastro and Barker's (1986) burial history diagram suggests that these rocks were near their maximum temperature from the end of the Eocene until the onset of cooling in the Pliocene. Given that long a heating duration, it is unlikely that apatite in WWH-13 could have retained fission tracks if it had been at temperatures much higher than about 110–115 °C prior to cooling. Therefore, assuming the adjusted temperature for WWH-13 of 90 °C is correct, it is unlikely that total cooling since 4–2 Ma has exceeded about 20–25 °C.

Neither the rate nor exact time of cooling can be determined precisely because of the large analytical uncertainty in the apatite ages in this part of the drill hole (table 2). However, the temperature of sample WWH-24, which yielded an apatite age of ~ 4 Ma and is at or just above the top of the cooling zone, is sufficiently low (96 °C) that it is unlikely the apatite has undergone significant age reduction as a result of postcooling annealing. Within the analytical uncertainty, it therefore is unlikely that the period of rapid cooling began significantly earlier than ~ 4 Ma. If the cooling occurred in response to the

combined effect of uplift and erosion, however, then the actual uplift may have begun somewhat earlier.

Pollastro and Barker (1984a, b, 1986) studied the thermal history in the Wagon Wheel well by using several other paleotemperature indicators. Depth-temperature curves determined from mean random vitrinite reflectance measured in thin coaly seams in the rocks and from illite/smectite transformations in the sandstone and shale layers are in good agreement and indicate that the rocks were subjected to temperatures 30–50 °C higher sometime in the past. The vitrinite reflectance data suggest that cooling of the rocks resulted from uplift and erosion rather than from a major decrease in geothermal gradient (Pollastro and Barker, 1984a, 1986).

The fission-track data indicate that an event resulting in approximately 20–25 °C cooling began in this area about 4–2 Ma. The timing of the cooling as indicated by the fission-track data is consistent with evidence (reviewed in Dickinson, this volume) for widespread uplift and erosion in the Green River basin beginning in the late Pliocene. Fission-track dating of apatite from rocks in other parts of the basin should help clarify the extent and magnitude of this uplift and erosion, but initial attempts at such a study in the Pacific Creek area (fig. 1) were unsuccessful because the rocks yielded insufficient apatite for fission-track analysis.

PROVENANCE OF THE SEDIMENTS

In most of the rocks sampled in the Wagon Wheel No. 1 well, the minimal variation in the range of ages of individual zircons in the detrital grain suites and in the proportion of grains of various ages suggests that the dominant source of sediments in the Pinedale anticline remained unchanged through most of the Late Cretaceous and earliest Paleocene.

Apparent exceptions are samples WWH-17, WWH-3, and WWH-1. Independent evidence suggests that the young age of zircon in WWH-17 results, at least in part, from the provenance of this sandstone rather than from postdepositional annealing. Sample WWH-17 was collected from the upper part of the Ericson Sandstone. Mineralogically and petrographically the Ericson Sandstone, particularly the upper part of the unit, is very different from most other Upper Cretaceous units in the northern Green River basin (Rice and Gautier, 1983; Edman and Surdam, 1986; Law and others, 1986; Pollastro, this volume). It has been suggested that these differences, although partly diagenetic in origin, can largely be explained by a major change in detrital source material for this unit (Rice and Gautier, 1983, p. 4–24; D.L. Gautier, U.S. Geological Survey, oral commun., 1984; Pollastro, this volume). In the Wagon Wheel well, the upper part of the Ericson Sandstone is further

distinguished from the other Upper Cretaceous sandstones that were sampled for fission-track analysis by the fact that it yielded little or no detrital apatite.

Another possible explanation for younger zircon in the Ericson Sandstone is that the zircon was slightly annealed at some time during the burial history by localized anomalously high temperatures. However, this interpretation seems unlikely because illite/smectite transformation and vitrinite reflectance data from sandstone and shale in the upper part of the Ericson Sandstone in the Wagon Wheel well show no evidence for anomalously high temperatures in this unit (Pollastro and Barker, 1986; R.M. Pollastro, oral commun., 1989; Dickinson, this volume).

The anomalous zircon ages of WWH-1 and WWH-3 may indicate changes in source terrane related to the structural evolution of the Wind River Mountains to the northeast. Uplift of this range began as part of the major Laramide activity in the latest Cretaceous, and by early to middle Paleocene this uplift and erosion had breached the crystalline core of the Wind River Mountains and produced an influx of arkosic material into the Green River basin (Prensky, 1984; Law and Johnson, this volume). A strong anomaly in the gamma-ray log for the Wagon Wheel well at 7,225 ft (2,202 m), between the depths at which samples WWH-3 and WWH-5 were collected, has been attributed to this arkose influx (Prensky, 1984, this volume). The decrease in young zircons and the increase in percentage of metamict grains in WWH-3 relative to WWH-5 are probably a direct consequence of this change in sediment source, which culminated in domination of the zircon suite in WWH-1 by metamict grains.

CONCLUSIONS

Vitrinite reflectance and illite/smectite transformation measurements in the Wagon Wheel No. 1 well suggest that present-day temperatures are about 30–50 °C cooler than the maximum paleotemperature (Pollastro and Barker, 1984a, b, 1986). Fission-track apatite ages of sandstones from the well support the hypothesis of higher paleotemperatures and suggest that the latest phase of cooling of the rocks began about 4 to 2 Ma, during the Pliocene, and has produced a relatively rapid temperature decrease of at least 20 °C.

Zircon ages from the well suggest that the dominant source of sediments in the Pinedale anticline did not change through most of the Late Cretaceous and earliest Paleocene. A significant change in provenance during the Paleocene was probably related to unroofing of the crystalline core of the Wind River Mountains to the northeast.

REFERENCES CITED

- Baldwin, S.L., and Harrison, T.M., 1985, Fission track dating of detrital zircons from the Scotland Formation, Barbados, W.I. [abs.]: *Nuclear Tracks and Radiation Measurements*, v. 10, p. 402.
- Baldwin, S.L., Harrison, T.M., and Burke, K., 1986, Fission track evidence for the source of accreted sandstones, Barbados: *Tectonics*, v. 5, p. 457–468.
- Bostick, N.H., Cashman, S.M., McCulloh, T.H., and Waddell, C.T., 1978, Gradients of vitrinite reflectance and present temperature in the Los Angeles and Ventura basins, California, in Oltz, D.F., ed., *Low temperature metamorphism of kerogen and clay minerals: Pacific Section, Society of Economic Paleontologists and Mineralogists*, p. 65–96.
- Carpenter, B.S., and Reimer, G.M., 1974, Standard reference materials; calibrated glass standards for fission track use: National Bureau of Standards Special Publication 260–49, 16 p.
- Cerveny, P.F., 1986, Uplift and erosion of the Himalaya over the past 18 million years; evidence from fission track dating of detrital zircons and heavy mineral analysis: Hanover, N.H., Dartmouth College, M.S. thesis, 198 p.
- Cerveny, P.F., Naeser, N.D., Zeitler, P.K., Naeser, C.W., and Johnson, N.M., 1988, History of uplift and relief of the Himalaya during the past 18 million years; evidence from fission-track ages of detrital zircons from sandstones of the Siwalik Group, in Kleinspehn, K.L., and Paola, C., eds., *New perspectives in basin analysis: New York, Springer-Verlag*, p. 43–61.
- Dickinson, W.W., and Law, B.E., 1985, Burial history of Upper Cretaceous and Tertiary rocks interpreted from vitrinite reflectance, northern Green River basin, Wyoming [abs.]: *American Association of Petroleum Geologists Bulletin*, v. 69, no. 5, p. 846.
- Duddy, I.R., and Gleadow, A.J.W., 1982, Thermal history of the Otway Basin, southeastern Australia, from geologic annealing of fission tracks in detrital volcanic apatites: *Fission-Track Dating Workshop, International Conference on Geochronology, Cosmochronology, and Isotope Geology*, 5th, Nikko National Park, Japan, 1982, Abstracts, p. 13–16.
- Edman, J.D., and Surdam, R.C., 1986, Organic-inorganic interactions as a mechanism for porosity enhancement in the Upper Cretaceous Ericson Sandstone, Green River basin, Wyoming, in Gautier, D.L., ed., *Roles of organic matter in sediment diagenesis: Society of Economic Paleontologists and Mineralogists Special Publication 38*, p. 85–109.
- Gleadow, A.J.W., Duddy, I.R., Green, P.F., and Hegarty, K.A., 1986, Fission track lengths in the apatite annealing zone and the interpretation of mixed ages: *Earth and Planetary Science Letters*, v. 78, p. 245–254.
- Gleadow, A.J.W., Duddy, I.R., Green, P.F., and Lovering, J.F., 1986, Confined fission track lengths in apatite; a diagnostic tool for thermal history analysis: *Contributions to Mineralogy and Petrology*, v. 94, p. 405–415.

- Gleadow, A.J.W., Duddy, I.R., and Lovering, J.F., 1983, Fission track analysis; a new tool for the evaluation of thermal histories and hydrocarbon potential: *Australian Petroleum Exploration Association Journal*, v. 23, pt. 1, p. 93-102.
- Green, P.F., Duddy, I.R., Gleadow, A.J.W., and Lovering, J.F., 1989, Apatite fission-track analysis as a paleotemperature indicator for hydrocarbon exploration, *in* Naeser, N.D., and McCulloh, T.H., eds., *Thermal history of sedimentary basins; methods and case histories*: New York, Springer-Verlag, p. 181-195.
- Harrison, T.M., 1985, A reassessment of fission-track annealing behavior in apatite: *Nuclear Tracks and Radiation Measurements*, v. 10, p. 329-333.
- Harrison, T.M., Armstrong, R.L., Naeser, C.W., and Harakal, J.E., 1979, Geochronology and thermal history of the Coast Plutonic Complex, near Prince Rupert, British Columbia: *Canadian Journal of Earth Sciences*, v. 16, p. 400-410.
- Hood, A., Gutjahr, C.C.M., and Heacock, R.L., 1975, Organic metamorphism and the generation of petroleum: *American Association of Petroleum Geologists Bulletin*, v. 59, no. 6, p. 986-996.
- Hurford, A.J., 1985, On the closure temperature for fission tracks in zircon [abs.]: *Nuclear Tracks and Radiation Measurements*, v. 10, p. 415.
- Hurford, A.J., Fitch, F.J., and Clarke, A., 1984, Resolution of the age structure of the detrital zircon populations of two Lower Cretaceous sandstones from the Weald of England by fission track dating: *Geological Magazine*, v. 121, no. 4, p. 269-277.
- Johnson, S.Y., 1984, Stratigraphy, age, and paleogeography of the Eocene Chuckanut Formation, northwest Washington: *Canadian Journal of Earth Sciences*, v. 21, p. 92-106.
- Kehle, R.O., 1972, Geothermal survey of North America 1971 annual progress report: American Association of Petroleum Geologists Research Committee, Unpublished report, 31 p.
- Kehle, R.O., Schoepel, R.J., and Deford, R.K., 1970, The AAPG geothermal survey of North America: Geothermics, Special Issue, 1970, p. 358-367.
- Law, B.E., 1984a, Introduction, *in* Law, B.E., ed., *Geological characteristics of low-permeability Upper Cretaceous and lower Tertiary rocks in the Pinedale anticline area, Sublette County, Wyoming*: U.S. Geological Survey Open-File Report 84-753, p. 1-5.
- _____, 1984b, Structure and stratigraphy of the Pinedale anticline, Wyoming, *in* Law, B.E., ed., *Geological characteristics of low-permeability Upper Cretaceous and lower Tertiary rocks in the Pinedale anticline area, Sublette County, Wyoming*: U.S. Geological Survey Open-File Report 84-753, p. 6-15.
- _____, 1984c, Relationships of source-rock, thermal maturity, and overpressuring to gas generation and occurrence in low-permeability Upper Cretaceous and lower Tertiary rocks, Greater Green River basin, Wyoming, Colorado, and Utah, *in* Woodward, Jane, Meissner, F.F., and Clayton, J.L., *Hydrocarbon source rocks of the greater Rocky Mountain region*: Rocky Mountain Association of Geologists, p. 469-490.
- Law, B.E., Pollastro, R.M., and Keighin, C.W., 1986, Geologic characterization of low-permeability gas reservoirs in selected wells, Greater Green River basin, Wyoming, Colorado, and Utah, *in* Spencer, C.W., and Mast, R.F., eds., *Geology of tight gas reservoirs: American Association of Petroleum Geologists Studies in Geology* 24, p. 253-269.
- Lindsey, D.A., Naeser, C.W., and Shawe, D.R., 1975, Age of volcanism, intrusion, and mineralization in the Thomas Range, Keg Mountains, and Desert Mountain, western Utah: *U.S. Geological Survey Journal of Research*, v. 3, p. 597-604.
- Märk, E., Pahl, M., Purtscheller, F., and Märk, T.D., 1973, Thermische ausheilung von uran-spaltspuren in apatiten, alterskorrekturen und beiträge zur geochronologie [Thermal annealing of uranium tracks in apatite, age corrections, and implications for geochronology]: *Tschermaks Mineralogische und Petrographische Mitteilungen*, v. 20, p. 131-154.
- McCulloh, T.H., and Beyer, L.A., 1979, Geothermal gradients, *in* Cook, H.E., ed., *Geologic studies of the Point Conception deep stratigraphic test well OCS-CAL 78-164 No. 1, outer continental shelf, southern California, United States*: U.S. Geological Survey Open-File Report 79-1218, p. 43-48.
- McGee, V.E., Johnson, N.M., and Naeser, C.W., 1985, Simulated fissioning of uranium and testing of the fission-track dating method: *Nuclear Tracks and Radiation Measurements*, v. 10, p. 365-379.
- Naeser, C.W., 1967, The use of apatite and sphene for fission track age determinations: *Geological Society of America Bulletin*, v. 78, no. 12, p. 1523-1526.
- _____, 1976, Fission track dating: U.S. Geological Survey Open-File Report 76-190, 65 p.
- _____, 1979a, Fission-track dating and geologic annealing of fission tracks, *in* Jäger, E., and Hunziker, J.C., eds., *Lectures in isotope geology*: New York, Springer-Verlag, p. 154-169.
- _____, 1979b, Thermal history of sedimentary basins; fission-track dating of subsurface rocks, *in* Scholle, P.A., and Schluger, P.R., eds., *Aspects of diagenesis: Society of Economic Paleontologists and Mineralogists Special Publication* 26, p. 109-112.
- _____, 1981, The fading of fission tracks in the geologic environment; data from deep drill holes: *Nuclear Tracks*, v. 5, p. 248-250.
- Naeser, C.W., and Faul, H., 1969, Fission track annealing in apatite and sphene: *Journal of Geophysical Research*, v. 74, no. 2, p. 705-710.
- Naeser, C.W., Hurford, A.J., and Gleadow, A.J.W., 1977, Fission-track dating of pumice from the KBS Tuff, East Rudolf, Kenya: *Nature*, v. 267, p. 649.
- Naeser, N.D., 1986, Neogene thermal history of the northern Green River basin, Wyoming; evidence from fission-track dating, *in* Gautier, D.L., ed., *Roles of organic matter in sediment diagenesis: Society of Economic Paleontologists and Mineralogists Special Publication* 38, p. 65-72.
- Naeser, N.D., Naeser, C.W., and McCulloh, T.H., 1989, The application of fission-track dating to the depositional and thermal history of rocks in sedimentary basins, *in* Naeser, N.D., and McCulloh, T.H., eds., *Thermal history of sedimentary basins; methods and case histories*: New York, Springer-Verlag, p. 157-180.

- Obradovich, J.D., and Cobban, W.A., 1975, A time-scale for the Late Cretaceous of the Western Interior of North America: Geological Association of Canada Special Paper 13, p. 31-54.
- Palmer, A.R., compiler, 1983, The Decade of North American Geology 1983 geologic time scale: *Geology*, v. 11, no. 9, p. 503-504.
- Pollastro, R.M., and Barker, C.E., 1984a, Geothermometry from clay minerals, vitrinite reflectance, and fluid inclusions; applications to the thermal and burial history of rocks cored from the Wagon Wheel No. 1 well, Green River basin, Wyoming, *in* Law, B.E., ed., Geological characteristics of low-permeability Upper Cretaceous and lower Tertiary rocks in the Pinedale anticline area, Sublette County, Wyoming: U.S. Geological Survey Open-File Report 84-753, p. 78-94.
- _____, 1984b, Comparative measures of paleotemperature; an example from clay-mineral, vitrinite reflectance, and fluid inclusion studies, Pinedale anticline, northern Green River basin, Wyoming: Society of Economic Paleontologists and Mineralogists Annual Midyear Meeting, San Jose, Calif., 1984, Abstracts, p. 65-66.
- _____, 1986, Application of clay-mineral, vitrinite reflectance, and fluid inclusion studies to the thermal and burial history of the Pinedale anticline, Green River basin, Wyoming, *in* Gautier, D.L., ed., Roles of organic matter in sediment diagenesis: Society of Economic Mineralogists and Paleontologists Special Publication 38, p. 73-83.
- Prensky, S.E., 1984, A gamma-ray log anomaly associated with the Cretaceous-Tertiary boundary in the northern Green River basin, Wyoming, *in* Law, B.E., ed., Geological characteristics of low-permeability Upper Cretaceous and lower Tertiary rocks in the Pinedale anticline area, Sublette County, Wyoming: U.S. Geological Survey Open-File Report 84-753, p. 22-35.
- Price, P.B., and Walker, R.M., 1963, Fossil tracks of charged particles in mica and the age of minerals: *Journal of Geophysical Research*, v. 68, no. 16, p. 4847-4862.
- Reimer, G.M., 1972, Fission track geochronology; method for tectonic interpretation of apatite studies with examples from the central and southern Alps: Philadelphia, University of Pennsylvania, Ph.D. thesis, 85 p.
- Rice, D.D., and Gautier, D.L., 1983, Patterns of sedimentation, diagenesis, and hydrocarbon accumulation in Cretaceous rocks of the Rocky Mountains: Society of Economic Paleontologists and Mineralogists Short Course 11, 339 p.
- Roberts, J.A., Gold, R., and Armani, R.J., 1968, Spontaneous-fission decay constant of ^{238}U : *Physical Review*, v. 174, p. 1482-1484.
- Sanford, S.J., 1981, Dating thermal events by fission track annealing, Cerro Prieto geothermal field, Baja California, Mexico: Riverside, University of California, M.S. thesis, 105 p.
- Shuster, M.W., 1986, The origin and sedimentary evolution of the northern Green River basin, western Wyoming: Laramie, University of Wyoming, Ph.D. thesis, 323 p.
- Shuster, M.W., and Steidtmann, J.R., 1983, Origin and development of northern Green River basin; a stratigraphic and flexural study [abs.]: *American Association of Petroleum Geologists Bulletin*, v. 67, no. 8, p. 1356.
- Waples, D.W., 1980, Time and temperature in petroleum formation; application of Lopatin's method to petroleum exploration: *American Association of Petroleum Geologists Bulletin*, v. 64, no. 6, p. 916-926.
- Weimer, R.J., 1961, Uppermost Cretaceous rocks in central and southern Wyoming, and northwest Colorado: Wyoming Geological Association Annual Field Conference, 16th, Casper, 1961, Guidebook, p. 17-28.
- Yim, W.W.-S., Gleadow, A.J.W., and van Moort, J.C., 1985, Fission track dating of alluvial zircons and heavy mineral provenance in Northeast Tasmania: *Journal of the Geological Society of London*, v. 142, p. 351-356.
- Zeitler, P.K., 1985, Closure temperature implications of concordant $^{40}\text{Ar}/^{39}\text{Ar}$ potassium feldspar and zircon fission-track ages from high-grade terranes [abs.]: *Nuclear Tracks and Radiation Measurements*, v. 10, p. 441-442.
- Zeitler, P.K., Johnson, N.M., Briggs, N.D., and Naeser, C.W., 1982, History of uplifts in northwestern Himalayas using a study of fission track ages of detrital Siwalik zircons: Geological Society of China Symposium on Mesozoic and Cenozoic Geology, 60th Anniversary Symposium, Beidaihe, China, 1982, Abstracts, p. 108-109.
- _____, 1986, Uplift history of the NW Himalaya as recorded by fission-track ages on detrital Siwalik zircons, *in* Jiqing, H., ed., Proceedings of the Symposium on Mesozoic and Cenozoic Geology: Beijing, China, Geological Publishing House, p. 481-494.
- Zimmermann, R.A., and Gaines, A.M., 1978, A new approach to the study of fission-track fading, *in* Zartman, R.E., ed., Short papers of the Fourth International Conference, Geochronology, Cosmochronology, Isotope Geology: U.S. Geological Survey Open-File Report 78-701, p. 467-468.

Chapter F

Analysis of Vitrinite Maturation and Tertiary Burial History, Northern Green River Basin, Wyoming

By WARREN W. DICKINSON

Prepared in cooperation with the U.S. Department of Energy

U.S. GEOLOGICAL SURVEY BULLETIN 1886

GEOLOGY OF TIGHT GAS RESERVOIRS IN THE PINEDALE ANTICLINE AREA, WYOMING,
AND AT THE MULTIWELL EXPERIMENT SITE, COLORADO

CONTENTS

Abstract	F1
Introduction	F1
Depositional and tectonic history	F1
Geothermal gradients	F5
Vitrinite reflectance data	F6
Burial and thermal reconstructions	F6
Recent folding	F8
Elevated paleogeothermal gradient	F9
Vitrinite maturation models	F9
Summary and conclusions	F11
References cited	F11
Appendix 1. Vitrinite reflectance values for Wagon Wheel, WASP, and Pacific Creek wells and equations used to calculate paleotemperatures	F16

FIGURES

1. Map showing areas of peneplained surfaces on southwestern flank of Wind River Mountains, northern Green River basin F2
2. Chart showing burial history for WASP, Wagon Wheel, and Pacific Creek wells F2
3. Cross sections showing general geologic structures and projected surfaces of Wind River peneplain F4
4. Graphs showing vitrinite reflectance values and Lopatin reconstructions for top of Ericson Sandstone at WASP, Wagon Wheel, and Pacific Creek wells F7
5. Cross section showing relationships between stratigraphy, structure, thermal maturation, and burial in northern Green River basin F8
6. Lopatin reconstruction diagram for a local increase in geothermal gradient in Wagon Wheel area F9
7. Graphs showing linear regression least-squares fits of maximum paleotemperatures for WASP, Wagon Wheel, and Pacific Creek wells calculated by using selected vitrinite maturation models F10

Analysis of Vitrinite Maturation and Tertiary Burial History, Northern Green River Basin, Wyoming

By Warren W. Dickinson¹

Abstract

Vitrinite reflectance data from three wells in the northern Green River basin are used in conjunction with a Lopatin thermal maturation model to evaluate Tertiary burial history. Geologic evidence suggests that, on a regional scale, present and past geothermal gradients in the Green River basin are similar and that heating or cooling of the rocks has occurred as the result of surface temperature changes, burial and erosion, or vertical movement of subsurface waters. After early Eocene time, little deposition occurred at the northern end of the basin, but on the southwestern flank of the Wind River mountains about 600 m of sediments was deposited. Regional erosion occurred during and after Pliocene time. The Lopatin model and the vitrinite reflectance surface intercept generally support the geologic evidence.

High vitrinite reflectance values in the area of the Pinedale anticline suggest erosion of more than 1,200 m of basin fill, a significantly greater amount than stratigraphic evidence can account for. Isoreflectance lines, which parallel the anticlinal structure, suggest that these high vitrinite reflectance values were either physically elevated into place by recent folding or generated by hotter than present-day temperatures around the anticline. The choice between these alternatives is not clear, but if the paleogeothermal gradient was 2 °C/km hotter than the present-day gradient, results of maturation modeling support geologic data.

Vitrinite reflectance data are used in several vitrinite maturation models to calculate paleotemperature gradients. Time-independent models show anomalously high paleogeothermal gradients, and time-dependent models yield gradients more similar to the present-day gradient and more in accord with the geologic evidence.

INTRODUCTION

In the northern Green River basin of Wyoming (fig. 1), much of the tectonic and depositional history since early Eocene time has been lost to erosion. In spite

of this loss, recently acquired stratigraphic and geochemical data provide considerable insight into this history. An understanding of the geologic history of the basin and adjacent thrust belt is important to the exploration of hydrocarbon resources.

Vitrinite reflectance (R_m) data for a large number of wells in the basin recently have been collected and mapped by Law (1984), Pawlewicz and others (1986), Merewether and others (1987), and Lickus and others (this volume). Vitrinite reflectance records thermal history, which is, in turn, a function of burial history and present and past geothermal gradients. Models of vitrinite maturation can be used to evaluate the burial history of the basin determined from other geologic evidence.

The WASP (Wyoming Atomic Stimulation Project), Wagon Wheel, and Pacific Creek wells (fig. 1) were used in this study because they penetrate Upper Cretaceous and Tertiary rock sequences that are representative of the basin and because vitrinite reflectance data for the wells are abundant. The goals of this study were threefold: (1) to synthesize published stratigraphic and geochemical data into a Tertiary burial history for the northern Green River basin; (2) to evaluate the depth and duration of burial by using the Lopatin model of vitrinite maturation; and (3) to test time-independent and time-dependent models of vitrinite maturation by comparing predicted paleogeothermal gradients and present-day thermal gradients.

DEPOSITIONAL AND TECTONIC HISTORY

Structurally, the deepest part of the northern Green River basin contains about 10,000 m of sedimentary rocks and is east of the Pinedale anticline (Law and Johnson, this volume, fig. 1). About 7,000 m of these rocks are Late Cretaceous, Paleocene, and Eocene in age and include the Hilliard Shale, Rock Springs Formation, Ericson Sandstone, and Lance, Fort Union, and Wasatch Formations. Most of these formations have been truncated by thrust faults and are not exposed

¹Research School of Earth Science, Victoria University
P.O. Box 600, Wellington, New Zealand

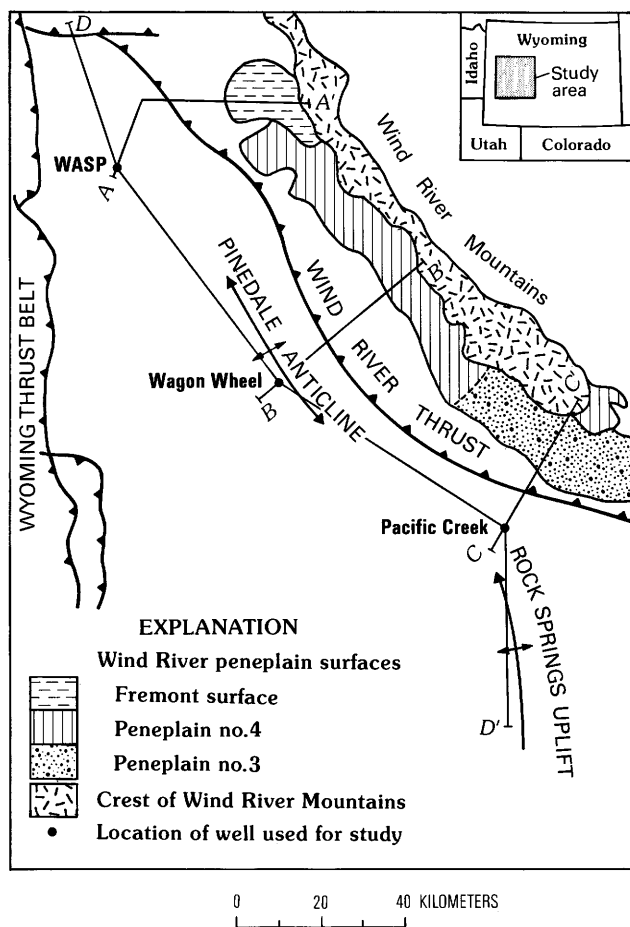


Figure 1. Areas of penneplained surfaces on the southwestern flank of the Wind River Mountains (Westgate and Branson, 1913; Blackwelder, 1915; Baker, 1946), northern Green River basin. Penneplained surfaces on northeastern flank of mountains are not as extensive. Lines of section A-A', B-B', C-C' (fig. 3) and D-D' (fig. 5) and locations of WASP, Wagon Wheel and Pacific Creek wells also shown.

along the margins of the basin; lower and middle Eocene rocks cover most of the surface.

Studies by Armstrong and Oriel (1965) and Dorr and others (1977) indicate that large volumes of the Upper Cretaceous and Tertiary sediments accumulated during periods of tectonic activity and uplift around the basin. Profile modeling by Shuster and Steidtmann (1984) suggests that basin subsidence occurred when the lithosphere was depressed by the weight of the Darby and Prospect thrust plates on the west and the Wind River thrust plate on the east. Erosion of these rising thrust plates and subsequent deposition in the adjacent depression redistributed this weight and modified the basin into its present shape. Burial histories for the three study wells (fig. 2) were synthesized from West (1969), Zeller and Stephens (1969), Dorr and others (1977), Law (1981), R. Bottjer (University of Wyoming, written commun., 1982), Naeser (1984), and Steidtmann and others (1986).

WASP well	Wagon Wheel well	Pacific Creek well
Time (m.y.)	Time (m.y.)	Time (m.y.)
0	0	0
Eroded by regional uplift, 470 m; 600 m of structural erosion and uplift possible	Eroded by regional uplift, 470 m; 600 m of structural erosion and uplift possible	Eroded by regional uplift, 600 m
0	3	3
Eroded by regional uplift < 150 m	3	17
3	17	17
Miocene, undivided 165 m	Pliocene and Miocene, undivided, and Arikaree Formation 335 m	24
12	24	24
Camp Davis Formation < 150 m	24	47
17	48	47
PRESENT-DAY SURFACE	PRESENT-DAY SURFACE	PRESENT-DAY SURFACE
51	50	48
Pass Peak Formation 460 m	Wasatch Formation 1,370 m	Green River and Wasatch Formations 1,140 m
53	54	54
Hoback Formation 1,250 m	Paleocene, undivided 926 m	Paleocene, undivided 1,530 m
60	65	65
Erosion ≈ 100 m	Erosion ≈ 100 m	Erosion ≈ 100 m
65	68	68
Upper Cretaceous, undivided 1,847 m	Lance Formation 1,685 m	Lance Formation 1,155 m
73	73	73
Ericson Sandstone 102 m	Ericson Sandstone 122 m	Ericson Sandstone 146 m
76	76	76
Sohare Formation and Bacon Ridge Sandstone 1,071 m	Rock Springs Formation 1,295 m	Rock Springs Formation 725 m
86	86	86
Hilliard Shale	Hilliard Shale	Baxter Shale

Figure 2. Burial history for WASP, Wagon Wheel, and Pacific Creek wells. Stratigraphy modified from West (1969), Zeller and Stephens (1969), Dorr and others (1977), Law (1981), R.J. Bottjer (University of Wyoming, written commun., 1982), Naeser (1984), Steidtmann and others (1986). Corrected elevation for the top of the Ericson Sandstone of -1,176 m mean sea level (B.E. Law, written commun., 1986) used for the WASP well. Thicknesses and time spans not shown in correct proportions. Hatching indicates hiatus. Location of wells shown in figure 1.

From the latest Cretaceous up to the present time, the area of the Green River basin has been an intermontane basin and the site of sporadic synorogenic deposition. Erosion and depositional rates are highly variable throughout the basin because the basin receives sediment from the west, north, and east at a rate in accordance

with local tectonic activity. For example, unconformities on the Rock Springs uplift suggest that major erosional events occurred between deposition of Cretaceous and Paleocene rocks and Paleocene and Eocene rocks (Roehler, 1978). In the Pinedale area, there is evidence for an unconformity between Cretaceous and Paleocene rocks (Law and Nichols, 1982; Law and Johnson, this volume). For purposes of burial reconstruction, 100 m of Cretaceous rocks is estimated to have been eroded before deposition of Tertiary rocks (fig. 2).

The amount of deposition after early Eocene time is difficult to determine because of the current cycle of widespread erosion. Post-Eocene deposition occurred at various rates and times throughout the basin, but it was minimal because major tectonism ended by mid-Eocene. Dorr and others (1977) and Shuster and Steidtmann (1984) suggested that no deposition occurred in the northern end of the basin after early Eocene time, probably because of the rapid filling of the narrow northern end of the basin and subsequent bypassing of sediment into the broad southern end. It is not coincidental, therefore, that the age of the surficial sediments in the basin (excluding Pleistocene and Holocene deposits) generally becomes younger toward the southeast along the Wind River Mountains.

In the southern part of the basin, post-Eocene deposition apparently continued at a slow rate. The crest of the Wind River Mountains may have been uplifted in Oligocene time by as much as 2,000 m, and erosion of this uplift could produce the observed Oligocene and Miocene tectogenic conglomerates (Steidtmann and others, 1986; Steidtmann, 1987). Zeller and Stephens (1964) measured a maximum of 335 m of Miocene and possibly Pliocene deposits in the area of the Pacific Creek well, and farther to the east Denson and Pippingos (1974) measured a maximum of 922 m of Oligocene, Miocene, and possibly Pliocene rocks. Careful scrutiny of all post-Eocene depositional data is necessary because burial depths affect the temperature of the rocks and hence maturation modeling.

In the area of the WASP well, the lower Eocene (about 51 Ma) Pass Peak Formation covers the surface, and, except for Pleistocene deposits, rocks younger than early Eocene are absent from the northern end of the basin (Dorr and others, 1977). A thin veneer of Miocene and Pliocene deposits, such as the Miocene Camp Davis Formation (fig. 2), possibly extended into the WASP area, but most of these deposits are in areas adjacent to uplifts in the north and east (Dorr and others, 1977).

West (1969) mapped surface rocks in the Wagon Wheel area as the western facies of the New Fork Tongue of the Wasatch Formation, which is early Eocene in age (about 50 Ma). In the Wagon Wheel area, about 305 m of lower and middle Eocene rocks presumably was eroded from the surface because, directly to the east and

stratigraphically above, West (1969) measured roughly 105 m of Wasatch and Green River Formations and about 90 m of lower Bridger Formation, and McGrew (1959) measured 110 m of upper Bridger Formation. These thicknesses may be slightly excessive if the Pinedale anticline was structurally high during early and middle Eocene time. With the exception of about 30 m of post-Bridger conglomerate (McGrew, 1959; Bottjer, 1984), evidence for post-middle Eocene deposition is lacking in the Wagon Wheel area. Bottjer correlated this conglomerate to the South Pass Formation, which Steidtmann and others (1986) and Zeller and Stephens (1969) recognized as Miocene in age. If we assume, however, that the amount of post-Eocene deposition increased from the WASP to Pacific Creek areas, then some deposition probably occurred in the area between them, in the Wagon Wheel area. A conservative estimate for the amount of this deposition is 165 m, about one-half of the amount measured at Pacific Creek (fig. 2). The total thickness of post-Eocene rocks that could be missing from the Wagon Wheel area is about 470 m.

In the Pacific Creek area, Zeller and Stephens (1969) mapped the surface rocks as undivided Wasatch Formation and placed them about 20 m stratigraphically below the base of the Laney Member of the Green River Formation of middle Eocene age (48 Ma). They also measured about 45 m of Laney Member and about 200 m of Bridger Formation. These thicknesses, together with a maximum thickness of 335 m for Miocene and possibly Pliocene rocks, suggest that about 600 m of sediments has been removed from the Pacific Creek area.

In a number of early studies (Westgate and Branson, 1913; Blackwelder, 1915; Baker, 1946), the Wind River peneplain was used to help interpret the amount of post-Eocene deposition around the Wind River Mountains. The peneplain is a broad dissected plateau, 30–50 km wide, parallel with almost the entire western and southern flanks of the mountain range. The peneplain slopes to the southwest, having gradients of from 40 to 10 m/km away from the crest of the range, and to the southeast, parallel with the crest of the range. Present-day elevations of the peneplain range from 3,700–3,300 m to 2,400–2,100 m (fig. 3). Although the peneplain is composed of as many as five, difficult to recognize terracelike steps, each of which represents an erosional subcycle (Westgate and Branson, 1913; Baker, 1946), it is essentially the result of a single, major erosional event.

Blackwelder (1915) interpreted the Wind River peneplain as a Pliocene (more recent epoch) erosional feature that stands in relief because of selective denudation of basin sediments during the Quaternary (glacial epoch). If his interpretation is correct, then a projection of the peneplained surface over the basin should yield an estimate of pre-Pliocene basin fill. Dorr and others (1977)

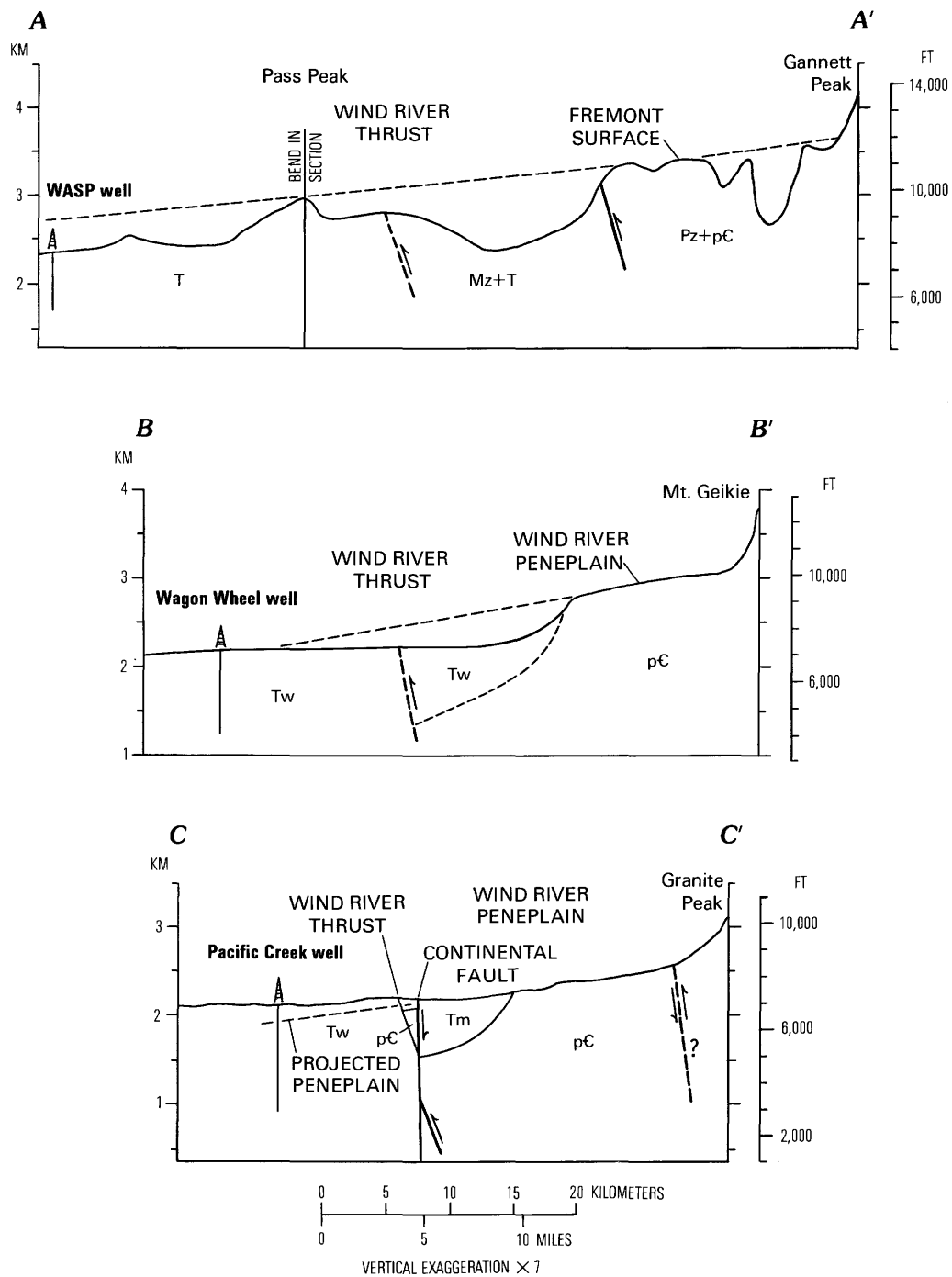


Figure 3. Cross sections showing general geologic structures and projected surfaces of the Wind River peneplain (dashed lines). Projected surface in section A-A' indicates that about 350 m of pre-Pliocene fill has been eroded from area of WASP well. Projected surfaces in sections B-B' and C-C' indicate that estimated amounts of basin fill are inconsistent with stratigraphic and vitrinite reflectance data. Section A-A' modified from Dorr and others (1977). Seismic studies (Basham and Martin, 1985) used to ascertain structural and stratigraphic relationships in section C-C'; true dip on Wind River thrust in section C-C' about 25°. pC, Precambrian rocks; Pz, Paleozoic rocks; Mz, Mesozoic rocks; T, Tertiary rocks; Tw, Wasatch Formation; Tm, Miocene rocks. Lines of section shown in figure 1.

projected the Fremont surface (summit peneplain of Westgate and Branson, 1913) and showed a minimal amount of basin fill in the area of the WASP well at the northern end of the basin (cross section *A-A'*, fig. 3). Projection of the equivalent surface (Wind River peneplains -4 and -3 of Westgate and Branson, 1913) over the areas of the Wagon Wheel and Pacific Creek wells, however, yields amounts of pre-Pliocene fill inconsistent with stratigraphic data (cross sections *B-B'* and *C-C'*, fig. 3). These inconsistencies probably result because the peneplain slopes to the southeast and is near the level of the basin in the Pacific Creek area.

If the peneplain is an erosional feature, then it must have been lowered in the southeast sometime after its formation during the Pliocene. Dondropping may have occurred along the Continental fault and a fault proposed by Steidtmann and others (1984) that separates the peneplain from the crest of the range (cross sections *B-B'* and *C-C'*, fig. 3). Alternatively, the southwestern end of the Wind River range may have been dondropped along the Continental fault after Pliocene time (Love, 1954; Zeller and Stephens, 1969). A seismic interpretation by Basham and Martin (1985) shows that post-Eocene rocks, which include those of the peneplain, north of the Continental fault in the Pacific Creek area have been lowered about 460 m relative to rocks south of the fault. Nace (1939) and Zeller and Stephens (1969) estimated similar displacements. If we raise the elevation of the peneplain by 460 m, then its projected surface indicates about 300 m of pre-Pliocene fill over the Pacific Creek well. This amount of fill generally agrees with the amount of missing section measured by Zeller and Stephens (1969) but is slightly less than the 650 m of Miocene sediments indicated in the seismic cross sections of Basham and Martin (1985).

Strong circumstantial evidence suggests that the current cycle of erosion, which has exhumed many intermontane basins in the Rocky Mountains, began in the late Pliocene when the region of the Green River basin was uplifted by more than 1,000 m (Blackwelder, 1915; Love, 1960; Dorr and others, 1977), and maturation modeling in this study generally supports this observation. Moore (1960) estimated that during deposition of the Hoback Formation in Paleocene time the basin was only 300–450 m above sea level, much lower than its present elevation of 2,100 m. During Paleocene time, the climate was subtropical (15 °C) and it probably remained warm until the Pliocene, when uplift decreased the average surface temperature of the basin to its present-day level of 4 °C (Dorr and others, 1977).

GEOHERMAL GRADIENTS

An understanding of past and present geothermal gradients is important when constructing maturation models because vitrinite reflectance depends mostly on the

heating of the rocks. A map of uncorrected borehole temperatures (Law and Smith, 1983) shows that the average geothermal gradient for the northern Green River basin is 25 °C/km. Geothermal gradients for the three study wells were calculated by using regression analysis of the mean annual surface temperature (4 °C for the basin) and the temperatures measured for drill-stem tests and geophysical logs. The nonmarine rocks in the basin are, on a large scale, lithologically homogeneous, and significant kinks in the geothermal gradients caused by differences in thermal conductivity were neither expected nor observed. The slightly higher gradient at the WASP well (28.4 °C) as compared to the Wagon Wheel (22.3 °C/km) and Pacific Creek (23.6 °C/km) wells may be related to the high geothermal gradient in the Yellowstone area about 150 km to the north. For comparison, uncorrected borehole temperatures in the Jackson Hole area to the south, halfway between the WASP well and Yellowstone National Park, yield an average gradient of 36 °C/km.

In general, data for the study wells are insufficient to correct disequilibrium temperatures measured during open-hole testing. Naeser (1984) reported corrected borehole temperatures for the Wagon Wheel well that yield a gradient of 23.5 °C/km, or about 1 °C/km hotter than the uncorrected gradient. The study wells were extensively tested and no abnormally high temperatures were reported; presumably, the use of corrected borehole temperatures would not significantly modify the uncorrected gradients.

No geologic evidence exists for a regional heat source near the basin from about 40 to 2 Ma. The Absaroka volcanic event began in southern Montana about 55 Ma and migrated southeast into Wyoming, where it ended about 44 Ma (Smedes and Prostka, 1972). Volcanism in the Yellowstone area, at the northeast end of the Cordilleran Thermotectonic Anomaly described by Eaton and others (1976), began about 2 Ma and has continued sporadically until the present time (Christiansen and Blank, 1972). Although both of these events occurred more than 150 km north of the north end of the basin, they may have had a small effect on the geothermal gradient. For example, heating associated with Yellowstone volcanism currently should be at its maximum, and the gradient at the WASP well (the closest) is slightly higher than gradients in other parts of the basin. Miocene and Pliocene volcanoclastic rocks in the Jackson Hole area (Love and others, 1973) and Pleistocene alkalic rocks at the north end of the Rock Springs uplift (Love and Christiansen, 1985) represent local heating events, yet no evidence for these events is found in the regional pattern of vitrinite maturation (Lickus and others, this volume).

Theoretically, the vertical movement of subsurface waters is very effective in altering geothermal gradients. Hitchon (1984) successfully demonstrated a relationship

between coal rank, geothermal gradient, and hydrodynamics in the Alberta basin of Canada, but Gretener (1981) found many claims of such a relationship to be tenuous. Although geothermal gradients in several areas of the Green River basin appear to have been modified by subsurface waters (B.E. Law, written commun., 1986), such modification is very difficult to document without extensive hydrodynamic data.

Fission track annealing studies of sandstones (Naeser, 1984, 1986) show that a 20–30 °C cooling event occurred 2 to 4 Ma in the area of the Wagon Wheel well. This cooling event coincides with a period of regional uplift that resulted in widespread erosion and a drop of approximately 10 °C in surface temperature. Theoretical calculations show the thermal diffusivity of sandstones is such that a 10 °C change in the surface temperature can produce, in a period of 3 m.y., a similar change in the temperature of rocks 3 km deep (Stegna and Dovenyi, 1983). In the same time and depth range, the geothermal gradient can also reequilibrate after as much as 1,000 m of surface erosion. Paleotemperatures modeled for the subsurface therefore must account for changes in surface temperature as well as for deposition and erosion.

VITRINITE REFLECTANCE DATA

Vitrinite reflectance (R_m) data used in this study are from Law and others (1980), Law (1984), and Pawlewicz and others (1986). Pyrolysis and atomic ratio analysis indicate the kerogen of these samples is dominantly humic or type III in composition (Law, 1984). For reflectance measurements, woody or coaly fragments from core were handpicked and supplemented with concentrates of dispersed organic matter from core and drill cuttings. Because of the nature of the kerogen, the quality of vitrinite was good, and reflectance measurements yielded relatively narrow histograms (M.J. Pawlewicz, written commun., 1984).

Vitrinite reflectance data for the WASP, Wagon Wheel, and Pacific Creek wells were used for burial reconstruction because the wells are the most extensively cored wells in the northern Green River basin. Vitrinite reflectance gradients (fig. 4) in the wells are similar to those of Dow (1977) for low geothermal gradients and young geologic sections. The Wagon Wheel well has the most core over the largest depth interval and shows the strongest correlation between log R_m and depth (fig. 4). The vitrinite reflectance gradient for the Wagon Wheel well (fig. 4B) is almost identical to that obtained independently by Pollastro and Barker (1984). The WASP well also shows a good correlation between log R_m and depth, but the four uppermost samples are from drill cuttings and may bias the linear fit (fig. 4). The Pacific Creek well actually includes reflectance measurements from core

and drill cuttings in three closely spaced wells; selective sampling for vitrinite was limited, and the correlation between log R_m and depth is inferior to that of the other two wells because most of the available samples consist of drill cuttings and random core chips from shale and siltstone (fig. 4).

BURIAL AND THERMAL RECONSTRUCTIONS

In this study, vitrinite reflectance data were combined with maturation models to evaluate the Tertiary burial history of the basin. The evaluation depends on the quality of the reflectance data, an understanding of the geothermal gradient, and the validity of the maturation model. Results from several models were compared, but the Lopatin model of Waples (1980) offers the easiest way to test depth and duration of burial against measured reflectance data. The amount of section known to be missing at each well was compared to the maximum burial depth determined by projecting the vitrinite reflectance gradient to 0.2 percent, a value most workers (notably, Dow, 1977) consider to be the surface intercept in un-eroded terrain (fig. 4).

The geologic history (fig. 2) was used to construct burial curves for the Cretaceous-Tertiary boundary, the top of the Ericson Sandstone, and the tops of the Blair and Hilliard Shales (fig. 4). The total organic maturity or time-temperature index (TTI) for these horizons was calculated according to Waples (1980). By using the TTI- R_m calibration of Waples (1980), the average R_m value for each horizon was converted to a measured TTI value for comparison with the calculated TTI value. Thus, burial history may be used to evaluate maturation models, or conversely, burial curves and geothermal gradient may be altered to match calculated and measured TTI values.

The Ericson Sandstone is the best horizon with which to compare measured and calculated TTI because it is the most traceable time-correlative horizon in the basin and also the one for which there is the most R_m data. Wherever the match for one horizon is good, the model of Waples (1980) does not accurately predict the maturation of the other two horizons (fig. 4). These inaccurate predictions may result from errors in R_m measurements, errors in the TTI- R_m relationship of Waples, errors in modeling the rate of vitrinite maturation, or errors in estimating the value and shape of the paleogeothermal gradient.

Burial curves for the WASP and Pacific Creek wells, as determined by stratigraphic analysis, generally agree with the R_m surface intercept and produce a reasonable match between calculated and measured TTI values for the Ericson Sandstone (fig. 4), except that the measured TTI value for the Ericson at the WASP well is somewhat lower than the calculated value. The

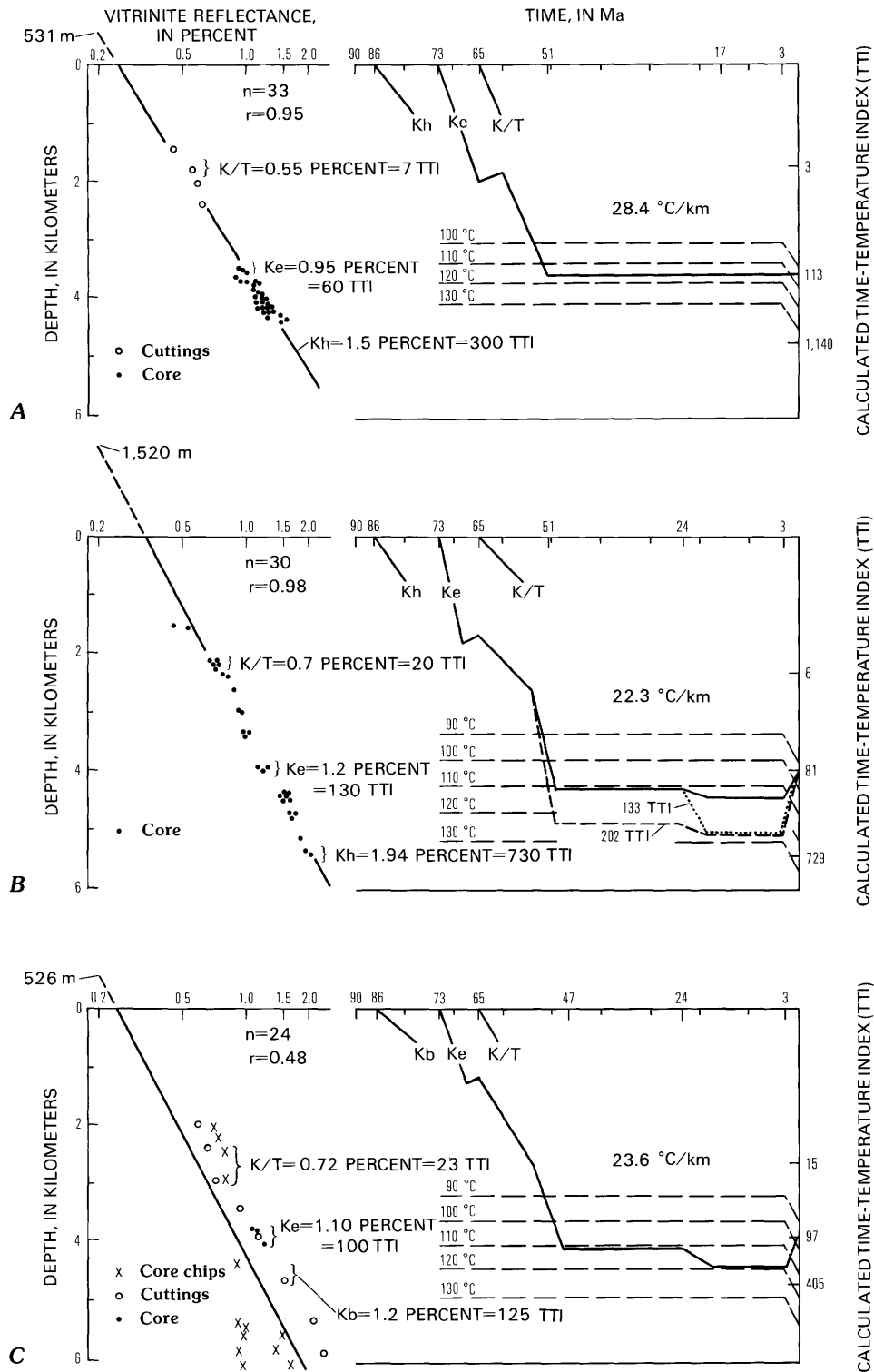


Figure 4. Vitrinite reflectance values and Lopatin reconstructions for the top of Ericson Sandstone (Ke) at the WASP (A), Wagon Wheel (B), and Pacific Creek (C) wells. Burial curves for the tops of the Baxter (Kb) and Hilliard (Kh) Shales and for the Cretaceous-Tertiary boundary (K/T) (fig. 2) are parallel with that for the Ericson Sandstone. For these horizons, calculated TTI values (right side) may be compared to measured TTI values (converted from measured vitrinite reflectance data (see appendix) by using method of Waples (1980)). Constant geothermal gradients use a surface temperature of 15 °C, which has decreased to 4 °C from 3 Ma to the present time. Plots of vitrinite reflectance versus depth show the elevation of the extrapolated intercept with 0.2 percent reflectance. Modified from Law and others (1980) and Law (1984).

difference in TTI values for the WASP well reflect high present-day geothermal gradients in the Yellowstone and Jackson Hole areas that may have caused a recent increase in the gradient at the WASP well. The Rm surface intercept at the WASP well predicts slightly hotter paleotemperatures than can be explained by burial and the Lopatin model, but this may result from the four shallow measurements from cuttings, which may bias the Rm gradient.

At the Wagon Wheel well, extrapolation of the Rm line to 0.2 percent reflectance indicates that 600–1,000 m of section has been eroded in addition to the 470 m that is missing from the stratigraphic section (fig. 4). If we assume that present-day and paleogeothermal gradients are similar, then the Ericson must have been buried 1,100–1,500 m deeper than at present. Stratigraphic data indicate, however, that no more than 470 m of section has been eroded from the area, and two interpretations are possible for this discrepancy.

Recent Folding

Cross sections in Lickus and others (1984, this volume) and in figure 5 show that isoreffectance lines are parallel with the Pinedale structure and suggest that the present-day Rm values in the Wagon Wheel well may have been physically elevated into their position by uplift

on the anticline sometime after maximum maturation or uplift and cooling during the Pliocene. The anticline has about 600 m of structural relief (Law, 1984; Law and Johnson, this volume), and local erosion resulting from uplift on the anticline could account for the additional missing section required by the reflectance data. Presumably, both local (600 m) and regional (470 m) erosion occurred during the cooling event indicated by the fission-track data (Naeser, 1984).

Some independent data support recent uplift on the Pinedale anticline. A listric normal fault penetrated by Wagon Wheel core probably was associated with uplift of the Pinedale anticline. Both petrographic and isotopic evidence (Dickinson, 1985) suggest that fractures associated with this fault are filled with relatively recent cements. In addition, fluid inclusion studies suggest that quartz in some of these fractures precipitated at or near the present-day formation temperature (Pollastro and Barker, 1984). In view of post-Pliocene movement on the Continental fault (Love, 1954; Zeller and Stephens, 1969), recent folding at Pinedale would not have been an isolated tectonic event.

In spite of the above evidence, some expected indications of recent folding are lacking. The Pinedale anticline is poorly defined at the surface, whereas recent structural features should be easily recognized. In addition, the listric normal fault associated with the anticline in the subsurface does not appear to penetrate Eocene

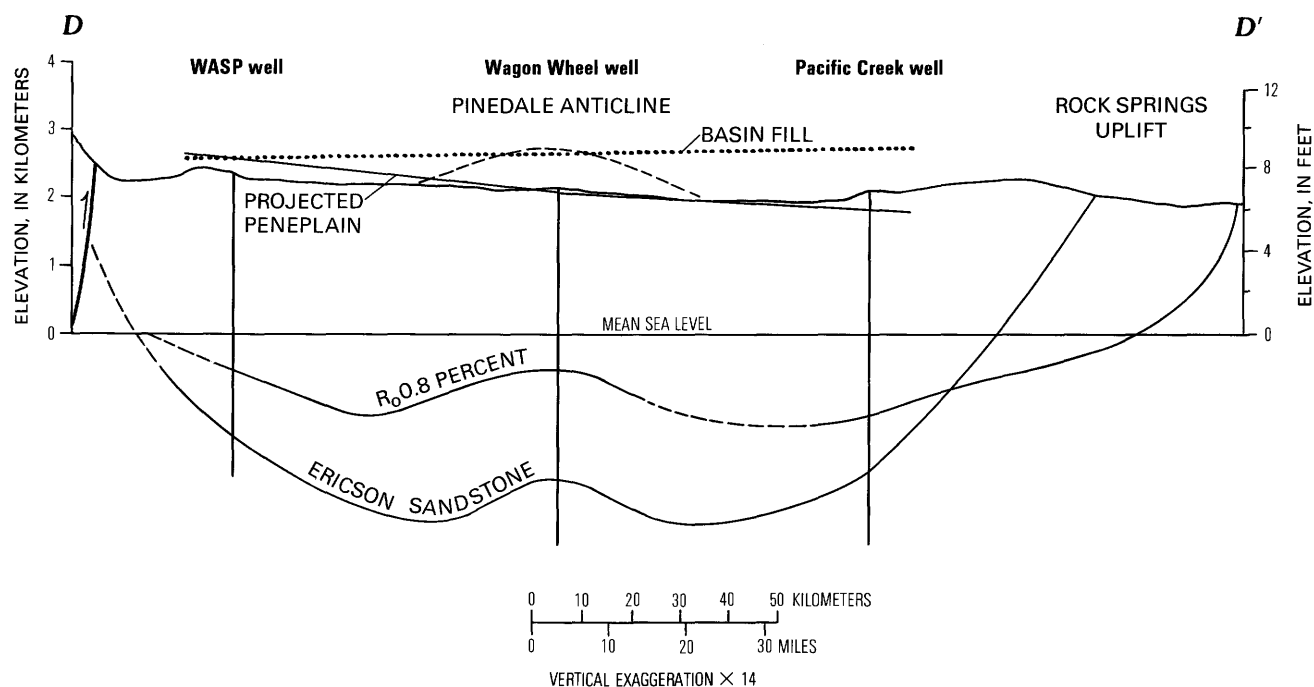


Figure 5. Cross section showing relationships between stratigraphy, structure, thermal maturation, and burial in northern Green River basin. Wind River peneplain projected into plane of cross section (fig. 3) to show its present relationship with basin fill. Stratigraphic data modified from Law (1981); Rm data from Pawlewicz and others (1986). Line of section shown on figure 1.

rocks at the surface. Structural details may be obscured, however, by the lack of traceable beds in the arkosic facies of the Wasatch Formation and by the poorly cemented and unconsolidated nature of this formation at the surface.

The stratigraphic age of the 600 m of missing section that may have been lost to local erosion of the anticline is unclear and is not indicated by the Lopatin maturation model. If post-Eocene deposition was minimal, as suggested by stratigraphic evidence, and an additional 600 m of Wasatch Formation was eroded, then the calculated TTI for the Ericson Sandstone would be 202 (dashed burial curve, fig. 4), much higher than the measured TTI of 130. On the other hand, if 600 m of Miocene rocks was eroded, a supposition not supported by stratigraphic evidence, then the measured (130) and calculated (133) TTI values for the Ericson Sandstone are in good agreement (dotted burial curve, fig. 4).

Elevated Paleogeothermal Gradient

The second interpretation for the discrepancy in amount of missing section is that a local heating event elevated the vitrinite reflectance values around the Pinedale anticline. If we assume that the Pinedale anticline is Laramide in age (Law and Johnson, this volume), then the paleotemperature gradient needs to be increased from the Eocene to the Pliocene by only 2 °C/km over the present-day gradient in order for calculated and measured TTI values in the Ericson Sandstone to agree (fig. 6). The uncorrected borehole temperature gradient is probably not in error by this amount because the temperature map of Law and Smith (1983), which uses the adjacent wells, shows no thermal anomaly that might explain the relationship between isorefectance lines and structure. Upward migration of hot fluids along faults and fractures associated with folding on the anticline could have locally increased the gradient, but there is no evidence to explain why the migration of hot fluids suddenly stopped or why the geothermal gradient decreased to the present level. Possible hydrothermal fluids, which can cause thermal anomalies, are presently inactive.

The 20–30 °C of recent cooling required by the fission-track data (Naeser, 1984) can be more easily explained if the paleogeothermal gradient was higher than the present-day gradient. If an additional 600 m of sediments was eroded as the result of uplift on the anticline, then about 40 °C of cooling would have occurred since the Pliocene (fig. 4B); however, if the geothermal gradient prior to the Pliocene was higher, then the amount of cooling would be about 25 °C, more similar to the amount of cooling predicted by fission-track annealing (fig. 6).

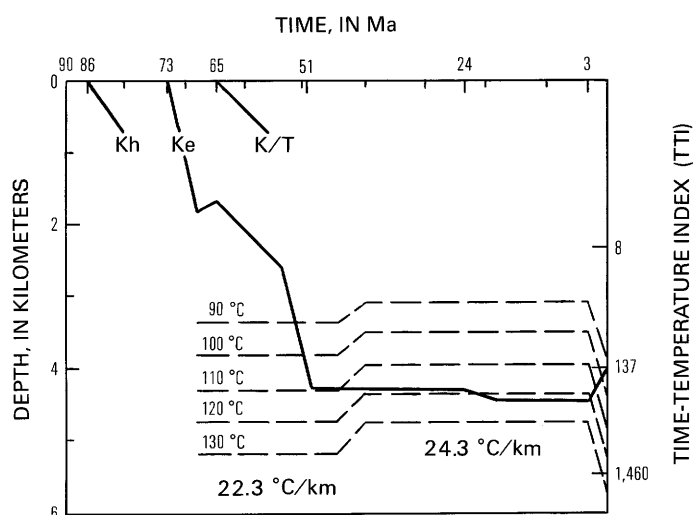


Figure 6. Lopatin reconstruction for a local increase in geothermal gradient in the Wagon Wheel area. Burial curves for the tops of the Ericson Sandstone (Ke) and Hilliard Shale (Kh) and for the Cretaceous-Tertiary boundary (K/T) same as in figure 4B, except without 600 m of structural uplift and erosion. Geothermal gradient increases shortly after possible Laramide folding of Pinedale anticline, then decreases back to 22.3 °C/km at 3 Ma. Modeled using method of Waples (1980).

In support of this explanation, Meyer and McGee (1985) observed elevated thermal gradients associated with structure in 15 of the 22 oil and gas fields they examined in the Rocky Mountain region. They attributed the elevated gradients to upward migration of fluids. On the Rock Springs uplift, the 0.8-percent reflectance line dips more steeply than structure on the Ericson Sandstone (fig. 5) (Pawlewicz and others, 1986), and this steep dip may result from the upward migration of hydrothermal fluids along fractures and faults (B.E. Law, written commun., 1986).

VITRINITE MATURATION MODELS

Vitrinite maturation models are used to predict the maximum temperature to which organic-rich sediments have been exposed. Although much progress has been made toward the refinement of these models, the relationship between the rate of maturation and temperature remains uncertain because independent calibration of maximum rock temperature is lacking and because subtle differences exist in the chemical and physical properties of the vitrinite macerals. For example, Price (1983) argued that vitrinite maturation follows high-order reaction kinetics, whereas most workers believe it follows first-order reaction kinetics. These differences of opinion have led to the development of essentially two categories

of models: (1) time-dependent models, which require time or length of heating in the maturation process, and (2) time-independent models, which discount the time factor and suggest that vitrinite is an absolute paleogeothermometer.

The time-dependent model of vitrinite maturation developed by Waples (1980) was used in this study mainly because it is widely accepted and allows for easy adjustment of burial curves. In view of the uncertainties, however, a comparison of this model and several other vitrinite models on a common basis with the known geologic history of the basin seems necessary. The comparison was done at each well, similar to the method of Bostick and Freeman (1984), by using selected models to calculate maximum paleotemperatures from measured R_m values (fig. 7). Paleotemperature gradients predicted by a regression analysis of these temperatures were compared to present-day temperature gradients and estimates of basin fill. If present-day and paleotemperature gradients are similar and stratigraphic estimates of basin fill are correct, the ideal paleotemperature gradient should be parallel with the present-day temperature gradient and intercept the elevation of the estimated basin fill at about 15 °C, the estimated surface temperature of the basin at the time of maximum burial.

For each well, the time-independent models of Price (1983) and Barker and Pawlewicz (1985) predict

significantly higher paleogeothermal gradients than can be accounted for by geologic evidence (fig. 7). In addition, these high paleogeothermal gradients do not agree with fission-track annealing data for the Wagon Wheel well. The lack of annealing in zircon in the deepest fission-track samples (4,557 m) indicates that temperatures in the surrounding rocks could not have been hotter than 175–200 °C, the minimum temperature at which zircon begins to anneal (Naeser, 1984). The present-day temperature at this depth is 113 °C and would have been only 126 °C had the paleogeothermal gradient been 2 °C/km hotter than the present-day gradient. In contrast, the temperature calculated from measured R_m data at this depth is 241 °C for the model of Price (1983) and 205 °C for the model of Barker and Pawlewicz (1985).

The time-dependent models of Hood and others (1975) and Middleton (1982) provide the best agreement between R_m data, present-day temperature gradient, and estimated burial at each well (fig. 7). The equations in the appendix show that these two models define temperature in different ways. The model of Hood and others (1975) predicts the maximum paleotemperature by using the amount of time (t_{eff}) at which burial is within 15 °C of the maximum temperature. In this study, t_{eff} was determined as a single value for each well according to the burial curves shown in figure 4. In the model of Middleton (1982), temperature is constant for a given length

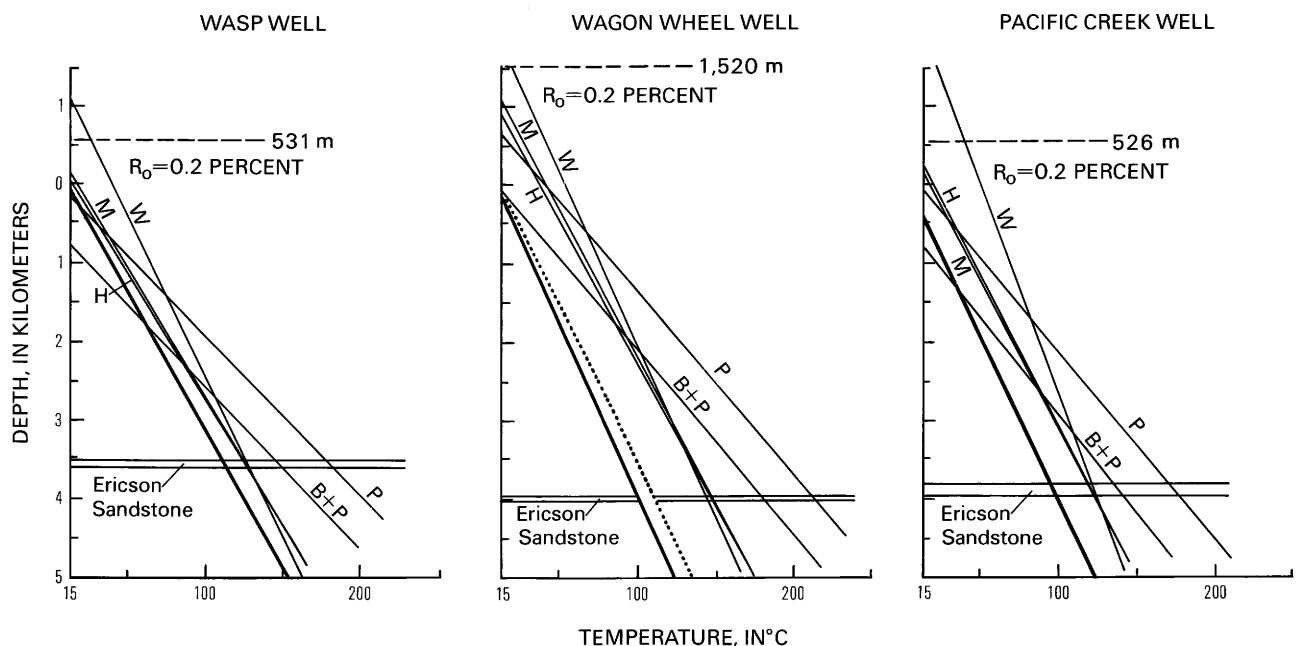


Figure 7. Linear regression least-squares fits of maximum paleotemperatures for the WASP, Wagon Wheel, and Pacific Creek wells calculated by using selected vitrinite maturation models and vitrinite reflectance values and equations shown in appendix. Present-day uncorrected temperature gradients (heavy solid lines) calculated from drill-stem tests and

geophysical logs; paleogeothermal gradient (dotted line) from Lopatin reconstruction (fig. 6). Estimated surface temperature of basin during maximum burial 15 °C. Vitrinite maturation models: H, Hood and others (1975); W, Waples, (1980); M, Middleton (1982); P, Price (1983); B+P, Barker and Pawlewicz (1985).

of time, the age of the rock. The two models give similar results, probably because the rocks were buried rapidly and were subjected to a long period of constant heating at or near maximum temperatures. In the MWX wells of the Piceance basin, Bostick and Freeman (1984) showed that predictions from numerous time-dependent models are similar and fit the geologic data better than those from time-independent models.

Paleotemperature gradients predicted by using the model of Waples (1980) are slightly lower than present-day gradients. These lower gradients, and the high elevations of the intercepts at 15 °C, reflect the low TTI values for the Cretaceous-Tertiary horizons and the high TTI values for the Hilliard and Baxter horizons calculated for the burial reconstructions (figs. 4, 6). The three time-dependent models predict almost identical temperatures for the Ericson Sandstone in each well (fig. 7), temperatures close to the maximum temperatures predicted by the burial curves (figs. 4, 6).

It is not clear why the Lopatin model of Waples (1980) predicts paleogeothermal gradients that are lower than present-day gradients; either geothermal gradients must change significantly with depth or burial curves must differ at each horizon. Both of these alternatives seem less likely than error in the model of Waples (1980). Variations of the Lopatin model (Koncz, 1983) that use different Rm-TTI relationships also predict low paleogeothermal gradients. The solution, therefore, is not a simple calibration of the Rm-TTI relationship for the Green River basin, as suggested by Issler (1984), but perhaps a reevaluation of the basic time-temperature relationship used in the model.

Discrepancies between thermal gradients do not necessarily discredit those models that do not fit the observed geologic data, but they do point out the need for evaluating several vitrinite maturation models at any specific location. Until the uncertainties of vitrinite maturation modeling are clarified, we may find that no model is universally applicable and that different models work better in different situations.

SUMMARY AND CONCLUSIONS

Analysis of vitrinite reflectance data in the northern Green River basin agrees with geologic evidence for depth and duration of burial. Extrapolation of the vitrinite reflectance profiles to 0.2 percent in the WASP and Pacific Creek wells yields elevations of basin fill that are consistent with stratigraphic evidence: only a minor amount of post-Eocene sediments has been removed in the northern end of the basin, and about 600 m of sediments has been removed by post-Pliocene erosion of the basin near the southern end of the Wind River Mountains. The duration of maximum burial (middle Eocene

to Pliocene), as indicated by time-dependent models of vitrinite maturation, agrees well with the depositional history of the basin and the fission-track data of Naeser (1984).

Available geologic evidence indicates that the amount of post-Eocene deposition (165 m) in the Wagon Wheel area should be intermediate between that in the WASP (no deposition) and Pacific Creek (335 m) areas. Using the present-day geothermal gradient, however, this intermediate amount of fill cannot account for the high reflectance values measured in the area. These high values probably result either from recent folding of the Pinedale anticline or from a local increase in the paleotemperature gradient, but stratigraphic, fission-track, and maturation data cannot completely resolve this choice. The Lopatin model is more in accord, however, with stratigraphic and fission-track data if the paleogeothermal gradient was 2 °C/km higher than the present-day gradient.

Comparison of maturation models clearly indicates that time plays an important role in vitrinite maturation. Errors in the geothermal gradient are not as crucial if time-independent models are used because such models yield unrealistically high gradients at each of the three areas. The differences in results produced by different time-dependent models indicates uncertainty about the role of time. At the WASP well, vitrinite maturation does not appear to reflect the present-day geothermal gradient, which may be at a maximum because of heating to the north, but independent data such as fission-track annealing are needed to support this conclusion.

REFERENCES CITED

- Armstrong, F.C., and Oriel, S.S., 1965, Tectonic development of Idaho-Wyoming thrust belt: *American Association of Petroleum Geologists Bulletin*, v. 49, no. 11, p. 1847-1866.
- Baker, C.L., 1946, Geology of the northwestern Wind River Mountains, Wyoming: *Geological Society of America Bulletin*, v. 57, no. 6, p. 565-596.
- Barker, C.E., and Pawlewicz, M.J., 1985, The correlation of vitrinite reflectance with maximum temperature in humic organic matter: Society of Economic and Paleontologic Mineralogists Midyear Meeting, Golden, Colo., 1985, Abstracts, p. 8.
- Basham, W.L., and Martin, W.F., 1985, Seismic line across the Wind River thrust fault, Wyoming, *in* Gries, R.R., and Dyer, R.C., eds., *Seismic exploration of the Rocky Mountain region: Rocky Mountain Association of Geologists*, p. 59-66.
- Blackwelder, E., 1915, Post Cretaceous history of the mountains of central western Wyoming: *Journal of Geology*, v. 23, p. 97-117, 193-217, 307-340.
- Bostick, N.H., and Freeman, V.L., 1984, Tests of vitrinite reflectance and paleotemperature models at the Multiwell Experiment site, Piceance Creek basin, Colorado, *in* Spencer, C.W., and Keighin, C.W., eds., *Geologic studies*

- in support of the U.S. Department of Energy Multiwell Experiment, Garfield County, Colorado: U.S. Geological Survey Open-File Report 84-757, p. 110-120.
- Bottjer, R., 1984, Depositional environments and tectonic significance of the South Pass formation, southern Wind River Range, Wyoming: Laramie, University of Wyoming, M.S. thesis, 229 p.
- Christiansen, R.L., and Blank, H.R., Jr., 1972, Volcanic stratigraphy of the Quaternary rhyolite plateau in Yellowstone National Park: U.S. Geological Survey Professional Paper 729-B, 18 p.
- Denson, N.M., and Pipiringos, G.M., 1974, Geologic map and sections showing areal distribution of Tertiary rocks near the southeastern terminus of the Wind River Range, Fremont and Sweetwater Counties, Wyoming: U.S. Geological Survey Miscellaneous Investigations Map I-835.
- Dickinson, W.W., 1985, Isotope geochemistry of carbonate minerals in nonmarine rocks, northern Green River basin, Wyoming: U.S. Geological Survey Open-File Report 85-532, 103 p.
- Dorr, J.A., Spearing, D.R., and Steidtmann, J.R., 1977, Deformation and deposition between a foreland uplift and an impinging thrust belt, Hoback basin, Wyoming: Geological Society of America Memoir 177, 82 p.
- Dow, W.G., 1977, Kerogen studies and geological interpretations: *Journal of Geochemical Exploration*, v. 7, p. 79-99.
- Eaton, G.P., Prostka, H.J., Oriol, S.S., and Pierce, K.L., 1976, Cordilleran thermal tectonic anomaly; geophysical and geological evidence of coherent late Cenozoic intraplate magmatism and deformation: *Geological Society of America Abstracts with Programs*, v. 8, no. 6, p. 850.
- Gretnere, P.E., 1981, Geothermics; using temperature in hydrocarbon exploration: *American Association of Petroleum Geologists Continuing Education Course Note Series 17*, 170 p.
- Hitchon, Brian, 1984, Geothermal gradients, hydrodynamics, and hydrocarbon occurrences, Alberta, Canada: *American Association of Petroleum Geologists*, v. 68, no. 6, p. 713-743.
- Hood, A., Gutjahr, C.C.M., and Heacock, R.L., 1975, Organic metamorphism and the generation of petroleum: *American Association of Petroleum Geologists Bulletin*, v. 59, no. 6, p. 986-996.
- Issler, D.R., 1984, Calculation of organic maturation levels of offshore eastern Canada; implications for general application of Lopatin's method: *Canadian Journal of Earth Sciences*, v. 21, no. 4, p. 477-488.
- Koncz, I., 1983, Comparison of the Lopatin methods and their critical evaluation: *Acta Mineralogical-Petrographica*, Szeged, v. 26, no. 1, p. 51-71.
- Law, B.E., 1981, Section C-C; subsurface correlations of some Upper Cretaceous and Tertiary rocks, northern Green River basin, Wyoming: U.S. Geological Survey Open-File Report 81-663, 1 sheet.
- _____, 1984, Relationships of source-rock, thermal maturity, and overpressuring to gas generation and occurrence in low-permeability Upper Cretaceous and lower Tertiary rocks, greater Green River basin, Wyoming, Colorado, and Utah, *in* Woodward, Jane, Meissner, F.F., and Clayton, J.L., eds., *Hydrocarbon source rocks of the greater Rocky Mountain region: Rocky Mountain Association of Geologists*, p. 469-490.
- Law, B.E., and Nichols, D.J., 1982, Subsurface stratigraphic correlations of some Upper Cretaceous and lower Tertiary rocks, northern Green River basin, Wyoming [abs.], *in* Steidtmann, J.R., ed., *Subsurface practices in geology and geophysics: Laramie, University of Wyoming, Department of Geology and Geophysics, Earth Science Bulletin 15*, p. 17.
- Law, B.E., and Smith, C.R., 1983, Subsurface temperature map showing depth to 180 °F in the Greater Green River basin, Wyoming, Colorado, and Utah: U.S. Geological Survey Miscellaneous Field Studies Map MF-504.
- Law, B.E., Spencer, C.W., and Bostick, N.H., 1980, Evaluation of organic matter, subsurface temperature, and pressure with regard to gas generation in low-permeability Upper Cretaceous and lower Tertiary sandstones in Pacific Creek area, Sublette and Sweetwater Counties, Wyoming: *The Mountain Geologist*, v. 17, no. 2, p. 23-25.
- Lickus, M.R., Pawlewicz, M.J., Law, B.E., and Dickinson, W.W., 1984, Thermal maturity map, northern Green River basin, Wyoming, *in* Law, B.E., ed., *Geological characteristics of low-permeability Upper Cretaceous and lower Tertiary rocks in the Pinedale anticline area, Sublette County, Wyoming: U.S. Geological Survey Open-File Report 84-753*, p. 60-65.
- Love, J.D., 1954, Periods of folding and faulting during Late Cretaceous and Tertiary time [abs.]: *American Association of Petroleum Geologists Bulletin*, v. 38, no. 3, p. 1311-1312.
- _____, 1960, Cenozoic sedimentation and crustal movement in Wyoming: *American Journal of Science*, v. 285-A, p. 204-214.
- Love, J.D., and Christiansen, A.C., compilers, 1985, Geologic map of Wyoming: U.S. Geological Survey, 3 sheets, scale 1:500,000.
- Love, J.D., Reed, J.C., Christiansen, R.L., and Stacey, J.R., 1973, Geologic block diagram and tectonic history of the Teton region, Wyoming-Idaho: U.S. Geological Survey Miscellaneous Geological Investigations Map I-730.
- McGrew, P.O., 1959, The geology and paleontology of the Elk Mountain and Tabernacle Butte area, Wyoming: *American Museum of Natural History Bulletin*, v. 117, art. 3, p. 117-176.
- Merewether, E.A., Krystinik, K.B., and Pawlewicz, M.J., 1987, Thermal maturity of hydrocarbon-bearing formation in southwestern Wyoming and northwestern Colorado: U.S. Geological Survey Miscellaneous Investigations Map I-1831, scale 1:500,000.
- Meyer, H.J., and McGee, H.W., 1985, Oil and gas fields accompanied by geothermal anomalies in the Rocky Mountain region: *American Association of Petroleum Geologists Bulletin*, v. 69, no. 9, p. 933-945.
- Middleton, M.F., 1982, Tectonic history from vitrinite reflectance: *Royal Astronomical Society Geophysics Journal*, v. 68, p. 121-132.
- Moore, R.G., 1960, A Paleocene fauna from the Hoback Formation, Wyoming: *Ann Arbor, University of Michigan, Ph.D. thesis*, 169 p.

- Nace, R. H., 1939, Geology of the northwest part of the Red Desert, Sweetwater and Fremont counties, Wyoming: Wyoming Geological Survey Bulletin 27, 51 p.
- Naeser, N.D., 1984, Fission-track ages from the Wagon Wheel No. 1 well, northern Green River basin, Wyoming; evidence for recent cooling, *in* Law, B.E., ed., Geological characteristics of low-permeability Upper Cretaceous and lower Tertiary rocks in the Pinedale anticline area, Sublette County, Wyoming: U.S. Geological Survey Open-File Report 84-753, p. 66-77.
- _____, 1986, Neogene thermal history of the northern Green River basin, Wyoming; evidence from fission-track dating, *in* Gautier, D.L., ed., Roles of organic matter in sediment diagenesis: Society of Economic Paleontologists and Mineralogists Special Publication 38, p. 65-72.
- Pawlewicz, M.J., Lickus, M.R., Law, B.E., Dickinson, W.W., and Barclay, C.S.V., 1986, Thermal maturity map showing subsurface elevation of 0.8 percent vitrinite reflectance in the Greater Green River basin of Wyoming, Colorado, and Utah: U.S. Geological Survey Miscellaneous Field Studies Map MF-1890, scale 1:500,000.
- Pollastro, R.M., and Barker, C.E., 1984, Geothermometry from clay minerals, vitrinite reflectance, and fluid inclusions; applications to the thermal and burial history of rocks cored from the Wagon Wheel No. 1 well, Green River basin, Wyoming, *in* Law, B.E., ed., Geological characteristics of low-permeability Upper Cretaceous and lower Tertiary rocks in the Pinedale anticline area, Sublette County, Wyoming: U.S. Geological Survey Open-File Report 84-753, p. 78-94.
- Price, L.C., 1983, Geologic time as a parameter in organic metamorphism and vitrinite reflectance as an absolute paleogeothermometer: *Journal of Petroleum Geology*, v. 6, p. 5-38.
- Roehler, H.W., 1978, Correlation of coal beds in the Fort Union, Lance, and Almond Formations in measured sections on the east flank of the Rock Springs uplift, Sweetwater County, Wyoming: U.S. Geological Survey Open-File Report 78-248, 1 sheet.
- Shuster, M.W., and Steidtmann, J.R., 1984, Origin and development of northern Green River basin; a stratigraphic and flexural study [abs.]: American Association of Petroleum Geologists Bulletin, v. 68, no. 4, p. 527.
- Smedes, H.W., and Prostka, H.J., 1972, Stratigraphic framework of the Absaroka volcanic supergroup in the Yellowstone National Park region: U.S. Geological Survey Professional Paper 729-C, 33 p.
- Stegena, L., and Dovenyi, P., 1983, Procedure to correct measured temperatures and temperature gradients for geological effects: *Zentralblatt für Geologie und Paläontologie*, v. 1, no. 1/2, p. 25-34.
- Steidtmann, J.R., 1987, The "Wyomide Event;" Oligocene deformation in the Rocky Mountain foreland of Wyoming: Geological Society of America Abstracts with Programs, v. 19, no. 7, p. 855.
- Steidtmann, J.R., Hurst, D.J., and Shuster, M.W., 1984, Structural evolution of part of the Wyoming thrust belt and foreland; a sedimentary-tectonic approach: Geological Society of America Abstracts with Programs, v. 16, no. 6, p. 667.
- Steidtmann, J.R., Middleton, L.T., Bottjer, R.J., Jackson, K.E., McGee, L.C., Southwell, E.H., and Lieblang, S., 1986, Geometry, distribution, and provenance of tectogenic conglomerates along the southern margin of the Wind River Range, Wyo., *in* Peterson, J.A., ed., Paleotectonics and sedimentation in the Rocky Mountain region, United States: American Association of Petroleum Geologists Memoir 41, p. 321-332.
- Waples, D.W., 1980, Time and temperature in petroleum formation; application of Lopatin's method to petroleum exploration: American Association of Petroleum Geologists Bulletin, v. 64, no. 6, p. 916-926.
- West, R.M., 1969, Geology and vertebrate paleontology of the northwestern Green River basin, Wyoming: Wyoming Geological Association Annual Field Conference, 21st, Casper, Wyo., 1969, Guidebook, p. 77-92.
- Westgate, L.G., and Branson, E.B., 1913, The later Cenozoic history of the Wind River mountains, Wyoming: *Journal of Geology*, v. 21, p. 142-159.
- Zeller, H.D., and Stephens, E.V., 1969, Geology of the Oregon Buttes area, Sweetwater, Sublette, and Fremont Counties, southwestern Wyoming: U.S. Geological Survey Bulletin 1256, 60 p.

APPENDIX 1

Appendix 1. Vitrinite reflectance values for Wagon Wheel, WASP, and Pacific Creek wells, northern Green River basin, and equations used to calculate paleotemperatures

A. Vitrinite reflectance values for study wells

[Depth in meters; vitrinite reflectance (Rm) in percent. Data from Law (1984)]

Wagon Wheel		WASP		Pacific Creek	
Depth	Rm	Depth	Rm	Depth	Rm
1,532.5	0.51	1,508.8	0.46	2,025.7	0.72
1,545.9	.46	1,815.1	.56	2,370.7	.72
2,148.2	.68	2,118.4	.57	2,557.9	.80
2,173.2	.74	2,421.6	.60	2,992.8	.80
2,175.4	.70	3,493.3	.93	4,438.5	.90
2,251.9	.72	3,558.5	.95	5,501.0	.91
2,254.0	.76	3,644.2	.97	5,681.2	.98
2,460.7	.78	3,708.5	.90	5,779.0	.96
2,479.5	.77	3,727.7	.92	5,779.0	1.43
2,738.3	.85	3,738.7	1.11	5,992.4	.91
3,092.2	.95	3,769.2	.99	5,992.4	1.39
3,100.7	.91	3,789.3	1.09	6,249.3	.92
3,360.1	.96	3,817.3	1.11	6,249.3	1.51
3,362.6	.98	3,952.3	1.05	3,876.1	1.05
3,368.3	1.03	3,970.9	1.16	3,880.4	1.05
3,992.0	1.22	4,042.0	1.13	4,105.0	1.20
4,005.4	1.15	4,059.3	1.10	1,979.7	.60
4,022.8	1.13	4,078.5	1.16	2,401.8	.64
4,542.1	1.47	4,087.1	1.11	3,032.8	.71
4,545.8	1.48	4,112.1	1.13	3,564.6	.91
4,547.0	1.53	4,187.3	1.15	3,977.6	1.10
4,548.5	1.48	4,205.6	1.21	4,709.2	1.50
4,550.7	1.55	4,207.8	1.23	5,471.2	2.00
4,554.3	1.49	4,231.8	1.18	5,903.4	2.28
4,897.5	1.61	4,264.5	1.28		
4,900.6	1.61	4,273.3	1.14		
4,907.6	1.65	4,291.9	1.31		
5,234.3	1.77	4,308.7	1.22		
5,474.2	1.98	4,321.8	1.24		
5,475.7	1.85	4,334.3	1.25		
		4,350.1	1.44		
		4,354.4	1.44		
		4,367.8	1.49		

B. Equations used to calculate paleotemperatures

1. Uncorrected borehole temperature gradients calculated by using data from geophysical logs and drill-stem tests in the following wells

Pacific Creek	T°C =	4.4 + 0.0236 (depth in meters)
Wagon Wheel	T°C =	2.2 + 0.0223 (depth in meters)
WASP 1-A	T°C =	8.9 + 0.0285 (depth in meters)

2. Price (1983)

$$T_{\max}(\text{°C}) = (302.97 \log R_0) + 187.33$$

3. Barker and Pawlewicz (1985)

$$\ln R_m = 0.0078 T_{\max}(\text{°C}) - 1.2, \text{ where}$$

R_m is mean random vitrinite reflectance as measured in oil

4. Hood and others (1975)

$$T_{\max}(\text{C°}) = 190 \log R_0 - 32.5 \log t_{\text{eff}} + 185$$

Level of maturation (LOM) converted to R_0 in unpublished nomogram of A. Hood (1976). t_{eff} = time (between 10 and 100 Ma) within 15 °C of T_{\max}

t_{eff} WASP	53 Ma
t_{eff} Wagon Wheel	48 Ma
t_{eff} Pacific Creek	49 Ma

5. Middleton (1982)

$$T_m(\text{C°}) = \ln(R_0^a - R^a/bt)/c, \text{ where}$$

a =	5.5
b =	2.8×10^{-6}
c =	0.065
R =	initial vitrinite reflectance (0.2 percent)
T_m =	constant temperature for a given time
t =	time (in millions of years)

6. Equation 35 of Koncz (1983) describes model of Waples (1980)

$$T_{\max}(\text{°C}) = 125.2(\log R_0 + 0.2645 \log e + 3.197) - 273, \text{ where}$$

e =	heating rate; °C/m.y. = $(T_i - T_0)/t_i$
T_i =	present-day temperature of rocks
T_0 =	initial temperature at burial (20 °C)
t_i =	age of rocks, in millions of years

Chapter G

Thermal Maturity Patterns in the Northern Green River Basin, Wyoming

By M.R. LICKUS, M.J. PAWLEWICZ, B.E. LAW, and
W.W. DICKINSON

Prepared in cooperation with the U.S. Department of Energy

U.S. GEOLOGICAL SURVEY BULLETIN 1886

GEOLOGY OF TIGHT GAS RESERVOIRS IN THE PINEDALE ANTICLINE AREA, WYOMING,
AND AT THE MULTIWELL EXPERIMENT SITE, COLORADO

CONTENTS

Abstract	G1
Introduction	G1
Methods	G1
Discussion	G2
Summary	G4
References cited	G5

FIGURES

1. Map showing depth to 0.8-percent vitrinite reflectance level in northern part of Green River basin of Wyoming G2
- 2-3. Linear regression plots of vitrinite reflectance values:
 2. Davis Granite Wash drill hole G2
 3. From 29 wells in northern part of Green River basin G3
4. Cross section showing structures, top of overpressured zone, and 0.8-percent isorefectance line in northern part of Green River basin G4
5. Sketches showing relationships between isorefectance lines and structural attitudes of sedimentary rocks G4

Thermal Maturity Patterns in the Northern Green River Basin, Wyoming

By M.R. Lickus¹, M.J. Pawlewicz, B.E. Law, and W.W. Dickinson²

Abstract

In the northern part of the Green River basin of Wyoming, thermal maturity patterns are similar to structural trends. In the Pinedale anticline area, thermal alteration effects caused by relatively hot fluids migrating upward along faults and fractures may render invalid techniques commonly used to determine the temporal relationships between structural growth and the development of thermal maturity.

INTRODUCTION

In recent years, thermal maturity studies have been increasingly utilized in basin analysis to study hydrocarbon generation and migration and to provide insight into the structural and burial history of a basin. Several methods are used to determine the level of thermal maturity, the most common of which is vitrinite reflectance.

In oil-prone source rocks, the thermal maturation window for oil generation is between 0.6 and 1.3 percent vitrinite reflectance. In gas-prone source rocks, vitrinite reflectance values for the initiation of thermogenic gas are poorly known, but values ranging from 0.5 to 0.8 percent have been reported (Law and others, 1979, 1980; Magoon and Claypool, 1983; Monnier and others, 1983; Law, 1984; Pitman and others, 1985). In the Pacific Creek area of the Green River basin, the generation of significantly large volumes of thermogenic gas begins at a vitrinite reflectance of about 0.8 percent (Law and others, 1979, 1980; Law and Spencer, 1981; Spencer and Law, 1981; Law, 1984).

In our study we attempt to determine the vitrinite reflectance level in the northern part of the Green River basin (fig. 1) and to provide information on the relationship between the thermal and structural history of the Pinedale anticline area. Our report expands on and supersedes the thermal maturity map of the northern part of the Green River basin by Lickus and others (1984).

METHODS

Vitrinite reflectance values for 138 samples from 29 drill holes (fig. 1) were used to construct a thermal maturity map; as many as 33 samples were collected from each drill hole. Coal samples were preferentially collected in order to minimize inclusion of recycled organic matter and to expedite sample preparation. Drill cuttings of shale and sandstone were processed by using an acid maceration technique (King and others, 1963; Saxby, 1970). Coal samples and cuttings samples were mounted in epoxy on petrographic slides and polished, and vitrinite reflectance was then measured under oil immersion. Vitrinite reflectance measurements were made by M.J. Pawlewicz, N.H. Bostick, and B.E. Law of the U.S. Geological Survey and by Robertson Research (U.S.) Incorporated, Houston, Tex.

Measurement of vitrinite reflectance of core samples presents few analytical problems; however, cuttings samples can be contaminated as a result of uphole sloughing or lignite drilling and additives. These effects can be minimized by altering the sample scanning method and by carefully selecting the organic matter from which vitrinite measurements are taken. For core samples, the least mature vitrinite is measured indiscriminantly; for cuttings samples, however, the most common material, or modal population, must be measured and choices must often be made between several populations or ranges of thermal maturity. Because of these constraints, the mean reflectance value was used to estimate the indigenous vitrinite population. In cases where the mean value did not accurately represent the vitrinite population, such as when vitrinite measurements were few and wide ranging, a pick was determined by the operator based on the polish of the slide and the quality of the organic matter. In almost all samples, the mean reflectance and the vitrinite reflectance of the pick are the same or almost the same.

The method used to determine 0.8-percent vitrinite reflectance for a drill hole depends on the number and stratigraphic distribution of samples within the hole. For drill holes containing more than four samples distributed

¹225 Old Bay Road, Bolton, MA 01740

²Research School of Earth Science, Victoria University
P.O. Box 600, Wellington, New Zealand

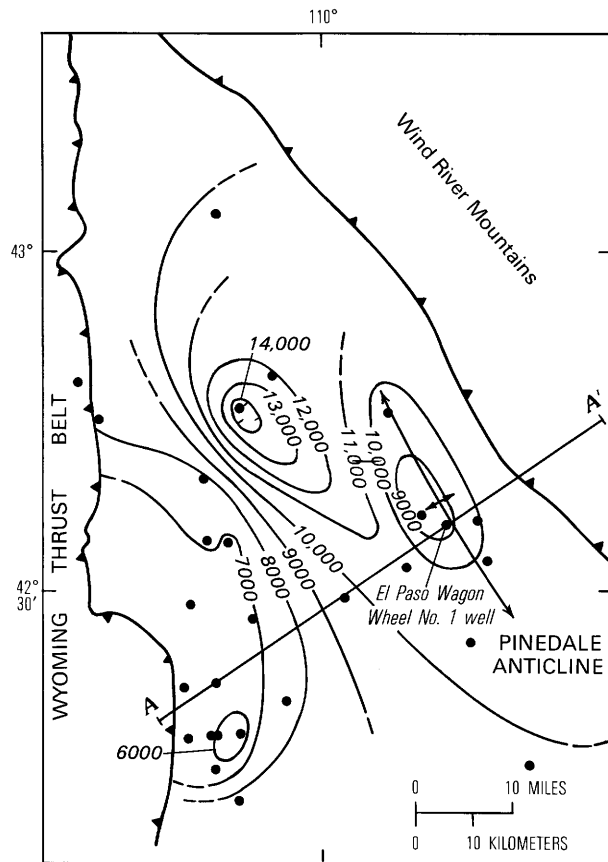


Figure 1. Depth to 0.8-percent vitrinite reflectance level (contour interval, 1,000 ft) in the northern part of the Green River basin of Wyoming. Thrust faults shown by heavy lines; saw-teeth on upper plate. Solid circles indicate drill holes from which samples for this study were collected. Line of section A-A' (fig. 4) also shown. Modified from Pawlewicz and others (1986).

over a significantly large depth interval, a linear regression plot of depth and the log of the vitrinite reflectance was constructed (Dow, 1977), and the depth to the 0.8-percent level in a given drill hole was calculated by using the least-squares regression line from the linear regression plot. For example, figure 2 shows data from the Davis Granite Wash well.

For drill holes containing fewer than 6 samples or for drill holes in which samples are distributed over a relatively narrow depth interval, data from all 29 drill holes in the northern part of the Green River basin were used to calculate a regional least-squares linear regression line (fig. 3). The slope of the regional regression line was then used to calculate the depth to the 0.8-percent vitrinite reflectance level in individual drill holes. For example, in a drill hole containing three samples, the depth to the 0.8-percent level was calculated for each sample by using the slope of the regional regression line, and the three calculated values were then averaged to produce a single value for the drill hole.

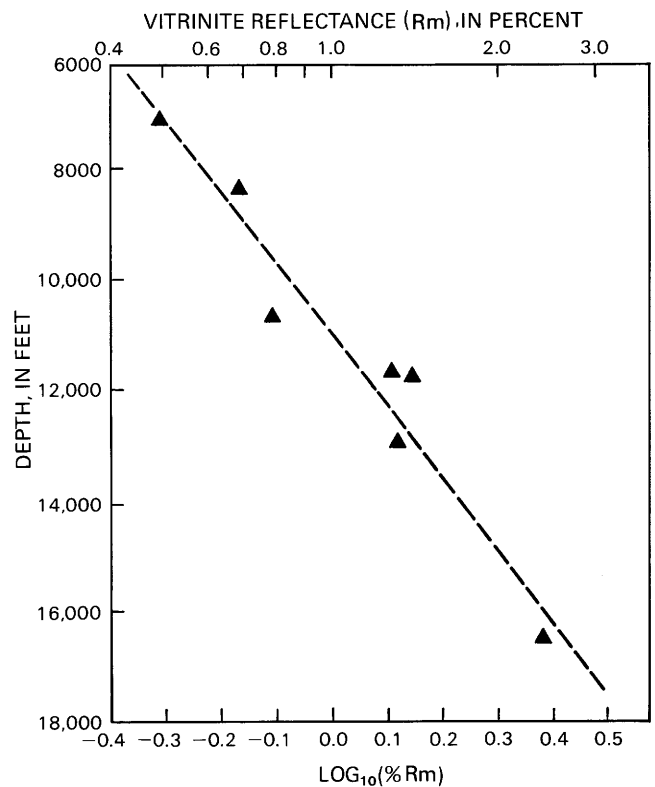


Figure 2. Linear regression plot of vitrinite reflectance (R_m) values, Davis Granite Wash drill hole (sec. 16, T. 29 N., R. 110 W.). (See Prenskey, this volume, fig. 1, for township-range map.) Linear and logarithmic scales shown. Dashed line is the least-squares linear regression line.

DISCUSSION

The thermal maturity map of the northern Green River basin (fig. 1) is modified from Pawlewicz and others (1986) and shows the depth to the 0.8-percent vitrinite reflectance level. This level was selected because observations in the Greater Green River basin indicate that significantly large volumes of gas begin to be generated at depths corresponding to vitrinite reflectance values of from 0.74 to 0.86 percent (Law and others, 1979, 1980; Law and Spencer, 1981; Law, 1984). The top of sustained gas shows is commonly associated with the top of overpressuring and an uncorrected (bottom-hole) subsurface temperature of about 180 °F (82 °C). Figure 4 shows, in cross section, the 0.8-percent isoreflexance line and the top of the overpressured zone. The depth to 180 °F (82 °C) was mapped by Law and Smith (1983).

In the area of the Pinedale anticline, the top of the overpressured zone is within the upper part of the Upper Cretaceous Lance Formation at a vitrinite reflectance of about 0.74 percent. The relationships between thermal maturity and overpressuring in the El Paso Wagon Wheel No. 1 well (fig. 4) have been discussed by Law (1984), Law and Dickinson (1985), and Spencer (1987, this volume). On

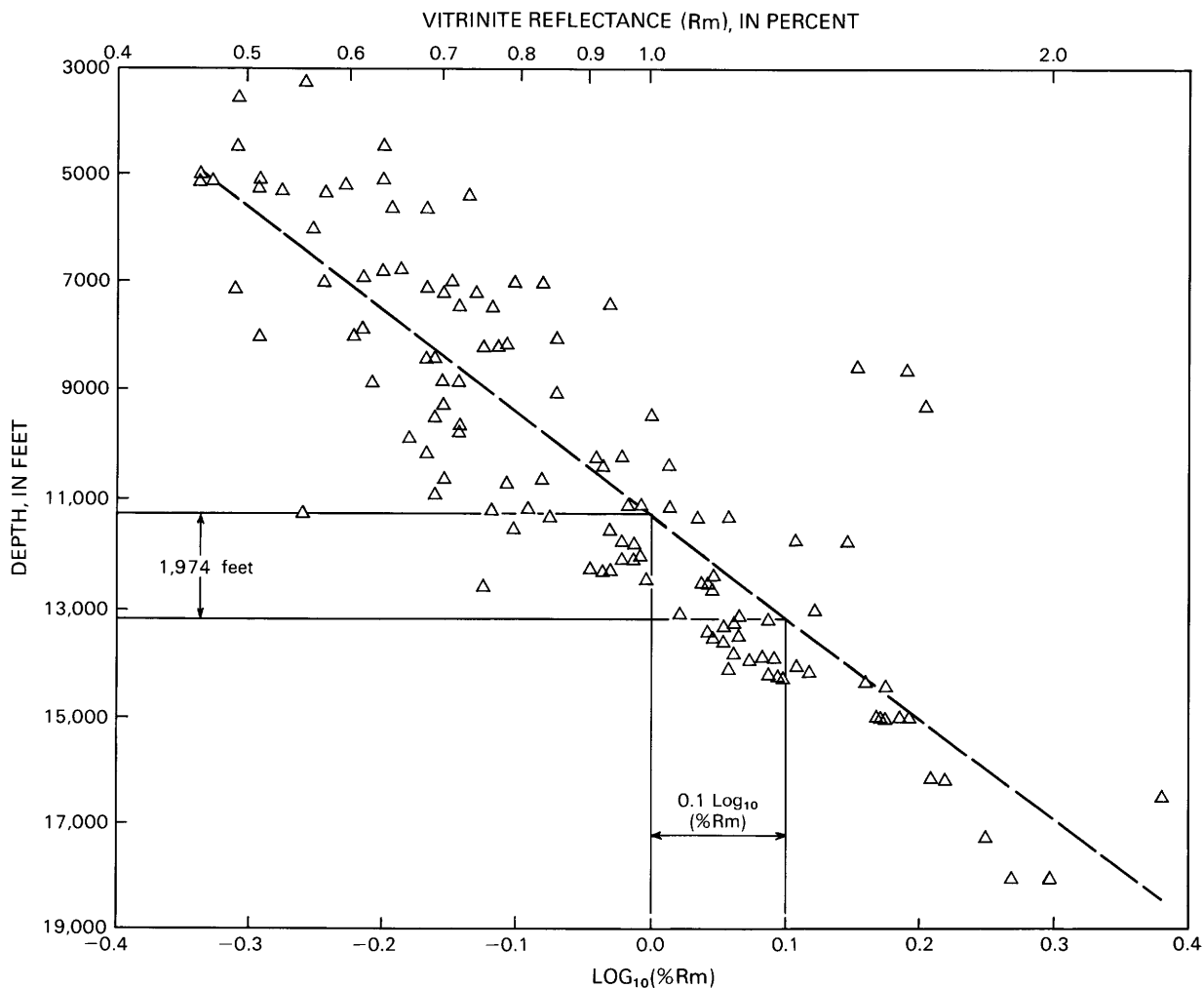


Figure 3. Linear regression plot of vitrinite reflectance (Rm) values from 29 wells in the northern part of the Green River basin. Slope of least-squares linear regression (dashed) is 19,740 ft/log₁₀Rm.

the LaBarge platform, the top of overpressuring is difficult to define but apparently is within the lower part of the Hilliard Shale at a vitrinite reflectance of less than 0.8 percent. The isoreflectance and top of overpressuring have similar configurations but are not coincident. One reason for the apparent lack of coincidence is the uncertainty in identifying the top of overpressuring. Another source of error is in the method used to calculate the depth of 0.8-percent vitrinite reflectance. The calculation assumes that thermal maturity (vitrinite reflectance) increases linearly with depth, but a recent study by Law and Nuccio (1986) and Law and others (1989) shows that vitrinite reflectance profiles in low-permeability rock sequences commonly are segmented and have one or more kinks or bends.

The configuration of thermal maturity contours in the area of the Pinedale anticline (fig. 1) is similar to the structural configuration (fig. 4). Along the line of section shown in figure 4, the stratigraphically highest

position of the 0.8-percent isoreflectance line is on the west flank of the Pinedale anticline. High vitrinite reflectance levels in this area may result from thermal alteration of organic matter by relatively hot fluids migrating upward along the fault. A similar area of unusually high thermal maturity has been observed in the Patrick Draw oil and gas field on the east side of the Rock Springs uplift in Wyoming and may result from hot fluids migrating upward along faults and fractures (Law and others, 1986).

Numerous attempts have been made to relate the configuration in cross section of an isoreflectance line and structural attitudes and to thereby infer the relative timing between thermal maturation and structural movement (Stach and others, 1975; Bustin and others, 1983). If isoreflectance lines are parallel with bedding (fig. 5A), thermal maturation is interpreted to have occurred prior to folding. If they are horizontal and cut across bedding planes (fig. 5B), maturation is believed to have occurred

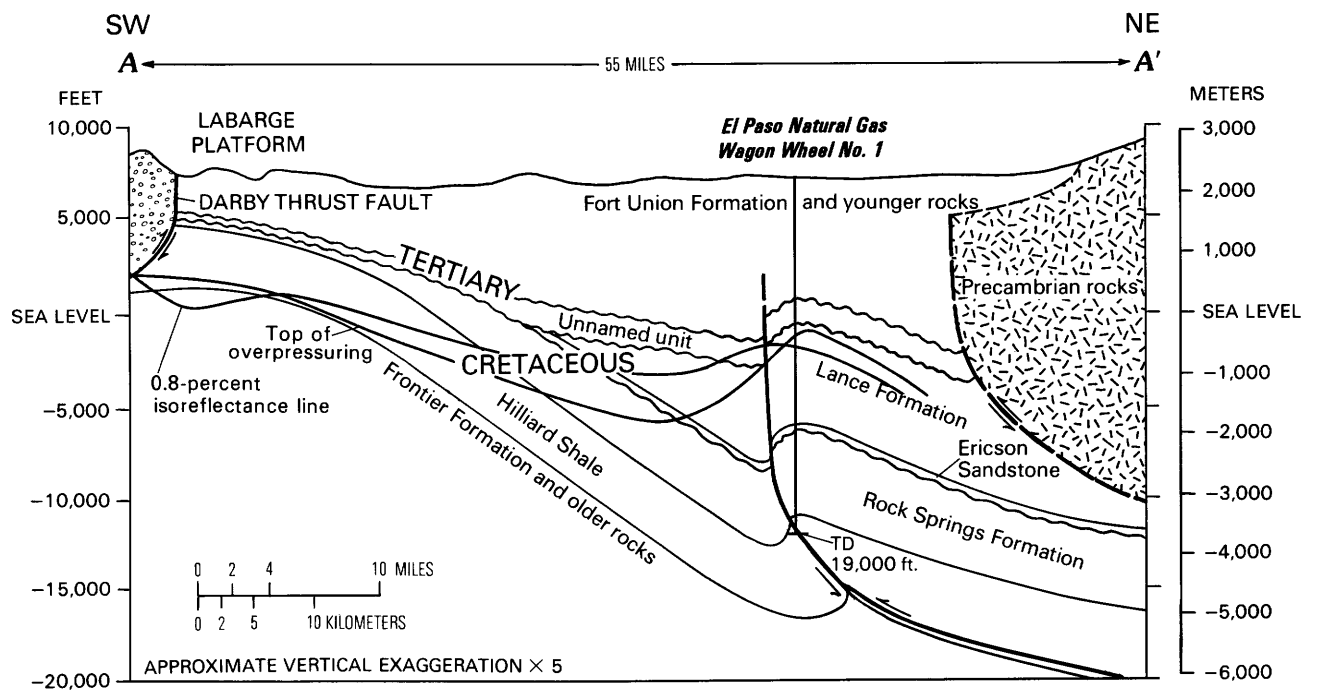


Figure 4. Cross section showing structures, top of overpressured zone, and 0.8-percent isorefectance line in the northern part of the Green River basin. Line of section A-A' shown in figure 1. Modified from Law and Johnson (this volume, fig. 2).

after folding. If they cut across bedding planes at a low angle and have a shallower dip than the bedding planes (fig. 5C), maturation and folding are interpreted to have occurred simultaneously.

Along the cross section shown in figure 4, isorefectance lines cut across bedding planes but have a steeper dip than bedding planes. This case is shown in figure 5D and may result from hot fluids ascending along already structurally deformed zones. The Pinedale anticline and associated structures may have acted as a focus for the movement of hot fluids and locally affected thermal maturation. We conclude that attempts to establish the timing of thermal maturation with respect to structural movement that are based on the cross sectional relationship between structure and isorefectance are not valid in the Pinedale anticline area.

SUMMARY

The configuration of the 0.8-percent vitrinite reflectance contours in the northern part of the Green River basin is similar to the configuration of Tertiary structures, but because of the possible influences of migrating hot fluids, interpretation of the relative timing of thermal maturation and structural events in the Pinedale anticline area by using cross sectional relationships may be misleading.

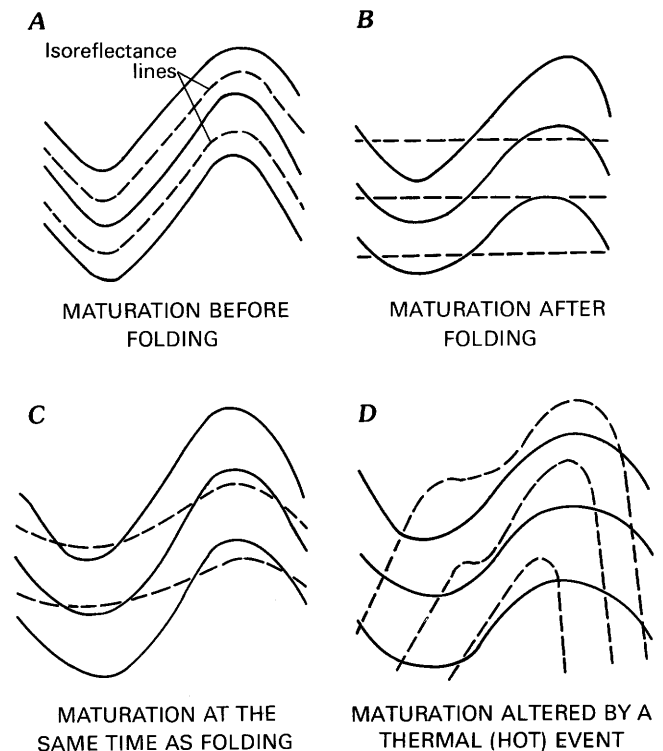


Figure 5. Relationships between isorefectance lines (dashed) and structural attitudes of sedimentary rocks. Modified from Bustin and others (1983). Bedding planes shown by solid lines. A, Thermal maturation prior to folding. B, Maturation after folding. C, Maturation at the same time as folding. D, Maturation altered by a thermal (hot) event.

REFERENCES CITED

- Bustin, R.M., Cameron, A.R., Grieve, D.A., and Kalkreuth, W.D., 1983, Coal petrology, its principles, methods, and applications: Geological Association of Canada Short Course Notes, v. 3, p. 161-169.
- Dow, W.G., 1977, Kerogen studies and geological interpretations: *Journal of Geochemical Exploration*, v. 7, no. 2, p. 79-99.
- King, L.H., Goodspeed, F.E., and Montgomery, D.S., 1963, A study of sedimented organic matter and its natural derivatives: Canada Department of Mines and Technical Surveys, Mines Branch Research Report R-114, 68 p.
- Law, B.E., 1984, Relationships of source rock, thermal maturity, and overpressuring to gas generation and occurrence in low-permeability Upper Cretaceous and lower Tertiary rocks, Greater Green River basin, Wyoming, Colorado, and Utah, *in* Woodward, Jane, Meissner, F.F., and Clayton, J.L., eds., Hydrocarbon source rocks of the greater Rocky Mountain region: Rocky Mountain Association of Geologists, p. 469-490.
- Law, B.E., and Dickinson, W.W., 1985, Conceptual model for origin of abnormally pressured gas accumulation in low-permeability reservoirs: *American Association of Petroleum Geologists Bulletin*, v. 69, p. 1295-1304.
- Law, B.E., Lickus, M.R., and Pawlewicz, M.J., 1986, Fluid migration pathways; evidence from thermal maturity mapping in southwestern Wyoming, *in* Carter, L.M.H., ed., USGS research on energy resources, 1986; programs and abstracts: U.S. Geological Survey Circular 974, p. 35.
- Law, B.E., and Nuccio, V.F., 1986, Segmented vitrinite reflectance profile from the Deep Seam project, Piceance Creek basin, Colorado; evidence of previous high pore pressure: *American Association of Petroleum Geologists Bulletin*, v. 70, no. 8, p. 1047.
- Law, B.E., Nuccio, V.F., and Barker, C.E., 1989, Kinky vitrinite of reflectance profiles; evidence of paleopore pressure in low-permeability, gas-bearing sequences in Rocky Mountain foreland basins: *American Association of Petroleum Geologists Bulletin*, v. 73, no. 8, p. 999-1010.
- Law, B.E., and Smith, C.R., 1983, Subsurface temperature map showing depth to 180 °F in the Greater Green River basin, Wyoming, Colorado, and Utah: U.S. Geological Survey Miscellaneous Field Studies Map MF-1504, scale 1:500,000.
- Law, B.E., and Spencer, C.W., 1981, Abnormally high-pressured, low-permeability, Upper Cretaceous and Tertiary gas reservoirs, northern Green River basin, Wyoming [abs.]: *American Association of Petroleum Geologists Bulletin*, v. 65, no. 5, p. 948.
- Law, B.E., Spencer, C.W., and Bostick, N.H., 1979, Preliminary results of organic maturation, temperature, and pressure studies in the Pacific Creek area, Sublette County, Wyoming: U.S. Department of Energy Symposium on Enhanced Oil and Gas Recovery and Improved Drilling Methods, 5th, Tulsa, Okla., 1979, Proceedings, v. 33, Petroleum Publishing Company, p. K2/1-2/13.
- _____, 1980, Evaluation of organic matter, subsurface temperature, and pressure with regard to gas generation in low-permeability Upper Cretaceous and lower Tertiary sandstones in Pacific Creek area, Sublette and Sweetwater Counties, Wyoming: *The Mountain Geologist*, v. 17, no. 2, p. 23-35.
- Lickus, M.R., Pawlewicz, M.J., Law, B.E., and Dickinson, W.W., 1984, Thermal maturity map, northern Green River basin, Wyoming, *in* Law, B.E., ed., Geological characteristics of low-permeability Upper Cretaceous and lower Tertiary rocks in the Pinedale anticline area, Sublette County, Wyoming: U.S. Geological Survey Open-File Report 84-753, p. 60-65.
- Magoon, L.B., and Claypool, G.E., 1983, Petroleum geochemistry of the North Slope of Alaska; time and degree of thermal maturity, *in* Bjoroe, M., and others, eds., Advances in organic geochemistry, 1981: International Meeting on Organic Geochemistry, 10th, Bergen, Norway, 1981, John Wiley, p. 28-38.
- Monnier, F., Powell, T.G., and Snowden, L.R., 1983, Qualitative and quantitative aspects of gas generation during maturation of sedimentary organic matter; examples from Canadian frontier basins, *in* Bjoroe, M., and others, eds., Advances in organic geochemistry, 1981: International Meeting on Organic Geochemistry, 10th, Bergen, Norway, 1981, John Wiley, p. 487-495.
- Pawlewicz, M.J., Lickus, M.R., Law, B.E., Dickinson, W.W., and Barclay, C.S.V., 1986, Thermal maturity map showing subsurface elevation of 0.8 percent vitrinite reflectance in the Greater Green River basin of Wyoming, Colorado, and Utah: U.S. Geological Survey Miscellaneous Field Studies Map MF-1890, scale 1:500,000.
- Pitman, J.K., Anders, D.E., Fouch, T.D., and Nichols, D.J., 1985, Depositional environments, diagenesis, and the origin of hydrocarbons in nonmarine Upper Cretaceous and lower Tertiary rocks, eastern Uinta basin, Utah [abs.]: *American Association of Petroleum Geologists Bulletin*, v. 69, no. 5, p. 860.
- Saxby, J.D., 1970, Isolation of kerogen in sediments by chemical methods: *Chemical Geology*, v. 6, no. 3, p. 173-184.
- Spencer, C.W., 1987, Hydrocarbon generation as a mechanism for overpressuring in Rocky Mountain region: *American Association of Petroleum Geologists Bulletin*, v. 71, p. 368-388.
- Spencer, C.W., and Law, B.E., Overpressured, low-permeability gas reservoirs in Green River, Washakie, and Great Divide basins, southwestern Wyo. [abs.]: *American Association of Petroleum Geologists Bulletin*, v. 65, no. 33, p. 569.
- Stach, E., Mackowsky, M.-th., Teichmuller, M., Teichmuller, R., Murchison, D.G., Taylor, G.H., and Zierke, F., 1975, Stach's textbook of coal petrology [translated by D.G. Murchison]: Berlin, Gebruder Borntraeger, 535 p.

Chapter H

Gamma-Ray Well-Log Anomaly in the Northern Green River Basin of Wyoming

By STEPHEN E. PRENSKY

Prepared in cooperation with the U.S. Department of Energy

U.S. GEOLOGICAL SURVEY BULLETIN 1886

GEOLOGY OF TIGHT GAS RESERVOIRS IN THE PINEDALE ANTICLINE AREA, WYOMING,
AND AT THE MULTIWELL EXPERIMENT SITE, COLORADO

CONTENTS

Abstract	H1
Introduction	H1
Gamma-ray anomaly	H1
Regional correlation	H3
Method	H4
Results and interpretation	H7
Areal distribution of the arkosic facies	H7
Discussion	H11
Relation to the Cretaceous-Tertiary boundary	H12
Conclusions	H19
References cited	H19

FIGURES

1. Map showing structure contours for top of Lower Cretaceous Dakota Sandstone, northern Green River basin H2
2. Chart showing generalized stratigraphic section and plot of gamma-ray log for Rainbow Resources No. 1-34 Pacific Creek Federal well H3
3. Cross section across northern Green River basin showing truncation of Upper Cretaceous and lower Tertiary rocks westward onto La Barge platform H4
4. Chart showing open-hole total gamma-ray log and potassium and uranium and thorium values derived from natural gamma-ray spectrometry log, Wexpro No. 1 Mesa well H8
5. North-south gamma-ray log cross section, *J-J'* H9
- 6-13. West-east gamma-ray log cross sections:
 6. *A-A'* H10
 7. *B-B'* H11
 8. *C-C'* H12
 9. *D-D'* H13
 10. *E-E'* H14
 11. *F-F'* H14
 12. *G-G'* H15
 13. *H-H'* H15
- 14-16. North-south gamma-ray log cross sections:
 14. *K-K'* H16
 15. *L-L'* H18
 16. *M-M'* H20

TABLES

1. List of study wells, northern Green River basin H5
2. Wells distant from the Wind River Mountains in the Green River basin from which arkose or feldspar has been reported H19

Gamma-Ray Well-Log Anomaly in the Northern Green River Basin of Wyoming

By Stephen E. Prenskey

Abstract

An abrupt increase in gamma-ray intensity in lower Tertiary nonmarine clastic rocks relative to underlying Cretaceous rocks in the northern Green River basin of Wyoming results from an abrupt increase in the volume of arkose and potassium feldspar in these rocks due to the unroofing and erosion of the granitic core of the Wind River Mountains during the Laramide orogeny. In order to study this anomaly, gamma-ray well-logs for selected wells were digitized, and plots having a greatly compressed depth scale were computer generated. A series of east-west and north-south cross sections were constructed to facilitate identification and correlation of the anomaly. Although changes in facies and a paucity of deep wells prevents a definitive correlation, this gamma-ray event extends northward into the Hoback basin, westward to the Wyoming thrust belt, and southward out of the study area. The anomaly may be useful in studying lower Tertiary fluvial drainage systems in the basin and, in combination with palynological data, may assist in reconstructing the timing of movement on the Prospect-Hogback thrust.

INTRODUCTION

The northern Green River basin in southwestern Wyoming is a foreland basin (Gries, 1983; Lowell, 1983) between the Wyoming thrust belt to the west and the Wind River Mountains to the east (fig. 1). It developed as a flexural response to loading caused by concurrent overthrusting to the west and uplift to the east (Hagen and others, 1985). The thick sedimentary sequence in the basin consists of Upper Cretaceous and lower Tertiary nonmarine low-permeability sandstones and shales overlying Upper and Lower Cretaceous marine sandstones and shales and older rocks of mixed lithology (fig. 2). The Tertiary and Upper Cretaceous section is thickest along the Wind River thrust: it is thicker than 20,000 ft in the Pacific Creek area (figs. 1, 2) and thins westward toward the La Barge platform (figs. 1, 3). Throughout the basin, varying amounts of uppermost Cretaceous and lowermost Tertiary rocks have been removed by the widespread and prolonged erosion during Laramide time (fig. 3). In some areas on the La Barge platform,

Tertiary rocks rest unconformably on the Upper Cretaceous Hilliard Shale.

An abrupt shift in gamma-ray intensity in the lower Tertiary clastic rocks in the Pinedale area of the northern Green River basin (fig. 1) was identified in plots of gamma-ray well-log data (Prenskey, 1984; Prenskey and Dickinson, 1986). Subsequent to that identification, additional data were examined to determine the extent of the anomaly throughout the basin.

Gamma-ray logs for more than 170 wells were put into digital form in order to produce computer-generated displays (Prenskey, 1988). Ninety-five of these logs (table 1) were selected for presentation in subsurface cross sections. They were chosen on the basis of location, total depth, and the availability of gamma-ray log data for the entire drilled interval. Gamma-ray logs for many wells in desirable locations, especially along the basin axis, are not available either because these wells were drilled prior to widespread availability of the open-hole gamma-ray logging tool in the middle 1960's or because this tool was considered an unnecessary expense by the well operator.

Acknowledgments.—The following companies provided data used in this study: American Hunter, American Quasar, Amoco, Apache Corporation, Belco Petroleum, Blackhawk Resources, Carollo Hay and Associates, Chevron, Enron, Davis Oil, Energetics, Gas and Oil Management Company, Home Petroleum, IGR, Primary Fuels, Rainbow Resources, Wexpro, and Woods Petroleum. C.W. Keighin and C.W. Spencer provided valuable comments. This study was funded in part by the U.S. Department of Energy's Western Tight Gas Sand Program.

GAMMA-RAY ANOMALY

The total gamma-ray log from the Wexpro No. 1 Mesa well (well 62, table 1) obtained from a single open-hole log run is shown in figure 4. At a depth of about 8,000 ft, there is an abrupt shift in the data and a similar shift is present in data for other wells along the Pinedale anticline (wells 70, 62, 63, 58, 52, 53, table 1) (fig. 5). The abrupt change in the total gamma-ray log corresponds to sudden changes in apparent potassium and

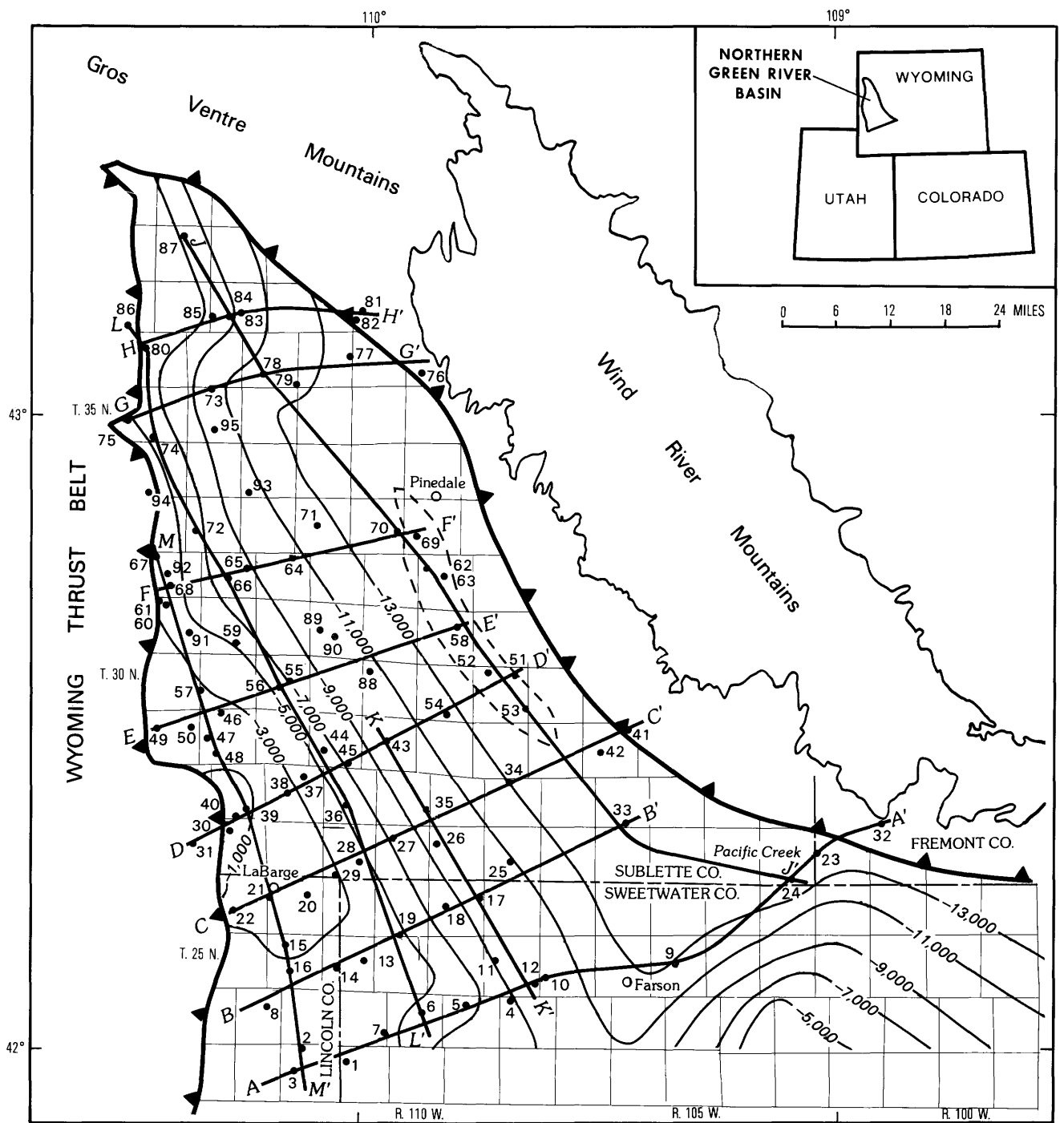


Figure 1. Structure contours (interval 2,000 ft) for the top of the Lower Cretaceous Dakota Sandstone, northern Green River basin, Wyoming. Dashed line delineates Pinedale anticline. Location of study wells (solid circles) and lines of sections also shown. Additional information for wells shown in table 1 by well number. Structure from Petroleum Information Corporation (1983).

thorium contents as shown in the spectral gamma-ray log (fig. 4). Petrographic examination of core from wells in the Pinedale area shows that the potassium feldspar content of sandstones abruptly changes from as much as 25 percent in Tertiary rocks (lithic arkose) to essentially zero in Cretaceous rocks (Butcher, 1971; Greenfield, 1981;

Keighin, 1984; Law and others, 1986; Pollastro, this volume). X-ray diffraction studies of core from the El Paso Natural Gas No. 1 Wagon Wheel well (well 52, table 1) confirm these results and also indicate the presence of potassium micas in the Tertiary rocks (Pollastro, 1985, this volume).

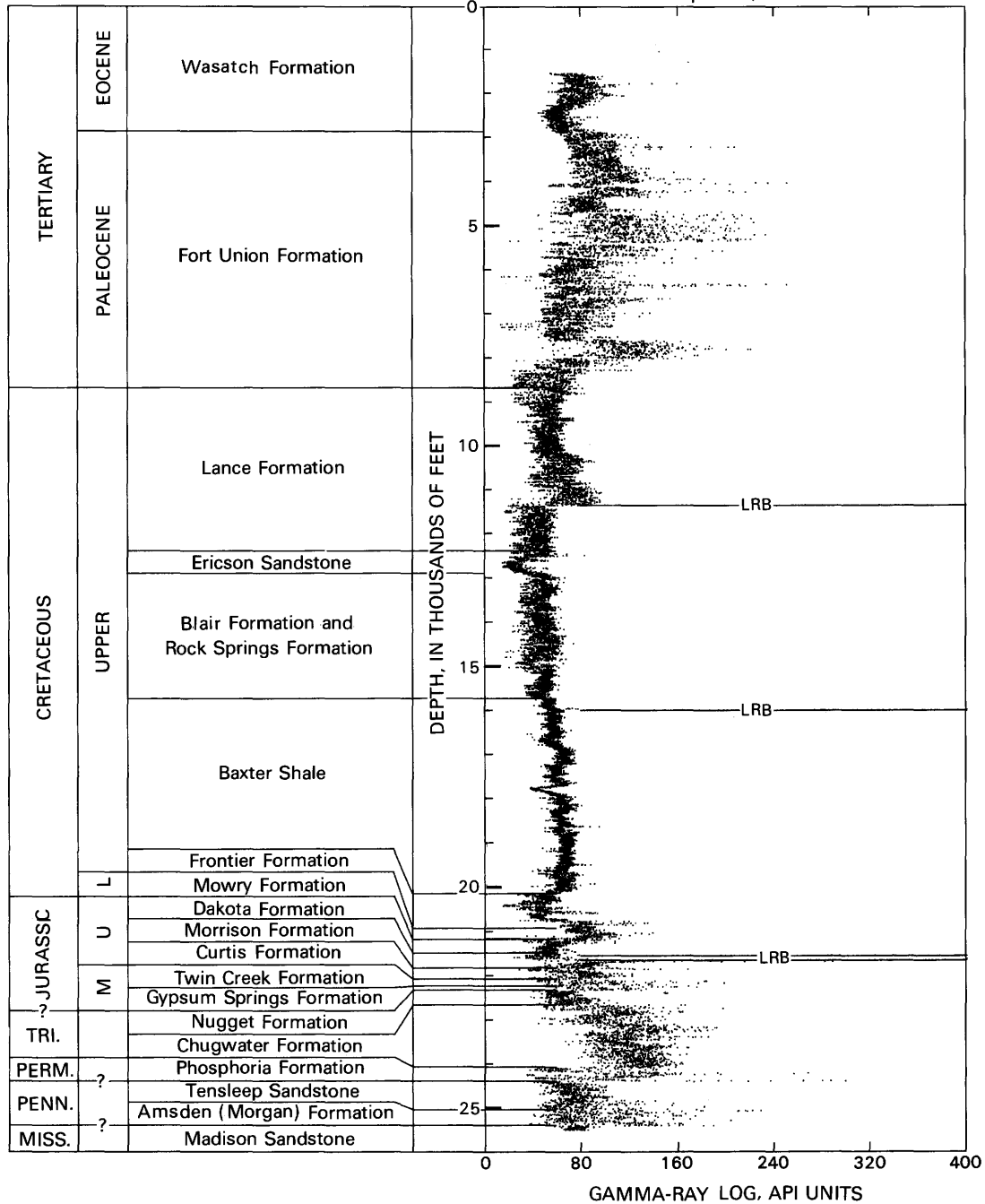


Figure 2. Generalized stratigraphic section and plot of gamma-ray log for Rainbow Resources No. 1-34 Pacific Creek Federal well (well 24, table 1, fig. 1). Intermediate casing points and log-run breaks (LRB) are noted for purpose of identifying data artifacts. Formation tops from Petroleum Information Corporation (1987).

Regional Correlation

Large-scale lithologic and stratigraphic trends can be examined by using compressed-scale plots of well-log data; that is, data plots on which both the vertical (depth)

and horizontal scales are much smaller than in standard presentations of well-log data (Prensky, 1986; Prensky and Dickinson, 1986). In areas where strong contrasts in lithology exist, such as the northern Green River basin, stratigraphic units can be identified by their different

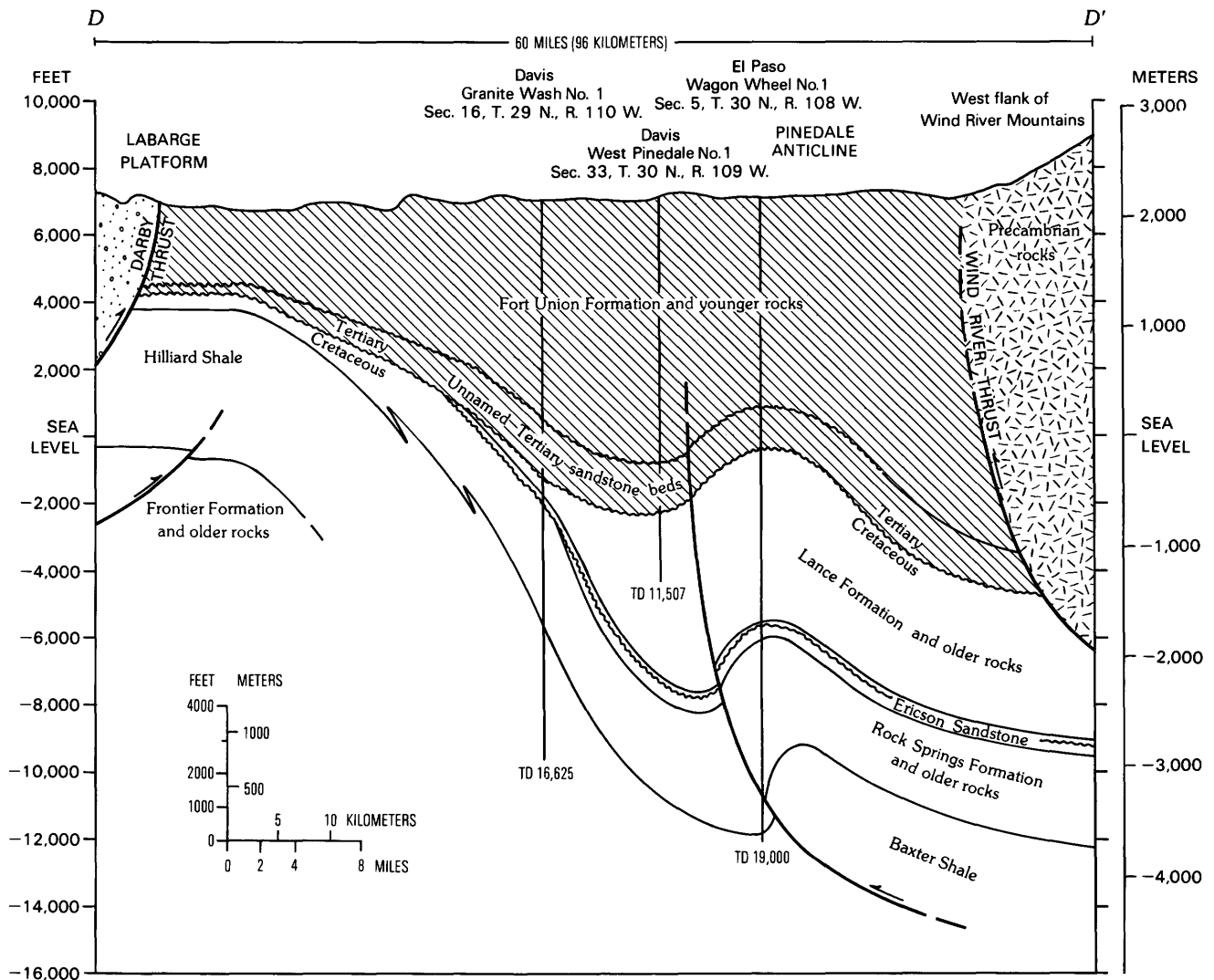


Figure 3. Cross section across northern Green River basin showing truncation of Upper Cretaceous and lower Tertiary rocks westward onto La Barge platform. Line of section D-D' shown in figure 1. Modified from Law (1984).

well-log "signatures" or patterns (fig. 2) and regional correlations can be made on the basis of these differing signatures. Particularly distinctive signatures in the northern Green River basin include the high API (American Petroleum Institute) gamma unit tail in the nonmarine lower Tertiary rocks, which is mostly produced by potassium feldspar, and a similar tail in the marine Mowry Shale (figs. 2, 4). These two patterns form the basis for the correlations of the gamma-ray anomaly and of the Second Frontier sandstone of local informal usage (Merewether and others, 1984) shown in the sections (figs. 5-16). The Second Frontier sandstone has a distinctive signature and is present in deep wells throughout the basin; thus it provides a reliable stratigraphic correlation.

Method

Data for the selected wells were digitized in 1-ft increments from total natural gamma-ray logs (table 1). Data entry was accomplished either through the manual digitization of copies of analog prints or directly from well-logging service company digital tapes. Compressed-scale plots for each well were then computer generated.

The plotted gamma-ray log data were not corrected for borehole size and mud weight. If the original log was run prior to the use of standard API gamma units, an approximate conversion to API units was made. For a few wells, only cased-hole gamma-ray logs are available and no corrections were applied. Depths for casing and log-run splices (table 1) are provided to help identify data

Table 1. List of study wells, northern Green River basin

[Data from well-log headers and from Petroleum Information (1987). Well locations shown by number on figure. Location given in section, township, and range; grid shown on figure 1. Well names may be abbreviated. Completion date in month, day, and year. Depths and elevations in feet. Leaders (--) indicate not applicable; OWDD indicates old well, drilled deeper]

Map no.	Well name	Location	Completion date	Total depth	Kelly Bushing elevation	Casing depth	Data splices log depth
1	Davis Oil 10 Storm Shelter	08, 23N, 111W	02/10/78	10,500	6,423	3,856	None
2	Texaco 1 Government-Matthews	04, 23N, 112W	08/14/85	11,750	6,748	1,485	None
3	Amoco 10 Shute Creek	20, 23N, 112W	08/21/82	11,900	6,523	1,519	None
4	R. Lacy 1 USA Government	05, 24N, 108W	08/13/64	8,995	6,854	326	None
5	General Petroleum 62-A-9 Buckhorn	09, 24N, 109W	10/30/55	9,275	6,635	1,698	None
6	Chorney Oil 1-10 Broken Hand	10, 24N, 110W	09/02/69	7,200	6,547	335	None
7	Davis Oil 1 Paparone Federal	25, 24N, 111W	09/02/76	10,621	6,518	528	None
8	FMC 1-11 Pomeroy Draw	11, 24N, 113W	11/16/80	11,425	6,905	1,005	None
9	Pan American Petroleum 1 State I	16, 25N, 105W	11/23/63	8,441	6,708	172	None
10	American Hunter 1 Enterprise	30, 25N, 107W	04/20/82	17,045	6,764	1,486	None
						11,056	11,000
11	American Hunter 1 Faraway	17, 25N, 108W	10/26/81	16,525	7,022	1,554	None
						10,278	10,200
12a	Davis Oil 1 Sandy Unit	25, 25N, 108W	10/31/78	10,825	6,811	168	None
b	Davis Oil 1 Simpson Unit (OWDD)	25, 25N, 108W	08/17/79	17,034	6,816	5,002	None
c	Merged data	25, 25N, 108W	---	17,034	6,811	5,002	10,550
13	Energetics 23-14 Federal	14, 25N, 111W	03/16/79	10,480	6,885	1,038	None
14	Natural Gas Corp. of Calif. 2-20 Federal	20, 25N, 111W	01/07/83	9,350	6,914	920	None
15	Natural Gas Corp. 33-4E Fontenelle Fed.	04, 25N, 112W	10/01/85	8,450	6,803	850	None
16	Natural Gas Corp. of Calif. 34-21E Federal	21, 25N, 112W	10/21/82	9,150	6,542	4,196	4,140
17	Davis Oil 1 Parrish Mark	12, 26N, 109W	01/27/79	15,872	6,907	5,005	None
18	Davis Oil 1 18-Mile Canyon	17, 26N, 109W	07/13/65	8,004	6,968	278	None
19	Energetics 32-33 Ferguson Federal	33, 26N, 110W	07/16/78	11,555	7,037	1,028	None
20	Belco Petroleum 8-11 Stead Canyon	11, 26N, 112W	04/05/82	8,535	6,936	326	None
21	Belco Petroleum 84-18 Green River Bend	18, 26N, 112W	04/25/83	7,610	6,635	1,209	None
22	Mobil Oil T21-21G Hogsback	21, 26N, 113W	04/15/69	8,300	6,919	503	None
23a	Ferguson 1 Government	18, 27N, 102W	02/01/68	8,421	7,154	522	None
b	Woods Petroleum 18, 1-A Govt (OWDD)	18, 27N, 102W	06/26/69	12,492	7,157	522	None
c	Merged data	18, 27N, 102W	---	12,492	7,154	522	8,300
24	Rainbow Resources Pacific Creek 1-34	34, 27N, 103W	09/10/82	25,764	7,080	1,533	None
						11,409	11,370
						---	16,000
						---	21,550
						21,670	21,650
25	Davis Oil 1 Bright Trail	21, 27N, 108W	06/04/79	18,000	6,905	4,975	None
26	Davis Oil 1 Yellow Point Ridge	07, 27N, 109W	10/15/78	15,772	7,085	3,932	None
27	Energetics 20-8 Federal	08, 27N, 110W	08/25/81	14,405	7,225	994	13,400
28	Energetics 30-23 East Bird Canyon	23, 27N, 111W	06/20/79	11,750	7,243	1,010	None
29	Energetics 10-32 Federal	32, 27N, 111W	07/22/80	9,730	7,235	820	None
30	Belnorth 32-5 North LaBarge Unit	05, 27N, 113W	10/04/84	7,385	7,494	313	None
31	Exxon 1 Graphite	16, 27N, 114W	10/13/81	17,317	9,214	60	None
						4,885	4,850
						13,191	13,150
						---	15,800
32	American Quasar 1 Skinner Federal	32, 28N, 101W	11/06/75	15,040	7,581	375	None
						2,505	2,450
						13,010	12,950
33	California Oil 1 Government	34, 28N, 106W	08/30/62	8,502	6,989	750	None
34	Home Petroleum 1-4 Jonah Federal	04, 28N, 108W	1987	12,594	7,139	2,550	None
35	Woods Petroleum 2 Cutlass	24, 28N, 110W	10/30/82	17,700	7,102	4,000	None
						14,000	13,980
36	Energetics 30-21 Chorney Federal	21, 28N, 111W	07/14/83	12,150	7,038	998	None
37	Belco Petroleum 1-2 Chapel Canyon	02, 28N, 112W	10/13/81	11,075	6,782	1,002	None

Table 1. Continued

Map no.	Well name	Location	Completion date	Total depth	Kelly Bushing elevation	Casing depth	Data spllices log depth
38	Energetics 13-16 Dry Piney-State	16, 28N, 112W	07/05/81	9,738	6,952	815	None
39	Mobil Oil T63X-27P Tip Top	27, 28N, 113W	08/21/84	7,300	7,182	827	None
40	Belnorth Petroleum 36-33 North LaBarge	33, 28N, 113W	12/22/84	7,700	8,038	822	None
41	Husky Oil 8-2 Federal	02, 29N, 106W	10/02/73	12,944	7,208	1,943	6,380
						---	11,650
42	Quadrant Oil 14-16 State	16, 29N, 106W	08/12/72	10,050	7,113	499	None
43	Davis Oil 1 Granite Wash	16, 29N, 110W	11/30/77	16,625	7,018	4,016	None
44	Primary Fuels 24-20 Van Buren Federal	20, 29N, 111W	09/27/82	12,394	6,870	2,025	None
45	Chandler 1 Ideen Government	35, 29N, 111W	08/19/69	6,206	6,815	231	None
46	Belco Petroleum 4-4 BUDD	04, 29N, 113W	03/13/80	3,250	7,359	230	None
47	Mobil Oil T72-19G Tip Top	19, 29N, 113W	07/03/79	8,610	7,517	887	7,850
48	Mobil Oil F12-33G Tip Top	33, 29N, 113W	10/04/77	7,900	7,542	788	None
49	American Quasar 8-24 Riley Ridge	08, 29N, 114W	09/24/80	16,000	7,760	69	None
						1,990	2,050
						9,865	9,800
						15,450	15,420
50	Terra Resources 1-12 North Tip Top	12, 29N, 114W	02/28/82	11,590	7,709	2,220	10,300
51	American Hunter 2 New Fork	02, 30N, 108W	07/08/81	11,986	7,282	4,425	None
52	El Paso Natural Gas 1 Wagon Wheel	05, 30N, 108W	08/01/71	19,000	7,089	2,479	5,065
						---	7,121
						12,086	12,090
						---	15,200
53	American Hunter 1 New Fork	25, 30N, 108W	07/10/81	10,989	7,338	4,068	None
54	Davis Oil 1 West Pinedale	33, 30N, 109W	11/18/75	11,507	7,052	478	None
55	Chandler 1 James Mickelson	15, 30N, 112W	10/30/69	6,288	6,954	222	None
56	General Petroleum 63-21 Bar Cross X	21, 30N, 112W	08/20/54	8,270	7,008	306	None
57	Mountain Fuel Supply 3 Johnson Ridge	19, 30N, 113W	07/04/72	4,837	7,562	202	None
58	Hay-Carollo 2 Jensen	11, 31N, 109W	08/10/83	10,302	6,925	1,046	None
59	Belco Petroleum 2-27 Mason	27, 31N, 113W	03/14/83	13,340	7,295	2,504	None
60	Pacific Transmission 13-4 Federal	04, 31N, 114W	08/01/75	12,586	8,437	1,025	None
						10,925	10,880
61	Natural Gas Calif. 13-5 Castle Creek	05, 31N, 114W	03/03/81	7,058	8,698	226	None
62	Mountain Fuel Supply (Wexpro) 1 Mesa	07, 32N, 109W	07/15/81	12,050	7,524	1,033	None
63	Wexpro 2 Mesa	16, 32N, 109W	06/22/81	12,190	7,474	1,023	None
64	Phillips Petroleum 4 Marbleton Unit	10, 32N, 112W	02/15/60	11,565	7,380	506	11,150
65	Ray Smith Drilling 1 Fear Ranch Unit	13, 32N, 113W	07/20/58	9,318	7,564	312	None
66a	Davis Oil 1 Aspen Ridge	22, 32N, 113W	06/15/74	7,854	7,902	378	None
b	Davis Oil 1 Aspen Ridge (OWDD)	22, 32N, 113W	04/23/76	14,940	7,891	2,010	None
c	Merged data	22, 32N, 113W	---	14,940	7,902	378	None
						2,010	None
						7,550	7,800
67	Belco Petroleum 3-8 Ote Creek	08, 32N, 114W	11/17/80	5,575	8,058	394	None
68	S. Louisiana (Celeron) 21-28 Castle Creek	08, 32N, 114W	07/22/82	11,875	8,167	1,400	None
						10,600	10,540
69	Mountain Fuel Supply 8 Pinedale Unit	20, 33N, 109W	01/06/64	10,500	7,448	1,009	None
70	Blackhawk Resources 21-24 Baumgartner	24, 33N, 110W	12/12/81	11,238	7,344	800	None
71	Phillips Petroleum 1 Daniel	21, 33N, 111W	04/04/56	16,531	7,307	529	None
72	Union Texas Natural Gas 1 Federal-Pure	20, 33N, 113W	11/11/60	7,268	7,827	451	None
73	Depco 7-4 Federal	04, 35N, 113W	09/13/71	5,510	7,843	336	None
74	Davis Oil 1 Bacon Ridge	33, 35N, 114W	09/06/78	11,820	8,937	840	None
						8,256	9,290
75	Pacific Trans Supply 24-24 Federal	24, 35N, 115W	10/22/75	14,999	9,778	1,005	None
						8,340	8,290

Table 1. Continued

Map no.	Well name	Location	Completion date	Total depth	Kelly Bushing elevation	Casing depth	Data splices log depth
76	Anadarko Production 1 Willow Lake Unit	29, 36N, 109W	11/24/70	11,753	8,633	10,237	None
77	Pacific Transmission Supply 33-13 Fed.	13, 36N, 111W	02/12/74	11,153	7,743	1,020 9,943	None 9,910
78a	Inexco A, 1 WASP	28, 36N, 112W	11/14/70	14,363	7,812	30 1,844	None 2,050
b	Belco Petroleum 3-28 Merna Unit (OWDD)	28, 36N, 112W	02/24/77	18,124	7,815	10,182 16,209 6,209	10,180 14,350 16,200
c	Merged data	28, 36N, 112W	---	18,124	7,812	16,978 30 1,844	16,950 None 2,050
						10,182 16,209 16,209 16,978	10,180 14,350 16,200 16,950
79	Apache Corporation 36-1 Robbins	36, 36N, 112W	09/27/85	16,480	7,625	1,590 10,545	None 10,515
80a	Rainbow Resources 1-7 Cliff Creek	07, 36N, 114W	10/04/77	11,548	7,649	486 2,905 8,628	None 2,950 8,590
b	Chevron Rainbow 1-7 Federal (OWDD)	07, 36N, 114W	07/19/81	15,561	7,659	15,531	13,510
c	Merged data	07, 36N, 114W	---	15,561	7,649	486 2,905 8,628	None 2,950 8,590
						15,531	13,510
							(cased-hole gamma-ray neutron log)
81	Home Petroleum 34-23 New Forks Carney	23, 37N, 110W	12/06/84	4,750	7,649	55	2,750
82	Home Petroleum 32-27 New Forks Black	27, 37N, 110W	12/19/85	5,050	7,655	785	None
83	Pure Oil 1 Bondourant Unit	22, 37N, 112W	10/19/64	5,202	7,200	378	None
84	Pure Oil 2 Bondourant Unit	29, 37N, 112W	11/06/64	4,570	7,118	326	None
85	Pan American 1 Empire State	25, 37N, 113W	11/09/63	4,509	6,900	303	None
86	Chevron 31-33C Cabin Creek Federal	33, 37N, 114W	07/28/86	11,305	8,041	494 3,483 ---	490 3,450 7,880
						9,008	9,000
87	Depco 1 Bondourant Unit	09, 38N, 113W	03/12/71	13,300	7,127	1,050 5,077	None 6,650
							Wells added after preparation of initial list
88	Gas & Oil Management GOMI 1-7 Federal	07, 30N, 110W	1987	9,600	7,033	531	None
89	BWAB 20-24	20, 31N, 111W	02/21/86	7,300	7,153	675	None
90	Gas Oil Management 1-28 New Tech Fed.	28, 31N, 111W	1988	9,570	6,982	1,067	None
91	Skyline 1 Piney Creek	23, 31N, 114W	11/21/82	5,300	7,876	410	None
92	Natural Gas Corp of Calif. 23-16A State	16, 32N, 114W	08/14/81	7,201	7,971	34	None
93	Pure Oil 1 USA Broady Draw	31, 34N, 112W	08/21/64	5,170	7,529	396	None
94	Gulf-U.S. 1 West Side Federal	32, 34N, 114W	11/01/72	8,487	8,254	782	None
95	Depco 5-27 Federal	27, 35N, 113W	09/30/71	5,490	8,094	329	None

shifts that are artifacts resulting from the change from cased-hole to open-hole conditions or vice versa or from changes in logging tools or calibrations.

All depths have been corrected to true elevation relative to sea level. Despite the schematic nature of these sections (they lack true horizontal scale), gross structural and stratigraphic elements within the study area can be observed.

RESULTS AND INTERPRETATION

Areal Distribution of the Arkosic Facies

The data are presented in figures 6-13 as transverse sections *A* through *H* and in figures 5 and 14-16 as longitudinal sections *J* through *M*. As mentioned earlier, these data, at least those for the Pinedale anticline, reflect

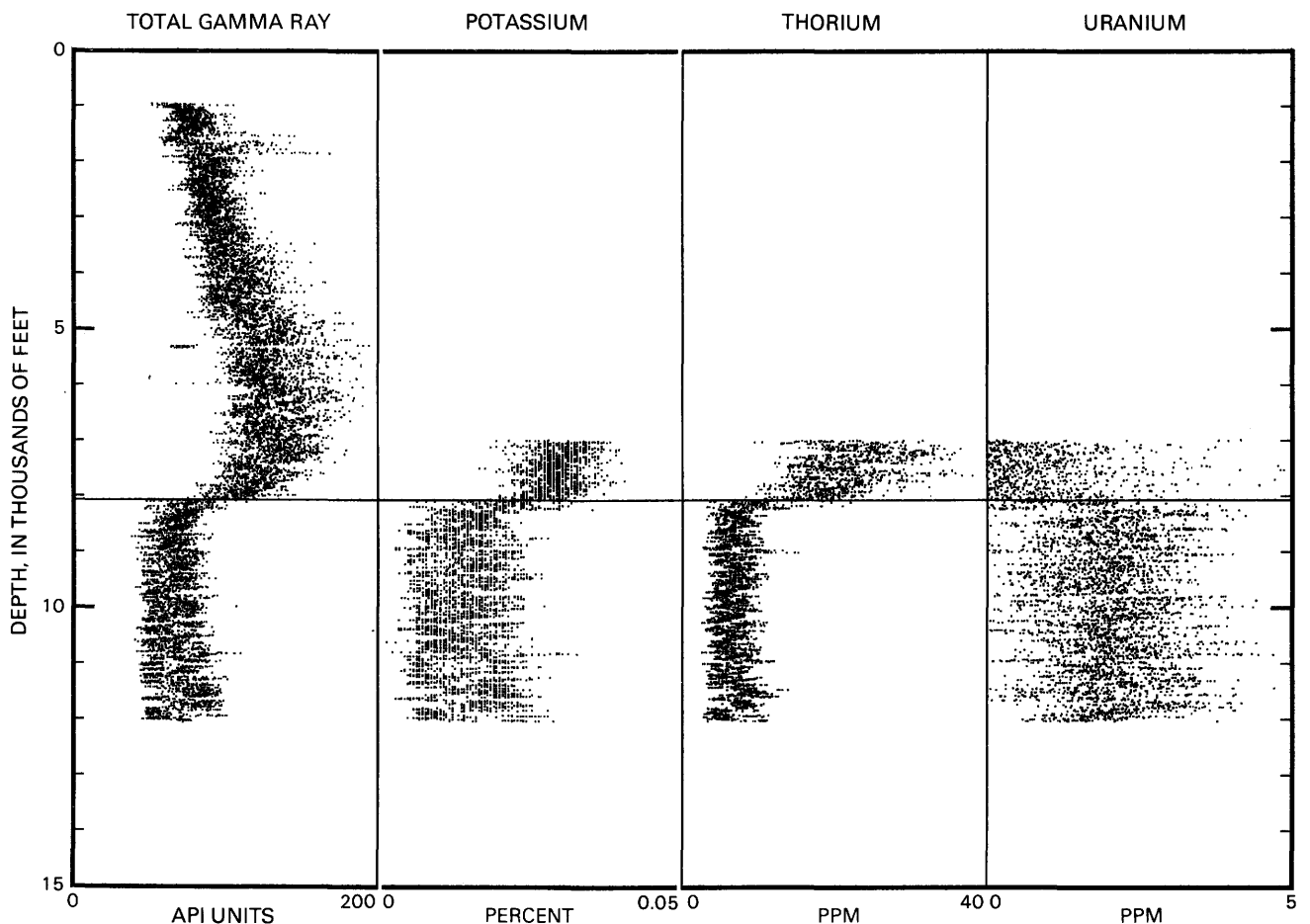


Figure 4. Open-hole total gamma-ray log (API gamma units), and potassium (percent) and uranium and thorium (ppm) values derived from natural gamma-ray spectrometry log, Wexpro No. 1 Mesa well (well 62, table 1, fig. 1). Horizontal line indicates position of gamma-ray anomaly. Note arcuate pattern of increasing and then decreasing API gamma unit intensity in total gamma-ray log just above anomaly indicated by solid line.

the presence and relative amounts of postassium feldspar and mica in that the magnitude of gamma-ray intensity (as indicated by API value) is directly related to the percentage of these constituents. At a given locality, the volume of potassium minerals, which are present in arkosic sandstones, is related to proximity to source terrain and to stream gradient. Consequently, gamma-ray intensity may be an indication of relative stream gradients; these, in turn, ultimately reflect tectonic uplift or subsidence. The gamma-ray anomaly is most striking in wells on the Pinedale anticline (fig. 5), and the magnitude of the anomaly (or shift) diminishes westward away from the Wind River Mountains (figs. 6-12). Absolute gamma-ray intensities in granitic intervals (wells 32 and 41, table 1) are extremely high and decrease with distance from the Wind River Mountains, especially across the Wind River thrust where the igneous granite facies changes to a detrital lithic arkosic facies (figs. 6, 8). The proximity and areal distribution of the arkosic facies relative to these mountains indicate that the Precambrian core of the

Wind River Mountains was the source of the arkose (Shuster, 1986).

Gamma-ray log data for the Mesa well (fig. 4) form an arclike pattern of high API values with the API shift at the lower part of the arc. In this pattern, gamma-ray intensity rises rapidly to a maximum value and then gradually decreases. The pattern, as well as the absolute gamma-ray intensity discussed above, becomes more subdued with distance from the presumed source terrane (figs. 6-13). The pattern may parallel major Laramide activity, which began in latest Cretaceous time (Love, 1960) and coincides with uplift of the Wind River Mountains. By middle to late Paleocene time, the crystalline core of the Wind River Mountains had been breached (Berg, 1961; Keefer, 1965; Merin and Lindholm, 1986) and erosion had begun. Deformation continued to intensify through early Eocene time (Love, 1960) and began to diminish by middle and late Eocene time (Love, 1960; Dorr and others, 1977). By Eocene time, deposition of arkose in Rocky Mountain basins was widespread (Love, 1960; Vine and Tourtelot, 1970).

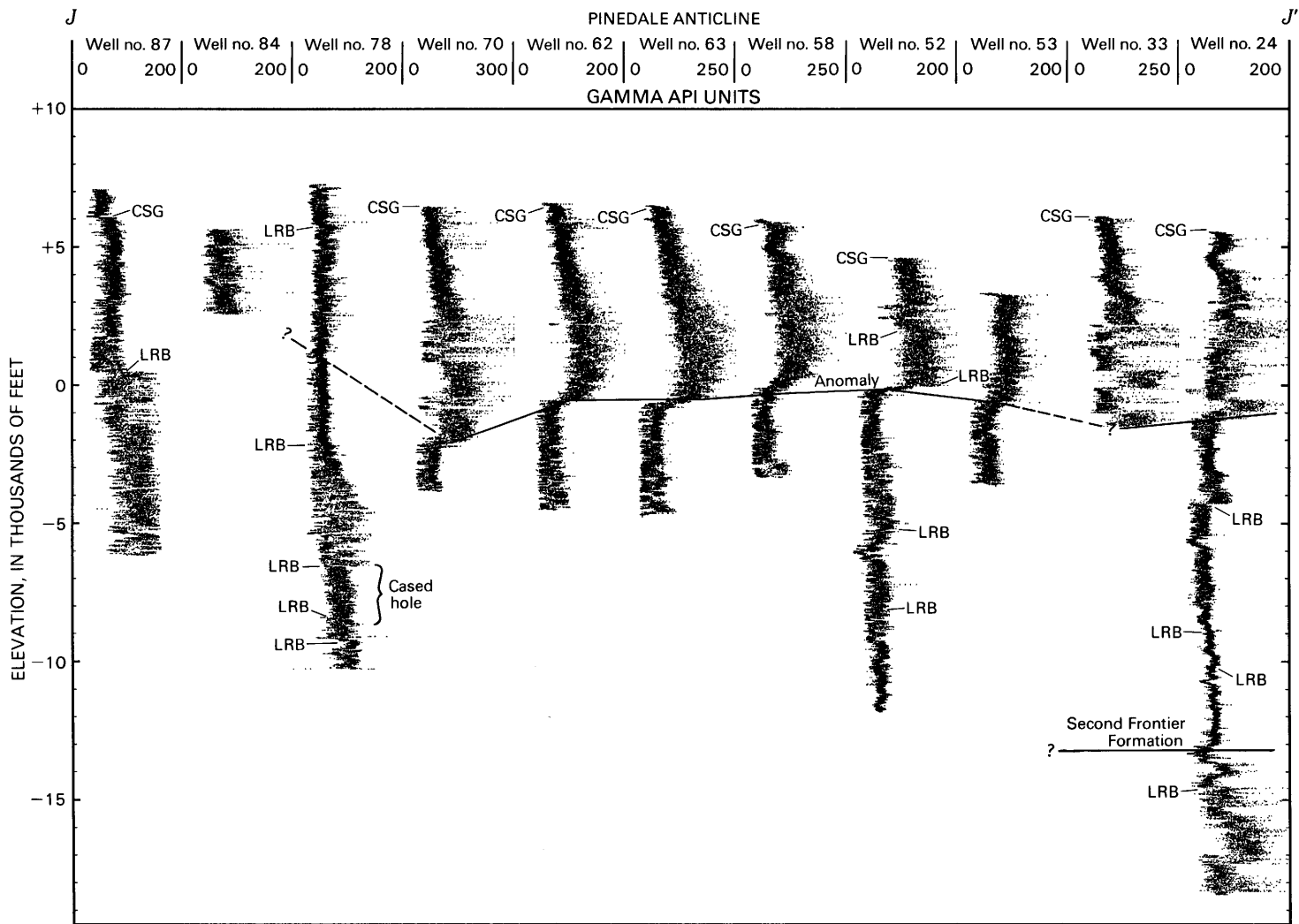


Figure 5. North-south gamma-ray log cross section *J-J'*, northern Green River basin. Casing points (CSG) and log-run breaks (LRB) indicated. Solid line indicates position of gamma-ray anomaly; dashed, queried line indicates position of anomaly is uncertain. Wells listed by number in table 1 and shown in figure 1. Line of section shown on figure 1. Datum is sea level.

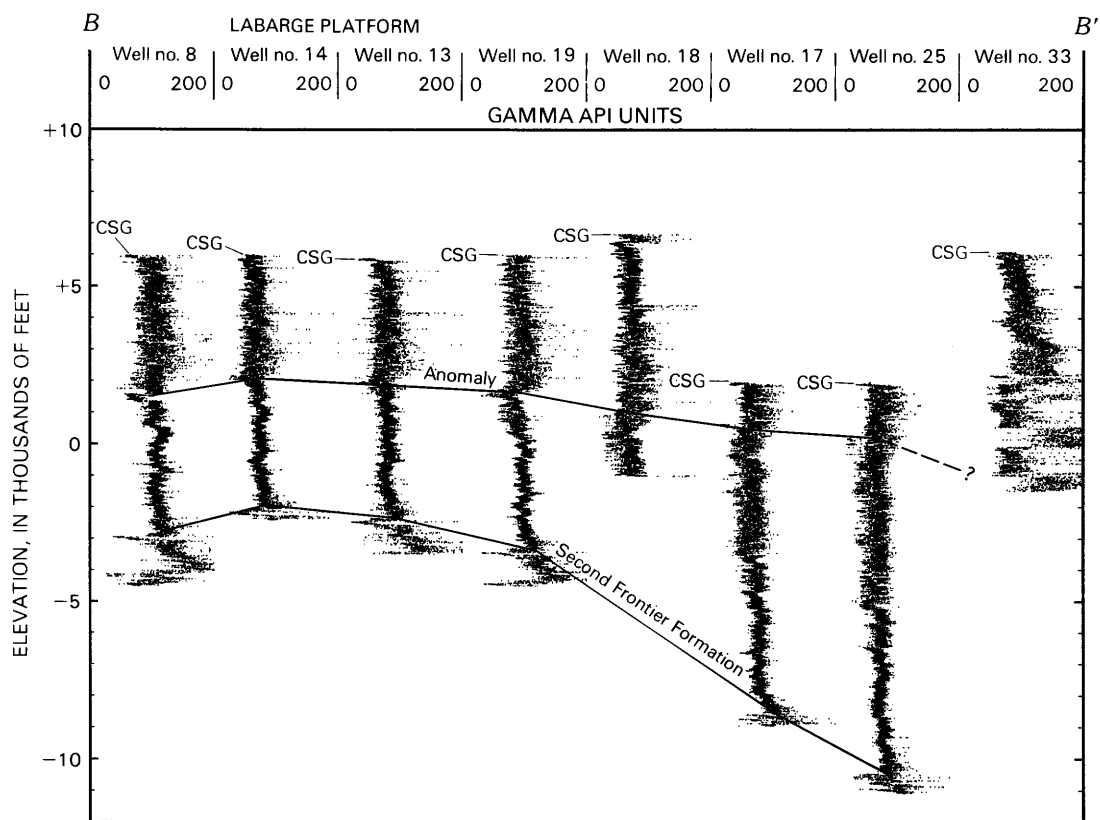


Figure 7. West-east gamma-ray log cross section *B-B'*, northern Green River basin. Casing points (CSG) and log-run breaks (LRB) indicated. Solid line indicates position of gamma-ray anomaly; dashed, queried line indicates position of anomaly is uncertain. Wells listed by number in table 1 and shown in figure 1. Line of section shown on figure 1. Datum is sea level.

Discussion

Arkosic sandstones have been reported in wells in the Pinedale, La Barge and Big Sandy areas (Berg, 1961, 1962; Asquith, 1966; Martin and Shaughnessy, 1969; Shuster, 1986). Shuster (1986) discussed the petrology and provenance of Upper Cretaceous and lower Tertiary rocks (primarily from outcrop) in the northern Green River basin and suggested that the feldspathic nature of the lower Paleocene rocks (Hoback Formation, Fort Union Formation, Chappo Member of the Wasatch Formation, unnamed unit of Law (Law and Nichols, 1982)) indicates a granitoid source, probably the northern Wind River Mountains. The Gros Ventre uplift probably served as a secondary and more localized source of Hoback Formation granitic debris.

Examination of lithologic logs (American Stratigraphic Company, Denver, Colo.) indicates that arkose has been reported in wells throughout the basin. In the logs of many wells, particularly those on the La Barge platform, arkose has not been specifically reported, but feldspar grains (presumably potassium feldspar) have been reported (table 2). Lithologic logs do not provide

definitive evidence for the presence or absence of these constituents, in part because of inconsistencies in identification and reporting on the logs and in part because they are not available for most drilled wells. Despite these problems, the logs can aid interpretations. The gamma-ray shift is at or below the deepest reported occurrence of arkose or feldspar.

Although the only analyzed core data available for this study are from the Pinedale area, the above-mentioned reports of arkose and feldspar suggest that, during lower Tertiary time, westward-draining fluvial patterns reached as far west as Rs. 112 and 113 W. Paleogeographic reconstructions of the northern Green River basin by Shuster (1986) indicate a southerly drainage in the basin throughout Upper Cretaceous and lower Tertiary times, and Shuster believed that the amount of detritus supplied from the Wind River and Gros Ventre Mountains was sufficient to force drainage westward toward the basin margin. In fact, arkosic material may exist farther west than the present-day margin of the basin. Reports of Tertiary sedimentary rocks underlying the leading edge of the Eocene-to Paleocene-age Prospect-Hogsback thrust, along which 31 mi of crustal

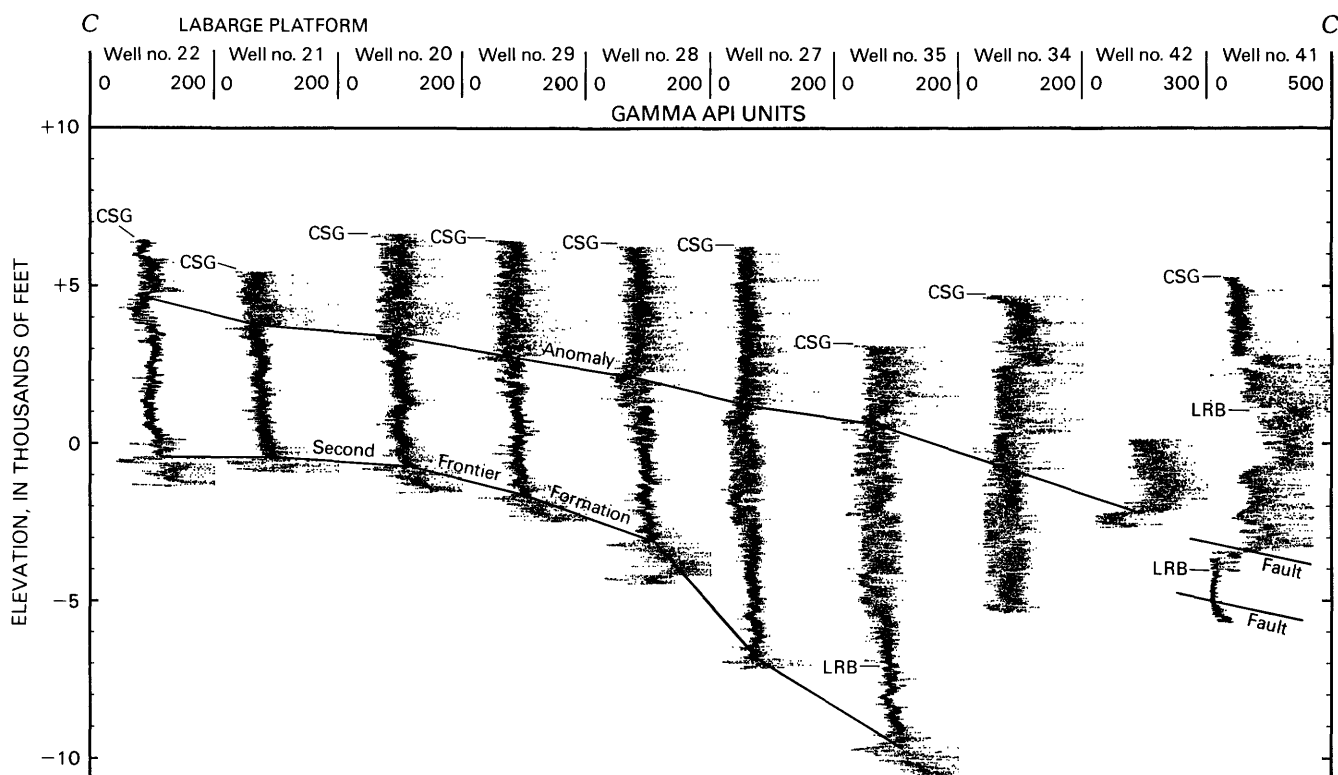


Figure 8. West-east gamma-ray log cross section C-C', northern Green River basin. Casing points (CSG) and log-run breaks (LRB) indicated. Solid line indicates position of gamma-ray anomaly; dashed, queried line indicates position of anomaly is uncertain. Wells listed by number in table 1 and shown in figure 1. Line of section shown in figure 1. Datum is sea level.

shortening has been proposed (Dixon, 1982), suggest the existence of a much broader east-west fluvial plain during lowermost Tertiary time than is indicated by present-day conditions. In addition, 15 mi of crustal shortening may have occurred on the Wind River thrust (Hagen and others, 1985).

Relation to the Cretaceous-Tertiary Boundary

The preliminary report on this gamma-ray log anomaly (Prensky, 1984) suggests a possible relationship between the anomaly and the Cretaceous-Tertiary boundary in the basin. This boundary has been dated by using palynological determinations from core samples and, in a few cases, drill cuttings. Unpublished data (D.J. Nichols, U.S. Geological Survey, to B.E. Law, written commun., 1984) indicate that in the Pinedale area, where little or no erosion of lower Tertiary and uppermost Cretaceous rocks (El Paso No. 1 Wagon Wheel and Wexpro No. 1 Mesa; wells 52 and 62, table 1) has occurred, the gamma-ray anomaly is time transgressive. In the western part of the basin, the depths of the gamma-ray log anomaly and the Cretaceous-Tertiary boundary converge to within a short distance of about 100 ft (General Petroleum No. 62-A-9 Buckhorn and No. 63-21 Bar

Cross X; wells 5 and 56, table 1) as a result of erosional truncation of the lower Tertiary and uppermost Cretaceous rocks.

A facies change occurs in lower Tertiary rocks from the northwestern margin of the basin (Hoback Formation) to the eastern margin of the basin (Wasatch and Fort Union Formations) (fig. 12). The part of the Hoback Formation in the Hoback Basin (northernmost Green River basin) is middle Paleocene in age (Dorr, 1952, 1958; Guennel and others, 1973; Dorr and others, 1977) and is composed of nonarkosic, recycled Mesozoic rocks derived from the Hoback Range (Spearing, 1969). The arkosic facies in the northern Green River Basin is generally assigned to the Eocene Wasatch Formation or its equivalents (Martin and Shaughnessy, 1969; West, 1969; Dorr and others, 1977), but arkose deposition may have begun earlier. In the vicinity of the Rock Springs uplift, the Fort Union Formation is assigned a middle Paleocene age based on vertebrate fossils, and Fort Union sandstones have been described as containing minor coarse-grained feldspars (Berg, 1961); an unnamed pre-Fort Union Tertiary arkosic sequence has been correlated northward from the Rock Springs area to the Merna area (Law, 1979; Law and Johnson, this volume). Definitive subsurface resolution of this facies change is hindered by a lack of deep wells between Ts. 34 and 38 N. and further

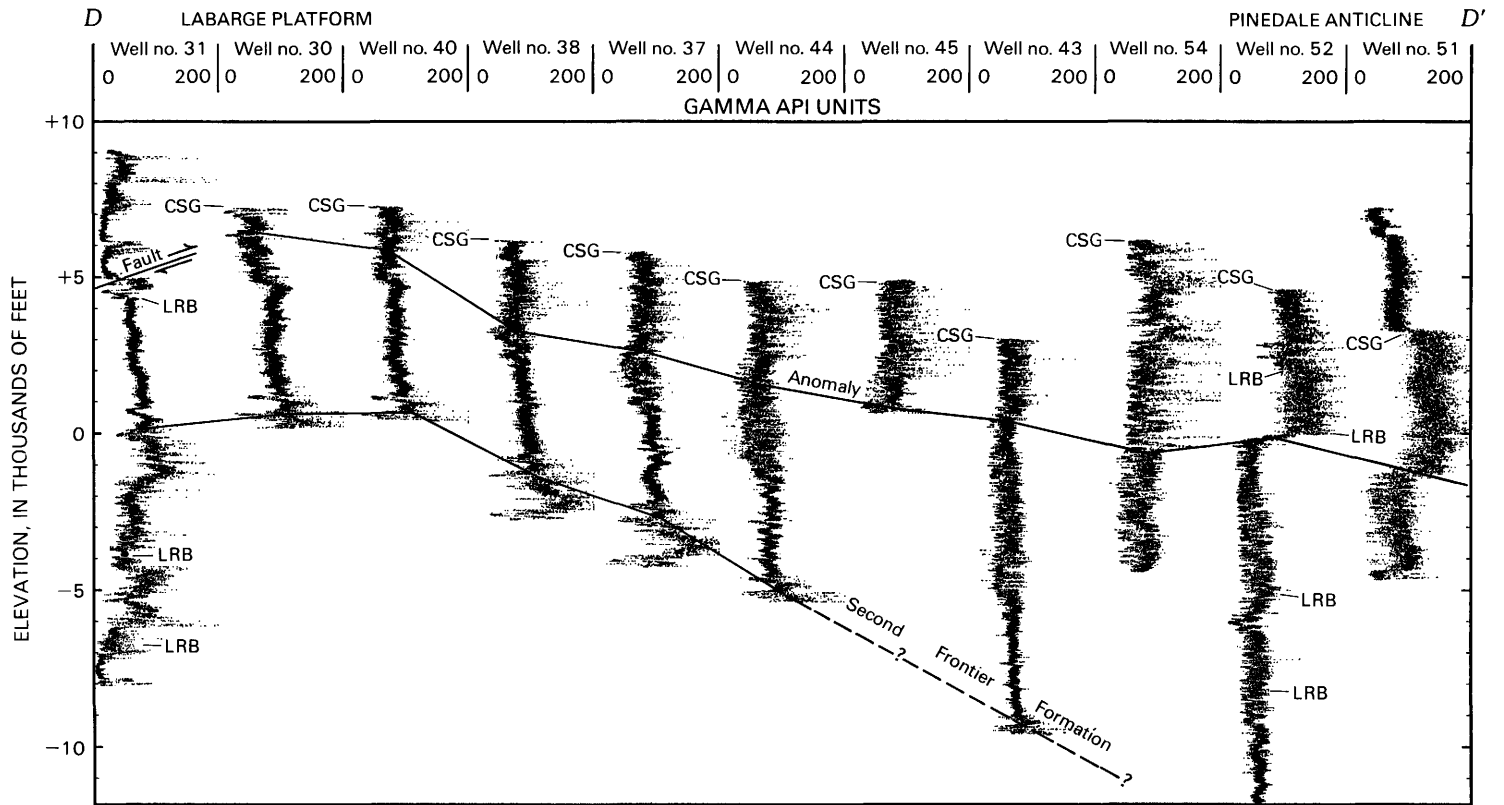


Figure 9. West-east gamma-ray log cross section D-D', northern Green River basin. Casing points (CSG) and log-run breaks (LRB) indicated. Solid line indicates position of gamma-ray anomaly; dashed, queried line indicates position of anomaly is uncertain. Wells listed by number in table 1 and shown in figure 1. Line of section shown on figure 1. Datum is sea level.

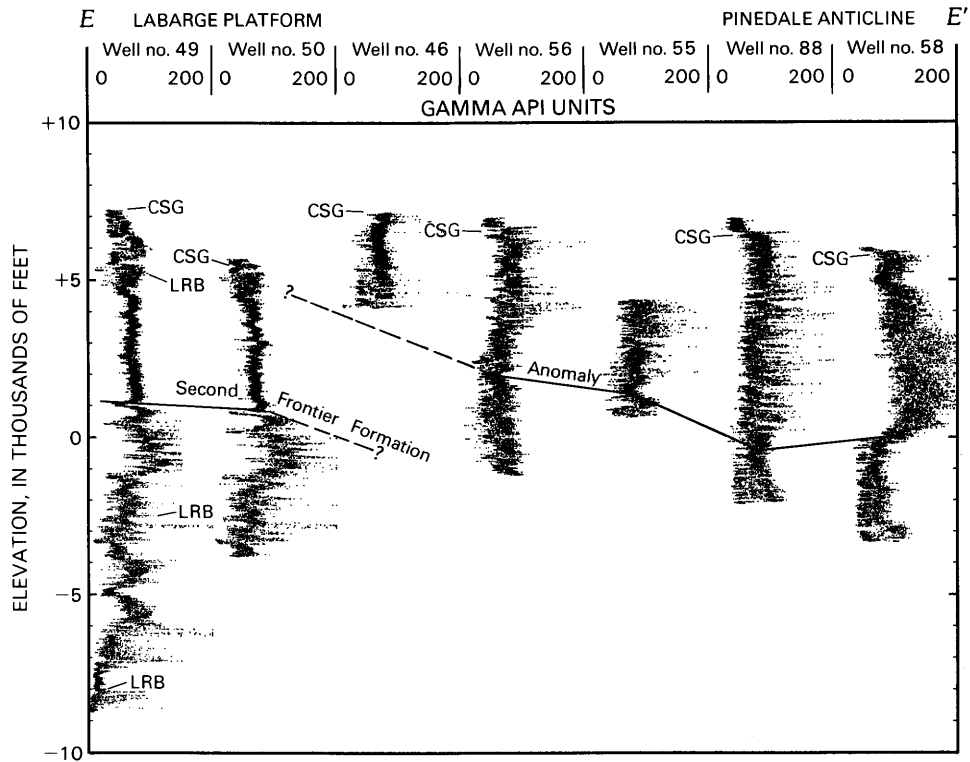


Figure 10. West-east gamma-ray log cross section $E-E'$, northern Green River basin. Casing points (CSG) and log-run breaks (LRB) indicated. Solid line indicates position of gamma-ray anomaly; dashed, queried line indicates position of anomaly is uncertain. Wells listed by number in table 1 and shown in figure 1. Line of section shown on figure 1. Datum is sea level.

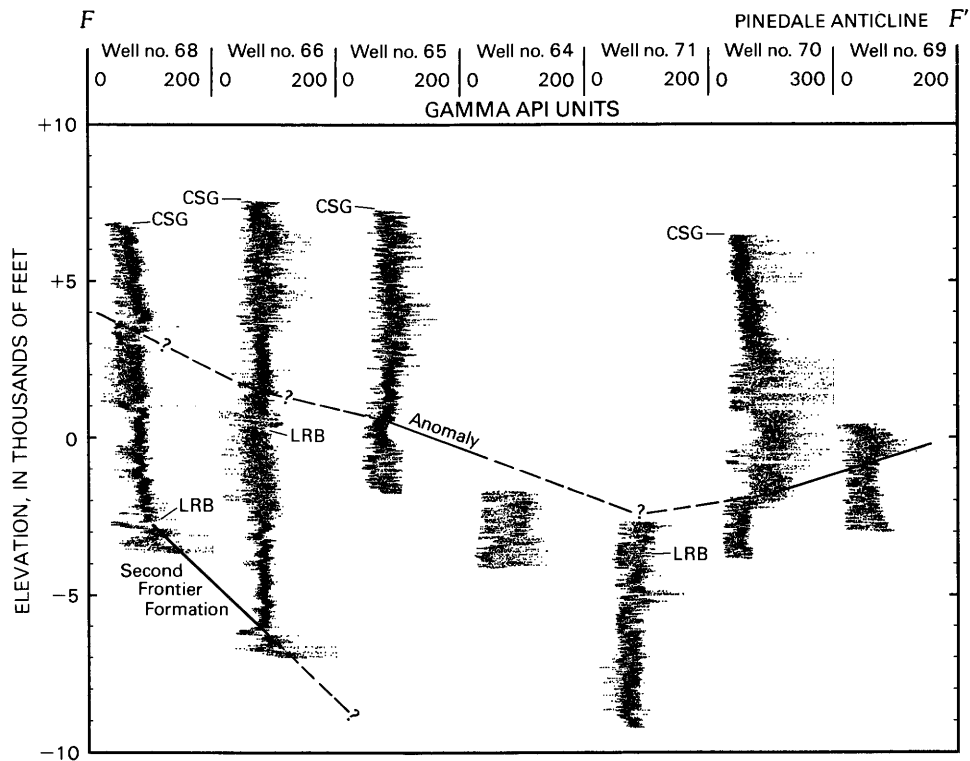


Figure 11. West-east gamma-ray log cross section $F-F'$, northern Green River basin. Casing points (CSG) and log-run breaks (LRB) indicated. Solid line indicates position of gamma-ray anomaly; dashed, queried line indicates position of anomaly is uncertain. Wells listed by number in table 1 and shown in figure 1. Line of section shown on figure 1. Datum is sea level.

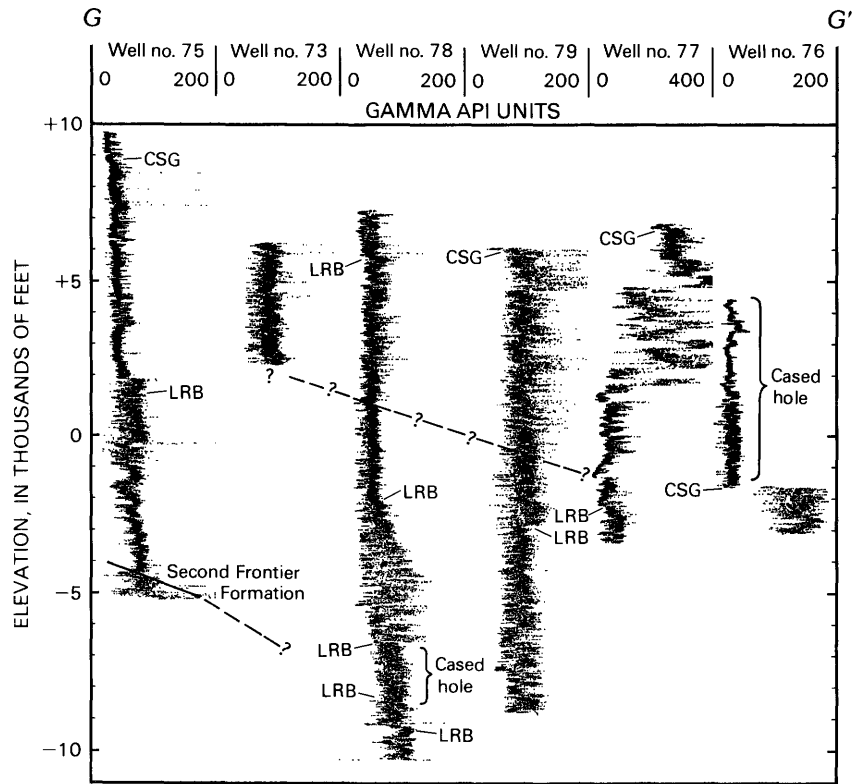


Figure 12. West-east gamma-ray log cross section *G-G'*, northern Green River basin. Casing points (CSG) and log-run breaks (LRB) indicated. Solid line indicates position of gamma-ray anomaly; dashed, queried line indicates position of anomaly is uncertain. Wells listed by number in table 1 and shown in figure 1. Line of section shown on figure 1. Datum is sea level.

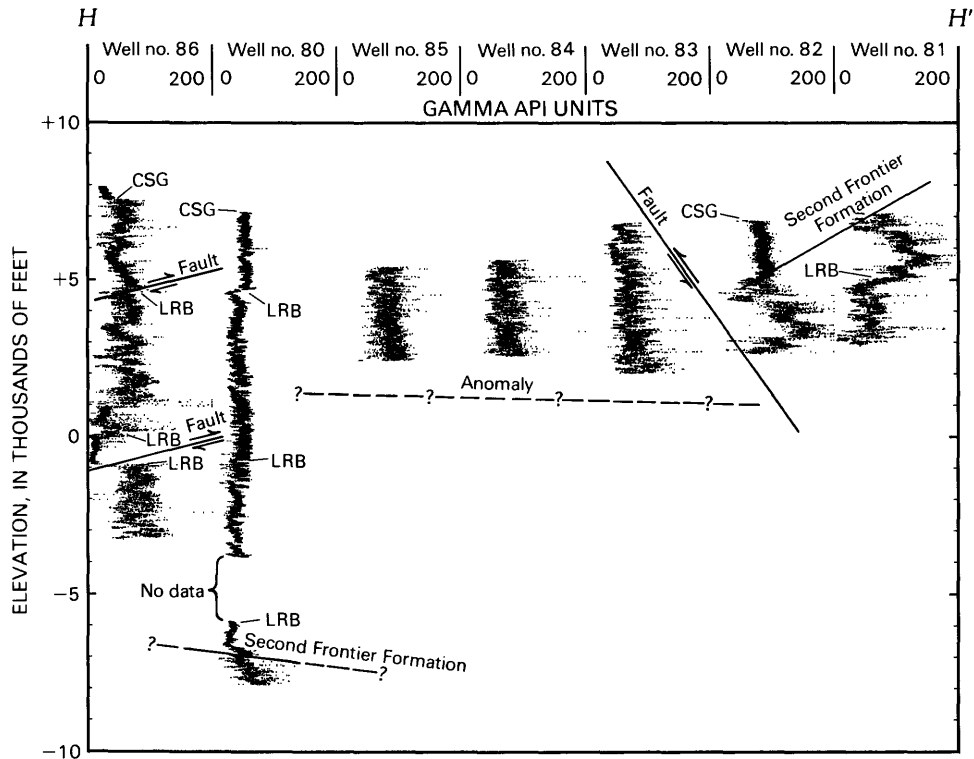


Figure 13. West-east gamma-ray log cross section *H-H'*, northern Green River basin. Wind River thrust shown schematically. Casing points (CSG) and log-run breaks (LRB) indicated. Solid line indicates position of gamma-ray anomaly; dashed, queried line indicates position of anomaly is uncertain. Wells listed by number in table 1 and shown in figure 1. Line of section shown on figure 1. Datum is sea level.

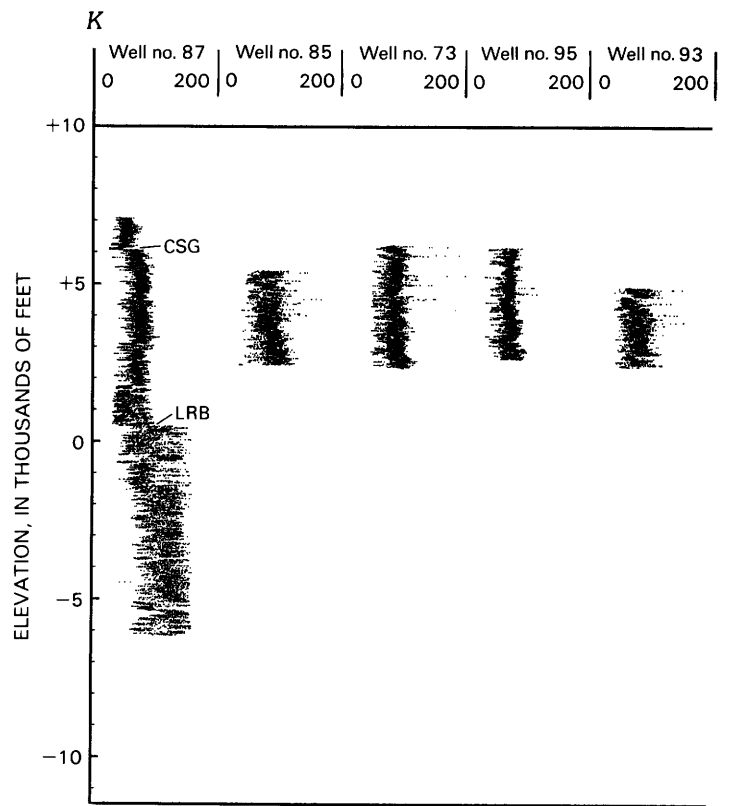
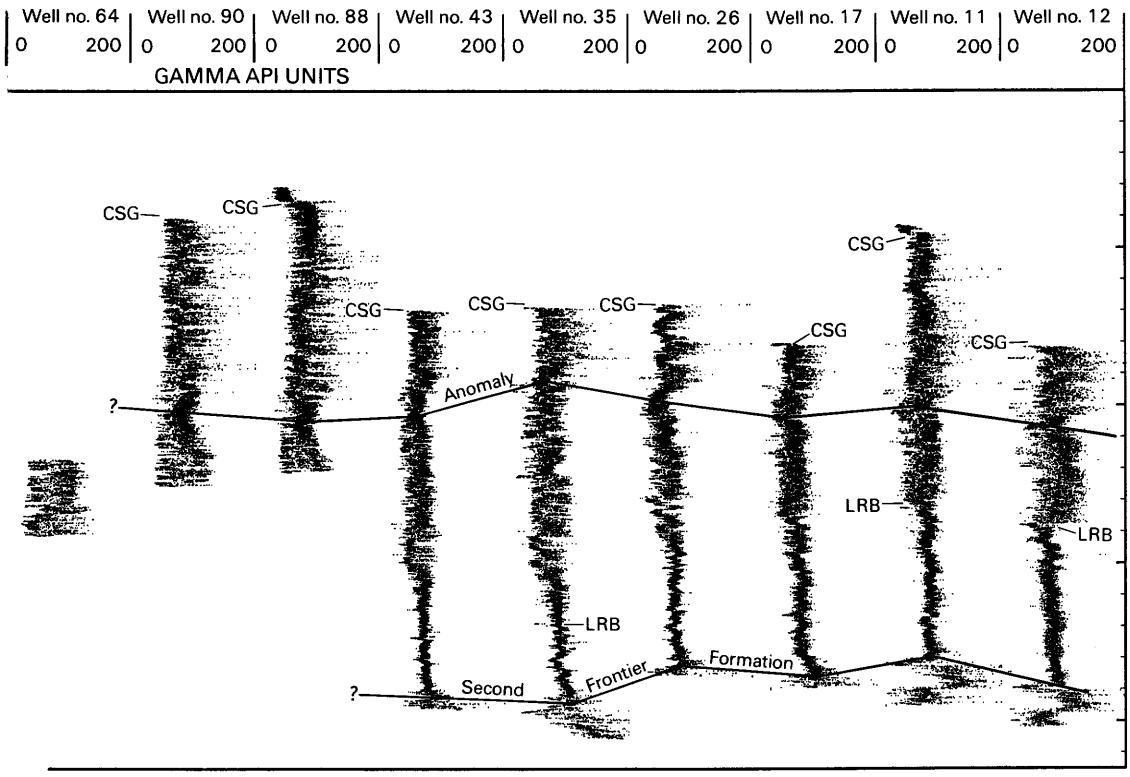


Figure 14. North-south gamma-ray log cross section K-K', northern of gamma-ray anomaly; dashed, queried line indicates position of Datum is sea level.



Green River basin. Casing points (CSG) and log-run breaks (LRB) indicated. Solid line indicates position anomaly is uncertain. Wells listed by number in table 1 and shown in figure 1. Line of section shown on figure 1.

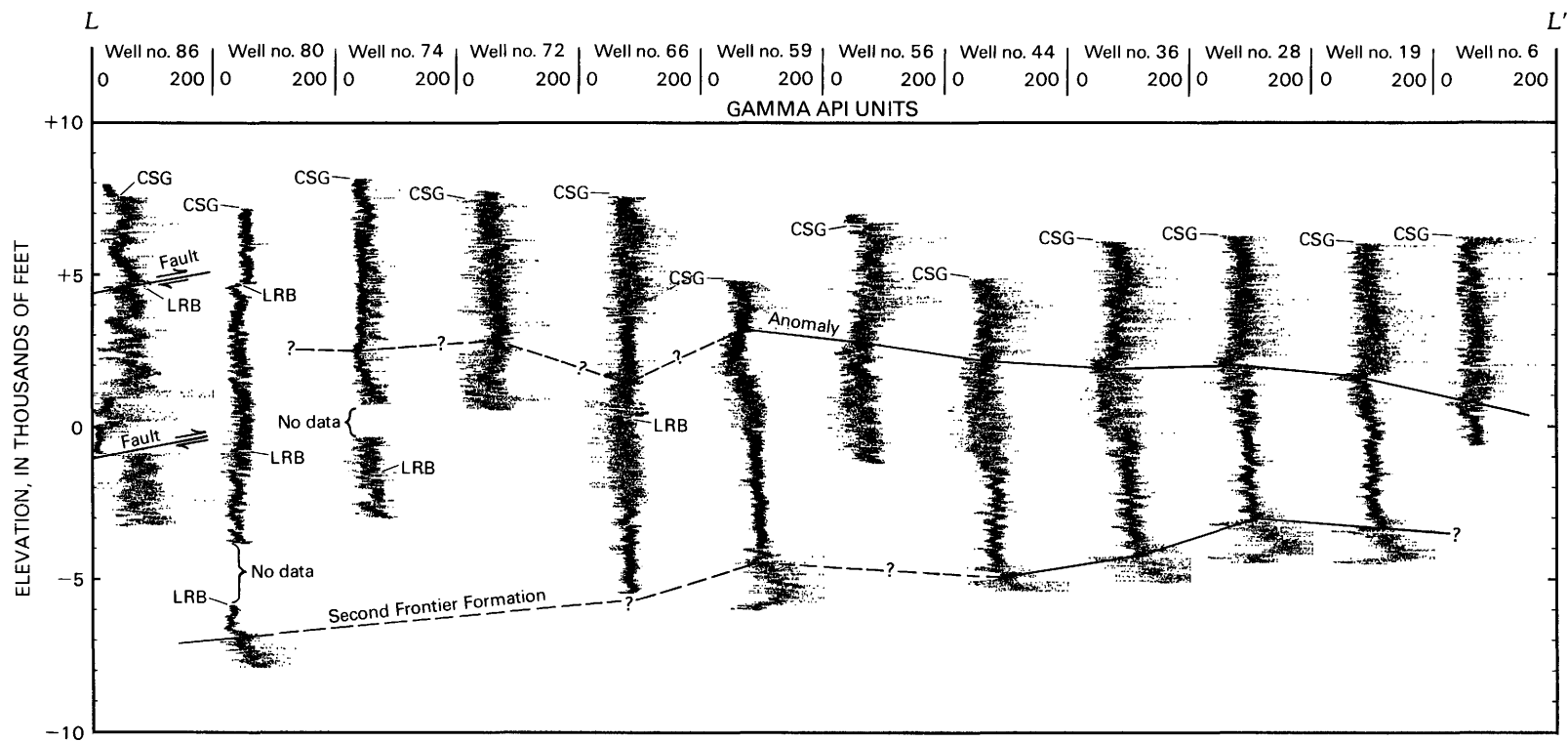


Figure 15. North-south gamma-ray log cross section L-L', northern Green River basin. Casing points (CSG) and log-run breaks (LRB) indicated. Solid line indicates position of gamma-ray anomaly; dashed, queried line indicates position of anomaly is uncertain. Wells listed by number in table 1 and shown in figure 1. Line of section shown on figure 1. Datum is sea level.

Table 2. Wells distant from the Wind River Mountains in the Green River basin from which arkose or feldspar has been reported

[Data from American Stratigraphic Company, Denver, Colo. Location in section, township (north), and range (west); township-range grid shown in figure 1]

Direction from		Well name	Constituent
Wind River Mountains	Location		
Northwest	23, 37, 113	Kerr McGee No. 1 Bondourant	Arkose
	23, 37, 113	Pan American No. 1 Raspberry Ridge	Arkose
West	24, 35, 114	Pacific Transmission Supply No. 24-24 Federal	Feldspar
	32, 34, 114	Gulf Oil No. 1 West Side Federal	Feldspar
	13, 33, 113	Ray Smith No. 1 Fear Ranch Unit	Arkose
	02, 33, 113	Texas Gulf No. 1 Horse Creek Federal	Arkose
	28, 31, 113	Belco No. 1 Goat Hill	Arkose
	34, 26, 113	Belco No. 2 Rocking Chair Ranch	Arkose, feldspar
	09, 26, 113	Belfer No. 35 BNG	Feldspar
Southwest	34, 24, 113	Amoco No. 1 Gravel Unit	Arkose

complicated by a sediment contribution from the Gros Ventre Mountains to the north (figs. 12, 13). Available data suggest that in many parts of the northern Green River basin the earliest preserved Tertiary rocks are probably arkosic. In these areas, the gamma-ray anomaly may mark the approximate location of the Cretaceous-Tertiary boundary.

CONCLUSIONS

A strong anomaly in gamma-ray intensity has been observed in lower Tertiary rocks of the northern Green River basin, in the subsurface adjacent to and parallel with the Wind River thrust. The anomaly can be identified in wells throughout the northern Green River basin, despite its reduction in amplitude with increasing distance from the Wind River Mountains. The anomaly results from detrital potassium feldspars and micas that have eroded from the Precambrian granitic core of the Wind River Mountains. The presence of arkose and feldspar in wells along the Wyoming thrust belt and on the La Barge platform implies that lower Tertiary fluvial drainage from the Wind River Mountains extended at least that far to the west. Limited palynologic data suggest that in some areas of the basin, particularly along its western flank, the gamma-ray anomaly is near the Cretaceous-Tertiary boundary. If additional data support this contention, the anomaly may prove useful in dating the timing of the Prospect-Hogsback thrusting.

REFERENCES CITED

Asquith, D.O., 1966, Geology of Late Cretaceous Mesaverde and Paleocene Fort Union oil production, Birch Creek Unit, Sublette County, Wyoming: American Association

of Petroleum Geologists Bulletin, v. 50, no. 10, p. 2176-2184.

Berg, R.B., 1961, Laramide tectonics of the Wind River Mountains, in Wiloth, G.J., ed., Symposium on Late Cretaceous rocks, Wyoming and adjacent areas: Wyoming Geological Association Field Conference, 16th, 1961, Guidebook, p. 70-80.

_____, 1962 Mountain flank thrusting in Rocky Mountain foreland, Wyoming and Colorado: American Association of Petroleum Geologists Bulletin, v. 46, p. 2019-2032.

Butcher, R.H., 1971, Modal analysis of petrographic study in Project Wagon Wheel technical studies report, December 31, PNE-WW1: El Paso Natural Gas Company, p. 203-206.

Dixon, J.S., 1982, Regional structural synthesis, Wyoming salient of western overthrust belt: American Association of Petroleum Geologists Bulletin, v. 66, p. 1560-1580.

Dorr, J.A., Jr., 1952, Early Cenozoic stratigraphy and vertebrate paleontology of the Hoback Basin, Wyoming: Geological Society of America Bulletin, v. 63, no. 1, p. 59-94.

_____, 1958, Early Cenozoic vertebrate paleontology, sedimentation, and orogeny in central western Wyoming: Geological Society of America Bulletin, v. 69, no. 10, p. 1217-44.

Dorr, J.A., Jr., Spearing, D.R., and Steidtmann, J.R., 1977, Deformation and deposition between a foreland uplift and impinging thrust belt, Hoback basin, Wyoming: Geological Society of America Special Paper 177, 82 p.

Greenfield, H., 1981, Resource evaluation and production research on tight sands in the Pinedale unit, Sublette County, Wyoming: Gas Research Institute, Final report for contract 5080-321-0328, 157 p.

Gries, Robbie, 1983, North-south compression of Rocky Mountain foreland structures, in Lowell, J.D., and Gries, Robbie, eds., Rocky Mountain foreland basins and uplifts: Rocky Mountain Association of Geologists, p. 9-32.

Guennel, G.K., Spearing, D.R., and Dorr, J.R., Jr., 1973, Palynology of the Hoback Basin, in Schell, E.M., ed. Symposium and core seminar on the geology and mineral

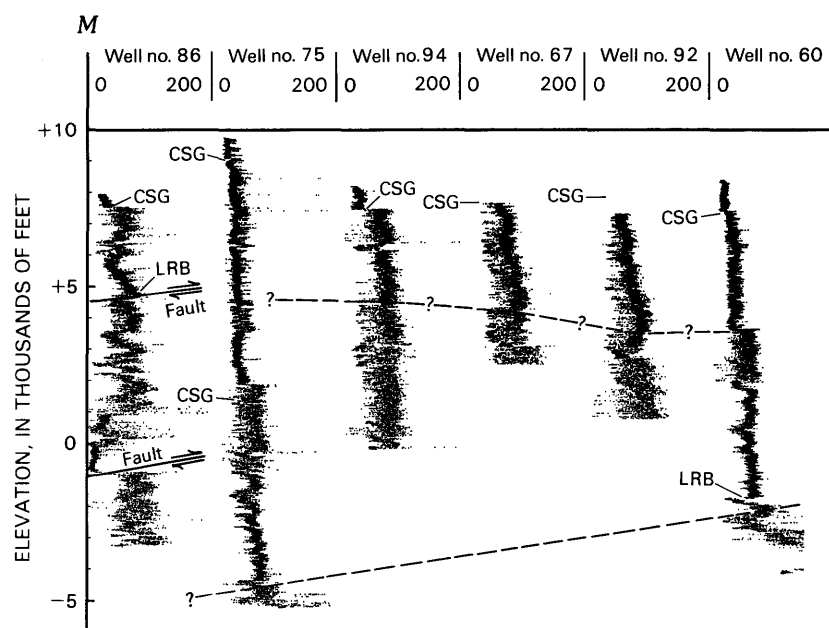


Figure 16. North-south gamma-ray log cross section M-M', northern Green River line indicates position of anomaly is uncertain. Wells listed by number in table 1

resources of the greater Green River basin: Wyoming Geological Association Field Conference, 25th, Guidebook, p. 173-185.

Hagen, E.S., Shuster, M.W., and Furlong, K.P., 1985, Tectonic loading and subsidence of intermontane basins; Wyoming foreland province: *Geology*, v. 13, no. 8, p. 585-588.

Keefer, W.R., 1965, Stratigraphy and geologic history of the uppermost Cretaceous, Paleocene, and lower Eocene rocks in the Wind River basin, Wyoming: U.S. Geological Survey Professional Paper 495-A, 77 p.

Keighin, C.W., 1984, Petrographic and selected reservoir characteristics of some Tertiary and Cretaceous sandstones, Pinedale anticline, Sublette County, Wyoming, *in* Law, B.E., ed., Geological characteristics of low-permeability Upper Cretaceous and lower Tertiary rocks in the Pinedale anticline area, Sublette County, Wyoming: U.S. Geological Survey Open-File Report 84-753, p. 16-21.

Law, B.E., 1979, Section B-B'; subsurface and surface correlations of some Upper Cretaceous and Tertiary rocks, northern Green River basin, Wyoming: U.S. Geological Survey Open-File Report 79-1689, 2 sheets.

_____, 1984, Relationships of source rock, thermal maturity, and overpressuring to gas generation and occurrence in low-permeability Upper Cretaceous and lower Tertiary rocks, greater Green River basin, Wyoming, Colorado and Utah, *in* Woodward, J., Meissner, F.F., and Clayton, J.L., eds., Hydrocarbon source rocks in the greater Rocky Mountain region: Rocky Mountain Association of Geologists, p. 468-490.

Law, B.E. and Nichols, D.J., 1982, Subsurface stratigraphic correlations of some Upper Cretaceous and lower Tertiary rocks, northern Green River basin, Wyoming [abs.], *in* Steidtmann, J.R., ed., Subsurface practices in geology and

geophysics: Laramie, University of Wyoming, Department of Geology and Geophysics, Earth Science Bulletin 15, p. 17.

Law, B.E., Pollastro, R.M. and Keighin, C.W., 1986, Geologic characterization of low-permeability gas reservoirs, *in* Spencer, C.W., and Mast, R.F., eds., Geology of tight gas reservoirs: American Association of Petroleum Geologists Studies in Geology 24, p. 253-269.

Love, J.D., 1960, Cenozoic sedimentation and crustal movement in Wyoming: *American Journal of Science*, v. 258-A, p. 204-214.

Lowell, J.D., 1983, Foreland deformation, *in* Lowell, J.D., and Gries, R., eds., Rocky Mountain foreland basins and uplifts: Rocky Mountain Association of Geologists, p. 1-8.

Martin, W.B. and Shaughnessy, J., 1969, Project Wagon Wheel, *in* Symposium on Tertiary rocks of Wyoming: Wyoming Geological Association Field Conference, 21st, Guidebook, p. 145-152.

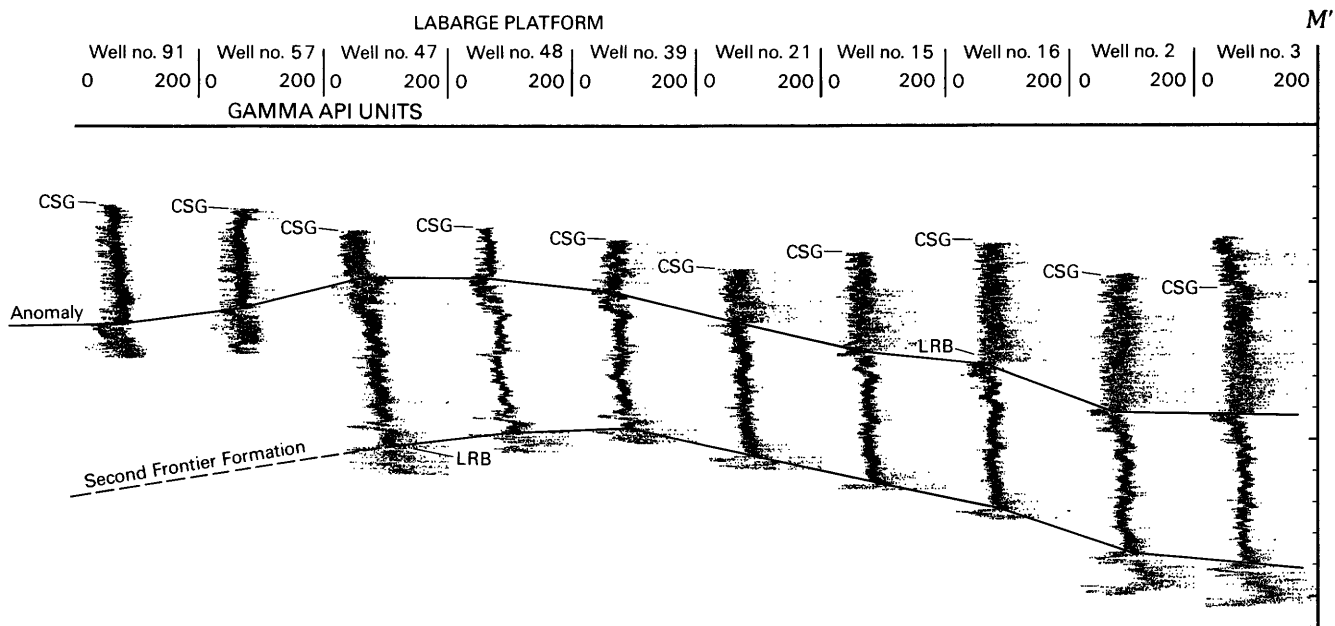
Merewether, E.A., Blackman, P.D., and Webb, J.C., 1984, The Mid-Cretaceous Frontier Formation near the Moxa arch, southwestern Wyoming: U.S. Geological Survey Professional Paper 1290, 29 p.

Merin, I.S. and Lindholm, R.C., 1986, Evidence that the crystalline cores of uplifts adjacent to the Powder River Basin were breached during Paleocene time: *The Mountain Geologist*, v. 23, no. 4, p. 128-131.

Petroleum Information Corporation, 1983, Structure contour map of the NW1/4 Green River basin, Wyoming: Denver, 1 sheet.

_____, 1987, Well history control system well completion records, Wyoming: Denver, microfiche.

Pollastro, R.M., 1985, Mineralogical and morphological evidence for the formation of illite at the expense of illite/smectite: *Clay and Clay Minerals*, v. 33, no. 4, p. 265-274.



basin. Casing points (CSG) and log-run breaks (LRB) indicated. Solid line indicates position of gamma-ray anomaly; dashed, queried and shown in figure 1. Line of section shown on figure 1. Datum is sea level.

Prensky, S.E., 1984, A gamma-ray anomaly associated with the Cretaceous-Tertiary boundary in the northern Green River basin, Wyoming, *in* Law, B.E., ed., *Geological characteristics of low-permeability Upper Cretaceous and lower Tertiary rocks in the Pinedale anticline area, Sublette County, Wyoming*: U.S. Geological Survey Open-File Report 84-753, p. 22-35.

_____, 1986, Geologic implications of large-scale trends in well-log response, northern Green River basin, Wyoming: *Society of Professional Well Log Analysts Annual Logging Symposium, 27th, Houston, Transactions*, paper EEE, 24 p.

_____, 1988, *Catalog of gamma-ray logs for selected wells in the northern Green River basin, Wyoming, presented as compressed depth-scale X-Y plots*: U.S. Geological Survey Open-File Report 89-82, 180 p.

Prensky, S.E., and Dickinson, W.W., 1986, Computer-generated well-log data plots assist regional subsurface evaluation: *Geobyte*, v. 1, no. 2, p. 52-58.

Shuster, M.W., 1986, *The origin and sedimentary evolution of the northern Green River basin, western Wyoming*: Laramie, Wyo., University of Wyoming, Ph.D. thesis, 323 p.

Spearing, D.R., 1969, *Stratigraphy and sedimentation of the Paleocene-Eocene Hoback Formation, western Wyoming*, *in* Barlow, J.A., ed., *Symposium on Tertiary rocks of Wyoming*: Wyoming Geological Association Field Conference, 21st, Guidebook, p. 65-76.

Vine, J.D., and Tourtelot, E.B., 1970, Preliminary geochemical and petrographic analysis of lower Eocene fluvial sandstones in the Rocky Mountain region, *in* Enyert, R.L., ed., *Symposium on Wyoming sandstones*: Wyoming Geological Association Field Conference, 22nd, Guidebook, p. 251-263.

West, R.M., 1969, *Geology and vertebrate paleontology of the northeastern Green River basin, Wyoming*, *in* Barlow, J.A., Jr., ed., *Symposium on Tertiary rocks of Wyoming*: Wyoming Geological Association Field Conference, 21st, Guidebook, p. 77-92.

Chapter I

Quantitative Model for Overpressured Gas Resources of the Pinedale Anticline, Wyoming

By R.R. CHARPENTIER, B.E. LAW, and S.E. PRENSKY

Prepared in cooperation with the U.S. Department of Energy

U.S. GEOLOGICAL SURVEY BULLETIN 1886

GEOLOGY OF TIGHT GAS RESERVOIRS IN THE PINEDALE ANTICLINE AREA, WYOMING,
AND AT THE MULTIWELL EXPERIMENT SITE, COLORADO

CONTENTS

Abstract	I1
Introduction	I1
Gas-bearing rocks	I1
General method of resource calculation	I2
Structure	I3
Calculation of gas concentrations	I4
Lithology	I4
Porosity	I5
Water saturation	I5
Pressure	I6
Temperature	I7
z factor	I7
Gas concentrations and volumes	I7
Distributions of concentrations	I8
Resource estimations	I9
Uncertainty of estimate	I10
Conclusions	I10
References cited	I10

FIGURES

1. Cross section from Wyoming thrust belt northeast to Wind River Mountains showing top of overpressuring I2
2. Map showing structure contours of top of Cretaceous in area of Pinedale anticline I3
- 3-6. Diagrams showing:
 3. Amount of sandstone in the Wagon Wheel well as determined by using gamma-ray log values I4
 4. Regression of sandstone porosity on depth in Wagon Wheel well I5
 5. Well pressures and temperature gradients in Wagon Wheel well I6
 6. Depth of top of overpressuring versus depth to top of Cretaceous for nine wells in Pinedale anticline area I7
7. Cross section showing concentration of natural gas per cubic foot of sandstone I9
8. Graph showing concentration of natural gas per cubic foot of sandstone versus depth I10
9. Cross section showing concentration of natural gas per cubic foot of rock I11
10. Map showing concentration of natural gas in assessed part of Pinedale anticline I12

TABLES

1. Average composition of gas for several wells on the Pinedale anticline, northern Green River basin I8
2. Estimate of in-place overpressured natural gas resource of the Pinedale anticline area I12

Quantitative Model for Overpressured Gas Resources of the Pinedale Anticline, Wyoming

By R.R. Charpentier, B.E. Law, and S.E. Prenskey

Abstract

The Pinedale anticline in the northern part of the Green River basin of Wyoming contains a large accumulation of overpressured natural gas within a low-permeability sequence of Upper Cretaceous rocks. The more important geologic factors that determine the vertical and horizontal distribution of gas have been incorporated into a quantitative model of the accumulation. Within the 197-mi² (317 km²) structure, sandstones of the 10,000-ft-thick (3,048 m) section of overpressured gas-bearing reservoirs are estimated to contain 159 trillion cubic feet (4.50×10^{12} m³) of in-place natural gas. Only a small part of this resource may be recoverable.

INTRODUCTION

The Pinedale anticline is a large thrust-rooted fold in the northern part of the Green River basin of Wyoming (Law and Johnson, this volume, fig. 1). Data obtained from wells drilled on the anticline demonstrate the occurrence of a thick (about 10,000 ft, 3,048 m) low-permeability gas-bearing interval below a depth of about 8,000 ft (2,438 m).

Prior to 1978, almost all aspects of the nature of large unconventional low-permeability gas accumulations were poorly understood; subsequently, numerous studies have been conducted that clarify the nature of these accumulations (Meissner, 1978, 1980, 1981; Masters, 1979; Spencer, 1983, 1987; Law and Dickinson, 1985). In the Pinedale area, relevant studies include those by Law and others (1979, 1980), Law and Spencer (1981), Spencer and Law (1981), Law (1984a, b), and Spencer (1984, 1987, this volume). Because these investigations are quite recent, most resource evaluations of low-permeability gas reservoirs have not incorporated these data and, in some instances, have utilized irrelevant or incomplete geologic criteria.

The primary purpose of our study, therefore, is to provide a more objective, geologically based model for the assessment of low-permeability gas reservoirs and, specifically, to evaluate the gas resources contained in low-permeability sandstone reservoirs in the Pinedale anticline area.

Acknowledgments.—This work was funded by the U.S. Department of Energy under Interagency Agreement DE-A121-83MC20422. The authors thank B. Hassler, Celcius Energy Company, and D. Reffert, Mountain Fuel Supply Company, for conversations concerning exploration, drilling, and production in the Pinedale area. The authors also thank K.B. Krystinik, U.S. Geological Survey, for help with the robust regression technique and G.L. Dolton and C.W. Spencer, U.S. Geological Survey, for helpful comments on the manuscript.

GAS-BEARING ROCKS

The gas accumulation in the Pinedale area is a deep-basin or basin-centered type, similar to that originally described by Masters (1979). This type of accumulation commonly is very large, occupies the deeper part of a basin, is abnormally pressured, and is downdip from water-bearing rocks. The reservoirs are almost always low-permeability (<0.1 mD) sandstones. The characteristics of these accumulations are important because they form the essential geologic elements of the resource analysis.

The gas accumulation in the Pinedale anticline is a small part of a much larger accumulation that occupies the deeper part of the Greater Green River basin of Wyoming, Colorado, and Utah. In the El Paso Natural Gas Company Wagon Wheel No. 1 well (Law and Spencer, this volume, fig. 2), the top of the gas-bearing interval is in Upper Cretaceous sandstone reservoirs at a depth of about 8,000 ft (2,438 m), coincident with the top of abnormally high pressures. The gas-bearing interval extends downward through the Upper Cretaceous Ericson Sandstone into the Rock Springs Formation (Law and Johnson, this volume). According to Law and Spencer (1981), Law (1984a, b), Spencer (1984, 1987, this volume), and Law and Dickinson (1985), the high pressures are caused by active or recently active gas generation. The low permeability of the sandstone reservoirs does not allow pressure to equilibrate to hydrostatic levels.

The seals for these low-permeability accumulations are not well understood. Conventional seals such as shale, evaporites, or some other relatively impermeable lithology are not significant, and the occurrence of these unconventional accumulations is not completely controlled by structure and stratigraphy. The relationship between structure, stratigraphy, and overpressuring, as shown in cross section (fig. 1), indicates that the top of gas-bearing overpressured rocks cuts across structural and stratigraphic boundaries. The more important aspects of these accumulations are temperature, thermal maturity, organic richness, and permeability, all of which have been determined to have a pronounced effect on the occurrence and magnitude of pressure variations in the Wagon Wheel well (Law, 1984a, b).

GENERAL METHOD OF RESOURCE CALCULATION

Both structural and stratigraphic boundaries were

used to delimit the volume of rock in the Pinedale anticline assessed for gas resources. The areal limits of the anticline are defined as the -2,000-ft (-610 m) contour on the top of the Cretaceous rocks and the high-angle reverse or thrust fault on the southwest flank of the anticline (fig. 2). The top of the assessed volume of rocks is defined as the top of the overpressured interval and the base of the assessed volume as the base of the Rock Springs Formation and the curving surface of the southwest-bounding fault.

Calculation of gas resources in the anticline was accomplished by dividing the anticline into about 8,000 cells and calculating the gas concentration and volume for each cell. Areal, land-survey section outlines (1 mi² each) were used to define cell boundaries. The column of rock under each of the 241 sections was divided into 25 intervals, each 500 ft (152 m) thick. The uppermost interval of each section began at an elevation 500 ft (152 m) below sea level and the lowermost ended 13,000 ft (3,962 m) below sea level. In order to facilitate separate estimations of gas resources for the Lance Formation, Ericson

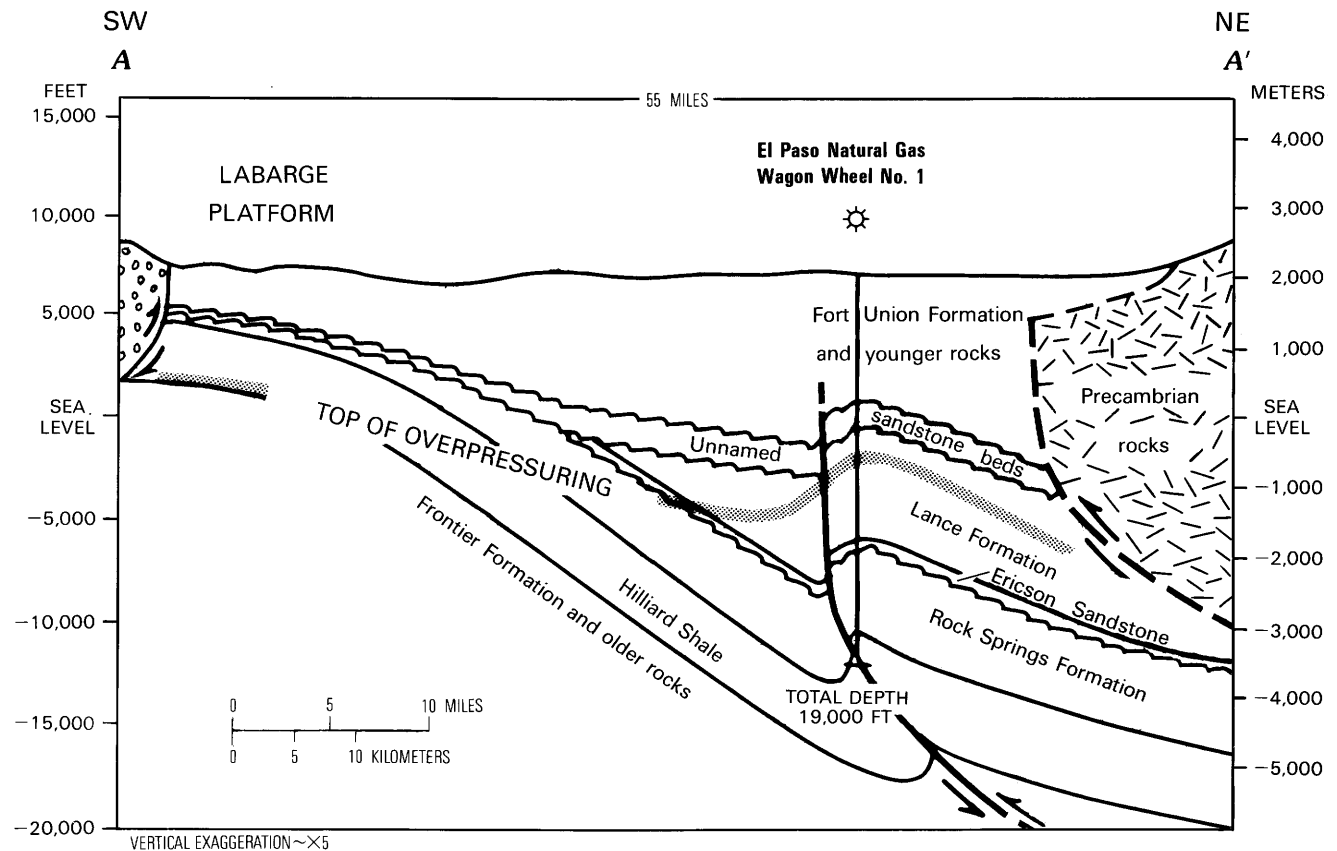


Figure 1. Cross section from Wyoming thrust belt northeast to Wind River Mountains. High-angle reverse fault on west side of Pinedale anticline from Martin and Shaughnessy (1969) and Shaughnessy and Butcher (1973, 1974). Line of section A-A' shown on figure 1 of Law and Johnson (this volume).

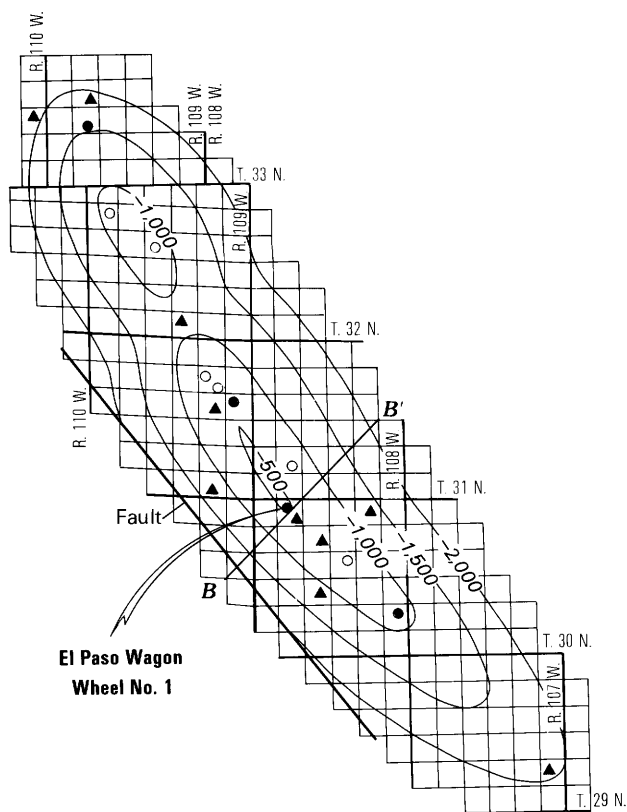


Figure 2. Structure contours of the top of the Cretaceous in the area of the Pinedale anticline. Contour interval, 500 ft; areal limits of assessed structure delimited by -2,000-ft contour. Wells: open circle, producing; solid circle, shut-in; triangle, all others, drilled and abandoned. Line of section B-B' (figs. 7,9) also shown.

Sandstone and Rock Springs Formation, some of the intervals between -5,500 and -8,000 ft (-1,676-2,438 m) were divided into two or three cells, one for each stratigraphic unit. For example, between -5,500 and -6,000 ft (-1,676-1,829 m), the Lance Formation and possibly the Ericson Sandstone can be within the interval, depending on the particular section. Thus, this interval was divided into two cells, one for the Lance from -5,500 to -6,000 ft and one for the Ericson. If for a particular section there is no Ericson at that depth, the volume of rock in the latter cell was set to zero. This procedure resulted in a total of 33 cells in each section. Section corners were digitized and used in combination with grid files of structural surfaces in order to allow computer calculation of section areas and cell volumes. Especially as one approaches the outer edge of the anticline, many of the cells fall above or below the limiting boundaries. These cells were given a cell volume of zero.

An alternative method would be to employ a regular grid instead of the slightly irregular section grid. If a regular grid is used, calculation of areas and volumes is simplified; however, straight outlines for the assessment boundaries are required, a disadvantage that results either in some loss of resolution or in a large increase in the number of cells and the number of calculations. Use of the section grid allows results to be related easily to lease areas and other land-use categories.

STRUCTURE

The structural configuration of the Pinedale anticline is shown in figure 1 of Law and Johnson (this volume). The structural datum is the top of the Cretaceous rocks. In the Green River basin, the boundary between Cretaceous and Tertiary rocks is unconformable and in many areas its location is uncertain. In the area of the Pinedale anticline, it has been identified on the basis of palynology and subsurface correlations (Law, 1979; Law and Nichols, 1982), but because it is an unconformable surface, some uncertainty remains as to the structural significance of the datum. Examination of all the well logs in the Pinedale area indicates little evidence of significant erosional truncation of the underlying Cretaceous rocks, and we believe that the Cretaceous-Tertiary datum in this area accurately portrays the structural configuration.

The computer representation of anticlinal structure is based on a hand-contoured map of structure of the top of the Cretaceous (fig. 2). Because initial trials of computer contouring on picks of the top of the Cretaceous in 20 wells did not adequately represent the structure, points were digitized from the hand-contoured map and a regular grid calculated. Reference to a proprietary seismic section suggests that the structural horizons are reasonably parallel, and grids for other structural horizons were calculated by subtracting a constant from each grid node value of the original (top of Cretaceous) grid.

For purposes of calculation, if depth relative to the top of Cretaceous was needed in an equation, the average elevation of the top of the Cretaceous was calculated for each section. The volume of the cells in a section from sea level down to the top of the Cretaceous was calculated and then divided by the area of the section. This procedure gave the average depth below sea level of the top of the Cretaceous for the particular section.

The configuration of the southwest-bounding fault was digitized in a manner similar to that of the top of the Cretaceous. A hand-contoured map of the fault surface was used, points digitized from the contour lines, and a grid calculated.

CALCULATION OF GAS CONCENTRATIONS

Lithology

The gas-bearing interval in the Pinedale anticline consists of interbedded sandstone, siltstone, and shale and minor amounts of carbonaceous rocks. Although all lithologies in the gas-bearing interval most likely are gas saturated, only the gas contained in sandstones was evaluated in this study. Based on examination of cores from the Wagon Wheel and other wells on the Pinedale anticline, the sandstones were grouped into those from the Lance and Rock Springs Formations and those from the Ericson Sandstone. The cored intervals in the Wagon Wheel well and their corresponding geologic units are shown in figure 3 of Law and Johnson (this volume).

The Lance and Rock Springs Formations consist of generally very fine to fine grained, poorly to moderately sorted lithic sandstones. Many of the sandstones have conglomeratic bases that fine upward. In the Lance Formation, many pores are partly to completely filled with authigenic clays (Keighin, 1984; Pollastro, this volume). The Ericson Sandstone consists of quartz-rich sandstones that are in places conglomeratic. The sandstones commonly contain more than 90 weight percent quartz (Law and others, 1986; Pollastro, this volume); grain size is very fine to coarse, sorting is poor to good. Detailed descriptions of the sandstone mineralogy are in Keighin (1984), Pollastro and Barker (1984), and Pollastro (this volume).

The percentage of sandstone in the gas-bearing interval is difficult to determine, but the proportion of sandstone, as determined from a visual examination of well logs, is 37–45 percent. In an attempt to increase precision of this value, we correlated core-derived lithology and the core-gamma log in the Wagon Wheel well. This correlation is good, in general, but a consistent source of error resulted from our inability to distinguish intraformational conglomeratic sandstones on the core-gamma log. Almost all the clasts in the conglomeratic beds are shale, mudstone, or shaly siltstone and, consequently, give a shale response on the core-gamma log.

The wireline gamma-ray log was corrected for the influence of borehole diameter and mud density, and the core-gamma log was linearly depth shifted to provide the best fit with the wireline gamma-ray log. Core lithology, as determined from visual and petrographic examination, was used to select a core-gamma sandstone cutoff value. Although the two gamma-ray logs are similar in character, they are not similar in absolute values and the core-gamma cutoff was transferred to the wireline gamma log in a proportional manner. The gamma-ray sandstone discriminator used corrected gamma values of 47 API from 8,000 to 12,099 ft (2,438–3,688 m) and 70 API from 12,100 to 17,840 ft (3,688–5,438 m). The change in API values occurs at a break in log runs.

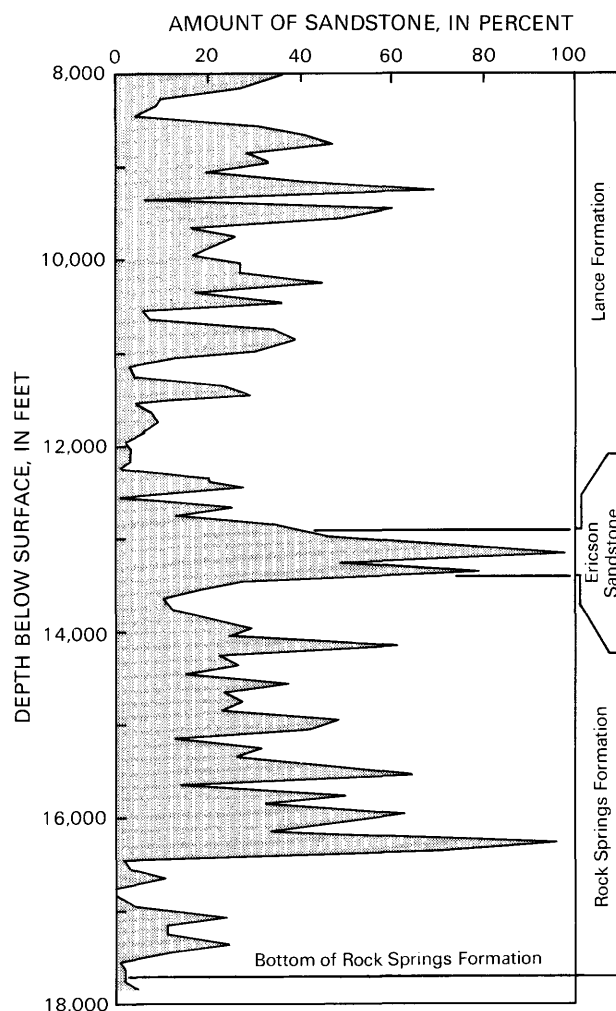


Figure 3. Amount of sandstone in the Wagon Wheel well as determined by using gamma-ray log values.

The wireline gamma-ray log was digitized in 1-ft increments, and from 8,024 to 17,840 ft (2,446–5,438 m) depth in the Wagon Wheel well determinations of lithology were made for each increment. The average percentage of sandstone for each 100-ft interval was summarized (fig. 3) and entered into the appraisal program as a table.

In order to calculate the percentage of sandstone for a particular cell, the depth of the center of the cell relative to the top of the Cretaceous was determined. The percentage of sandstone for the cell was calculated as the average percentage of sandstone for a 500-ft-thick (152 m) interval in the Wagon Wheel well centered at the same depth below the top of the Cretaceous. The geologic assumption behind this procedure is that the trends in sandstone percents obtained by averaging for 500-ft intervals are relatively consistent in the area of the Pinedale structure. This assumption cannot be firmly established, however, because only the Wagon Wheel well penetrated

the entire assessed interval. For cases in which the 500-ft interval included part of a different formation, only that part of the interval in the formation of interest was used.

Porosity

Three types of porosity measurements were made in the Wagon Wheel well: acoustic, density, and sidewall neutron. The latter two utilize pad tools that require good contact with the borehole wall and thus are affected by hole rugosity. Severe borehole washout, as indicated by the caliper log, is encountered throughout much of the Upper Cretaceous interval between 7,000 and 16,000 ft (2,134–4,877 m). It occurs preferentially in shaly zones (as defined by gamma-ray logs) between 7,000 and 12,000 ft (2,134–3,658 m) and frequently in sandstone intervals (as defined by gamma-ray logs) between 12,000 and 17,000 ft (3,658–5,182 m). Although the preferred porosity log for low-permeability gas sandstones is the density log, it was not used because its overall quality as measured by the density correction curve was highly variable.

Porosity determinations were made by using the borehole-compensated sonic log. Acoustic traveltime was converted to porosity by using a matrix traveltime of 55.5 microseconds/ft (182 microseconds/m). This matrix-derived value correlates best with core-derived data from the well (Prensky and Dickinson, 1986). Data affected by borehole washout generally were excluded through the

use of the gamma-ray sandstone cutoff, and the remaining high acoustic porosities may result from the presence of gas. The sonic log also may have underestimated the fracture porosity.

Sonic-derived porosity values for the sandstone intervals were regressed on depth (fig. 4), but, because of borehole washout, porosity values for many intervals were unreasonably high. A robust regression program written by K.B. Krystinik and W.F. Dumler (U.S. Geological Survey) was used to give a more reasonable fit to the data. The first step of the program is a least-squares regression on all the points. This regression is followed by a weighted least-squares regression that gives less weight to the points having large deviations from the regression. The procedure is repeated until an adequate fit is obtained. For this particular data set, points having large deviations are those having unreasonably high porosity values and thus those most reasonable to downweight. Comparison of the two regressions (fig. 4) indicates that the robust regression gives a more reasonable fit and that the original least-squares regression overestimates porosity by about 2 percent.

Water Saturation

The derivation of reliable water saturation values in low-permeability reservoirs is an unresolved problem. Log-derived values commonly are higher than core-derived values. Calculation of water saturation from well logs requires a value for formation water resistivity (R_w), which normally is computed by using the spontaneous potential (SP) curve. This method is unreliable in the Wagon Wheel well because of the poor character of the SP curve. The deflection amplitude of the curve varies from very low to flat, and the SP reverses; this character is a result of adverse changes in R_w relative to the mud-filtrate resistivity (R_{mf}). R_w can be obtained independently from analysis of formation water samples obtained during drill-stem or production testing, but water generally is not recovered from these low-permeability reservoirs, and the origin of the small amounts of water that have been recovered is somewhat uncertain.

Observations by Law and others (1979, 1980) in the Pacific Creek area of the Green River basin (Spencer, this volume, fig. 1) indicate that these gas-bearing low-permeability reservoirs contain little or no recoverable water, and wells in the Pinedale anticline area commonly do not produce water. These empirical relationships indicate that, in these reservoirs, water is immobile and is in very small pores and capillaries as irreducible water. For purposes of our calculations, we therefore assume that water in these reservoirs occurs at irreducible saturation levels.

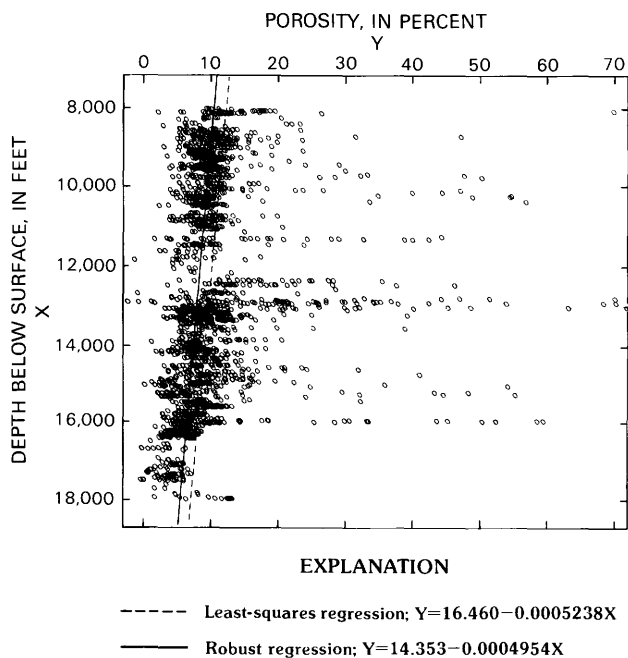


Figure 4. Regression of sandstone porosity on depth in Wagon Wheel well. For ease of viewing, independent variable (depth) shown on vertical axis.

During the original evaluation of data from the Wagon Wheel well by El Paso Natural Gas Company, analyses of cores from depths of 8,100 to 10,985 ft (2,469–3,348 m) indicate that water saturations are from 27.6 to 54.9 percent, with most values from 40 to 54.9 percent. These measurements agree well with results of mercury capillary pressure tests from similar sandstone reservoirs at the U.S. Department of Energy Multiwell Experiment site in the Piceance basin of Colorado. Because irreducible water saturation probably increases as porosity and permeability decrease with depth and because there are no measurements of water saturation deeper than 11,000 ft (3,353 m) in the Pinedale anticline, we chose a water saturation value of 50 percent for the gas-bearing interval.

Pressure

Overpressuring in the Pinedale area was initially reported by Rathbun (1968) and later discussed by Rathbun and Dickey (1969), Law and Spencer (1981), Law (1984a, b), Spencer (1984, 1987, this volume), Law and Dickinson (1985), and Prensky (1986). Rathbun concluded that tectonism was the cause of overpressuring, but subsequent investigations attributed the abnormally high pressures to the thermal generation of gas from coal and carbonaceous rocks interbedded with low-permeability sandstone reservoirs. The latter explanation of overpressuring in these rocks is more compatible with available data than is the former.

The pressure gradient in the Wagon Wheel well (fig. 5) is based on mud-weight data from mud logs, well logs, and drill-stem tests. Because gas is the pressuring phase, the total gas-bearing interval was divided into three pressure-related intervals that are defined on the basis of specific geologic conditions (Law, 1984a; Spencer, this volume).

The uppermost interval in the Wagon Wheel well, referred to as the inactive zone (Law, 1984a), extends from a depth of 8,035 to about 10,500 ft (2,449–3,200 m), at which point the pressure gradient abruptly increases. The inactive zone corresponds to an interval in which significantly large volumes of gas previously have been thermally generated. As a result of a cooling event that occurred 2–4 Ma (Naeser, 1984, 1986, this volume), thermal generation of gas has either ceased or diminished to such low rates that it is lost from the reservoirs faster than it accumulates.

The active zone (Law, 1984a) is below the inactive zone and is subdivided into two intervals. Within the active zone, thermogenic gas is thought to be actively generated. The upper part of the active zone extends from a depth of about 10,500 to about 14,700 ft (3,200–4,481 m), at which point the pressure gradient again abruptly increases. The pressure gradient in the upper part of the

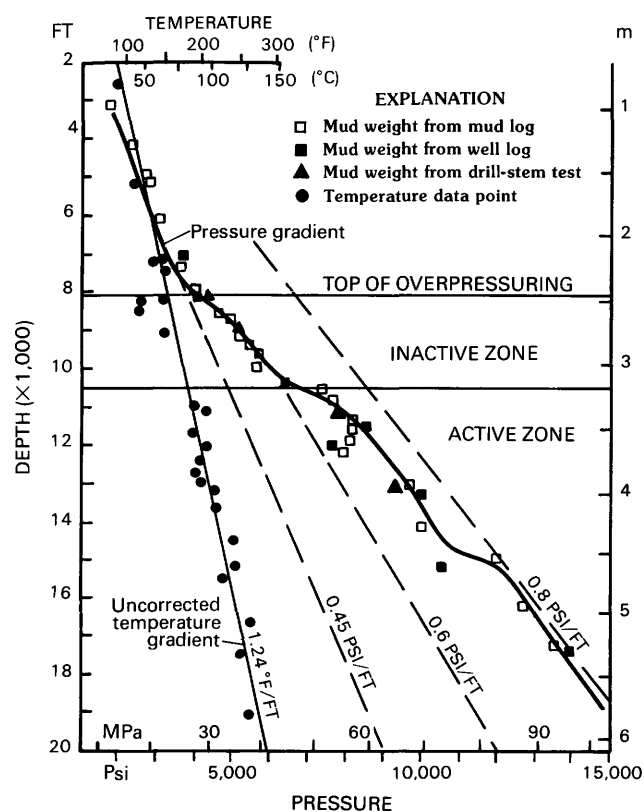


Figure 5. Well pressures and temperature gradients in Wagon Wheel well. Pressure gradients as interpreted by C.W. Spencer (oral commun., 1986). Temperature data from Wagon Wheel No. 1 and Pinedale No. 5 wells.

active zone probably is the result of a thermal effect described by Law (1984a). The lower part of the active zone extends from a depth of about 14,700 ft to the base of the Rocks Springs Formation at 17,700 ft (4,481–5,395 m). The increase in pressure gradient in the lower part of the active zone coincides with the top of a coal-bearing (organic-rich) zone. The elevated pressure gradient through this interval has been interpreted to result from the increased gas generation capacity of the coal zone (Law, 1984a).

The top of overpressuring in wells was determined primarily by using mud-weight data. If the top of overpressuring as determined by using mud weights is plotted versus the elevation of the top of the Cretaceous as determined by using palynological and sedimentological data, a strong correlation ($R^2=0.8732$) is evident (fig. 6) and indicates that the surface of the top of overpressuring dips in the same directions as that of the structure. This relationship indicates a probable genetic link between thermal maturity and the structural deformation. The slope of the regression is greater than one, however, and indicates that the surface of the top of overpressuring dips more steeply than the structural surface (Lickus and others, this volume). Results of this regression were used

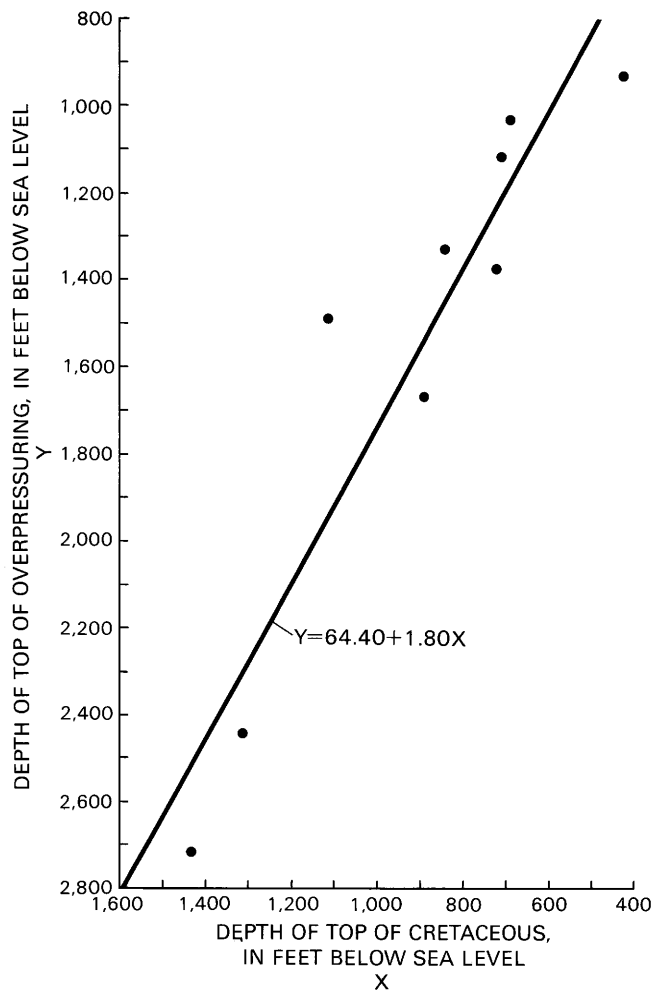


Figure 6. Depth of top of overpressuring versus depth to top of Cretaceous for nine wells in Pinedale anticline area.

in conjunction with the grid of the top of the Cretaceous surface to create a grid of the surface of the top of overpressuring.

In order to calculate the average pressure for a cell, the depth below the surface was multiplied by an appropriate pressure gradient, the product of which was then added to atmospheric pressure of 14.73 psi (101.6 kPa). The three zones each have specific pressure gradients. The inactive zone was assigned a pressure gradient of 0.55 psi/ft (12.45 kPa/m), the upper part of the active zone a gradient of 0.70 psi/ft (15.83 kPa/m), and the lower part of the active zone a gradient of 0.78 psi/ft (17.64 kPa/m). These zones are separated from each other by surfaces that correspond to the inflection points in the pressure/depth plot for the Wagon Wheel well (fig. 5). The inactive zone and the upper part of the active zone are separated by a horizontal plane at 3,311 ft (1,009 m) below sea level, and the upper and lower parts of the active zone are separated by a surface parallel with structure 7,180 ft (2,188 m) below the top of the Cretaceous.

Temperature

Temperature is an important aspect of overpressured gas accumulations, but reliable temperature data are difficult to obtain. Most temperature data are from measurements recorded during well-log runs (bottom-hole temperatures); they generally are not in equilibrium with true formation temperatures and are therefore minimal temperatures. Correction of bottom-hole temperatures to true formation temperatures requires information often not available.

The bottom-hole thermal gradient for the Pinedale area is 1.24 °F/100 ft (2.26 °C/100 m). T.H. McCulloh (Mobil Exploration and Producing Services, written commun., 1981) calculated a corrected thermal gradient based on these bottom-hole temperatures, and this gradient (converted to degrees Rankine (°R)) was used in our resource calculations. The corrected subsurface temperature (°R) from the surface to a depth of 10,000 ft (3,048 m) is defined as

$$T = 1.8 * [10 + 0.0079 * \text{Depth}] + 491.69 \quad (1)$$

and from 10,000 ft (3,048 m) to total depth as

$$T = 1.8 * [89 + 0.00645 * (\text{Depth} - 10,000)] + 491.69. \quad (2)$$

Present-day subsurface temperatures in the Pinedale area are lower than paleotemperatures. Studies involving vitrinite reflectance (Law and Spencer, 1981; Law, 1984a; Pollastro and Barker, 1984, 1986), clay transformations (Pollastro and Barker, 1984, 1986), and apatite fission-track dating (Naeser, 1984, 1986, this volume) show that present-day temperatures are 36–90 °F (20–50 °C) cooler than paleotemperatures and that a cooling event occurred 2–4 Ma.

z Factor

The derivation of the gas compressibility factor (z) is based on the average composition of gas recovered from several wells on the Pinedale anticline (table 1). Although there is some uncertainty as to the depths from which the gas was recovered, most of the gas recovered from wells on the anticline has been from depths of 10,000 to 11,500 ft (3,048–3,505 m). Because of the uncertainties as to changes in gas composition with depth, we calculated an average z of 1.34 for the entire gas-bearing interval.

Gas Concentrations and Volumes

The gas concentration for each cell was calculated in a stepwise manner such that both gas quantity per unit volume of sandstone and gas quantity per unit volume

Table 1. Average composition of gas for several wells on the Pinedale anticline, northern Green River basin

[Data from El Paso Natural Gas Company (1971)]

Components	Mole percent
Nitrogen	0.54
Carbon dioxide	.26
Methane	92.14
Ethane	4.71
Propane	1.39
I-butane	.29
N-butane	.28
I-pentane	.16
N-pentane	.07
Hexanes plus	.16

of total rock could be derived. Initially, the concentration in sandstone was calculated by using the equation

$$\begin{aligned} &\text{Concentration per cubic foot of sandstone} \\ &= (0.14353 - 0.000004954 * \text{Depth}) * 0.5 \\ &\quad * (\text{Reservoir pressure} / 14.696) \\ &\quad * (519.69 / \text{Reservoir temperature}) * (1 / 1.34). \end{aligned} \quad (3)$$

The concentration in total rock was then calculated by using the equation

$$\begin{aligned} &\text{Concentration per cubic foot of rock} \\ &= \text{Concentration per cubic foot of sandstone} \\ &\quad * \text{Percent sandstone}. \end{aligned} \quad (4)$$

Both types of gas concentrations were used to study the distribution of gas resources within the structure. The gas volume for a cell was calculated by using the equation

$$\begin{aligned} &\text{Volume of gas in a cell} \\ &= \text{Concentration per cubic foot of rock} \\ &\quad * \text{Volume of rock in cell}. \end{aligned} \quad (5)$$

A gas volume was calculated for each cell, these were then summed for each section; the total gas volume was then divided by the area of the section to give the gas concentration by surface area. The gas volumes per section were summed to give a total volume of gas-in-place for the entire structure. The volume for each formation was also tallied separately.

DISTRIBUTION OF CONCENTRATIONS

Gas concentrations per cubic foot of sandstone in a cross section through the Pinedale anticline at approximately the site of the Wagon Wheel well are shown in figure 7. These concentrations depend on five main factors: water saturation, porosity, pressure, temperature, and gas compressibility. Both water saturation and gas compressibility are held constant and thus do not

contribute to the pattern shown in figure 7. Pressure increases with depth and thus contributes to an increased concentration with depth. Porosity decreases with depth and temperature increases with depth; both contribute to a decrease in concentration with depth.

The interaction of these trends is better shown in figure 8, in which concentration is plotted as a function of depth. The concentrations used are based primarily on results for sec. 5, T. 30 N., R. 108 W., an area that includes the Wagon Wheel well. Concentrations increase gradually with depth and dramatically increase at 3,500 ft (1,067 m) below sea level. This increase corresponds to the top of the active zone and a substantial increase in pressure gradient. The gas concentration again dramatically increases at 7,500 ft (2,286 m) below sea level, where the pressure gradient changes at the boundary between the upper and lower parts of the active zone. These jumps in concentration follow the surfaces that define the boundaries between zones: a horizontal boundary between the active and inactive zone and a boundary parallel with structure between the upper and lower parts of the active zone (fig. 7).

Within each zone, the gas concentration changes more gradually. In the inactive zone and in the uppermost part of the active zone, the increase in concentration indicates that the effect of pressure outweighs those of decreasing porosity and increasing temperature. Below about 5,500 ft (1,676 m) below sea level, the decrease in concentration indicates that the effects of porosity and temperature outweigh that of pressure. If a water saturation is used that increases with decreasing porosity (and thus increases with depth) instead of a constant saturation, gas concentrations would further decrease with depth. Not only will the actual slopes in figure 8 change, but the point at which the slope changes probably will be closer to the surface.

The concentration of gas per cubic foot of total rock is shown in figure 9. Comparison of figures 9 and 3 shows that the concentration of gas is more strongly controlled by lithologic variation than by variation in concentration per cubic foot of sand. The high concentrations in the Ericson Sandstone are especially striking. The second most prominent trend of high concentration is between about 7,500 and 10,000 ft (2,286–3,048 m) below sea level, an interval in which a group of sandstone beds in the Rock Springs Formation has high concentrations per cubic foot of sandstone because of the increase in pressure in the lower part of the active zone. In the Lance Formation, gas concentrations are generally higher in the upper part of the formation because of higher proportions of sandstone.

The concentration of gas per square mile is shown in figure 10. Two trends are evident, and both probably are primarily related to thickness of assessed section. A minor trend is evident over most of the structure,

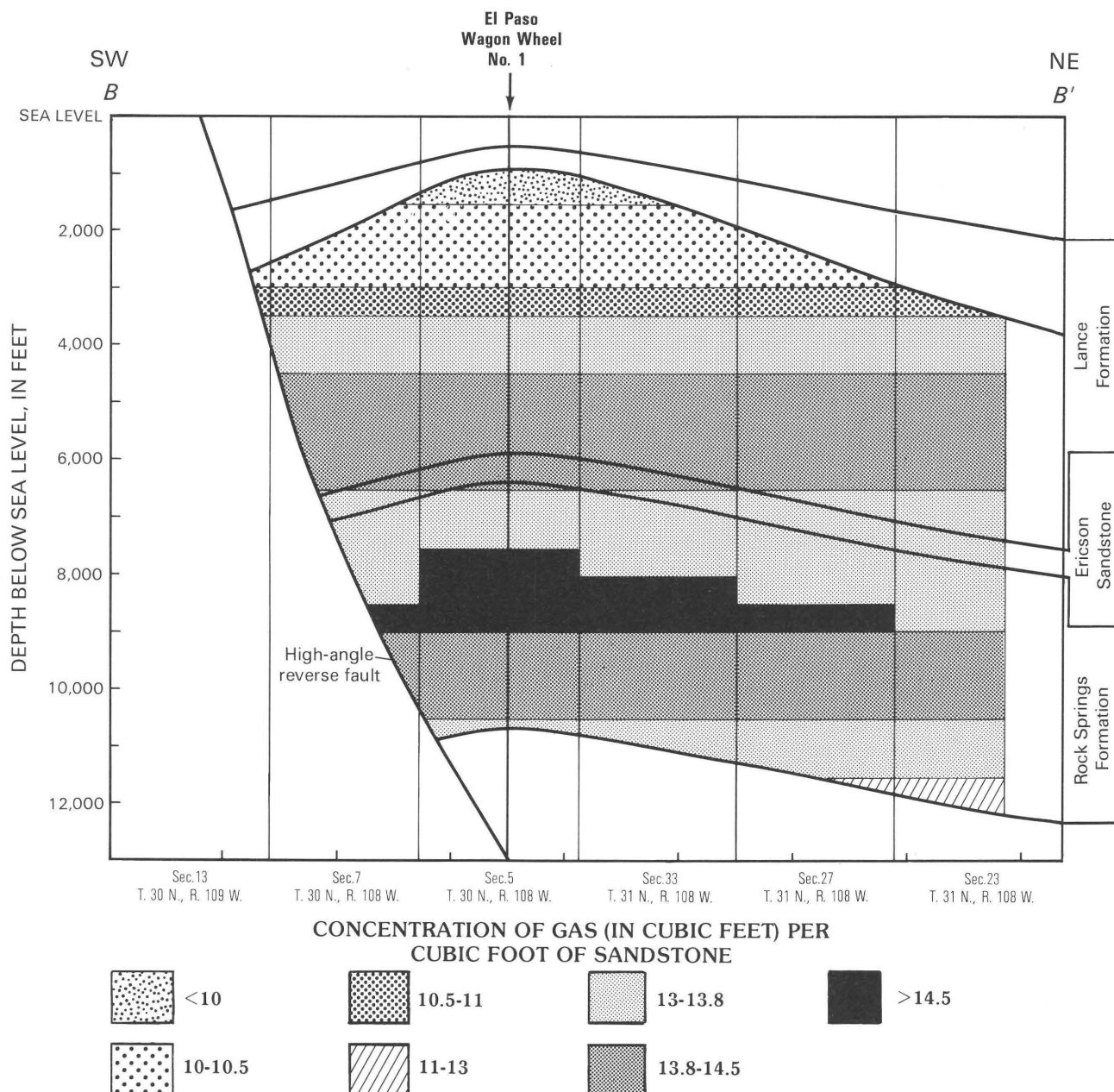


Figure 7. Cross section showing concentration of natural gas per cubic foot of sandstone. Line of section B-B' shown in figure 2.

especially to the northeast where concentration decreases downdip. This trend is probably the result of decreases in assessed thickness owing to the steeper dip of the top of overpressuring. A much more prominent trend is evident on the southwest flank of the structure where the assessed section is truncated by the thrust fault (fig. 9).

RESOURCE ESTIMATIONS

The results of the resource estimation are shown in table 2. The total in-place overpressured gas resource

for the sandstone reservoirs is 159 trillion cubic feet (4.50×10^{12} m³). It must be stressed that this is an estimate of gas in-place, not recoverable resources. Recoverable amounts of gas would be considerably less.

Other estimates of resources in the Pinedale anticline have been made, but because of differences in such factors as area assessed, stratigraphic interval assessed, and in-place versus recoverable amounts estimated, the estimates cannot be directly compared.

El Paso Natural Gas Company (1971) estimated an in-place resource of 252.3 billion cubic feet (7.1×10^9 m³) for an area of only 640 acres (2.59 km²) around the

Wagon Wheel well and only for depths from 7,983.5 to 11,796.5 ft (2,433–3,596 m). In the El Paso study, the interval was assigned to the Fort Union Formation, but we now know that it is generally correlative to the sandy part of the Lance Formation (fig. 3) (Law, 1979, 1984c; Law and Nichols, 1982).

Greenfield and others (1981) estimated a total recoverable resource of 2.8 trillion cubic feet (79.3×10^9 m³) for the Pinedale field. Their estimate was for an area slightly smaller (90,000 acres, 364 km²) than that used in our study (more than 126,000 acres, 510 km²) and having a somewhat different boundary. They also only estimated gas resources for selected intervals within the Lance.

UNCERTAINTY OF ESTIMATE

Despite all the sources of uncertainty in the input variables, some comments regarding the uncertainty of the results can be made. Because water saturation and gas compressibility are treated as constants, the concentrations and amounts of gas can be easily calculated for different constants. For a water saturation of X , gas concentrations and volumes will change by a factor of $[(1-X)/0.5]$. For a compressibility factor (z) of Y , gas concentrations and volumes will change by a factor of $[1.34/Y]$. The effect of variation in either of these factors with depth would be more difficult to calculate.

A number of factors are not included in our model. Gas volumes from porosity in silt and shale were not assessed, and gas dissolved in formation water or sorbed on organic material was excluded from the analysis. As mentioned, fracture porosity and formation pressures may have been underestimated. All in all, estimates for in-place gas resources may be conservative. On the other hand, gas from the shaly and silty intervals is less likely to ever be producible, and thus the estimate of 159 trillion cubic feet from the sandstone reservoirs is probably of more interest and use than an estimate for all lithologies.

CONCLUSIONS

The in-place resources of natural gas within the overpressured part of the Upper Cretaceous in the Pinedale anticline is estimated to be 159 trillion cubic feet (4.50×10^{12} m³), but a number of factors suggest that this estimate may be conservative. Only a small part of this gas may be recoverable using currently available recovery technology. In our study, the characteristics of these unconventional accumulations have been related to specific geologic conditions that facilitate the resource evaluation, and we believe the methodology used in this study is, in general, applicable to similar gas accumulations elsewhere.

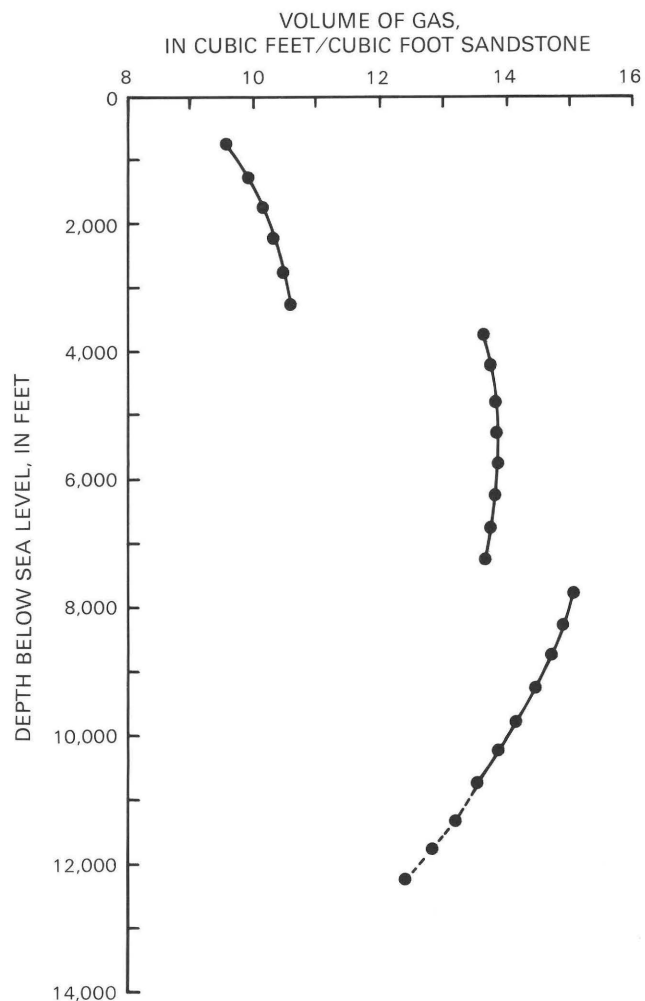


Figure 8. Concentration of natural gas per cubic foot of sandstone versus depth. Data primarily from sec. 5, T. 30 N., R. 108 W.; the three deepest values from sec. 23, T. 31 N., R. 108 W.

REFERENCES CITED

- El Paso Natural Gas Company, 1971, Project Wagon Wheel, technical studies report: El Paso, Tex., 248 p.
- Greenfield, H., Ahmed, U., Holland, M.T., and Schatz, J.F., 1981, Resource evaluation and production research on tight sands in the Pinedale Unit, Sublette County, Wyoming: Gas Research Institute GRI-81/0049, 157 p.
- Keighin, C. W., 1984, Petrographic and selected reservoir characteristics of some Tertiary and Cretaceous sandstones, Pinedale anticline, Sublette County, Wyoming, *in* Law, B.E., ed., Geological characteristics of low-permeability Upper Cretaceous and lower Tertiary rocks in the Pinedale anticline area, Sublette, County, Wyoming: U.S. Geological Survey Open-File Report 84-753, p. 16–21.
- Law, B.E., 1979, Section B-B'; subsurface and surface correlations of some Upper Cretaceous and Tertiary rocks, northern Green River basin, Wyoming: U.S. Geological Survey Open-File Report 79-1689, 2 sheets.

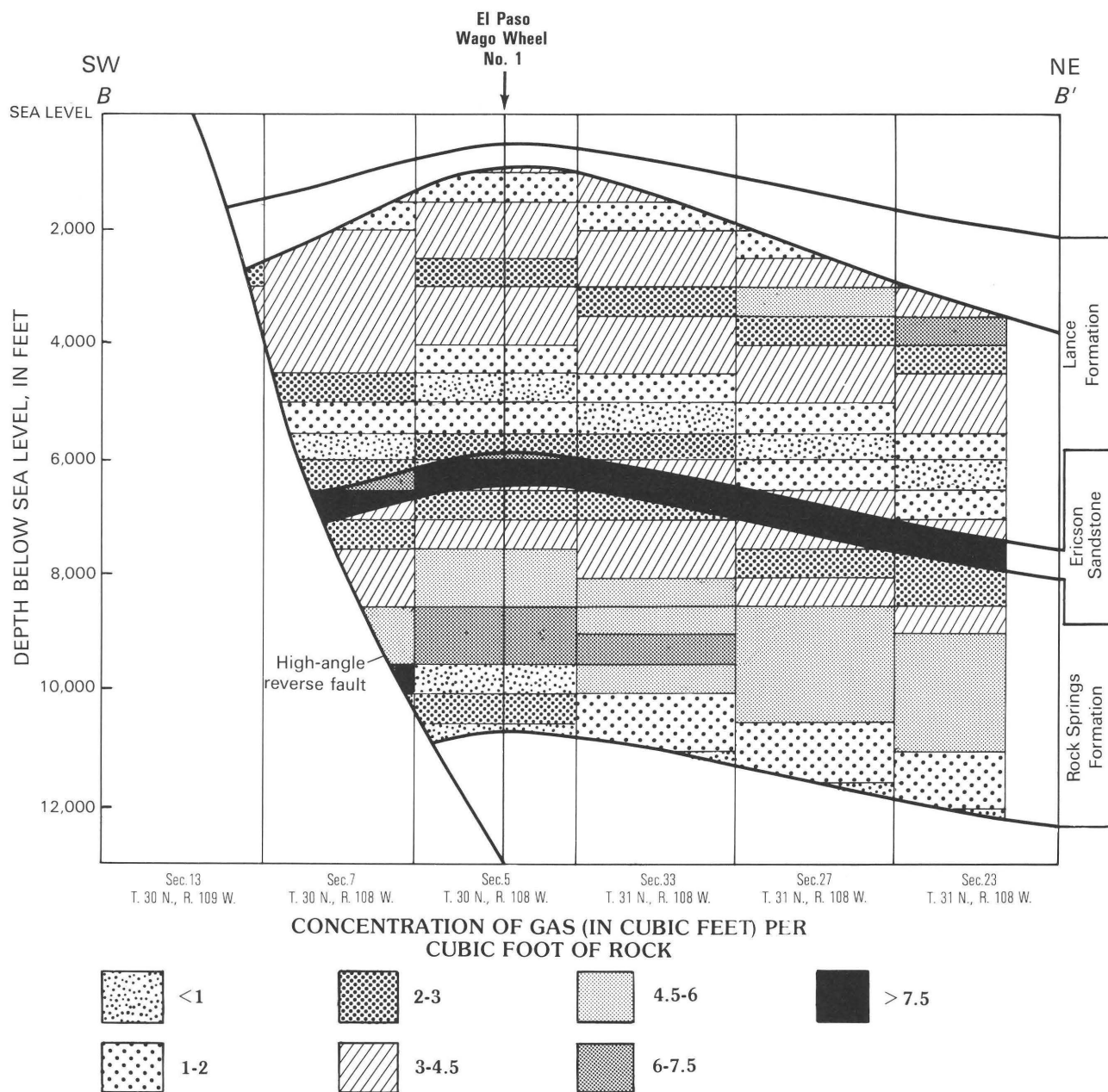


Figure 9. Cross section showing concentration of natural gas per cubic foot of rock. Line of section B-B' shown in figure 2.

____ 1984a, Relationships of source-rock, thermal maturity, and overpressuring to gas generation and occurrence in low-permeability Upper Cretaceous and lower Tertiary rocks, Greater Green River basin, Wyoming, Colorado, and Utah, in Woodward, J., Meissner, F.F., and Clayton, J.L., eds., Hydrocarbon source rocks of the greater Rocky Mountain region: Rocky Mountain Association of Geologists, p. 469-490.

____ 1984b, Source-rock evaluation of Upper Cretaceous and lower Tertiary rocks in the Pinedale anticline area, Sublette County, Wyoming, in Law, B.E., ed., Geological characteristics of low-permeability Upper Cretaceous and lower Tertiary rocks in the Pinedale anticline area, Sublette County, Wyoming: U.S. Geological Survey Open-File Report 84-753, p. 36-50.

____ 1984c, Structure and stratigraphy of the Pinedale anticline, Wyoming, in Law, B.E., ed., Geological characteristics of low-permeability Upper Cretaceous and lower Tertiary rocks in the Pinedale anticline area, Sublette County, Wyoming: U.S. Geological Survey Open-File Report 84-753, p. 6-15.

Law, B.E., and Dickinson, W.W., 1985, Conceptual model for origin of abnormally pressured gas accumulations in low-permeability reservoirs: American Association of Petroleum Geologists Bulletin, v. 69, no. 8, p. 1295-1304.

Law, B.E., and Nichols, D.J., 1982, Subsurface stratigraphic correlations of some Upper Cretaceous and lower Tertiary rocks, northern Green River basin, Wyoming [abs.], in Steidtmann, J.R., ed., Subsurface practices in geology and geophysics: Laramie, Wyo., University of Wyoming,

CONCENTRATION OF GAS
(IN BILLIONS OF CUBIC FEET)
PER SQUARE MILE

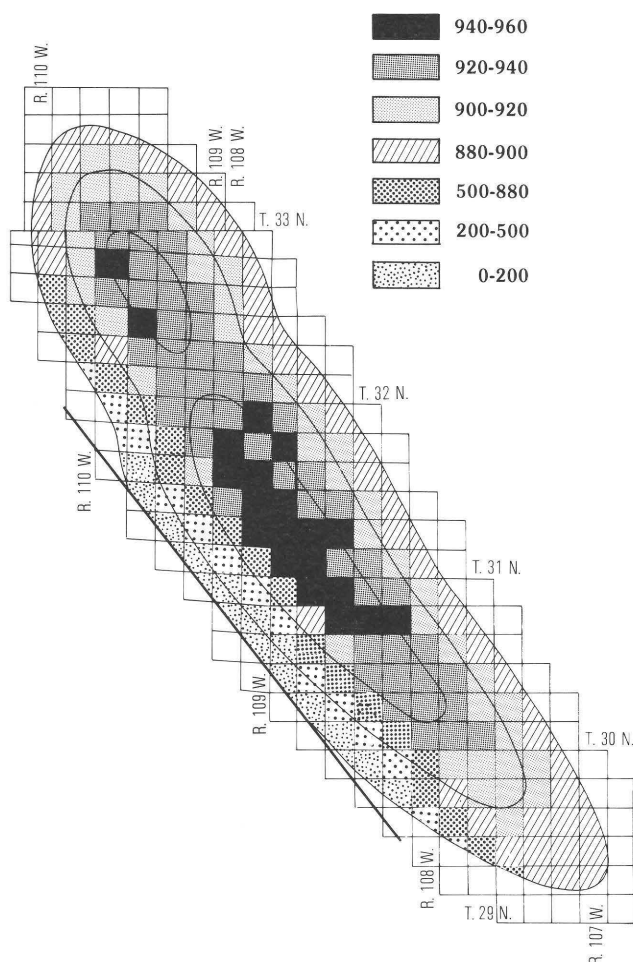


Figure 10. Concentration of natural gas in assessed part of Pinedale anticline.

Department of Geology and Geophysics, Earth Science Bulletin 15, p. 17.

- Law, B.E., Pollastro, R.M., and Keighin, C.W., 1986, Geologic characterization of low-permeability gas reservoirs in selected wells, Greater Green River Basin, Wyoming, Colorado, and Utah, in Spencer, C.W., and Mast, R.F., eds., *Geology of tight gas reservoirs*: American Association of Petroleum Geologists Studies in Geology 24, p. 253-270.
- Law, B.E., and Spencer, C.W., 1981, Abnormally high-pressured, low-permeability, Upper Cretaceous and Tertiary gas reservoirs, northern Green River basin, Wyoming [abs.]: *American Association of Petroleum Geologists Bulletin*, v. 65, no. 5, p. 948.
- Law, B.E., Spencer, C.W., and Bostick, N.H., 1979, Preliminary results of organic maturation, temperature, and pressure studies in the Pacific Creek area, Sublette County, Wyoming: U.S. Department of Energy Symposium on Enhanced Oil and Gas Recovery and Improved Drilling Methods, 5th, Tulsa, Okla., 1979, p. K2/1-K2/13.

Table 2. Estimate of in-place overpressured natural gas resources of the Pinedale anticline area

Stratigraphic unit	Amount of gas (trillion cubic feet)
Lance Formation	62
Ericson Formation	23
Rock Springs Formation	75
Entire structure	159

- _____, 1980, Evaluation of organic matter, subsurface temperature, and pressure with respect to gas generation in low-permeability Upper Cretaceous and lower Tertiary sandstones in Pacific Creek area, Sublette and Sweetwater Counties, Wyoming: *The Mountain Geologist*, v. 17, no. 2, p. 23-35.
- Martin, W.B., and Shaughnessy, J., 1969, Project Wagon Wheel, in *Symposium on Tertiary rocks of Wyoming: Wyoming Geological Field Conference, 21st, Casper, Wyo., 1969, Guidebook*, p. 145-152.
- Masters, J.A., 1979, Deep basin gas trap, western Canada: *American Association of Petroleum Geologists Bulletin*, v. 63, no. 2, p. 152-181.
- Meissner, F.F., 1978, Patterns of source-rock maturity in non-marine source rocks of some typical Western Interior basins: *Rocky Mountain Association of Geologists Continuing Education Lecture Series*, chapter IX, p. 1-37.
- _____, 1980, Examples of abnormal fluid pressure produced by hydrocarbon generation [abs.]: *American Association of Petroleum Geologists Bulletin*, v. 64, no. 5, p. 749.
- _____, 1981, Abnormal pressures produced by hydrocarbon generation and maturation and their relation to processes of migration and accumulation [abs.]: *American Association of Petroleum Geologists Bulletin*, v. 65, no. 11, p. 2467.
- Naeser, N.D., 1984, Fission-track ages from the Wagon Wheel No. 1 well, northern Green River basin, Wyoming; evidence for recent cooling, in Law, B.E., ed., *Geological characteristics of low-permeability Upper Cretaceous and lower Tertiary Rocks in the Pinedale anticline area, Sublette County, Wyoming*: U.S. Geological Survey Open-File Report 84-753, p. 66-77.
- _____, 1986, Neogene thermal history of the northern Green River basin, Wyoming; evidence from fission-track dating, in Gautier, D.L., ed., *Roles of organic matter in sediment diagenesis*: Society of Economic Paleontologists and Mineralogists Special Publication 38, p. 65-72.
- Pollastro, R.M., and Barker, C.E., 1984, Geothermometry from clay minerals, vitrinite reflectance, and fluid inclusions; applications to the thermal and burial history of rocks cored from the Wagon Wheel no. 1 well, Green River basin, Wyoming, in Law, B.E., ed., *Geological characteristics of low-permeability Upper Cretaceous and lower Tertiary rocks in the Pinedale anticline area, Sublette County, Wyoming*: U.S. Geological Survey Open-File Report 84-753, p. 78-94.

- _____ 1986, Application of clay-mineral, vitrinite reflectance, and fluid inclusion studies to the thermal and burial history of the Pinedale anticline, Green River basin, Wyoming, *in* Gautier, D.L., ed., Roles of organic matter in sediment diagenesis: Society of Economic Paleontologists and Mineralogists Special Publication 38, p. 73-83.
- Prensky, S.E., 1986, Geologic implications of large-scale trends in well-log response, northern Green River basin, Wyoming: SPWLA Annual Logging Symposium, 27th, Paper EEE, p. 1-24.
- Prensky, S.E., and Dickinson, W.E., 1986, Computer-generated well-log data plots assist in regional subsurface evaluation: *Geobyte*, v. 1, no. 2, p. 52-58.
- Rathbun, F.C., 1968, Abnormal pressures and conductivity anomaly, northern Green River basin, Wyoming: Society of Petroleum Engineers, Annual Fall Meeting, 43rd, SPE Paper 2205, p. 1-8.
- Rathbun, F.C., and Dickey, P., 1969, Abnormal pressures and conductivity anomaly, northern Green River basin, Wyoming: *The Log Analyst*, v. 10, no. 4, p. 3-8.
- Shaughnessy, J., and Butcher, R.H., 1973, Geology of Project Wagon Wheel Nuclear Stimulation Project, *in* Fassett, J.E., ed., Cretaceous and Tertiary rocks of the southern Colorado Plateau: Durango, Colo., Four Corners Geological Society, p. 185-196.
- _____ 1974, Geology of Wagon Wheel Nuclear Stimulation Project, Pinedale field, Wyoming: American Association of Petroleum Geologists Bulletin, v. 58, no. 11, p. 2250-2259.
- Spencer, C.W., 1983, Geologic aspects of tight gas reservoirs in the Rocky Mountain region: Society of Petroleum Geologists/U.S. Department of Energy Joint Symposium on Low-Permeability Gas Reservoirs, Denver, Colo., 1983, Proceedings, p. 399-408.
- _____ 1984, Overpressured tight gas reservoirs in the Pinedale anticline area, Sublette County, Wyoming, *in* Law, B.E., ed., Geological characteristics of low-permeability Upper Cretaceous and lower Tertiary Rocks in the Pinedale anticline area, Sublette County, Wyoming: U.S. Geological Survey Open-File Report 84-753, p. 51-59.
- _____ 1987, Hydrocarbon generation as a mechanism for overpressuring in rocky Mountain region: American Association of Petroleum Geologists Bulletin, v. 71, no. 4, p. 368-388.
- Spencer, C.W., and Law, B.E., 1981, Overpressured, low-permeability gas reservoirs in Green River, Washakie, and Great Divide basins, southwestern Wyo. [abs.]: American Association of Petroleum Geologists Bulletin, v. 65, no. 3, p. 569.

Chapter J

Petrology and Isotope Geochemistry of Mineralized Fractures in Cretaceous Rocks— Evidence for Cementation in a Closed Hydrologic System

By JANET K. PITMAN and WARREN W. DICKINSON

Prepared in cooperation with the U.S. Department of Energy

U.S. GEOLOGICAL SURVEY BULLETIN 1886

GEOLOGY OF TIGHT GAS RESERVOIRS IN THE PINEDALE ANTICLINE AREA, WYOMING,
AND AT THE MULTIWELL EXPERIMENT SITE, COLORADO

CONTENTS

Abstract	J1
Introduction	J1
Origin and distribution of fractures	J4
Fracture mineralization	J5
Carbon and oxygen isotopes	J8
Carbon	J8
Oxygen	J10
Discussion	J11
Temperature	J11
Pore water $\delta^{18}\text{O}$	J11
Water/rock ratio	J12
Pore water $\delta^{13}\text{C}$	J13
Summary and conclusions	J13
References cited	J14

FIGURES

1. Photographs showing mode of natural fractures in sandstone and shale, MWX wells **J2**
2. Photomicrographs illustrating paragenetic relationships of fracture-fill minerals in study wells **J6**
3. Scatter diagram of $\delta^{13}\text{C}$ versus $\delta^{18}\text{O}$ for fracture-fill calcite **J9**
4. Crossplots of isotopic composition and depth **J9**
- 5-6. Graphs showing:
 5. Variation in oxygen isotope composition of water in equilibrium with calcite of fixed isotopic composition, 120-300 °F **J12**
 6. Calculated $\delta^{18}\text{O}$ and $\delta^{13}\text{C}$ compositions for calcite as a function of water/rock ratio in closed system at 120 °F (50 °C) **J13**

TABLE

1. Isotopic compositions and estimated temperatures for fracture-fill calcite, Piceance basin, Colorado, and northern Green River basin, Wyoming **J10**

Petrology and Isotope Geochemistry of Mineralized Fractures in Cretaceous Rocks— Evidence for Cementation in a Closed Hydrologic System

By Janet K. Pitman and Warren W. Dickinson¹

Abstract

Well-developed, partly mineralized, vertical extension fractures containing abundant calcite and minor quartz, dickite, barite, and bitumen commonly occur in overpressured gas-bearing sandstones of Cretaceous age in the Green River basin of Wyoming and the Piceance basin of Colorado. Methane inclusions in calcite (C.E. Barker, U.S. Geological Survey, 1987, oral commun.) and the occurrences of bitumen indicate that fracture cementation took place during hydrocarbon generation. Periods of tectonism and sediment loading also contributed to fracture development. Stable-isotope studies of fracture calcite from three wells show a narrow range in carbon and oxygen compositions (average $\delta^{13}\text{C}$, -2.98 per mil PDB; average $\delta^{18}\text{O}$, 15.07 per mil SMOW) over a thick stratigraphic interval (5,000–18,000 ft; 1,500–5,500 m). Typically, $\delta^{13}\text{C}$ and $\delta^{18}\text{O}$ compositions display a slight enrichment trend with increased burial depth and temperature and, at any given depth, approximate the $\delta^{13}\text{C}$ and $\delta^{18}\text{O}$ compositions of matrix carbonate in the enclosing sandstones. The isotopic trends, together with a knowledge of the burial and pressure history of the rocks, indicate that fracture carbonate inherited its isotopic composition from matrix carbonate through a process of dissolution and reprecipitation in a closed hydrologic system dominated by low water/rock ratios. The primary source of carbon in fracture calcite was from dissolved detrital marine carbonate grains that are ubiquitous in adjacent rocks. Increased $\delta^{18}\text{O}$ compositions with depth suggest that, at greater burial depths and temperatures, fracture calcite crystallized from $\delta^{18}\text{O}$ -enriched pore waters. On the basis of estimated formation temperatures, the calculated composition of formation waters in isotopic equilibrium with fracture calcite varies from -8 to $+2$ per mil SMOW, values consistent with calcite crystallization in a rock-buffered diagenetic system.

INTRODUCTION

Thermogenic gas in the Piceance basin of Colorado and the Green River basin of Wyoming is widespread in Upper Cretaceous rocks. Most of the gas-bearing rocks

are nonmarine and consist of lenticular, low-permeability sandstone interbedded with siltstone, kerogenous mudstone, and discontinuous beds of coal. The economic production of gas from these rocks depends either on the presence of artificially induced (hydraulic) fractures or on a network of open, interconnected natural fractures to increase effective permeability. Because artificial fracture enhancement is generally not cost effective, the exploitation of natural fractures may provide a possible alternative for economic gas recovery.

This paper describes mineralized fractures from widely spaced wells in the Green River and Piceance basins and characterizes the hydrologic and thermal regime that existed during fracture development and mineralization. Cores from the El Paso Natural Gas Company Wagon Wheel No. 1 well and the Belco Petroleum WASP No. 1-A well (Law, 1984) in the Green River basin show numerous mineralized fractures in the Upper Cretaceous Lance Formation, Ericson Sandstone, and Rock Springs Formation. Abundant open and partly mineralized fractures are also present in core from the Mesaverde Formation (Upper Cretaceous) in the two wells from the U.S. Department of Energy's Multiwell Experiment (MWX) in the Piceance basin (Law and Spencer, this volume, fig. 1).

High pore-fluid pressures, which formed during the maturation of hydrocarbons, together with tectonism and sediment loading, may have generated stresses that initiated the formation of fractures. Knowledge of the factors controlling the opening, orientation, and mineralization of fractures is necessary before fractures can be successfully exploited for gas recovery. Mineralized fractures provide evidence of the chemical and thermal conditions that govern fracture cementation. In this study, petrographic and stable isotope techniques were used to identify the occurrence and distribution of discrete generations of fracture-fill minerals and to postulate the geochemical conditions that existed during fracture mineralization. The degree of rock-water interaction during fracture mineralization and the relative timing of fracture cementation also were evaluated.

¹Research School of Earth Science, Victoria University
P.O. Box 600, Wellington, New Zealand

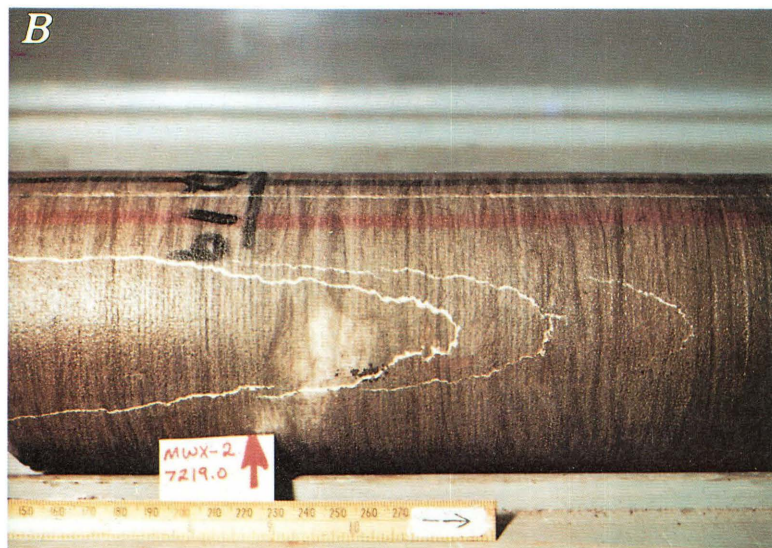
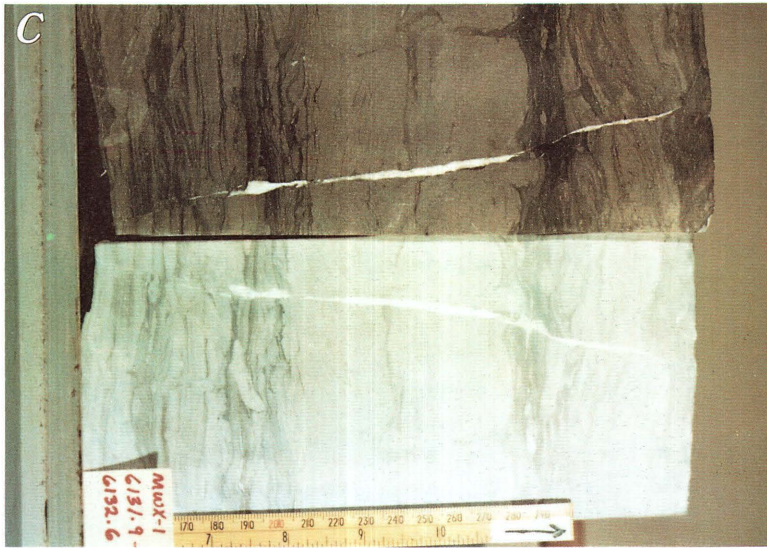


Figure 1 (above and facing page). Mode of natural fractures in sandstone and shale, MWX wells. Scale in inches and millimeters. *A*, Open fracture in sandstone perpendicular to bedding; parallel vertical fracture displays calcite along fracture face. *B*, Multiple en echelon vertical fractures in sandstone filled with calcite cement. *C*, Calcite-filled fracture in sandstone becomes closed and nonmineralized at shale interbeds. *D*, Fracture face in sandstone coated with tiny euhedral crystals of calcite. *E*, Fracture in shale displaying a polished slickensided surface.



Results from this study suggest that the precipitation of fracture-fill carbonate was controlled by the dissolution and reprecipitation of matrix carbonate in a closed diagenetic environment characterized by low water/rock ratios. The fluids that precipitated fracture carbonate do not appear to have been in equilibrium with matrix carbonate. Results from this study may be applicable to fractured rocks that formed in similar depositional and diagenetic settings in other geographic areas.

Acknowledgments.—This study was funded by the U.S. Geological Survey Evolution of Sedimentary Basins Program and by the U.S. Department of Energy Morgantown Energy Technology Center. Carbon and oxygen isotope analyses were determined by the U.S. Geological Survey, Branch of Isotope Geology, and by Coastal Sciences Laboratory through Mobil Oil Company.

ORIGIN AND DISTRIBUTION OF FRACTURES

With few exceptions, the occurrence and distribution of fractures are similar in Upper Cretaceous rocks in the study wells. Fractures may be either open (non-mineralized) or partly to completely cemented with calcite, dickite, quartz, or barite. In general, open non-mineralized fractures are rare in core from the Wagon Wheel and WASP wells and are locally abundant in the MWX wells (fig. 1A). It is uncertain why some fractures are open and others are mineralized; however, the open fractures may be younger than the mineralized fractures and simply not have had sufficient time to become filled with cement. Verbeek and Grout (1984a) have shown that the oldest fractures in Tertiary rocks in the Piceance basin commonly contain more discrete generations of calcite than do the youngest fractures. No evidence exists for carbonate dissolution in partly cemented fractures in Cretaceous sandstones, and thus it is likely that the fractures are in the initial process of cement filling rather than cement removal.

In sandstone and siltstone, fractures typically are single or multiple, subvertical extension features that extend across several beds and usually terminate at a change in lithology (figs. 1B, C). The fractures commonly are cemented by fine- to coarse-crystalline calcite (fig. 1D). Permeability is locally enhanced in these otherwise low-permeability rocks wherever fractures are open as a result of incomplete development of carbonate cement. Fractures in shale are rare in the WASP and Wagon Wheel wells but numerous and mostly nonmineralized and closed in the MWX wells. The low angle to bedding of most fractures in shale suggest that the fractures may have formed during compaction and dewatering of mud shortly after deposition within a few feet of the surface (Verbeek and Grout, 1984a). The polished and

slickensided surfaces of some fractures (fig. 1E) suggest that the fractures originated in shear.

Fractures in Cretaceous rocks may have resulted from stresses associated with tectonism and sediment loading in conjunction with high pore-fluid stresses generated during burial diagenesis. Secor (1965) has demonstrated that high fluid pressures resulting from progressive loading of low-permeability sediments can play a significant role in the initiation and propagation of fractures at depth. Many Upper Cretaceous rocks in the Piceance and Green River basins contain beds of low-permeability shale that enclose and, hence, effectively isolate more permeable sandstone lenses. During burial and compaction, these shale beds may have functioned as barriers to fluid movement between lenticular sandstones and thereby caused high pore-fluid pressures to develop internally (Pitman and Sprunt, 1984).

Law and others (1980), Law (1984), Law and Dickinson (1985), and McPeck (1981) have attributed abnormally high pore pressures in the Green River basin to the thermal generation of gas from coals and kerogenous mudstone. Law and others (1980) found that generation of significant thermogenic gas begins at temperatures of about 190–200 °F (88–93 °C), which correspond to a mean vitrinite reflectance (R_m) of about 0.80 percent. Overpressuring develops when gas is produced from local source rocks at a rate that exceeds the rate at which it can escape. Stresses associated with overpressuring may create new fractures or possibly reopen preexisting fractures that developed during burial and compaction. Under high pore-fluid pressures, fracturing by tectonism and sediment loading requires less effective stress than does fracturing under normal (hydrostatic) pressures.

In each well, fractures occur in rocks that are now overpressured or were overpressured in the past. Fractures in the MWX wells are present from a depth of about 4,000 ft (1,219 m) to the bottom of the hole at about 8,000 ft (2,438 m); however, no cores were shallower than 4,000 ft (1,219 m). Although the top of overpressuring is at a depth of about 5,600 ft (1,707 m), an R_m of 0.80 percent occurs at about 4,000 ft (1,219 m). Studies by Bostick and Freeman (1984) show that in the area of the MWX wells approximately 5,000 ft (1,520 m) of strata was eroded during late Tertiary development of the Colorado River drainage system. During this erosional event, temperatures and the rate of gas generation decreased, which allowed high pore pressures to dissipate to a normal pressure regime. As the overlying sediments were eroded, the top of the overpressured zone was lowered from 4,000 to 5,600 ft (1,219–1,707 m).

Although the MWX wells are in a structurally undeformed area, some extension fractures in Upper Cretaceous rocks may have formed as a result of stresses that developed during periods of epeirogenic uplift and

erosion. Studies by Verbeek and Grout (1984b) indicate that regional fracture orientation patterns on the Grand Hogback along the eastern margin of the Piceance basin are very similar to those in MWX core. In addition, Laramide tectonism caused widespread differential erosion of sediment that is reflected in a regional unconformity separating Cretaceous and Tertiary strata throughout much of the basin. Fractures in these Cretaceous rocks may record stresses that occurred during the early stages of Laramide tectonism or during later periods of tectonic activity associated with the development of the White River plateau and the Grand Hogback monocline, which border the eastern margin of the basin.

In the Wagon Wheel well, situated on the Pinedale anticline in the Green River basin, the top of overpressuring (0.74 percent Rm) was lowered from 8,030 to 10,400 ft (2,450–3,170 m) because of a decrease in temperature (Law, 1984). Fractures were observed in all of the cored intervals below the top of overpressuring (8,030 ft, 2,450 m), but none were found in the 200 ft (61 m) of core above this depth. An increase in the number or frequency of fractures with increasing depth below the top of the overpressuring may be the result of different lithologies or of faults at depth. Many fractures in the Wagon Wheel well formed, at least in part, from stresses caused by tectonism. The highest concentration of fractures is between 16,000 and 18,000 ft (4,877–5,486 m). Seismic data (Martin and Shaughnessy, 1969) and steeply dipping beds in core indicate that these fractures are associated with a fault and thus are of probable tectonic origin.

In the WASP well, the top of overpressuring is at about 10,600 ft (3,200 m) (Law, 1984). Fractures were not observed in the 100 ft (30 m) of core above the top of overpressuring but are common in cored intervals (11,329–14,900 ft, 3,453–4,542 m) within the overpressured zone. Because there is no evidence for widespread uplift and erosion in the area of this well during the late Tertiary, the top of overpressuring is presumed to have remained relatively constant since maximum burial.

FRACTURE MINERALIZATION

Fractures in the Upper Cretaceous rocks are partly to completely cemented by a mineral assemblage that is common to all wells and consists of quartz, dickite, calcite, and barite. Fine- to coarse-crystalline calcite is most abundant, dickite occurs in moderate amounts, and quartz and barite are present in minor amounts. Two minerals commonly coexist in a single fracture, but rarely are all found together. In addition to these minerals, a bituminous residue coats many crystals in fractures in the Wagon Wheel and WASP wells. Textural relations

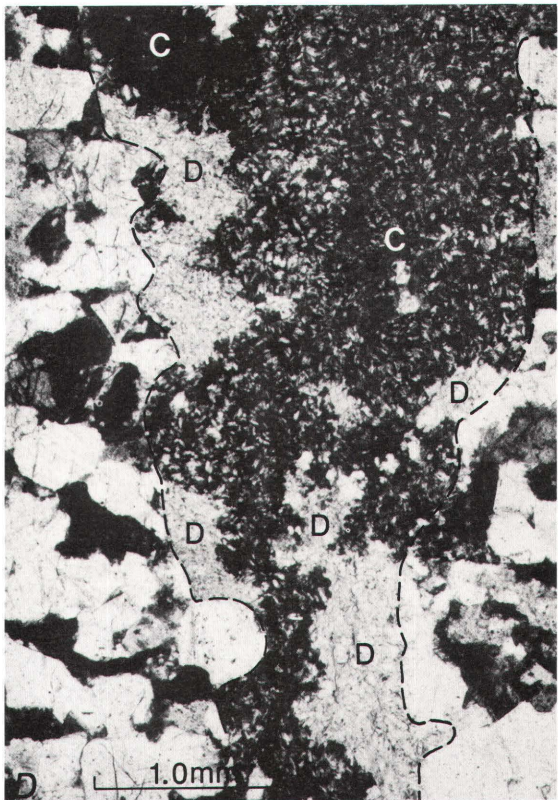
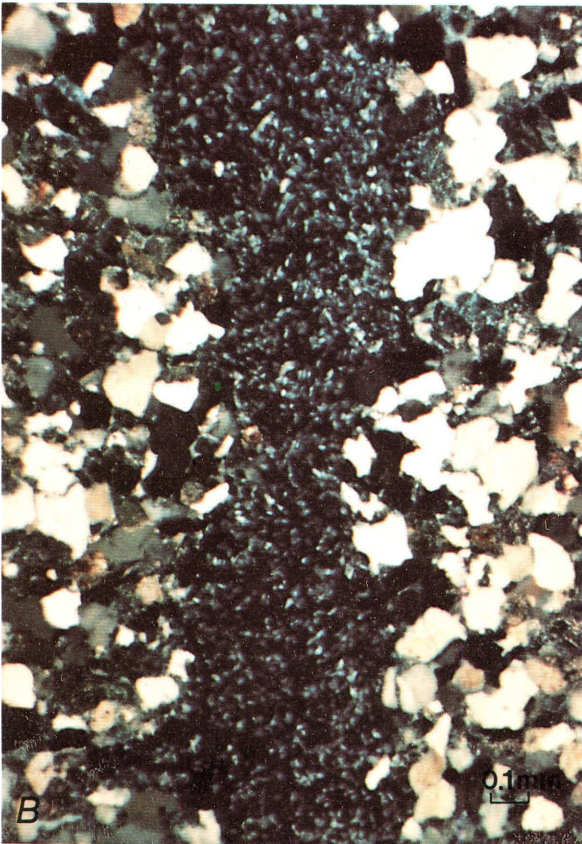
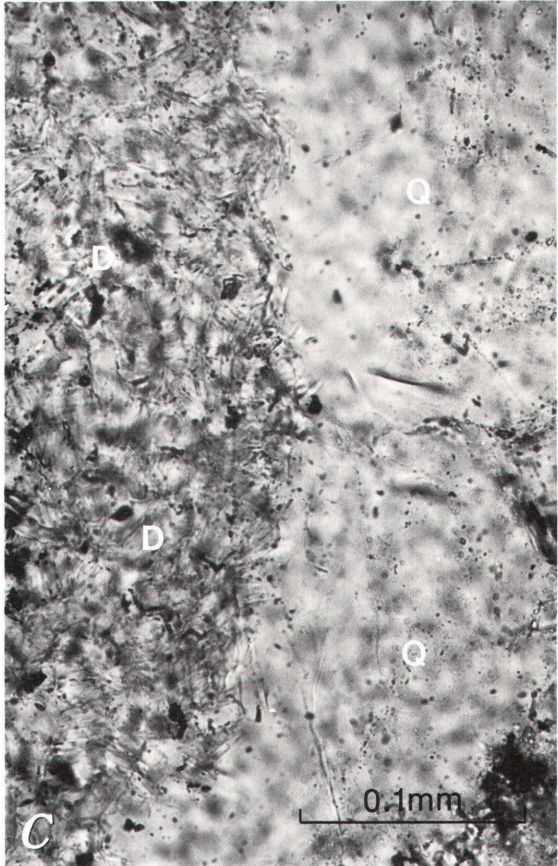
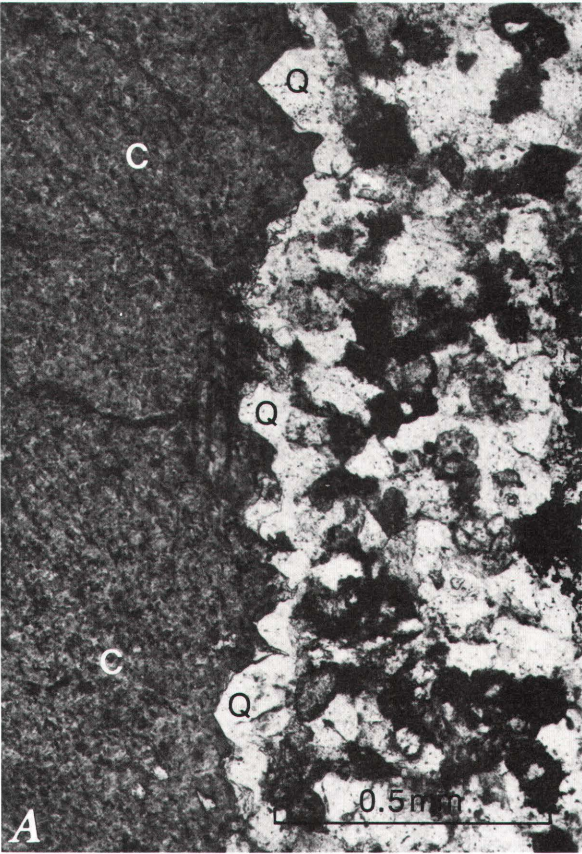
between these discrete mineral phases are shown in figure 2.

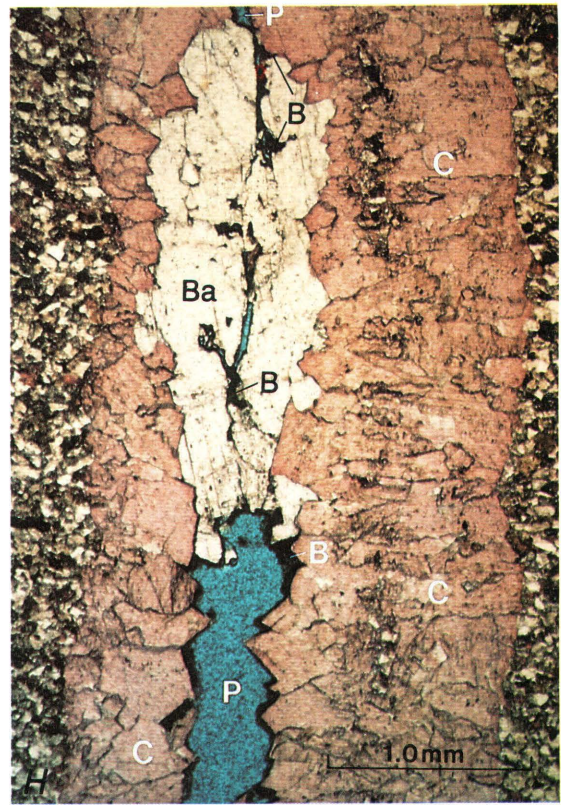
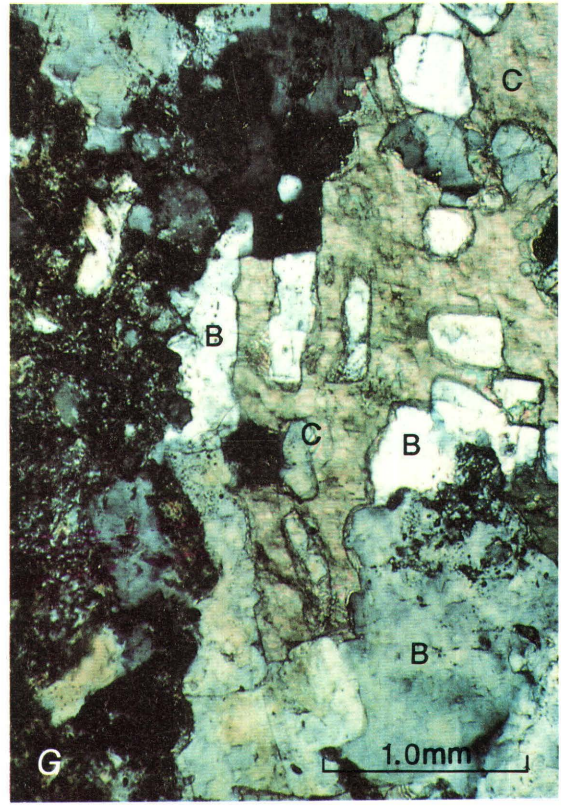
The distribution of fracture-fill minerals, particularly calcite and dickite, appears to be controlled by the mineralogic composition of the surrounding rock. Calcite-filled fractures are abundant in sandstone containing authigenic matrix calcite and detrital limestone grains but rare or absent in rocks devoid of these minerals. Dickite occurs locally in fractures for which there is evidence for pore-fill and replacement kaolinite in the surrounding sandstone. In Wagon Wheel core, fractures in the Ericson Sandstone, a quartzarenite, are filled only with dickite, probably because there are no carbonate minerals in the surrounding rocks. No apparent correlation exists between the fracture-fill minerals quartz and barite and the matrix composition of the enclosing sandstone.

The paragenetic sequence of minerals in fractures is similar among the wells. Quartz, the earliest mineral to precipitate, commonly occurs as euhedral crystals lining the walls of fractures that are subsequently infilled by either dickite or calcite (fig. 2A). The presence of euhedral, syntaxial quartz overgrowths attached to detrital grain surfaces suggests that some fractures were open and permeable to fluids before the onset of carbonate precipitation. In one fracture from the Wagon Wheel well, large euhedral quartz crystals surrounded by calcite suggest that quartz was the last mineral phase to precipitate.

Dickite is morphologically identical to kaolinite and has been identified by X-ray diffraction in several fractures from the Wagon Wheel and MWX wells (R.M. Pollastro, 1986, oral commun.). We assume that in many fractures the kaolin mineral, which has not been X-rayed, also is dickite. Macroscopic dickite occurs as a well-crystallized, soft, white mineral along fracture faces (fig. 2B). In thin section, it forms discrete pseudo-hexagonal platelets that commonly surround crystals of quartz. Both quartz and dickite typically are well crystallized, and textural relations between the two minerals suggest that they

Figure 2 (next two pages). Photomicrographs illustrating paragenetic relationships of fracture-fill minerals in the study wells. *A*, Equant crystals of quartz (Q) lining fracture walls; proximal part of fracture is filled with calcite (C). *B*, Well-crystallized dickite filling fracture. *C*, Fracture containing intergrown quartz (Q) and dickite (D). *D*, Calcite (C) replacing early-formed dickite (D) within fracture; dashed lines indicate fracture walls. *E*, Fracture-fill calcite composed of elongate crystals having planar and curved intercrystalline boundaries. *F*, Fracture filled with ferroan calcite (Fc) cutting feldspar grain (F); note occurrence of iron-free matrix calcite (C). *G*, Fracture-fill calcite cement (C) replaced by multiple generations of barite (B). *H*, Early calcite (C) along fracture walls and late-stage barite (Ba) filling central part of fracture; voids (P) are lined with bitumen (B).





may have formed simultaneously during a single diagenetic event rather than by replacement. Moreover, quartz shows no evidence of corrosion by dickite (fig. 2C). In fractures from the MWX wells, dickite clearly has been replaced by calcite, whereas in the WASP and Wagon Wheel wells calcite and dickite interpenetrate one another (fig. 2D). Although paragenetic relations between calcite and dickite are somewhat obscure, it seems most likely that crystallization of dickite postdates development of quartz but predates precipitation of calcite. It is possible that reaction of kaolinite in nearby sandstones with high-temperature pore fluids resulted in recrystallization of kaolinite to dickite in fractures; however, the reported coexistence of nacrite, dickite, and kaolinite in ore hydrothermal deposits (Hanson and others, 1981) indicates that no unique environmental indicators can be used to predict the conditions governing the precipitation of these minerals. The crystallization of dickite may be controlled by trace amounts of heavy metals such as mercury, lead, zinc, and copper (Hanson and others, 1981).

Fine- to coarse-crystalline calcite fills most fractures and is composed of discrete, tabular or equant crystals that coalesce to form a cement. In some fractures, calcite crystallization apparently occurred during a single episode, inasmuch as individual crystals of calcite extend from one fracture wall to the other and their long axes are oriented perpendicular to the face of the fracture (fig. 2E). The intercrystalline boundaries commonly are either slightly curved or planar. In other fractures, aggregates of calcite crystals are intergrown and exhibit different optic orientations; in these fractures, more than one episode of calcite precipitation may have occurred in the same fracture. There is no evidence in any of the wells to suggest that fracture calcite has undergone extensive dissolution and recrystallization. The sharp, planar boundaries of voids within discrete calcite crystals indicate incomplete carbonate cementation rather than a period of dissolution.

Some features in calcite from the MWX wells were not evident in calcite from the Wagon Wheel and WASP wells. Potassium ferricyanide staining indicates that calcite in fractures from MWX locally is enriched in iron (fig. 2F); thus, the chemical composition of pore fluids that precipitated calcite probably changed through time. In addition, crystals of calcite may exhibit multiple sets of twin lamellae reflecting stress gradients possibly caused by an increase in overburden pressure resulting from either progressive burial or periods of local tectonism.

Barite in fractures is recognized by its moderate relief, blocky cleavage, and low birefringence. In the MWX wells, barite occurs locally as patches replacing calcite and dickite; individual barite crystals commonly display a sharp contact with these minerals (fig. 2G). In the Wagon Wheel well, barite typically occupies the central part of a fracture (fig. 2H). Although paragenetic

relations between barite and the other minerals are unclear, barite probably was the last mineral to precipitate in the fractures.

Bitumen coats crystals of quartz, dickite, calcite, and barite in many fractures in the Wagon Wheel and WASP wells. Characteristically, it lines these crystals and was deposited parallel with the fracture walls (fig. 2H); local cementation probably was episodic, at least during the formation of the bitumen. Numerous inclusions of methane were also detected in calcite (C.E. Barker, 1985, oral commun.) and indicate that interbedded humic-rich source rocks were generating thermogenic gas during the time calcite was infilling fractures.

CARBON AND OXYGEN ISOTOPES

Representative samples of calcite in fractures from the study wells were analyzed for their carbon and oxygen isotope compositions in order to determine the conditions governing fracture mineralization. The calcite was scraped and drilled from the fractures and reacted with anhydrous phosphoric acid to produce carbon dioxide gas for analysis (McCrea, 1950). The results, summarized in table 1, are reported in per mil relative to the PDB standard for carbon and the SMOW standard for oxygen. For comparison between wells, $\delta^{13}\text{C}$ and $\delta^{18}\text{O}$ compositions are shown in a scatter diagram (fig. 3) and are plotted against depth (fig. 4). Calcite from fractures in all three wells shows little isotopic variation; the average carbon composition is -2.98 per mil, and the average oxygen composition is 15.07 per mil. The isotopic variation that does occur in fracture calcite may reflect the wide range in burial depth and temperature of formation in the different wells.

In natural systems, the carbon and oxygen in calcite originate from different sources and are fractionated by different processes. Predominantly, equilibrium processes fractionate oxygen, whereas kinetic processes fractionate carbon. Although both $\delta^{13}\text{C}$ and $\delta^{18}\text{O}$ compositions of fracture calcite become slightly enriched with increasing burial depth (fig. 4), the factors that influence each trend are different.

Carbon

Carbon isotopic ratios in pore waters are a function of pH, CO_2 partial pressure, and the dominant source of carbon in the reservoir. In turn, the $\delta^{13}\text{C}$ composition of the pore water and, to a lesser extent, the temperature at the time of crystallization control the isotopic composition of carbon in calcite. Isotopically light carbon derived from organic matter (<-20 per mil) and isotopically heavy carbon derived from limestones

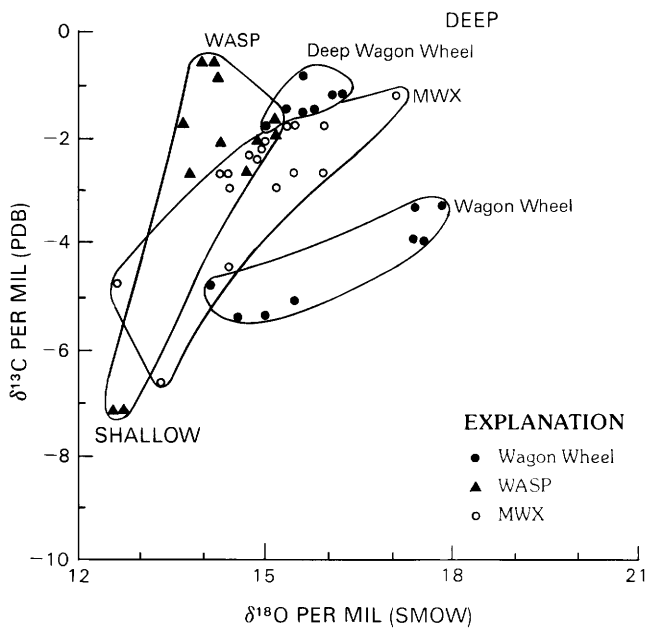


Figure 3. Scatter diagram of $\delta^{13}\text{C}$ versus $\delta^{18}\text{O}$ for fracture-fill calcite.

and dolomites (about zero per mil) as well as from various inorganic minerals can be distinguished by the $\delta^{13}\text{C}$ composition of calcite. The isotopic composition of sedimentary carbonate minerals commonly reflects a mixing or dominance of carbon from these sources. With the exception of the samples denoted by asterisks in table 1, most $\delta^{13}\text{C}$ compositions for fracture calcite are within the range reported for freshwater and marine limestones (+2.0 to -6.6 per mil PDB; Keith and Weber, 1964), suggesting that the carbon in the diagenetic fluids precipitating fracture calcite originated primarily from these sources.

The $\delta^{13}\text{C}$ composition of fracture calcite generally becomes more positive with increasing depth of burial (table 1, fig. 4A). This shift may be interpreted as resulting from a similar shift in $\delta^{13}\text{C}$ composition of the formation waters. In the northern Green River basin, the average $\delta^{13}\text{C}$ composition for inorganic carbon in shallow aquifers (mean depth 164 ft, 50 m) is -8.6 per mil (B.A. Kimball, U.S. Geological Survey, 1984, written commun.). As burial depth increases, the relative concentration of ^{13}C in formation waters moving down a flow path may increase if there is a progressive addition of ^{13}C from the dissolution of detrital carbonate grains and (or) if there is a decrease in the volume of near-surface water (usually depleted in ^{13}C) penetrating the deeper sandstones. Calcite depleted in ^{13}C also may reflect sandstone cement that contains a component of soil CO_2 that formed during meteoric diagenesis associated with the development of an erosion surface (Pitman and Sprunt, 1987). Allan and Matthews (1982)

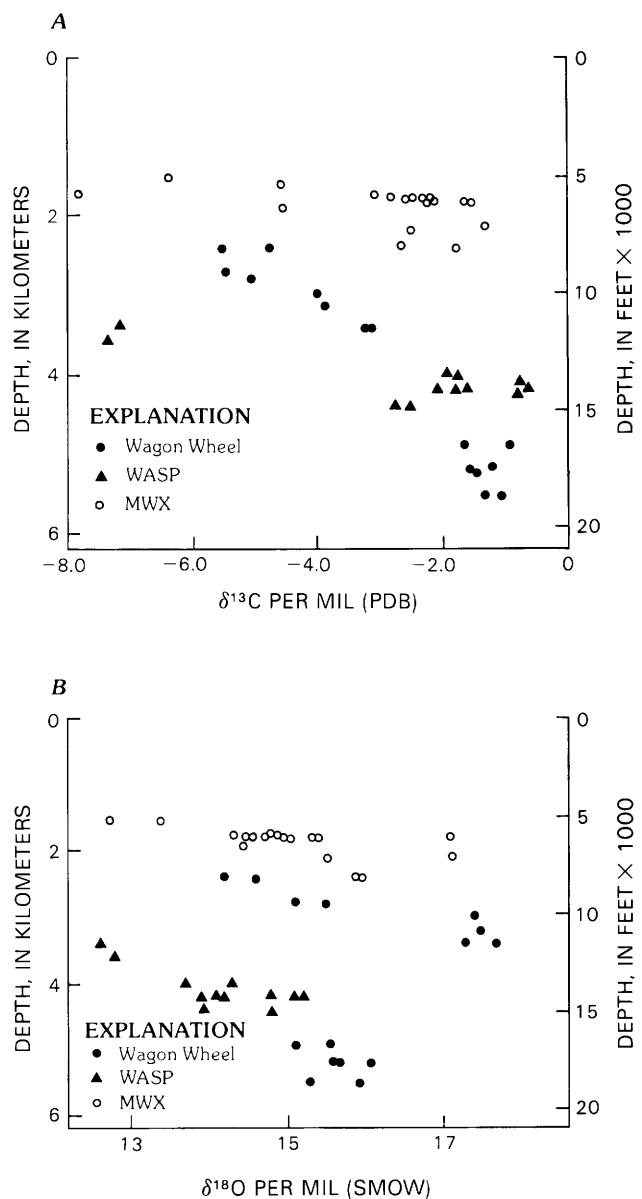


Figure 4. Crossplots of isotopic composition and depth. A, $\delta^{13}\text{C}$. B, $\delta^{18}\text{O}$.

have documented that as much as 4 to 6 per mil carbon depletion can occur in rocks near an exposure surface.

In each well, the $\delta^{13}\text{C}$ composition of fracture calcite at any given depth approximates the $\delta^{13}\text{C}$ composition of calcite cement in the host sandstone (J.K. Pitman, 1984, unpub. data; Dickinson, 1985). The general correlation in $\delta^{13}\text{C}$ composition between fracture and matrix calcite strongly suggests that the dominant source of carbon in fracture calcite was sandstone cement, and the slight shift in fracture calcite to lighter values indicates that the carbon reservoir underwent some modification during burial. Emrich and others (1970) have demonstrated that the carbon-isotope equilibrium between

Table 1. Isotopic compositions and estimated temperatures for fracture-fill calcite in three wells, Piceance basin, Colorado, and northern Green River basin, Wyoming

[Asterisk (*) indicates value more negative than average range for freshwater and marine limestones. Paleotemperatures estimated from Lopatin burial history models. Location of wells shown in Law and Spencer (this volume, figs. 2, 3)]

Depth (feet)	Depth (meters)	Temperature (°F)		$\delta^{13}\text{C}$	$\delta^{18}\text{O}$	Depth (feet)	Depth (meters)	Temperature (°F)		$\delta^{13}\text{C}$	$\delta^{18}\text{O}$
		Past	Present	(per mil)	(per mil)			Past	Present	(per mil)	(per mil)
MWX wells, Piceance basin											
5,018.0	1,534.0	243	153	-6.58	13.33	6,076.0	1,857.0	266	176	-1.72	15.29
5,475.3	1,674.0	253	163	-4.71	12.60	6,076.0	1,857.0	266	176	-1.72	15.29
5,731.0	1,752.0	259	169	-3.09	15.08	6,076.5	1,865.0	266	176	-1.72	15.39
5,734.0	1,753.0	259	169	-2.90	14.46	6,131.6	1,874.0	266	176	-2.29	14.77
5,744.6	1,756.0	259	169	-2.62	14.25	6,312.0	1,929.0	270	180	-4.57	14.36
5,780.7	1,766.0	259	169	-2.55	14.46	7,181.4	2,194.0	298	208	-1.27	17.14
5,792.9	1,771.0	259	169	-10.38	17.14	7,219.0	2,206.0	300	210	-2.59	15.49
5,828.7	1,782.0	261	171	-2.36	14.67	8,114.2	2,479.0	334	244	-2.69	15.90
5,867.0	1,793.0	261	171	-2.18	14.87	8,124.5	2,482.0	334	244	-1.83	15.90
5,868.0	1,793.0	261	171	-2.17	14.98						
Wagon Wheel well, northern Green River basin											
8,096.1	2,467.7	198	153	-5.50	14.53	16,120.7	4,913.6	297	252	-0.92	15.65
8,128.0	2,477.4	198	153	-4.85	14.16	16,119.1	4,913.1	297	252	-1.67	15.06
8,944.2	2,726.2	208	163	-5.05	15.50	17,169.0	5,233.1	309	264	-1.26	16.16
8,959.0	2,730.7	208	163	-5.49	15.06	17,176.2	5,235.3	309	264	-1.43	15.65
10,154.9	3,095.2	223	178	-4.04	17.44	17,178.5	5,236.0	309	264	-1.48	15.71
10,234.9	3,119.6	225	180	-3.96	17.57	17,960.0	5,474.2	318	273	-1.37	15.27
10,993.1	3,350.7	234	189	-3.19	17.38	17,965.9	5,476.0	318	273	-1.12	15.99
11,000.0	3,352.8	234	189	-3.33	17.80						
WASP well, northern Green River basin											
11,333.0	3,454.3	225	225	-7.14*	12.53	13,611.9	4,148.9	261	261	-0.68	14.05
11,591.9	3,533.2	230	230	-7.34*	12.68	13,986.9	4,263.2	269	269	-0.82	14.20
13,025.9	3,970.3	252	252	-1.79	13.62	14,032.2	4,277.0	269	269	-2.15	14.82
13,433.1	4,094.4	259	259	-1.97	14.25	14,043.0	4,280.3	269	269	-1.77	15.19
13,482.0	4,109.3	259	259	-1.69	15.09	14,192.9	4,326.0	270	270	-2.63	14.73
13,590.9	4,142.5	261	261	-0.75	13.87	14,198.2	4,327.6	270	270	-2.69	13.82

calcite and dissolved bicarbonate in pore fluids is temperature dependent. Although temperature may have been an important factor governing the isotopic composition of carbon during the precipitation of fracture calcite, the crystallization of calcite in fractures at temperatures lower than those at which matrix carbonate precipitated is unlikely. More likely, the slight $\delta^{13}\text{C}$ depletion exhibited in fracture calcite reflects pore waters containing a component of isotopically light carbon associated with the generation of hydrocarbons rather than a significant temperature decrease. Inclusions of methane occurring locally in calcite and quartz (C.E. Barker, 1985, oral communication) are good evidence that interbedded source rocks attained high levels of thermal maturity (>0.76 per cent Rm) during fracture cementation.

Oxygen

$\delta^{18}\text{O}$ compositions for calcite from MWX and shallow Wagon Wheel fractures form a trend that is distinct from those for the WASP and deep Wagon Wheel

fractures (fig. 4B). Except for the deep fractures in the Wagon Wheel well, $\delta^{18}\text{O}$ compositions generally become enriched by 1 to 3 per mil as burial depth increases. Variations in $\delta^{18}\text{O}$ compositions of fracture calcite with depth may reflect changes in both the $\delta^{18}\text{O}$ composition of pore waters and the temperature of precipitation. The $\delta^{18}\text{O}$ composition of calcite as it undergoes recrystallization during burial will shift toward the $\delta^{18}\text{O}$ composition of the pore water in response to the decreasing isotopic fractionation that occurs between calcite and water as temperature increases.

The degree of openness of the rock-water system influences the control of mineral-water reactions on the isotope composition of pore water. In a closed system in which the water/rock ratio is low, mineral-water reactions can significantly modify the $\delta^{18}\text{O}$ composition of the pore waters. The remarkable similarity between the $\delta^{18}\text{O}$ isotope compositions of calcite in fractures and those of matrix calcite in sandstones (J.K. Pitman, unpub. data, 1984; Dickinson, 1985) and the apparent control by the mineralogic composition of the surrounding rock on the fracture mineralogy strongly suggest that,

similar to $\delta^{13}\text{C}$ compositions, local wall-rock materials were the dominant source of oxygen in fracture-fill calcite. Thus, it is probable that a large component of the oxygen in fracture calcite was inherited from matrix carbonate through a process of dissolution and reprecipitation in a closed, rock-dominated system. Detrital and authigenic clay minerals such as illite and chlorite also may have contributed some oxygen to the system during diagenesis.

The $\delta^{18}\text{O}$ composition of fracture calcite typically is depleted by 1 to 4 per mil relative to that of calcite cements in the surrounding sandstones (J.K. Pitman, unpub. data, 1984; Dickinson, 1985). If fracture calcite crystallized from pore fluids that were in isotopic equilibrium with those that precipitated matrix calcite, then the difference in $\delta^{18}\text{O}$ compositions may reflect burial temperatures that were higher during the crystallization of fracture calcite than during the formation of calcite cement in adjacent sandstones. This mechanism of ^{18}O depletion is consistent with the hypothesis that the development and cementation of fractures may have taken place under the influence of an overpressured regime at elevated temperatures. Petrographic studies demonstrate that mineralization of fractures followed emplacement and subsequent dissolution of matrix carbonate in sandstones. In the MWX well, $\delta^{18}\text{O}$ -enriched fracture calcite (about 13 per mil; table 1) occur locally and has approximately the same $\delta^{18}\text{O}$ compositions as matrix calcite in rocks of the same age and origin in other areas of the basin. These similar compositions suggest that fracture calcite may have precipitated at temperature conditions and pore-water chemistries similar to those from which matrix carbonate dissolved.

The $\delta^{18}\text{O}$ compositions of calcite (15.64 per mil average) in the deep Wagon Wheel fractures, which are associated with a fault system, are depleted relative to the depth trend of enrichment established by the shallow Wagon Wheel fractures (fig. 4B). These isotopically light $\delta^{18}\text{O}$ compositions may reflect either high water/rock ratios associated with groundwater recharge through open and interconnected fractures or possibly deep basin brines that migrated upward through the fracture network.

DISCUSSION

The $\delta^{18}\text{O}$ composition of water, $\delta^{18}\text{O}$ composition of carbonate, and temperature are important variables in a $^{18}\text{O}/^{16}\text{O}$ equilibrium carbonate system. Although the physiochemical conditions that govern fracture cementation are poorly understood, some constraints can be placed on the temperature and isotopic composition of the pore waters that may have characterized an overpressured restricted hydrologic regime during Late Cretaceous and early Tertiary time in the Piceance and Green River basins.

Temperature

Temperatures in the Piceance and Green River basins during the precipitation of fracture calcite were estimated from modified Lopatin burial history models and are reported in table 1, together with corresponding present-day temperatures. Based on these models, fracture calcite precipitated over a wide temperature range if cementation occurred at temperatures equal to or greater than present-day temperatures. Paleotemperatures for Cretaceous rocks in the MWX well are estimated to have varied from 240 to 330 °F (116–166 °C) during maximum burial 10 to 40 Ma. Bostick and Freeman (1984) postulated that about 5,000 ft (1,400 m) of erosion has taken place in the area of MWX during the past 10 million years. Assuming that the geothermal gradient has not changed from the Late Cretaceous to the present, we estimate that burial temperatures declined about 122 °F (50 °C) in response to this late stage of uplift and erosion.

In the vicinity of the Wagon Wheel well, maximum burial temperatures of about 200–300 °F (90–160 °C) occurred between 48 and 4 Ma ago; during the last 2 to 4 million years, the rocks cooled by 68–86 °F (20–30 °C) (Naeser, 1984). This temperature range is in good agreement with temperatures determined by Pollastro and Barker (1984) for fluid inclusions in fracture-fill quartz from the deep Wagon Wheel fractures, which formed late in the burial history. Pollastro and Barker estimated a minimum temperature of 266 °F (130 °C) for quartz precipitation, about 50 °F (10 °C) hotter than the present burial temperature. Uplift and erosion in the area of the WASP well has been minimal for the last 50 million years (Dorr and others, 1977), and there is no evidence to suggest that the geothermal gradient varied significantly through time. Formation temperatures in the Cretaceous section (225–270 °F; 110–130 °C) probably remained relatively constant during this period.

Pore Water $\delta^{18}\text{O}$

The oxygen isotope composition of pore fluids that may have existed during precipitation of fracture calcite in the Piceance and Green River Basins was determined from the calcite-water fractionation equation of Friedman and O'Neil (1977) using estimated paleotemperatures from burial history models (table 1) and measured isotopic ratios of fracture calcite. Figure 5 shows the range in oxygen isotopic composition of pore waters in equilibrium with calcite over a temperature span of 120–300 °F (50–150 °C). It is evident that formation waters in isotopic equilibrium with fracture calcite at the estimated temperatures of precipitation become enriched from about -8 to +2 per mil as burial depth increases (fig. 5). Based on studies by Dickinson (1987), these

waters are isotopically more similar to modeled waters for a closed system than to those for an open system.

The $\delta^{18}\text{O}$ composition of near-surface meteoric water in the northern Green River basin is about -20 per mil (B.A. Kimball, 1984, unpublished data), whereas in the Piceance Creek basin, some 62 mi (100 km) north of the MWX well, the $\delta^{18}\text{O}$ composition of recharge groundwater is about -17 per mil (Kimball, 1984). Formation water data from the Wagon Wheel and WASP wells are not available, but the $\delta^{18}\text{O}$ composition of water from the paludal zone, 3,973 ft (1,211 m) below the Cretaceous-Tertiary boundary, in one of the MWX wells is -7.5 per mil (B.A. Kimball, 1986, written commun.). Based on the fractionation equation of Friedman and O'Neil (1977), this water is not in isotopic equilibrium with fracture calcite (about 14 per mil $\delta^{18}\text{O}$) at the present-day temperature of 230 °F (110 °C) (fig. 5). To be in equilibrium with this water, the calcite would have had to precipitate at 122 °F (50 °C), which is unlikely because the estimated temperature of precipitation is about 352 °F (160 °C), hotter than the present temperature of 230 °F (110 °C). The oxygen isotope composition of water recovered from this MWX well probably represents a mixing of enriched formation water and depleted meteoric water.

Compared to the measured compositions of formation water from one of the MWX wells, the estimated compositions of formation fluids that may have existed during fracture cementation are significantly enriched in $\delta^{18}\text{O}$. Isotopically heavy pore waters may be expected in a closed hydrologic system for which water/rock ratios are low, such as in these low-permeability, overpressured sandstone. Part of this enrichment may reflect elevated temperatures resulting from deep burial, but the large component of $\delta^{18}\text{O}$ in the pore waters should compensate for a negative shift in $\delta^{18}\text{O}$ of calcite that might result from increasing temperatures. It is plausible that some fraction of the heavy oxygen represents a component of enriched meteoric water. Taylor (1974) estimated that meteoric waters present in the Rocky Mountain region from the Eocene to the Pliocene were enriched by 2 to 3 per mil in $\delta^{18}\text{O}$ relative to present-day waters.

Water/Rock Ratio

Calculation of the mole ratio of water to rock (W/R) following the method of Taylor (1977) can be used to model conditions governing fracture mineralization. The W/R ratio in atom percent is the isotopic shift in the rock divided by the isotopic shift in the water and can be determined by estimating the initial isotopic composition of the water and calcite in the system prior to alteration by dissolution and subsequent precipitation in fractures. Because isotopic composition of fracture calcite

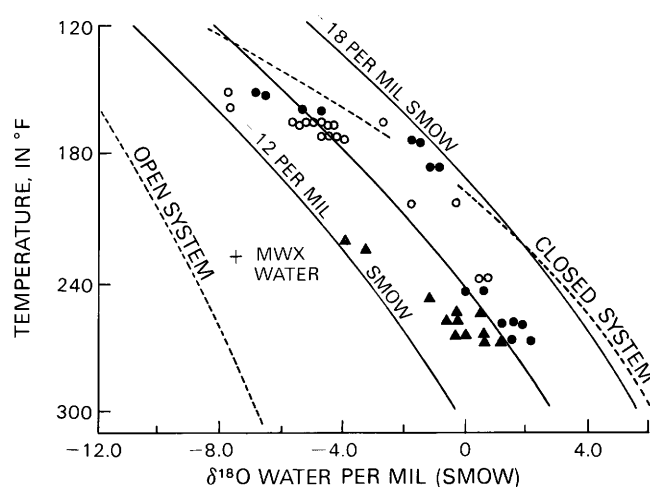


Figure 5. Variation in oxygen isotope composition of water in equilibrium with calcite of fixed isotopic composition in temperature range 120–300 °F (50–150 °C.) (Based on fractionation equation of Friedman and O'Neil, 1977.) $\delta^{18}\text{O}$ compositions of calcite are read from the curves ($\delta^{18}\text{O} = 18, 15, 12$ per mil), which depict relationship between temperature and water in equilibrium with calcite of indicated $\delta^{18}\text{O}$ composition. Estimated paleotemperatures used to calculate $\delta^{18}\text{O}$ (SMOW) of formation waters are from table 1. Dashed lines show range in isotope composition for waters in open and closed systems; closed system model of Dickinson (1987) uses $\delta^{18}\text{O}$ value of 18.5 for surface water; open system water uses mixing factor of 0.3 for the same water. Solid circles, Wagon Wheel well; open circles, MWX wells; closed triangles, WASP well.

not only changes with depth but also reflects the original composition of detrital limestone grains in sandstone, meteoric water compositions ($\delta^{13}\text{C}$, -8.6; $\delta^{18}\text{O}$, 18.5) and detrital limestone compositions ($\delta^{13}\text{C}$, -0.33; $\delta^{18}\text{O}$, 21) are best estimates for prealteration or initial values. When these initial values are used, W/R ratios calculated from the measured carbon and oxygen values in fracture calcite are generally similar and decrease in value with increasing depth. This trend probably reflects the decreasing porosity and permeability of the associated sandstones.

The isotopic compositions of calcite, calculated as a function of W/R ratios at constant temperature and superimposed on the measured compositions of fracture calcite, are shown in figure 6. Values for present-day meteoric waters (line B) are bracketed by heavier and lighter values (lines A and C); all calculated lines converge toward the isotopic composition selected for the initial rock. The use of isotopic values for initial water, such as the water at depth in the MWX well, which is heavy in both carbon and oxygen, cause the calculated lines to rotate clockwise around values for the initial rock and away from the measured isotopic compositions of fracture calcite. To compensate for this rotation, lighter values for the initial rock must be used to bring the

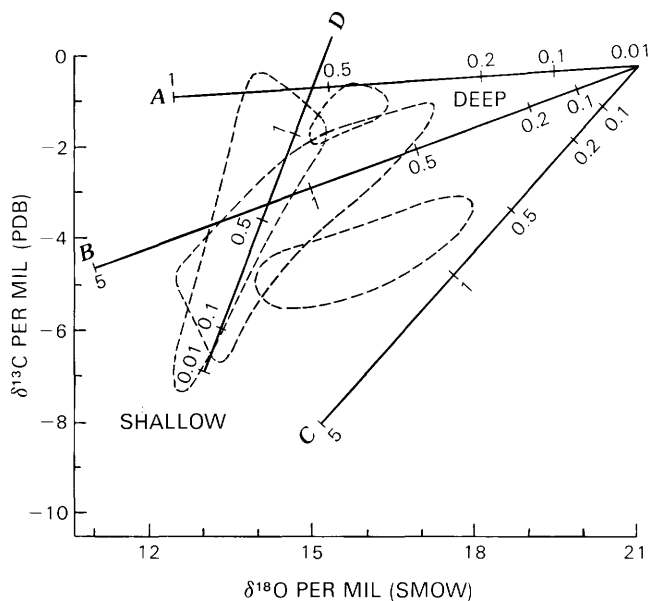


Figure 6. Calculated $\delta^{18}\text{O}$ and $\delta^{13}\text{C}$ compositions for calcite as a function of the water/rock ratio (atom percent) in closed system at 120 °F (50 °C) superimposed on data fields for calcite cement (fig. 3). Water/rock ratios calculated according to Taylor (1977). For initial water, values for $\delta^{18}\text{O}$ and $\delta^{13}\text{C}$ are, respectively, as follows: line A, 20, -4; line B, 18.5, -8.6; line C, 10, -12; line D, 7.5, -1. For initial rock, values of $\delta^{18}\text{O}$ and $\delta^{13}\text{C}$ are, respectively, as follows: lines A, B, and C, 21, -0.33; line D, 13, -7. For example, a calcite on line C having $\delta^{18}\text{O}$ composition of 15 and $\delta^{13}\text{C}$ composition of -8 precipitated from a system having water-rock ratio of 5 if the initial water had $\delta^{18}\text{O}$ of 10 and $\delta^{13}\text{C}$ of -12 and the initial rock had $\delta^{18}\text{O}$ of 21 and $\delta^{13}\text{C}$ of -0.33. At water/rock ratios below 5, the differences between open and closed systems (as defined by Taylor, 1977) are negligible.

calculated values (line D, fig. 6) close to the measured values; the use of these lighter values causes the W/R ratios to increase toward the deep samples.

The relationship between the calculated water/rock ratios and the measured isotopic compositions of the calcite cements places constraints on the conditions governing fracture cementation. For example, it is evident that the isotopic composition of the initial water from which the cements precipitated is similar to present-day meteoric values, although it is possible that the initial water may have been somewhat lighter in carbon and heavier in oxygen than assumed in the model. The fracture cements could not have precipitated from deep-seated or isotopically heavy water unless the initial calcite was isotopically light in both carbon and oxygen, which is unlikely. In addition, carbon or oxygen isotope trends in calcite for all three wells correlate closely with the isotopic composition of meteoric water as the water/rock ratio decreases with increasing burial depth. These calculations alone, however, cannot determine whether

the diagenetic system in which fracture cementation occurred evolved from a closed to an open state.

Pore Water $\delta^{13}\text{C}$

Dissolved bicarbonate in water from the paludal zone in one MWX well has a $\delta^{13}\text{C}$ composition of +1.16 per mil. This heavy carbon most likely reflects dissolved marine carbonate that originated in sandstone and shale beds. Assuming a temperature of about 230 °F (110 °C), which corresponds to the present-day burial depth at the top of the paludal zone, fracture calcite from this interval should be enriched in ^{13}C by approximately 2.5 per mil relative to dissolved HCO_3^- and CO_2^- . Fracture calcite in equilibrium with this water should have a $\delta^{13}\text{C}$ composition of about +4 per mil rather than the measured -2.1 per mil average. The difference of approximately -6 per mil suggests that these fluids may contain a component of organically derived carbon.

SUMMARY AND CONCLUSIONS

Overpressured gas-bearing rocks of Upper Cretaceous age in Wyoming and Colorado contain abundant, open and partly mineralized natural fractures that may serve to enhance permeability in these otherwise tight rocks. Identification of the factors that control the occurrence and distribution of fracture-fill cements and the hydrologic regime that existed during fracture mineralization is important in order to predict the presence of fractures in rocks of the same age and origin in other geographic areas that have undergone similar burial and diagenetic histories. Fractures in sandstones from three study wells are cemented with abundant calcite and lesser amounts of quartz, dickite, and barite. Most of the fractures were filled late in the burial history when the rocks were at greater burial depths and higher temperatures than at present.

Stable isotope studies reveal systematic $\delta^{13}\text{C}$ and $\delta^{18}\text{O}$ patterns in fracture calcite with depth that are similar to those in matrix carbonate. These trends suggest that host sandstones acted as the dominant carbon and oxygen reservoir during fracture cementation. In all three wells, the $\delta^{13}\text{C}$ compositions for fracture calcite are enriched with depth and in the range reported for marine carbonate, suggesting that the source of most of the carbon was from detrital grains of marine carbonate in the host sandstones. The $\delta^{18}\text{O}$ compositions for fracture calcite are consistently light (15 per mil average); in the MWX, WASP, and shallow Wagon Wheel fractures, oxygen is slightly enriched (1-3 per mil) with increasing burial depth. This trend reflects increased temperatures with greater depth of burial. The small difference in $\delta^{18}\text{O}$

compositions between the wells argues for a broad geographic control on the geochemical conditions governing fracture cementation.

The isotope trends, together with a knowledge of the burial history of the rocks, indicate that fracture calcite formed through a process of dissolution and reprecipitation of matrix carbonate. In addition, methane inclusions in fracture calcite are evidence for fracture cementation in a thermal regime dominated by the active generation of hydrocarbons and high pore-fluid pressures. The slight enrichment in $\delta^{18}\text{O}$ of fracture calcite with increasing depth and temperature suggests that precipitation occurred in a closed system in which the oxygen of the pore waters became sufficiently enriched with increasing depth to offset the decrease in isotopic fractionation between calcite and water.

Most fractures in Cretaceous rocks probably were opened and cemented at different times in the burial history rather than during a single event. Variations in the isotopic composition of calcite in closely spaced fractures suggest that most fractures, except those in the deepest part of the Wagon Wheel well, were not open and interconnected during mineralization. If the fractures had been connected at depth, the isotopic compositions of the calcite cement would be homogeneous between individual fractures. The isotopic differences, together with petrographic evidence that indicates carbonate dissolution and reprecipitation did not occur following fracture cementation, imply that fracture-fill calcite underwent no significant postdepositional isotopic exchange during burial.

Formation water from the paludal zone in one MWX well has a $\delta^{18}\text{O}$ composition of -7.5 per mil and a $\delta^{13}\text{C}$ bicarbonate composition of $+1.6$ per mil. The calcite-water fractionation equation of Friedman and O'Neil (1977) indicates that the $\delta^{18}\text{O}$ of water having this isotopic composition is not in equilibrium with fracture calcite in the same zone at its present-day temperature (230°F ; 110°C). We postulate that the water sample represents a mixing of enriched formation water and depleted near-surface meteoric water. Based on paleotemperature estimates from burial history models, calculated formation waters in equilibrium with fracture calcite become enriched in $\delta^{18}\text{O}$ from -8 to $+2$ per mil with increasing burial depth. These systematically heavier values, together with dissolved bicarbonate values on the order of $+1.6$ per mil, are consistent with fracture calcite precipitation in a closed rock-buffered diagenetic system.

REFERENCES CITED

- Allan, J.R., and Matthews, R.K., 1982, Isotope signatures associated with early meteoric diagenesis: *Sedimentology*, v. 29, no. 6, p. 797-817.
- Bostick, N.H. and Freeman, V.L., 1984, Tests of vitrinite reflectance and paleotemperature models at the Multiwell Experiment site, Piceance Creek basin, Colorado, *in* Spencer, C.W., and Keighin, C.W., eds., *Geologic studies in support of the U.S. Department of Energy Multiwell Experiment, Garfield County, Colorado: U.S. Geological Survey Open-File Report 84-757*, p. 110-120.
- Dickinson, W.W., 1985, Isotope geochemistry of carbonate minerals in nonmarine rocks, northern Green River basin, Wyoming: U.S. Geological Survey Open-File Report 85-532, 103 p.
- , 1987, An oxygen isotope model for interpreting carbonate diagenesis in nonmarine rocks, Green River basin, Wyoming: *Chemical Geology (Isotope Geoscience Section)*, v. 65, p. 103-116.
- Dorr, J.A., Spearing, D.R., and Steidman, J.R., 1977, Deformation and deposition between a foreland uplift and an impinging thrust belt, Hoback Basin, Wyoming: *Geological Society of America Special Paper 177*, 82 p.
- Emrich, K., Ehhalt, D.H., and Vogel, J.C., 1970, Carbon isotope fractionation during the precipitation of calcium carbonate: *Earth and Planetary Science Letters*, v. 8, p. 363-371.
- Friedman, I., and O'Neil, J.R., 1977, Compilation of stable isotope fractionation factors of geochemical interests, *in* Fleischer, M., ed., *Data of geochemistry (6th ed.)*: U.S. Geological Survey Professional Paper 440-KK, p. KK1-KK12.
- Hanson, R.F., Zamora, R., and Keller, W.D., 1981, Nacrite, dickite, and koolinite in one deposit in Nayarit, Mexico: *Clay and Clay Minerals*, v. 29, no. 6, p. 451-453.
- Keith, M.L., and Weber, J.N., 1964, Carbon and oxygen isotopic composition of selected limestones and fossils: *Geochimica et Cosmochimica Acta*, v. 28, no. 11, p. 1787-1816.
- Kimball, B.A., 1984, Ground water age determinations, Piceance Creek basin, Colorado, *in* Hitchon, Brian, and Wallick, E.I., eds., *Practical applications of ground water geochemistry: First Canadian/American Conference on Hydrogeology, Banff, Alberta, June 1984, Proceedings*, p. 267-283.
- Law, B.E., 1984, Relationships of source-rock, thermal maturity, and overpressuring to gas generation and occurrence in low-permeability Upper Cretaceous and lower Tertiary rocks, Greater Green River basin, Wyoming, Colorado, and Utah, *in* Woodward, Jane, Meissner, F.F. and Clayton, J., eds., *Hydrocarbon source rocks of the greater Rocky Mountain region: Rocky Mountain Association of Geologists*, p. 469-490.
- Law, B.E., and Dickinson, W.W., 1985, Conceptual model for the origin of abnormally pressured gas accumulations in low-permeability reservoirs: *American Association of Petroleum Geologists Bulletin*, v. 69, no. 8, p. 1295-1304.
- Law, B.E., Spencer, C.W., and Bostick, N.H., 1980, Evaluation of organic matter, subsurface temperature, and pressure with regard to gas generation in low-permeability Upper Cretaceous and lower Tertiary sandstones in Pacific Creek area, Sublette and Sweetwater Counties, Wyoming: *The Mountain Geologist*, v. 17, no. 2, p. 23-25.

- Martin, W.B., and Shaughnessy, J., 1969, Project Wagon Wheel, *in* Symposium on Tertiary rocks of Wyoming: Wyoming Geological Association Field Conference, 21st, 1969, Guidebook, p. 145-152.
- McCrea, J.M., 1950, The isotopic chemistry of carbonates and a paleo-temperature scale: *Journal of Chemistry and Physics*, v. 18, p. 849-855.
- McPeck, L.A., 1981, Eastern Green River basin, a developing giant gas supply from deep, overpressured Upper Cretaceous sandstones: *American Association of Petroleum Geologists Bulletin*, v. 65, no. 6, p. 1078-1098.
- Naeser, N.D., 1984, Fission-track ages from the Wagon Wheel No. 1 well, northern Green River basin, Wyo.; evidence for recent cooling, *in* Law, B.E., ed., Geological characteristics of low-permeability Upper Cretaceous and lower Tertiary rocks in the Pinedale anticline area, Sublette County, Wyoming: U.S. Geological Survey Open-File Report 84-753, p. 66-77.
- Pitman, J.K., and Sprunt, E.S., 1984, The origin and occurrence of fracture-filling cements in the Upper Cretaceous Mesa-verde Formation at MWX, Piceance Creek basin, Colorado, *in* Spencer, C.W., and Keighin, C.W., eds., Geologic studies in support of the U.S. Department of Energy Multiwell Experiment, Garfield County, Colorado: U.S. Geological Survey Open-File Report 84-757, p. 87-101.
- Pollastro, R.M., and Barker, C.E., 1984, Geothermometry from clay minerals, vitrinite reflectance, and fluid inclusions; applications to the thermal and burial history of rocks cored from the Wagon Wheel No. 1 well, Green River basin, Wyoming, *in* Law, B.E., ed., Geological characteristics of low-permeability Upper Cretaceous and lower Tertiary rocks in the Pinedale anticline area, Sublette County, Wyoming: U.S. Geological Survey Open-File Report 84-753, p. 78-94.
- Secor, D.T., Jr., 1965, Role of fluid pressure in jointing: *American Journal of Science*, v. 263, p. 633-646.
- Taylor, H.P., Jr., 1974, The application of oxygen and hydrogen isotope studies to problems of hydrothermal alterations and ore deposition: *Economic Geology*, v. 69, no. 6, p. 843-883.
- _____, 1977, Water/rock interactions and the origin of H₂O in granitic batholiths: *Geological Society of London Journal*, v. 133, pt. 6, p. 509-558.
- Verbeek, E.R., and Grout, M.A., 1984a, Fracture studies in Cretaceous and Paleocene strata in and around the Piceance basin, Colorado; preliminary results and their bearing on a fracture-controlled natural-gas reservoir at the MWX site: U.S. Geological Survey Open-File Report 84-156, 30 p.
- _____, 1984b, Prediction of subsurface fracture patterns from surface studies of joints; an example from the Piceance Creek basin, Colorado, *in* Spencer, C.W., and Keighin, C.W., eds., Geologic studies in support of the U.S. Department of Energy Multiwell Experiment, Garfield County, Colorado: U.S. Geological Survey Open-File Report 84-757, p. 75-86.

Chapter K

Reservoir Sedimentology of Rocks of the Mesaverde Group, Multiwell Experiment Site and East-Central Piceance Basin, Northwest Colorado

By JOHN C. LORENZ

Prepared in cooperation with the U.S. Department of Energy

U.S. GEOLOGICAL SURVEY BULLETIN 1886

GEOLOGY OF TIGHT GAS RESERVOIRS IN THE PINEDALE ANTICLINE AREA, WYOMING,
AND AT THE MULTIWELL EXPERIMENT SITE, COLORADO

CONTENTS

Abstract	K1
Introduction	K1
Fluvial deposits	K2
Example of fluvial reservoir	K4
Nonchannel deposits	K7
Delta-plain deposits	K11
Example of an upper delta-plain reservoir	K13
Examples of lower delta-plain reservoirs	K16
Shoreline-marine deposits	K16
Reservoirs in the Mancos Shale	K19
Summary	K22
References cited	K23

FIGURES

1. Diagrammatic map showing depositional environments of sandstones at MWX site **K2**
2. Chart showing reservoir characteristics of rocks from different depositional environments encountered in MWX wells and geophysical logs **K3**
3. Well-to-well gamma-ray log correlation of reservoir sandstones in fluvial part of Williams Fork Formation in MWX wells **K4**
4. Cross section showing detailed lithologic description of slabbed core and gamma-ray logs for typical fluvial reservoir in Williams Fork Formation in MWX wells **K5**
5. Charts showing porosity and permeability characteristics of meander-belt fluvial sandstone reservoir in Williams Fork Formation in MWX wells **K6**
6. Schematic cross section of flood-deposit sandstone (unnamed sandstone bed of Williams Fork Formation) **K7**
7. Core and gamma-ray logs showing lateral variation of floodplain deposits in fluvial zone of Williams Fork Formation in MWX wells and schematic diagrams showing depositional environments **K8**
8. Schematic cross section of point-bar deposits in single-story lenticular sandstone in lower delta-plain deposits of Williams Fork Formation **K11**
9. Well-to-well gamma-ray log correlation of reservoir sandstones in delta-plain interval of Williams Fork Formation in MWX wells **K12**
10. Cross section showing detailed lithologic description of slabbed core and gamma-ray logs for composite reservoir in upper delta-plain environment (coastal zone of Williams Fork Formation) in MWX wells **K14**
11. Charts showing porosity and permeability characteristics of upper delta-plain distributary-channel sandstone reservoirs in Williams Fork Formation in MWX wells **K15**
12. Cross section showing detailed lithologic description of slabbed core and gamma-ray logs for lenticular distributary-channel sandstone and thick splay deposit in lower delta-plain environment of Williams Fork Formation in MWX wells **K17**

13. Charts showing porosity and permeability characteristics of distributary channel sandstone reservoir and laterally variable splay sandstone reservoir in lower delta-plain environment of Williams Fork Formation in MWX-1 and MWX-2 wells **K18**
14. Well-to-well gamma-ray log correlation of sandstones in shoreline-marine interval of Iles Formation of Mesaverde Group in MWX wells **K20**
15. Cross section showing detailed lithologic description of slabbed core and gamma-ray logs for Cozzette Sandstone Member of Iles Formation of Mesaverde Group in MWX-1 and MWX-2 wells **K21**
16. Charts showing porosity and permeability characteristics of blanket-marine sandstones (lower and upper sandstone units of Cozzette Sandstone Member of Iles Formation) in MWX-1 and MWX-2 wells **K22**
17. Diagrams showing lithology and setting of offshore-marine deposits in Mancos Shale along the Book Cliffs **K23**

Reservoir Sedimentology of Rocks of the Mesaverde Group, Multiwell Experiment Site and East-Central Piceance Basin, Northwest Colorado

By John C. Lorenz¹

Abstract

Three types of low-permeability sandstone reservoirs are encountered in Upper Cretaceous rocks of the Mesaverde Group in the U.S. Department of Energy's Multiwell Experiment (MWX) wells in the east-central Piceance basin, northwest Colorado. Reservoir characteristics of each type of sandstone are determined by the environment in which the sandstone was deposited. The lower Mesaverde Group consists of a series of blanket sandstone reservoirs deposited in regressive wave-dominated delta and shoreline environments and interbedded with nonmarine coal and marine shale. Above the blanket sandstone reservoirs, distributary channel reservoirs were deposited on a delta plain as elongate lenticular sandstone bodies. These are associated with mudstone in the upper delta plain (coastal) facies and with mudstone and coal in the lower delta plain (paludal) facies. Irregular sandstone bodies composed of stacked point bars were deposited in the overlying fluvial environment. Estimates of reservoir morphology, dimensions, trends, and internal characteristics for each environment can be made on the basis of sedimentological models and by using characteristics observed both in core and in outcrops near the MWX site.

INTRODUCTION

The U.S. Department of Energy conducted field-laboratory studies designed to characterize low-permeability sandstones and to assess different technologies for the production of natural gas from these reservoirs. The laboratory consisted of three closely spaced wells drilled into the Upper Cretaceous Mesaverde Group in the east-central Piceance basin of northwest Colorado (Law and Spencer, this volume, fig. 1). It was designated the Multiwell Experiment (MWX), and the three wells were designated MWX-1, MWX-2, and MWX-3. The purpose of this report is to summarize reservoir characteristics of the various types of sandstones encountered within the Mesaverde Group in these wells.

These characterizations are supported by extensive field studies of Mesaverde outcrops around the Piceance basin, most notably at Rifle Gap, approximately 12 mi (20 km) northeast of the MWX site.

The MWX wells penetrated rocks deposited in four distinct environments in the 4,000-ft-thick (1,220 m) Mesaverde Group. Three of these environments are part of a progradational sequence and are, from the stratigraphic base up, shoreline marine, delta plain (including coastal and paludal), and fluvial. The spatial arrangement of these environments at any given time is depicted in figure 1. As progradation occurred, the deposits were superimposed vertically. Variations in local subsidence and uplift rates significantly influenced the thickness and percentage of sandstone in the formation in different parts of the basin, but the primary control on local reservoir geometry and internal complexity was depositional environment (fig. 2).

The fourth type of environment has been recognized in the Ohio Creek Member, found at the top of the Mesaverde Group (Lorenz and Rutledge, 1987). This marine-influenced paralic environment records a major change from the overall regressive succession recorded in the rest of the formation to deposition associated with the ensuing Lewis transgression. The rocks do not contain significant amounts of gas in the MWX wells and will not be described in this report, although they may constitute a significant reservoir facies elsewhere in the basin (Lorenz and Rutledge, 1985a, b).

Most of the MWX reservoir properties, including porosity, matrix permeability, and gross reservoir morphology, size, and internal heterogeneity, are governed by the sedimentary characteristics described in this paper. Although overall reservoir permeability is controlled by the system of natural fractures and in situ stresses found in the Mesaverde strata at the MWX site (Lorenz and others, 1988), the different sedimentary characteristics of the different reservoirs exert significant control on the distribution and character of the natural fractures. Moreover, the sedimentology or primary depositional

¹Sandia National Laboratories, Albuquerque, N. Mex. 87185

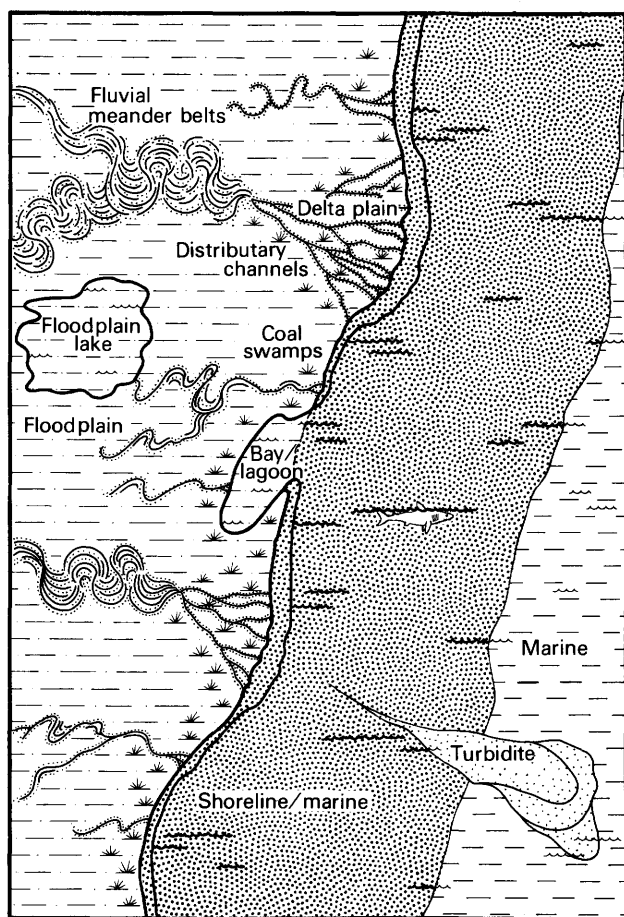


Figure 1. Depositional environments of sandstones at the MWX site in the east-central Piceance basin of northwest Colorado. Lateral migration of the system during progradation resulted in stacked fluvial deposits above delta-plain and marine deposits. Modified from Fisher and McGowen's (1969) interpretation of Eocene deposits of Texas Gulf Coast. Depositional environments of Mesaverde Group deposits are believed to be analogous.

environment of a reservoir in large part dictates the petrologic characteristics of grain size, sorting, and maturity that affect the primary and secondary (diagenetic) development of porosity and permeability (Lorenz, Sattler, and Stein, 1989).

Acknowledgments.—This work was performed for the U.S. Department of energy under contract DE-ACOH-76DP00769.

FLUVIAL DEPOSITS

Rocks of the fluvial interval (MWX depths 4,400–6,000 ft, 1,340–1,830 m) of the Mesaverde Group were deposited in an environment of meandering fluvial systems (fig. 2). Most of these systems were relatively small and probably originated on the alluvial plain rather

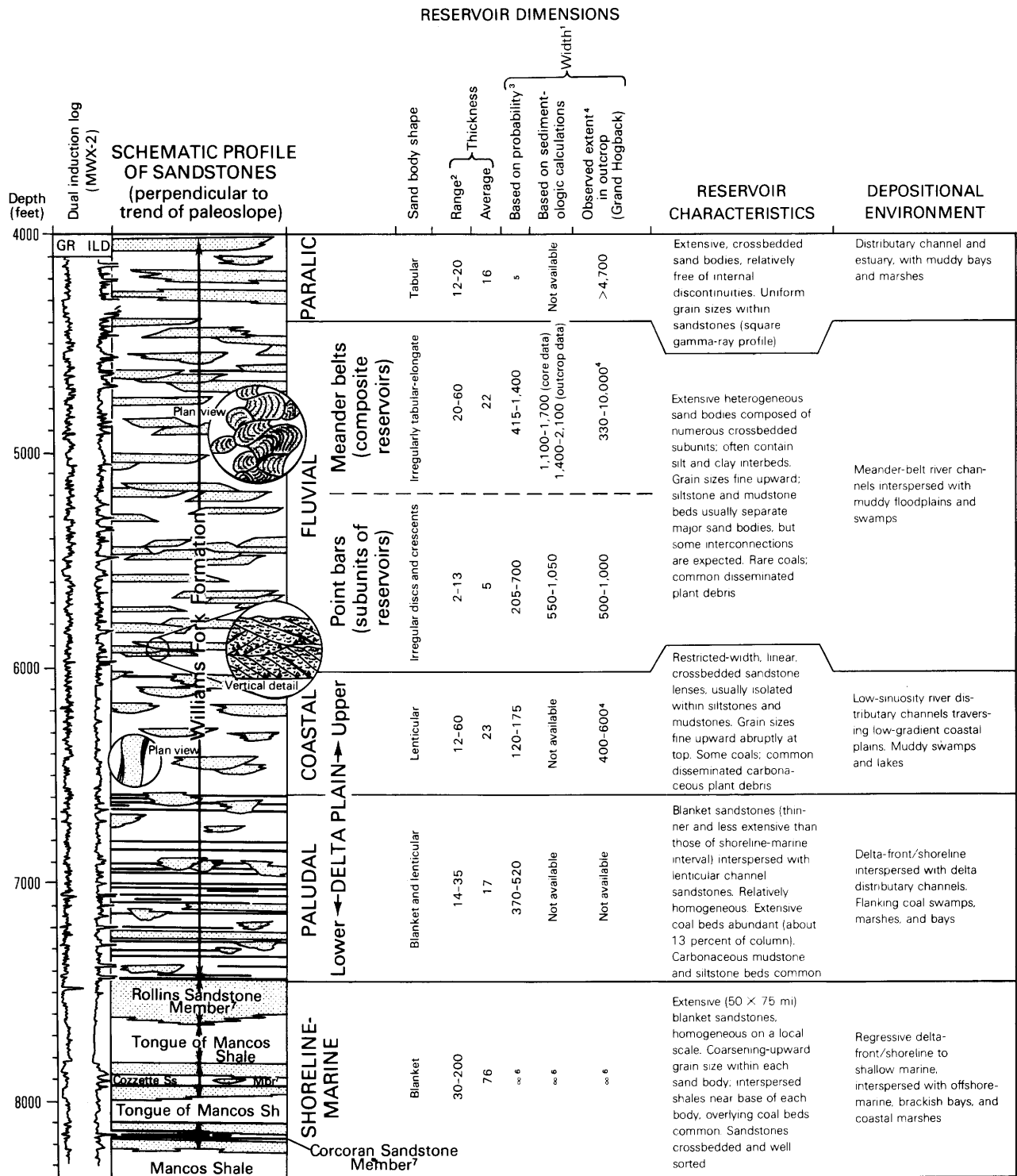
than in the distant, contemporaneous fold and thrust belt of central Utah. The presence at the mid-fluvial level at Rifle Gap of a small coal deposit and a sandstone lens that contains several fossil logs with the trace fossil *Teredolithus* suggests that a minor transgression may have occurred at this time in the east-central part of the basin, and that the seaward edge of this progradational episode was never far beyond the Rifle Gap area.

Study of outcrops along the Grand Hogback near Rifle indicates that most of the fluvial sandstones were deposited as arcuate point bars on the inside of river bends during lateral migration of rivers. A sandstone deposited as a point bar is commonly partially eroded and replaced when subsequent point bars migrate over the same area. Each individual point-bar unit in the MWX reservoirs fines upward, and the composite unit also commonly fines upward as a result of lowered gradients of maturing rivers.

Sedimentologic models of depositional environments suggest that each point-bar deposit is arcuate in plan view. Reconstructions (Lorenz and others, 1985) suggest that the Mesaverde point bars were about 700 ft (200 m) wide and 2–13 ft (0.6–4 m) thick. These point-bar units commonly are stacked on top of each other in random orientations and form composite meander-belt sandstone reservoirs that are 20–60 ft (6–13 m) thick and on the order of 1,000–2,000 ft (300–600 m) wide. The reservoirs generally are elongate parallel with paleoslope and have irregular edges. At the MWX site, they are significantly wider than the well spacings of 120–200 ft (37–61 m), and therefore well-to-well correlation of individual sandstone reservoirs is excellent (fig. 3).

Internally, these complex reservoirs are composed of a series of fining-upward sequences, each of which corresponds to the deposit of one point bar. As many as seven fining-upward sequences occur within one reservoir. In general, each cycle has a basal scour surface (the floor of the ancient channel) overlain by fine- to medium-grained, crossbedded sandstone. The crossbedded sandstone grades upward into fine to very fine grained, usually rippled sandstone. Some of the sequences continue upward into siltstone or even thin mudstone, but many of the upper channel and channel-margin deposits were eroded by scouring at the base of the next channel as it migrated across the area.

Figure 2 (on facing page). Reservoir characteristics of rocks from different depositional environments encountered in the MWX wells. Meander belts within the fluvial zone are composed of point bars. Geophysical logs: GR, gamma ray; ILD, deep induction log. Thicknesses (range and average) from MWX downhole geophysical logs. Methods used to calculate reservoir widths described in Lorenz and others (1985). Outcrop widths measured along Grand Hogback, 12 mi (20 km) north-east of MWX site. N.A. indicates not available.



- Crossbedding, ripples
- Clay ripup clasts
- Bedding plane (clay surfaced)
- Coal

- ¹ Lengths are indeterminant » widths
- ² Sand and silt beds as thin as 2 ft can be seen on logs but are economically unimportant
- ³ Probable width varies with estimate of borehole separation at depth
- ⁴ Outcrop dimensions are apparent widths that may include significant portions of length
- ⁵ Data insufficient to make valid calculation
- ⁶ Infinite with respect to effective well-bore drainage
- ⁷ Of Iles Formation

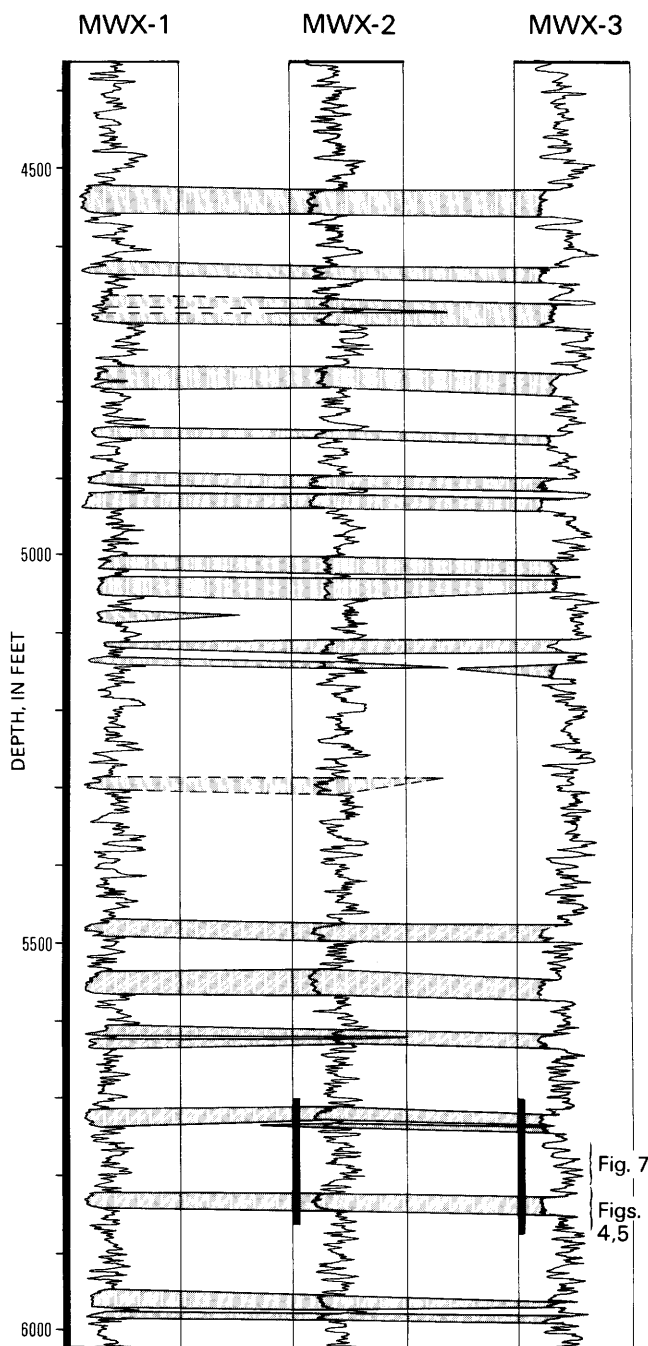


Figure 3. Well-to-well gamma-ray log correlation of reservoir sandstones (pattern) in fluvial part of the Williams Fork Formation in the MWX wells. Correlation between wells is excellent as a result of large lateral extent of these reservoirs relative to well spacing. Solid bar indicates cored intervals; dashed line indicates tentative correlations.

Although some of the individual fining-upward units may be attributed to lateral accretion of diagonally inclined point-bar beds, there is evidence for channel-base scour surfaces below many of the units. Moreover, the erratic thickness of the units reflects the irregularities of

partial erosion rather than the more uniform changes in thickness indicative of superimposed lower, middle, and upper point-bar facies. These stacked units therefore are inferred to be multistoried, superimposed point-bar deposits.

The vertical trend across an entire reservoir is shown well in gamma-ray profile and commonly fines upward. Upper-channel siltstone and mudstone are preserved near the top of the reservoir and are overlain by siltstone and mudstone of levee and floodplain environments. Penetration of these uppermost zones by roots of plants commonly has obscured or destroyed bedding.

Example of Fluvial Reservoir

Lateral heterogeneity of reservoirs in the fluvial facies is illustrated in figure 4, which shows the lithologies of core in the three MWX wells for a typical MWX fluvial reservoir. On a gross scale, this sandstone is one of the more uniform lenses in the fluvial zone. Bedding characteristics in the core show, however, that the reservoir is heterogeneous in detail, in that each well contains multiple partial point-bar sequences. The thickest point-bar sequence is in the basal part of MWX-2; it is about 10 ft (3 m) thick and is inferred to be relatively complete.

The 10-ft (3 m) thickness can be used to reconstruct a minimum meander-belt width of 1,000 ft (300 m) (technique of Lorenz and others, 1985). Dipmeter and oriented core data from MWX-3 provide two instances of northerly paleoflow in two point bars, and crossbeds in MWX-2 core (oriented by using paleomagnetic measurements) indicate northwest paleoflow. The base of the sandstone is about 5 ft (1.5 m) lower in MWX-1 than in the other two wells; the channel probably was initially located in the area of MWX-1, subparallel with the MWX-2/MWX-3 axis. Such a location restricts possible reservoir-axis orientations to a generally north-south alignment, although data are insufficient to be definitive.

Partially eroded mudstone drapes and the clay plugs that filled abandoned channels created irregularly spaced lithologic discontinuities that are permeability barriers within the matrix rock. Natural fractures are the dominant permeability mechanism in these tight reservoirs, but the extent of individual fractures is strongly controlled by lithologic discontinuities within the reservoirs (Lorenz and Smock, 1986; Finley and Lorenz, 1989; Lorenz, Branagan and others, 1989). Similar internal complexities in fluvial reservoirs elsewhere in the basin have also been described (Jones, 1984; Jones and others, 1984).

Porosity and permeability within the fluvial reservoirs follow erratic but generally decreasing upward trends consistent with lithologic heterogeneity caused by the amalgamation of multiple point-bar deposits. Measurements from core of MWX-1 and MWX-3 (fig. 5)

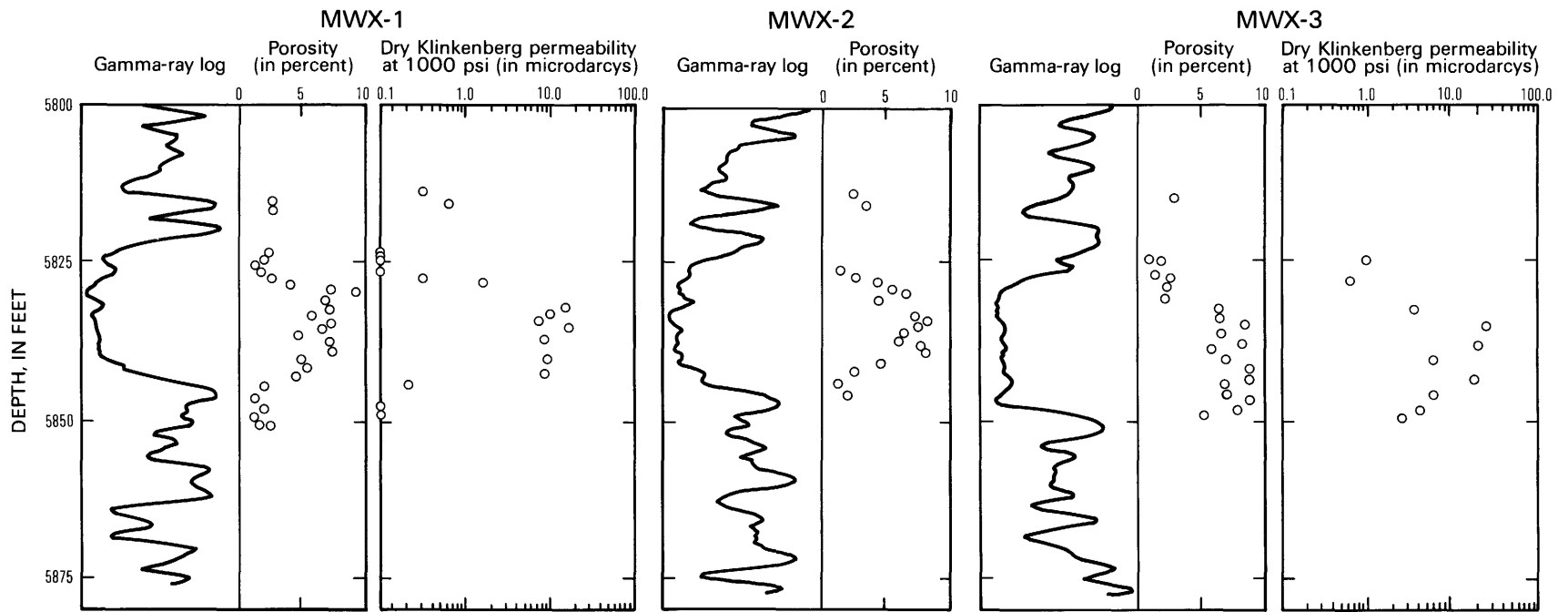


Figure 5. Porosity and permeability characteristics of a meander-belt fluvial sandstone reservoir in the Williams Fork Formation in the MWX wells. Reservoir quality is highly variable in sandstones deposited in this type of environment. Note logarithmic scale of permeability graphs.

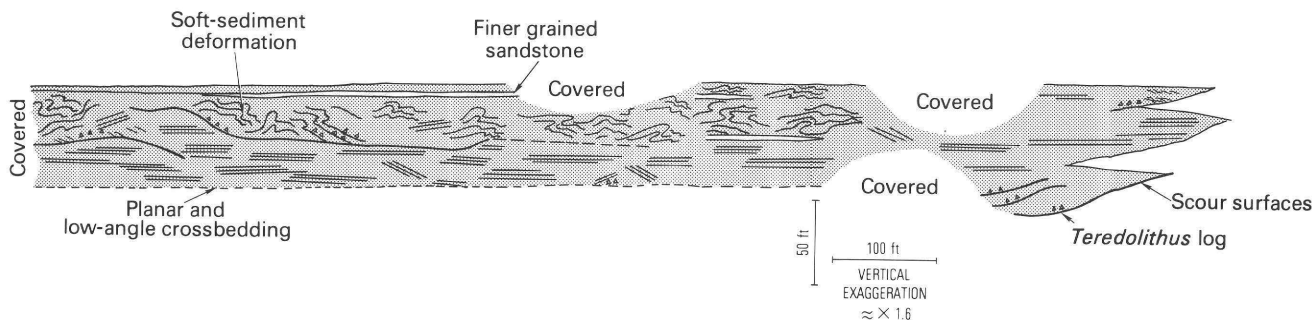


Figure 6. Schematic cross section of a flood-deposit sandstone (unnamed sandstone bed of Williams Fork Formation) in Estes Gulch, about 1 mi (1.6 km) west of Rifle Gap. Planar-horizontal bedding predominates; subunits represent multidepositional events. Adjacent fine-grained deposits are covered.

show abrupt increases in porosity and permeability at the bases of fluvial reservoirs and erratic but generally high values through the main parts. The variability in these measurements correlates well with grain size, increasing with each new coarse-grained basal point-bar deposit and decreasing above it. Near the top of a reservoir, where it becomes silty, there is a gradual but marked decrease in porosity and permeability.

Porosity in core from MWX-2 shows a similar pattern, except for a more gradual initial increase at the base of the reservoir. In this well, numerous claystone ripup clasts were incorporated into the basal sandstones (fig. 4) and may have inhibited the development of good porosity.

Average porosity in this reservoir is about 8 percent, and average dry Klinkenberg permeability at 1,000 lbs/in.² (6.9 MPa) net confining stress is about 7–8 microdarcys (A.R. Sattler, Sandia National Laboratories, oral commun., 1986).

Nonchannel Deposits

A wide, homogeneous sandstone body of probable flood origin (unnamed sandstone bed of the Williams Fork Formation) (fig. 6) has been observed in outcrops of the fluvial facies at Estes Gulch, just west of Rifle Gap. The closest modern analogs to this deposit are inferred to be the fan deltas of Scott and others (1969). These multistory/multidepositional event deposits result from storm-related torrential rainfall and flooding in local drainage basins. The abrupt increase in the percentage of sandstone in the Mesaverde Group above the flood deposit in Estes Gulch suggests that the storm events that caused the flooding also may have caused avulsion of a fluvial system into the Estes Gulch area.

This fan-delta environment produced primarily planar-horizontal bedding in the thicker central sections of the sandstone body. The presence of a single fossil log burrowed with *Teredolithus* trace fossils suggests that the shoreline was not distant. The deposit is at about the same

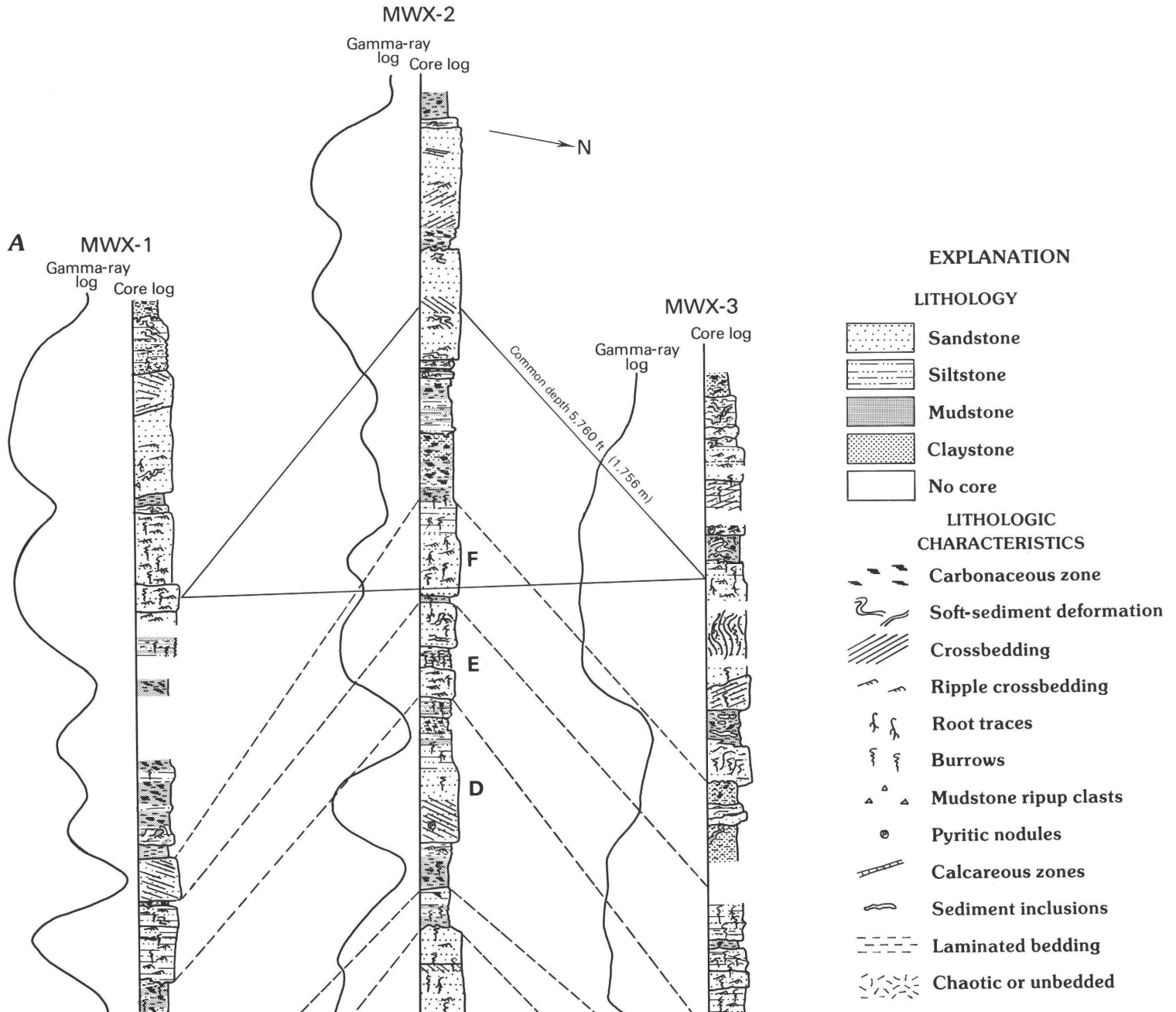
stratigraphic interval as the coal and the burrowed log noted previously. It is also possible, however, that the log was swept far inland during the storm event. The absence of associated shoreline deposits may indicate that the sandstone was deposited in an inland lacustrine basin.

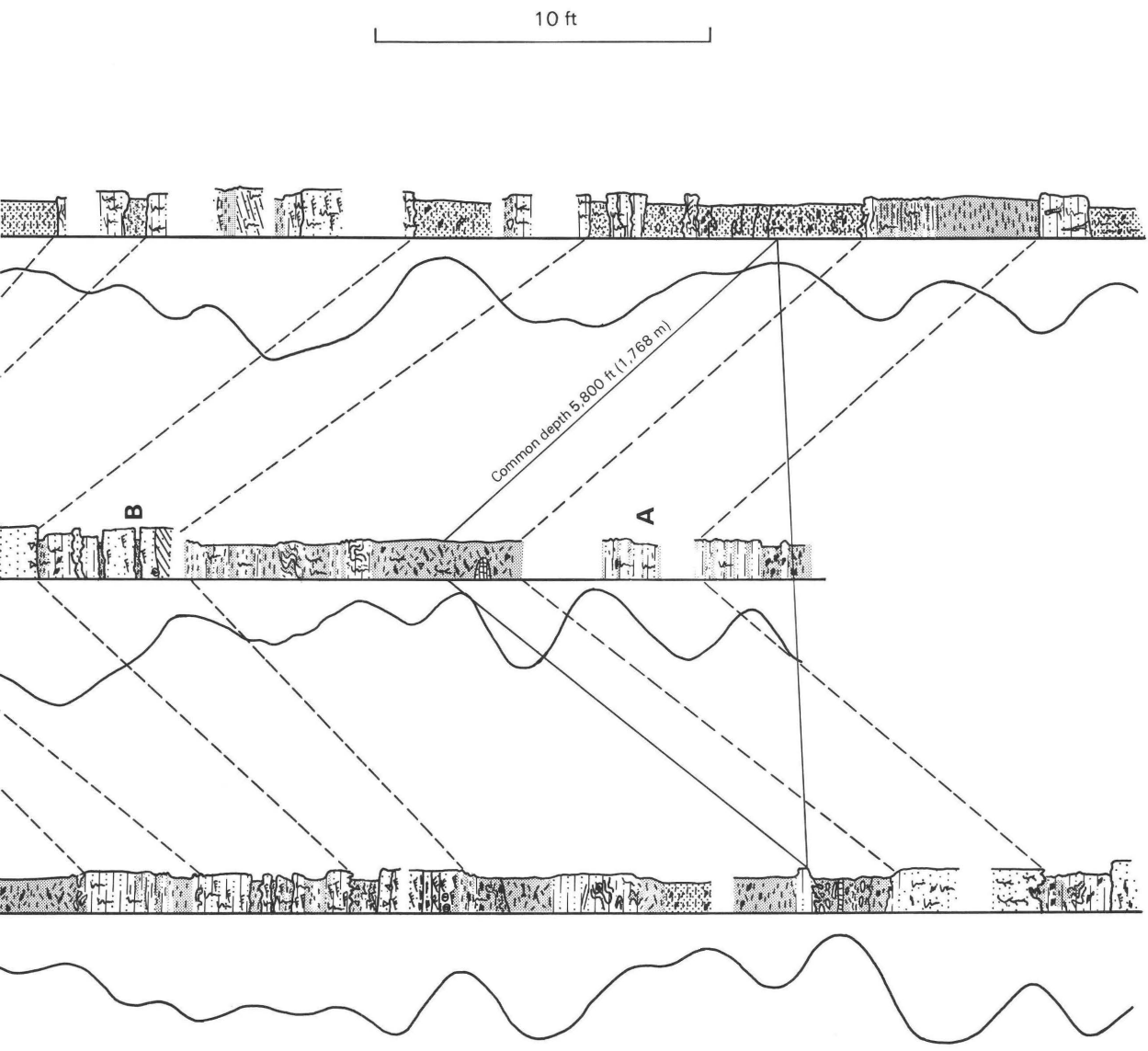
Such flood deposits should be excellent reservoirs. They may be significantly different in size from the more common meander-belt sandstone deposits, but their morphologies and internal compositions are less complex. Deposits of this type have not been recognized in core from the MWX wells but probably are not rare in the Mesaverde Group as a whole.

Lacustrine claystone and thinly bedded, rooted and rippled siltstone and mudstone levee and splay deposits are common between the channel sandstones. The non-sandy deposits also include rooted and burrowed swamp mudstones that are carbonaceous and probably provided an immediate, though perhaps diluted, source for reservoir gas. These mudstones are composed of mixed clays and silts and should also provide good reservoir seals, even in fractured reservoirs, because the fractures that dominate reservoir permeability commonly terminate at contacts with these adjacent mudstones in both core and outcrops.

The fine-grained nonchannel sediments were deposited as lateral facies equivalents of the sandy meander-belt complexes. Paleosols are rarely found in the floodplain deposits, and the abundance of soft-sediment deformation, burrowing, and preserved organic matter indicates that the Mesaverde floodplain environments were rarely desiccated. The limited extent of the different floodplain environments is suggested by the rapid lateral lithologic variations in the short distances between the three MWX wells (Lorenz, 1985a) (fig. 7).

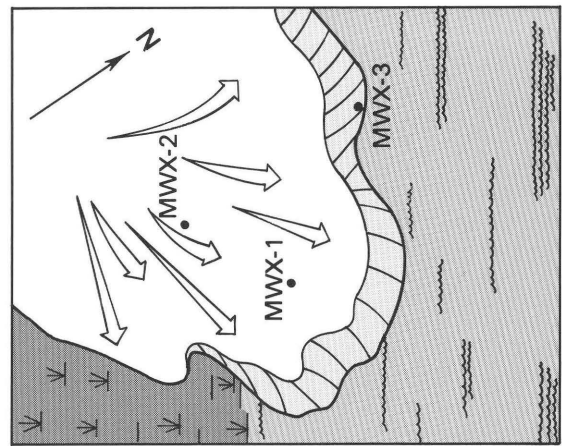
Figure 7 (next three pages). Lateral variation of floodplain deposits in the fluvial zone of the Williams Fork Formation in the MWX wells. Alphabetic labels refer to units discussed in text. Location of interval shown in figure 3. A, Fence diagram of detailed logs for part of MWX wells. B, Schematic diagrams showing depositional environments.



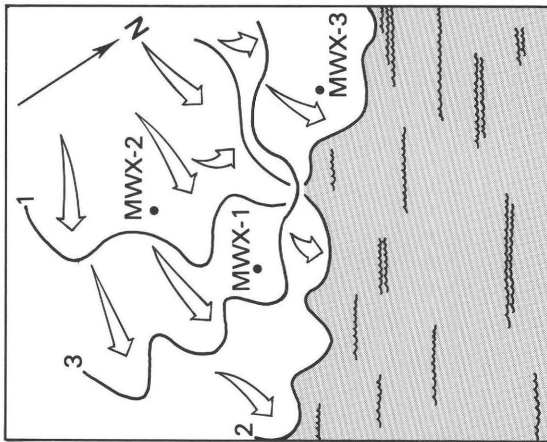




UNIT C



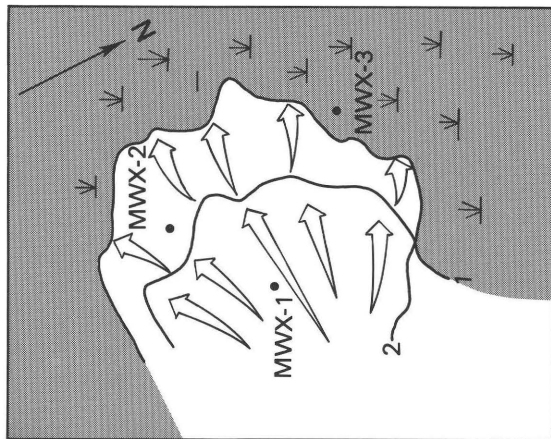
UNIT F



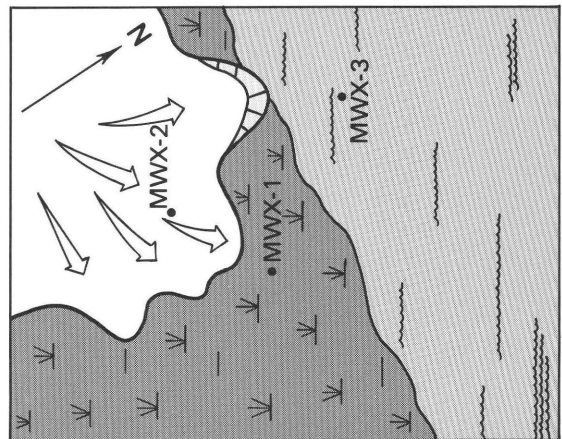
UNIT B



UNIT E



UNIT A



UNIT D

B

Unit A of the floodplain deposits shown in figure 7 is a rooted and burrowed levee splay deposit in MWX-1 that grades distally into swampy deposits in MWX-2 and into probable lacustrine deposits in MWX-3. Unit B probably records multiple depositional events on a splay that later abandoned the MWX-3 area, being replaced by a lacustrine environment. Unit C may record overlapping environments: a crossbedded and rippled levee and channel-margin deposit in MWX-3 grades into thin, subaqueous, burrowed and rippled siltstone in MWX-1, whereas the equivalent deposits in MWX-2 record a proximal splay derived from an entirely different source.

Unit D records extreme facies changes: carbonaceous mudstone of a paludal environment in MWX-1 is equivalent to the dark, organic claystone of a lacustrine environment in the MWX-3 area. In the area of MWX-1, sandstone splay deposits encroached into these environments. More laterally extensive, but still variable, multiple splay deposits occur in all three wells in unit E, whereas unit F contains lacustrine claystone in MWX-3, rippled splay sandstone in MWX-2, and what are interpreted to be the inclined siltstone foresets of a lacustrine delta in MWX-1.

DELTA-PLAIN DEPOSITS

Rocks of the coastal (6,000–6,600 ft, 1,830–2,010 m) and paludal (6,600–7,455 ft, 2,010–2,270 m) zones in MWX were deposited in upper and lower delta-plain environments, respectively. On a delta plain, numerous relatively straight to slightly sinuous distributary channels radiate outward from the main river channels to the shoreline across low-gradient coastal swamps and marshes. Several distributary channels serve one fluvial system, and the channels are small relative to the meander-belt channel that feeds them. The width to depth ratios of the

channels are commonly less than those of meander-belt fluvial channels, and therefore channel depths in the coastal and paludal zones may be greater than those in the fluvial zone even though channel widths are less. The channels lack lateral erosive power, the gradient of the coastal plain is low, and the channels usually do not migrate or meander significantly. Coals form on the lower delta plain, and the better drained upper delta-plain (coastal) interval is differentiated from the lower delta-plain interval primarily by the absence of coals.

In the subsurface, upper delta-plain deposits would be difficult to distinguish from the overlying fluvial deposits without closely spaced wells that highlight the narrower sand-body widths of the coastal distributary channels. The sedimentology of the core, however, provides some clues; delta-plain sandstones in the MWX wells contain fewer internal scour surfaces and more authigenic pyrite than do fluvial sandstones.

The delta-plain rocks are poorly exposed in the outcrops at Rifle Gap, but several lenticular sandstones can be seen and the presence of coal is well documented within the lower strata (Collins, 1976). However, there are excellent outcrops of delta-plain rocks in Coal Canyon, north of Cameo on the western side of the basin. These outcrops confirm both the lenticular shape and limited widths of the channel sandstones of this environment, despite locally well developed lateral-accretion (point-bar) surfaces (fig. 8). Internally amorphous, crossbedded, lenticular sandstones are equally abundant and probably correspond to straighter reaches of the distributary channels. Geophysical logs from the closely spaced MWX wells also document the restricted width of sandstones in the delta-plain environment (fig. 9), and core shows an internal structure composed of crossbedding, ripple bedding, and soft-sediment deformation.

Mudstone associated with sandstone reservoirs in the delta-plain interval in the MWX wells is highly

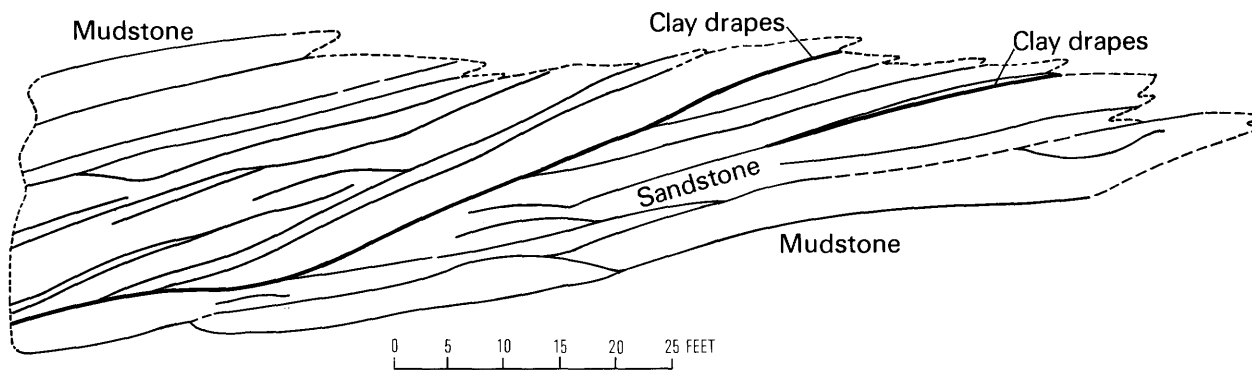


Figure 8. Cross section (traced from photograph) of point-bar deposits in a 300-ft (90 m) wide, single-story lenticular sandstone in coal-bearing, lower delta-plain deposits of the Williams Fork Formation in Coal Canyon, west of Cameo on the southwestern edge of the Piceance basin. Heavy line indicates clay drapes; dashed line indicates approximate edge of sandstone unit.

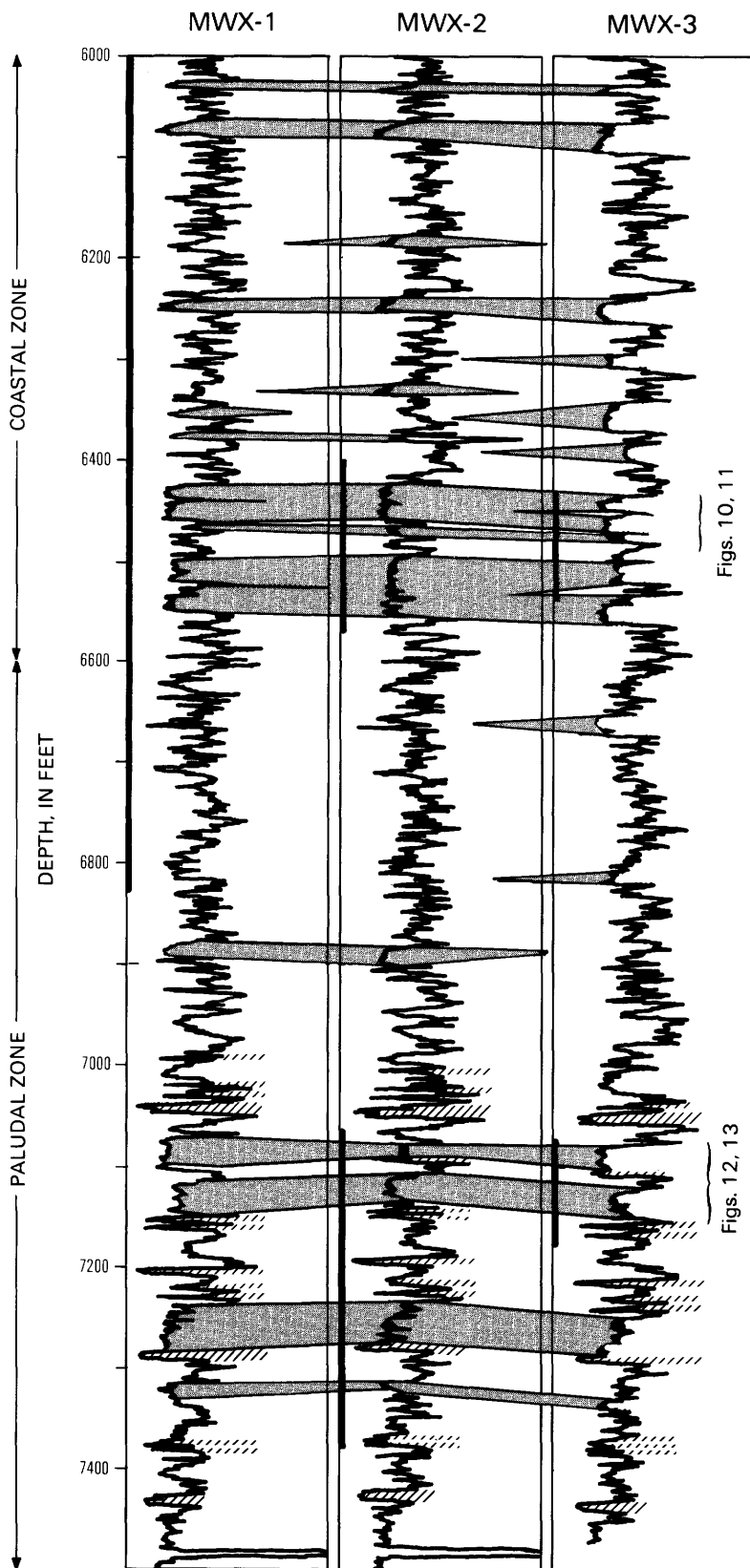


Figure 9. Well-to-well gamma-ray log correlation of reservoir sandstones (pattern) in the delta-plain interval of the Williams Fork Formation in the MWX wells. Correlation between wells is poorer than for fluvial part of formation (fig. 3) because reservoir widths are smaller. Solid bar indicates cored interval; hachured pattern indicates coal beds.

carbonaceous, and the amount of coalified plant debris increases downhole until it is locally concentrated into coal beds in the paludal (lower delta plain) zone. Many of the rooted sandstones and siltstones were deposited from floods that breached channel levees and inundated adjacent swamps as splays. Although the sediments originally were rippled, many of the structures have been destroyed by plant roots. Roots also grew into the mudstone, leaving it structureless or with a churned texture.

Sandstone reservoirs are isolated within mudstones and coals because of the avulsive behavior of distributary channels. Internally, the reservoirs are heterogeneous. Clay partings, which formed during periods of slack water, act as incomplete vertical permeability barriers and affect both reservoir conductivity and fracture distribution. Abrupt changes in grain size and sedimentary structures also disrupt vertical permeability.

The lower boundary of delta-plain sandstone reservoirs is most commonly an abrupt sandstone-mudstone contact at the channel-base scour surface. The upper boundary is marked by an abrupt decrease in grain size from sandstone to mudstone over a vertical distance of 1–2 ft, a change commonly made indistinct by root penetration.

The unfractured ductile mudstones and carbonaceous mudstones that are interbedded with paludal and coastal reservoir sandstones provide good reservoir seals. The mudstones are probably the source of the gas in the associated sandstones, but reservoir volumes are relatively small in this facies.

The average delta-plain reservoir width was determined on the basis of probability and sandstone-bed correlations between two closely spaced wells, using the assumption that a greater percentage of the reservoirs will correlate between the wells if the reservoirs are wider. Subsurface widths of 370–520 ft (133–159 m) (fig. 2) for the paludal zone are similar to those measured on outcrop. Limited subsurface data from the coastal zone suggest that reservoir widths in this area are 120–175 ft (37–53 m), although outcrops suggest that reservoir widths in the coastal zone are, in fact, similar to those of the paludal zone (Lorenz, 1985b). The delta-plain sandstone bodies are lenticular in cross section and of variable orientation.

Detailed observations of core from the delta-plain sandstones allow for a tentative reconstruction of orientation of specific reservoirs. Orientations were interpreted from spatial relationships of the three wells at depth and the specific subenvironments (main channel, channel margin, overbank) penetrated by each well. Crossbedding information obtained from high-resolution dipmeter measurements in MWX-3 and from oriented core supplemented the conclusions.

Example of an Upper Delta-Plain Reservoir

A typical upper delta-plain (coastal zone) reservoir is shown in figure 10. Two main sandstone bodies (units A and B) are separated by 3–4 ft (1 m) of mudstone in MWX-1 and MWX-3 but interconnect in MWX-2, where unit A has scoured down into unit B. A third bed (unit C) is not obviously connected but is separated from unit B by only 3–5 ft (1–2 m) of mudstone in each well.

In all three wells, unit A is a clean, crossbedded sandstone that is rippled near the top. Using outcrop thickness to width relationships (Lorenz, 1985b), its thickness in MWX-2 suggests a minimum width of 200 ft (61 m). Unit A thins in MWX-1 and MWX-3, and the channel center may lie between these two wells and MWX-2 and trend northwest. Limited data (crossbeds in oriented core and a dipmeter log in MWX-3) suggest west to northwest paleoflow, although this direction is away from the interpreted paleoshoreline. A slight angling of the axis of the bed toward the northwest allows all three wells to be encompassed within the 200-ft (61 m) minimum width. Unit A is interpreted to be a channel deposit superimposed locally on unit B. Units A and B are probably unrelated and in plane view separate beyond the MWX site.

Unit B also is a channel sandstone, and its central part is penetrated by MWX-2 and MWX-3. Oriented crossbeds and dipmeter data indicate east to southeast paleoflow, the reverse of that for unit A. Overall channel trend is best estimated to be east to southeast, based on paleoflow vectors and the penetration of main channel deposits along the axis of MWX-2 and MWX-3.

The thickness of unit B is about 25 ft (7.6 m), as reconstructed by estimating the amount of the top of unit B removed by scour during superposition of unit A in MWX-2. This thickness yields a minimum width estimate of 300 ft (91 m).

Unit C is a splay or channel-margin deposit that consists primarily of rippled sandstone and siltstone in all three wells. Dipmeter data from MWX-3 suggest northeast paleoflow from a source southwest of MWX-2. This direction may be corroborated by the slightly thicker deposits of unit C in MWX-2.

The porosity and permeability of lenticular channel sandstones of the upper delta plain are typified by this composite reservoir (fig. 11). In general, both the porosity and permeability of the two main-channel units (A and B) decrease upward. The trends are not uniform but neither are they as erratic as those in the multistoried fluvial reservoirs discussed previously. Porosity and permeability decrease abruptly within the silty to muddy intervals near the top and base of the reservoir.

Porosity and permeability of unit A are slightly less than those of unit B, even in MWX-2 where the two units are directly superimposed. The multistory nature of the

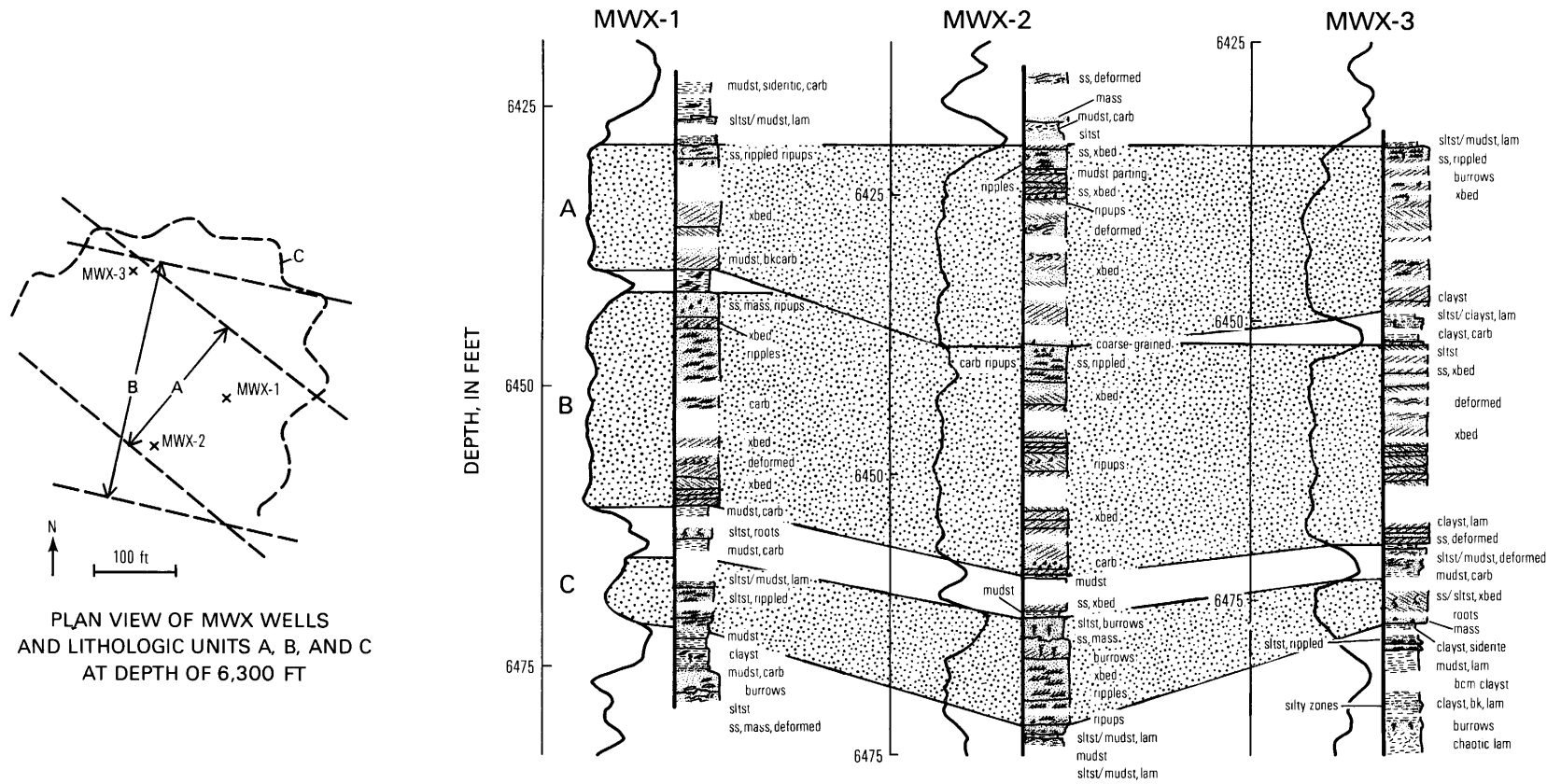


Figure 10. Detailed lithologic description of slabbed core and gamma-ray logs for a composite reservoir (pattern) in the upper delta-plain environment (coastal zone of Williams Fork Formation) in the MWX wells. The sandstone reservoir consists of two superimposed channel sandstones (units A and B) and an underlying thin splay deposit (unit C). Abbreviations: bk, black; carb, carbonaceous; clayst, claystone; lam, laminated; mass, massive; mudst, mudstone; sltst, siltstone; ss, sandstone; xbed, crossbedded.

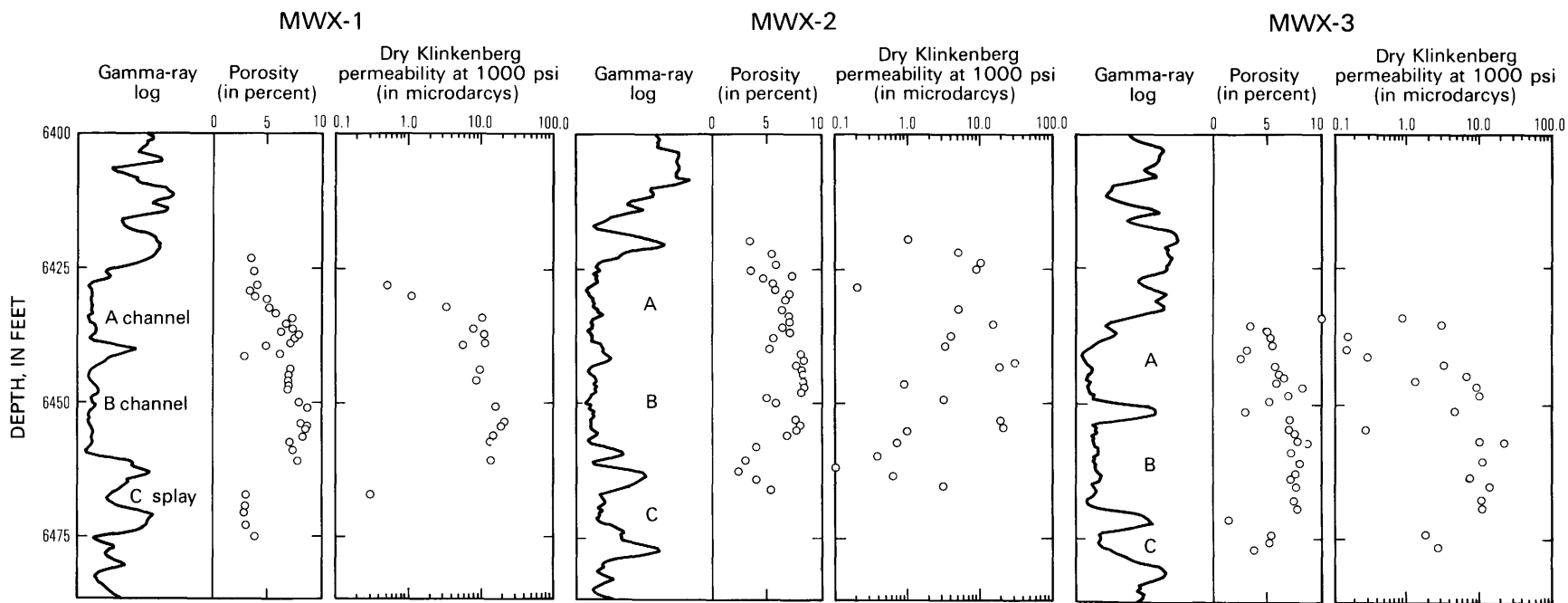


Figure 11. Porosity and permeability characteristics of upper delta-plain distributary-channel sandstone reservoirs in the Williams Fork Formation in the MWX wells. Reservoir quality is slightly less heterogeneous in these reservoirs than in the meander-belt reservoirs. Note logarithmic scale of permeability graphs.

reservoir would be difficult to detect in MWX-2 without core or without the adjacent wells, both of which show the two distinct sandstones. Average porosity in units A and B is 6–7 percent. Average dry Klinkenberg permeability, measured at 3,000 lb/in.² (20.7 MPa) net confining stress, is 3–5 microdarcys (A.R. Sattler, oral commun., 1986).

Examples of Lower Delta-Plain Reservoirs

An example of a lenticular distributary-channel reservoir, similar to the upper delta-plain reservoirs, is shown by the lower sandstone unit (zone 3) in figure 12. Core from MWX-2 shows a sequence of crossbedded and rippled sandstones and a few mudstones. This sequence, as well as basal scour surfaces and clay-ripup conglomerates, suggests penetration by the well of a main channel. Core from this interval in MWX-3 shows a similar but thinner sandstone body that probably is also part of the main channel but closer to its edge. This interval was not cored in MWX-1, but the gamma-ray log indicates a sandy main-channel sequence. The channel probably trends east-northeast, generally parallel with and centered on the line between MWX-1 and MWX-2 but encompassing MWX-3 at its edge. Based on its thickness of 28 ft (8.5 m), its minimum width should be about 350 ft (107 m).

The upper sandstone shown in figure 12 (zone 4) is a different type of lower delta-plain reservoir. Core of this interval from MWX-3 consists almost entirely of rippled and carbonaceous sandstones, without the cross-bedding indicative of main channels. This type of rippled sandstone occurs primarily in splays, the flood deposits adjacent to channels. The interval is split in MWX-2 by a coaly mudstone, and only the lower half of the interval was cored, but the core displays the thinly laminated and extensively burrowed deposits typical of the subaqueous distal edges of splays. The gamma-ray log from MWX-1 for the interval is similar in shape and thickness to that of MWX-3, and thus the interval is interpreted to be similar to the splay sandstones in MWX-3. The splay deposit thins rapidly in the direction of MWX-2, and the parent channel may be a few hundred feet to the north and east of the MWX wells.

Porosity and permeability characteristics of the lenticular reservoirs of the lower delta plain (paludal zone) are shown in figure 13 and are similar to those of the upper delta plain (coastal zone). The primary control on these petrophysical parameters is the sedimentology of the deposits (fig. 12). Porosity and permeability are low in the basal and upper zones of the reservoirs, where interbedded sandstone, siltstone, and mudstone form a heterogeneous lithology. They are higher and more uniform in the homogeneous and coarser grained crossbedded sandstones of the main-channel environment.

The reservoir characteristics of the splay deposits are significantly different and vary rapidly between the distal and mid-to proximal regions. Porosity in the distal regions of the typical splay (upper unit of MWX-2) (fig. 13) is uniformly low, and permeability of the interlaminated sandstone-mudstone deposit is too low to be measured. In the more proximal splay deposits, however, porosity and permeability are of reservoir quality through most of the sandstone; porosity is about 8–10 percent and Klinkenberg permeability is about 7 microdarcys at 2,000 lb/in.² (13.7 MPa) net confining stress (A.R. Sattler, oral commun., 1986). Reservoir quality decreases at the base and top and in a middle zone, where siltstone and mudstone are interbedded with the reservoir sandstone. The reservoir quality of the upper half of the splay deposit in MWX-3 is slightly better than that of the lower half. The upper and lower halves of this reservoir may have been deposited during different splay events or even from different channels, and the boundary between the two is marked by an interval of fine-grained sediments and poor reservoir quality. The two splay events deposited slightly different kinds of sediment, resulting in a composite reservoir having locally different properties.

SHORELINE-MARINE DEPOSITS

From the top of the Rollins Sandstone Member of the Iles Formation down to the Mancos Shale (7,455–8,350 ft, 2,270–2,545 m), the rocks of the Mesaverde Group in the MWX wells represent an irregularly cyclic series of environments, each cycle consisting (from the base up) of marine, shallow marine, shoreline, and paludal components (figs. 2, 14). The paludal zone previously described in the delta-plain section is actually the upper and considerably thickened component of the last of these cycles. The marine units are dark, fissile shales of the Mancos Shale, which were deposited offshore and below wave base in the interior seaway.

Irregularly coarsening upward shallow-marine deposits of thin-bedded shale, siltstone, and fine-grained sandstone overlie the Mancos Shale. This upward transition into the shoreline sandstone reservoirs is not well developed in the MWX wells, possibly because the sand may have been provided by longshore drift rather than from nearby distributary channels. A large volume of these deposits may therefore represent the interdeltic shoreface environments depicted in figure 1 rather than wave-dominated delta environments. Waves dispersed sand evenly along the shoreline, and progradation of the environments produced a blanket sandstone deposit.

In some places the cycle is completed by an uppermost coal-bearing paludal deposit, similar to that described previously. The upper sandstone of the Corcoran

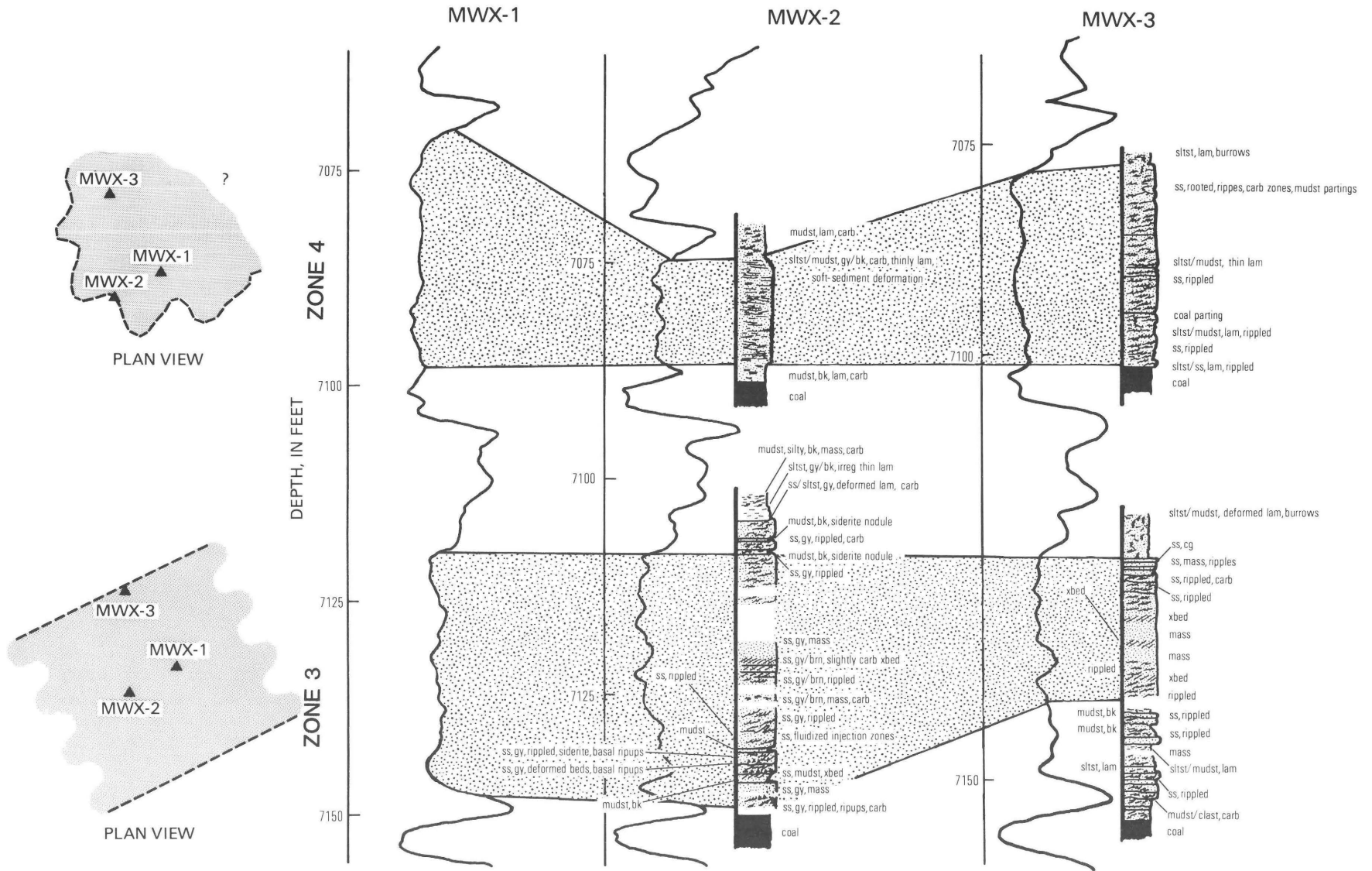


Figure 12. Detailed lithologic description of slabbed core and gamma-ray logs for a lenticular distributary-channel sandstone (zone 3) and a thick splay deposit (zone 4), both from the lower delta-plain environment of the Williams Fork Formation in the MWX wells. (No core was available for MWX-1.) Abbreviations: bk, black; brn, brown; carb, carbonaceous; cg, coarse grained; clayst, claystone; gy, gray; irreg, irregular; lam, laminations; mudst, mudstone; sltst, siltstone; ss, sandstone; xbed, crossbedded.

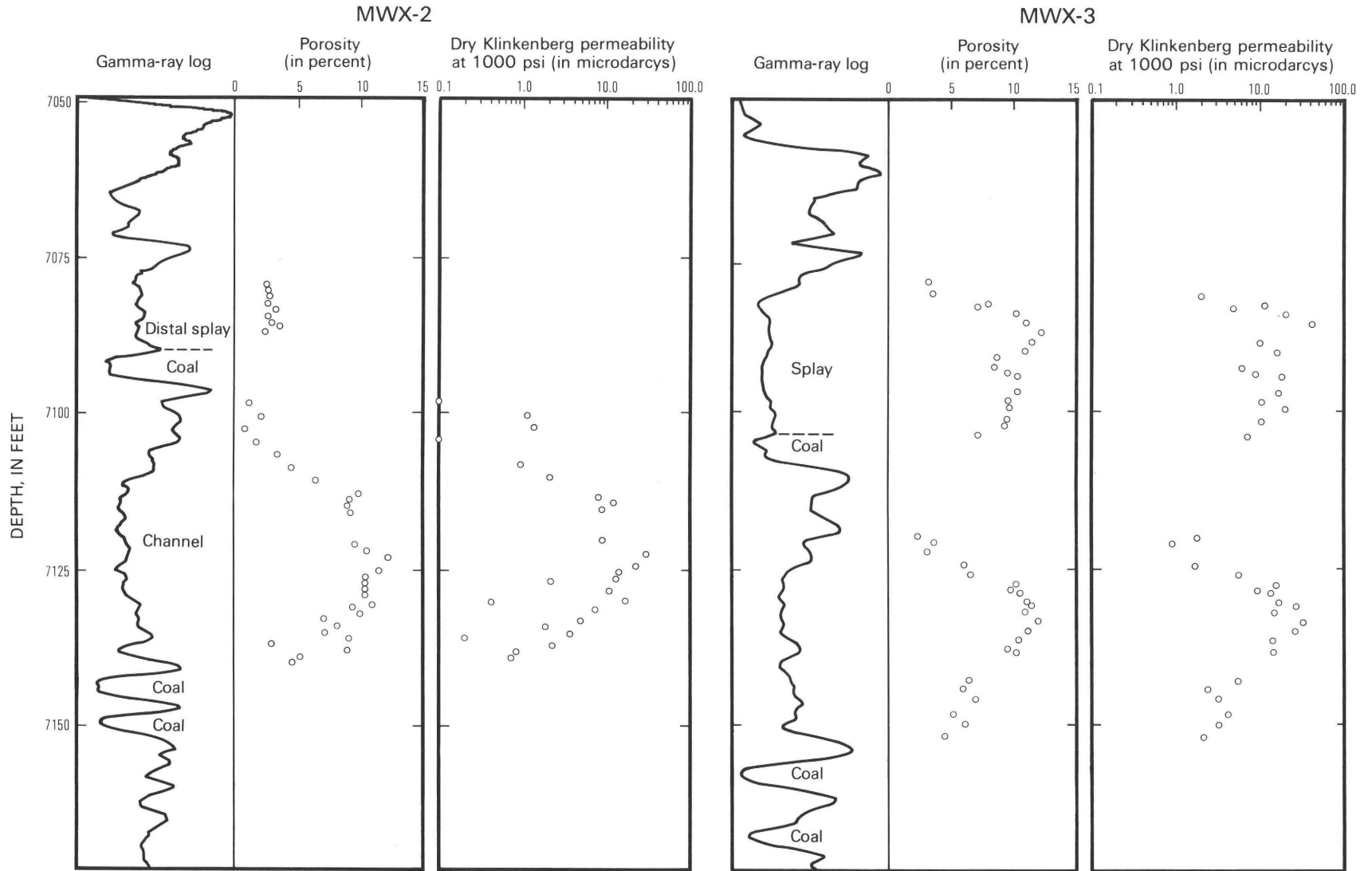


Figure 13. Porosity and permeability characteristics of a distributary-channel sandstone reservoir and a laterally variable splay sandstone reservoir in the lower delta-plain environment of the Williams Fork Formation in the MWX-1 and MWX-2 wells. Note logarithmic scale of permeability graphs.

Sandstone Member (fig. 14) in the MWX wells is in fact a laterally discontinuous distributary channel within lower delta-plain deposits. In other places at MWX (above the lower Corcoran and the upper Cozzette Sandstone Members), the ensuing marine transgression deposited marine shale directly above the shoreline sandstone.

Core of the Cozzette reservoir displays good shallow-marine and shoreline characteristics (fig. 15), including low-angle (possibly hummocky) crossbedding in well-sorted, fine-grained sandstone, and marine-type burrowing. Minor scour surfaces separate crossbed sets. The interval between the two sandstone units of the Cozzette Sandstone Member (fig. 15) consists of thin-bedded and burrowed shallow-marine shale, siltstone, and sandstone.

In this facies at MWX, reservoirs are limited to the thick, sandy shoreline deposits. These deposits are laterally extensive blanket-type sandstones that, for the most part, change little over a scale of miles. At the scale of spacing of the MWX wells, they have no axial trend and do not intersect. At MWX, the reservoirs are 30–100 ft (9–30.5 m) thick and are relatively homogeneous internally. Within the cored reservoir intervals, porosity and permeability are almost constant (fig. 16) and much more uniform than in the nonmarine sandstones. This uniformity results from well-sorted, clean sandstones that were reworked by and deposited in a wave-dominated, high-energy shoreline environment. Reservoir quality decreases in the lower part of each sandstone because of the increased siltstone and shale content associated with deeper marine environments. The heterogeneous sandstone-siltstone-shale lithofacies between the two sandstone units of the Cozzette Sandstone Member displays an erratic distribution of porosity and permeability.

Within the upper 20 ft (7.3 m) of the upper sandstone unit of the Cozzette Sandstone Member (fig. 16), porosity and permeability abruptly decrease to a slightly lower but still uniform level. More than half of the pore space within the sandstone of this interval is occupied by pyrobitumen (Pitman and Spencer, 1984). Water saturation increases by a factor of 2 to 3 in this zone of “cooked-out” oil, probably because of the retention of water by stronger capillary effects in the narrowed pores. This interval was not cored in MWX-1, but similar subtle changes in geophysical log response in MWX-1 and MWX-2 suggest that it is present there as well.

The shoreline reservoirs have no obvious lateral boundaries, but the presence of gas in the Corcoran and Cozzette Sandstone Members despite nearby outcrops suggests the existence of internal permeability barriers. Features such as the large-scale, seaward-dipping bedding planes noted by Balsley (1982) in excellent outcrops of similar rocks in the Book Cliffs of Utah or the updip relative permeability traps as described by Masters (1979) may have trapped the gas. High unstimulated production rates from these reservoirs at MWX (about a million cubic

feet per day) indicate the existence of an important natural fracture system (Lorenz and Finley, 1989).

The Rollins Sandstone Member presents an enigma in that it apparently does not contain gas despite its proximity to both coal beds and marine shale. The apparent lack of gas would suggest that the Rollins, the thickest of the blanket sandstones, has permeability continuity with the outcrops that occur as close as 12 mi (19 km) to the MWX site. However, the salinity of formation waters in the Rollins Sandstone Member is nominally marine, and the trend of overpressuring of the Mesaverde sequence is not interrupted at the Rollins; therefore, the zone is not a free-flowing aquifer with hydrologic continuity to meteoric waters. It may be that the clay content of the Rollins causes an erroneous log response indicating water saturation and this zone may in fact contain gas. It was not tested.

The interbedded mudstone and marine shale in this interval should provide good vertical permeability seals. Both the coals and the marine organic material within the marine shales are possible sources of gas, although measurements of geochemical parameters by D.D. Rice (U.S. Geological Survey, written commun., 1986) indicate that marine organic components are the principal source of gas in the Corcoran and Cozzette Sandstone Members at MWX.

Reservoirs in the Mancos Shale

Potential reservoir zones also may occur locally within the Mancos Shale, below the blanket-type shoreline-marine deposits. Offshore turbidite deposits derived from the Cretaceous shoreline during storm events are present elsewhere within the upper parts of the Mancos Shale (Balsley, 1982; Krystinik, 1983), and three types of offshore deposits were observed in the Mancos on the slopes of Mount Garfield, just east of Grand Junction on the western edge of the Piceance basin (fig. 17). These deposits previously have been either ignored, or briefly interpreted as remnants of recent landslide deposits (Lohman, 1965) or as remnants of a Pleistocene outwash terrace or pediment (Young and others, 1981). Unpublished microfossil data, however, indicate a Late Cretaceous age.

The potential reservoir facies within the Mancos Shale on Mount Garfield are composed of widespread thin beds of rippled and burrowed sandstone layers (unit A, fig. 17), large slump blocks of Mancos Shale (unit B, fig. 17), or less extensive lenses of millimeter- to meter-sized ripup clasts of Mancos Shale and larger blocks of sandstone in a silty mudstone matrix (unit C, fig. 17). These beds are slightly more resistant to erosion than the surrounding Mancos Shale and form a shelf that supports recent talus blocks of sandstone, which in turn further

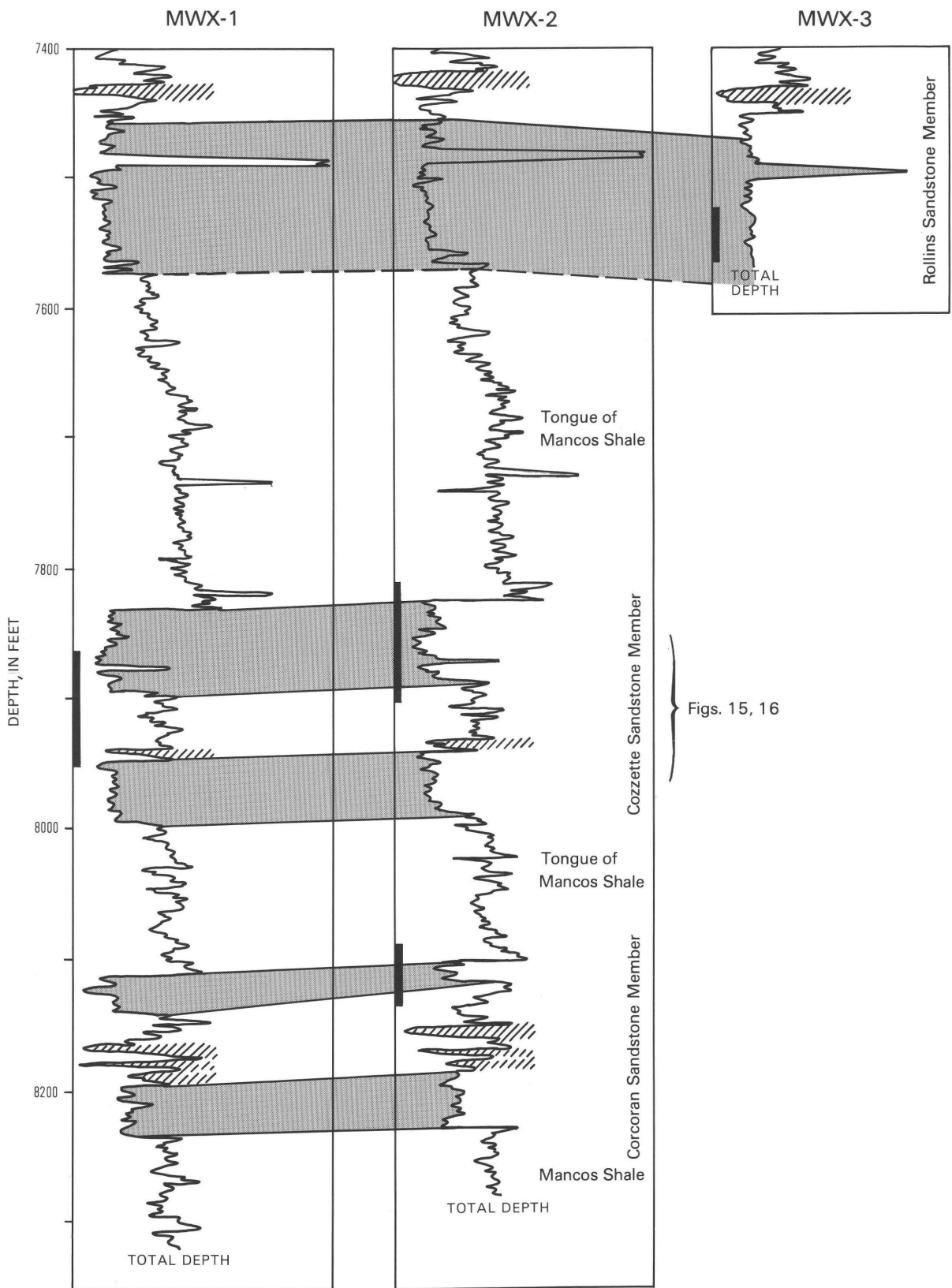


Figure 14 (facing page). Well-to-well gamma-ray log correlation of sandstones (pattern) in shoreline-marine interval of the Iles Formation of the Mesaverde Group in the MWX wells. Correlation of these widespread and uniform blanket-type sandstones is excellent, except for the upper sandstone unit of the Corcoran Sandstone Member, which is inferred to be a distributary channel. Solid bar indicates cored interval; hachures indicate coal beds; dashed line indicates tentative correlation.

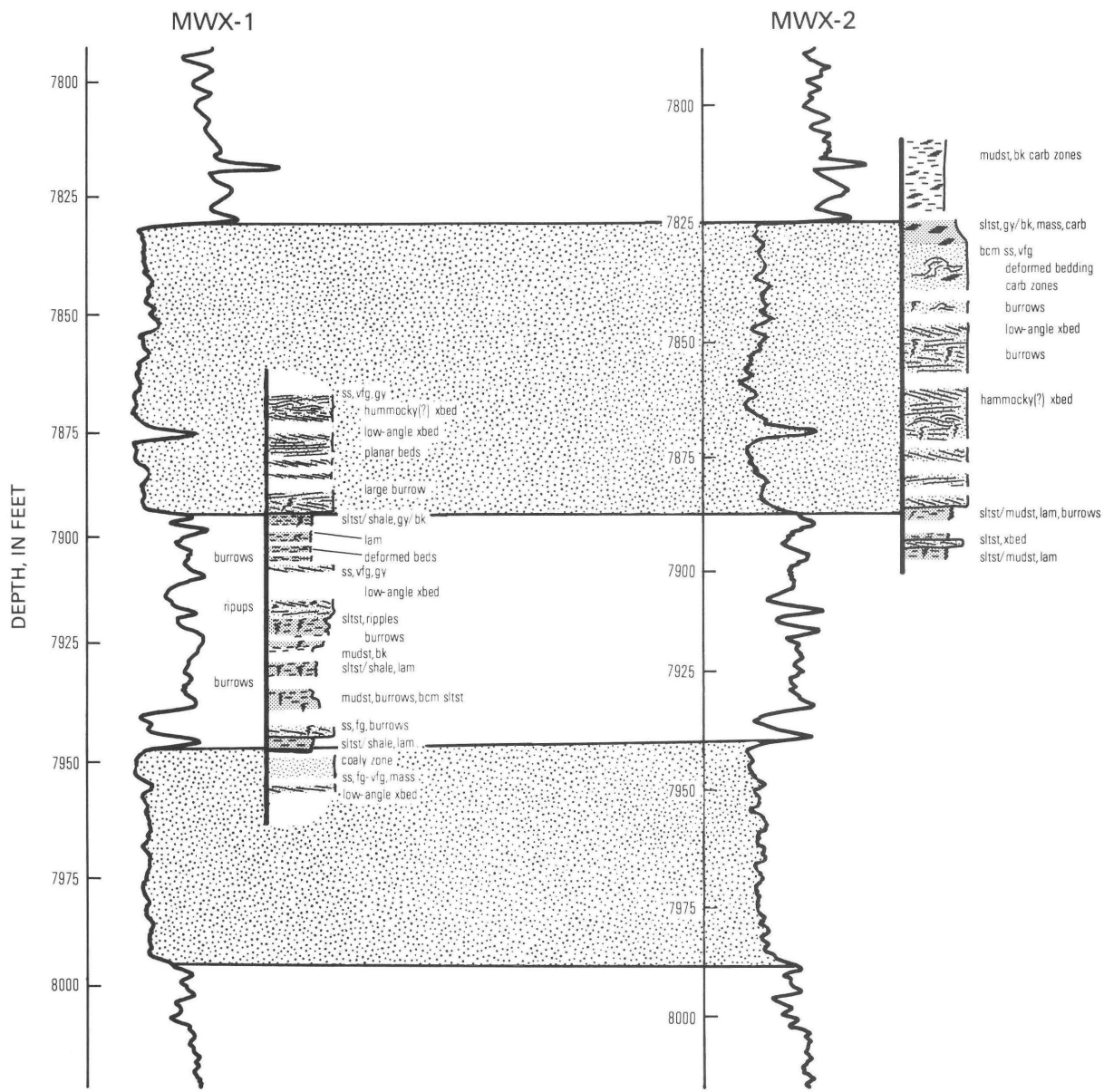


Figure 15. Detailed lithologic description of slabbed core and gamma-ray logs for the Cozzette Sandstone Member of the Iles Formation of the Mesaverde Group (pattern) in the MWX-1 and MWX-2 wells. Logs were correlated by using the top of the Cozzette Sandstone Member. Abbreviations: bcm, becomes; bk, black; carb, carbonaceous; fg, fine grained; gy, gray; lam, laminated; mass, massive; mudst, mudstone; sltst, siltstone; ss, sandstone; vfg, very fine grained; xbed, crossbedded.

increase the local erosional resistance. The beds are interpreted to represent submarine slump-block (unit B), submarine debris-flow (unit C), and distal turbidite environments (unit A) (Lorenz and Muhr, 1987).

Turbidite deposits have the greatest potential as reservoirs if their frequency, porosity, and permeability

are sufficient. The “Mancos B” productive interval of the Mancos Shale in the subsurface in the northwestern part of the basin may consist of similar deposits. Turbidite deposits have not been encountered in the MWX wells because little of the Mancos Shale was penetrated. Both the debris-flow and slump-block deposits have a

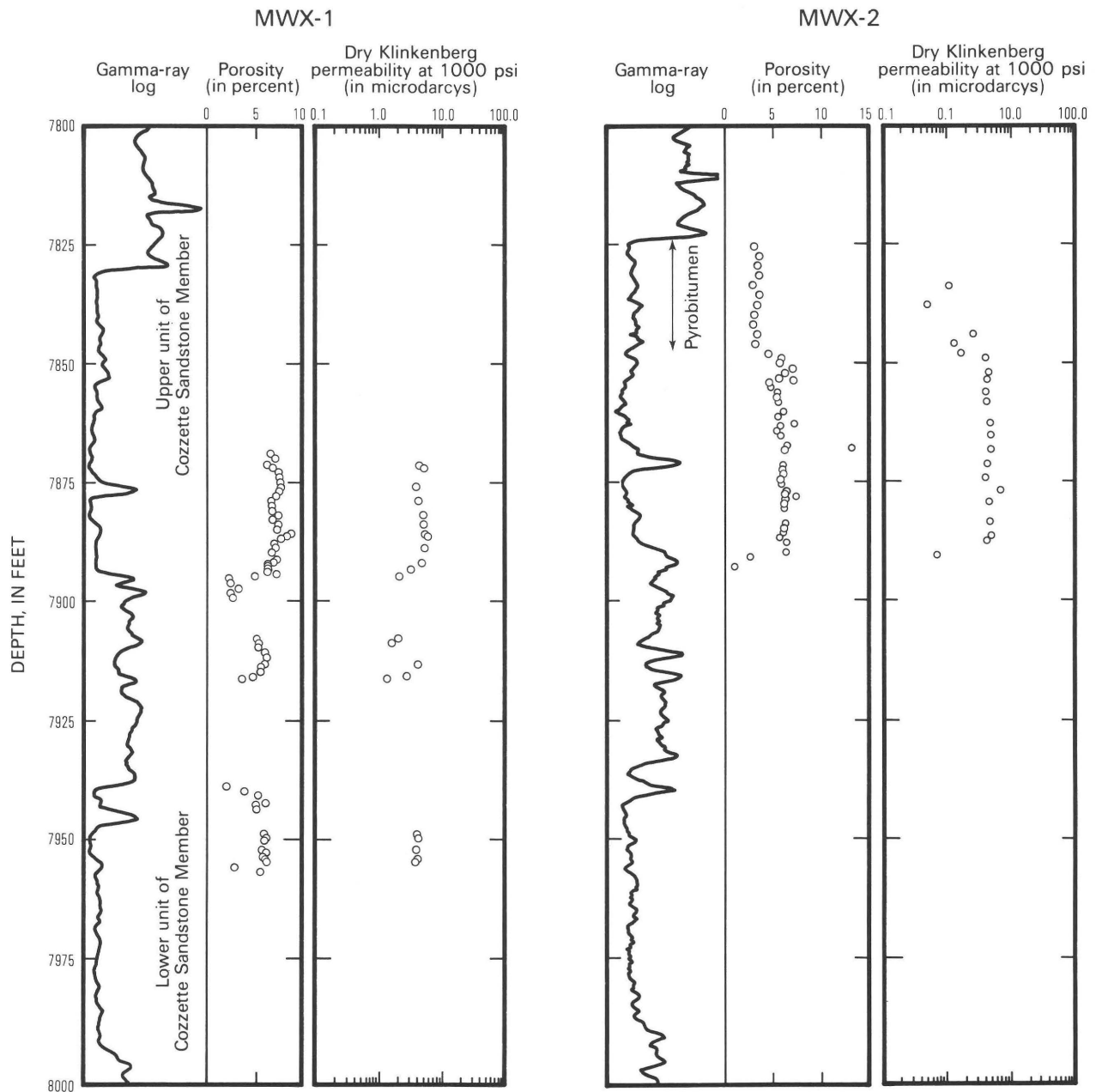


Figure 16. Porosity and permeability characteristics of blanket-marine sandstones (lower and upper sandstone units of Cozzette Sandstone Member of Iles Formation) in the MWX-1 and MWX-2 wells. Reservoir quality is relatively homogeneous as compared to that in overlying nonmarine sandstones. Note logarithmic scale of permeability graphs.

muddy matrix, and although in outcrop they are more fractured than the adjacent Mancos Shale, their reservoir potential may not be significantly greater than that of the shale.

SUMMARY

Three types of gas-bearing sandstone bodies were encountered in the MWX wells. Their reservoir morphologies are determined by the sedimentary environments

in which they were deposited. In the fluvial environment, highly irregular tabular-elongate reservoirs formed by amalgamation of point-bar deposits of meandering rivers. In the delta-plain environment, distributary channels deposited lenticular reservoirs that radiated out across the coastal plain. Near the shoreline, these channels traversed paludal environments and are interbedded with coal-swamp deposits. Splay deposits are also common in this environment.

The lowermost reservoirs at MWX were deposited during the initial regressions of the Cretaceous Interior

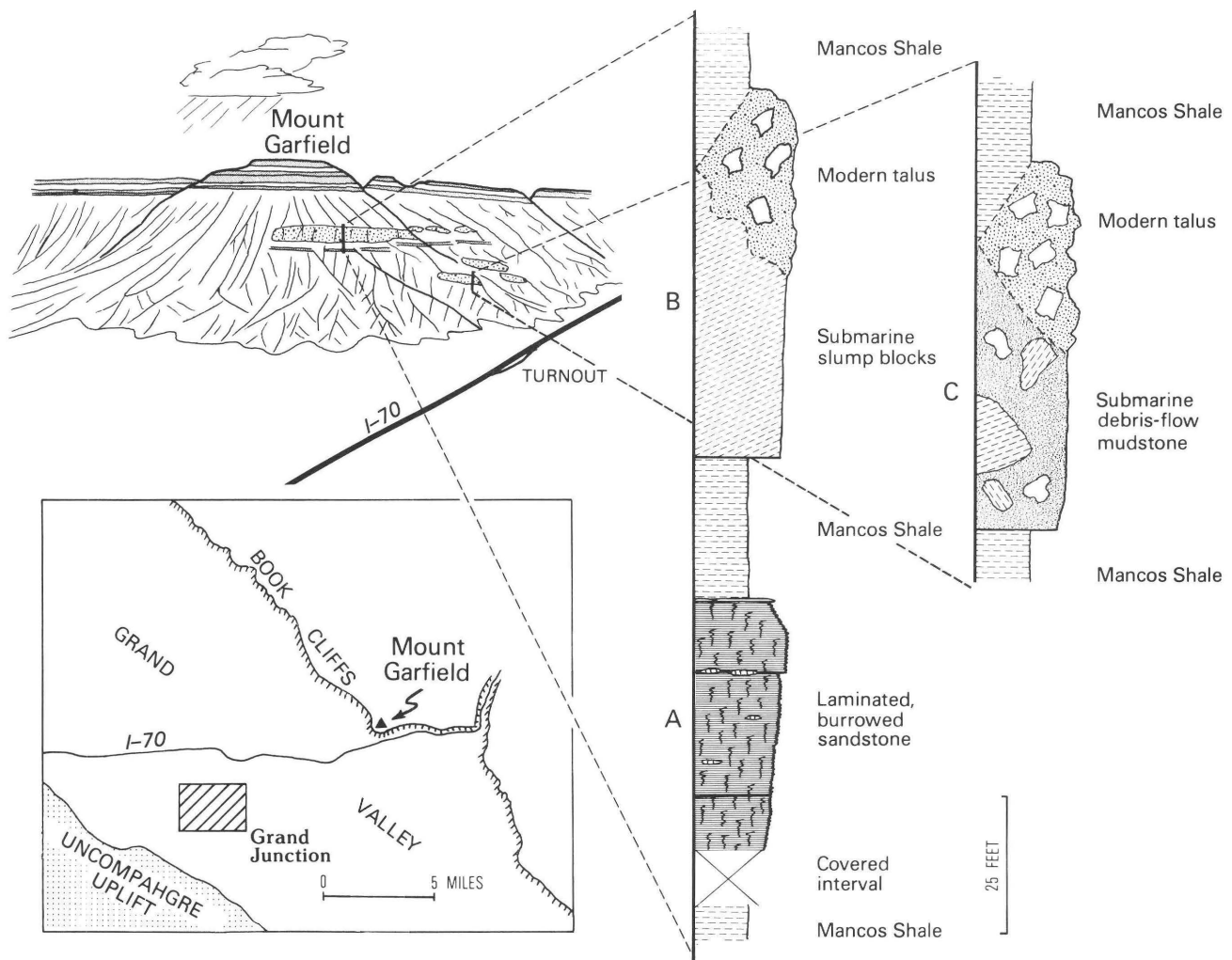


Figure 17. Offshore-marine deposits in the Mancos Shale along the Book Cliffs, east of Grand Junction, Colo. Inferred environments of deposition: A, submarine slump block; B, submarine debris flow; C, distal turbidite.

Seaway as shallow-marine and shoreline blanket sandstones in wave-dominated delta and coastline environments. Hydrocarbon traps in these reservoirs probably are internal permeability barriers associated with delta abandonment and reactivation.

Other potential Cretaceous reservoir facies in the Piceance basin include local turbidite sandstones in the Mancos Shale and flood-deposited sandstones in the non-marine parts of the Mesaverde Group. The uppermost unit of the Mesaverde Group, the Ohio Creek Member, may also be productive locally.

REFERENCES CITED

Balsley, J.K., 1982, Cretaceous wave-dominated delta systems; Book Cliffs, east-central Utah: American Association of Petroleum Geologists, 219 p.

Collins, B.A., 1976, Coal deposits of the Carbondale, Grand Hogback, and southern Danforth Hills coal fields, eastern Piceance Basin, Colorado: Colorado School of Mines Quarterly, v. 71, no. 1, 138 p.

Finley, S.J., and Lorenz, J.C., 1989, Characterization of natural fractures in Mesaverde reservoirs at the Multiwell Experiment site: Society of Petroleum Engineers Joint Rocky Mountain Regional Meeting and Low-Permeability Reservoir Symposium, Denver, Colo., 1989, SPE Proceedings 19007, p. 721-728.

Fisher, W.L., and McGowen, J.H., 1969, Depositional systems in the Wilcox Group (Eocene) of Texas and their relationship to occurrence of oil and gas: American Association of Petroleum Geologists Bulletin, v. 53, no. 1, p. 30-54.

Jones, J.R., Jr., 1984, Reservoir characterization of Mesaverde (Campanian) bedload fluvial meanderbelt sandstones, northwestern Colorado [abs.]: American Association of Petroleum Geologists Bulletin, v. 68, no. 4, p. 493.

- Jones, J.R., Jr., Scott, A.J., and Lake, L.W., 1984, Reservoir characterization for numerical simulation of Mesaverde meander belt sandstone, northwestern Colorado: Society of Petroleum Engineers Annual Technical Conference and Exhibition, 59th, Houston, Tex., 1984, SPE Proceedings 13502, 14 p.
- Krystinik, L.F., 1983, Turbidite fans in Upper Cretaceous Pierre Shale, Eagle Basin, Colorado; a new reservoir facies [abs.]: American Association of Petroleum Geologists Bulletin, v. 67, no. 3, p. 498.
- Lohman, S.W., 1965, Geology and artesian water supply of the Grand Junction area, Colorado: U.S. Geological Survey Professional Paper 451, 149 p.
- Lorenz, J.C., 1985a, Small-scale lateral variation in non-channel fluvial deposits, Mesaverde Formation, Colorado: International Fluvial Sedimentology Conference, 3rd, Fort Collins, Colo., 1985, Abstracts Volume, p. 26.
- _____, 1985b, Predictions of size and orientations of lenticular reservoirs in the Mesaverde Group, northwestern Colorado: Society of Petroleum Engineers/Department of Energy Joint Symposium on Low Permeability Reservoirs, Denver, Colo., 1985, Proceedings, p. 23-31.
- Lorenz, J.C., Branagan, P., Warpinski, N.R., and Sattler, A.R., 1989, Fracture characteristics and reservoir behavior of stress-sensitive fracture systems in flat-lying lenticular formations: Journal of Petroleum Engineering, v. 41, no. 6, p. 615-622.
- Lorenz, J.C., and Finley, S.J., 1989, Differences in fracture characteristics and related production of natural gas in different zones of the Mesaverde Formation, northwestern Colorado: Society of Petroleum Engineers Formation Evaluation, v. 4, p. 11-16.
- Lorenz, J.C., Heinze, D.M., Clark, J.A. and Searls, C.A., 1985, Determination of widths of meander-belt sandstone reservoirs from vertical downhole data, Mesaverde Group, Piceance Creek basin, Colorado: American Association of Petroleum Geologists Bulletin, v. 69, no. 5, p. 710-721.
- Lorenz, J.C., and Muhr, C.A., 1987, Submarine debris-flow, slump-block, and turbidite deposits in Mancos Shale (Cretaceous) of northwestern Colorado [abs.]: American Association of Petroleum Geologists Bulletin, v. 71, no. 5, p. 585.
- Lorenz, J.C., and Rutledge, A.K., 1985a, Facies relationships, reservoir potential of Ohio Creek interval across the Piceance Creek basin: Oil and Gas Journal, v. 83, p. 91-96.
- _____, 1985b, Facies relationships and reservoir potential of the Ohio Creek interval across the Piceance Creek basin, northwestern Colorado: Sandia National Laboratories Report SAND84-2610, 52 p.
- _____, 1987, Description of the Late Cretaceous Mesaverde Group outcrops at Rifle Gap, Piceance Creek basin, northwestern Colorado: Geological Society of America Centennial Field Guide 2, p. 307-310.
- Lorenz, J.C., Sattler, A.R., and Stein, C.L., 1989, Differences in reservoir characteristics of marine and nonmarine sandstones of the Mesaverde Group, northwestern Colorado: Sandia National Laboratories Report SAND 88-1963.
- Lorenz, J.C., and Smock, K., 1986, 3-D Characterization of fractures in Mesaverde reservoirs: or why the sugar cube reservoir model doesn't always work [abs.]: American Association of Petroleum Geologists Bulletin, v. 70, no. 5, p. 613.
- Lorenz, J.C., Warpinski, N.R., Teufel, L.W., Branagan, P.T., Sattler, A.R., and Northrop, D.A., 1988, In situ stresses, natural fractures, and other geologic controls on reservoirs: EOS, v. 69, p. 817, 825-826.
- Masters, J.A., 1979, Deep basin gas trap, western Canada: American Association of Petroleum Geologists Bulletin, v. 63, p. 152-181.
- Pitman, J.K., and Spencer, C.W., 1984, Petrology of selected sandstones in the MWX wells (northwest Colorado) and its relationship to borehole geophysical-log analysis and reservoir quality, in Spencer, C.W., and Keighin, C.W., eds., Geologic studies in support of the U.S. Department of Energy Multiwell Experiment, Garfield County, Colorado: U.S. Geological Survey Open-File Report 84-757, p. 33-66.
- Scott, A.J., Hoover, R.A., and McGowen, J.H., 1969, Effects of Hurricane "Beulah," 1967, on Texas coastal lagoons and barriers: UNAM-UNESCO Symposium, 1969, Lagunas Costeras, Mexico, p. 221-226.
- Young, R.G., Keighin, C.W., and Campbell, J.A., 1981, Second day; road log from Grand Junction to Glenwood Canyon and return to Grand Junction, in Epis, R.C., and Callender, J.F., eds., Western Slope, Colorado, western Colorado and eastern Utah: New Mexico Geological Society Field Conference, 32nd, Guidebook, p. 17-28.

Chapter L

Thermal History of Selected Coal Beds in the Upper Cretaceous Mesaverde Group and Tertiary Wasatch Formation, Multiwell Experiment Site, Colorado, In Relation to Hydrocarbon Generation

By VITO F. NUCCIO and RONALD C. JOHNSON

Prepared in cooperation with the U.S. Department of Energy

U.S. GEOLOGICAL SURVEY BULLETIN 1886

GEOLOGY OF TIGHT GAS RESERVOIRS IN THE PINEDALE ANTICLINE AREA, WYOMING,
AND AT THE MULTIWELL EXPERIMENT SITE, COLORADO

CONTENTS

Abstract	L1
Introduction	L1
Vitrinite reflectance profile for the MWX site	L2
Present-day temperatures at MWX	L2
Burial reconstruction of the Mesaverde Group at the MWX site	L2
Thermal histories for the six coals	L4
TTI modeling	L5
Source-rock potential and hydrocarbon-generation thresholds	L5
Results and discussion	L5
References cited	L7

FIGURES

1. Vitrinite reflectance profile for MWX site L2
- 2-3. Temperature logs for MWX-1 well, as measured by:
 2. Los Alamos National Laboratories L3
 3. Southern Methodist University L3
4. Diagram showing burial history for coals from Mesaverde Group and Wasatch Formation L4

TABLES

- 1-3. Results of TTI modeling at MWX site using:
 1. Maximum bottom-hole temperature of 244 °F (118.7 °C) for coals from Mesaverde Group and Wasatch Formation L6
 2. Maximum bottom-hole temperature of 266 °F (131 °C) for coals from Mesaverde Group and Wasatch Formation L6
 3. Geothermal gradient that best fits both predicted TTI values and measured Rm values for coals from Mesaverde Group and Wasatch Formation L6

Thermal History of Selected Coal Beds in the Upper Cretaceous Mesaverde Group and Tertiary Wasatch Formation, Multiwell Experiment Site, Colorado, In Relation to Hydrocarbon Generation

By Vito F. Nuccio and Ronald C. Johnson

Abstract

The burial and thermal histories of six coal beds in the Upper Cretaceous Mesaverde Group and Tertiary Wasatch Formation at the Multiwell Experiment (MWX) site in northwest Colorado were reconstructed and the timing of certain hydrocarbon-generation thresholds estimated by using time-temperature index (TTI) modeling. The thermal history reconstruction assumes that paleogeothermal gradients are the same as the present-day geothermal gradient. Two downhole temperature surveys were run at the site; however, these logs recorded somewhat different geothermal gradients and maximum bottom-hole temperatures. These differences probably result from different operators and instruments, not differences in equilibration times, because the surveys were conducted at approximately the same time. TTI values were calculated for each of the two surveys and vitrinite reflectance (Rm) values predicted by using TTI models were compared with measured values for each coal. Predicted vitrinite reflectance values for both temperature surveys are systematically higher than measured vitrinite reflectance values for the Mesaverde coals but lower than the measured value for the Wasatch coal, and we present a model that best fits a geothermal gradient to our measured vitrinite reflectance values.

Three hydrocarbon-generation thresholds were used: the onset of oil generation (TTI 10, 0.60 percent Rm), the beginning of gas generation (TTI 25, 0.73 percent Rm), and the point at which oil becomes unstable and breaks down to methane gas (TTI 180, 1.35 percent Rm). Each of the geothermal gradients yields different timing for the thresholds, yet all timings fall within a fairly narrow range. The stratigraphically shallowest coal achieved an Rm of 0.60 percent about 10 Ma and the stratigraphically deepest coal achieved an Rm of 0.60 percent between 51 and 49 Ma, an Rm of 0.73 percent between 49 and 46 Ma, and an Rm of 1.35 percent between 45 and 37 Ma.

Overestimation of Rm values for the Mesaverde Group coals and underestimation for the Wasatch coal predicted by using the TTI model may result from: (1) operator and laboratory bias in measuring vitrinite reflectance, (2) errors in reconstruction of burial history, (3) a recent increase in the heat

flow of the area, (4) "kinks" in the Rm curve resulting from heat transfer processes, or (5) problems in comparing TTI values with measured Rm values.

INTRODUCTION

Reconstructions of the burial and thermal histories of the area around the Multiwell Experiment (MWX) site in northwest Colorado (Law and Johnson, this volume, fig. 6) have recently been made (Bostick and Freeman, 1984; Johnson and Nuccio, 1984, 1986; Nuccio and Johnson, 1984), but, as yet, the petroleum generation history at the site has not been reconstructed. We present results of mean random vitrinite reflectance measurements (Rm) for six coals from the Upper Cretaceous Mesaverde Group and Tertiary Wasatch Formation at the MWX site, reconstruct their burial history, and use time-temperature index modeling (TTI) of the selected coals to reconstruct the petroleum generation history of Upper Cretaceous and Tertiary rocks at the MWX site.

Vitrinite reflectance measures the maximum level of thermal maturation of a rock, and TTI modeling (Waples, 1980) aids in estimating the timing of thermal maturation and hence the timing of hydrocarbon generation in the past. Geothermal gradients calculated from two different temperature logs measured at the MWX site were used in the TTI modeling, and vitrinite reflectance values predicted by using these two thermal gradients are compared with those measured on samples from the MWX wells. Using present-day geothermal gradients, TTI reconstructions significantly overestimate vitrinite reflectance values for the Mesaverde coals and underestimate the value for the Wasatch coal, so a geothermal gradient that best fits predicted values with our measured values is presented for each coal.

VITRINITE REFLECTANCE PROFILE FOR THE MWX SITE

Vitrinite reflectance data for the MWX site is available from Amoco Production Company (unpublished data), Bostick and Freeman (1984), and our measurements. We measured vitrinite reflectance on coal samples from core from the MWX-1 and MWX-2 wells, on shale cuttings from the Wasatch Formation in the MWX-3 well, and on coal from a Wasatch surface outcrop sample.

The coal was crushed and mounted in epoxy, then planed off and polished. Composite samples of shale required maceration, a technique used to extract the organic matter from a rock sample. The reflectance of randomly oriented vitrinite grains was measured under oil immersion by using reflected-light microscopy, and mean reflectance values were calculated from large sample populations (as many as 135 selected vitrinite grains) for several of the samples. The vitrinite reflectance profile (fig. 1) shows that values from all three sources agree fairly well, although our values are generally slightly lower than those of both Bostick and Freeman (1984) and Amoco (unpublished data), and those of Bostick and Freeman are generally lower than those of Amoco. These differences probably result from laboratory and operator bias. The Amoco data show some scatter in the interval between about 5,400 and 6,200 ft (1,646–1,890 m). In this interval, coal is scarce and the reflectance of vitrinite from carbonaceous shale was measured. Individual shale samples commonly have a greater range of vitrinite values than do coals, and the data show more scatter in profile. In this paper, we use R_m values; they range from 0.60 percent at the surface to 1.94 percent at 7,950 ft (2,423 m). A change in slope in the vitrinite reflectance profile occurs at about 4,500 ft. This break is coincident with, but not necessarily a result of, the Cretaceous-Tertiary boundary and will be discussed later.

PRESENT-DAY TEMPERATURES AT MWX

Two temperature logs were measured at the MWX-1 well about 7 months after circulation of drilling fluids ended. In the first log (fig. 2), measured by Los Alamos National Laboratory, a maximum bottom-hole temperature of 244 °F (118 °C), corresponding to a geothermal gradient of 2.37 °F/100 ft (43.5 °C/km), was measured. In the second log (fig. 3), measured by Southern Methodist University, a maximum bottom-hole temperature of 266 °F (131 °C), corresponding to a geothermal gradient of 2.63 °F/100 ft (48.4 °C/km), was recorded. By comparison, bottom-hole temperatures of 200 °F (94.1 °C) were recorded during some of the original logging runs shortly after circulation ended.

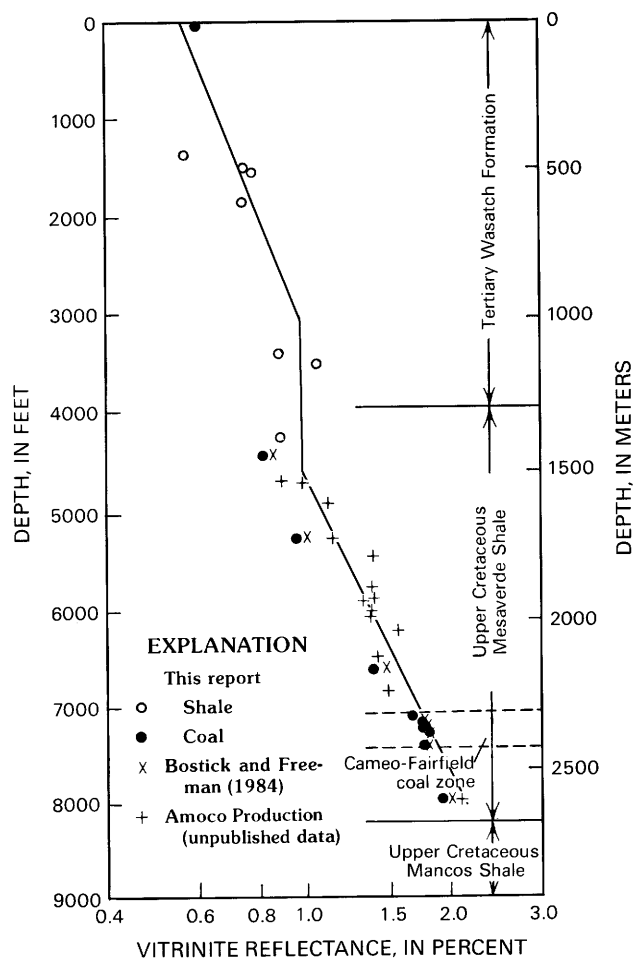


Figure 1. Vitrinite reflectance profile for the MWX site.

Both temperature logs show a distinct change in slope (increase in thermal gradient) through the Cameo-Fairfield coal zone of the Williams Fork Formation of the Mesaverde Group between depths of 7,040 and 7,400 ft (2,146–2,256 m) that corresponds to differences in thermal conductivity between carbonaceous shale and coal and the enclosing sandstone and shale. The logs were measured at about the same time, and variations resulting from equilibration are not a factor. Much of the variation between the two logs results from different operators and equipment.

BURIAL RECONSTRUCTION OF THE MESAVERDE GROUP AT THE MWX SITE

A detailed burial history of the MWX site was recently presented by Johnson and Nuccio (1986). The MWX site is in the Colorado River canyon, and much of the evidence for the burial history of the MWX site can be determined by studying exposures on the nearby

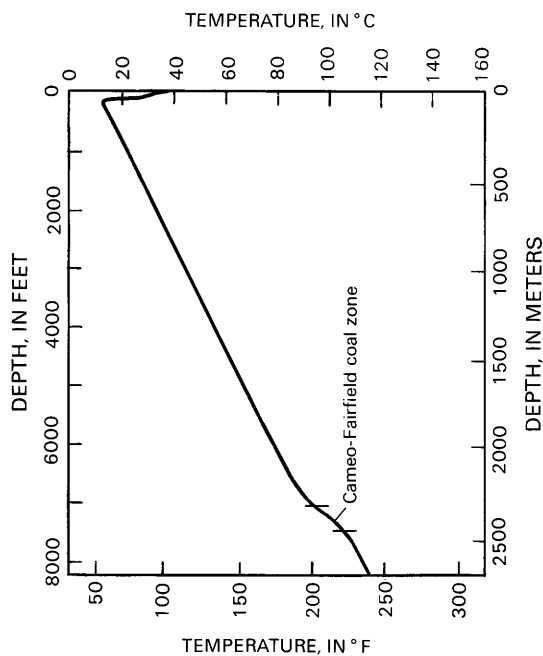


Figure 2. Temperature log for the MWX-1 well, as measured by Los Alamos National Laboratories (E.H. Horton, written commun. to N.H. Bostick, U. S. Geological Survey, 1982). Note maximum bottom-hole temperature of 244 °F (118.7 °C) and kink in gradient through Cameo-Fairfield coal zone.

canyon walls. The burial history of the six coals in this study is divided into seven time intervals (fig. 4): 74–66 Ma, 66–60 Ma, 60–50 Ma, 50–46 Ma, 46–35 Ma, 35–10 Ma, and 10 Ma to present.

From 74 to 66 Ma (late Campanian through Maestrichtian time), the MWX area was subsiding and the Upper Cretaceous Mesaverde Group was deposited. The rate of subsidence can be estimated by dividing the thickness of Mesaverde rocks by the approximate length of time of deposition. Between 66 and 60 Ma, a hiatus (represented by an unconformity) occurred at the top of the Mesaverde. Although erosion was significant in other parts of the Piceance basin, it probably was not significant near the structural trough of the basin where the MWX site is located, and the reconstruction presented in this paper does not include any erosion at MWX during this time period. Subsidence resumed during the period of 60 to 50 Ma, and about 5,225 ft (1,593 m) of sediment was deposited on the unconformable surface. The end of this time period is represented by the Long Point bed of the Eocene Green River Formation. From 50 to 46 Ma, an additional 2,200 ft (670 m) of lacustrine Green River Formation was deposited. The end of this interval is represented by the top of the Mahogany oil-shale ledge of the Green River Formation. The next time interval spans the period from 46 Ma (Eocene) to the end of basin subsidence at about 35 Ma (Oligocene).

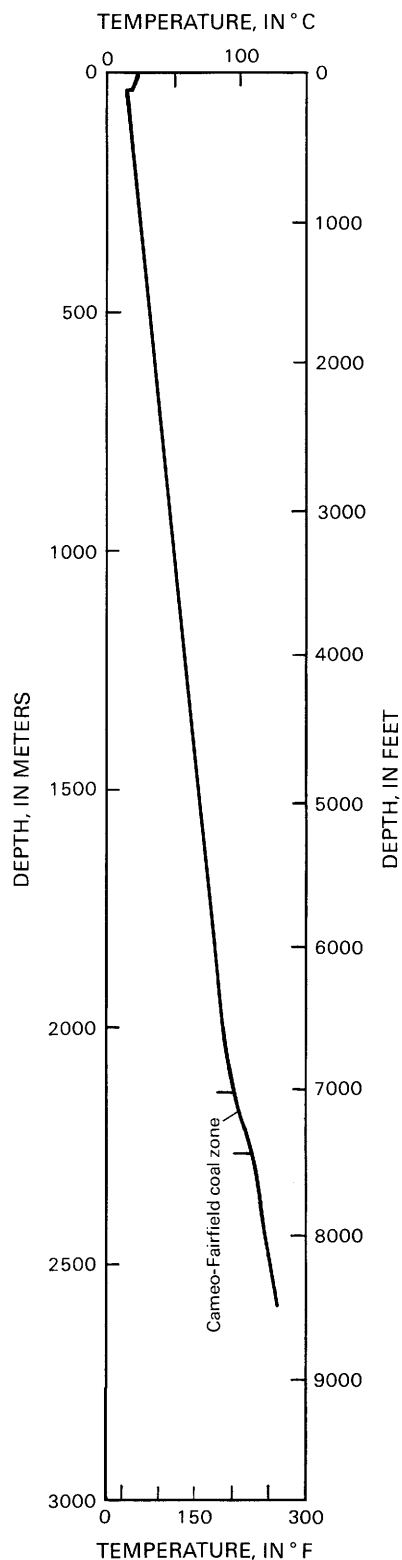


Figure 3. Temperature log for the MWX-1 well, as measured by Southern Methodist University (D.D. Blackwell, written commun. to A.R. Sattler, Los Alamos National Laboratories, 1982). Note maximum bottom-hole temperature of 266 °F (131 °C) and kink in gradient through Cameo-Fairfield coal zone.

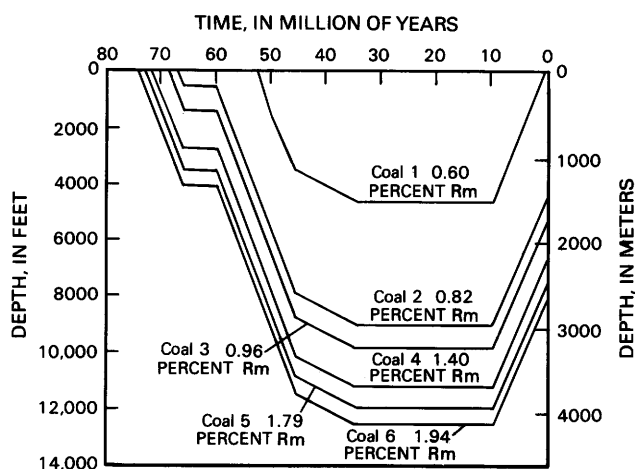


Figure 4. Burial history for coals from the Mesaverde Group (samples 2–6, tables 1–3) and Wasatch Formation (sample 1, tables 1–3). Rm is measured vitrinite reflectance (in percent).

Approximately 1,075 ft (328 m) of upper Eocene Green River Formation and Uinta Formation is preserved above the Mahogany ledge and beneath an erosion surface that is capped by a ledge of 9.7 ± 0.5 -million-year-old basalts (Marvin and others, 1966). During the latest Eocene and early Oligocene, widespread erosion occurred across much of the Rocky Mountain region (Epis and Chapin, 1975; Larson and others, 1975; Tweto, 1975; Hansen, 1984). The erosion surface beneath the basalts is thought to be part of this widespread complex of late Eocene-early Oligocene erosion surfaces (Larson and others, 1975; Johnson and Nuccio, 1986). If this is the case, then little sedimentation or erosion occurred in the MWX area between about 35 Ma, when the surface developed, and 9.7 Ma, when the basalts were deposited. The thickness of upper Eocene or possibly lower Oligocene rocks eroded during the development of this erosion surface is not known. Johnson and Nuccio (1986) suggested that during this time period erosion in the Piceance basin decreased from the basin margins inward and essentially no rock was removed near the axis of the basin where the MWX site is located. Regional uplift and erosion began about 10 Ma and has continued until the present. Approximately 4,600 ft (1,402 m) of section has been removed, and our reconstruction assumes that erosion has occurred at a constant rate.

THERMAL HISTORIES FOR THE SIX COALS

Present-day geothermal gradients were used to reconstruct the thermal history of coals from six stratigraphic levels in the Mesaverde Group and Wasatch Formation. The coals were collected both at the surface and to a depth of 4,050 ft (1,234 m) below the top of the

Mesaverde. The thermal histories of the coals were used to predict both present-day ranks of the coals and timing of hydrocarbon generation by using the model of Waples (1980). For our calculations, we assume that heat flow has been constant through time and that the low thermal conductivity in the Cameo-Fairfield coal zone, as indicated by temperature logs (figs. 2, 3), is the same as that in the past. Separate geothermal gradients were calculated for the two temperature logs measured at MWX-1. We assume that the thermal gradient for the 4,600 ft (1,402 m) of section eroded from the MWX site during the last 10 million years is the same as that measured through the 3,900 ft (1,189 m) of Wasatch Formation that overlies the Mesaverde Group at the MWX site. The thermal gradient through this interval is $2.12 \text{ }^\circ\text{F}/100 \text{ ft}$ ($38.6 \text{ }^\circ\text{C}/\text{km}$) in the LANL survey (fig. 2) and $2.22 \text{ }^\circ\text{F}/100 \text{ ft}$ ($40.6 \text{ }^\circ\text{C}/\text{km}$) in the SMU survey (fig. 3). Only about 1,325 ft (404 m) of the eroded section consisted of Wasatch Formation; the remaining 3,275 ft (998 m) consisted of about 2,700 ft (823 m) of Green River Formation and 575 ft (175 m) of Uinta Formation. The lithology of the lower 2,150 ft (655 m) of Green River Formation and the 575 ft (175 m) of Uinta Formation is generally similar to that of the Wasatch Formation and consists of interbedded sandstone, siltstone, claystone, and marlstone. The thermal conductivities of these intervals probably are similar to those of the underlying Wasatch Formation. The upper 550 ft (168 m) of the Green River Formation, however, consists mostly of oil shale, the thermal conductivity of which varies widely with different organic matter contents (DuBow and others, 1977) but is significantly lower than that of the typical mixed sandstone, siltstone, and shale section. If thermal gradients in the oil shale section are significantly higher than those in the underlying section, then temperatures in the Mesaverde Group at the MWX site at maximum burial may be underestimated by $10 \text{ }^\circ\text{F}$ ($6 \text{ }^\circ\text{C}$) or more.

The computer program used to calculate the TTI index of Waples could not accommodate variations in geothermal gradient with depth, such as those observed through the Cameo-Fairfield coal zone. This did not affect our calculations of TTI for coals above the Cameo-Fairfield coal zone because the geothermal gradient is relatively constant from the coal zone to the surface, but it did slightly affect TTI calculations for coals within the coal zone and below. If a constant gradient is assumed for the entire section, then the TTI value for the period of maximum burial between 35 and 10 Ma is slightly higher than actual TTI values obtained for those intervals when the basin was subsiding or being uplifted. The period of maximum burial and temperature between 35 and 10 Ma is by far the most significant number in the total TTI calculation for the coals, and the error induced by assuming a constant gradient is not significant.

TTI MODELING

The thermal history of the MWX site was reconstructed by using a slightly modified version (Waples, 1980) of Lopatin's time-temperature index (TTI) (Lopatin, 1971). We propose that the coals reached their maximum level of thermal maturity at the end of maximum burial, about 10 Ma. We calculated TTI values only to 10 Ma because after this time, temperatures began to drop as a result of uplift and erosion. The TTI model is one method of predicting when formations such as the Mesaverde and Wasatch entered or passed through oil and gas generation limits. In the TTI model, time and temperature are interchangeable and given sufficient time a relatively low temperature can produce a high level of maturity. No single temperature, therefore, can be assigned to a vitrinite reflectance value. It should be noted that a second time-independent model postulates that time does not have a significant effect on thermal maturity and that relatively soon (geologically speaking) after maximum temperature is attained organic matter stabilizes and reactions cease (Neruchev and Parparova, 1972; Barker, 1983; Price, 1983). If this second model is correct, then indicators of thermal maturity such as vitrinite reflectance can be used as absolute paleogeothermometers. Nuccio and Johnson (1984) suggested that at the MWX site inconsistencies exist with respect to both models because of problems in determining paleogeothermal gradients, but Bostick and Freeman (1984) concluded that the time-dependent model correlates more closely with vitrinite reflectance data. It is beyond the scope of this paper to debate the two models, and we used the TTI model and geothermal gradients calculated from temperature logs to estimate the timing of important thermal events at the MWX site.

SOURCE-ROCK POTENTIAL AND HYDROCARBON-GENERATION THRESHOLDS

In general, organic matter can be divided into three types: type I, sapropelic or fatty; type III, humic or coaly; and type II, intermediate between types I and III. Sapropelic organic matter is hydrogen rich; it occurs principally in rocks of marine origin and generates oil with some gas during thermal maturation. Humic organic matter is hydrogen poor and oxygen rich; it occurs mostly in nonmarine rocks and generates methane gas during maturation. Type II organic matter can be a source for both oil and gas (Tissot and others, 1974).

At the MWX site, the Mesaverde Group contains a basal marginal-marine section but is primarily a fluvial and deltaic section. The marginal-marine section, or Iles Formation of the Mesaverde Group, intertongues with the marine Mancos Shale and most likely contains a

mixture of types II and III organic matter. A "burned-out" oil zone identified in the Cozzette Member of the Iles Formation at MWX (C.W. Spencer, written commun., 1982) indicates the presence of some oil-prone source rocks. Hydrogen/carbon ratios determined by Rock-Eval pyrolysis confirm the presence of type II organic matter in some of the coals and carbonaceous shales in the Iles Formation. Multiple thick (as much as 10 ft) coal beds and associated carbonaceous shales in the Cameo-Fairfield coal zone in the lower part of the fluvial Mesaverde Group or Williams Fork Formation of the Mesaverde Group make this part of the Mesaverde an excellent source for gas.

The overlying Wasatch Formation consists mostly of organically lean, varicolored shales, and lenticular sandstones and a few thin carbonaceous shale and coal intervals. A thin, coaly interval in the Wasatch Formation exposed on fresh outcrops near the MWX site was sampled and analyzed for our study. Most of the organic matter in the Wasatch Formation is of type III origin, as determined petrographically.

Three important hydrocarbon-generation thresholds were recognized at the MWX site: TTI 10, 0.60 percent Rm, the point at which oil begins to be generated (Waples, 1980); TTI 25, 0.73 percent Rm, the approximate point at which methane gas begins to be generated (Juntgen and Karweil, 1966); and TTI 180, 1.35 percent Rm, the point at which liquid hydrocarbons break down to gas and condensate and the upper limit of the oil window (Waples, 1980). Methane gas is stable at relatively high temperatures, corresponding to 4.8 percent Rm and TTI 120,000–130,000 (Waples, 1980), a much higher level of maturation than at the MWX site.

RESULTS AND DISCUSSION

The results of TTI modeling for the six coals are shown in tables 1–3. Tables 1 and 2 show the two geothermal gradients calculated from the two temperature logs measured at MWX-1 and corresponding TTI and Rm values calculated for the end of maximum burial (10 Ma), the temperature at maximum burial, and the timing of hydrocarbon-generation events. Table 3 shows the geothermal gradient that best fits measured vitrinite reflectance values for the MWX site as well as the TTI value at maximum burial, the temperature at maximum burial, and the timing of hydrocarbon-generation thresholds.

The geothermal gradients based on measured temperature logs and the best-fit geothermal gradient yield different times for hydrocarbon generation for the coals. The stratigraphically highest coal in our study achieved a Rm value of 0.60 percent at 10 Ma. The stratigraphically lowest coal in our study achieved a Rm value of 0.60 percent between 51 and 49 Ma, 0.73

Table 1. Results of TTI modeling using a maximum bottom-hole temperature of 244 °F (118.7 °C) for coals from the Mesaverde Group and Wasatch Formation at the MWX site
 [Coal 1 from Wasatch Formation, 2-6 from Mesaverde Group. Time-temperature indices (TTI) and mean vitrinite reflectance (Rm) values for end of period of maximum burial; temperature at maximum burial. Time in Ma; NA indicates not attained]

Coal no.	Geothermal gradient	TTI	Calculated Rm (percent)	Temperature	Time of hydrocarbon generation		
					TTI 10 0.60 Rm	TTI 25 0.73 Rm	TTI 180 1.35 Rm
1	2.12 °F/100 ft 39.0 °C/km	2.1	0.45	147 °F 64.4 °C	NA	NA	NA
2	2.09 °F/100 ft 38.2 °C/km	63	.96	238 °F 115.4 °C	39	30	NA
3	2.07 °F/100 ft 37.8 °C/km	115	1.17	253 °F 123.8 °C	42	36	NA
4	2.10 °F/100 ft 38.4 °C/km	400	1.65	285 °F 141.7 °C	46	43	28
5	2.23 °F/100 ft 40.8 °C/km	1,350	2.19	318 °F 160.2 °C	49	47	39
6	2.25 °F/100 ft 41.1 °C/km	2,300	2.40	333 °F 168.6 °C	50	48	43

Table 2. Results of TTI modeling using a maximum bottom-hole temperature of 266 °F (131 °C) for coals from Mesaverde Group and Wasatch Formation at the MWX site
 [Coal 1 from Wasatch Formation, 2-6 from Mesaverde Group. Time-temperature indices (TTI) and mean vitrinite reflectance (Rm) values for end of period of maximum burial; temperature at maximum burial. Time in Ma; NA indicates not attained]

Coal no.	Geothermal gradient	TTI	Calculated Rm (percent)	Temperature	Time of hydrocarbon generation		
					TTI 10 0.60 Rm	TTI 25 0.73 Rm	TTI 180 1.35 Rm
1	2.22 °F/100 ft 40.08 °C/km	2.5	0.47	152 °F 67.2 °C	NA	NA	NA
2	2.19 °F/100 ft 40 °C/km	90	1.06	247 °F 120.4 °C	41	34	NA
3	2.21 °F/100 ft 40.4 °C/km	195	1.38	268 °F 132.2 °C	43.5	39	13
4	2.19 °F/100 ft 40 °C/km	580	1.81	295 °F 147.3 °C	47	44	32
5	2.35 °F/100 ft 43.3 °C/km	2,200	2.37	332 °F 168 °C	50	48	43
6	2.37 °F/100 ft 43.3 °C/km	4,100	2.77	347 °F 176.4 °C	51	49	45

Table 3. Results of TTI modeling using geothermal gradient that best fits both predicted TTI values and measured Rm values for coals from the Mesaverde Group and Wasatch Formation at the MWX site
 [Coal 1 from Wasatch Formation, 2-6 from Mesaverde Group. Time-temperature indices (TTI) and mean vitrinite reflectance (Rm) values for end of period of maximum burial; temperature at maximum burial. Time in Ma; NA indicates not attained]

Coal no.	Geothermal gradient	TTI	Calculated Rm (percent)	Temperature	Time of hydrocarbon generation		
					TTI 10 0.60 Rm	TTI 25 0.73 Rm	TTI 180 1.35 Rm
1	3.0 °F/100 ft 54.6 °C/km	10	0.60	188° F 87.3 °C	10	NA	NA
2	1.94 °F/100 ft 35.4 °C/km	38	.82	225 °F 108.1 °C	35	22.5	NA
3	1.92 °F/100 ft 35 °C/km	65	0.96	240 °F 116.5 °C	40	31	NA
4	1.95 °F/100 ft 35.6 °C/km	205	1.40	270 °F 133.3 °C	45	40	15
5	2.04 °F/100 ft 7.2 °C/km	550	1.79	298 °F 149 °C	48	46	32
6	2.02 °F/100 ft 36.8 °C/km	775	1.94	302 °F 151.2 °C	49	46	37

percent between 49 and 46 Ma, and 1.35 percent between 45 and 37 Ma.

Present-day Rm values predicted by using the geothermal gradients calculated from the two temperature logs are systematically higher than actual measured values for the five Mesaverde coals. These results are consistent with those of Johnson and Nuccio (1986), which show that the model of Waples (1980) overestimates coal ranks in all but the southernmost part of the Piceance basin. This overestimation may result from operator and laboratory bias in measuring Rm values, from a relatively recent increase in heat flow in the basin, or from a "kink" in the vitrinite reflectance profile (fig. 1).

Operator bias is clearly a problem in measuring vitrinite reflectance. For example, for the coal at a present-day depth of 5,226 ft (1,593 m), we measured an Rm value of 0.96 percent and Amoco measured a value of 1.14 percent. Amoco's value is quite close to the value we predict by using the lower bottom-hole temperature of 244 °F (118 °C). On the other hand, for the coal at a present-day depth of 7,950 ft (2,423 m), our measurement of 1.94 percent is much closer to Amoco's measurement of 2.11 percent. For this coal, the two temperature logs predict Rm values of 2.40 and 2.77 percent, respectively, values significantly greater than either of the actual measurements. Operator bias may explain some, but probably not all, of the difference between predicted and measured Rm values.

A relatively recent increase in heat flow at the MWX site, as well as throughout much of the rest of the Piceance basin, is an intriguing possibility that can be neither proven nor disproven at this time. In order to significantly lower TTI values for the five coals analyzed from the Mesaverde Group, the heat flow must have begun to increase no earlier than late in the period of maximum burial between 35 and 10 Ma. Furthermore, any increase in heat flow may have been more substantial than is suggested by a comparison of the temperatures shown in tables 1-3 because, as previously discussed, we minimized the calculated temperatures under maximum burial by assuming the lowest possible maximum burial depth and the lowest possible geothermal gradient through the eroded section.

Law and Nuccio (1986) and Law and others (1989) have described "kinks" in vitrinite reflectance profiles from several wells in Rocky Mountain basins, including the MWX wells. Law and others (1989) suggested that overpressuring associated with the maturation of coal beds and carbonaceous shale caused a vertical flow of relatively hot waters upward into normally pressured strata that raised the overlying vitrinite reflectance values. This convective heat transfer process is the most likely cause for our inability to model a straight-line time-temperature curve, hence underprediction of the Wasatch coal and overprediction for the Mesaverde coals.

We cannot assess the possibility of other unknown

problems in applying the TTI model of Waples (1980) to the Mesaverde coals of the Piceance basin. There is a great deal of scatter in the data that Waples used to calibrate TTI and Rm values, and our data is not anomalous when plotted on his curve.

REFERENCES CITED

- Barker, C.E., 1983, Influence of time on metamorphism of sedimentary organic matter in liquid-dominated geothermal systems, western North America: *Geology*, v. 11, no. 7, p. 384-388.
- Bostick, N.H., and Freeman, V.L., 1984, Tests of vitrinite reflectance and paleotemperature models at the Multiwell Experiment Site, Piceance Creek basin, Colorado, *in* Spencer C.W., and Keighin, C.W., eds., *Geologic studies in support of the U.S. Department of Energy Multiwell Experiment, Garfield County, Colorado: U.S. Geological Survey Open-File Report 84-757*, p. 110-120.
- DuBow, J., Nottenburg, R., Rajeshwar, K., and Rosenovold, R., 1977, Electrical and thermal transport properties of Green River oil shale heated in nitrogen: *Oil Shale Symposium, 10th, Golden, Colo., 1977, Proceedings*, p. 60-73.
- Epis, R.C., and Chapin, C.E., 1975, Geomorphic and tectonic implications of the post-Laramide, late Eocene erosion surface in the southern Rocky Mountains, *in* Curtis, B.F., ed., *Cenozoic history of the southern Rocky Mountains: Geological Society of America Memoir 144*, p. 45-74.
- Hansen, W.R., 1984, Post-Laramide tectonic history of the eastern Uinta Mountains, Utah, Colorado, and Wyoming: *The Mountain Geologist*, v. 21, no. 1, p. 5-29.
- Johnson, R.C., and Nuccio, V.F., 1984, Late Cretaceous through Early Tertiary general stratigraphy and structural geology of the Piceance Creek basin, Colorado, *in* Spencer, C.W., and Keighin, C.W., eds., *Geologic studies in support of the U.S. Department of Energy Multiwell Experiment, Garfield County, Colorado: U.S. Geological Survey Open-File Report 84-757*, p. 14-20.
- _____, 1986, Structural and thermal history of the Piceance Creek basin, western Colorado, in relation to hydrocarbon occurrence in the Mesaverde Group, *in* Spencer, C.W., and Mast, R.F., eds., *Geology of tight gas reservoirs: American Association of Petroleum Geologists Studies in Geology 24*, p. 165-206.
- Juntgen, H., and Karweil, J., 1966, Gasbildung und gasspeicherung in steinkohlenflozen, part I und II [Gas formation and storage in bituminous coal seams]: *Erdol and Kohle, Erdgas, Petrochemie*, v. 19, p. 251-258, 339-344.
- Larson, E.E., Ozima, Minoru, and Bradley, W.C., 1975, Late Cenozoic basic volcanism in northwestern Colorado and its implications concerning tectonism and the origin of the Colorado River system, *in* Curtis, B.F., ed., *Cenozoic history of the southern Rocky Mountains: Geological Society of America Memoir 144*, p. 155-178.
- Law, B.E., and Nuccio, V.F., 1986, Segmented vitrinite reflectance profile from the Deep Seam Project, Piceance Creek basin, Colorado; evidence of previous high pore pressure [abs.]: *American Association of Petroleum Geologists Bulletin*, v. 70, no. 8, p. 1047.

- Law, B.E., Nuccio, V.F., and Barker, C.E., 1989, Kinky vitrinite reflectance profiles; evidence of paleopore pressure in low-permeability gas-bearing sequences in Rocky Mountain foreland basins: *American Association of Petroleum Geologists Bulletin*, v. 73, no. 8, p. 999-1010.
- Lopatin, N.V., 1971, Temperature and geologic time as factors in coalification: *Akademiya nauk SSSR, Izvestiya Seriya Geologicheskaya*, no. 3, p. 95-106.
- Marvin, R.F., Mehnert, H.H., and Mountjoy, W.M., 1966, Age of basalt cap on Grand Mesa, *in Geological Survey Research 1966: U.S. Geological Survey Professional Paper 550-A*, p. A81.
- Neruchev, S.G., and Parparova, G.M., 1972, O roli geologicheskogo vremeni v protsessakh metamorfizma ugley i rasseyannogo organicheskogo veshchestva porod [The role of geologic time in processes of metamorphism of coal and dispersed organic matter in rocks]: *Akademiya nauk SSSR Sibirsk. Otdeleniye Geologiya i Geofizika*, no. 10, p. 3-10.
- Nuccio, V.F., and Johnson, R.C., 1984, Thermal maturation and burial history of the Upper Cretaceous Mesaverde Group, including the Multiwell Experiment (MWX), Piceance Creek basin, Colorado, *in Spencer, C.W., and Keighin, C.W., eds., Geologic studies in support of the U.S. Department of Energy Multiwell Experiment, Garfield County, Colorado: U.S. Geological Survey Open-File Report 84-757*, p. 102-109.
- Price, L.C., 1983, Geologic time as a parameter in organic metamorphism and vitrinite reflectance as an absolute paleogeothermometer: *Journal of Petroleum Geology*, v. 6, no. 1, p. 5-38.
- Tissot, B.P., Durand, B., Espatalie, J., and Combaz, A., 1974, Influence of nature and diagenesis of organic matter in formation of petroleum: *American Association of Petroleum Geologists Bulletin*, v. 58, no. 3, p. 499-506.
- Tweto, Ogden, 1975, Laramide (Late Cretaceous-Early Tertiary) orogeny in the southern Rocky Mountains, *in Curtis, B.F., ed., Cenozoic history of the southern Rocky Mountains: Geological Society of America Memoir 144*, p. 1-44.
- Waples, D.W., 1980, Time and temperature in petroleum formation; application of Lopatin's method to petroleum exploration: *American Association of Petroleum Geologists Bulletin*, v. 64, no. 6, p. 916-926.

Chapter M

Fluid Inclusion Evidence for Paleotemperatures within the Mesaverde Group, Multiwell Experiment Site, Piceance Basin, Colorado

By CHARLES E. BARKER

Prepared in cooperation with the U.S. Department of Energy

U.S. GEOLOGICAL SURVEY BULLETIN 1886

GEOLOGY OF TIGHT GAS RESERVOIRS IN THE PINEDALE ANTICLINE AREA, WYOMING,
AND AT THE MULTIWELL EXPERIMENT SITE, COLORADO

CONTENTS

Abstract	M1
Introduction	M1
Results of fluid inclusion studies	M2
Calcite veins	M2
Quartz druses	M2
Thermal history reconstruction	M3
Present temperature	M3
Peak paleotemperature	M3
Burial history	M3
Timing of coalification and gas generation	M4
Timing of cementation	M5
Discussion	M6
References cited	M6
Appendix 1. Fluid inclusion analysis	M10
Appendix 2. Paleotemperature from vitrinite reflectance	M11

FIGURES

- 1-2. Graphs showing:
 1. Homogenization temperatures of aqueous fluid inclusions, MWX-1 M3
 2. Reconstructed and measured geothermal gradients, MWX wells M4
 3. Diagram showing burial history reconstruction, MWX wells M5

Fluid Inclusion Evidence for Paleotemperatures within the Mesaverde Group, Multiwell Experiment Site, Piceance Basin, Colorado

By Charles E. Barker

Abstract

Gas-bearing aqueous fluid inclusions occur in veins cutting the Mesaverde Group in the MWX wells. The fluid inclusions in calcite decrepitate or reequilibrate when heated, and no quantitative homogenization temperature data can be obtained from them. Fluid inclusions in quartz-lined veins at depths of 5,578 ft (1,700 m) and 7,844 ft (2,390 m) were homogenized at about 285 °F (140 °C) and 315 °F (158 °C), respectively. Modified homogenization temperatures suggest that the fluid inclusions in quartz veins formed in a geothermal profile similar to the present-day near-surface temperature gradient of 2.1 °F/100 ft (38 °C/km).

Burial temperatures calculated from vitrinite reflectance values indicate a peak paleogeothermal gradient of 2.0 °F/100 ft (37 °C/km) above 4,400 ft (1,340 m), and a higher paleogeothermal gradient of 4.1 °F/100 ft (74 °C/km) from 4,400 to 7,950 ft (1,340–2,420 m). The shallow paleogeothermal gradient agrees with a geothermal gradient of 2.1 °F/100 ft (38 °C/km) measured at depths less than 6,600 ft (2,010 m). Below a depth of 6,600 ft (2,010 m), an increase in coal content causes a higher gradient of about 3.4 °F/100 ft (62 °C/km). Changes in slope of the measured temperature profile do not correspond to those in the rank profile or to the gradient suggested by the fluid inclusions. This difference suggests that the geothermal gradient has changed in portions of the well.

INTRODUCTION

The basis of thermal history reconstruction using fluid inclusions is that they are trapped as a mineral precipitates and can record the temperature and chemistry of the pore water present. Fluid inclusion salinity is measured by freezing point depression. The brine composition is inferred from the eutectic (first melting) temperature. The homogenization temperature of a fluid inclusion is related to its formation temperature (Roedder, 1984) if the fluid inclusion has not reequilibrated (Goldstein, 1986). These data are used to reconstruct the fluid temperature and composition in the rock when the inclusions formed. In the MWX wells, fractures formed in response to several episodes of

regional deformation. These fractures are now mineralized and contain fluid inclusions. Reconstruction of the regional stress history shows the time when fractures of a given orientation probably opened. Measurements of orientation bracket a geologic time when the temperatures shown by homogenization temperature could have existed. The sophistication of the temperature bracketing is increased by measurements from veins of a different orientation or by data from other geothermometers. Particularly useful are the peak temperatures indicated by vitrinite reflectance and the measured well temperatures. This method of comparative geothermometry shows a time-temperature history for the MWX site.

These comparative studies are important because fluid inclusion geothermometry is being discredited as a viable method in sedimentary rocks (Prezbindowski and Larese, 1987). Physical changes in fluid inclusions (reequilibration) during deeper burial cause averaged homogenization temperatures not to fit other geologic data. Actually, at fault is a defective approach in defining fluid inclusion origin and thermal history, leading to inclusions from different trapping events being reported as one population. Fluid inclusion geothermometry in sedimentary rocks can easily be misinterpreted and lead to erroneous conclusions. The inaccurate temperature information arises from: (1) reequilibration of fluid inclusions when they are heated to temperatures exceeding their trapping conditions; (2) the assumption that fluid inclusions of ambiguous origin are primary; (3) overemphasis of two-phase fluid inclusions and not considering evidence from single-phase fluid inclusions; (4) heating events not being recorded by the fluid inclusion population; and (5) insufficient composition data to properly evaluate the meaning of heating stage measurements. (See Roedder 1984, and Goldstein 1986, among others, for reviews.) In spite of these problems, careful fluid inclusion studies provide a strong tool useful in thermal diagenesis studies. The potential for misinterpretation of fluid inclusion data is mitigated in this study by using other paleogeothermometers and well temperature data to check results.

Acknowledgments.—V.F. Nuccio and R.C. Johnson helped with the geology of Piceance basin. J.C. Lorenz, Sandia National Laboratories, provided the quartz-lined fractures for the fluid inclusion study. C.W. Spencer and B.E. Law helped guide the investigation. V.F. Nuccio and C.W. Spencer reviewed the paper. M.J. Pawlewicz helped at a critical time by typing a corrected version of the paper.

RESULTS OF FLUID INCLUSION STUDIES

Fluid inclusions in the MWX core samples occur in calcite veins and quartz-lined fractures. Analysis of these vein samples proceeded by the methods outlined in appendix 1. These mineralized fractures have been further described by Verbeek and Grout (1984), Pitman and Sprunt (1984, 1986), Lorenz and Findlay (1986), and Pitman and Dickinson (this volume).

Calcite Veins

Aqueous inclusions are common in calcite veins cutting the Mesaverde Group. Homogenization temperatures for these inclusions cannot be determined because the inclusions decrepitate or reequilibrate when heated.

Vein samples from a shallow (5,018 ft, 1,530 m) and a deep (8,114 ft, 2,470 m) core were opened in a crushing stage (Roedder, 1984). The cleavage fragments are immersed in glycerin to check for noncondensable gas and then in kerosene to check for natural gas. The shallow sample contains secondary planes of two-phase fluid inclusions. Bubbles that evolved from these samples when they were cracked on the crushing stage did not dissolve in glycerin but rapidly disappeared in kerosene. Cleavage fragments from the deeper sample behaved similarly except that bubbling was more vigorous and a greater volume of gas emanated from inclusions of similar size. The larger volume of gas emitted from the deeper sample suggests that the gas in the inclusion was under greater pressure. The pressure difference is consistent with formation at a greater depth in the well. Because the gas bubbles rapidly dissolved in the kerosene, the gas is qualitatively identified as methane (Shepard and others, 1985). Fluorescence microscopy detected no oil in these inclusions.

Quartz Druses

An extensive search through hundreds of fractures in the MWX cores (performed by Sandia Laboratories, Los Alamos, N. Mex.) identified only a few fractures lined with quartz. In some cases, quartz precipitated with

calcite. Some of the euhedral quartz crystals that line fractures contain small rhombs (calcite ?) having high relief and birefringence. This occurrence may be a localized phenomena because Pitman and Dickinson (this volume), in a more extensive study of the fractures, reported that quartz precipitated before calcite.

Only euhedral quartz crystals or quartz overgrowth cements are considered usable because detrital quartz grains contain inherited fluid inclusions. A MWX-2 core sample collected from 5,572 ft (1,700 m) contains a near-vertical fracture lined with euhedral quartz crystals that have overgrown detrital grains. A core sample at 7,844 ft (2,390 m) contains euhedral quartz crystals that occur as druses growing on a curving, subhorizontal, slicken-sided fracture surface. Fluorescence microscopy detected no oil in these inclusions.

Aqueous inclusions in quartz did homogenize and provide (apparently) acceptable data. Some fluid inclusions selected for analysis are associated with inclusions with higher vapor to liquid ratios and homogenization temperatures exceeding 390 °F (200 °C). These latter inclusions were not measured because many had textures that suggest necking has occurred. In the sample from 7,844 ft (2,390 m), five inclusions had a homogenization temperature that exceeded 340–360 °F (170–180 °C). Cycling the heating stage at increasingly higher temperature did not cause homogenization in these inclusions (appendix 1). Heating was discontinued before damaging the sample. Both secondary fracture-bound inclusions and primary inclusions related to growth zones are in these samples. Although the secondary and primary inclusions formed at different times, their homogenization temperatures appear to be closely related and these values were combined to calculate an average.

The average homogenization temperature is about 285 °F (140 °C) at 5,578 ft (1,700 m) and 315 °F (158 °C) at 7,844 ft (2,390 m) (fig. 1). These temperatures suggest a apparent geothermal gradient of 1.4 °F/100 ft (26 °C/km). Modifications to the homogenization-temperature population show that the fluid inclusion data are consistent with the measured well temperature profile (fig. 2). The average homogenization temperature at 7,844 ft (2,390 m) is too low because I did not include the five inclusions having indeterminate homogenization temperatures (but definitely above 340–360 °F; 170–180 °C) in the calculations. The exclusion of these inclusions produces an artificially low average temperature in the deep sample. This is an important point, because if the average homogenization temperature at 7,844 ft (2,390 m) is increased by 14 °F (8 °C), the apparent geothermal gradient will increase to 2.1 °F/100 ft (38 °C/km) or equal to the present temperature profile.

The fluid inclusions in quartz at 7,844 ft may contain natural gas because they coexist with gas-bearing aqueous inclusions in calcite and are difficult to

homogenize. Crushing these inclusions did not clearly show that they contain natural gas. The crushing stage caused these small crystals to violently shatter. These violent movements can cause gas to exsolve from the immersion fluid and obscure any gas produced from the crystal. There was no continued bubbling of gas from the sample after cracking, which is strong qualitative evidence of natural gas in the fluid inclusions. Fluorescence microscopy detected no oil in these inclusions.

THERMAL HISTORY RECONSTRUCTION

Present Temperature

The MWX-1 borehole was spudded on September 13, 1981, and drilling operations ceased on December 18, 1981, and drilling operations ceased on December 18, 1981. Temperature logs (fig. 2) were run the following year on June 28 (LANL log) and September 9, 1982 (SMU log). The LANL log was measured 6 months after drilling ceased, enough time for well temperatures to reequilibrate (Bullard, 1947). The LANL log appears more accurate because the temperature profile changes correlate more closely with changes in lithology in the borehole (C.W. Spencer, oral commun., 1987). The geothermal gradient changes significantly at a depth of 6,600 ft (2,010 m). It is 2.1 °F/100 ft (38 °C/km) above 6,600 ft and 3.4 °F/100 ft (62 °C/km) below.

Peak Paleotemperature

Vitrinite reflectance (Nuccio and Johnson, this volume) is interpreted in this study as recording peak burial temperature (appendix 2). This analysis suggests peak paleotemperature increased from 190 °F (90 °C) in rocks now exposed at the surface to 280 °F (140 °C) at a depth of 4,400 ft (1,340 m) (2.0 °F/100 ft; 37 °C/km gradient). The gradient is higher from 4,400 to 7,950 ft (1,340–2,420 m). At 7,950 ft (2,420 m) (the deepest vitrinite reflectance measurement), the peak paleotemperature was 430 °F (220 °C) (4.1 °F/100 ft), corresponding to a paleogeothermal gradient of 4.1 °F/100 ft (74 °C/km) peak gradient.

Other qualitative evidence for the high paleogeothermal gradients includes relationships between temperature and the type of hydrocarbon present. The observed coexistence of pyrobitumens and gas within the MWX-1 well (Sattler and Lorenz, 1983) could be the result of burial temperatures exceeding 390 °F (200 °C) (Hunt, 1979, p. 102).

Burial History

The burial history (fig. 3) reconstructed by Johnson and Nuccio (1986) is used to estimate paleodepth for the period 74 to 10 Ma. For the period 10 Ma to present, their reconstruction is modified using data from Larson and others (1975). Larson and others asserted that no erosion

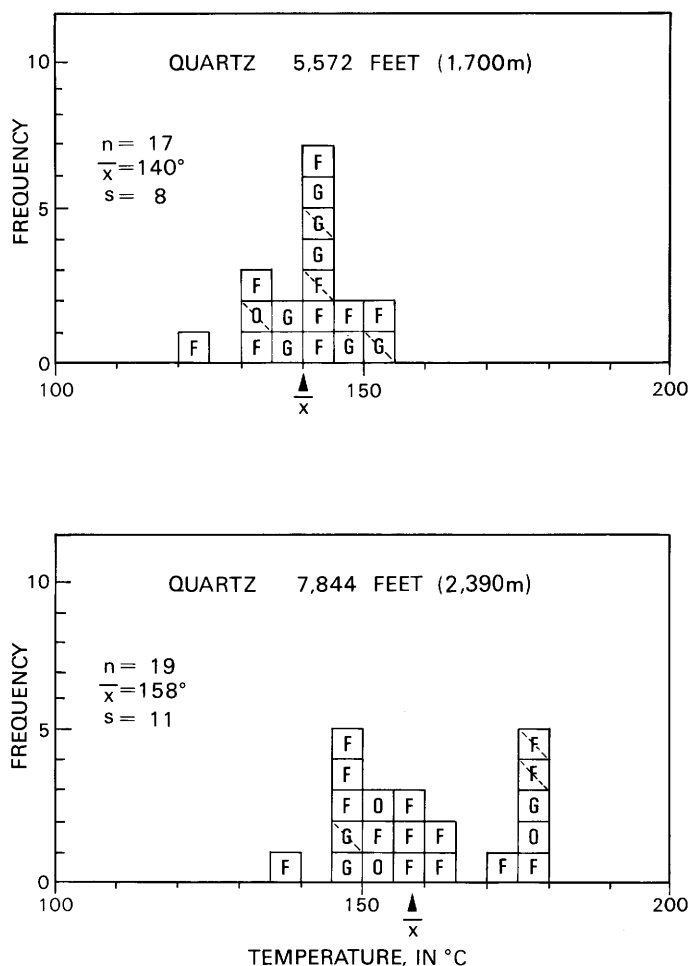


Figure 1. Homogenization temperatures of aqueous fluid inclusions, MWX-1. Fracture-bound fluid inclusions (F) are those trapped along a healed crack. Orphan inclusions (O) are those that have no apparent spatial or genetic relationship to other inclusions or crystal defects. Fluid inclusions in growth zones (G) are those that formed along quartz overgrowth contacts with a detrital quartz grain. Diagonal dashing across data symbol indicates difficult, suspect measurements.

occurred between 8 and 1.5 Ma in the Upper Colorado River system. This difference in the timing of erosion does not effect the maximum burial depth as reconstructed by Nuccio and Johnson, only the timing of erosion in the period 10 Ma to present. The timing of temperature decreases resulting from erosion can be useful in fixing the time of diagenetic events, in particular, the temperatures recorded in secondary fluid inclusions trapped along fracture planes during uplift.

Johnson and Nuccio (1986) assumed that minimal erosion occurred at unconformities in the MWX well because the area is near the axis of the Piceance basin. Because of this assumption, the burial history reconstruction of Johnson and Nuccio is a minimum estimate of maximum burial depth. Paleotemperature estimates based on this burial reconstruction are consequently minimum values.

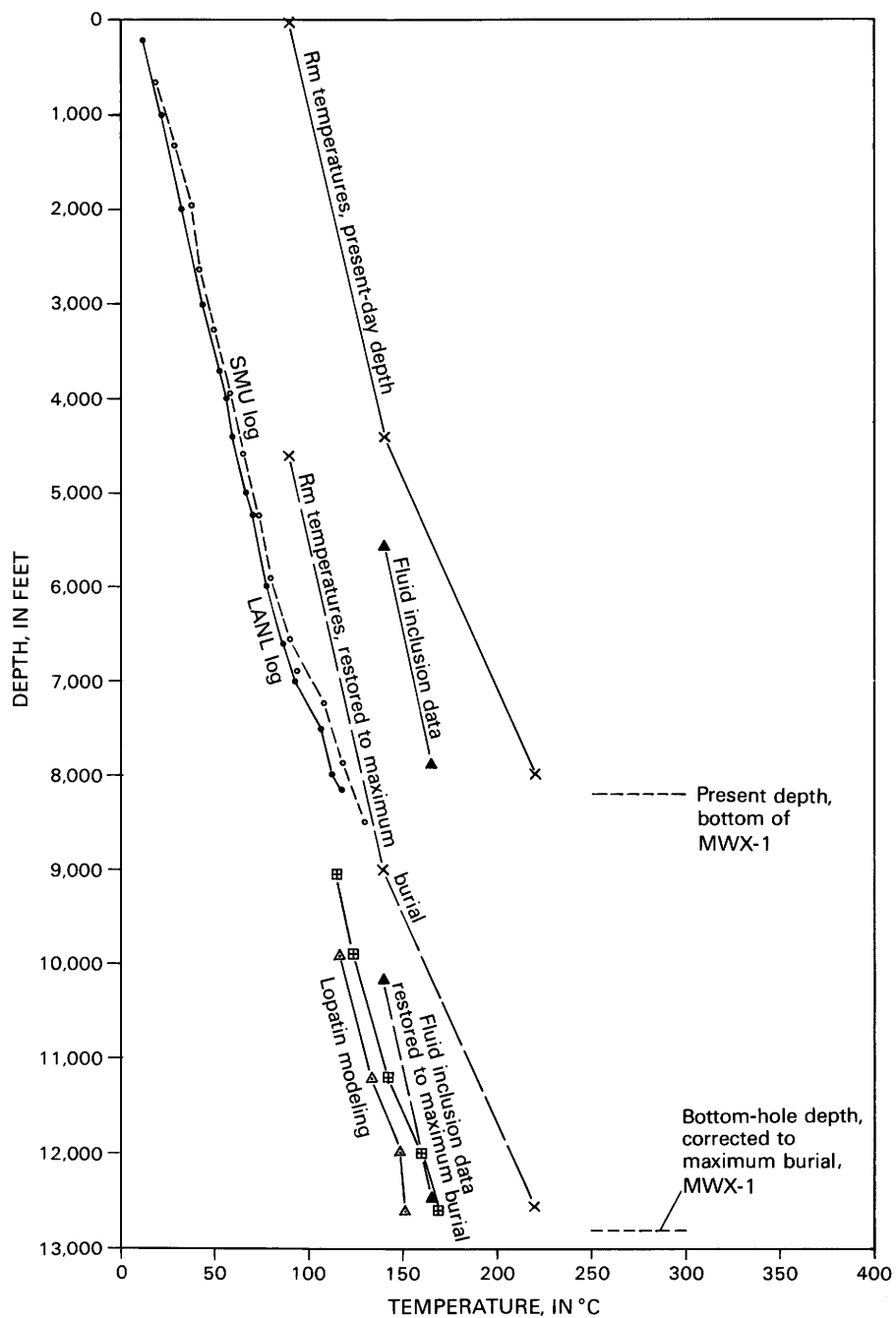


Figure 2. Reconstructed and measured geothermal gradients, MWX wells. Note that the paleotemperatures calculated from vitrinite reflectance data (Rm temperatures), when restored to maximum burial depth, fit well with the higher well temperatures in the coaly rocks near the bottom of well. Well temperatures from Sattler and Lorenz (1983). Lopatin modeling from Nuccio and Johnson (this volume).

Timing of Coalification and Gas Generation

Cross sections constructed by Johnson and Nuccio (1986) show that iso-vitrinite-reflectance lines in the vicinity of the MWX site only locally follow structure. This relationship infers that coalification is syntectonic (Stach and others, 1982). The final phase of deformation in the

Piceance basin that affected the coals occurred near the end of the Eocene (about 35 Ma; Johnson and Nuccio, 1986). Coalification was apparently completed during this time. Coals in the Mesaverde Group at the margins of the Piceance basin were uplifted and cooled in the late Eocene. The vitrinite reflectance of these uplifted coals is similar to the present-day rank of stratigraphically

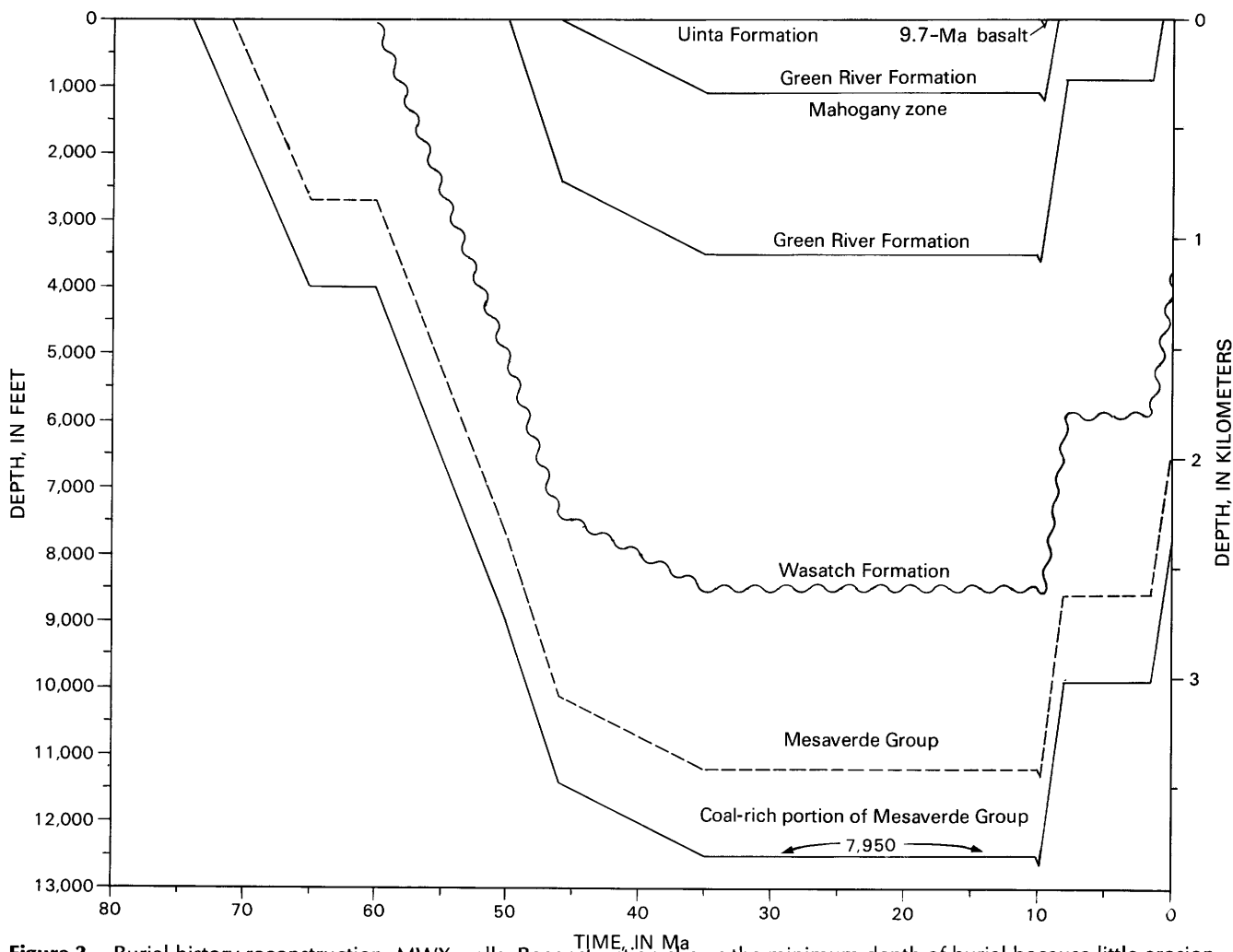


Figure 3. Burial history reconstruction, MWX wells. Reconstruction shows the minimum depth of burial because little erosion occurred at the unconformities older than 10 Ma. Since 10 Ma, erosion has removed a total of 4,600 ft (1,400 m) of rock. Modified from Johnson and Nuccio (1986) using evidence for timing of erosion from Larson and others (1975).

equivalent coals that are still deeply buried in the central part of the basin (Johnson and Nuccio, 1986). The similarity of rank between the shallow and deeply buried coals suggests that thermal maturation has not increased since the late Eocene. Consequently, gas generation must have decreased after thermal maturation stabilized (at about 35 Ma).

Timing of Cementation

The timing of fracturing is important because it represents the maximum age of the veins. Most fractures at the MWX site trend almost east-west, and Verbeek and Grout (1984) suggested that they opened before formation of the Grand Hogback at about 34 Ma. Fractures were available for cementation essentially during

the entire maximum burial phase from 35 to 9 Ma (fig. 3).

By restoring the 4,600 ft (1,400 m) of post-maximum-burial erosion, measured well temperatures can be projected to estimate peak paleotemperature. The restored temperature profile is an estimate of peak temperature if the heat flow has not changed. The peak temperatures must be adjusted for the middle Tertiary surface temperature of 70 °F (20 °C) (Savin, 1977). Samples from depths of less than 6,600 ft (2,010 m) now exist in a geothermal gradient of 2.1 °F/100 ft (38 °C/km). Samples below 6,600 ft exist in a higher gradient of 3.4 °F/100 ft (62 °C/km). Restored peak paleotemperature at 6,600 ft is 300 °F (150 °C). At 7,950 ft (2,420 m), it is 350 °F (175 °C).

Fluid inclusion temperature data roughly agree with restored peak paleotemperatures. Aqueous inclusions

in quartz-lined fractures from MWX-2 have an average homogenization temperature of about 280 °F (140 °C) at 5,578 ft (1,700 m) depth and 315 °F (158 °C) at 7,844 ft (2,390 m) (fig. 1). The restored peak paleotemperatures at these depths are 280 °F (140 °C) and 340 °F (170 °C), respectively. The agreement between restored peak paleotemperatures and fluid inclusion temperatures argues that the geothermal gradient has not changed since the quartz-lined fractures formed, sometime during the maximum burial phase 35 to 9 Ma.

Similar homogenization temperatures for secondary and primary fluid inclusions in the same samples of MWX quartz veins suggest that the microfractures containing the secondary inclusions likely opened and healed at near maximum burial.

DISCUSSION

Even allowing for cooling of the system as a result of erosion, the shape of the measured well temperature profile should be similar to that of the vitrinite reflectance profile. The difference between the two profiles suggests that the peak temperatures that set the vitrinite reflectance profile in the late Eocene have changed. The higher than present-day geothermal profile indicated by vitrinite reflectance apparently existed during only the early part of the maximum burial phase. By the time the quartz-lined fractures formed, the geothermal gradient had already decreased to present-day levels. The fluid inclusions appear to record conditions later in the maximum burial phase that existed from 35 to 9 Ma. Fluid inclusion evidence also infers that the present-day geothermal gradient was established before erosion commenced at about 9 Ma and decreased burial temperature.

REFERENCES CITED

- Barker, C.E., and Halley, R.B., 1986, Fluid inclusion, stable isotope, and vitrinite reflectance; evidence for the thermal history of the Bone Spring Limestone, southern Guadalupe Mountains, Texas, *in* Gautier, D.L., ed., Roles of organic matter in sediment diagenesis: Society of Economic Paleontologists and Mineralogists Special Publication 38, p. 189-203.
- Barker, C.E., and Pawlewicz, M.J., 1986, The correlation of vitrinite reflectance with maximum temperature in humic organic matter, *in* Buntbarth, G., and Stegena, L., eds., Paleogeothermics: New York, Springer-Verlag, p. 79-93.
- Barker, C.E., and Reynolds, T.J., 1984, Preparing doubly polished sections of temperature sensitive sedimentary rocks: *Journal of Sedimentary Petrology*, v. 54, no. 2, p. 635-636.
- Bullard, E.C., 1947, The time necessary for a borehole to attain temperature equilibrium: *Royal Astronomical Society Geophysical Supplement*, v. 5, p. 127-130.
- Christian, S.D., and Tucker, E.E., 1986, Linear least squares analysis with dependent and independent variable subject to error: *American Laboratory*, v. 18, p. 33-36.
- Goldstein, R.H., 1986, Reequilibration of fluid inclusions in low-temperature calcium-carbonate cement: *Geology*, v. 14, p. 792-795.
- Hanor, J.S., 1980, Dissolved methane in sedimentary basins; potential effect on the PVT properties of fluid inclusions: *Economic Geology*, v. 75, no. 4, p. 603-609.
- Hunt, J.M., 1979, *Petroleum geochemistry and geology*: San Francisco, Freeman, 617 p.
- Johnson, R.C., and Nuccio, V.F., 1986, Structural and thermal history of the Piceance basin, western Colorado, in relation to hydrocarbon occurrence in the Mesaverde Group, *in* Spencer, C.W., and Mast, R.F., eds., *Geology of tight gas reservoirs*: American Association of Petroleum Geologists Studies in Geology 24, p. 165-206.
- Larson, E.E., Ozima, M., and Bradley, W.C., 1975, Late Cenozoic basic volcanism in northwestern Colorado and its implications concerning tectonism and the origin of the Colorado River system, *in* Curtis, B.F., *Cenozoic history of the southern Rocky Mountains*: Geological Society of America Memoir 144, p. 155-178.
- Lorenz, J.C., and Findlay, S.J., 1986, Details of fractures in core from the MWX marine zones: Sandia National Laboratories Distribution Memorandum, September 23, 1986, 6 p.
- Love, K., 1987, Closing the trapdoors of regression analysis: *Geobyte*, v. 2, p. 18-21.
- Pitman, J.K., and Sprunt, E.S., 1984, Origin and occurrence of fracture-filling cements in the Upper Cretaceous Mesaverde Formation at MWX, Piceance Creek basin, Colorado, *in* Spencer, C.W., and Keighin, C.W., *Geologic studies in support of the U.S. Department of Energy Multiwell Experiment, Garfield County, Colorado*: U.S. Geological Survey Open-File Report 84-757, p. 87-101.
- _____, 1986, Origin and distribution of fractures in lower Tertiary and Upper Cretaceous rocks, Piceance Basin, Colorado, and their relation to the origin of hydrocarbons, *in* Spencer, C.W., and Mast, R.F., eds., *Geology of tight gas reservoirs*: American Association of Petroleum Geologists Studies in Geology 24, p. 221-234.
- Pollastro, R.M., and Barker, C.E., 1986, Application of clay-mineral, vitrinite reflectance, and fluid inclusion studies to the thermal and burial history of the Pinedale Anticline, Green River basin, Wyoming, *in* Gautier, D.L., ed., 1986, Roles of organic matter in sediment diagenesis: Society of Economic Paleontologists and Mineralogists Special Publication 38, p. 73-83.
- Prezbindowski, D.R., and Larese, R.E., 1987, Experimental stretching of fluid inclusions in calcite; implication for diagenetic studies: *Geology*, v. 19, p. 333-336.
- Roedder, E., 1984, Fluid inclusions: Mineralogical Society of America, *Reviews in Mineralogy*, v. 12, 644 p.
- Sattler, A.R., and Lorenz, J.C., 1983, Topical discussion of organic maturation at Multiwell Experiment site (MWX): Sandia National Laboratories Distribution Memorandum, March 24, 1983.
- Savin, S.M., 1977, The history of the earth's surface temperature during the past 100 million years: *Annual Reviews of Earth and Planetary Sciences*, v. 5, p. 319-355.

- Shepard, T.J., Rankin, A.H., and Alderton, D.H.M., 1985, A practical guide to fluid inclusion studies: London, Blackie, 239 p.
- Stach, E., Mackowsky, M.-Th, Teichmuler, M., Taylor, G., Chandra, D., and Teichmuler, R., 1982, Stach's textbook of coal petrology: Berlin, Gebruder Borntraeger, 535 p.
- Till, R., 1974, Statistical methods for the earth scientist; an introduction: London, Macmillan, 154 p.
- Verbeek, E.R., and Grout, M.A., 1984, Prediction of subsurface fracture patterns from surface studies of joints; an example from the Piceance Creek basin, Colorado, *in* Spencer, C.W., and Keighin, C.W., eds., Geologic studies in support of the U.S. Department of Energy Multiwell Experiment, Garfield County, Colorado: U.S. Geological Survey Open-File Report 84-757, p. 75-86.
- Werre, R.W., Jr., Bodnar, R.J., Bethke, P.M., and Barton, P.B., Jr., 1979, A novel gas-flow fluid inclusion heating/freezing stage: Geological Society of America Abstracts with Programs, v. 11, no. 7, p. 539.
- Woods, T.L., Bethke, P.M., Bodnar, R.J., and Werre, R.W., Jr., 1981, Supplementary components and operation of the U.S. Geological Survey gas-flow heating/freezing stage: U.S. Geological Survey Open-File Report 81-954, 21 p.

APPENDIXES 1, 2

Appendix 1. Fluid inclusion analysis

Sample Preparation

Quartz crystals lining the fractures are removed from the fracture surface by picking them off with a needle. These loose crystals are epoxy bonded on circular cover slips that fit directly into the heating stage. The mounting medium is a low-viscosity Epoxy (Epotek 301) that has an index of refraction close to that of quartz. This mounting method mutes the crystal boundaries and thus enhances observation of fluid inclusions in unpolished mounts.

The calcite veins are large enough to make doubly polished sections or to chip off thin cleavage fragments for analysis. These samples are naturally heated to over 170 °F (75 °C), and thermal alteration of the fluid inclusions during polishing is unlikely. The techniques of Barker and Reynolds (1984) required modification to correctly polish the calcite veins in a harder sandstone matrix. Polishing the calcite required planing the rock surface on 600-grit silicon carbide paper and polishing the sample for 60 seconds or less on a 1-micron diamond lap or on lapping film. This procedure replaces the 6-micron diamond paste step used by Barker and Reynolds.

Microscopy

Fluid-inclusion homogenization temperatures are measured in a gas-flow heating stage (Werre and others, 1979) rebuilt to the specifications of Fluid Incorporated. Calibration of this heating stage uses the procedures described in Barker and Halley (1986). The accuracy of temperature determinations is ± 1 °C in heating mode and ± 0.2 °C in freezing mode. The heating stage uses a Zeiss microscope equipped with a 100-watt quartz-halogen light source, Zeiss long-working-distance condenser, Lietz L-32 objective, and 12.5 X, 16 X, or 20 X oculars. The higher power oculars provide a larger, but less distinct image. A Zeiss epi-illuminator fitted with blue and ultraviolet filters provides incident fluorescence microscopy.

Often the fluid inclusions in the MWX samples are visible at high magnification with the heating stage chamber top off but become indistinct and immeasurable with the top on. Serial sections of specimens aid the search for larger and (or) more clearly observable small inclusions. These small inclusions occur in clean, solid inclusion-free parts of the crystal. Dark shadows in a fluid inclusion can be reduced by using oblique illumination produced by moving the inclusion off center in the field of view. Periodic cleaning of the microscope lenses and replacement of the stage windows is required to reduce interference by dust. Setting up the microscope for the Kohler illumination is required for each inclusion, and proper adjustment of the diaphragms on the condenser and on the L-32 objective is crucial in order to improve the fluid inclusion image. A polarizer can be inserted and rotated in the light path to cut out double refraction.

Each fluid inclusion is described by its petrographic characteristics and occurrence. Each inclusion is heated at least twice to homogenization temperature to check the measurement. Only two fluid inclusions in each fracture-bound set are measured in order to estimate consistency of the vapor to liquid ratios in the group without unnecessarily biasing the results toward the ubiquitous inclusions occurring in a few secondary planes. All primary fluid inclusions are measured.

Pressure Correction

The homogenization temperatures do not require pressure correction. The fluids are gas saturated and they apparently homogenize at temperatures at or near the bubble point. The homogenization temperature of natural-gas-bearing aqueous fluid inclusions can be used as a minimum temperature of entrapment (Hanor, 1980).

Dealing with Gas-Rich Inclusions

In these gas-rich fluid inclusions it is difficult to clearly observe homogenization. When heated, the bubble merely shrinks until it is no longer visible. Subsequent cooling causes the bubble to slowly grow back, often in the same position within the crystal. This phenomenon suggests that homogenization has not occurred. Normally, the vapor phase renucleates at about 20–30 °C below homogenization. Renucleation is an abrupt event marked by the sudden appearance of a relatively large bubble. This type of homogenization was not commonly observed in the MWX fluid inclusions. In the cycling method (Woods and others, 1981), the peak stage temperature increases by small increments until during the cooling cycle the vapor bubble suddenly reappears rather than slowly grows back into view. For many MWX inclusions, incrementally increasing the peak temperature did not cause homogenization. The vapor bubble slowly grew back into view during cooling, even if the point of bubble disappearance was exceeded by more than 50 °C. Initially, this behavior was thought to result from reequilibration. In many cases, the reappearance temperature of the bubble did not change, despite ever higher peak temperatures, an indication that the fluid inclusion was not re-equilibrating. Another indication of reequilibration is the increase of the diameter of the bubble after cooling to room temperature. The fluid inclusions in calcite did show this behavior and are not usable. Fluid inclusions in quartz did not reequilibrate when heated to less than 50 °C beyond the vapor-bubble disappearance.

If the gas-rich inclusions are ignored, serious distortion of the data can occur. There is a tendency to not use difficult to measure two-phase or single-phase inclusions. In this study, the temperature at which the bubble disappears to the observer gives a crude and subjective minimum homogenization temperature estimate. This technique is only used if homogenization could not be directly observed, and the estimated temperatures are not included in the calculation of average homogenization temperature. The temperature at which the bubble first grows back into view should also be noted because if this temperature continues to creep upward during heating cycles, the inclusion may be reequilibrating. Reequilibration is confirmed if upon cooling to room temperature, the diameter of the bubble has measurably increased.

Careful microscopy and repetition of measurements often permits determination of homogenization temperature. Sometimes if the inclusion is cooled slightly after the bubble apparently disappears, the bubble may move from where it is hidden. If the bubble is observed to move, the temperature is noted and heating resumed. Several heating cycles are required in order to ensure that the bubble truly has disappeared because the bubble may be hidden at the wall of the inclusion or it may have moved out of the focal plane. Often the inclusion can finally be observed to homogenize by making these small heating cycles. In these cases, the apparent disappearance temperature is within about 20 °C of the true homogenization temperature.

Appendix 2. Paleotemperature from vitrinite reflectance

Barker and Pawlewicz (1986) used the ordinary least-squares regression method to calibrate an empirical geothermometer based on vitrinite reflectance. However, because of measurement errors in both variables, this classical regression technique produces incorrect results. This problem was not detected in early tests of the empirical geothermometer. Barker and Halley (1986) and Pollastro and Barker (1986) used an equation that was computed from a smaller data set than was later published by Barker and Pawlewicz. Unfortunately, the final version of the equation published in Barker and Pawlewicz (1986) computes temperature estimates that are too hot for burial diagenesis.

A revised equation uses major-axis regression (Till, 1974) to compute the curve. Major-axis regression is better because it is difficult to measure peak temperature and vitrinite reflectance without error. Major-axis regression considers both variables to have measurement errors and adjusts the fitted curve

accordingly. In contrast, least-squares regression requires that one variable be known without error (Christian and Tucker, 1986; Love, 1987), an unrealistic requirement in this case. These problems indicate that a data set generated by consistent methods of measurement is needed to assure more accuracy in calibrating this geothermometer.

The major-axis regression equation is

$$\ln(R_m) = 0.00959(T_{\text{peak}}) - 1.42,$$

where R_m is the vitrinite reflectance and T_{peak} is the peak paleotemperature. This equation is used here to estimate peak paleotemperature by rounding to the nearest 10 °C (20 °F). Peak paleotemperature estimated from this equation is in better agreement with those from other geothermometers published in Barker and Halley (1986) and Pollastro and Barker (1986).

Regardless of the statistical theory and its constraints, Barker and Pawlewicz's (1986) conclusion that the effect of time on vitrinite reflectance cannot be large still holds. This conclusion is based on the strong correlation of vitrinite-reflectance and peak-temperature data from diverse geologic systems having a wide range of heating duration.

Chapter N

Rock-Eval Analysis of Sediments and Ultimate Analysis of Coal, Mesaverde Group, Multiwell Experiment Site, Piceance Basin, Colorado

By CHARLES E. BARKER

Prepared in cooperation with the U.S. Department of Energy

U.S. GEOLOGICAL SURVEY BULLETIN 1886

GEOLOGY OF TIGHT GAS RESERVOIRS IN THE PINEDALE ANTICLINE AREA, WYOMING,
AND AT THE MULTIWELL EXPERIMENT SITE, COLORADO

CONTENTS

Abstract N1

Introduction N1

Rock-Eval pyrolysis N1

Results N2

Conclusions N2

References cited N2

Appendix 1. Rock-Eval pyrolysis data, MWX-1, -2, and -3 N8

Appendix 2. Coal analysis data, MWX-1 N11

FIGURES

1-4. Graphs showing:

1. Hydrogen index versus oxygen index from Rock-Eval pyrolysis, MWX-1, -2, and -3 N3
2. Hydrogen and oxygen indices versus depth, MWX-1, -2, and -3 N4
3. Van Krevelen diagram of coal ultimate analyses, MWX-1 N5
4. Rock-Eval Tmax, vitrinite reflectance, and vitrinite reflectance equivalent versus depth, MWX-1, -2, and -3 N5

Rock-Eval Analysis of Sediments and Ultimate Analysis of Coal, Mesaverde Group, Multiwell Experiment Site, Piceance Basin, Colorado

By Charles E. Barker

Abstract

Rock-Eval data indicate that rocks in the Multiwell Experiment boreholes have a moderate to high total organic carbon content, an indication of good source-rock richness. Rock-Eval and coal ultimate analysis data both suggest that the organic matter is mature to overmature. The slope of the Rock-Eval Tmax profile confirms the high thermal maturity gradient in the Mesaverde Group indicated by vitrinite reflectance studies. Although the rocks have a moderate to high total organic carbon content, the generally thermally overmature organic matter and its low hydrogen content indicate little remaining petroleum-generating potential.

INTRODUCTION

As part of the multidisciplinary studies of the Multiwell Experiment (MWX) boreholes in the Piceance basin of northwest Colorado (Law and Spencer, this volume, fig. 1), Rock-Eval analysis of selected core samples was contracted by Sandia Laboratories, Los Alamos, N. Mex., to Core Laboratories, Dallas, Tex. The coal samples were analyzed by the U.S. Geological Survey. These data were intended to screen the samples for subsequent geochemical or other analysis (Sattler and Lorenz, 1983) and were not interpreted. This report presents the geochemical data (appendix 1) and an interpretation of the results.

Acknowledgments.—J.C. Lorenz, Sandia National Laboratories, sampled the MWX boreholes and arranged for the Rock-Eval analysis. C.W. Spencer and B.E. Law helped guide the investigation and provided funding through the U.S. Department of Energy.

ROCK-EVAL PYROLYSIS

Rock-Eval pyrolysis and measurement of total organic carbon (TOC) qualitatively evaluate organic-matter geochemistry and thermal maturity. Rock-Eval pyrolysis must be used with caution in rocks having low TOC and

if organic contamination is present (Peters, 1986). In clay-rich rocks containing humic organic matter, with less than 0.5 weight percent TOC, the hydrogen index (HI) is likely to be too low and the temperature of maximum-hydrocarbon generation (Tmax) too high. (See Peters, 1986, for a discussion of terminology.)

Organic drilling mud additives can increase HI. Because MWX-1 and MWX-2 were drilled with an oil-base mud and MWX-3 with a potassium chloride polymer-base mud (Spencer, 1984), such contamination could be a problem. However, no samples contaminated by particulate mud additives were detected by examination under a binocular microscope. The possibility of contamination was further reduced before analysis by pulverizing the core chips, washing them in hot hydrochloric acid for 2 hrs to remove carbonate, and then rinsing them with distilled water.

Rock-Eval pyrolysis also is influenced by migrated oil or bitumen. Migrated oil in a sample produces an S1 peak greater than 2 mg hydrocarbon (HC)/g of rock, an anomalously high transformation ratio and low Tmax as compared to adjacent samples, and a bimodal S2 peak. The migration factor must be considered because pyrobitumen has been observed at the top of the Cozzette Sandstone Member of the Iles Formation at 2,370 m (7,830 ft) in MWX-2 (C.W. Spencer, *in* Sattler and Lorenz, 1983). Oil contamination is probably not a generally important factor because the pyrobitumen is a localized occurrence in the MWX boreholes. Only 10 of 109 samples (9 percent) have a S1 peak greater than 2, and except for 2 of the 10 samples all seem to have transformation ratios and Tmax values that agree with those of adjacent samples. Four other samples have bimodal S2 peaks, but the corresponding S1 peaks are all less than 0.1 mg HC/g of rock. Some samples, especially those from the shallow part of the borehole, have relatively low Tmax values. These samples also generally have a low TOC. The low Tmax may be related to weak S2 peaks resulting from low TOC values and not to organic contamination.

RESULTS

Rock-Eval pyrolysis of carbonaceous mudrock, coal, and sandstone core samples indicates that the organic matter is mature to overmature and has moderate to high transformation ratios and moderate to high TOC (appendix 1), and low residual hydrogen and oxygen contents (figs. 1, 2). The mature to overmature organic matter indicated by the Rock-Eval pyrolysis data is confirmed by ultimate analysis of five coal samples (appendix 2, fig. 3).

Tmax data from Rock-Eval pyrolysis generally are consistent with the other organic geochemical data in that they indicate moderate to high thermal maturation (fig. 4), but several Tmax values are anomalously low, as compared to the general trend of the data, and may result from contamination in these samples. If these anomalously low points are ignored, the trend of the clustered Tmax data indicates an increase in thermal maturation as depth increases. Computation of vitrinite reflectance equivalents (VRE) from Tmax (fig. 4) confirms the general level of rank shown in the Van Krevelen diagram (fig. 3) and a somewhat higher rank than indicated by the vitrinite reflectance (Rm) measurements (Nuccio and Johnson, this volume). The differences between Rm and VRE values are not considered significant because the calibration between Rm and Tmax is diffuse and can vary from basin to basin. The VRE-depth profile confirms the relatively high vitrinite reflectance gradient in the Mesaverde Group (Nuccio and Johnson, this volume).

CONCLUSIONS

The data presented here support the following conclusions:

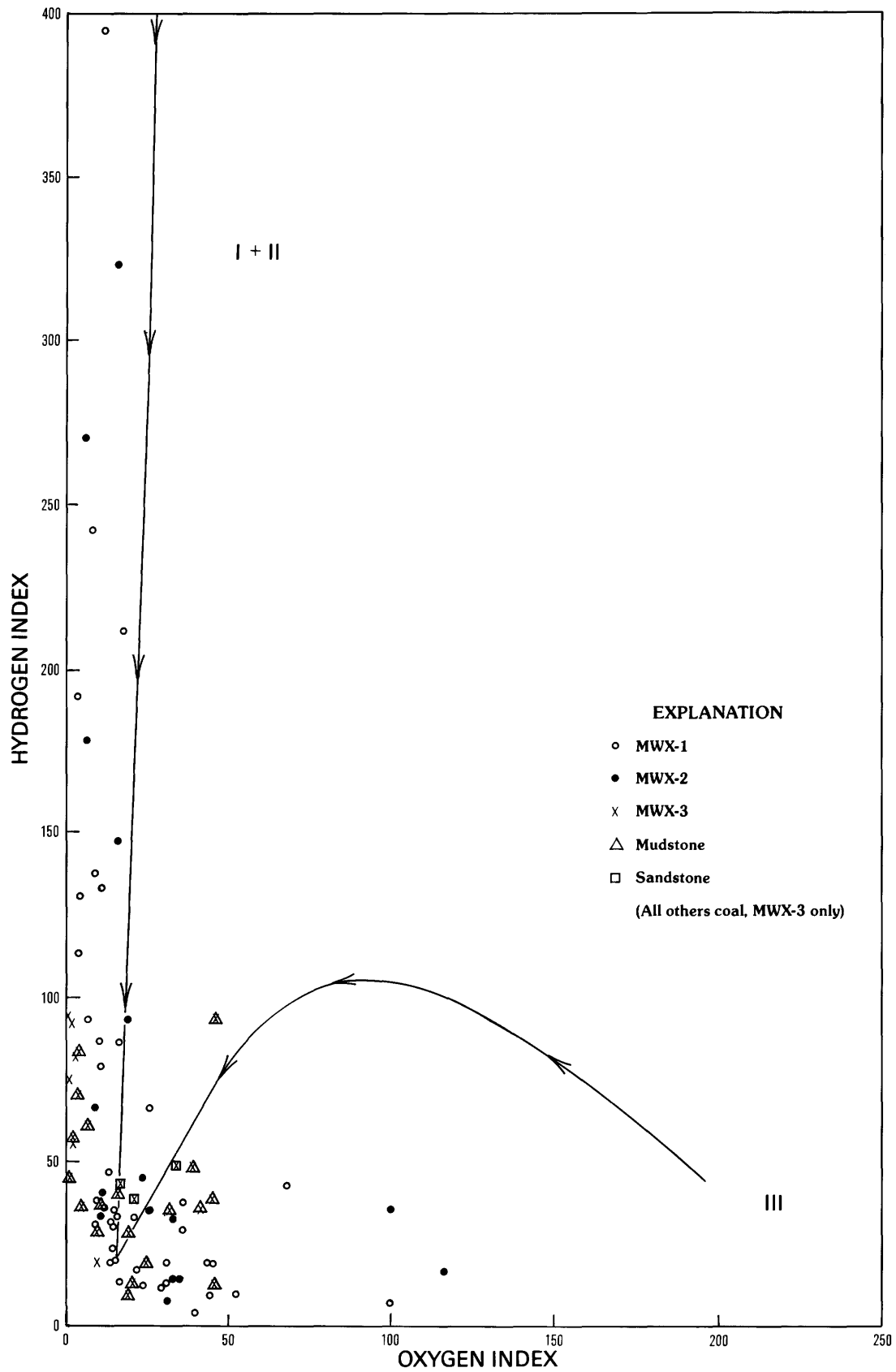
1. Rock-Eval data indicate that the organic matter in the MWX boreholes has moderate to high TOC, an indication of good source-rock richness.

2. Rock-Eval Tmax and ultimate coal analysis data suggest that the organic matter is mature to overmature.
3. The generally low hydrogen content of the organic matter infers that little petroleum-generating potential remains.
4. The slope of the Rock-Eval Tmax profile when converted to the VRE indicates a high thermal maturity gradient in the Mesaverde Group.

REFERENCES CITED

- Jones, R.W., and Edison, T.A., 1978, Microscopic observations of kerogen related to geochemical parameters with emphasis on thermal maturation, *in* Oltz, D.F., ed., *Low temperature metamorphism of kerogen and clay minerals: Society of Economic Paleontologists and Mineralogists, Pacific Section*, p. 1-12.
- Peters, K.E., 1986, Guidelines for evaluating petroleum source rock using programmed pyrolysis: *American Association of Petroleum Geologists Bulletin*, v. 70, no. 3, p. 318-329.
- Spencer, C.W., 1984, Overview of U.S. Department of Energy Multiwell Experiment, Piceance Creek basin, Colorado, *in* Spencer, C.W., and Keighin, C.W., eds., *Geologic studies in support of the U.S. Department of Energy Multiwell Experiment, Garfield County, Colorado: U.S. Geological Survey Open-File Report 84-757*, p. 1-14.
- Sattler, A.R., and Lorenz, J.C., 1983, Topical discussion of organic maturation at Multiwell Experiment site (MWX): *Sandia National Laboratories Distribution Memorandum*, March 24, 1983.

Figure 1 (facing page). Hydrogen index versus oxygen index from Rock-Eval pyrolysis, MWX-1, -2, and -3, Piceance basin, Colorado. Thermal maturation paths for type I, II, and III sedimentary organic matter from Peters (1986). Data provided by J.C. Lorenz (Sandia National Laboratories, written commun., 1984).



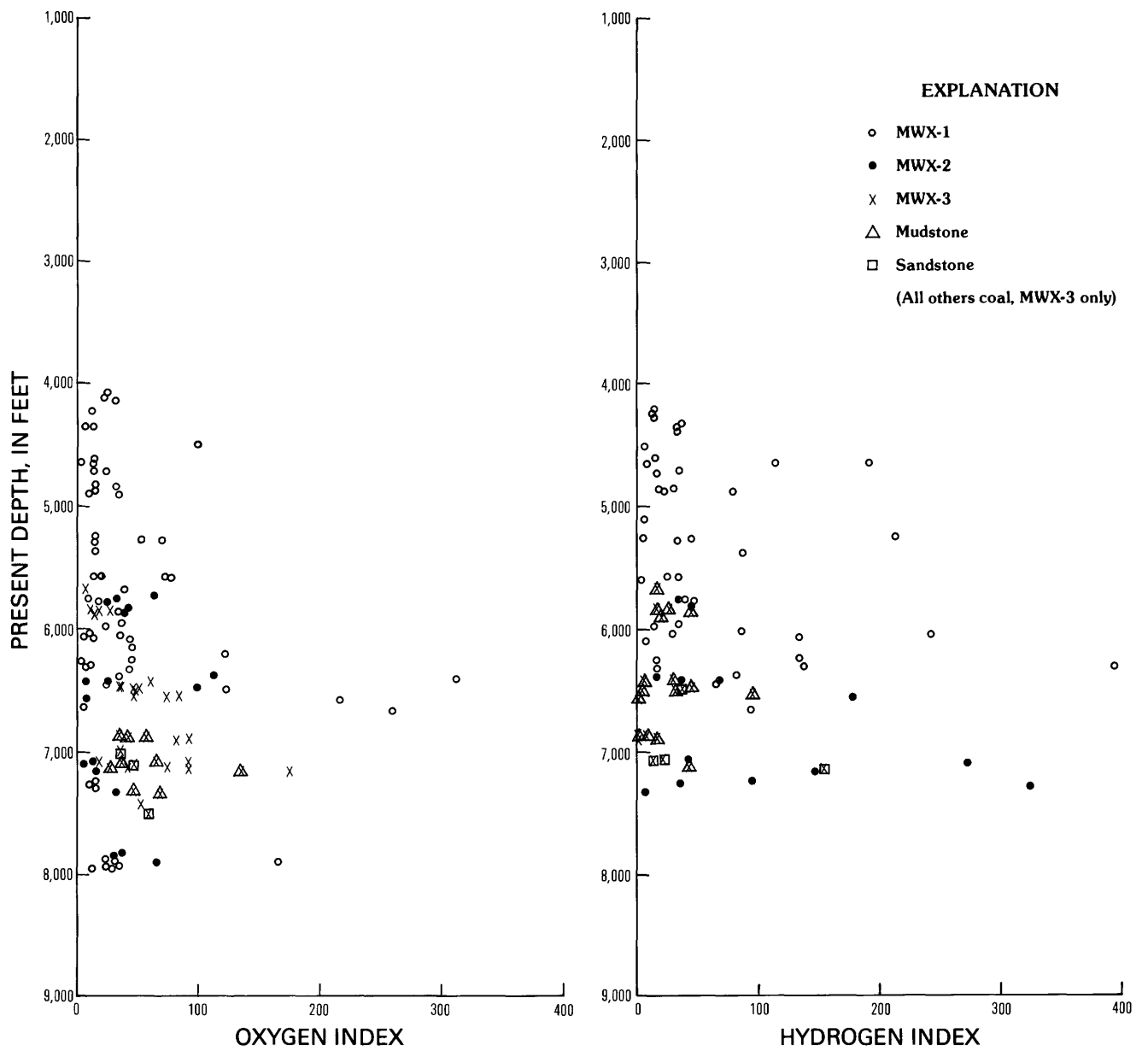


Figure 2. Hydrogen and oxygen indices versus depth, MWX-1, -2, and -3, Piceance basin, Colorado. More than one data point per sample is indicated by a number.

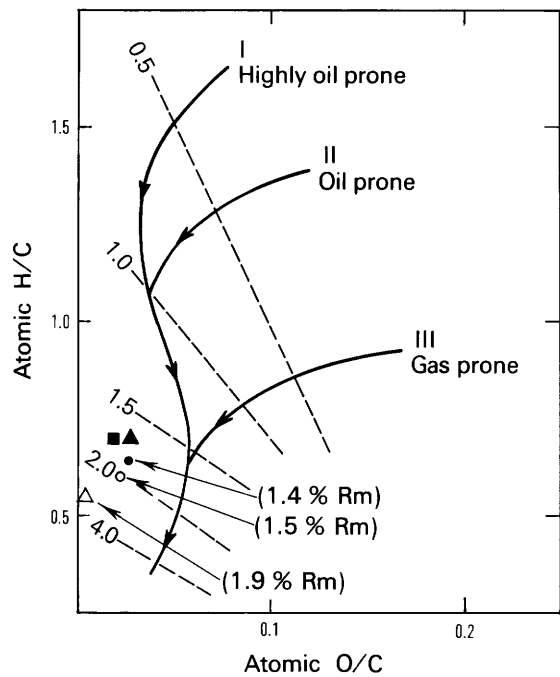
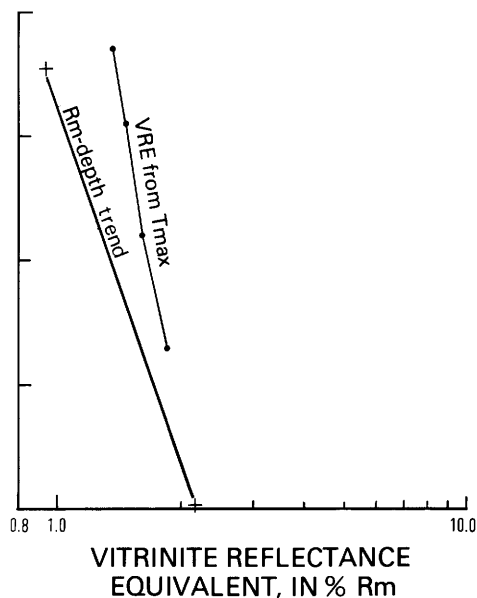
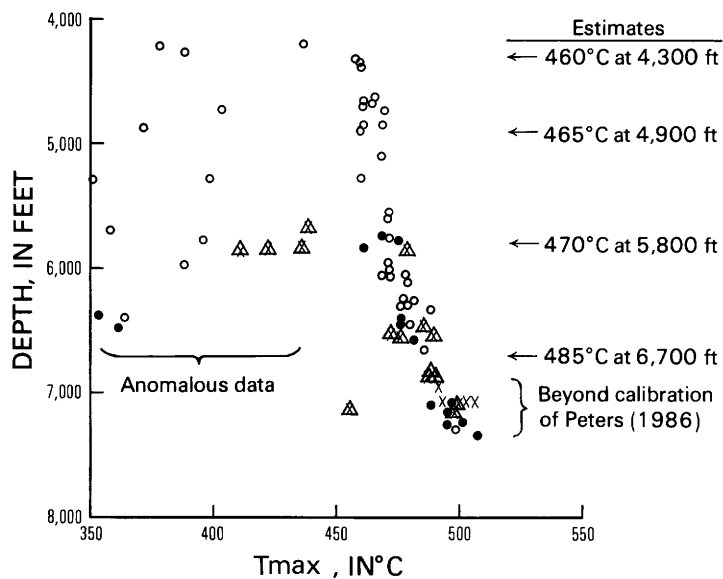


Figure 3. Van Krevelen diagram of coal ultimate analyses, MWX-1, Piceance basin, Colorado. Chemical analysis data in appendix 2. Mean vitrinite reflectance (Rm, in percent) shown for each sample. Thermal maturation paths (solid lines) and iso-vitrinite reflectance contours (dashed lines) from Jones and Edison (1978).

EXPLANATION

Sample	Depth (feet)
●	5,433
▲	6,601
■	6,647
○	6,827
△	7,950

Figure 4 (below). Rock-Eval Tmax, vitrinite reflectance (Rm, in percent) and vitrinite reflectance equivalent (VRE) versus depth, MWX-1, -2, and -3. Piceance basin, Colorado. Vitrinite reflectance profile from Nuccio and Johnson (this volume). Conversion of Tmax to VRE by using a line drawn through the midrange of Peters' calibration (1986, fig. 14).



EXPLANATION

○	MWX-1	} More than one data point per sample shown by number
●	MWX-2	
x	MWX-3	
△	Mudstone	} MWX-3 only
□	Sandstone	
	All others coal	

APPENDIXES 1, 2

Appendix 1. Rock-Eval pyrolysis data, MWX wells, Piceance basin, Colorado

[Data provided by J.C. Lorenz, Sandia National Laboratories. Analyses performed on a Delsi Rock-Eval system. See Peters (1986) for discussion of terminology. Total organic carbon (TOC) analyses of sample splits performed in a Leco WR-12 carbon determinator. Hydrogen index (HI) = (S2/TOC)X100. Oxygen index (OI) = (S3/TOC)x100. Transformation ratio = S1/(S1+S2). TOC, S1, S2, and S3 in mg/g; Tmax in °C. Asterisk (*) indicates Tmax value considered by analyst to be unreliable due to low concentration of S2. Leaders (--) indicate sample did not produce a complete pyrogram, and this parameter could not be computed]

Depth (meters)	Depth (feet)	TOC	S1	S2	S3	HI	OI	Trans- formation ratio	Tmax
MWX-1									
1,280	4,198.0	0.38	0.02	0.05	0.10	13.2	26.3	0.29	437*
1,283	4,210.0	0.33	0.01	0.04	0.08	12.1	24.2	0.20	379*
1,298	4,260.0	0.37	0.01	0.05	0.12	13.5	32.4	0.17	387*
1,322	4,336.0	0.68	0.01	0.25	0.08	36.8	11.8	0.04	458
1,330	4,363.0	0.58	0.01	0.18	0.05	31.0	8.6	0.05	460
1,331	4,368.5	0.57	0.01	0.18	0.08	31.6	14.0	0.05	460
1,375	4,510.0	0.15	0.02	0.01	0.15	6.7	100.0	0.67	285*
1,405	4,610.0	0.31	0.01	0.04	0.05	12.9	16.1	0.20	465*
1,416	4,647.0	3.26	0.64	3.70	0.15	113.5	4.6	0.15	461
1,417	4,647.5	21.88	4.67	41.93	0.75	191.6	3.4	0.10	461
1,419	4,654.0	0.21	0.02	0.02	0.03	9.5	14.3	0.50	465*
1,435	4,707.5	0.40	0.02	0.14	0.06	35.0	15.0	0.13	404
1,436	4,710.0	0.41	0.03	0.99	0.10	17.1	24.4	0.30	470
1,475	4,840.0	0.83	0.06	0.25	0.12	30.1	14.5	0.19	468
1,480	4,856.0	0.32	0.01	0.06	0.10	18.8	31.3	0.14	462
1,486	4,875.0	0.33	0.02	0.07	0.05	21.2	15.2	0.22	372*
1,489	4,884.0	0.63	0.08	0.50	0.07	79.4	11.1	0.14	460
1,555	5,101.0	0.14	0.01	0.01	0.05	7.1	35.7	0.50	469*
1,597	5,240.0	0.34	0.35	0.72	0.06	211.8	17.6	0.33	317
1,605	5,266.0	0.21	0.01	0.01	0.11	4.8	52.4	0.50	350*
1,608	5,275.1	1.08	0.34	0.47	0.76	43.5	70.4	0.42	460
1,608	5,277.0	0.39	0.07	0.13	0.06	33.3	15.4	0.35	399
1,641	5,386.0	0.49	0.22	0.43	0.08	87.8	16.3	0.34	312
1,698	5,570.5	0.43	0.04	0.14	0.09	32.6	20.9	0.22	472
1,702	5,584.2	1.08	0.34	0.47	0.76	43.5	70.4	0.42	460
1,702	5,585.0	0.41	0.03	0.10	0.06	24.4	14.6	0.23	471
1,702	5,585.0	0.43	0.01	--	0.34	--	79.1	--	--
1,736	5,697.0	0.25	0.01	0.01	0.10	4.0	40.0	0.50	359*
1,751	5,744.0	0.88	0.09	0.34	0.08	38.6	9.1	0.21	471
1,759	5,771.0	0.50	0.06	0.24	0.09	48.0	18.0	0.20	396
1,815	5,953.5	0.86	0.27	0.32	0.33	37.2	38.4	0.46	471
1,821	5,974.5	0.39	0.01	0.05	0.09	12.8	23.1	0.17	389*
1,831	6,006.0	2.36	0.92	2.05	0.25	86.9	10.6	0.31	472
1,841	6,041.0	1.58	0.38	0.46	0.56	29.1	35.4	0.45	478
1,847	6,059.7	4.43	1.97	10.74	0.35	242.4	7.9	0.15	468
1,847	6,060.0	5.21	1.49	6.99	0.60	134.2	11.5	0.18	472
1,859	6,099.0	1.01	0.22	0.10	0.45	9.9	44.6	0.69	479
1,870	6,134.0	0.78	0.09	--	0.37	--	47.4	--	--
1,890	6,200.0	0.33	0.03	--	0.40	--	121.2	--	--
1,899	6,231.0	7.93	1.71	10.39	0.33	131.0	4.2	0.14	477
1,908	6,259.0	1.02	0.17	0.19	0.46	18.6	45.1	0.47	481
1,919	6,294.7	23.76	13.15	93.86	2.85	395.0	12.0	0.12	476
1,919	6,294.8	14.90	3.45	20.50	1.39	137.6	9.3	0.14	478
1,928	6,324.0	1.56	0.28	0.30	0.69	19.2	44.2	0.48	489
1,949	6,395.0	0.91	0.68	0.74	0.34	81.3	37.4	0.48	364

Appendix 1. Continued

Depth (meters)	Depth (feet)	TOC	SI	S2	S3	HI	OI	Trans- formation ratio	Tmax
1,950	6,398.0	0.60	0.29	--	1.87	--	311.7	--	--
1,964	6,443.0	1.35	0.86	0.90	0.35	66.7	25.9	0.49	480
1,974	6,478.0	0.42	0.36	--	0.52	--	123.8	--	--
2,000	6,562.0	0.60	0.59	--	1.31	--	218.3	--	--
2,025	6,645.0	7.89	2.20	7.33	0.57	92.9	7.2	0.23	486
2,028	6,653.0	0.58	0.18	--	1.51	--	260.3	--	--
2,407	7,898.0	0.93	0.09	--	0.21	--	22.6	--	--
2,408	7,899.0	0.12	0.05	--	0.20	--	166.7	--	--
2,415	7,923.5	0.77	0.29	--	0.20	--	26.0	--	--
2,420	7,938.0	1.42	0.15	--	0.19	--	13.4	--	--
2,423	7,948.0	0.98	0.17	--	0.28	--	28.6	--	--
MWX-2									
1,739	5,707.0	0.45	0.06	--	0.29	--	64.4	--	--
1,750	5,741.0	0.71	0.20	0.23	0.23	32.4	32.4	0.47	469
1,761	5,776.0	0.90	0.16	0.41	0.21	45.6	23.3	0.28	475
1,775	5,825.0	0.33	0.05	--	0.14	--	42.4	--	--
1,784	5,854.0	0.51	0.06	--	0.20	--	39.2	--	--
1,784	5,854.1	0.54	0.12	--	0.19	--	35.2	--	--
1,948	6,390.0	0.35	0.22	0.06	0.41	17.1	117.1	0.79	354
1,951	6,401.0	0.97	0.16	0.35	0.25	36.1	25.8	0.31	476
1,953	6,408.0	4.32	1.03	2.90	0.38	67.1	8.8	0.26	477
1,979	6,492.0	0.33	1.03	0.12	0.33	36.4	100.0	0.90	361
2,003	6,570.0	5.59	1.88	9.98	0.46	178.5	8.2	0.16	480
2,158	7,081.0	3.69	0.99	1.54	0.44	41.7	11.9	0.39	497
2,164	7,100.1	21.55	14.91	58.27	1.30	270.4	6.0	0.20	489
2,179	7,148.0	13.83	2.74	20.44	2.19	147.8	15.8	0.12	495
2,203	7,228.0	8.24	3.95	7.74	1.49	93.9	18.1	0.34	503
2,207	7,241.0	4.20	1.24	1.46	0.44	34.8	10.5	0.46	495
2,222	7,290.0	12.27	6.77	39.62	1.98	322.9	16.1	0.15	498
2,229	7,313.0	1.68	0.34	0.13	0.53	7.7	31.5	0.72	515
2,385	7,825.0	0.81	0.13	--	0.31	--	38.3	--	--
2,387	7,830.0	0.73	0.02	--	0.22	--	20.1	--	--
2,407	7,898.0	0.97	0.10	--	0.29	--	29.9	--	--
2,408	7,900.0	0.58	0.20	--	0.38	--	65.5	--	--
2,409	7,905.0	0.62	0.40	--	0.20	--	32.3	--	--
MWX-3									
1,773	5,817.2	0.33	0.09	0.06	0.08	18.2	24.2	0.60	436*
1,782	5,847.5	0.77	0.24	0.22	0.15	28.6	19.5	0.52	479*
1,783	5,849.9	0.24	0.05	0.03	0.11	12.5	45.8	0.63	423*
1,787	5,863.2	0.39	0.04	0.05	0.08	12.8	20.5	0.44	412*
1,960	6,431.5	2.10	0.37	1.30	0.15	61.9	7.1	0.22	476
1,975	6,480.2	1.10	0.25	0.39	0.35	35.5	31.8	0.39	486
1,736	5,694.0	0.21	0.02	0.02	0.04	9.5	19.0	0.50	437*
1,976	6,483.2	0.93	0.38	0.37	0.42	39.8	45.2	0.51	485
1,978	6,488.2	0.99	0.46	0.48	0.39	48.5	39.4	0.49	484
1,979	6,493.2	0.73	0.38	0.36	0.25	49.3	34.2	0.51	485
1,987	6,519.2	1.38	0.44	0.64	1.30	46.4	94.2	0.41	490
1,987	6,520.5	3.40	0.79	2.83	0.16	83.2	4.7	0.22	473
1,990	6,528.3	2.91	0.64	2.04	0.10	70.1	3.4	0.24	476
2,098	6,883.2	8.09	1.23	4.62	0.20	57.1	2.5	0.21	488
2,098	6,882.4	1.85	0.20	0.70	0.18	37.8	9.7	0.22	490

Appendix 1. Continued

Depth (meters)	Depth (feet)	TOC	SI	S2	S3	HI	OI	Trans- formation ratio	Tmax
2,100	6,890.5	1.04	0.28	0.42	0.16	40.4	15.4	0.40	488
2,103	6,898.7	8.56	1.40	7.03	0.23	82.1	2.7	0.17	487
2,104	6,904.2	14.36	3.10	13.21	0.32	92.0	2.2	0.19	488
2,105	6,906.6	11.14	1.31	6.21	0.27	55.7	2.4	0.17	491
2,155	7,071.2	12.12	1.41	7.78	0.18	64.2	1.5	0.15	494
2,156	7,072.3	14.16	1.54	12.88	0.60	91.0	4.2	0.11	504
2,157	7,077.3	1.16	0.09	0.23	0.11	19.8	9.5	0.28	506
2,158	7,079.8	1.75	0.49	0.64	0.19	36.6	10.9	0.43	499
2,159	7,084.6	1.13	0.42	0.44	0.23	38.9	20.4	0.49	495
2,164	7,100.3	1.78	0.48	0.77	0.29	43.3	16.3	0.38	494
2,166	7,105.5	59.26	3.40	55.58	0.47	93.8	0.8	0.06	490
2,167	7,108.4	68.07	2.92	50.69	0.32	74.5	0.5	0.05	489
2,167	7,110.5	6.77	1.35	3.09	0.06	45.6	0.9	0.30	498

Appendix 2. Coal analysis data, MWX-1, Piceance basin, Colorado

[Rm, mean random vitrinite reflectance (in percent), except where noted mx (maximum). Elemental analysis: H, C,N in weight percent (d.a.f.); O in percent (d.a.f.) by difference; S in weight percent (as received; ash in percent (dry). Proximate analysis: moisture in percent (as received); volatile matter and fixed carbon in weight percent (d.a.f.); ash in percent (dry); heating value in BTU/pound. N.R., not reported; N.D., not determined. Data from Sattler and Lorenz (1983)]

Depth		Elemental analysis							Atomic		Proximate analysis				
(meters)	(feet)	Rm	H	C	O	N	S	Ash	H/C	O/C	Moisture	Volatile matter	Fixed carbon	Ash	Heating value
1,656	5,433	1.52mx 1.43	4.90	90.05	3.22	1.33	0.5	N.R.	0.65	0.27	0.88	23.47	76.53	11.90	15,779
2,012	6,601	N.D.	5.23	88.35	3.20	2.07	1.15	38.05	0.705	0.0272	0.83	24.25	75.75	38.05	15,374
2,026	6,647	N.D.	5.21	88.96	2.32	2.00	1.51	16.22	0.698	0.0195	0.72	21.68	78.32	16.22	15,590
2,081	6,827.2	1.50	4.62	89.55	2.55	1.91	1.17	8.66	0.615	0.0214	0.74	21.13	78.87	8.68	15,779
2,423	7,950.1	2.07	4.19	88.92	0.50	1.51	4.87	17.68	0.561	0.00418	0.72	14.39	95.61	17.68	15,298

Chapter O

Azimuthal Vertical Seismic Profiles at the Multiwell Experiment Site, Northwest Colorado

By MYUNG W. LEE

Prepared in cooperation with the U.S. Department of Energy

U.S. GEOLOGICAL SURVEY BULLETIN 1886

GEOLOGY OF TIGHT GAS RESERVOIRS IN THE PINEDALE ANTICLINE AREA, WYOMING,
AND AT THE MULTIWELL EXPERIMENT SITE, COLORADO

CONTENTS

Abstract	01
Introduction	01
Data acquisition and processing	02
Discussion	02
Interpretation	06
Identification of coastal sandstone reservoirs	06
Geometry of coastal sandstone bodies	011
Conclusions	013
References cited	014

FIGURES

1. Map showing configuration of seismic study and topography of area, MWX site 01
2. Flow chart showing processing steps for far-offset vertical seismic profile data 03
- 3-4. Logs showing:
 3. Stacked vertical-component data for MWX-3 well 04
 4. Processed vertical seismic profile data for MWX-3 well 05
5. Schematic diagram of ray path for truncated body 06
6. Diagram showing spatial distribution of sandstone bodies and trace of gamma-ray logs for the coastal zone of MWX-1, -2, and -3 wells 07
7. Relative impedance log in two-way travel time for MWX-3 well 08
8. Synthetic seismograms generated by using impedance log and various zero-phase bandpass filters 09
9. Diagrams showing identification of lower coastal zone at MWX-3 from source location 1 010
- 10-11. Logs showing laterally stacked and cumulatively summed vertical-component data at MWX-3 from:
 10. Source location 1 011
 11. Source location 2 012
12. Log showing laterally stacked and cumulatively summed, horizontally polarized shear wave component data at MWX-3 from source location 2 013
- 13-14. Logs showing laterally stacked and cumulatively summed vertical-component data at MWX-3 from:
 13. Source location 3 014
 14. Source location 4 015
15. Log showing laterally stacked vertical-component data at MWX-3 from source location 2 016
16. Schematic interpretation of geometry of lower coastal sandstone bodies in MWX-3 well 016

TABLE

1. Summary of vertical seismic profile data 03

Azimuthal Vertical Seismic Profiles at the Multiwell Experiment Site, Northwest Colorado

By Myung W. Lee

Abstract

An azimuthal vertical seismic profile (VSP) experiment was conducted at the U.S. Department of Energy Multiwell Experiment site to delineate lenticular, very low permeability (tight), gas-bearing sandstone bodies in the Mesaverde Group in the southern Piceance basin of northwest Colorado. Profiles of two wells were created by using a triaxial, three-component downhole geophone and a 450-in.³ surface airgun source at four different locations. The azimuthal VSP data were analyzed and interpreted by using the laterally stacked vertical component of the VSP data, one- and three-dimensional seismic modeling, and a geological interpretation of the area.

Individual sandstone bodies in the coastal interval were difficult to identify or delineate because of the lack of high-frequency components in the seismic data. The lower coastal sandstone bodies could be mapped, however, by using the azimuthal VSP data. One lower coastal sandstone probably trends northeast and has an average width of 800 ft, and a second probably trends northwest and has an average width of 600 ft. The results of this study are similar to those from a sedimentological study of the coastal interval and suggest that azimuthal VSP surveys may be used to detect and delineate bodies of finite extent such as reservoirs.

INTRODUCTION

Three wells were drilled at the U.S. Department of Energy Multiwell Experiment (MWX) site about 9 mi southwest of Rifle, Colo., and are designated MWX-1, -2, and -3 (fig. 1) (Law and Spencer, this volume, fig. 1). The purpose of the experiment was to delineate both the character of sandstone lenses within the Upper Cretaceous Mesaverde Group in western Colorado and the geometry of significant tight-gas reservoirs in order to better analyze these unconventional gas resources in the Piceance basin. To this end, a comprehensive three-phase seismic program was initiated to determine how well seismic studies can map these discontinuous sandstone bodies. The program included a high-resolution three-dimensional survey, a vertical seismic profile, and a hole-to-hole survey (Searls and others, 1983). My studies focus on the second phase of the seismic program, vertical seismic profiling.

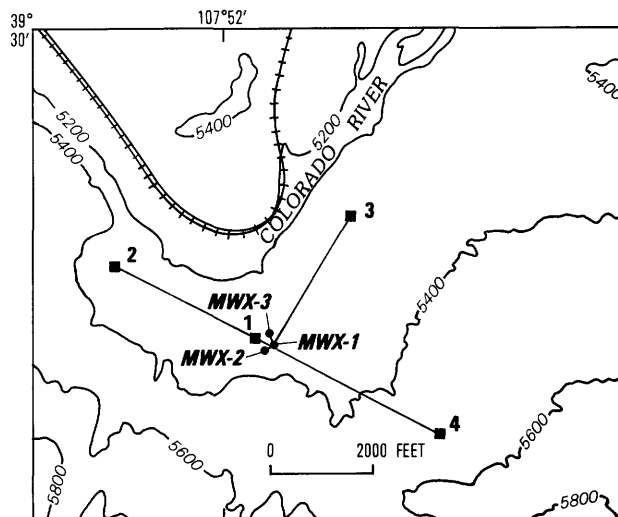


Figure 1. Configuration of seismic study and topography of area, MWX site, northwest Colorado. Solid circle indicates location of well; solid square indicates seismic study source location. Contour interval, 200 ft. Source location 1 is on drill pad of MWX-2.

Vertical seismic profile (VSP) data were collected during two separate field operations. In May 1982 data were collected from two source locations using the MWX-1 and -2 wells (Lee, 1984a), and in April 1984 data were collected simultaneously from four different source locations using the MWX-2 and -3 wells.

The primary objective of the 1982 field operation was to collect VSP data that could be correlated to three-dimensional high-resolution surface seismic data previously collected. The VSP and three-dimensional data would then be used to delineate the lateral extent of the tight-gas sandstone reservoirs (Searls and others, 1983). Analysis of the surface seismic data indicated that the spatial distribution of the sandstone bodies is difficult to map because only low-frequency seismic events were recorded at the surface. Analysis of the VSP data indicated, however, some possibilities for delineating lenticular sandstone bodies.

After an extensive feasibility study of the mapping of lenticular sandstone bodies by using VSP techniques (Lee, 1984b), an azimuthal VSP survey (one near-offset profile and three far-offset profiles) was conducted in April 1984 to determine the lateral extent of the coastal sandstone reservoirs. This paper presents an interpretation of this second survey.

The quality of the VSP data is not as good as desired because of extremely bad weather conditions and time limitations. Although the lack of high-frequency reflections made it impossible to identify or delineate individual sandstone bodies in the coastal zone, two lower coastal sandstone lenses were identified. These lenses are most likely the Yellow and Red zones of J.C. Lorenz (Sandia National Laboratories, written commun., 1985; Sattler and others, 1986); that is, the VSP study delineated the top of Lorenz's Yellow A zone and the bottom of his Red B zone. The orientation of these sandstone bodies was determined by using laterally stacked VSP data, geologic information (J.C. Lorenz, written commun., 1985), and three-dimensional seismic modeling.

Acknowledgments.—My sincere appreciation is extended to the CER Corporation, Sandia National Laboratories, and U.S. Department of Energy for their support of this investigation. Particular appreciation is expressed to C.A. Searls and A.L. Sattler of Sandia National Laboratories, to J.J. Miller, J. Leinbach, N. Zihlman, D. Smith and H. Oliver of the U.S. Geological Survey for their assistance in the data collection under adverse field conditions, and especially to Keith Westhusing of the U.S. Department of Energy, Morgantown, W. Va., who originally suggested this research and provided encouragement and support throughout the project.

DATA ACQUISITION AND PROCESSING

VSP data at MWX-2 and -3 were digitally recorded on a MDS-10 seismic recording system using a sampling interval of 1 millisecond and a record length of 5 seconds. The seismic sources were two Bolt LSS-1T land airguns, each capable of delivering 1,500 tons of force into the ground. The seismic signal was detected in each well simultaneously by using a triaxial three-component wall-locking geophone (one vertical and two horizontal components, oriented orthogonally), designed and provided by Sandia National Laboratories.

Data from each component were amplified in two stages (high and low gain). The output of each stage modulated a constant-bandwidth (4 kHz), voltage-controlled oscillator. The eight modulated signals were frequency-division multiplexed and transmitted along a single conductor wire line in each well to the surface instruments where they were demodulated.

Four source locations were distributed around the two wells (fig. 1). Because only two airguns were available, each well was profiled twice and a sampling interval of 25 ft was used. In the initial source configuration, one source was located at source location 1 and another at source location 3. Each source was energized alternately, four times per geophone level.

This experiment was planned originally for late autumn or early winter of 1983 in order to take advantage of optimum field conditions; that is, cool weather and dry ground. The experiment was delayed, however, until April 1984. During this time period, the ground was wet from spring snowmelt and runoff and the weather unpredictable. In addition, local ranchers had opened up their irrigation ditches a week previously, and the fields in which the airguns were located became muddy quagmires.

Because of the weight and impact force of the airgun trucks, deep holes were dug into the muddy ground and the operators were forced to move the trucks as often as every 20 shots to avoid becoming stuck; on two occasions, a bulldozer was needed to free the trucks. Because the trucks were moved as far as 200 ft from their original locations, timing discrepancies and waveform variability resulting from the large number and distribution of source locations caused serious processing and interpretation problems. Source location 1, located on the drill pad of MWX-2 and reinforced with gravel, was the only source location not moved extensively.

A flow sheet showing the processing steps for far-offset VSP data is shown in figure 2. Details of data acquisition and processing are in Lee and Miller (1985), and a summary of the VSP data is shown in table 1.

DISCUSSION

One method proposed to delineate the lenticular sandstone bodies is to analyze the variation in reflection amplitude with respect to lateral distance from a well by using laterally stacked VSP data (Lee, 1984b). In this technique, the amplitude, arrival time, frequency content of reflected events, and propagation modes all are considered.

One of the biggest problems during data acquisition was the extremely soft ground, particularly at source locations 3 and 4, which necessitated frequently moving the surface airgun source. The raw stacked vertical-component VSP data from source location 4 is shown in figure 3A. While this profile was being made, the source was moved at least 24 times. These moves show on the record either as abrupt changes of first arrival times or as substantial changes in reverberation patterns. The abrupt changes in arrival times may result from gradual compaction of the near-surface medium during

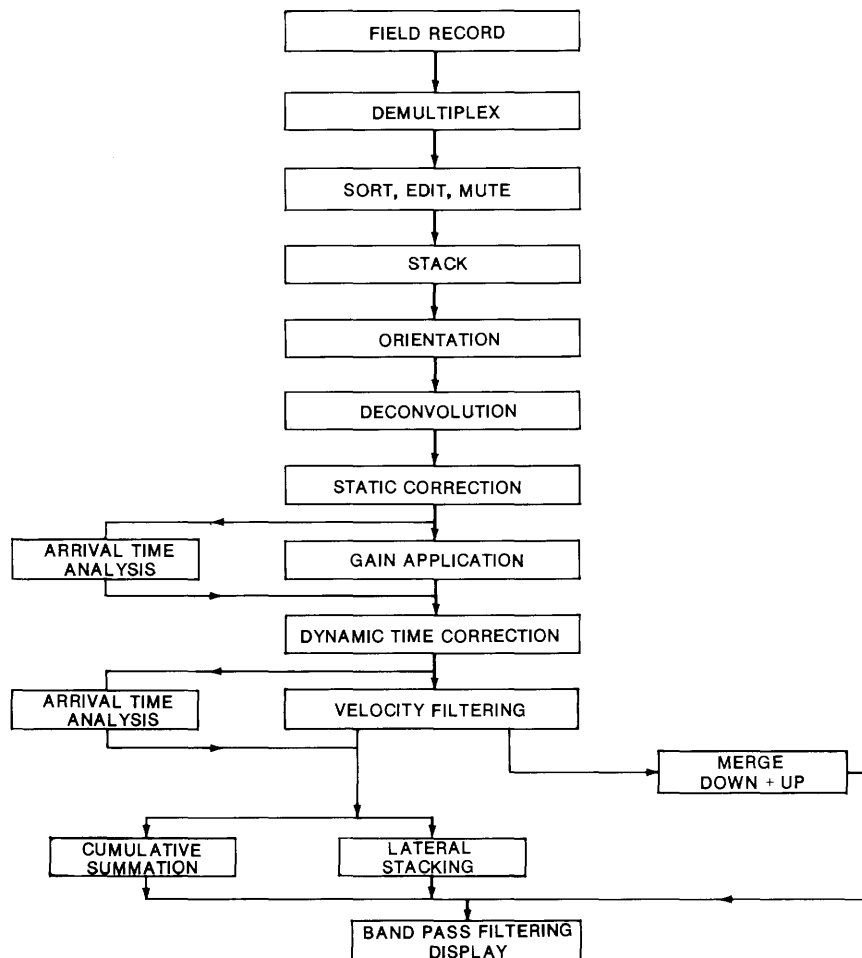


Figure 2. Processing steps for far-offset vertical seismic profile (VSP) data.

Table 1. Summary of vertical seismic profile (VSP) data
[Configuration of seismic study shown in figure 1]

Source location	Timing error	Reflection amplitude	Dominant frequency	Maximum source movement within source location	Airgun used*
1	Small	Reliable	35	Small	1
2	Small	Reliable	35	200 ft, parallel with source-to-well azimuth	1
3	Some	Probable	25	200 ft, perpendicular to source-to-well azimuth	2
4	May be substantial	Probable	25	200 ft, in random directions	2

*Airgun 1 performed without problems during fieldwork; airgun 2 malfunctioned and was not resynchronized.

the shooting, changes in distance between the well and the individual source point, or a combination of the first two. As mentioned in Lee and Miller (1985), no reliable monitor records are available to correct or compensate for the above-mentioned source variations, and some errors in timing and amplitude exist for all processed VSP data, particularly those from source location 4.

Figure 3B shows the raw stacked vertical-component data from source location 2. Arrival times at this location are quite different from those at source location 4. For example, at a well-seismometer depth of 2,000 ft, the arrival time of the trough following onset

is 447 milliseconds at source location 4 and 331 milliseconds at source location 2. Some part of this time difference may result from low-velocity surface material at source location 4. (This source location was completely water saturated.) Most of this large time difference cannot be explained, however, unless a constant time delay difference existed between the two airgun firing circuits, and such a delay was not noticed during the fieldwork.

In addition to the time-uncertainty problem, the low-frequency content of the source signal limits interpretation of the VSP data. The low-frequency content of VSP data from source locations 3 and 4 most probably

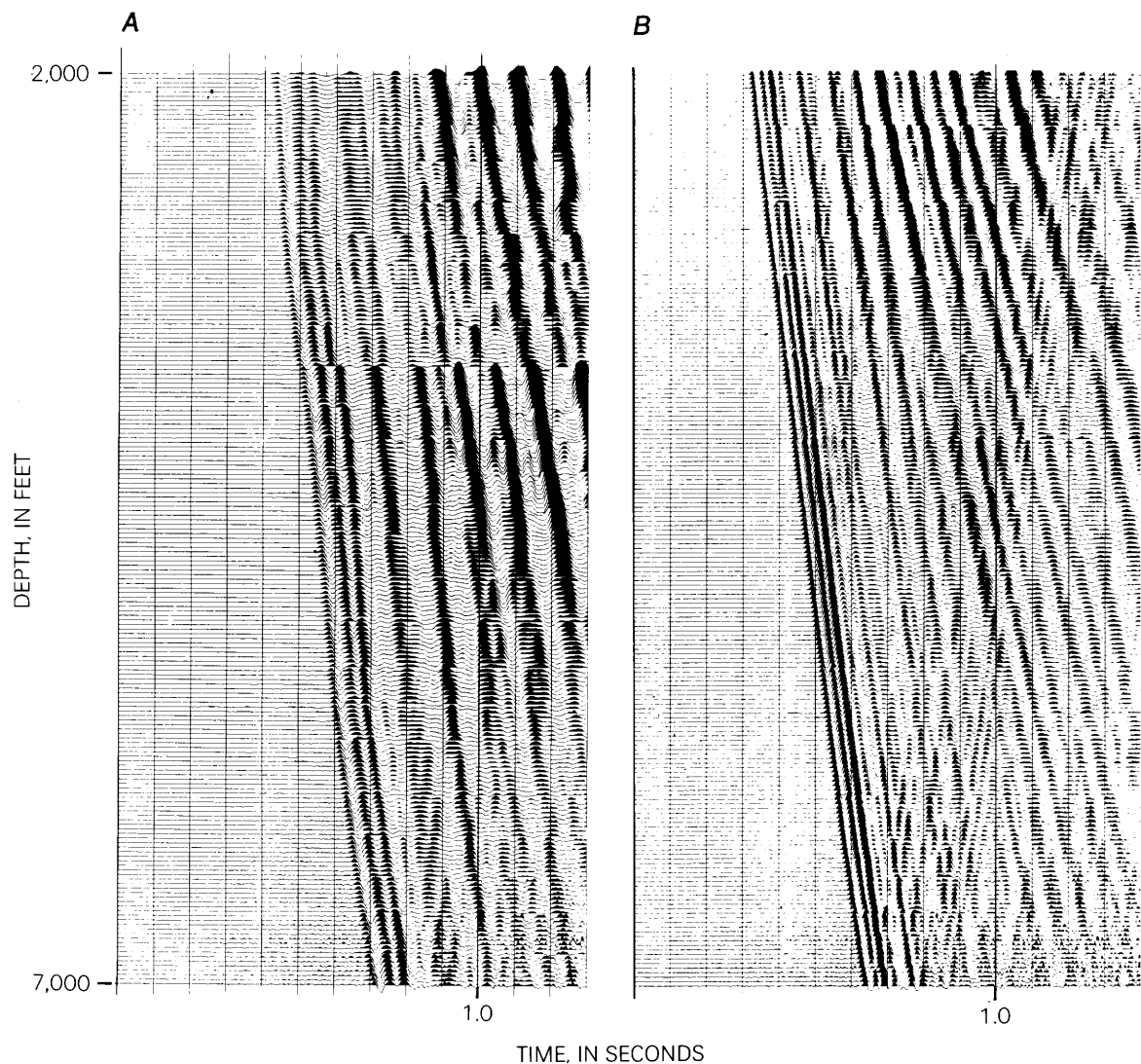


Figure 3. Stacked vertical-component data for the MWX-3 well. *A*, Source location 4. *B*, Source location 2.

results from poor source coupling to the ground. Deconvolution provided for adequate contraction of the complicated and slowly decaying reverberatory downgoing signal and broadening of the amplitude spectrum, and the usable frequency content could be extended as high as 75 Hz for source location 2 (Lee, 1985). Although deconvolution of data at source location 4 substantially improved the data, the overall frequency content is less than for source location 2.

The foregoing discussion indicates that good ground coupling of the source in the field can substantially improve the overall quality of the VSP data; unfortunately, during this investigation less-than-desirable source location position was dictated by the soft ground that resulted from rain and snow.

The far-offset VSP data show complicated wave interference patterns, particularly in the upper part of the section. Figure 4 shows an example of the processed VSP

data at MWX-3 from a source (location 2) about 3,000 ft northwest of the well. Figure 4*A* was processed to emphasize mode conversions at the acoustic boundaries, and figure 4*B* was processed to enhance converted upgoing shear waves. Figure 4 also shows that the surface airgun source generated substantial amounts of shear (*S*) waves (note complicated wave fields). Near the Tertiary-Cretaceous unconformity, at a depth of about 3,900 ft, converted, transmitted, and reflected *S*-waves can be seen in addition to transmitted and reflected longitudinal (*P*) waves. The mode conversions at the boundary affect not only processing but also interpretation.

Shear waves on the VSP profiles provide both advantages and disadvantages for interpretation. The advantages should be fully utilized, and most of the disadvantages can be handled by careful processing. One advantage of analyzing converted vertically polarized shear (*SV*) waves is shown in figure 5. Figure 5*A* shows

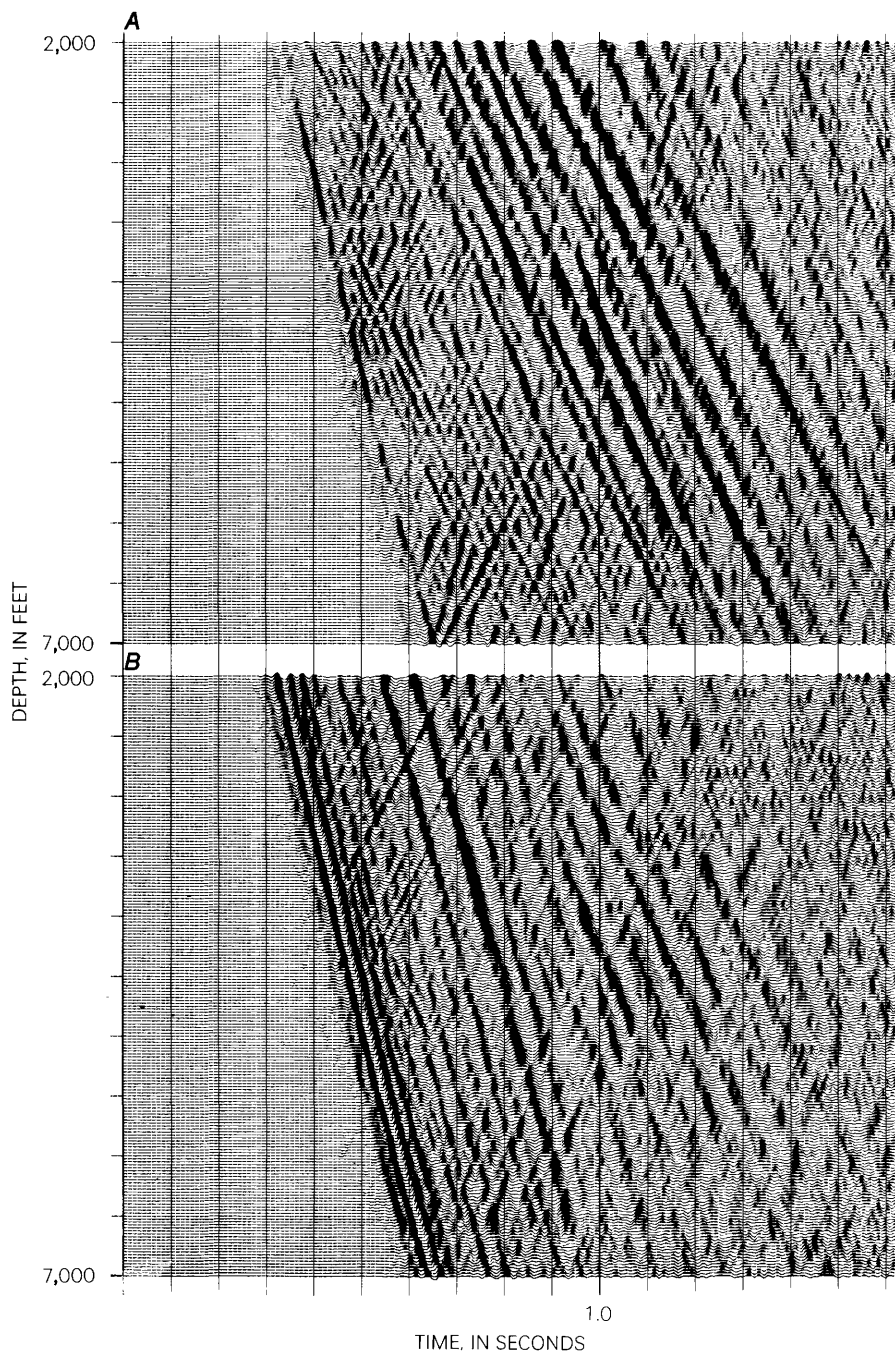


Figure 4. Processed vertical seismic profile data for the MWX-3 well from source location 2. *A*, Data processed in order to analyze mode conversions at the acoustic boundary. *B*, Data processed in order to analyze converted upgoing shear (*SV*) wave.

a schematic ray-path diagram for a truncated body. The downgoing P -wave is reflected at the edge of the body and propagates as both a P -wave and a converted SV -wave. The specular reflection ray path of the P -wave is recorded as the reflected event at a well-seismometer depth of Z_p , and SV -wave at Z_s . The depth of Z_s is shallower than Z_p by Snell's law.

The kinematics of the different arrival times are shown schematically in figure 5B. If the edge of the sandstone body is identified at the well-recording depth Z_p by P -wave analysis and the converted SV -wave extends vertically greater than the P -wave event (in the direction of the shallow well-phone depth), then the edge of the truncated body can be interpreted with higher reliability. Identification of converted SV -waves at the acoustic boundary may also help reduce the incidence of selecting erroneous reflected events.

Analysis of far-offset VSP data confirms the presence of converted SV -waves at the acoustic boundaries of interest. The extension of SV -wave events beyond P -wave events is not confirmed, partly because the SV -waves were attenuated higher than the P -waves and partly because interference patterns in the upper section are very complicated.

Horizontally polarized shear (SH) waves are also useful in interpreting VSP data, and the reliability of interpreting SH -wave information derived from good VSP data shot by a surface source is documented by Lee (1984b). In this study, SH -wave analysis was not used,

except at source location 2, because of the low signal-to-noise ratio of SH -waves in this azimuthal VSP survey.

In order to estimate the frequency needed to delineate the lower coastal sandstone bodies, a one-dimensional model was studied. The lower coastal interval below 6,420 ft in the MWX-3 well contains five sandstone lenses; they have a two-way time thickness of about 20 milliseconds.

The model study indicates that unambiguous identification of individual sandstone reservoirs can be made if the dominant frequency is about 200 Hz. In addition, the synthetic seismogram with the extracted source wavelet is very similar to that of the 30-Hz Ricker wavelet. This similarity implies that the dominant frequency of the observed VSP data is about 30 Hz, well below that needed to resolve individual sandstone bodies (Lee, 1985).

INTERPRETATION

Identification of Coastal Sandstone Reservoirs

Identification of the coastal sandstone lenses by using the seismic sections is difficult because of the lack of impedance contrast between intervening shales, the thinness of the lenses, and the lack of high-frequency content. Figure 6 shows the spatial distribution of individual sandstone bodies near the well sites, as determined by

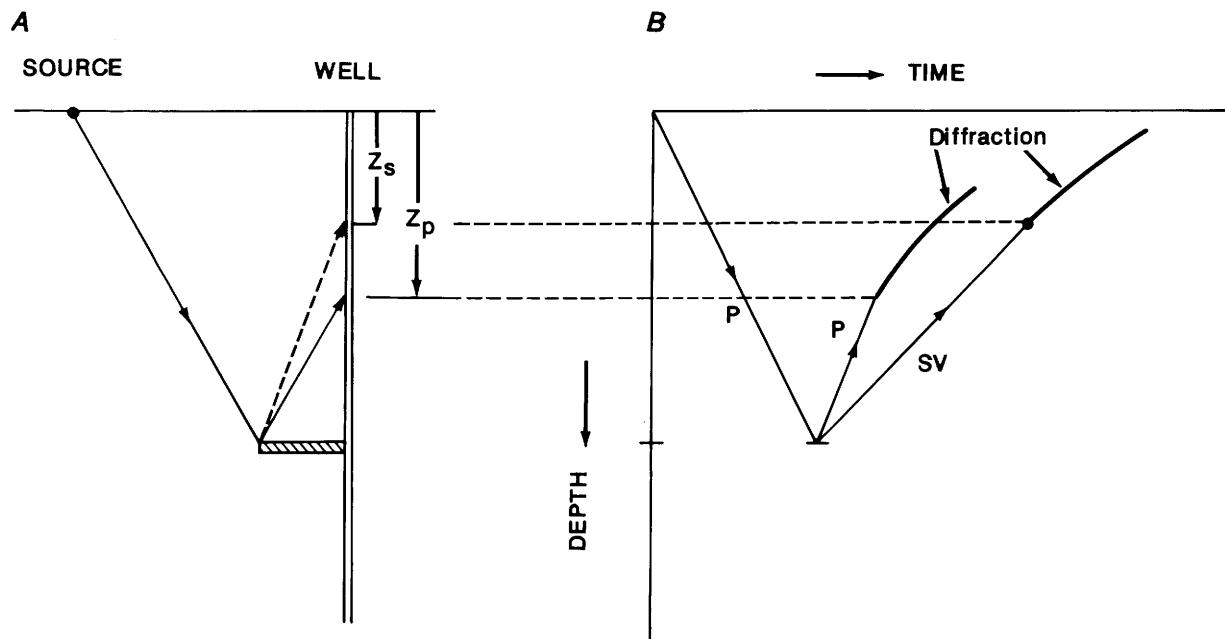


Figure 5. Schematic diagram of ray path for a truncated body (patterned area). A, Ray path for converted shear (SV) (dashed line) and longitudinal (P) (solid line) waves. Z_p and Z_s are well-seismometer depths of P and SV waves, respectively. B, Arrival time for reflected P - and SV -waves.

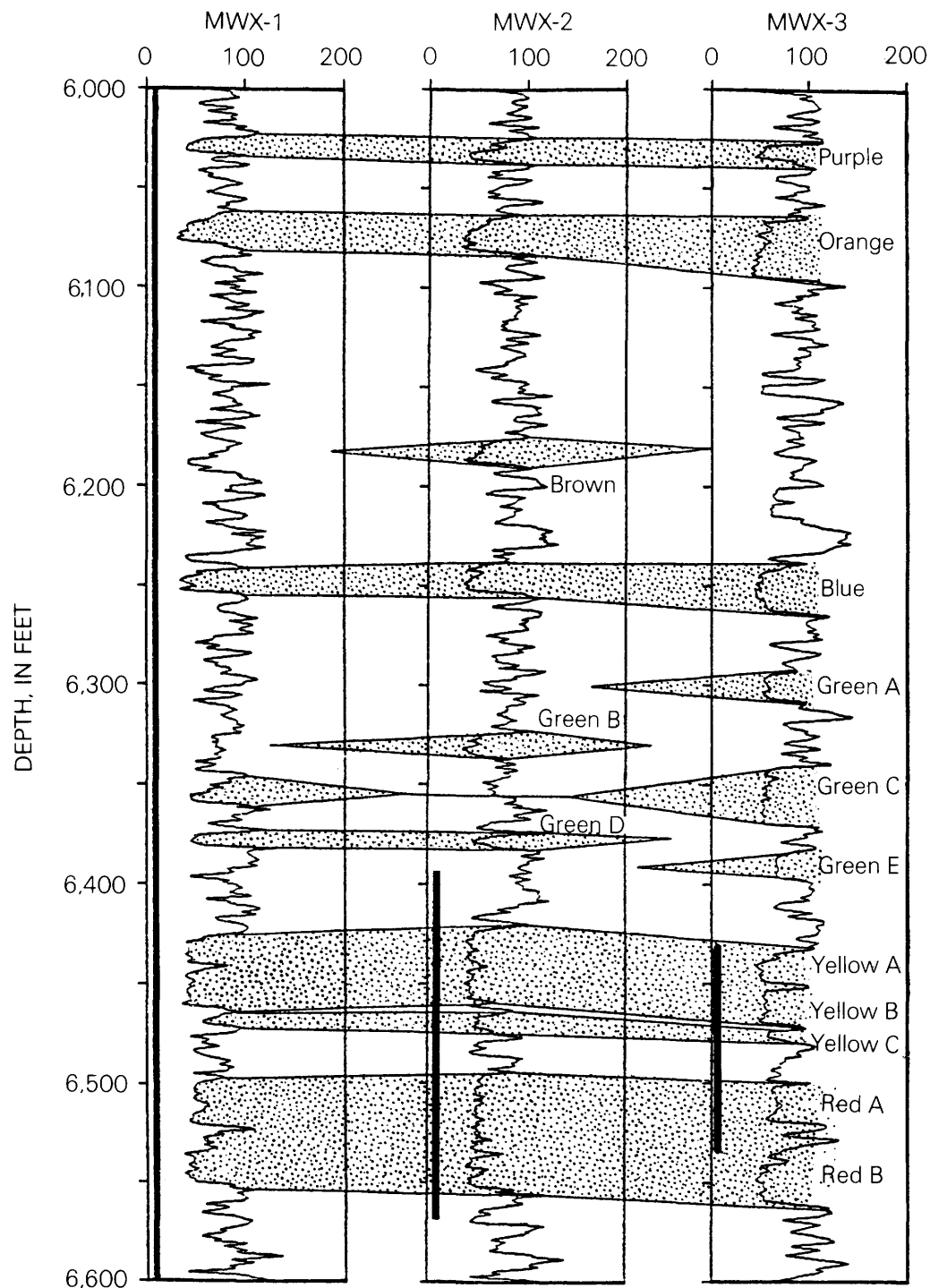


Figure 6. Spatial distribution of sandstone bodies (stippled pattern) and trace of gamma-ray logs for the coastal zone of the MWX-1, -2, and -3 wells. Modified from J.C. Lorenz (written commun., 1984) and Sattler and others (1986).

J.C. Lorenz (written commun., 1984; Sattler and others, 1986).

Results of a previous VSP study by Lee (1984a) indicate that seismic responses of the upper coastal sandstones above a depth of 6,400 ft are too weak to interpret

because of the thinness of the lenses, and data from the present study confirm this conclusion. My interpretation focuses, therefore, on the lower coastal sandstone bodies, the Yellow and Red zones of J.C. Lorenz (1984, written commun.).

Figure 7 shows the relative impedance log, in two-way travel time, derived from the sonic and density logs at the MWX-3 well between depths of 6,000 and 7,000 ft. From this impedance log, synthetic seismograms were generated by using various zero-phase bandpass filters (fig. 8).

The lowermost panel of figure 8 shows the seismic response obtained by using a 2/4–250/300-Hz wavelet bandpass filter. The top of the Yellow A sandstone appears as a strong peak, the top of the Red A as a small peak, and the bottom of Red B as a small trough. If the frequency content is lowered, the character of the seismic response changes dramatically. The second panel from the bottom of figure 8 shows the seismic response using 2/4–72/100-Hz wavelet bandpass filter; most of the seismic energy observed in the high-frequency section has disappeared and overall amplitudes are much lower than those in the higher frequency version. The third panel from the bottom shows the same response plotted using a different gain, and the top panel of figure 8 shows the response obtained by using a 4/8–52/62-Hz wavelet bandpass filter.

If the frequency content is lowered, the base of the Red B sandstone is the strongest trough in the seismogram and the peak that represents the top of the Yellow A sandstone in the high-frequency version is shifted to a later time. The overall seismic response in the frequency range of 4/8–52/62 Hz represents only the complicated interference peaks and troughs, and all of the lower coastal sandstone bodies are within 3/4 of the dominant period.

The rather obvious question is how much do the sandstone lenses in the lower coastal interval contribute to the overall seismic character shown in the top panel of figure 8. In an attempt to answer this question, the lower part of the near-offset VSP data (source location 1) was reprocessed very carefully. An inversion method that includes three depth intervals was used to extract outgoing waves in order to minimize spatial mixing of the outgoing waves during multichannel velocity filtering.

The downgoing wave and its amplitude spectrum at a well-seismometer depth of 6,000 ft are shown in figure 9A; the outgoing wave field was shifted in order to align coherent events between depths of 5,925 and 7,000 ft (fig. 9B). The peak-trough combination shown in the top panel of figure 8 can be seen in the processed VSP data, and the overall seismic character near the coastal sandstone lenses is very similar to that derived from the impedance log.

In the VSP section (fig. 9), the trough corresponding to the base of the Red B sandstone timewise appears to start at about 6,550 ft, the depth of the base of the Red B sandstone. The preceding peak appears to start at about 6,425 ft, the depth of the top of the Yellow A sandstone. The sharpness of the downgoing wave at 6,000 ft (fig. 9A) suggests that the preceding peak is not likely the result of the side lobe of the strong trough.

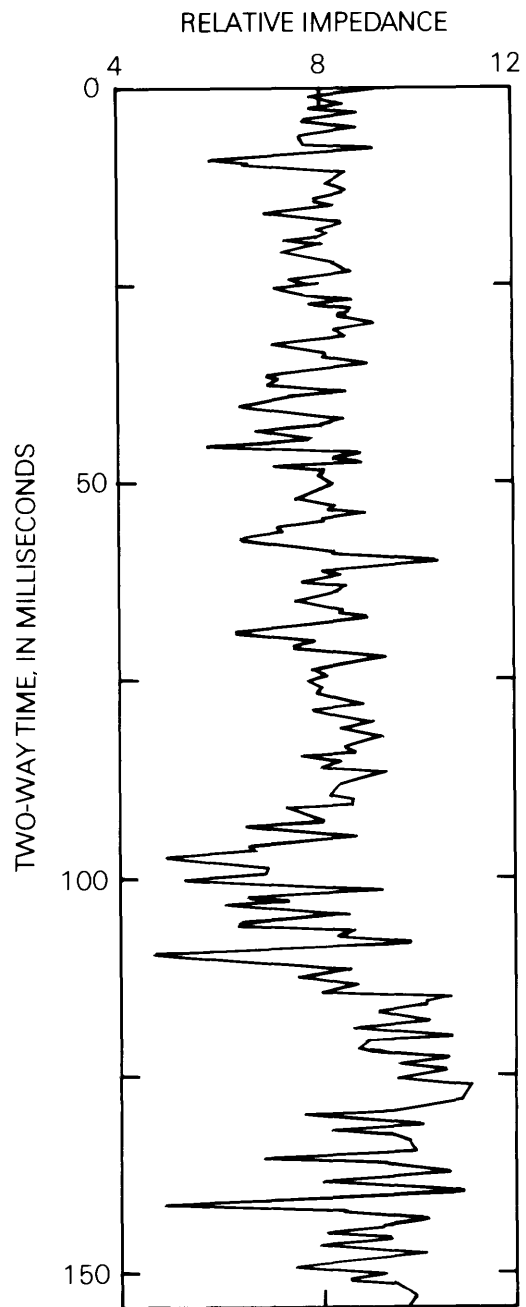


Figure 7. Relative impedance log in two-way travel time for the MWX-3 well between depths of 6,000 and 7,000 ft.

Based on the above analyses and observations, I conclude that the peak amplitude within the lower coastal interval is caused by the presence of the Yellow A sandstone and that the following trough represents the base of the Red B sandstone. I am unable to estimate the contribution of individual sandstone bodies in the Yellow (Yellow A, B, and C, fig. 6) and Red (Red A and B, fig. 6) zones to the overall seismic response, and I believe that the peak in the lower coastal interval represents the average

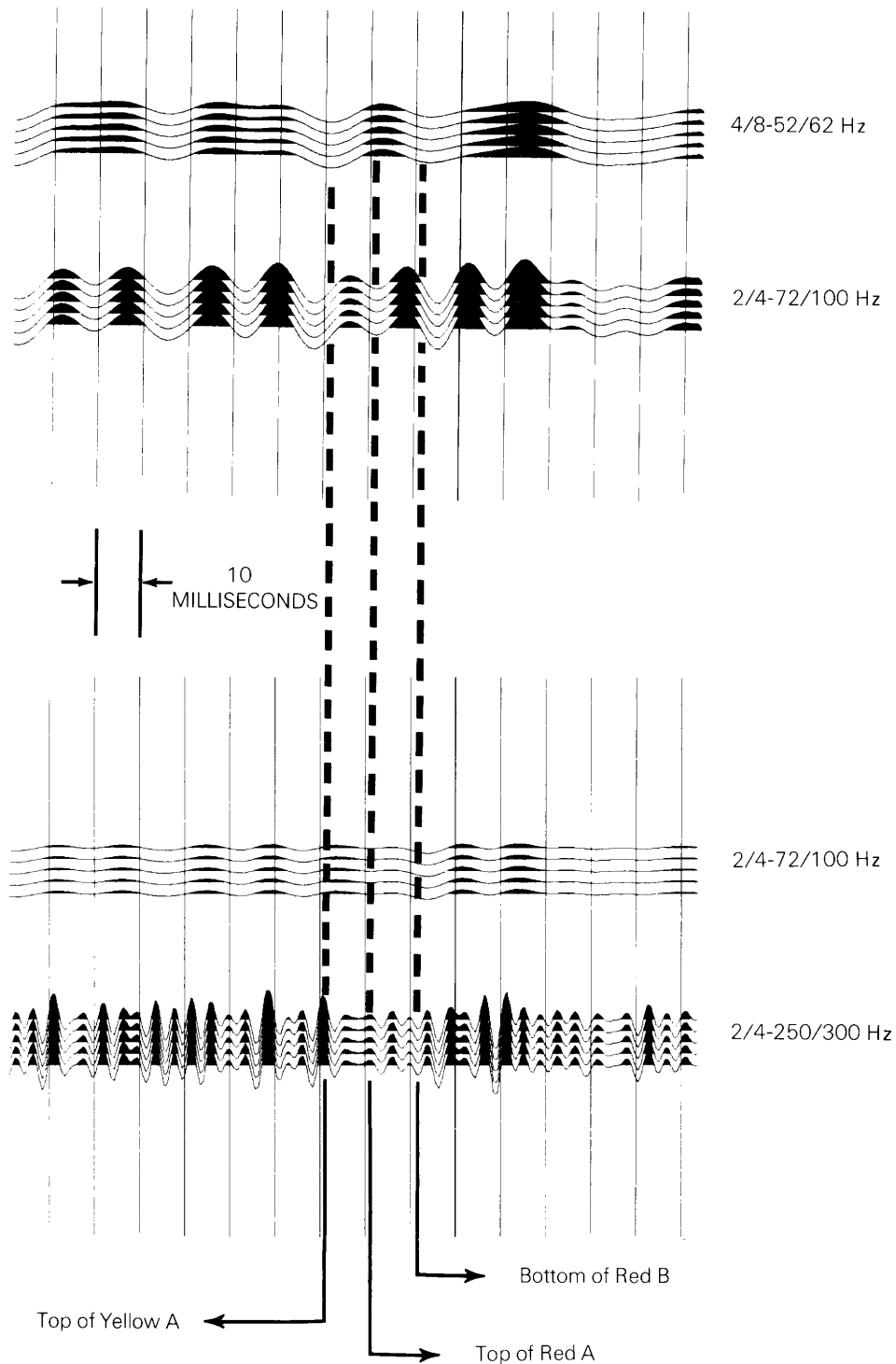


Figure 8. Synthetic seismograms generated by using impedance log shown in figure 7 and various zero-phase bandpass filters.

seismic response from all Yellow sandstone bodies and the trough represents the average response of all Red sandstone bodies. This peak-trough combination can be seen throughout the study.

In an attempt to identify the seismic character of the lower coastal interval at other source locations, down-

going and upgoing waves between depths of 6,000 and 6,250 ft were vertically summed to improve signal-to-noise ratios, and various bandpass filters were applied. The same peak-trough combination is at all source locations at the correct time, and differences in the peak-trough amplitude between source locations are possibly

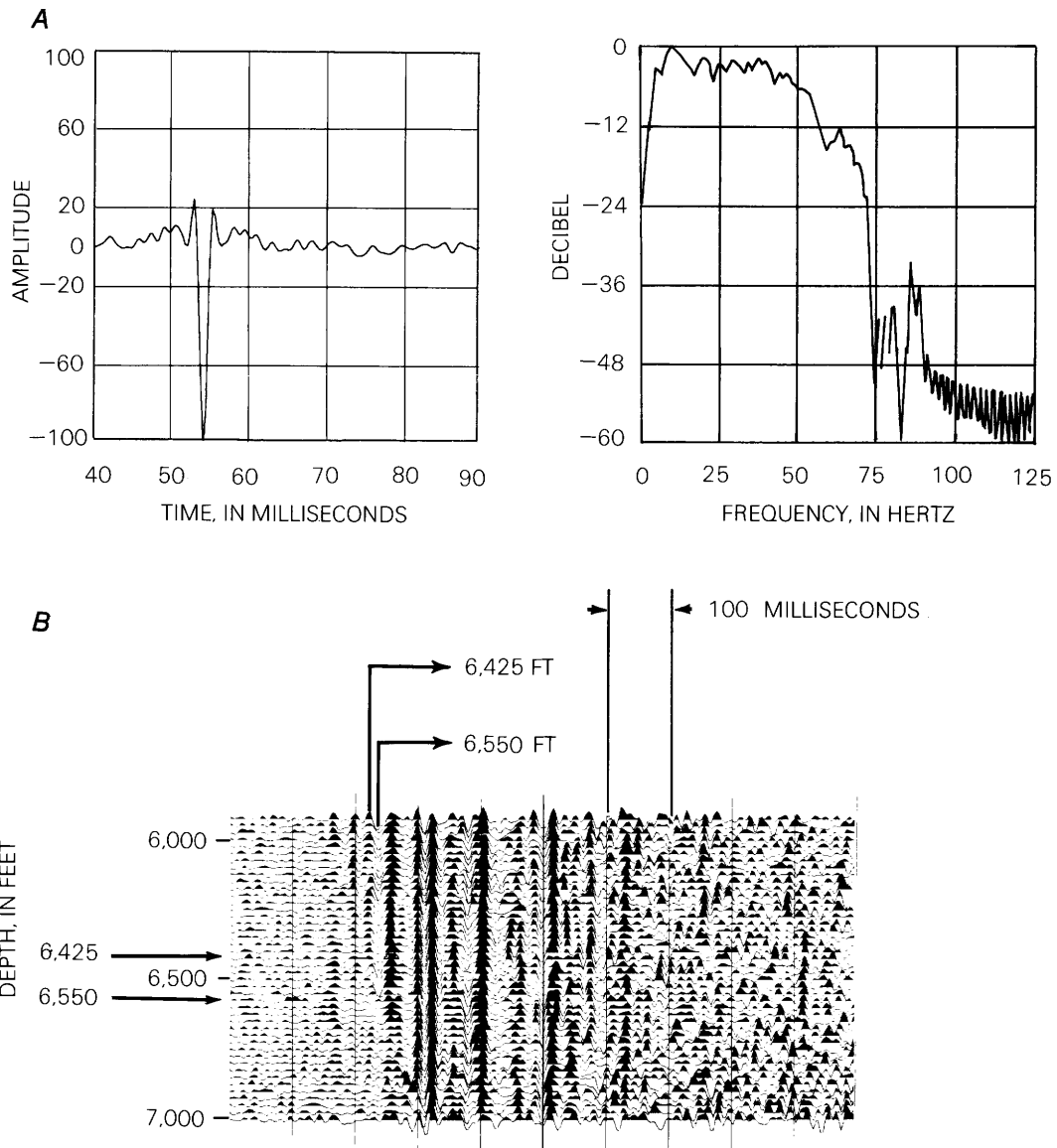


Figure 9. Identification of the lower coastal zone at MWX-3 from source location 1. *A*, Down-going wave and its amplitude spectrum at well-seismometer depth of 6,000 ft. *B*, Vertically aligned upgoing wave field shifted to align coherent events between depths of 5,925 and 7,000 ft by using inversion method.

caused by the spatial distribution of the lower coastal sandstone reservoirs around the well.

Although the peak-trough combination is the result of sandstone reservoirs near the well, it would be very interesting and helpful to analyze other possible acoustic impedance distributions that might result in similar peak-trough combinations farther away from the well. A synthetic seismogram generated by replacing the lower coastal impedance by a constant relative impedance of 8 (corresponding to the average relative impedance of shale within the lower coastal zone) fits the observed peak-trough combination quite well. This good fit implies

that if a sandstone near the well site pinches out progressively away from the well into shale, it would be very difficult to detect truncation of the sandstone, even though the amplitude response of shale is slightly less than that of sandstone.

Different spatial distributions of sandstones and shales might provide some indication of the sandstone distribution, but the small amplitude variation may be quite difficult to analyze in real vertical seismic data. The possibility of a facies change into shale should be retained, therefore, in the interpretation of the sandstone bodies.

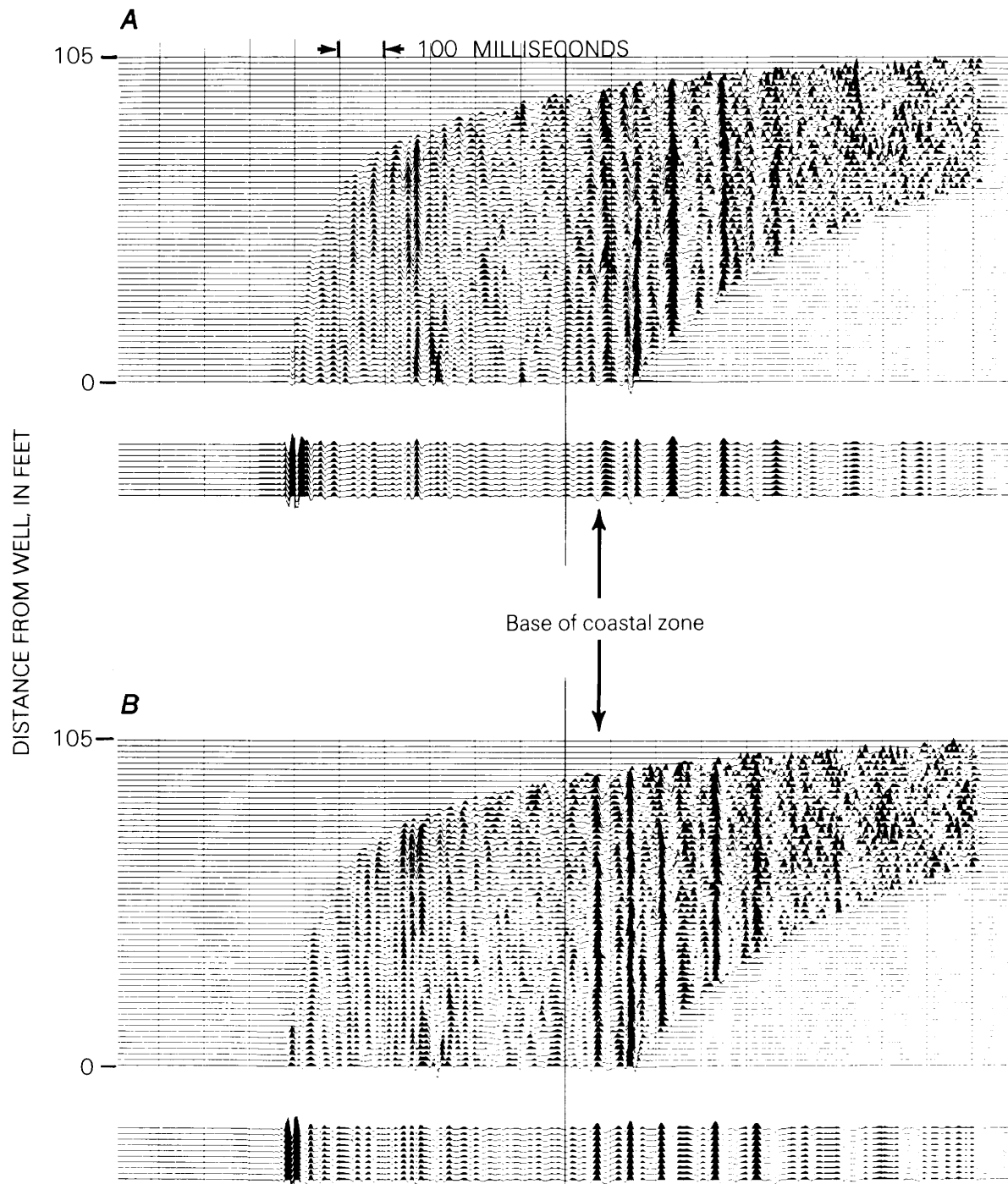


Figure 10. Laterally stacked and cumulatively summed vertical-component data at MWX-3 from source location 1. A, Normal polarity. B, Reverse polarity.

Geometry of Coastal Sandstone Bodies

The spatial distribution of the lower coastal sandstones was interpreted by using laterally stacked vertical seismic profiles (figs. 10–14), the geologic interpretation of J.C. Lorenz (written commun., 1984, 1985), well logs, one- and three-dimensional seismic modeling, and other

available vertical seismic profiles. The following procedure was used.

1. Identification of peak-trough combination for the lower coastal interval.
2. Examination of continuity and character of peak-trough combination for laterally stacked data and other available vertical seismic profiles.

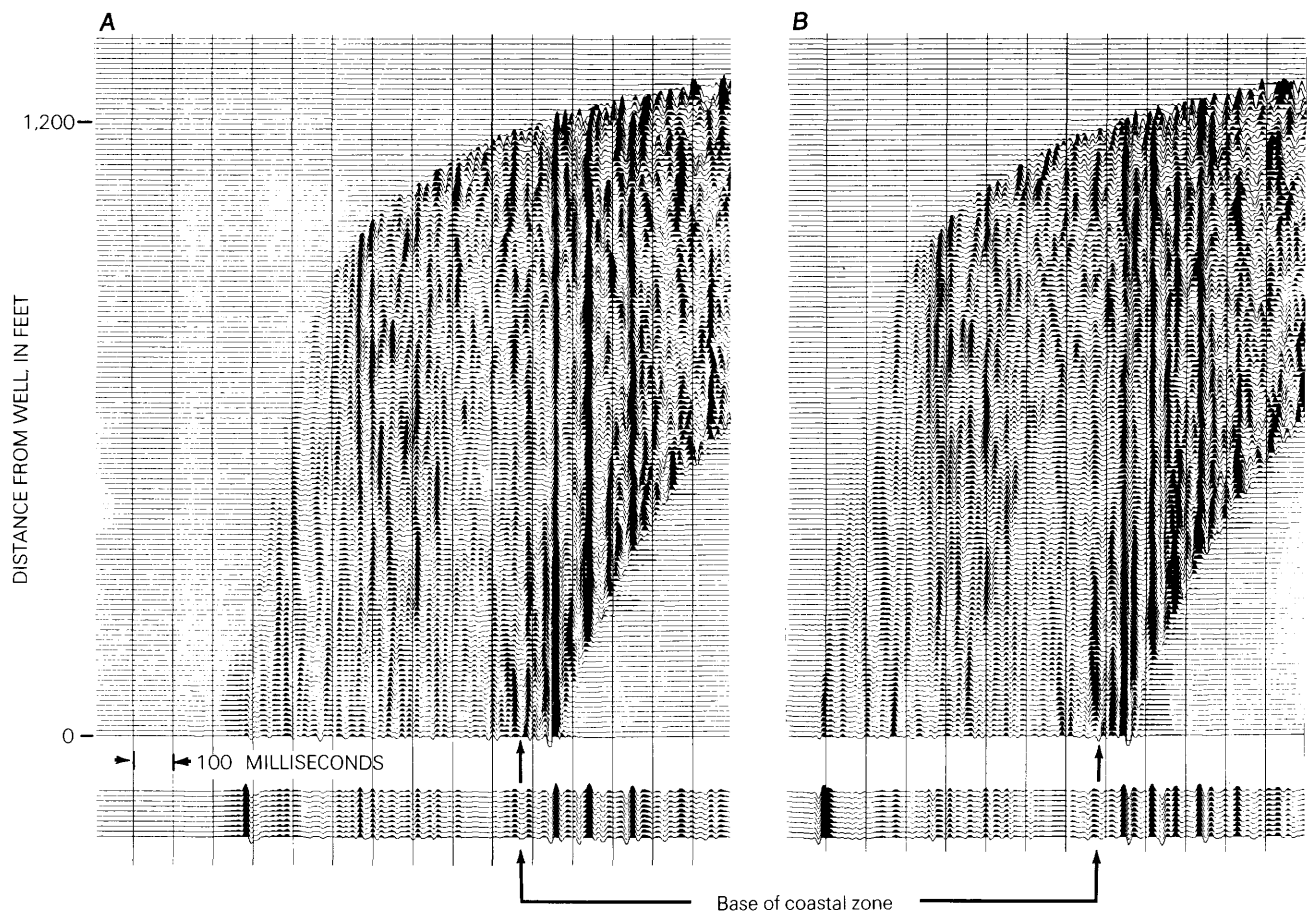


Figure 11. Laterally stacked and cumulatively summed vertical-component data at MWX-3 from source location 2. A, Normal polarity. B, Reverse polarity.

3. Interpretation of the geometry of the Yellow and Red sandstone bodies by using amplitude variation near their edges and available geologic information.
4. Creation of three-dimensional seismic model based on results of step 3, and comparison of model results and real data for all four source locations. In the three-dimensional modeling, a lenticular sandstone body is modeled as a rectangular body (Lee, 1985).
5. Adjustment of model parameters as necessary to fit real data.

The peak-trough combination that represents the seismic response of the lower coastal interval was identified for all source locations by using vertically summed traces. Confirmation of the same peak-trough combination in laterally stacked data should increase the reliability of both data processing and interpretation. Thus, the laterally stacked VSP data about 800 ft from MWX-3 in the direction of source location 2 were replaced by the vertically summed traces from source location 1 (fig. 15). This procedure is very similar to the conventional technique of inserting vertical seismic data

into surface seismic data in order to make accurate stratigraphic interpretations (Balch and others, 1982). The remarkable match of the key stratigraphic horizons between the two data sets should rule out any ambiguity in identification of the lower coastal interval, and the gross error in the processing should be small.

The northwest edge of the base of the Red sandstone zone was located primarily by using the interference pattern and amplitude reduction of the laterally stacked *SH*-wave from source location 2 (fig. 12) and is about 400 ft from the MWX-3 well. A similar seismic character can be observed in the vertical-component data (fig. 11). The northeast and southeast edges of the Red sandstone zone were located by using the amplitude reduction of the base of coastal reflection and are about 600 ft from the well (figs. 13, 14). The length of the sandstone body cannot be estimated directly because the VSP is not offset to the southwest but was estimated by adjusting model parameters (step 5 of interpretation procedure).

The location and geometry of the Yellow zone were more difficult to determine, possibly because of the zone's

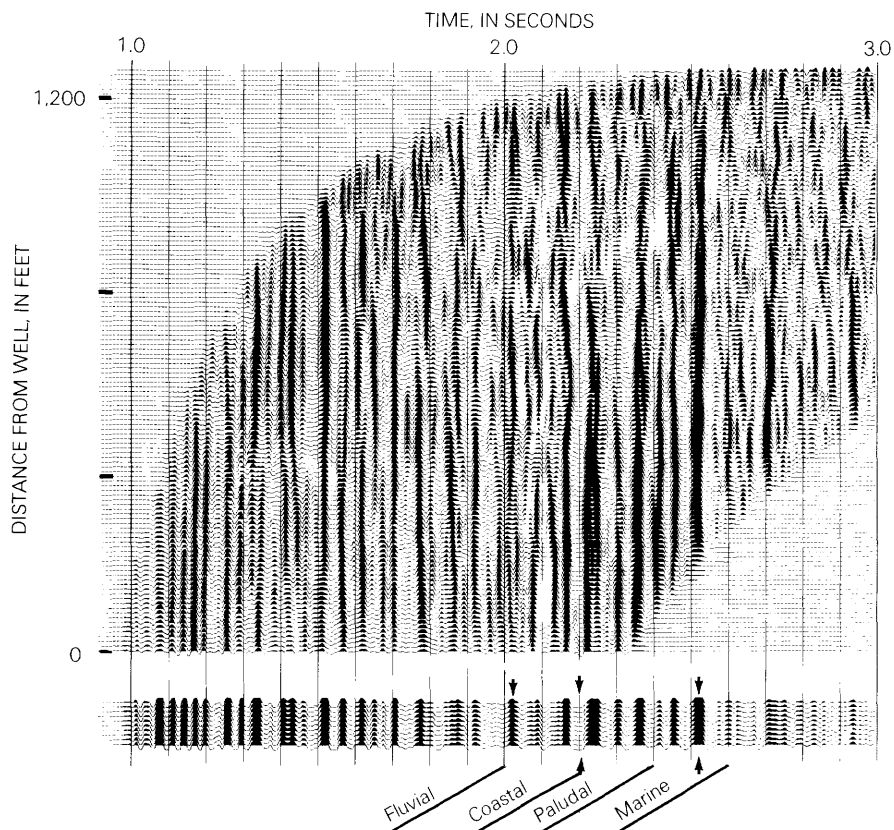


Figure 12. Laterally stacked and cumulatively summed, horizontally polarized shear wave (*SH*) component data at MWX-3 from source location 2.

low reflection amplitude as compared to that from the base of the Red sandstone body and because of interferences with the upper coastal sandstone bodies. By using the continuity of the peak reflection (fig. 11), the northwest edge of the Yellow zone was interpreted to be beyond the maximum lateral distance investigated by the azimuthal survey; that is, more than 1,200 ft from the well. The southeast edge of the Yellow zone was located by using an amplitude reduction (fig. 13) and is about 250 ft from the well.

By performing interpretative steps 4 and 5 and taking into consideration the above observations, I interpreted the shape and location of the lower coastal sandstone bodies (fig. 16). My interpretation is similar to that of J.C. Lorenz (written commun., 1985), which is based on the sedimentology of the sandstones.

The similar amplitude variation between the three-dimensionally modeled and real near-offset VSP data (fig. 10) suggests that estimates for the average widths of the Yellow and Red sandstone bodies are reasonable. Comparison of real and synthetic data for source location 2 indicates a similar amplitude character of trough reflections. For source location 3, the three-dimensional model

does not indicate any amplitude reduction within 600 ft of the lateral distance, whereas the actual VSP data do.

In addition, numerous discrepancies were observed between the real and synthetic data. The synthetic model may be too simple to explain the observed data, or the observed data may be contaminated by noise.

CONCLUSIONS

Detection of the edges of the lower coastal sandstone bodies at the MWX site by using an azimuthal VSP survey was difficult because:

1. The quality of VSP data acquired under adverse field conditions was substantially degraded.
2. The high-frequency seismic data required to map individual sandstone bodies could not be attained even by using very modern technology because of the lack of impedance contrast between sandstone and shale and because of the small size of the sandstone bodies.

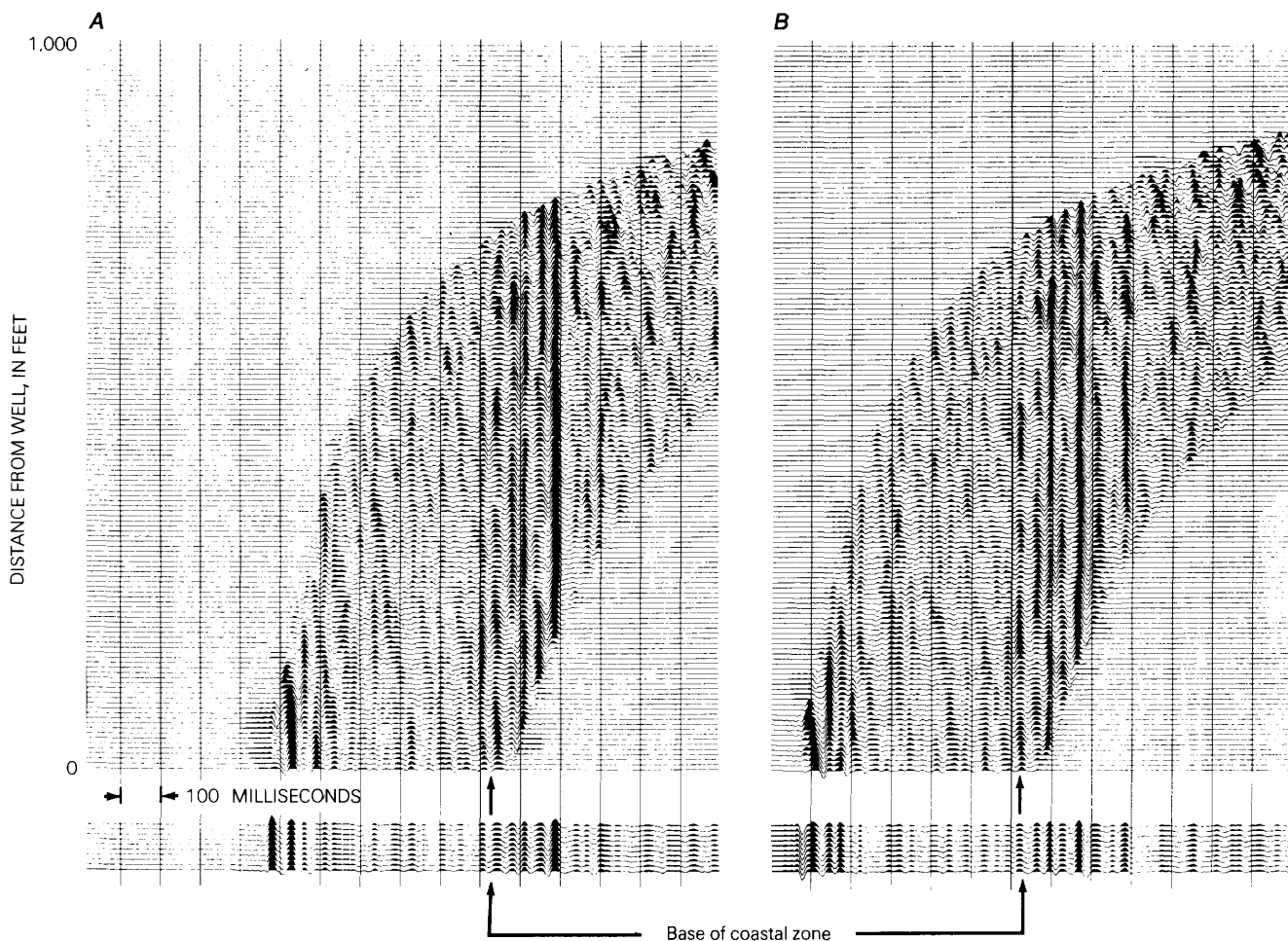


Figure 13. Laterally stacked and cumulatively summed vertical-component data at MWX-3 from source location 3. *A*, Normal polarity. *B*, Reverse polarity.

Although some uncertainty in the interpretation exists, the following conclusions can be derived by using the results of the survey at the MWX-3 well.

1. The lower sandstone bodies (Yellow and Red zones) were identified with a high level of confidence for all source locations.
2. The Yellow sandstone zone may extend more than 1,200 ft to the northwest of the well and have an average width of 600 ft. The truncation edge of the zone may be about 400 ft southeast of the well site.
3. The Red sandstone zone probably is oriented northeast, has an average width of 800 ft, and may be truncated about 500 ft from the MWX-3 well site in the direction of source location 3. The position of the other edge of the Red sandstone zone could not be estimated directly by using the VSP data because there is no source location opposite to source location 3. A three-dimensional model indicates that the zone may extend more than 2,000 ft to the southwest of the MWX site.

4. The extent of the upper coastal sandstone bodies cannot be resolved because of their low and discontinuous amplitude responses and because they are smaller or thinner than the lower coastal sandstone bodies.

5. The general orientation of the Yellow and Red zones, as determined by the azimuthal VSP survey, is similar to that determined by a sedimentological study of these zones.

6. Azimuthal VSP techniques may be applicable for the delineation of sandstone reservoirs.

REFERENCES CITED

- Balch, A.H., Lee, M.W., Miller, J.J., and Ryder, R.T., 1982, The use of vertical seismic profiles in seismic investigations of the Earth: *Geophysics*, v. 47, no. 6, p. 906-918.
- Lee, M.W., 1984a, Vertical seismic profiles at the Multiwell Experiment site, Garfield County, Colorado: U.S. Geological Survey Open-File Report 84-168, 57 p.

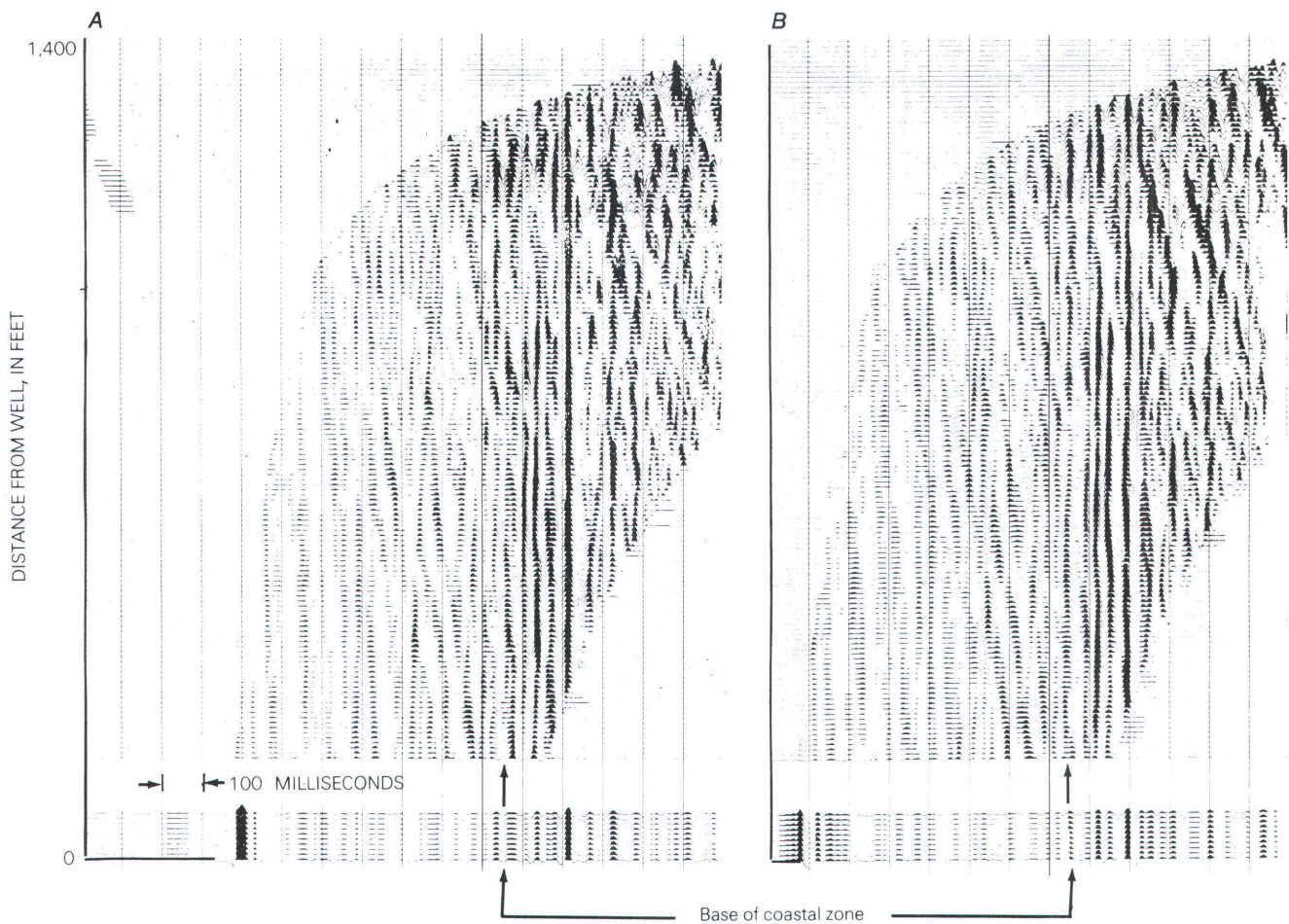


Figure 14. Laterally stacked and cumulatively summed vertical-component data at MWX-3 from source location 4. *A*, Reverse polarity. *B*, Normal polarity.

____ 1984b, Delineation of lenticular-type sand bodies by the vertical seismic profiling method: U.S. Geological Survey Open-File Report 84-265, 92 p.

____ 1985, Interpretation of azimuthal vertical seismic profile survey at Multi-well Experimental site, Garfield County, Colorado: U.S. Geological Survey Open-File Report 85-428, 44 p.

Lee, M.W., and Miller, J.J., 1985, Acquisition and processing of azimuthal vertical seismic profiles at Multi-well Experiment site, Garfield County, Colorado: U.S. Geological Survey Open-File Report 85-427, 36 p.

Sattler, A.R., Hudson, P.J., Raible, C.J., Gall, B.L., and Maloney, D.R., 1986, Laboratory studies for the design and analysis of hydraulic fractured stimulations in lenticular tight gas reservoirs: Society of Petroleum Engineers Unconventional Gas Technology Symposium, Louisville, Ky., 1983, Proceedings, p. 437-447.

Searls, C.A., Lee, M.W., Miller, J.J., Albright, J.N., Fried, Jonathan, and Applegate, J.K., 1983, A coordinated seismic study of the Multi-well Experiment site: Society of Petroleum Engineers/Department of Energy Symposium on Low Permeability Gas Reservoirs, Denver, Colo., 1983, Proceedings, p. 115-120.

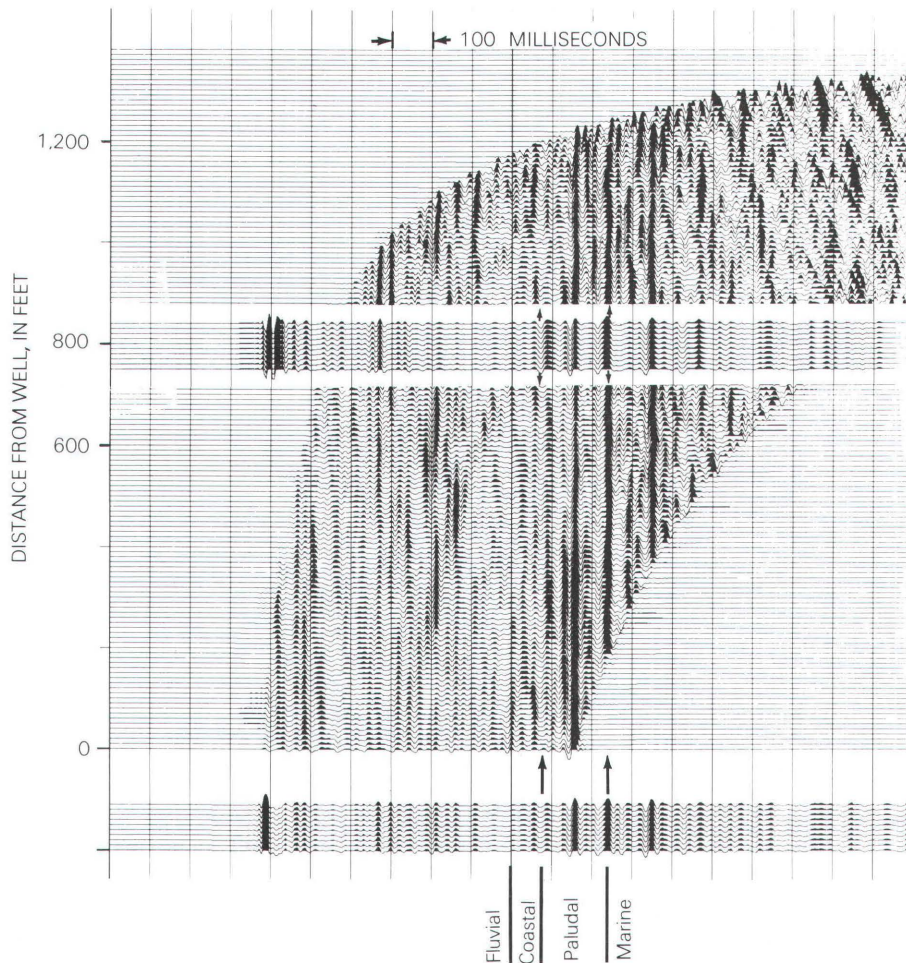


Figure 15. Laterally stacked vertical-component data at MWX-3 from source location 2. Laterally stacked data at a distance of 800 ft from the MWX-3 well was replaced by cumulatively summed data from source location 1.

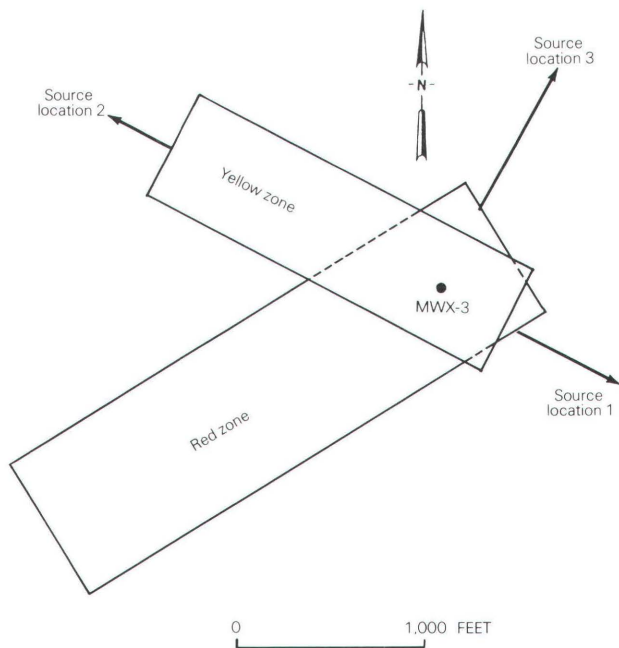


Figure 16. Schematic interpretation of the geometry of the lower coastal sandstone bodies in the MWX-3 well.



